NOVEL COMBINATION THERAPIES FOR THE TREATMENT OF SOLID CANCERS

EDITED BY: Khalid A. El Sayed and Nehad M. Ayoub

PUBLISHED IN: Frontiers in Oncology and Frontiers in Pharmacology

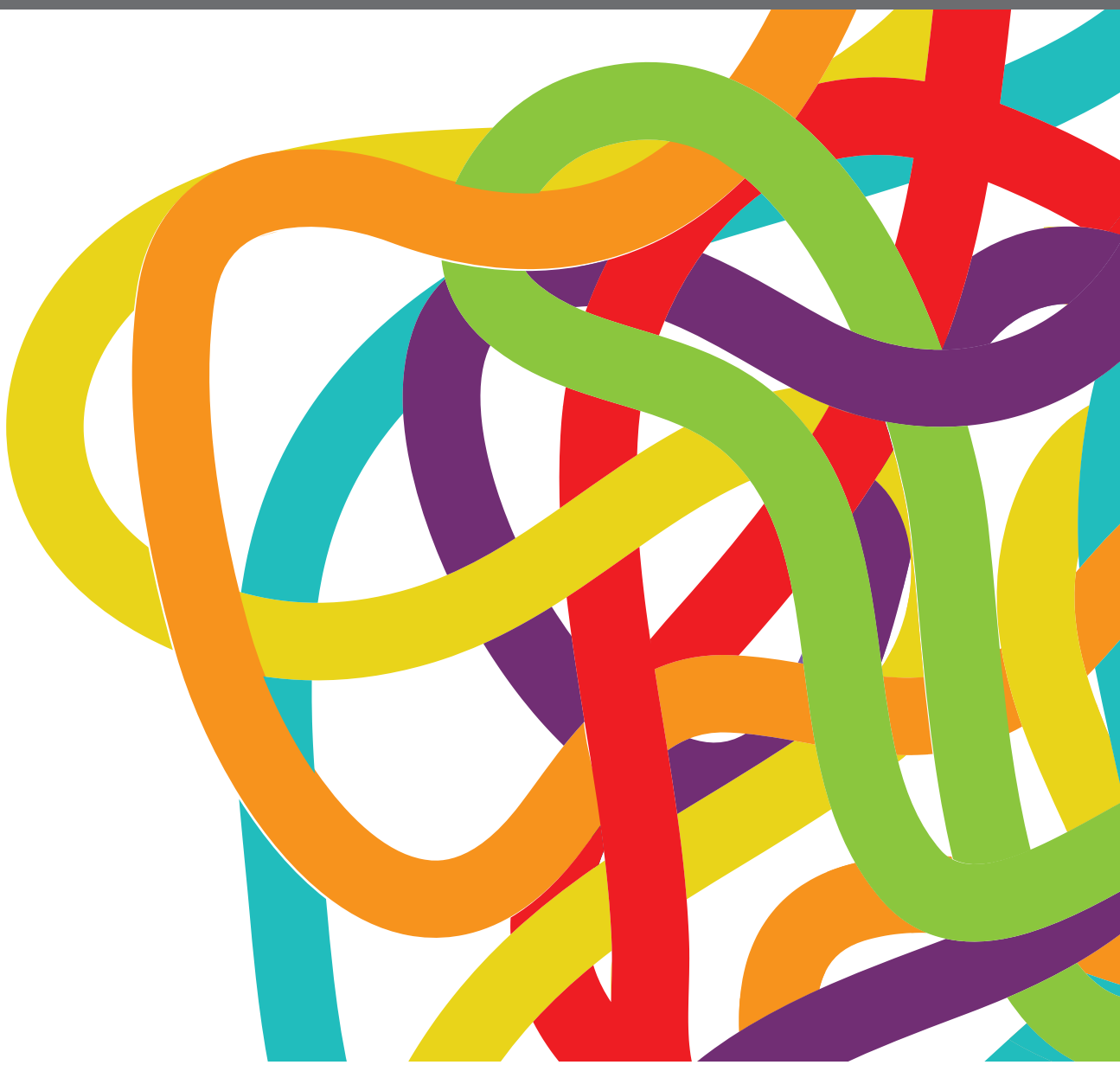

frontiers Research Topics

ISSN 1664-8714
ISBN 978-2-88971-857-3
DOI 10.3389/978-2-88971-857-3

About Frontiers

Frontiers is more than just an open-access publisher of scholarly articles: it is a pioneering approach to the world of academia, radically improving the way scholarly research is managed. The grand vision of Frontiers is a world where all people have an equal opportunity to seek, share and generate knowledge. Frontiers provides immediate and permanent online open access to all its publications, but this alone is not enough to realize our grand goals.

Frontiers Journal Series

The Frontiers Journal Series is a multi-tier and interdisciplinary set of open-access, online journals, promising a paradigm shift from the current review, selection and dissemination processes in academic publishing. All Frontiers journals are driven by researchers for researchers; therefore, they constitute a service to the scholarly community. At the same time, the Frontiers Journal Series operates on a revolutionary invention, the tiered publishing system, initially addressing specific communities of scholars, and gradually climbing up to broader public understanding, thus serving the interests of the lay society, too.

Dedication to Quality

Each Frontiers article is a landmark of the highest quality, thanks to genuinely collaborative interactions between authors and review editors, who include some of the world's best academicians. Research must be certified by peers before entering a stream of knowledge that may eventually reach the public - and shape society; therefore, Frontiers only applies the most rigorous and unbiased reviews.
Frontiers revolutionizes research publishing by freely delivering the most outstanding research, evaluated with no bias from both the academic and social point of view. By applying the most advanced information technologies, Frontiers is catapulting scholarly publishing into a new generation.

What are Frontiers Research Topics?

Frontiers Research Topics are very popular trademarks of the Frontiers Journals Series: they are collections of at least ten articles, all centered on a particular subject. With their unique mix of varied contributions from Original Research to Review Articles, Frontiers Research Topics unify the most influential researchers, the latest key findings and historical advances in a hot research area! Find out more on how to host your own Frontiers Research Topic or contribute to one as an author by contacting the Frontiers Editorial Office: frontiersin.org/about/contact

NOVEL COMBINATION THERAPIES FOR THE TREATMENT OF SOLID CANCERS

Topic Editors:
Khalid A. El Sayed, University of Louisiana at Monroe, United States
Nehad M. Ayoub, Jordan University of Science and Technology, Jordan

Citation: El Sayed, K. A., Ayoub, N. M., eds. (2021). Novel Combination Therapies For The Treatment of Solid Cancers. Lausanne: Frontiers Media SA. doi: 10.3389/978-2-88971-857-3

Table of Contents

05 ***Editorial: Novel Combination Therapies for the Treatment of Solid Cancers***
Nehad M. Ayoub

08 ***Repositioning Aspirin to Treat Lung and Breast Cancers and Overcome Acquired Resistance to Targeted Therapy***
Ling Li, Mengdi Hu, Tao Wang, Hongzhuan Chen and Lu Xu

18 ***Clinical and Immunological Outcomes in High-Risk Resected Melanoma Patients Receiving Peptide-Based Vaccination and Interferon Alpha, With or Without Dacarbazine Preconditioning: A Phase II Study***
Francesca Urbani, Virginia Ferraresi, Imerio Capone, Iole Macchia, Belinda Palermo, Carmen Nuzzo, Angela Torsello, Patrizio Pezzotti, Diana Giannarelli, Anna Fausta Pozzi, Mariano Santaquilani, Paolo Roazzi, Silvia Bastucci, Caterina Catricalà, Antonia La Malfa, Giuseppe Vercillo, Novella Gualtieri, Carla Buccione, Luciano Castiello, Francesco Cognetti, Paola Nisticò, Filippo Belardelli, Federica Moschella and Enrico Proietti

34 ***Sitravatinib, a Tyrosine Kinase Inhibitor, Inhibits the Transport Function of ABCG2 and Restores Sensitivity to Chemotherapy-Resistant Cancer Cells*** **in vitro**
Yuqi Yang, Ning Ji, Qiu-Xu Teng, Chao-Yun Cai, Jing-Quan Wang, Zhuo-Xun Wu, Zi-Ning Lei, Sabrina Lusvarghi, Suresh V. Ambudkar and Zhe-Sheng Chen

48 ***M3814, a DNA-PK Inhibitor, Modulates ABCG2-Mediated Multidrug Resistance in Lung Cancer Cells***
Zhuo-Xun Wu, Zheng Peng, Yuqi Yang, Jing-Quan Wang, Qiu-Xu Teng, Zi-Ning Lei, Yi-Ge Fu, Ketankumar Patel, Lili Liu, Lizhu Lin, Chang Zou and Zhe-Sheng Chen

62 ***Protective Role of Enalapril in Anthracycline-Induced Cardiotoxicity: A Systematic Review***
Yili Zhang, Junjie Liu, Yuan Li, Nannan Tan, Kangjia Du, Huihui Zhao, Juan Wang, Jian Zhang, Wei Wang and Yong Wang

72 ***Chemotherapeutic Effectiveness of Combining Cetuximab for Metastatic Colorectal Cancer Treatment: A System Review and Meta-Analysis***
Rong Li, Minqing Liang, Xiao Liang, Lu Yang, Min Su and Keng Po Lai

82 ***Targeting SphK2 Reverses Acquired Resistance of Regorafenib in Hepatocellular Carcinoma***
Weiwei Shi, Shan Zhang, Ding Ma, Dongliang Yan, Guang Zhang, Yin Cao, Zhongxia Wang, Junhua Wu and Chunping Jiang

99 ***Phosphodiesterase Type 5 Inhibitors Synergize Vincristine in Killing Castration-Resistant Prostate Cancer Through Amplifying Mitotic Arrest Signaling***
Jui-Ling Hsu, Wohn-Jenn Leu, Lih-Ching Hsu, Chen-Hsun Ho, Shih-Ping Liu and Jih-Hwa Guh

113 ***Overcoming Limitations of Cisplatin Therapy by Additional Treatment With the HSP90 Inhibitor Onalespib***
Anja Charlotte Lundgren Mortensen, Tabassom Mohajershojai, Mehran Hariri, Marika Pettersson and Diana Spiegelberg

128 ***Activity of Birinapant, a SMAC Mimetic Compound, Alone or in Combination in NSCLCs With Different Mutations***
Marika Colombo, Mirko Marabese, Giulia Vargiu, Massimo Broggini and Elisa Caiola

139 ***Suppression of Esophageal Cancer Stem-like Cells by SNX-2112 Is Enhanced by STAT3 Silencing***
Dan-dan Xu, Su-hong Chen, Peng-jun Zhou, Ying Wang, Zhen-dong Zhao, Xia Wang, Hui-qing Huang, Xue Xue, Qiu-ying Liu, Yi-fei Wang and Rong Zhang

155 ***Novel Combination Therapies for the Treatment of Bladder Cancer***
Mei Peng, Di Xiao, Yizhi Bu, Jiahui Long, Xue Yang, Shuhe Lv and Xiaoping Yang

168 ***Doubling the Dose of Bevacizumab Beyond Progression in Metastatic Colorectal Cancer—the Experience of a Tertiary Cancer Center***
Călin Căinap, Ovidiu-Vasile Bochiş, Cătălin Vlad, Raluca Popita, Patriciu Achimaş-Cadariu, Andrei Havasi, Andreea Vidrean, Alexandra Dranca, Andra Piciu, Anne-Marie Constantin, Tiberiu Tat, Maniu Dana, Ovidiu Crişan, Cosmin Vasile Cioban, Ovidiu Bălăcescu, Ovidiu Coza, Loredana Bălăcescu, Monica Mihaela Marta, Madalina Bota and Simona Căinap

frontiers in Oncology

EDITORIAL
published: 18 June 2021
doi: 10.3389/fonc.2021.708943

Editorial: Novel Combination Therapies for the Treatment of Solid Cancers

Nehad M. Ayoub *

Department of Clinical Pharmacy, Faculty of Pharmacy, Jordan University of Science and Technology (JUST), Irbid, Jordan

Keywords: combination, resistance, repositioning, synergy, efflux transporters

Editorial on the Research Topic

Combination Therapies for the Treatment of Solid Cancers

The concept of combination therapy was first introduced in 1965 when Emil Frei et al. launched the first-ever combination chemotherapy in pediatric patients with acute leukemia (1). The success of this combination therapeutic approach had remarkably changed the landscape of clinical oncology ever since (2). Consequently, much emphasis in cancer research was directed to investigating combination therapies that target different pathways to generate a favorable anticancer activity (3). In line with this, advancements in cancer cell genomics, epigenomics, transcriptomics, and proteomics have paved the way to identifying new molecular targets and the development of selective targeted anticancer therapies (4). Targeted therapies have substantially expanded the options for combinational anticancer treatments that can be combined with other targeted therapies or chemotherapeutic drugs (5).

The combination of anticancer therapies is clinically appealing for several reasons. Firstly, combination therapy improves treatment outcomes and results in superior therapeutic effects, especially when a synergistic anticancer activity is achieved (6). Secondly, the combinational approach overcomes clonal heterogeneity which is further associated with improved response rates (7). Thirdly, combined drug regimens reduce the toxicity of the regimen as it allows using individual drugs at reduced dosages at maintained therapeutic efficacy (6). Another advantage of combination therapies is reducing the emergence of drug resistance (6). In this context, combination therapy enables concurrent targeting of several molecular pathways essential for cancer cell survival and abolish cellular mechanisms associated with adaptive resistance (8). Despite the advantages of combination cancer treatments, several challenges accompany the development and utilization of combined therapies. A challenging aspect of combination therapies is the potential drug interactions and the pharmacokinetics of co-administered agents that could influence the therapeutic activity of the regimen (2, 9). Besides, the administration of suboptimal doses of drugs in the combination may be necessary to avoid toxicity (9). The definition of synergism is inconclusive, particularly in clinical studies, and its prediction is challenging (10).

Historically, the development of most drug combinations was conducted using empirical experimental or clinical settings (7, 8). In such a case, a detailed mechanistic analysis is rarely performed for the prediction of effective combinations (7). Therefore, the development of strategies

Edited and reviewed by:
Olivier Feron,
Université catholique de Louvain, Belgium

***Correspondence:**
Nehad M. Ayoub
nmayoub@just.edu.jo

Specialty section:
This article was submitted to Pharmacology of Anti-Cancer Drugs, a section of the journal Frontiers in Oncology

Received: *12 May 2021*
Accepted: *04 June 2021*
Published: *18 June 2021*

Citation:
Ayoub NM (2021) Editorial: Novel Combination Therapies for the Treatment of Solid Cancers. Front. Oncol. 11:708943. doi: 10.3389/fonc.2021.708943

for the prediction and identification of combinations that exhibit synergy is imperative (7, 8). In this regard, Narayan et al. used a new approach called '*drug atlas*' to identify novel synergistic combination therapies (8). This strategy allows the identification of independent processes for which the tumor might be particularly vulnerable when attacked by two drugs on a pan-cancer scale. A restrictive combination of drugs is another approach that is gaining attention in cancer therapy (3). This restrictive approach is based on the differences between cancer cells and normal cells and focuses on strategic dosing and drug administration to spare normal cells while targeting cancer cells (3, 11). Besides, Tolcher et al. have demonstrated the use of the '*CombiPlex*' technology platform as a valuable tool for developing drug combinations to predict the likelihood of clinical activity of anticancer therapies (9). The *CombiPlex* platform improves drug combinations by identifying synergistic drug ratios and directing drug exposure to target tissues (9).

In this Research Topic, several studies have investigated the impact of novel anticancer combinations and strategies in the treatment of solid cancers. Colombo et al. studied the anticancer activity of birinapant, an inhibitor of the inhibitor of apoptosis proteins, in non-small-cell lung cancer. The activity of birinapant was demonstrated in liver kinase B1 (LKB1)-deleted clone but not LKB1-wild type cancer cells. In addition, the combination of birinapant with the p38 inhibitor, ralimetinib, restored the sensitivity of LKB1- and KRAS-mutated cell lines to birinapant. In another study, Mortensen et al. investigated the impact of the novel heat shock protein 90 (HSP90) inhibitor, onalespib to enhance the activity and reverse resistance of cisplatin in ovarian and head and neck cancer cells. The results of the study showed that the combination of onalespib and cisplatin restored therapeutic activity and enhanced the antiproliferative, antimigratory, and apoptotic effects of the chemotherapeutic drug. Shi et al. showed that sphingosine kinase 2 (SphK2) mediated regorafenib resistance in hepatocellular carcinoma through NF-kB and STAT3 activation. The authors also reported that sensitivity to regorafenib was restored with the combination of regorafenib and the SphK2 inhibitor ABC294640 in both *in vitro* and xenograft animal models of hepatocellular carcinoma. Xu et al. showed that the combination of the HSP90, SNX-2112 with the knockdown of STAT3 is associated with enhanced antiproliferative and apoptotic anticancer activity in esophageal cancer stem-like cells in culture and animal models.

The multidrug resistance of cancer cells is strongly linked to the overexpression of ATP-binding cassette (ABC) efflux transporters (12). In this Research Topic, Yang et al. and Wu et al. evaluated the use of ABC efflux transporter inhibitors as chemosensitizing agents to improve the activity of anticancer drugs. Yang et al. demonstrated the inhibitory effect of sitravatinib, a broad-spectrum tyrosine kinase inhibitor, on ABCG2 efflux transporters. Sitravatinib treatment blocked the efflux function of ABCG2 efflux transporters and restored the antineoplastic effect of various anticancer drugs known as ABCG2 substrates. In a second study by Wu et al., nedisertib (M3814), a potent and selective inhibitor of DNA-dependent protein kinase, attenuated the efflux activity of ABCG2 transporter without affecting the expression or cell surface localization of the pump. Nedisertib treatment increased the accumulation of the ABCG2 substrate drugs mitoxantrone and doxorubicin restoring their sensitivity in cancer cells.

Drug repurposing (also known as drug repositioning) is an increasingly recognized therapeutic approach in cancer therapy. Drug repurposing utilizes existing non-cancerous drugs to be used for cancer treatment (3). This approach is very attractive as it utilizes FDA-approved pharmaceutical agents with known safety and pharmacokinetic profiles as a source of new anticancer drugs at a reduced financial burden (3, 13). Li et al. found that aspirin inhibited proliferation and promoted apoptosis of lung and breast cancer cells. In addition, the authors reported that aspirin treatment delayed and overcame resistance to targeted therapy using *in vitro* and *in vivo* models. Hsu et al. demonstrated a synergistic anticancer activity for the combination of sildenafil, a phosphodiesterase inhibitor, and vincristine treatment against castration-resistant prostate cancer (CRPC). The authors showed that sildenafil synergistically potentiated vincristine-induced mitotic arrest and mitochondrial damage *in vitro* and synergized with vincristine on suppressing tumor growth in a xenograft animal model of CRPC. In a systematic review by Zhang et al., the cardioprotective effect of enalapril against anthracycline-induced cardiotoxicity was examined across 626 studies. Preliminary evidence showed that enalapril treatment was associated with reduced cardiac enzymes and improved left ventricular ejection fraction in cancer patients treated with anthracyclines.

In a meta-analysis by Li et al., the authors evaluated 12 randomized controlled trials for the clinical effectiveness of combining cetuximab treatment with chemotherapy for treating metastatic colorectal cancer (mCRC). They revealed an improved progression-free and overall survival for the combination of cetuximab with chemotherapy in wild-type KRAS patients. In a review by Peng et al., the combination of immunotherapy, particularly the immune checkpoint inhibitors, with other drug therapies or radiation was discussed as a novel approach in the treatment of bladder cancer. In this e-book, a phase II study by Urbani et al. evaluated the impact of dacarbazine treatment with peptide-based vaccination in combination with IFN-α2b in melanoma patients. No significant differences were observed between patients who received or did not receive dacarbazine treatment for relapse-free and overall survival. Căinap et al. conducted a retrospective analysis for patients with mCRC who were treated with bevacizumab as first- or second-line therapy and who received bevacizumab beyond the first progression (BYP). They report that doubling the dose of bevacizumab BYP improved overall survival in mCRC patients, and that bevacizumab was a suitable partner in combination with both oxaliplatin- and irinotecan-based regimens.

The use of combined chemotherapy becomes the standard practice in medical oncology. Taking into consideration the tremendous number of available chemotherapeutic and targeted anticancer drugs, the prediction, and development of novel drug combinations is a challenging task. Hence, it is

mandatory to explore the tools necessary to predict the combinations with synergistic anticancer activity. Articles in this Research Topic contributed to the field of novel drug combinations in several aspects including the combinations intended to overcome cancer resistance and enhance anticancer drug activity, repurposing of drugs in combination regimens, and providing insights from human studies on novel combinational approach. Collectively, the future of novel combinations to treat solid cancers is promising with endless potentials for combination therapies on the horizon.

AUTHOR CONTRIBUTIONS

The author confirms being the sole contributor of this work and has approved it for publication.

ACKNOWLEDGMENTS

We are grateful to all authors who contributed to this Research Topic.

REFERENCES

1. Frei E3rd, Karon M, Levin RH, Freireich EJ, Taylor RJ, Hananian J, et al. The Effectiveness of Combinations of Antileukemic Agents in Inducing and Maintaining Remission in Children With Acute Leukemia. *Blood* (1965) 26 (5):642–56. doi: 10.1182/blood.V26.5.642.642
2. Ismail M, Khan S, Khan F, Noor S, Sajid H, Yar S, et al. Prevalence and Significance of Potential Drug-Drug Interactions Among Cancer Patients Receiving Chemotherapy. *BMC Cancer* (2020) 20(1):335. doi: 10.1186/s12885-020-06855-9
3. Bayat Mokhtari R, Homayouni TS, Baluch N, Morgatskaya E, Kumar S, Das B, et al. Combination Therapy in Combating Cancer. *Oncotarget* (2017) 8 (23):38022–43. doi: 10.18632/oncotarget.16723
4. Falzone L, Salomone S, Libra M. Evolution of Cancer Pharmacological Treatments at the Turn of the Third Millennium. *Front Pharmacol* (2018) 9:1300. doi: 10.3389/fphar.2018.01300
5. Kwak EL, Clark JW, Chabner B. Targeted Agents: The Rules of Combination. *Clin Cancer Res* (2007) 13(18 Pt 1):5232–7. doi: 10.1158/1078-0432.CCR-07-1385
6. Bukowska B, Gajek A, Marczak A. Two Drugs Are Better Than One. A Short History of Combined Therapy of Ovarian Cancer. *Contemp Oncol (Pozn)* (2015) 19(5):350–3. doi: 10.5114/wo.2014.43975
7. Palmer AC, Chidley C, Sorger PK. A Curative Combination Cancer Therapy Achieves High Fractional Cell Killing Through Low Cross-Resistance and Drug Additivity. *Elife* (2019) 8:e50036. doi: 10.7554/eLife.50036
8. Narayan RS, Molenaar P, Teng J, Cornelissen FMG, Roelofs I, Menezes R, et al. A Cancer Drug Atlas Enables Synergistic Targeting of Independent Drug Vulnerabilities. *Nat Commun* (2020) 11(1):2935. doi: 10.1038/s41467-020-16735-2
9. Tolcher AW, Mayer LD. Improving Combination Cancer Therapy: The CombiPlex((R)) Development Platform. *Future Oncol* (2018) 14(13):1317–32. doi: 10.2217/fon-2017-0607
10. Chou TC. Drug Combination Studies and Their Synergy Quantification Using the Chou-Talalay Method. *Cancer Res* (2010) 70(2):440–6. doi: 10.1158/0008-5472.CAN-09-1947
11. Blagosklonny MV. Targeting the Absence and Therapeutic Engineering for Cancer Therapy. *Cell Cycle* (2008) 7(10):1307–12. doi: 10.4161/cc.7.10.6250
12. Choi YH, Yu AM. ABC Transporters in Multidrug Resistance and Pharmacokinetics, and Strategies for Drug Development. *Curr Pharm Des* (2014) 20(5):793–807. doi: 10.2174/13816128005140214165212
13. Yang EJ, Wu C, Liu Y, Lv J, Sup Shim J. Revisiting Non-Cancer Drugs for Cancer Therapy. *Curr Top Med Chem* (2016) 16(19):2144–55. doi: 10.2174/1568026616666160216154441

Conflict of Interest: The author declares that the research was conducted in the absence of any commercial or financial relationships that could be construed as a potential conflict of interest.

frontiers in Oncology

ORIGINAL RESEARCH
published: 14 January 2020
doi: 10.3389/fonc.2019.01503

Repositioning Aspirin to Treat Lung and Breast Cancers and Overcome Acquired Resistance to Targeted Therapy

Ling Li[1†], *Mengdi Hu*[1†], *Tao Wang*[1], *Hongzhuan Chen*[1,2*] *and Lu Xu*[1*]

[1] *Department of Pharmacology and Chemical Biology, Shanghai Jiao Tong University School of Medicine, Shanghai, China,*
[2] *Institute of Interdisciplinary Integrative Biomedical Research, Shanghai University of Traditional Chinese Medicine, Shanghai, China*

Background: The major limitation of targeted cancer therapy is development of acquired resistance. Intratumoral heterogeneity and coexist of multiple resistance mechanisms make combination therapies targeting one specific mechanism inefficient.

Methods: Transcriptional signature obtained from GEO was used to reposition FDA-approved drugs to treat lung and breast cancers as well as overcome acquired resistance to EGFR TKIs in lung cancer and to tamoxifen in breast cancer via CMap. *In vitro* and *in vivo* models were used to examine candidate drugs for their anti-cancer and anti-resistance efficacy and underlying mechanisms.

Results: We found that aspirin, the most commonly used drug, not only inhibited proliferation and promoted apoptosis of cancer cells, but also delayed and overcame acquired resistance to targeted therapy using *in vitro* and *in vivo* models. The underlying mechanism could be attributed to enhanced cancer stemness and activated NF-κB signaling in acquired resistant tumors, both of which were suppressed by aspirin and rendered resistant tumors more sensitive to aspirin.

Conclusions: Our data identify aspirin as a potential candidate for combination therapy for lung and breast cancers.

Keywords: aspirin, lung cancer, breast cancer, targeted therapy, EGFR TKIs, tamoxifen, CMap, reposition

OPEN ACCESS

Edited by:
Khalid A. El Sayed, University of Louisiana at Monroe, United States

Reviewed by:
Weicheng Liang, The Chinese University of Hong Kong, China
Rafael Rosell, Catalan Institute of Oncology, Spain

***Correspondence:**
Hongzhuan Chen
hongzhuan_chen@hotmail.com
Lu Xu
luxuluxu@yahoo.com

[†]*These authors have contributed equally to this work*

Specialty section:
This article was submitted to Pharmacology of Anti-Cancer Drugs, a section of the journal Frontiers in Oncology

Received: *25 September 2019*
Accepted: *16 December 2019*
Published: *14 January 2020*

Citation:
Li L, Hu M, Wang T, Chen H and Xu L (2020) Repositioning Aspirin to Treat Lung and Breast Cancers and Overcome Acquired Resistance to Targeted Therapy. Front. Oncol. 9:1503. doi: 10.3389/fonc.2019.01503

BACKGROUND

Cancer is the leading cause of death worldwide. Treatment for cancer includes surgery, chemotherapy, and radiation therapy. Recently, the emergence of targeted therapy, which directly targets molecules that are uniquely or abnormally expressed in cancer cells, has changed dramatically the treatment of cancer. For example, tamoxifen was the first targeted therapy using estrogen receptor (ER) as the target, which is present in about 80% of all breast cancer (ER-positive), and reduces greatly the incidence of breast cancer death and recurrence in ER-positive patients. Epidermal growth factor receptor (EGFR) is another effective target for treatment of many epithelial cancers, especially non-small cell lung cancer in which 10–55% patients have EGFR mutation. EGFR tyrosine kinase inhibitors (TKIs) have been approved for the first line-treatment for EGFR-mutant lung cancer patients. However, the limitation of targeted therapy is acquired resistance developed during the treatment course. The one major mechanism of acquired resistance to targeted therapy is the alterations in the target itself (on-target),

such as second mutation T790M in EGFR in EGFR-mutant lung cancer or loss of ER function/expression in ER+ breast cancer. Next-generation drugs targeting altered targets need to be developed to overcome on-target acquired resistance. The other type of mechanisms is compensatory activation of downstream or parallel signaling pathways (off-target), such as RAS-RAF-MEK-ERK, PI3K-PTEN-AKT-mTOR, IGF1R pathway, NF-κB pathway et al., which were common in both lung and breast cancer with acquired resistance to respective targeted therapy (1–4) and could be overcome by combination therapies. Unfortunately, intratumoral heterogeneity which has been linked to treatment resistance and tumor recurrence as well as coexist of multiple resistance mechanisms render combination therapy targeting one specific molecule or pathway inefficient (5, 6).

Drug repositioning or repurposing is to apply an existing drug for another indication than it was originally approved for and has recently gained popularity as an alternative strategy to *de novo* drug synthesis, which is a time-consuming and costly process (7, 8). Systematic repurposing approaches can be subdivided into computational approaches and experimental approaches, both of which are often used synergistically. Signature matching is one of the most commonly used computational approaches, which is based on the comparison of the signature of a drug against that of another drug or disease. Connectivity map (CMap, http://www.broad.mit.edu/cmap/) is a transcriptional expression database containing compound-perturbed gene expression profiles of cultured human cell lines. Of the 1309 compounds included in CMap, most of them are currently used in clinic or well-developed. By comparison of the transcriptome of human cells treated with compound with that of a disease, which can be easily accessed through public databases like Gene Expression Omnibus (GEO), some old drugs have been successfully repositioned. For example, using glioblastoma gene signatures collected from GEO to query CMap and then cell-based screening of 65 candidate drugs, Cheng et al. found that thioridazine, a DRD2 antagonist/antipsychotic drug, had anticancer stem cell effects (9). A phase I trial has been conducted on acute myeloid leukemia (AML) patients to evaluate thioridazine in combination with cytarabine and preliminary results suggest that DRD2 represents a potential therapeutic target for AML (10).

Aspirin is the most common used non-steroidal anti-inflammatory drug (NSAID) and daily intake of 75–1,200 mg aspirin per day has been reported to reduce the incidence of colorectal cancer (11). However, the anticancer mechanisms of aspirin, the most commonly used drug and emerging candidate of drug repositioning, have not been yet clear.

The aim of this study was to reposition FDA-approved drugs as part of combination therapy to overcome acquired resistance to EGFR TKIs in lung cancer and to tamoxifen in breast cancer, targeting their common mechanisms underlying off-target acquired resistance. We searched GEO database to obtain gene signatures associated with lung/breast cancer and acquired resistance to EGFR TKIs/tamoxifen to query CMap. The top-ranked candidate aspirin was examined for its anticancer and antiresistance effects on *in vitro* cells and *in vivo* animal models and the underlying mechanisms were also explored.

Abbreviations: A, aspirin; T, tamoxifen; G, gefitinib; O, osimertinib; CMap, Connectivity map; CSC, cancer stem cell; EGFR TKI, epidermal growth factor receptor tyrosine kinase inhibitor; ER, estrogen receptor; GEO, Gene Expression Omnibus; NSCLC, non-small cell lung cancer; PARP, poly ADP-ribose polymerase.

MATERIALS AND METHODS

Reagents

Gefitinib, osimertinib and tamoxifen were purchased from Selleck (Shanghai, China). Aspirin was purchased from Sangon Biotech (Shanghai, China). Gefitinib, osimertinib, tamoxifen, and aspirin were dissolved in DMSO.

Drug Screening via the CMap

Nine datasets from GEO (GSE19804, GSE42568, GSE15852, GSE10797, GSE7670, GSE74575, GSE38310, GSE67916, and GSE122005) were used in this study, all of which were generated using Affymetrix HG-U133A gene chips. Two-fold change with $P < 0.05$ was used as the cut-off criterion for up and down probe sets, which were used to query CMap. Compounds with $P < 0.05$ and enrichment score <-0.5 were retained.

Cell Culture and Establishment of Resistant Cancer Cell Lines *in vitro*

HCC827, 16HBE, and MCF-7 cells were purchased from Cell Bank of Type Culture Collection of the Chinese Academy of Sciences (Shanghai, China). MCF-10A cells were gifts from Dr. Zhaoyuan Hou in Shanghai Jiao Tong University School of Medicine. The cell lines were cultured under standard condition and tested by certified third-party laboratories for authenticity using short tandem repeat analysis and examined for mycoplasma regularly. Gefitinib-, osimertinib-, and tamoxifen-resistant cells were established by the stepwise escalation method and maintained as previously described (12). Briefly, parental cells were cultured with stepwise escalation of concentration of gefitinib, osimertinib or tamoxifen from 5 to 5 μM over 6 months. Resistant cell lines are capable of proliferating normally in the presence of 5 μM gefitinib, osimertinib or tamoxifen. Cell viability was used to confirm resistance after allowing the cells to grow in drug-free medium for 5–7 days. Upon confirming resistance, resistant cell lines were cultured without gefitinib, osimertinib, or tamoxifen and their resistance was examined periodically.

Cell Viability Assay

Cell viability was determined using the Cell Counting Kit-8 (CCK-8) colorimetric assay (Dojindo, Shanghai, China) and the IncuCyte ZOOM® system (Essen BioScience) as previously described (12). Briefly, for CCK8 assay, cells were seeded at a density of 2,000–3,000 cells/well in 96-well plates. After incubated with serum-free DMEM for 24 h, the cells were treated with indicated concentrations of drug for 48–72 h. Cells treated with solvent (DMSO) were used as a control, with viability set at 100%. For IncuCyte assay, 3,000 cells were seeded into 96-well plates containing DMEM supplemented with 10% FBS in the presence or absence of indicated concentrations of drug. The plates were placed into an IncuCyte Zoom (Essen Bioscience)

that automatically takes phase-contrast images of each well every 2 h over the course of 2–5 days and utilizes software to measure confluence as a proxy for cell viability.

Western Blot and Immunofluorescence Analyses

The expression levels of proteins were examined by Western blot and immunofluorescence staining analyses as previously described (12). The list of antibodies used is available in **Table S2**.

Colony Formation Assay

A total of 800–1,000 viable cells were placed in six-well plates and cultured in complete medium for 2–3 weeks. Colonies were fixed, stained with crystal violet and then counted.

Mouse Xenograft Models, Combination Treatment, and Tumorigenic Assay

Athymic BALB/c nude mice were purchased from Shanghai Laboratory Animal Center (Chinese Academy of Sciences, Shanghai, China) and housed in environmentally controlled, specific pathogen-free conditions for 1 week before the study. All experimental procedures were reviewed and approved in accordance with the guidelines for the care and use of laboratory animals at Shanghai Jiao Tong University.

To establish mouse xenograft models, same amount of indicated tumor cells was injected subcutaneously into both flanks of each mouse. The tumor volume was measured after 1 week from injection and then every other day or twice a week. Tumor volumes (mm^3) were calculated as length $\times$width^2/2.

For combination treatment experiments, when the volumes of xenograft tumors reached ~200 mm^3, mice were given daily PBS, 12.5 mg/kg gefitinib, 100 mg/kg aspirin, or combination of 12.5 mg/kg gefitinib and 100 mg/kg aspirin by garage. At the end of experiments, mice were sacrificed and tumors were dissected, weighted and photographed.

For tumorigenic assay, HCC827 cells were treated with aspirin for 12 h and then different amount of viable cells (1×10^6, 5×10^5, 2×10^5, 1×10^5) in 50 μl PBS were injected subcutaneously into each mouse. Xenograft tumor initiation and growth were examined every 5 days.

Statistical Analysis

All data are presented as the mean±SEM. Statistical analysis was conducted using GraphPad Prism 5.0 software (La Jolla, CA, USA). Differences between groups were examined using Student's *t*-test. Differences were considered significant if P was <0.05.

RESULTS

Using Gene Signatures to Identify Drugs for Lung and Breast Cancers via CMap

It is currently acknowledged that transcriptional programs can be used to identify therapeutic targets to treat cancer. If a drug treatment could reverse the gene signature of a certain disease, it might have the potential to treat the disease. The Connectivity Map (CMap) database comprised a large reference collection of gene expression profiles from cultured human cells treated with 1,309 drugs. The database can be queried with a gene signature of interest to identify those drugs that induce desired gene expression changes. In order to identify drugs to treat the two most common cancers lung and breast cancers, as well as overcome acquired resistance to targeted therapy, first, we searched the Gene Expression Omnibus (GEO) database for lung cancer or breast cancer vs. respective normal tissue, EGFR TKI-sensitive vs. acquired resistant lung cancer, and tamoxifen-sensitive vs. acquired resistant breast cancer. We obtained five datasets for cancer vs. normal and four for targeted-therapy sensitive vs. acquired resistant. The data sources were summarized in **Tables 1**, **2** and data analysis was described in the Material and methods section. All nine datasets were published previously (13–21). Then, differentially expressed genes from each dataset were individually queried with CMap. As shown in **Figure 1A**, intersection of five normal vs. cancer datasets and four targeted-therapy sensitive vs. acquired resistant datasets yielded 83 and 76 drugs, respectively. Both of those two groups of drugs contained the same 12 FDA-approved drugs and the names of these drugs were listed in **Table S1**.

Aspirin Inhibited Proliferation and Promoted Apoptosis of Cancer Cells

First, we tested the effects of these drugs on the proliferation and apoptosis of lung and breast cancer cells. As shown in **Figure 1B**, in a dose-dependent manner, aspirin promoted apoptosis of lung cancer HCC827 and breast cancer MCF-7 cells by increasing the expression of cleaved PARP or caspase-3. Flow cytometry also showed significantly increased percentage of apoptotic cells when treated with aspirin (**Figure 1C**). Then, we treated HCC827 cells with EGFR TKIs (gefitinib or osimertinib) and MCF-7 cells with tamoxifen in combination with aspirin (A). Cell viability assays (**Figures 1D–F**, upper panels) and IncuCyte

TABLE 1 | Summary of five datasets (normal vs. tumor samples) used for CMap analysis.

GEO #	GSE7670	GSE10797	GSE15852	GSE19804	GSE42568
Pubmed ID	17540040	18373191	20097481	20802022	23740839
Up probe sets #	21	7	18	9	4
Down probe sets #	109	110	47	47	103
Normal #	27	10	43	60	17
Tumor #	27	56	43	60	104

TABLE 2 | Summary of four datasets (sensitive vs. resistant cells) used for CMap analysis.

GEO #	GSE38310	GSE74575	GSE122005	GSE67916
Pubmed ID	22751098	27108960	30609749	24882577
Up probe sets #	13	48	33	13
Down probe sets #	30	29	41	11
Sensitive #	3	3	3	8
Resistant #	3	3	3	10

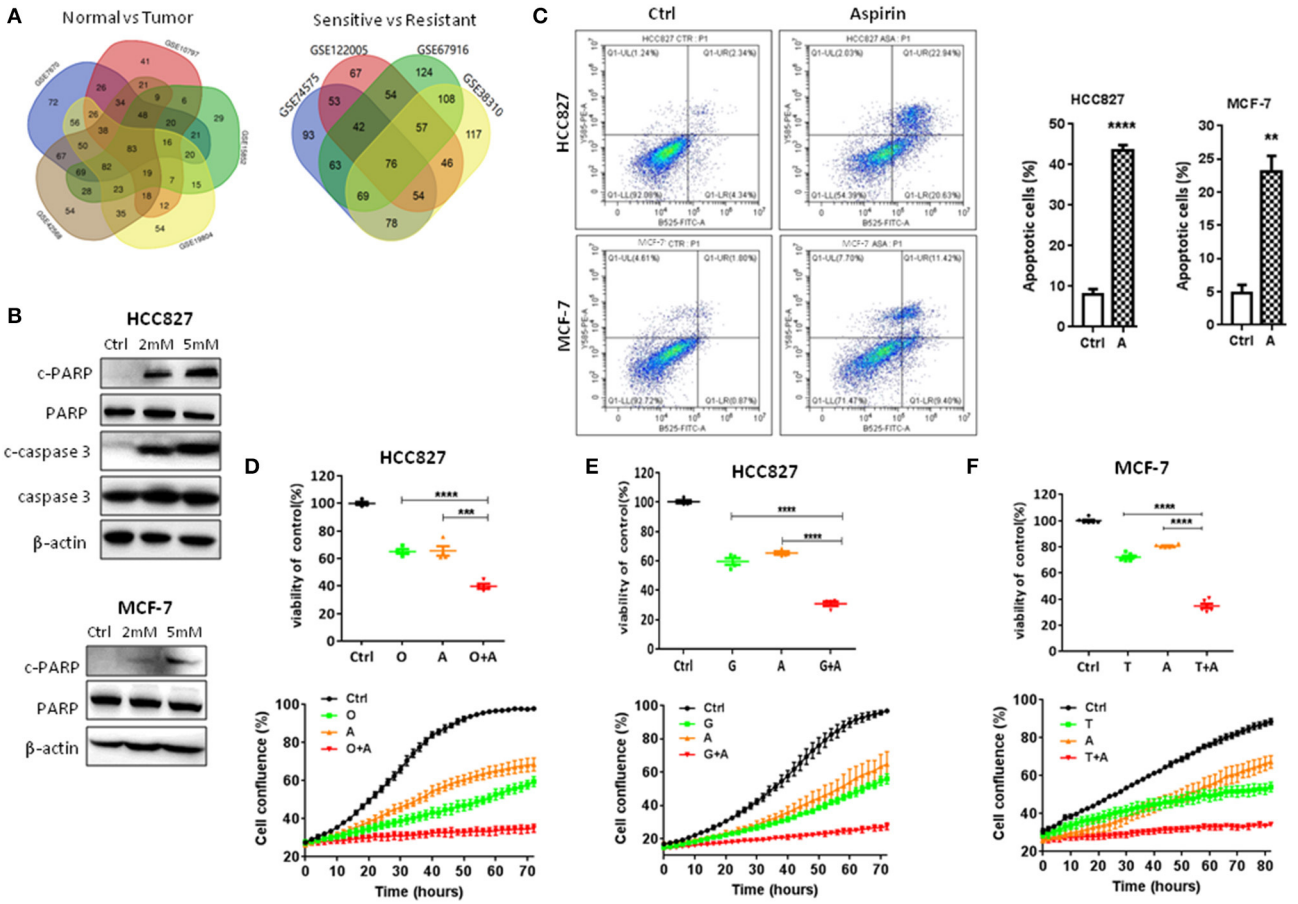

FIGURE 1 | Aspirin inhibited proliferation and promoted apoptosis of lung and breast cancer cells. **(A)** The Venn diagram represents the number of drugs using five data sets (GSE19804, GSE42568, GSE15852, GSE10797, and GSE7670) or four data sets (GSE74575, GSE38310, GSE67916, GSE122005) to query the CMap. **(B)** Western blot analysis of cleaved-caspase 3 (c-caspase 3), caspase 3, cleaved-PARP (c-PARP), and PARP in HCC827 and MCF-7 cells treated with indicated concentrations of aspirin for 72 h. β-actin was used as loading control. **(C)** Flow cytometry analysis of apoptosis of HCC827 treated with 2 mM aspirin and of MCF-7 cells treated with 2 mM aspirin for 72 h (left panels). Quantitative analysis of apoptotic cells identified by flow cytometry (right panels). Data were obtained from three independent experiments. **(D–F)** Cell viability by CCK8 assay (upper panels) and IncuCyte growth curves (lower panels) of indicated cells treated with 10 nM osimertinib (O), 10 nM gefitinib (G), 2 mM aspirin (A), 2 μM tamoxifen (T), O+A, G+A, or T+A for 72 h as indicated. The data are presented as the means ± SEM. Student's *t*-test was used. $^{*}P < 0.05$; $^{**}P < 0.01$; $^{***}P < 0.001$; $^{****}P < 0.0001$.

growth curves (**Figures 1D–F**, lower panels) both showed that combination of aspirin with targeted drugs dramatically inhibited proliferation of cancer cells. However, single agents including targeted therapies and aspirin, or combination of targeted therapies and aspirin had no effects on the proliferation of normal lung (16HBE) or breast epithelial cells (MCF-10A) (**Figure S1**).

Aspirin Overcame Acquired Resistance to Targeted Therapy

Next, we determined to test the effects of aspirin on the acquired resistance to targeted therapy in lung and breast cancers. First, we established *in vitro* cell models of acquired resistance to targeted therapy by culturing sensitive cancer cells in targeted drugs with escalating concentration as we previously reported (12). Then we examined the effects of aspirin on the cell viability in normal epithelium cells, sensitive and resistant cells using CCK8 assay. As shown in **Figures S2A,B**, resistant cells such as HCC827GR, HCC827OR, and MCF-7TR cells were more sensitive to aspirin than their respective sensitive cells, HCC827 cells and MCF-7 cells, while sensitive cells were more sensitive to aspirin than normal epithelium cells, 16HBE and MCF-10A. Therefore, we chose 1 or 2 mM aspirin to treat resistant cells and 2 or 5 mM to treat sensitive cells in this study. We found that aspirin promoted apoptosis by increasing the percentages of apoptotic cells (**Figure 2A** and **Figure S2C**) and the expression of cleaved PARP and caspase-3 (**Figure 2B**). Similarly, we treated resistant cells with targeted drugs in combination with aspirin. Cell viability assays (**Figures 2C–E**, left panels) and IncuCyte growth curves (**Figures 2C–E**, right panels) both showed that combination of aspirin with targeted drugs dramatically inhibited proliferation of resistant cells. To extend our findings to *in vivo*, we

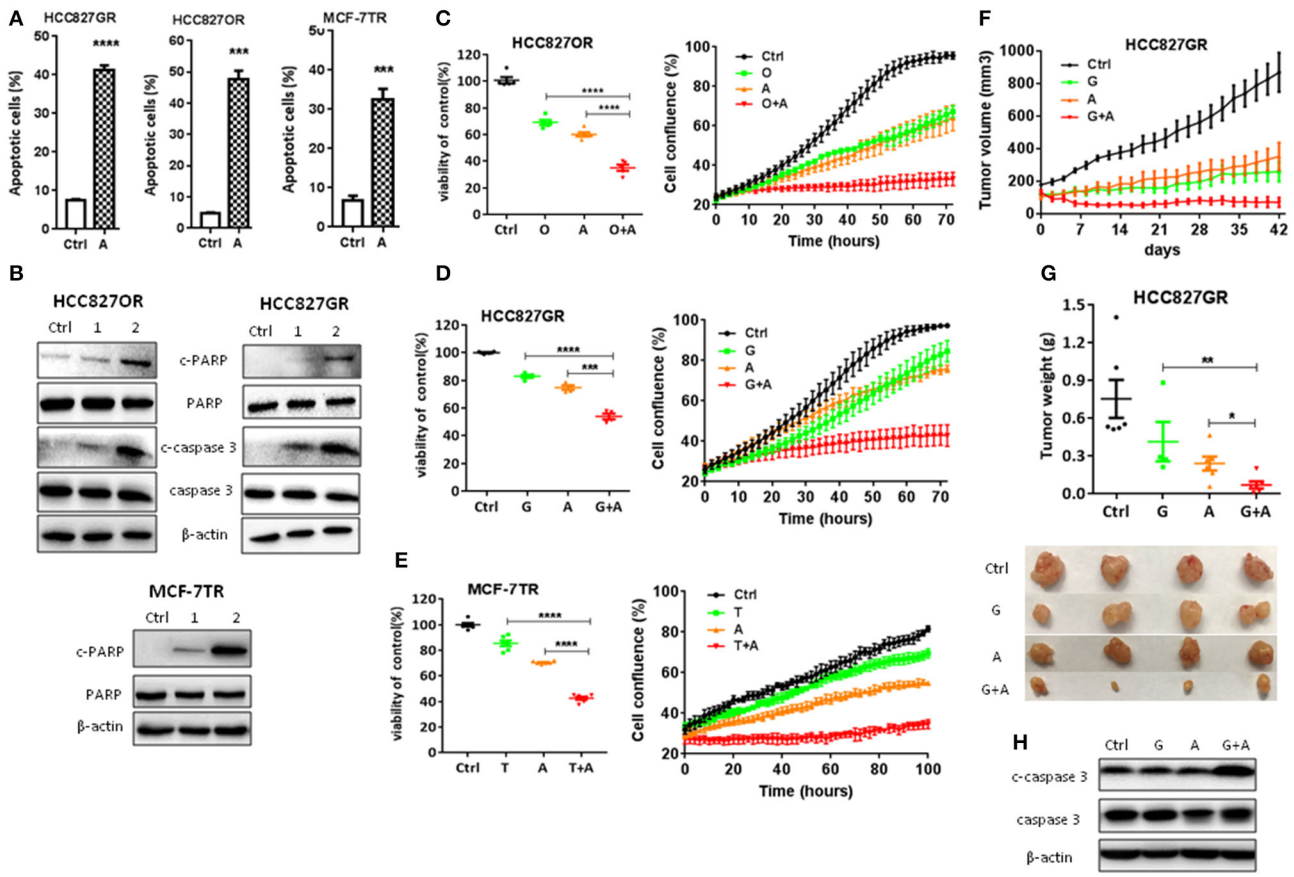

FIGURE 2 | Aspirin overcame acquired resistance to targeted therapy in lung and breast cancers. **(A)** Quantitative analysis of apoptotic cells in the indicated cells treated with 1 mM aspirin for 72 h identified by flow cytometry. Data were obtained from three independent experiments. **(B)** Western blot analysis of c-caspase 3, caspase 3, c-PARP, and PARP in HCC827OR, HCC827GR, and MCF-7TR cells treated with indicated concentrations (mM) of aspirin for 72 h. **(C–E)** Cell viability by CCK8 assay (left panels) and IncuCyte growth curves (right panels) of indicated cells treated with 10 μM osimertinib (O), 10 μM gefitinib (G), 1 mM aspirin (A), 8 μM tamoxifen (T), O+A, G+A, or T+A for 72 h as indicated. **(F–H)** HCC827GR-derived xenograft tumors were treated with PBS, 12.5 mg/kg/day gefitinib (G), 100 mg/kg/day aspirin (A), or G+A. The growth curve **(F)**, and the weight and photographs of tumors **(G)**. **(H)** Western blot analysis of c-caspase 3 and caspase 3. β-actin was used as loading control. The data are presented as the means ± SEM. Student's *t*-test was used. $^{*}P < 0.05$; $^{**}P < 0.01$; $^{***}P < 0.001$; $^{****}P < 0.0001$.

subcutaneously injected HCC827GR cells into both flanks of nude mice. And when tumor cells formed solid, palpable tumor with an average volume of 150–200 mm^3, we treated mice with gefitinib (12.5 mg/kg/day) in combination with aspirin (100 mg/kg/day). As shown in **Figures 2F–H**, combination therapy dramatically inhibited tumor growth (**Figures 2F,G**) and promoted apoptosis compared to single agent therapy (**Figure 2H**).

Aspirin Delayed the Emergence of Acquired Resistance to Targeted Therapy

To determine whether aspirin could prevent or delay the occurrence of acquired resistance to targeted therapy, we assessed the emergence of acquired resistance to targeted drugs. Low confluence cells (200–500/well) were seeded and treated in a 96-well plate, and wells of 50% or greater confluence were scored as positive weekly (22). We found that gefitinib- and osimertinib-resistant colonies began to appear within 1 week, while tamoxifen-resistant colonies appeared within 2 weeks (**Figures 3A–C**). Aspirin alone didn't delay the emergence of resistance while combination of aspirin with targeted drugs significantly delayed the emergence of acquired resistance and reduced the incidence of resistant colonies (**Figures 3A–C**). To recapitulate the *in vitro* results *in vivo*, nude mice harboring HCC827-xenograft tumors were treated with gefitinib (12.5 mg/kg/day), aspirin (100 mg/kg/day), or combination of thereof. During the course of treatment, aspirin alone slightly inhibited tumor growth while gefitinib alone or in combination with aspirin led to significant tumor regression (**Figures 3D–F**). However, gefitinib alone was not able to prevent tumor regrowth after about 3-week treatment, indicating emergence of acquired resistance, while combination of gefitinib with aspirin effectively suppressed tumor regrowth up to 8 weeks. Moreover, combination therapy dramatically promoted apoptosis compared to single agent therapy (**Figure 3G**).

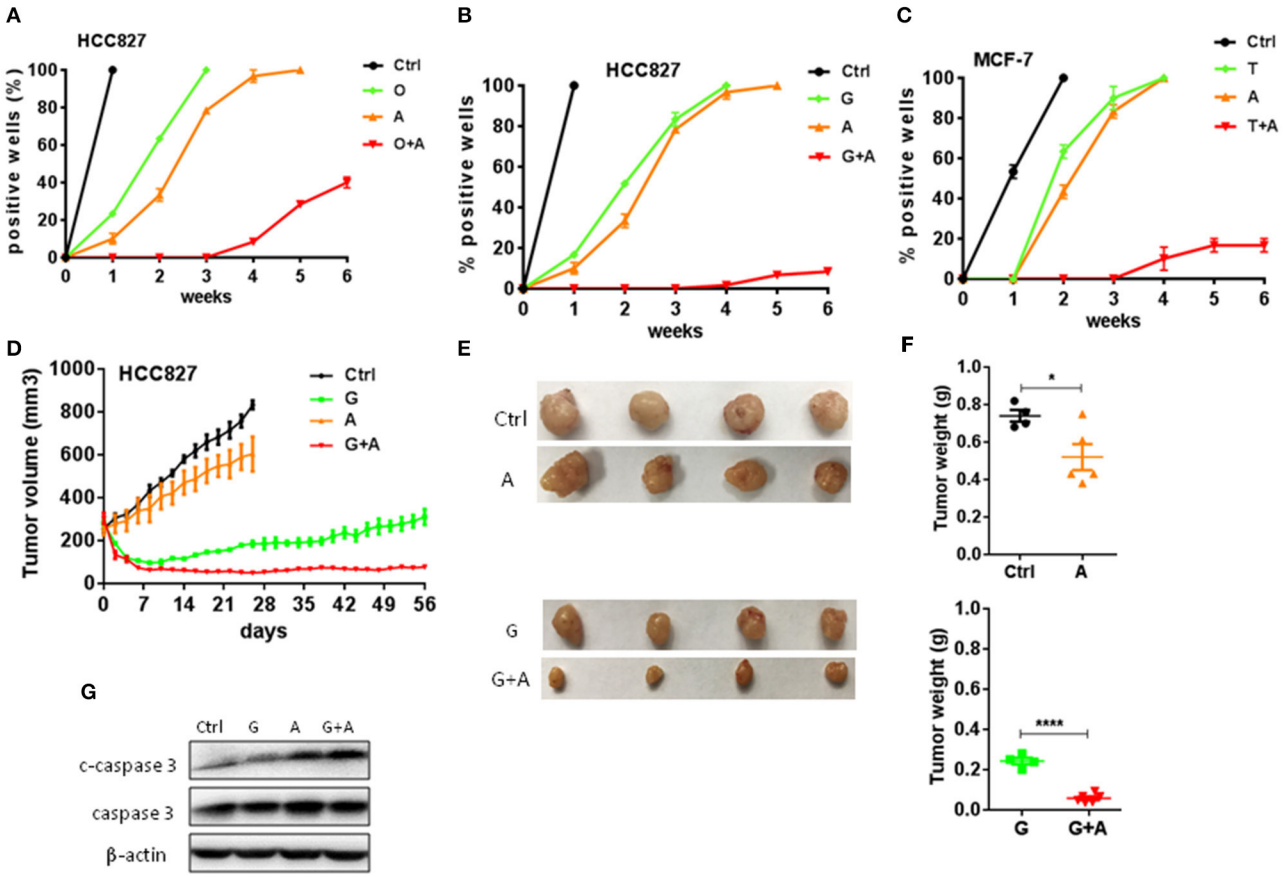

FIGURE 3 | Aspirin delayed the emergence of acquired resistance to targeted therapy in lung and breast cancers. **(A–C)** The indicated cells (200–500/well) were seeded and treated in a 96-well plate, and wells of 50% or greater confluence were scored as positive weekly and graphed means ± SEM. Each experiment was repeated two times. **(A)** HCC827 cells were treated with 10 nM O, 2 mM A, or O+A. **(B)** HCC827 cells were treated with 10 nM G, 2 mM A, or G+A. **(C)** MCF-7 cells were treated with 2 μM T, 2 mM A, or T+A. **(D–F)** HCC827-derived xenograft tumors were treated with PBS, 12.5 mg/kg/day G, 100 mg/kg/day A, or G+A. The growth curve **(D)**, the photographs **(E)** and the weight of tumors **(F)**. **(G)** Western blot analysis of c-caspase 3 and caspase 3. β-actin was used as loading control. The data are presented as the means ± SEM. Student's *t*-test was used. $^{*}P < 0.05$; $^{****}P < 0.0001$.

Aspirin Suppressed Cancer Stemness of Lung and Breast Cancers

Cancer stem cells (CSC) are considered to play a pivotal role in therapy resistance and relapse of cancer (23). Next, we sought to examine the effects of aspirin on cancer stemness of lung and breast cancers. Cancer cells with acquired resistance to targeted therapy have been reported with enhanced cancer stemness (24). So, we treated resistant cancer cells with aspirin and then examined the expression of CSC markers CD44 by immunofluorescence analysis. As shown in **Figure 4A**, the expressions of CD44 in HCC827GR, HCC827OR and MCF-7TR were decreased by aspirin treatment. Western blot also showed that the expressions of CD44 as well as ALDH1A1, which is another well-known cancer stem cell marker, were repressed in HCC827OR and HCC827GR cells treated with aspirin (**Figure 4B**). Furthermore, colony formation assay showed that aspirin suppressed self-renewal capacity of both sensitive and resistant cells *in vitro* (**Figure 4C**). To examine *in vivo* tumorigenic capacity, HCC827 cells were treated with aspirin for 12 h, after which 1×10^6, 2×10^5, or 1×10^5 viable cells were implanted subcutaneously into nude mice. Pretreatment with aspirin led to a significant reduction in tumor incidence and tumor volume (**Figures 4D,E**). Overall, these results demonstrated that aspirin suppressed cancer stemness of lung and breast cancers.

Aspirin Suppressed NF-κB Signaling Pathway

Activation of NF-κB signaling has been linked to various aspects of cancer, including inflammation, transformation, proliferation, angiogenesis, metastasis, treatment resistance, and cancer stemness (25, 26). As we previously reported that NF-κB signaling was activated in HCC827GR cells (12), we determined to examine whether aspirin could suppress NF-κB signaling. Consistent with our previous study (12), we found that acquired EGFR TKI-resistant cells HCC827GR and HCC827OR had higher levels of NF-κB activity compared to their parental, sensitive cells HCC827 (**Figures 5A,B** and

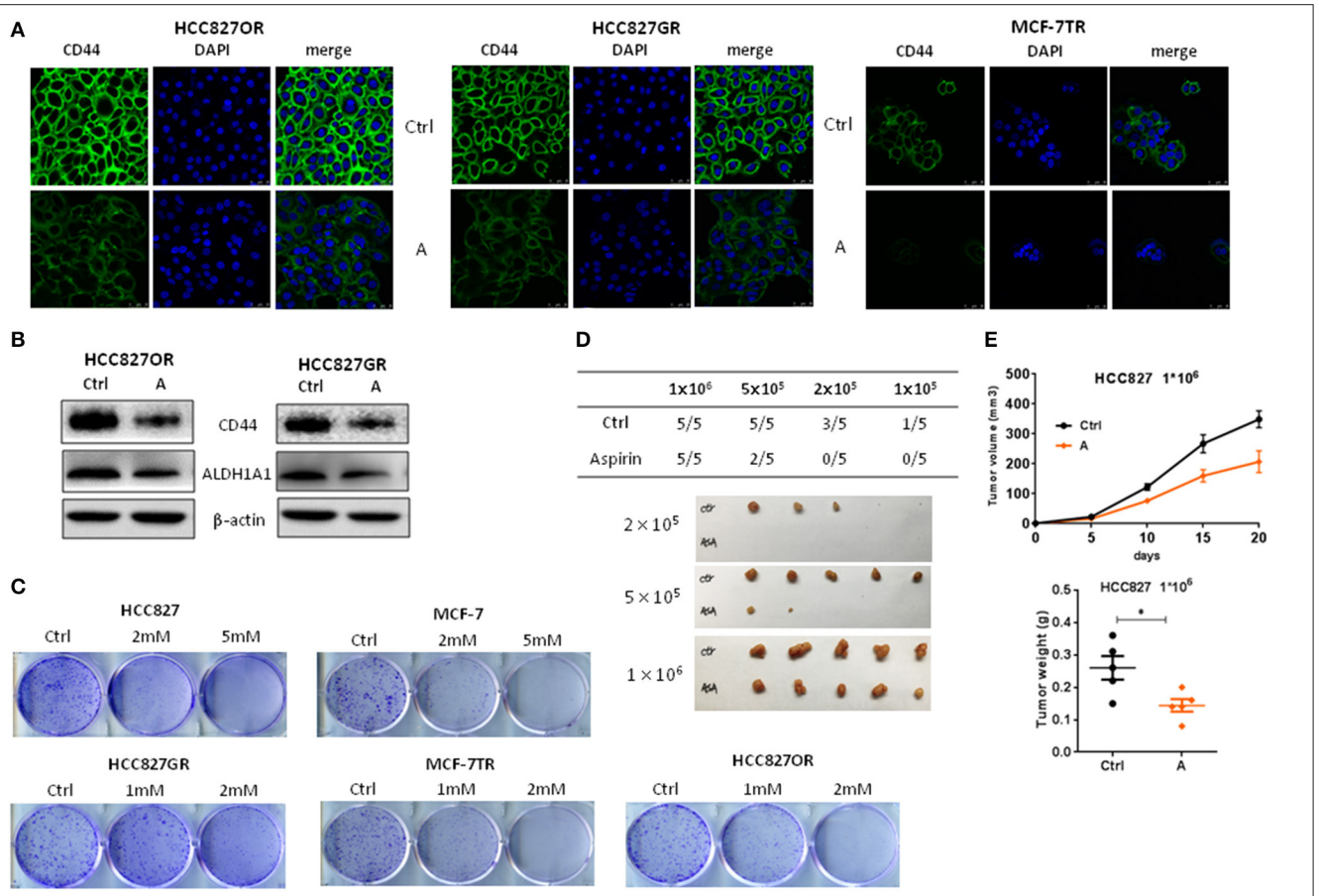

FIGURE 4 | Aspirin suppressed cancer stemness of lung and breast cancers. **(A,B)** The indicated cells were treated with 1 mM aspirin for 72 h. CD44 expression was analyzed by immunofluorescence staining **(A)**. Nuclei were observed with DAPI staining. Scale bar, 50 μm. **(B)** The expressions of CD44 and ALDH1A1 were examined by Western blot. **(C)** Colony formation assay of indicated cells treated with indicated concentrations of aspirin. **(D,E)** Limiting dilution transplantation assay. HCC827 cells were treated with 2 mM aspirin for 12 h prior to transplantation. The indicated numbers of viable HCC827 cells were transplanted subcutaneously into nude mice. The incidence and the photograph of tumors **(D)**. The growth curve and weight of tumors from 1×10^6 HCC827 cells **(E)**. The data are presented as the means ± SEM. Student's *t*-test was used. $^*P < 0.05$.

Figures S3A,C,E). NF-κB activity was assessed by the levels of phosphorylated NF-κB p65 by Western blot and p65 nuclear translocation by immunofluorescence. Similarly, tamoxifen resistant MCF-7TR cells had a higher level of NF-κB activity compared to parental, sensitive MCF-7 cells (**Figures 5A,B** and **Figure S3E**). After HCC827 and MCF-7 cells were treated with targeted drugs gefitinib/osimertinib and tamoxifen for 72 h, respectively, NF-κB activity was also increased (**Figures 5B,C** and **Figures S3A,C,E**). These results demonstrated that targeted therapy increased NF-κB activity in cancer cells, which may contribute to the development of acquired resistance. Next, we treated cancer cells with aspirin. As shown in **Figures 5D–F** and **Figures S3B,D,F**, aspirin decreased NF-κB activity in both sensitive and resistant cells. These results demonstrated that aspirin suppressed NF-κB signaling. Aspirin also decreased targeted therapy-induced NF-κB activity in HCC827 and MCF-7 cells (**Figure 5G**). Furthermore, HCC827 and MCF-7 cells were treated with NF-κB activator TNF-α in the presence or absence of aspirin. As shown in **Figure 5H**, TNF-α increased the level of phosphorylated NF-κB p65 while aspirin abrogated TNF-α-induced p65 phosphorylation, further demonstrating that aspirin suppressed NF-κB signaling.

DISCUSSION

Acquired resistance to targeted drugs limits the long-term clinical efficacy of these drugs. Therefore, novel therapies such as new drugs or combination of old drugs are needed to overcome or delay the emergence of acquired resistance to targeted drugs. Since new drug development is a time-consuming and expensive process, repositioning old drugs for new indications seems attempting and has set some successful examples (27, 28). In this study, we aimed to reposition FDA-approved drugs to treat lung and breast cancers as well as overcome or delay the emergence of acquired resistance to targeted lung and breast cancer therapies. We searched GEO database for tumor-associated gene signatures (tumor vs. normal) and acquired

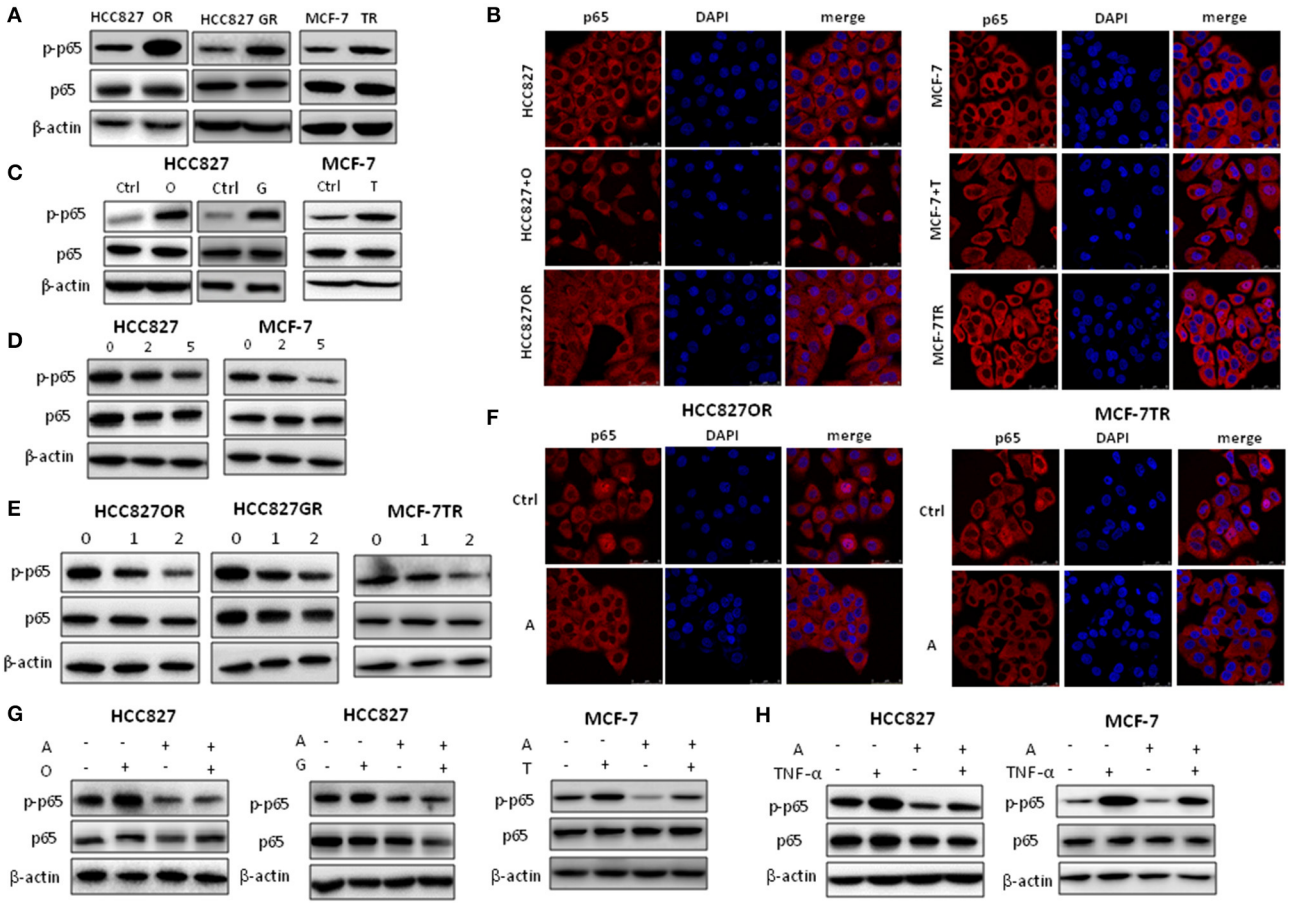

FIGURE 5 | Aspirin suppressed NF-κB activity in cancer cells. **(A)** Western blot analysis of p-NF-κB p65 (p-p65) and NF-κB p65 (p65) in HCC827, HCC827OR (OR), HCC827GR (GR), MCF-7 and MCF-7TR (TR) cells. **(B)** Immunofluorescence staining analysis of p65 in HCC827, HCC827OR, or HCC827 cells treated with 10 nM O for 72 h (left panels) and in MCF-7, MCF-7TR, or MCF-7 cells treated with 2 μM T for 72 h (right panels). **(C)** Western blot analysis of p-p65 and p65 in HCC827 cells treated with 10 nM O or 10 nM G for 72 h (left panels) and in MCF-7 cells treated with 2 μM T for 72 h. **(D)** Western blot analysis of p-p65 and p65 in HCC827 and MCF-7 cells treated with indicated concentration (mM) of aspirin for 72 h. **(E)** Western blot analysis of p-p65 and p65 in HCC827OR, HCC827GR, and MCF-7TR cells treated with indicated concentration (mM) of aspirin for 72 h. **(F)** Immunofluorescence staining analysis of p65 in HCC827OR or MCF-7TR cells treated with 1 mM A for 72 h. Nuclei were observed with DAPI staining. Scale bar, 50 μm. **(G)** Western blot analysis of p-p65 and p65 in HCC827 or MCF-7 cells pretreated with A (2 mM) for 2 h and then subjected to 10 nM O, 10 nM G, or 2 μM T as indicated for 72 h. **(H)** Western blot analysis of p-p65 and p65 in HCC827 or MCF-7 cells pretreated with 2 mM A for 70 h and then subjected to 10 ng/ml TNF-α as indicated for 2 h. β-actin was used as loading control.

resistant tumor-associated gene signatures (resistant vs. sensitive) to query the CMap, respectively. Through CMap data mining, we identified 12 candidate drugs. Among these candidate drugs, we found that aspirin has potent antitumor effects on lung and breast cancers and can re-sensitize acquired resistant tumors to targeted therapies as well as delay the emergence of acquired resistance when combined with targeted therapies.

CMap was created to identify compounds that induce a similar or opposite gene-expression signature to diseases of interest. So, it is a useful tool to identify new applications for "old" drug. From GEO, one of the largest gene expression data repositories, we chose lung and breast cancer datasets that contain normal vs. tumor and sensitive/before targeted therapy vs. acquired resistant/after targeted therapy and used selected gene signatures constructed from each dataset to query CMap. Comparing the significant drugs obtained using individual gene signatures, there were 83 overlapping drugs from five normal vs. tumor datasets and 76 from four sensitive vs. resistant datasets. Among these, we found 12 common FDA-approved drug candidates, which have the potential to kill both lung and breast cancers as well as lung and breast cancers with acquired resistance to targeted therapy. Indeed, our results demonstrated that one of these 12 FDA-approved drugs, aspirin, which is widely used and safe, could be repositioned to treat lung and breast cancers.

Epidemiological data have shown that use of aspirin has been associated with lower cancer risk. *In vitro* and *in vivo* studies have also revealed the anticancer activities of aspirin and plausible mechanisms (29–32). Consistently, we found that aspirin inhibited proliferation and promoted apoptosis of lung and breast cancer cells. On the contrary, aspirin has no effects on normal lung and mammary epithelial cell proliferation at concentrations used on lung and breast cancer

cells. When combined with targeted drugs gefitinib, osimertinib, or tamoxifen, aspirin had synergistic effects on cancer cell proliferation. More importantly, our results showed that aspirin dramatically increased the sensitivity of resistant tumors to targeted drugs and significantly delayed the emergence of acquired resistance *in vitro* and *in vivo*. In the meanwhile, interestingly, we found that resistant cells were more sensitive to aspirin treatment than parental, sensitive cells in terms of proliferation and apoptosis. Mechanistically, our data showed that resistant cancer cells had higher levels of NF-κB activity compared to their parental, sensitive cancer cells, while NF-κB is reported to be constitutively activated in a wide variety of tumor types including lung and breast cancers compared with their respective normal tissues or cells (33). Aspirin suppressed NF-κB signaling, which could explain the differences in sensitivity to treatment among different cells including normal epithelial cells, sensitive or resistant cancer cells. That is, resistant cancer cells, which have the highest activity of NF-κB, are most sensitive to aspirin, while normal epithelial cells which have the lowest activity NF-κB are least sensitive to aspirin. NF-κB signaling is involved in various aspects of cancer including survival, metastasis, therapy resistance as well as cancer stemness. During the course of targeted therapy, survival tumor cells became resistant, and concomitantly acquired increased cancer stemness and NF-κB activity. Similarly, resistant cells were more sensitive to aspirin treatment than sensitive cells in terms of cancer stemness, which could also be due to increased NF-κB activity in resistant cells. Aspirin was also found to be able to abrogate NF-κB p65 activation induced by targeted drugs or TNF-α. Taken together, we proposed that aspirin could suppress NF-κB p65 signaling to inhibit tumor progression.

In this study, the concentration of aspirin used in *in vitro* experiments was ∼2 mM, which is similar to the plasma concentration of salicylate (metabolite of aspirin *in vivo*) observed in rheumatoid arthritis patients. The dose of aspirin used in *in vivo* experiments is 100 mg/kg. According to the Reagan-Shaw method (34), the dose of 100 mg/kg in mice is equal to 8.1 mg/kg in humans, which is the dose that used in clinic to treat inflammation. Thus, the dose in our study is safe for human patients.

CONCLUSIONS

In summary, our data identify aspirin as a potential candidate for combination therapy for lung and breast cancers. There only have been few stage III clinical trials of aspirin plus radiation therapy, chemotherapy, or targeted therapy to treat lung or breast cancer patients. We hope our study provides further molecular rationale and preclinical data to support combination of aspirin with targeted therapy to treat lung and breast cancers.

DATA AVAILABILITY STATEMENT

All datasets generated for this study are included in the article/**Supplementary Material**.

ETHICS STATEMENT

All animal experimental procedures were reviewed and approved in accordance with the guidelines for the care and use of laboratory animals at Shanghai Jiao Tong University.

AUTHOR CONTRIBUTIONS

LL, MH, TW, and LX designed all the experiments. LL, MH, and TW conducted the experiments, analyzed, and interpreted the results. LX and HC supervised the project. LL and LX wrote the draft manuscript. HC and LX reviewed and edited the manuscript. All authors read and approved the final manuscript.

FUNDING

This work was supported by National Natural Science Foundation of China (81773747 and 81372522), Science and Technology Commission of Shanghai Municipality (12ZR1416000 and 12140901400).

ACKNOWLEDGMENTS

We thank Dr. Zhaoyuan Hou for providing MCF-10A cells.

SUPPLEMENTARY MATERIAL

The Supplementary Material for this article can be found online at: https://www.frontiersin.org/articles/10.3389/fonc.2019.01503/full#supplementary-material

REFERENCES

1. Groenendijk FH, Bernards R. Drug resistance to targeted therapies:deja vu all over again. *Mol Oncol.* (2014) 8:1067–83. doi: 10.1016/j.molonc.2014.05.004
2. Rotow J, Bivona TG. Understanding and targeting resistance mechanisms in NSCLC. *Nat Rev Cancer.* (2017) 17:637–58. doi: 10.1038/nrc.2017.84
3. Furman C, Hao MH, Prajapati S, Reynolds D, Rimkunas V, Zheng GZ, et al. Estrogen receptor covalent antagonists:the best is yet to come. *Cancer Res.* (2019) 79:1740–5. doi: 10.1158/0008-5472.CAN-18-3634
4. Mills JN, Rutkovsky AC, Giordano A. Mechanisms of resistance in estrogen receptor positive breast cancer:overcoming resistance to tamoxifen/aromatase inhibitors. *Curr Opin Pharmacol.* (2018) 41:59–65. doi: 10.1016/j.coph.2018.04.009
5. McGranahan N, Swanton C. Clonal heterogeneity and tumor evolution:past, present, and the future. *Cell.* (2017) 168:613–28. doi: 10.1016/j.cell.2017.01.018
6. Jamal-Hanjani M, Wilson GA, McGranahan N, Birkbak NJ, Watkins TBK, Veeriah S, et al. Tracking the evolution of non-small-cell lung cancer. *N Engl J Med.* (2017) 376:2109–21. doi: 10.1056/NEJMoa1616288

7. Cha Y, Erez T, Reynolds IJ, Kumar D, Ross J, Koytiger G, et al. Drug repurposing from the perspective of pharmaceutical companies. *Br J Pharmacol.* (2018) 175:168–80. doi: 10.1111/bph.13798
8. Pushpakom S, Iorio F, Eyers PA, Escott KJ, Hopper S, Wells A, et al. Drug repurposing:progress, challenges and recommendations. *Nat Rev Drug Discov.* (2018) 18:41–58. doi: 10.1038/nrd.2018.168
9. Cheng HW, Liang YH, Kuo YL, Chuu CP, Lin CY, Lee MH, et al. Identification of thioridazine, an antipsychotic drug, as an antiglioblastoma and anticancer stem cell agent using public gene expression data. *Cell Death Dis.* (2015) 6:e1753. doi: 10.1038/cddis.2015.77
10. Aslostovar L, Boyd AL, Almakadi M, Collins TJ, Leong DP, Tirona RG, et al. A phase 1 trial evaluating thioridazine in combination with cytarabine in patients with acute myeloid leukemia. *Blood Adv.* (2018) 2:1935–45. doi: 10.1182/bloodadvances.2018015677
11. Drew DA, Cao Y, Chan AT. Aspirin and colorectal cancer:the promise of precision chemoprevention. *Nat Rev Cancer.* (2016) 16:173–86. doi: 10.1038/nrc.2016.4
12. Li L, Gu X, Yue J, Zhao Q, Lv D, Chen H, et al. Acquisition of EGFR TKI resistance and EMT phenotype is linked with activation of IGF1R/NF-kappaB pathway in EGFR-mutant NSCLC. *Oncotarget*. (2017) 8:92240–53. doi: 10.18632/oncotarget.21170
13. Casey T, Bond J, Tighe S, Hunter T, Lintault L, Patel O, et al. Molecular signatures suggest a major role for stromal cells in development of invasive breast cancer. *Br Cancer Res Treat.* (2009) 114:47–62. doi: 10.1007/s10549-008-9982-8
14. Clarke C, Madden SF, Doolan P, Aherne ST, Joyce H, O'Driscoll L, et al. Correlating transcriptional networks to breast cancer survival:a large-scale coexpression analysis. *Carcinogenesis.* (2013) 34:2300–8. doi: 10.1093/carcin/bgt208
15. Elias D, Vever H, Laenkholm AV, Gjerstorff MF, Yde CW, Lykkesfeldt AE, et al. Gene expression profiling identifies FYN as an important molecule in tamoxifen resistance and a predictor of early recurrence in patients treated with endocrine therapy. *Oncogene*. (2015) 34:1919–27. doi: 10.1038/onc.2014.138
16. Lu TP, Tsai MH, Lee JM, Hsu CP, Chen PC, Lin CW, et al. Identification of a novel biomarker, SEMA5A, for non-small cell lung carcinoma in nonsmoking women. *Cancer Epidemiol Biomarkers Prev.* (2010) 19:2590–7. doi: 10.1158/1055-9965.EPI-10-0332
17. Pau Ni IB, Zakaria Z, Muhammad R, Abdullah N, Ibrahim N, Aina Emran N, et al. Gene expression patterns distinguish breast carcinomas from normal breast tissues:the Malaysian context. *Pathol Res Pract.* (2010) 206:223–8. doi: 10.1016/j.prp.2009.11.006
18. Su LJ, Chang CW, Wu YC, Chen KC, Lin CJ, Liang SC, et al. Selection of DDX5 as a novel internal control for Q-RT-PCR from microarray data using a block bootstrap re-sampling scheme. *BMC Genom.* (2007) 8:140. doi: 10.1186/1471-2164-8-140
19. Wu SG, Chang TH, Tsai MF, Liu YN, Hsu CL, Chang YL, et al. IGFBP7 drives resistance to epidermal growth factor receptor tyrosine kinase inhibition in lung cancer. *Cancers.* (2019) 11:E36. doi: 10.3390/cancers11010036
20. Wu Y, Yu DD, Hu Y, Yan D, Chen X, Cao HX, et al. Genome-wide profiling of long non-coding RNA expression patterns in the EGFR-TKI resistance of lung adenocarcinoma by microarray. *Oncol Rep.* (2016) 35:3371–86. doi: 10.3892/or.2016.4758
21. Zhang Z, Lee JC, Lin L, Olivas V, Au V, LaFramboise T, et al. Activation of the AXL kinase causes resistance to EGFR-targeted therapy in lung cancer. *Nat Genet.* (2012) 44:852–60. doi: 10.1038/ng.2330
22. Tricker EM, Xu C, Uddin S, Capelletti M, Ercan D, Ogino A, et al. Combined EGFR/MEK inhibition prevents the emergence of resistance in EGFR-mutant lung cancer. *Cancer Discov.* (2015) 5:960–71. doi: 10.1158/2159-8290.CD-15-0063
23. Qiu GZ, Sun W, Jin MZ, Lin J, Lu PG, Jin WL. The bad seed gardener: deubiquitinases in the cancer stem-cell signaling network and therapeutic resistance. *Pharmacol Ther.* (2017) 172:127–38. doi: 10.1016/j.pharmthera.2016.12.003
24. Prasad S, Ramachandran S, Gupta N, Kaushik I, Srivastava SK. Cancer cells stemness: a doorstep to targeted therapy. *Biochim Biophys Acta Mol Basis Dis.* (2019) 2019:S0925–4439(19)30071–7. doi: 10.1016/j.bbadis.2019.02.019
25. Aggarwal BB, Sung B. NF-kappaB in cancer:a matter of life and death. *Cancer Discov.* (2011) 1:469–71. doi: 10.1158/2159-8290.CD-11-0260
26. Rinkenbaugh AL, Baldwin AS. The NF-kappaB pathway and cancer stem cells. *Cells.* (2016) 5:E16. doi: 10.3390/cells5020016
27. Li F, He B, Ma X, Yu S, Bhave RR, Lentz SR, et al. Prostaglandin E1 and its analog misoprostol inhibit human cml stem cell self-renewal via EP4 receptor activation and repression of AP-1. *Cell Stem Cell.* (2017) 21:359–73.e5. doi: 10.1016/j.stem.2017.08.001
28. Sleire L, Forde HE, Netland IA, Leiss L, Skeie BS, Enger PO. Drug repurposing in cancer. *Pharmacol Res.* (2017) 124:74–91. doi: 10.1016/j.phrs.2017.07.013
29. Gronich N, Rennert G. Beyond aspirin-cancer prevention with statins, metformin and bisphosphonates. *Nat Rev Clin Oncol.* (2013) 10:625–42. doi: 10.1038/nrclinonc.2013.169
30. Maresso KC, Tsai KY, Brown PH, Szabo E, Lippman S, Hawk ET. Molecular cancer prevention:Current status and future directions. *CA Cancer J Clin.* (2015) 65:345–83. doi: 10.3322/caac.21287
31. Saha S, Mukherjee S, Khan P, Kajal K, Mazumdar M, Manna A, et al. Aspirin suppresses the acquisition of chemoresistance in breast cancer by disrupting an NFkappaB-IL6 signaling axis responsible for the generation of cancer stem cells. *Cancer Res.* (2016) 76:2000–12. doi: 10.1158/0008-5472.CAN-15-1360
32. Song JM, Upadhyaya P, Kassie F. Nitric oxide-donating aspirin (NO-Aspirin) suppresses lung tumorigenesis *in vitro* and *in vivo* and these effects are associated with modulation of the EGFR signaling pathway. *Carcinogenesis.* (2018) 39:911–20. doi: 10.1093/carcin/bgy049
33. Prasad S, Ravindran J, Aggarwal BB. NF-kappaB and cancer:how intimate is this relationship. *Mol Cell Biochem.* (2010) 336:25–37. doi: 10.1007/s11010-009-0267-2
34. Reagan-Shaw S, Nihal M, Ahmad N. Dose translation from animal to human studies revisited. *FASEB J.* (2008) 22:659–61. doi: 10.1096/fj.07-9574LSF

Conflict of Interest: The authors declare that the research was conducted in the absence of any commercial or financial relationships that could be construed as a potential conflict of interest.

frontiers in Oncology

CLINICAL TRIAL
published: 06 March 2020
doi: 10.3389/fonc.2020.00202

Clinical and Immunological Outcomes in High-Risk Resected Melanoma Patients Receiving Peptide-Based Vaccination and Interferon Alpha, With or Without Dacarbazine Preconditioning: A Phase II Study

Francesca Urbani[1,2†], Virginia Ferraresi[3†], Imerio Capone[1], Iole Macchia[1], Belinda Palermo[4], Carmen Nuzzo[3], Angela Torsello[3], Patrizio Pezzotti[5], Diana Giannarelli[6], Anna Fausta Pozzi[7], Mariano Santaquilani[8], Paolo Roazzi[9], Silvia Bastucci[10], Caterina Catricalà[11], Antonia La Malfa[7], Giuseppe Vercillo[12], Novella Gualtieri[4], Carla Buccione[1], Luciano Castiello[13], Francesco Cognetti[3], Paola Nisticò[4], Filippo Belardelli[14], Federica Moschella[1†] and Enrico Proietti[1†]*

[1] Department of Oncology and Molecular Medicine, Istituto Superiore di Sanità, Rome, Italy, [2] Medical Biotechnology and Translational Medicine, Tor Vergata University, Rome, Italy, [3] Department of Medical Oncology 1, IRCCS Regina Elena National Cancer Institute, Rome, Italy, [4] Unit of Tumor Immunology and Immunotherapy, Department of Research, Advanced Diagnostics and Technological Innovation, IRCCS Regina Elena National Cancer Institute, Rome, Italy, [5] Department of Infectious Disease, Istituto Superiore di Sanità, Rome, Italy, [6] Biostatistical Unit, IRCCS Regina Elena National Cancer Institute, Rome, Italy, [7] Hospital Pharmacia, IRCCS Regina Elena National Cancer Institute, Rome, Italy, [8] Computer Control and Management, Istituto Superiore di Sanità, Rome, Italy, [9] Health Technology Assessement, Istituto Superiore di Sanità, Rome, Italy, [10] Clinical Trial Center, IRCCS Regina Elena National Cancer Institute, Rome, Italy, [11] Oncological Dermatology, San Gallicano Hospital, Rome, Italy, [12] Clinical Pathology, IRCCS Regina Elena National Cancer Institute, Rome, Italy, [13] FAST—Istituto Superiore di Sanità, Rome, Italy, [14] Institute of Translational Pharmacology, CNR, Rome, Italy

Clinical studies based on novel rationales and mechanisms of action of chemotherapy agents and cytokines can contribute to the development of new concepts and strategies of antitumor combination therapies. In previous studies, we investigated the paradoxical immunostimulating effects of some chemotherapeutics and the immunoadjuvant activity of interferon alpha (IFN-α) in preclinical and clinical models, thus unraveling novel rationales and mechanisms of action of chemotherapy agents and cytokines for cancer immunotherapy. Here, we carried out a randomized, phase II clinical trial, in which we analyzed the relapse-free (RFS) and overall survival (OS) of 34 completely resected stage III–IV melanoma patients, treated with peptide-based vaccination (Melan-A/MART-1 and NY-ESO-1) in combination with IFN-α2b, with (arm 2) or without (arm 1) dacarbazine preconditioning. All patients were included in the intention-to-treat analysis. At a median follow-up of 4.5 years (interquartile range, 15.4–81.0 months), the rates of RFS were 52.9 and 35.3% in arms 1 and 2, respectively. The 4.5-year OS rates were 68.8% in arm 1 and 62.7% in arm 2. No significant differences were observed between the two arms for both RFS and OS. Interestingly, the RFS and OS curves remained stable starting from 18 and 42 months, respectively. Grade 3 adverse events occurred in 5.9%

OPEN ACCESS

Edited by:
Nehad M. Ayoub, Jordan University of Science and Technology, Jordan

Reviewed by:
Lisa H. Butterfield, Parker Institute for Cancer Immunotherapy, United States
Zhihong Chi, Beijing Cancer Hospital, China

***Correspondence:**
Filippo Belardelli
filippo.belardelli@ift.cnr.it

[†] These authors have contributed equally to this work

Specialty section:
This article was submitted to Pharmacology of Anti-Cancer Drugs, a section of the journal Frontiers in Oncology

Received: *16 October 2019*
Accepted: *06 February 2020*
Published: *06 March 2020*

Citation:
Urbani F, Ferraresi V, Capone I, Macchia I, Palermo B, Nuzzo C, Torsello A, Pezzotti P, Giannarelli D, Pozzi AF, Santaquilani M, Roazzi P, Bastucci S, Catricalà C, La Malfa A, Vercillo G, Gualtieri N, Buccione C, Castiello L, Cognetti F, Nisticò P, Belardelli F, Moschella F and Proietti E (2020) Clinical and Immunological Outcomes in High-Risk Resected Melanoma Patients Receiving Peptide-Based Vaccination and Interferon Alpha, With or Without Dacarbazine Preconditioning: A Phase II Study. Front. Oncol. 10:202. doi: 10.3389/fonc.2020.00202

of patients, whereas grade 4 events were not observed. Both treatments induced a significant expansion of vaccine-specific $CD8^+$ T cells, with no correlation with the clinical outcome. However, treatment-induced increase of polyfunctionality and of interleukin 2 production by Melan-A–specific $CD8^+$ T cells and expansion/activation of natural killer cells correlated with RFS, being observed only in nonrelapsing patients. Despite the recent availability of different therapeutic options, low-cost, low-toxic therapies with long-lasting clinical effects are still needed in patients with high-risk resected stage III/IV melanoma. The combination of peptide vaccination with IFN-α2b showed a minimal toxicity profile and resulted in encouraging RFS and OS rates, justifying further evaluation in clinical trials, which may include the use of checkpoint inhibitors to further expand the antitumor immune response and the clinical outcome.

Clinical Trial Registration: https://www.clinicaltrialsregister.eu/ctr-search/search, identifier: 2008-008211-26

Keywords: immunotherapy, melanoma, combination therapy, chemotherapy, drug repurposing, interferon-α

INTRODUCTION

In the last decade, cancer immunotherapy has registered an impressive progress, mostly due to the clinical use of checkpoint inhibitors (CPIs), which showed long-term responses in a large variety of tumors. Because of its high immunogenicity, melanoma was the first cancer type in which CPIs were approved in metastatic (1) as well as in high-risk resected patients (2). Nevertheless, a subset of patients remains unresponsive to this therapy because of primary or secondary resistance (3). Further advances in cancer immunotherapy can only stem from a better understanding on how CPIs can be combined with additional treatments, including cancer vaccines (4).

In the history of cancer immunotherapy, many research efforts have been devoted to the development of active immunization strategies against tumor-associated antigens (TAAs), taking advantage of shared as well as neoantigens (5), with alternate cycles of optimism and discouragement. One main research challenge is how to increase the antitumor immune response to TAAs by using selected cytokines and/or drugs acting as effective immune adjuvants.

A long-standing preclinical work from our institution and other research groups had deepened our understanding for the basic mechanisms of the combined treatment of immunotherapy with chemotherapy and/or type I interferons (IFN-I) (6–8). Of note, certain chemotherapeutics (such as alkylating agents), given at defined dose and timing, may augment lymphocyte proliferation (9), reduce the number of regulatory T cells (10–12) and the expression of PD-1 on $CD8^+$ T cells, favor T helper 1 (T_H1) and T_H17 responses (11, 12), activate polyfunctional T helper cells (13), promote tumor infiltration by T cells (14), and reset dendritic cell (DC) homeostasis (15). Remarkably, type I IFN gene signature has been demonstrated in animal models, as well as in cancer patients following administration of alkylating agent (16–18).

Interferon (IFN)-α is a cytokine belonging to the IFN-I family and endowed with pleiotropic effects, including DC development/activation (19, 20), T_H1 cell differentiation, T cell memory turnover, and natural killer (NK) cell activation (21, 22). INF-α is the cytokine with the longest record of clinical use. For many years, the antitumor effects observed in patients with certain hematological malignancies (hairy cell leukemia and chronic myeloid leukemia) and solid tumors (including melanoma and renal cancer) contributed in maintaining a great interest of the scientific community, patients, and media on IFN-α. Today, the use of IFN-α has been largely replaced by new drugs (including targeted therapies), thought to be less toxic and more selective for cancer cells. Of note, IFN-I were used in cancer patients when their mechanisms of action were still largely unknown, as either conventional cytostatic drugs or nonspecific biological response modifiers. They were generally utilized at high dosages and administered continuously, assuming that such treatment regimens could result in more potent antitumor effects. Specific biological activities subsequently ascribed to IFN-I have poorly been considered for clinical use. As an example, an ensemble of data demonstrated that the interaction of IFN-α with specific types of immune cells, such as DC, is strictly instrumental for the induction of antitumor effects (21, 23, 24). Based on these premises, IFN-α has been used in a few clinical studies as a vaccine adjuvant in infective (25) as well as neoplastic diseases [reviewed in Rizza et al. (21)]. A pilot study showed that in stage IV advanced melanoma patients the vaccination with Melan-A/MART-1 (Melan-A) and gp100 peptides combined with low-dose IFN-α resulted in enhanced specific $CD8^+$ T cells and

Abbreviations: IFN, Interferon; RFS, relapse-free; OS, overall survival; CPIs, checkpoint inhibitors; IFN-I, type I interferons; TH, T helper; DC, dendritic cell; NK, natural killer; DTIC, Melan-A/MART-1 Melan-A, dacarbazine; ISS, Istituto Superiore di Sanità; IRE, Regina Elena National Cancer Institute; AJCC, American Joint Commission on Cancer; CT, computed tomography; eCRF, electronic case report forms; CTCAE, Common Terminology Criteria for Adverse Events; PE, phycoerythrin; FITC, fluorescein isothiocyanate; SEB, staphylococcal enterotoxin B; IL, interleukin; TNF, tumor necrosis factor; SE, standard error; NED, no evidence of disease; FDA, Food and Drug Administration; EMA, European Medicines Agency; TAAs, tumor-associated antigens.

monocyte/DC precursor activation (26). A subsequent phase I/II clinical study was conducted by our group in stage III/IV melanoma patients following surgery to evaluate the safety and immunogenicity of peptide-based vaccination with Melan-A and gp-100 in combination with low-dose IFN-α, preceded or not by a single administration of dacarbazine (DTIC) (16). Remarkably, three of five high-risk patients treated with DTIC plus IFN-α plus vaccination are up to now disease-free after more than 10 years (16). The triple combination proved safe and well tolerated and capable of inducing higher specific $CD8^+$ T cell responses than vaccination plus IFN-α alone. In responder patients, we found a progressive enhancement of the T cell receptor (TCR) repertoire diversity in highly avid Melan-A–specific $CD8^+$ T cells (27), accompanied by serine/threonine kinase (AKT)-activation (28).

In light of our results, we aimed to carry out an open-label, randomized, phase II trial on resected stage III, IVM1a, and IVM1b melanoma patients. Since in our previous phase I trial the immune responses to gp100 were much weaker than those to Melan-A (16), we replaced gp100 with the cancer-testis antigen NY-ESO-1, which represents a promising candidate for vaccine-based therapy given its ability to induce both cellular and humoral immune responses (29). The trial was designed to evaluate (a) whether peptide-based vaccination combined with IFN-α could improve relapse-free survival (RFS) and overall survival (OS) with respect to literature estimates available at the time of the study design; (b) whether preconditioning with DTIC could further increase the clinical outcome; (c) whether the immune response could predict the time to relapse; and (d) safety and tolerability of the investigated treatment approach.

MATERIALS AND METHODS

Patients and Enrollment

This study (EudraCT no. 2008-008211-26) was sponsored and coordinated by Istituto Superiore di Sanità (ISS, Rome, Italy) and was conducted in accordance with the International Conference on Harmonization E6 Guidelines for Good Clinical Practice and the Declaration of Helsinki. Patients were enrolled at Regina Elena National Cancer Institute (IRE) (Rome, Italy), after having signed an informed consent form approved by the IRE Ethical Committee. Patients with histologically confirmed stage III or IV (M1a or M1b) melanoma, according to the 2002 modified American Joint Commission on Cancer (AJCC) staging system, underwent surgical resection of nodal or metastatic disease. Inclusion criteria included histologically confirmed stage III or IV (M1a or M1b) melanoma; surgical resection of nodal or metastatic disease; no evidence of disease (NED), as assessed by computed tomography (CT) scan performed within 30 days before therapy; HLA-A*0201 positivity; age 18 years or older; adequate renal, hepatic, and hematologic functions; Eastern Cooperative Oncology Group (ECOG) score 0–1; and life expectancy of at least 6 months. Exclusion criteria included current or a previous diagnosis of carcinoma within 5 years; concomitant or prior chemotherapy, immunotherapy, or radiotherapy (within 4 years); severe cardiovascular disease; concomitant immunosuppressant therapy; active autoimmune disease; active or chronic infection (including human immunodeficiency virus, hepatitis C and B viruses); pregnancy; and breastfeeding. Patients were required to have a CT scan performed within 30 days before initiation of therapy, showing NED. Patients' characteristics are detailed in **Supplementary Table S1**.

Vaccine

Melan-A_{26-35} (A27L) (ELAGIGILTV) and NY-ESO-$1_{157-165}$ (SLLMWITQC) GMP-grade peptides were produced by Polypeptide Laboratories (Strasbourg, France) and emulsified with Montanide ISA-51 (Seppic, Milan, Italy) using a two-syringe method. The emulsion was obtained by using rubber/silicone-free syringes (B. Braun, Melsungen, Germany) and flexible connector devices specifically designed by Know Medical (Viadana, Italy).

Treatment

In arm 1, patients received the vaccine intradermally in combination with 6 MU IFN-α2b subcutaneously (IntronA®; Schering-Plough Corporation, Kenilworth, NJ, USA). Each peptide and 3 MU IFN-α2b were injected in close but separate sites near local lymph nodes in right or left alternating arms or legs. The immunization regimen consisted of six cycles (every 21 days) of two vaccine doses (7 days apart) (**Figure 1A**). Arm 2 patients received the same treatment of arm 1 patients, preceded (1 day before each vaccination cycle) by an intravenous infusion of 800 mg/m^2 DTIC (Deticene; Sanofi–Aventis Groupe, Paris, France) (**Figure 1A**).

Study Design

This was a single-center, open-label, randomized phase II study with the objective of gaining preliminary information regarding RFS and OS. The primary endpoint of the study was to assess whether the combination of vaccination and IFN-α2b, with or without DTIC, could increase the RFS of resected stage III/IV melanoma patients, with respect to literature estimates at the time of trial design (30). A single-stage design, as described by A'Hern (31), was used to calculate the sample size. For each arm, a sample size of 24 patients was considered sufficient to give an 80% probability of rejecting a 1-year distant metastases-free (or death-free) rate of 60% with an exact 10% one-sided significance test when the true response rate is 80%. Secondary endpoints were OS, safety and tolerability of the treatment, and immune responses analysis.

Randomization

Randomization was performed by a computer-generated random list, with block restriction of four. The list was hidden to the clinical center.

Patients Follow-Up

Patients' clinical status was monitored before, during, and after treatment. Complete blood count and full chemistry panel were done pretreatment and before each vaccination cycle. Total body CT scan was performed every 4 or 6 months according to the stage of disease. Locoregional lymph node ultrasound was carried out every 4–6 months. All data were recorded in electronic case

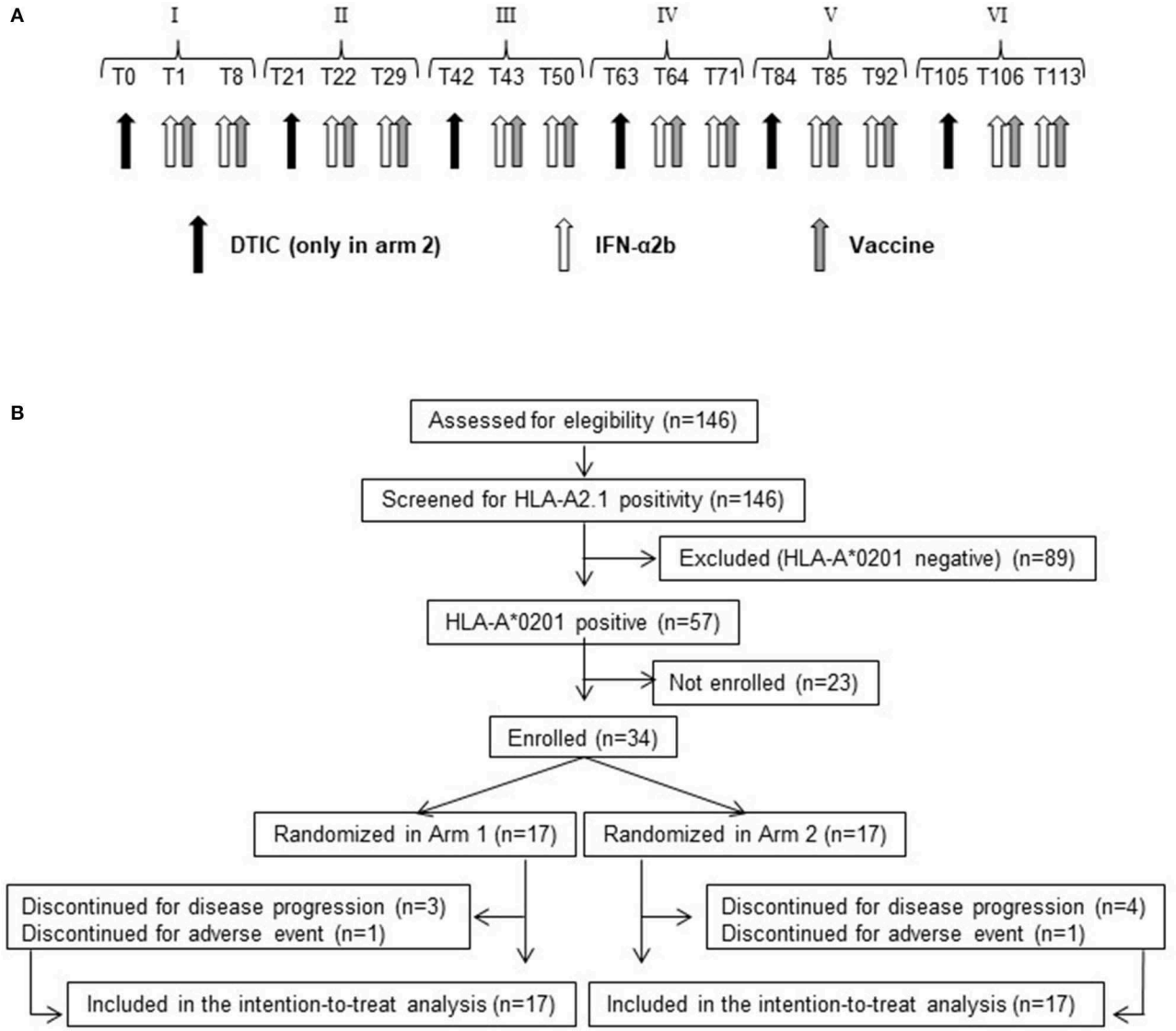

FIGURE 1 | Treatment schedule and CONSORT flow diagram. **(A)** Roman numbers indicate the cycle of treatment. Tn indicates the day after beginning of treatment. Black arrow, dacarbazine (DTIC) intravenous infusion. White arrow, IFN-α2b subcutaneous injection. Gray arrow, vaccine (Melan-A/MART-1 and NY-ESO-1 peptides emulsified with Montanide ISA-51) intradermal injection. **(B)** Flow diagram showing the progress of patients throughout the trial.

report forms (eCRF), designed by the information technology service at ISS.

Safety

Safety was evaluated by assessing incidence, severity, and nature of adverse events and graded according to NCI Common Terminology Criteria for Adverse Events (CTCAE) v4.0. The association of adverse events with treatment was determined by physicians. Adverse events were recorded in eCRF.

Immune Response Monitoring

Blood was collected at different time points before, during (21, 42, 63, 84, 92, and 105 days), and after (4 and 6 months) treatment. Peripheral blood mononuclear cells (PBMCs) were isolated and frozen as described in (32). MIATA and MIANKA guidelines (http://miataproject.org/miata-guidelines/final-guidelines-2/) were followed to implement the data quality level of flow cytometry assays. Live and dead cells were discriminated by trypan blue exclusion method, and samples showing viability less than 70% were not further processed. Current immunological monitoring uses advanced technologies that allow the evaluation of many parameters on a small number of cells (33). The flow cytometer available when the study was performed (FACSCanto) allowed the analyses of a limited number of parameters. Considering also the low number of cells obtained by patients, we focused our analyses on specific T cell

and NK cell responses as detailed below. The FACS analysis was performed on total PBMCs (1×10^6 cells) or magnetically sorted $CD8^+$ T cells (Miltenyi Biotech, Bergisch Gladbach, Germany), both *ex vivo* and after a short-term *in vitro* sensitization with Melan-A and NY-ESO peptides, by staining with phycoerythrin (PE)-labeled HLA-A*0201/peptide (Melan-A and NY-ESO-1) tetramers (Beckman Coulter, San Diego, CA, USA) (1 μg/10^6 cells, 30 min, room temperature) and fluorescein isothiocyanate (FITC)–conjugated anti-CD8 mAb (Miltenyi Biotech) (15 min, 4°C). Background fluorescence (0.01%) was assessed by means of iTAgTM HLA class I human negative tetramers SA-PE (Beckman Coulter).

A multicolor flow cytometry–based approach was used to monitor variations in the percentages of the major lymphocyte and NK subsets before, during, and after treatment by using different antibody panels (anti-CD3, anti–IFN-γ, anti-CD107, anti-CD56, anti-CD16) and a dead/live staining kit, as detailed in **Supplementary Table S2**. All samples showed a viability greater than 88%, and for this reason, no sample was excluded from the analysis.

Functional analysis of vaccine-specific T cell responses was performed on cryopreserved PBMCs isolated at baseline and at different time points before, during (92 days), and after (4 months) treatment, by a previously described functional multiparameter test (34), combining surface staining for CD8 and HLA-A*0201/Melan-A tetramer with staining for the cytotoxicity surrogate marker CD107a and intracellular cytokine staining for IFN-γ, interleukin 2 (IL-2), and tumor necrosis factor α (TNF-α). Briefly, after thawing in the presence of DNase, 2×10^6 PBMCs/well were stained with PE-labeled HLA-A*0201/Melan-A tetramer (0.5 μg/10^6 cells), washed, and cultured in 96-well round-bottom plates in the presence of the costimulatory antibodies anti-CD49d and anti-CD28 (Becton Dickinson, San Jose, CA, USA), for 6 h at 37°C in a 5% CO_2 incubator, in RPMI medium (Life Technologies, Gibco BRL, Grand Island, NY, US) added with 2% human serum (Euroclone, Pero, Italy), HEPES, penicillin, streptomycin, nonessential amino acids, L-glutamine, and DNase I (10 U/mL). Staphylococcal enterotoxin B (SEB; Sigma-Aldrich, Munich, Germany) (2 μg/mL) was used as positive control. During the incubation, PBMCs were stained with FITC-labeled anti-CD107a. To inhibit cytokine secretion and lysosome acidification, brefeldin A (Golgi Plug) and monensin (Golgi stop) (Becton Dickinson) were added after the first hour of incubation. After 6 h, 2 mM EDTA was added to each well and cells were incubated for 15 min. Cells were surface stained with PE/Cy7-conjugated anti-CD8 mAb (30 min at 4°C) and then washed, fixed, and permeabilized with BD intrasure kit (BD Biosciences, San Jose, CA, USA) and stained intracellularly with an antibody cocktail containing fluorescently labeled mAbs directed against IFN-γ, IL-2, and TNF-α. Fluorochromes, mAb clones, and manufacturers are detailed in **Supplementary Table S2**. The gating strategy is described in **Supplementary Figure S1**.

Natural killer cell effector functions were determined in a single-cell assay using CD107a mobilization assay and IFN-γ production. Cells were stimulated with K562 cells at 25:1 effector/target ratio or PMA (1.25 ng/mL) and ionomycin (1μg/mL) (Sigma-Aldrich, St. Louis, MO, USA) as positive control. In brief, 1×10^6 thawed PBMCs were cultured in U-bottom plates for 4 h at 37°C cells in the presence of monensin (Golgi Stop; BD Biosciences) and brefeldin A (Golgi Plug; BD Biosciences). Spontaneous degranulation ($CD107a^+$ percentage) and IFN-γ secretion were determined in the absence of targets and stimuli. Fluorescein isothiocyanate–labeled anti-CD107a was added at the beginning of incubation. After culturing, cells were labeled for 20 min at 4°C with anti-CD16, anti-CD56, and anti-CD3. Cells were then washed, lysed, and permeabilized with BD intrasure kit (BD Biosciences) and stained with anti–IFN-γ. A LIVE/DEAD Fixable Near-IR Dead Cell Stain Kit (Molecular Probes, Eugene, OR, USA) was used to determine the viability of cells prior to surface and intracellular staining. FcR blocking (BD Biosciences) was also included in order to avoid nonspecific staining of monoclonal antibodies to FcγRIII. The gating strategy for NK and NKT cells is described in **Supplementary Figure S2**.

Data acquisition was performed using a FACSCanto instrument (BD Biosciences) and analyzed by FACS DIVA or FlowJo version 10 (Tree Star, Ashland, OR, USA) or Kaluza (Beckman Coulter, Brea, CA, USA) software. For each sample, all labeled cells (up to 1,300,000 events) were acquired in order to give statistical significance to very low expressed or even rare populations. Abnormal or manifestly artifactual acquired samples were not further analyzed (e.g., light scatter or any fluorescence abnormal profile).

Statistical Analysis

The sample size was calculated for each treatment arm using a single-stage design as described by A'Hern (31). Based on the EORTC 18991, the expected 1-year RFS rate of untreated stage III resected melanoma patients was 60% (30). For each arm, a sample size of 24 patients was considered sufficient to give an 80% probability of rejecting the null hypothesis, with an exact 10% one-sided significance test when the true response rate is 80%.

Relapse-free survival and OS were evaluated by intention-to-treat analysis including all randomized patients.

Relapse-free survival was measured from the date of randomization until the date of relapse or death from any cause, and OS was measured from the date of randomization until death from any cause (**Supplementary Table S1**). For patients who were disease-free or alive at the time of data cutoff or for patients lost to follow-up, survival was censored on the last date of follow-up. The Kaplan–Meier method was used to estimate median survival, RFS, and OS distributions and the 95% confidence interval (CI) of these estimates [1.96 times the standard error (SE) in each direction], where the SE was computed with the Greenwood formula. The Brookmeyer and Crowley method was used to calculate the 95% CI of median RFS and OS. Stratified log-rank test, at a two-sided α level of 0.05, was used to compare distributions of OS and RFS between treatment arms.

A χ^2 test or Fisher exact test was used to compare different groups of patients for the analysis of toxicity.

Regarding immunological markers, comparisons between arm 1 vs. arm 2 and relapsing vs. disease-free patients were performed by independent nonparametric Mann-Whitney *U*-test.

TABLE 1 | Patient demographic and baseline characteristics.

Characteristics	*n*[a] (%) or Median (range)		
	All	**Arm 1**	**Arm 2**
Median age (range), years	52 (23–80)	55 (40–80)	46 (23–73)
Sex, *n* (%)			
Male	21 (62)	11 (65)	10 (59)
Female	13 (38)	6 (35)	7 (41)
Ethnicity, *n* (%)			
White	34 (100)	17 (100)	17 (100)
ECOG performance status, *n* (%)			
0	34 (100)	17 (100)	17 (100)
AJCC stage, *n* (%)			
IIIa	1 (3)	1 (6)	0 (0)
IIIb	4 (12)	2 (12)	2 (12)
IIIc	17 (50)	8 (47)	9 (53)
IV M1a	9 (27)	5 (29)	4 (24)
IV M1b	3 (8)	1 (6)	2 (12)
Median LDH,[b] range (U/L)	305 (197–433)	309 (197–433)	300 (260–432)

[a] *Data are n or median, as indicated. Percentage (%) or range in brackets.*
[b] *LDH normal range, 220–480 U/L.*

Wilcoxon nonparametric test for paired sample was used to analyze differences between time points.

Statistical analysis was performed using IBM-SPSS processor v25 (IBM Corporate New York, NY, USA) and STATA (StataCorp LLC 4905 Lakeway Drive, Texas, USA).

RESULTS

Patients' Characteristics and Treatment

From February 23, 2010, to August 10, 2012, 146 stage III, IVM1a, IVM1b melanoma patients, undergoing surgical resection of metastatic or nodal lesions and complying with all other eligibility criteria, were screened for HLA-A*0201 expression. A total of 57 patients were found HLA-A2 positive, and 34 were enrolled and randomly allocated to either arm 1 (17 patients) or arm 2 (17 patients) (**Figure 1B** and **Supplementary Table S1**).

Patients allocated in arm 1 were treated with peptide-based vaccination [Melan-A:26-35(27L) and NY-ESO-1:157-165, emulsified with Montanide ISA-51]. The immunization regimen consisted of six cycles (every 21 days) of two vaccine doses (7 days apart), administered in combination with 6 MU IFN-α2b (**Figure 1A**). Arm 2 patients received the same treatment of arm 1, preceded (1 day before each vaccination cycle) by DTIC (800 mg/m^2) (**Figure 1A**).

Table 1 and **Supplementary Table S1** show demographic and clinical characteristics of patients. Overall, 1 patient (3%) had stage IIIA, 4 (12%) had stage IIIB, 17 (50%) had stage IIIC, 9 (27%) had stage IVM1a, and 2 (8%) had stage IVM1b disease. Stage, age, gender, ethnicity, ECOG status, and LDH values were not significantly different between the two arms (**Table 1**). All patients showed an ECOG performance status of 0. Median LDH level before vaccination was 305 U/L (range, 197–433 U/L), falling within the reference range values.

Seven patients (20.6%) (three in arm 1 and four in arm 2) discontinued treatment because of disease progression. Two patients (5.9%) (one in arm 1 and one in arm 2) discontinued treatment because of adverse events (**Figure 1B**).

Clinical Results

On November 2018, clinical data cutoff date, the median follow-up duration was 55.1 months (4.5 years) (interquartile range, 15.4–81.0 months).

The intention-to-treat analysis is shown in **Figure 2** for both treatment arms (34 patients). In both treatment arms, all recurrences were observed within 18 months following randomization.

Of note, the probability of relapse was mostly concentrated in the first year (50%; 95% CI, 34.7–67.6%), although it became very low after this period and equal to zero after 17 months (**Figure 2A**).

Eighteen months following randomization, 9 of 17 patients treated with vaccination and IFN-α2b (arm 1) were still relapse-free and alive, and remarkably, no further relapses were observed thereafter. Therefore, the RFS rate was 52.9% (95% CI, 29.2%−76.6%) at 1.5 years and remained the same at 4.5 years (median follow-up duration), when five or more patients were still under observation and even beyond (fewer than 5 patients under observation) (**Figure 2A**). The median RFS was not reached (**Figure 2A**).

Of the 17 patients receiving preconditioning DTIC before vaccination (arm 2), six had NED at 18 months and remained disease-free until their last follow-up. The 4.5-year RFS rate was 35.3% (95% CI, 12.6%−58.0%), and the median RFS of this patient cohort was 9.3 months (95% CI, 2.3%−18.6%) (**Figure 2A**).

Although the sample size was not dimensioned to compare the two treatment arms, no significant differences were observed between them (**Figure 2A**). On the whole, 15 of 34 patients were still relapse-free at their last follow-up, and the cumulative 4.5-year RFS rate of all treated patients was 44.1% (95% CI, 27.4%−60.8%) (**Figure 2C**). The median RFS of all treated patients was 11.4 months (95% CI, 0–23.1 months) (**Figure 2C**).

After 4.5 years, some patients were lost to follow-up (≤12 patients at risk). Interestingly, at 6 years following randomization, 11 of 11 patients under observation were disease-free. Of particular relevance, a stage IV M1a patient (patient 4, arm 1) was NED up to 8 years (**Figure 2C** and **Supplementary Table S1**). Among patients who relapsed, one patient (patient 011) who relapsed 13 months after randomization had surgical removal of relapsed tumor and remained disease-free until the last follow-up (7.6 years). Patient 024 (arm 2), who relapsed 4 months after randomization, underwent a second surgery and relapsed again 22 months later. However, this patient (patient 024) displayed a complete response after treatment with dabrafenib and trametinib, which lasted until the last follow-up (4 years) (**Supplementary Table S1**).

The OS (secondary endpoint of the study) is shown in **Figures 2B,D**. In the cohort of patients treated with vaccination and IFN-α2b, 5 of 17 patients died. As shown in **Figure 2B** and **Supplementary Table S1**, the last death was observed at 40

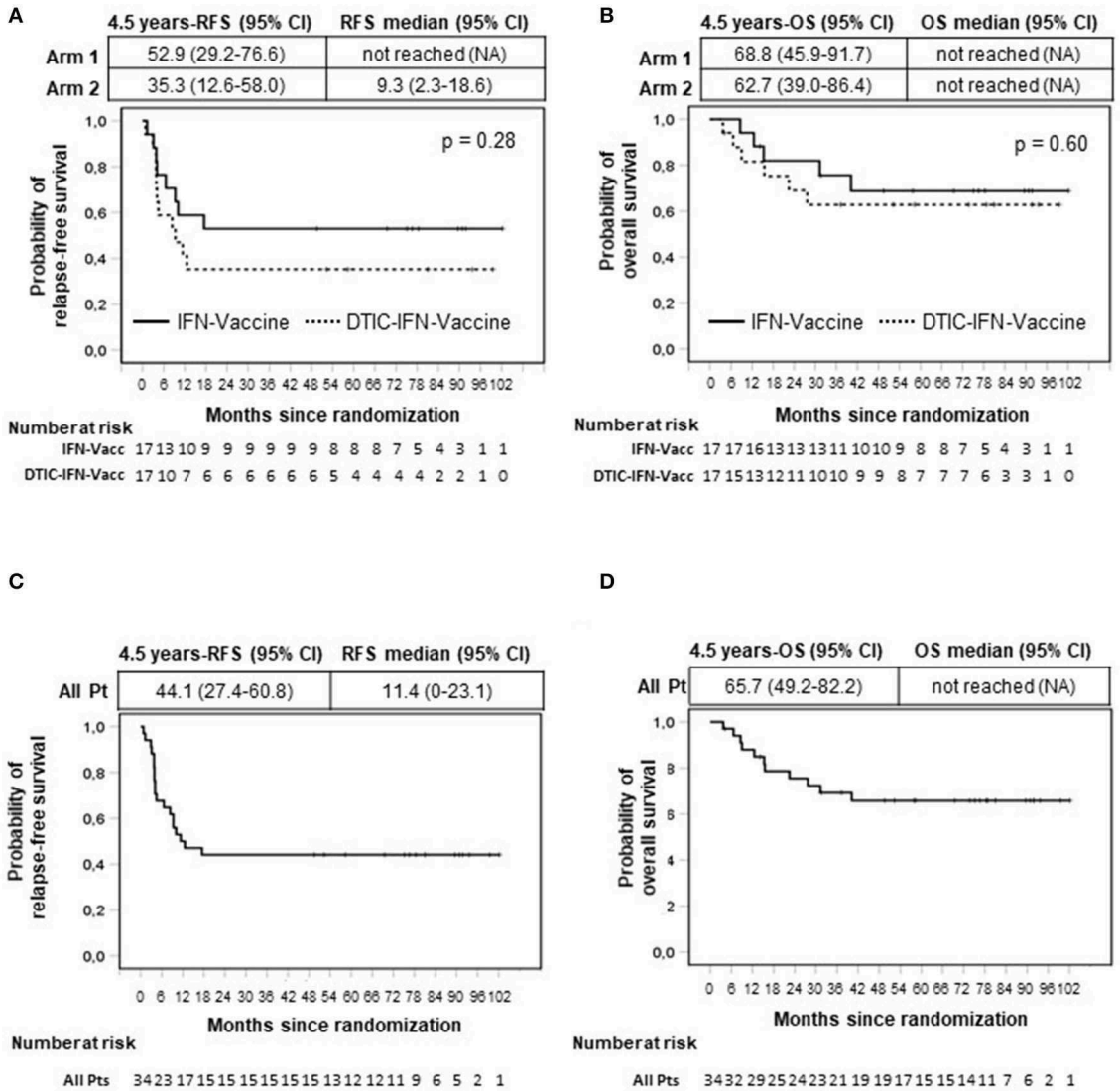

FIGURE 2 | Intention-to-treat analysis of relapse-free (RFS) **(A,C)** and overall survival (OS) **(B,D)** by Kaplan–Meier method. All enrolled patients were included in the analysis ($n = 34$). Months are calculated since time of randomization. Arm 1 patients (Pt) ($n = 17$) were treated with vaccination with Melan-A and NY-ESO-1 peptides (Vaccine) and interferon-α2b (IFN). Arm 2 patients ($n = 17$) received the same treatment of arm 1 patients with the addition of dacarbazine (DTIC) pretreatment. **(A,B)** Comparison between arms. **(C,D)** All patients ($n = 34$). p value by log-rank test.

months. The 4.5-year OS rate was 68.8% (95% CI, 46.1%−91.5%), and the OS curve remained stable later on. The median OS has not been reached. The OS rate at 4.5 years for patients treated with the combination of DTIC plus vaccination plus IFN-α2b was 62.7% (95% CI, 39.0%−86.4%) and remained stable thereafter (six deaths were reported). The median OS was not reached (**Figure 2B**). No statistically significant difference was found between the two treatment arms (**Figure 2B**), and the cumulative 4.5-year OS rate was 65.7% (95% CI, 49.2%−82.2%) (**Figure 2D**).

In **Supplementary Table S1**, the RFS and OS are reported for each patient along with demographic and disease characteristics.

Safety and Toxicity

Overall, the treatment was well tolerated. Adverse events for any cause are reported in **Table 2**. There were neither treatment-related deaths nor grade 4 adverse events during the treatment courses. Only two patients (5.9%) presented with grade 3 adverse events: severe musculoskeletal pain (arm 1) and severe asthenia (arm 2). These adverse events lead to patients' withdrawal from the trial. Other common adverse events (mostly grade 1) were fever (68%), musculoskeletal pain (27%), asthenia (24%), nausea (29%), and vomiting (18%) (**Table 2**). Noticeably, most of the reported adverse events were typical side effects of IFN-α treatment (i.e., fever, musculoskeletal pain, headache) and

TABLE 2 | Treatment-related adverse events.

Event	Grade[a] 1	Grade 2	Grade 3	Grade 4/5
	n (%)			
Fever	22 (65)	1 (3)	0	0
Nausea	9 (26)	1 (3)	0	0
Musculoskeletal pain	8 (24)	1 (3)	1 (3)	0
Vomiting	6 (18)	0	0	0
Asthenia	5 (15)	3 (9)	1 (3)	0
Headache	3 (9)	0	0	0
Injection site reaction/erythema	2 (6)	0	0	0
Bradycardia	1 (3)	0	0	0
Diarrhea	1 (3)	1 (3)	0	0
Nail dyschromia	1 (3)	0	0	0
Local pain	1 (3)	0	0	0
Epigastric pain	1 (3)	1 (3)	0	0
Injection site reaction/swelling	1 (3)	0	0	0
Herpes labialis	1 (3)	0	0	0
Injection site reaction/hyperemia	1 (3)	0	0	0
Hypotension	1 (3)	0	0	0
Mild visus decrease	1 (3)	0	0	0
Loss of appetite	1 (3)	0	0	0
Agitation	1 (3)	0	0	0
Vertigo	1 (3)	0	0	0
Anemia	0	1 (3)	0	0
Abdominal pain	0	1 (3)	0	0
Neutropenia	0	1 (3)	0	0
Persistent coughing	0	1 (3)	0	0

[a]*Grades of adverse events were defined according to the National Cancer Institute CTCAE, version 4.0.*

TABLE 3 | Nausea and vomiting in the different treatment arms.

		Arm		Total
		1	2	
Nausea and/or vomiting[a]	Not present	15	6	21
	Present	2	11	13
	Total	17	17	34

[a]*Nausea and/or vomiting were significantly associated to the treatment (Fisher exact test $p = 0.004$). Arm 1 patients were treated with vaccination and IFN-α2b. Arm 2 patients were treated with vaccination, IFN-α2b, and dacarbazine.*

persisted for no more than 1 day. Exceptionally, nausea and vomiting were significantly related to DTIC administration ($P = 0.004$) (**Table 3**).

Evaluation of the Vaccine-Specific Immune Response

To evaluate whether the vaccination with Melan-A and NY-ESO-1 peptides was able to induce or increase specific $CD8^+$ T cell responses and in order to characterize their functionality, peripheral blood samples were taken before, during, and after treatment in 29 patients evaluable for response (excluding patients who discontinued early the trial).

First, PBMCs were e*x vivo* analyzed by flow cytometry to assess the percentages of Melan-A/NY-ESO-1 tetramer–positive $CD8^+$ T cells. NY-ESO-1–specific T cell numbers were in most cases below the level of detection (data not shown). In case of Melan-A, the kinetic of response in one representative patient (patient 29) showed that the frequency of Melan-A–specific $CD8^+$ T cells doubled starting from T63 (i.e., after three treatment cycles) to reach a plateau at T84 (**Figure 3A**). Therefore, in all evaluable patients ($n = 29$), the T cell response was analyzed at T0 and between T84 and T105, depending on sample availability. Before treatment (pre), a low frequency (between 0.01 and 0.04%) of Melan-A–specific $CD8^+$ T lymphocytes was detectable in 23 patients. One patient (patient 14) had a high spontaneous Melan-A–specific T cell response (0.36%) (**Figure 3B**). A significant (twofold or greater) increase of Melan-A tetramer–positive $CD8^+$ T cell frequencies was observed in 20 of 29 patients analyzed (68.96%) following treatment (post) in both arms ($P = 0.003$ in arm 1 and $P = 0.001$ in arm 2) (**Figure 3B**). In particular, the combination of the vaccine with IFN-α2b and DTIC induced a T cell response in 12 of 15 patients (80%) ($P = 0.001$), whereas, 8 of 14 patients (57.2%) ($P = 0.003$) responded to the combination of the vaccine with IFN-α2b alone (**Figure 3B**). We then compared whether the response to Melan-A correlated with the patient clinical outcome. As shown in **Figure 3C**, a statistically significant increase of Melan-A–specific T cell frequencies was observed after treatment in both NED (81%) ($P = 0.001$) and relapsing patients (61%) ($P = 0.009$). However, the survival curves of responding and nonresponding patients were not significantly different (**Supplementary Figure S3**).

To determine their proliferative potential, lymphocytes were sensitized *in vitro* in the short term with Melan-A (**Figures 3D–F**) or NY-ESO-1 (**Figures 3G–I**) peptides and analyzed by tetramer staining. A significant expansion of T cells specific for both epitopes was observed in both treatment arms (**Figures 3D,G**) and in both NED and relapsing patients (**Figures 3E,H**). Staining of lymphocyte expanded by a short-term *in vitro* stimulation with Melan-A (F) and NY-ESO-1 (I) peptides is shown before (Pre) and after (Post, T105) treatment, for a representative patient (patient 09).

To assess whether disease-free and relapsing patients developed a T cell response with different functionalities, we analyzed the ability of Melan-A–specific cells to simultaneously produce CD107a, TNF-α, IL-2, and IFN-γ in selected patients (16 patients with available frozen samples and showing at least 0.01% of $CD8^+$ cells in both pre and post samples) (**Figure 4**). The gating strategy is shown in **Supplementary Figure S1**. Before treatment (pre), most of the Melan-A–specific cells in both NED (**Figure 4A**) and relapsing patients (**Figure 4B**) did not express any tested function (74%), ∼20% of cells expressed one function, ∼5% were double positive, ∼1% expressed three functions, and almost none expressed four functions. Remarkably, 92 days (i.e., after nine vaccinations) and 4 months following treatment onset, only in patients who

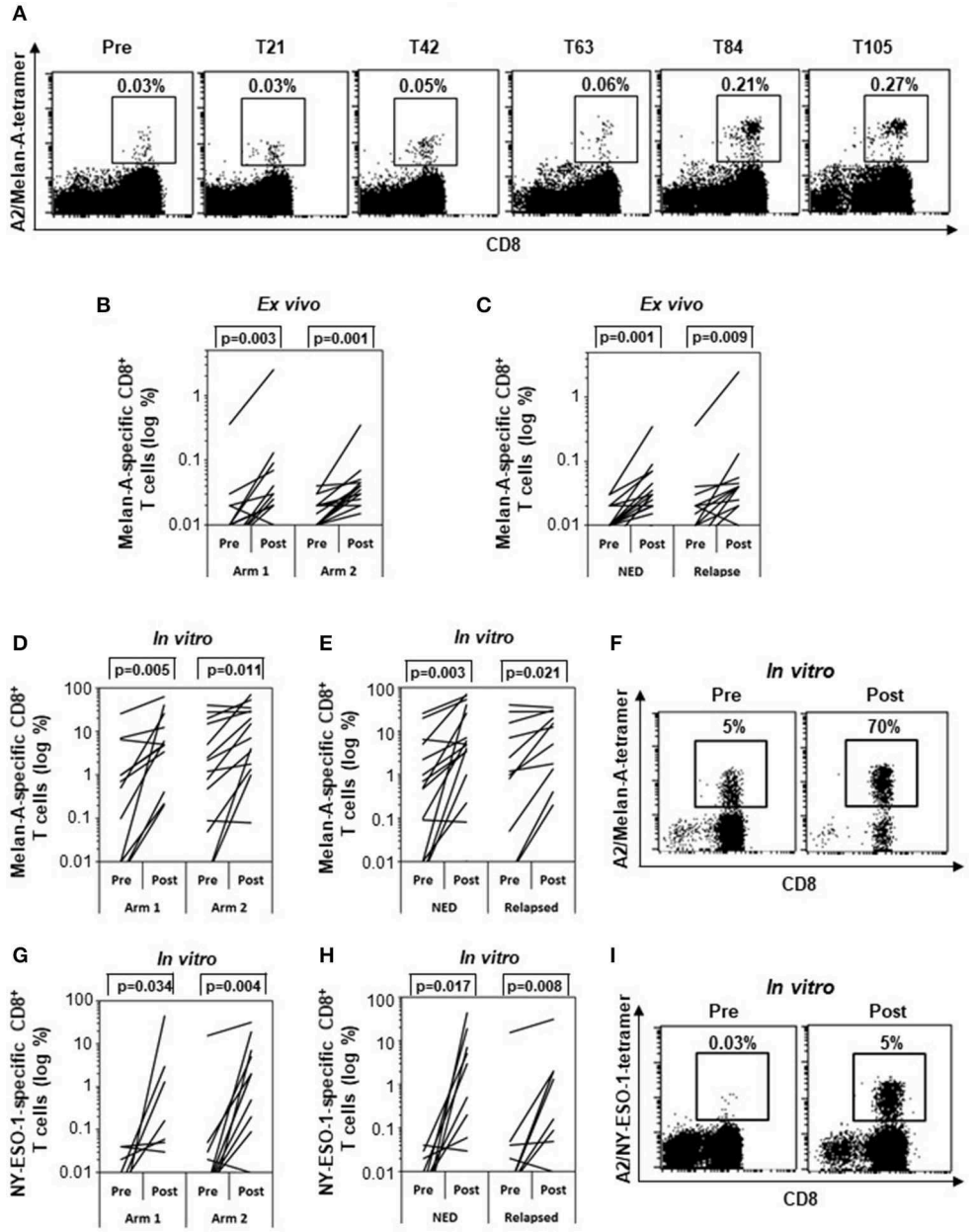

FIGURE 3 | Specific immune response. Frequencies of Melan-A– **(A–F)** and NY-ESO-1–specific **(G–I)** $CD8^+$ T cells analyzed by tetramer staining ($n = 29$). **(A)** Kinetic analysis of the frequency of Melan-A–specific T cells between pretreatment and posttreatment samples (T21, T42, T63, T84, T105) in one representative patient (patient 29). **(B,C)** Variation of Melan-A–specific T cell percentage between pretreatment and posttreatment *ex vivo* samples in arm 1 ($n = 15$) vs. arm 2 patients ($n = 14$) **(B)** and in patients with no evidence of disease (NED) ($n = 16$) vs. relapsed patients ($n = 13$) **(C)**. **(D,E,G,H)** Variation of Melan-A– ($n = 28$) **(D,E)** and NY-ESO-1–specific ($n = 26$) **(G,H)** T cell percentage after short term *in vitro* expansion, in arm 1 vs. arm 2 patients **(D,G)** and in patients with no evidence of disease (NED) vs. relapsed patients **(E,H)**. **(F,I)**. Representative staining (patient 09) of short term *in vitro* expansion before (pre) and after (post, T105) stimulation with Melan-A (F) and NY-ESO-1 (I) peptides. *p* values were calculated by Wilcoxon signed-rank test.

remained disease-free the Melan-A–specific cell functionality increased. In fact, the percentage of Melan-A–specific cells expressing none of the tested functions significantly diminished from the pretreatment level of 74 to 59.2% at T92 ($P = 0.046$) and 62.8% posttreatment ($P = 0.043$). The percentage of single positive cells increased from 20.4 to 30.1% at 4 months ($P = 0.043$). For double- and triple-positive cells, a trend of increase from 4.5 to 13.9% and from 1 to 5.4%, respectively, was observed at T92 (**Figure 4A**). Conversely, in relapsing patients, no changes in the percentages of zero-functional, monofunctional, and polyfunctional cells were observed (**Figure 4B**).

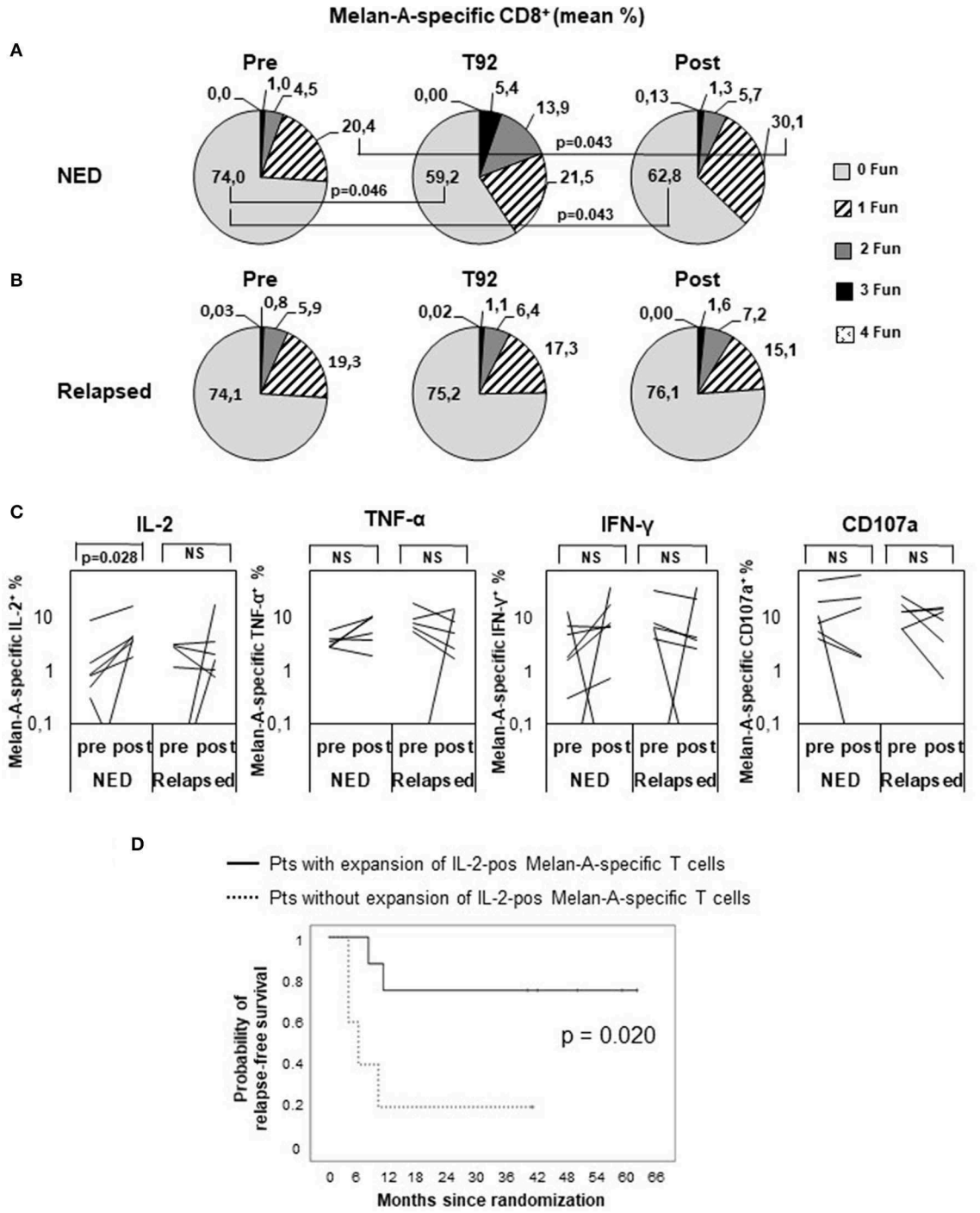

FIGURE 4 | Polyfunctional analysis of Melan-A–specific CD8$^+$ T cells. Peripheral blood mononuclear cells were analyzed by multiparameter flow cytometry after 5 h *in vitro* culture without peptide pulsing, followed by 1-h incubation with brefeldin A and monensin. CD8$^+$ Melan-A tetramer–positive T cells were gated as shown in **Supplementary Figure S1** and analyzed for their simultaneous expression of surface CD107a and intracellular IL-2, IFN-γ, and TNF-α. **(A,B)** Pie charts showing the proportion of cells expressing any combination of four (4 Fun), three (3 Fun), two (2 Fun), one (1 Fun), or zero (0 Fun) tested markers (CD107a, IL-2, IFN-γ, and TNF-α). Data are expressed as mean percentage of CD8$^+$ Melan-A tetramer–positive T cells. **(A)** Patients with no evidence of disease (NED). **(B)** Patients with disease recurrence (Relapsed). *p* values by Wilcoxon signed-rank test. **(C)** Variation of Melan-A–specific T cell percentage expressing intracellular IL-2, TNF-α, IFN-γ, or surface CD107a (logarithmic scale) between pretreatment and posttreatment (4 months) in patients with no evidence of disease (NED) ($n = 7$) vs. relapsed patients ($n = 6$). *p* values by Wilcoxon signed-rank test. **(D)** Kaplan–Meier plot comparing the relapse-free survival of patients (Pts) characterized, or not, by a twofold expansion of IL-2–positive Melan-A–specific T cells in post vs. pre samples. *p* value by log-rank test.

We then analyzed whether the modulation of any defined function (or combination of functions) correlated with the patient clinical outcome and found that the production of IL-2 by Melan-A–specific lymphocytes was significantly increased following treatment only in nonrelapsing patients ($P = 0.028$) (**Figure 4C**). Remarkably, the RFS curve of patients in which the percentage of IL-2^+ Melan-A–specific cells increased following treatment was significantly ($P = 0.020$) different from the curve of patients with no expansion of these cells (**Figure 4D**). Interestingly, in relapsing patients, a trend of reduction of TNF-α, IFN-γ, and CD107a producing cell percentages was observed after treatment (**Figure 4C**), thus highlighting a different functionality of peptide-specific T cells in patients with different clinical response. A similar set of analyses was conducted to compare whether Melan-A–specific T cells had a different functionality in arm 1 and arm 2 patients, and no significant differences were found (data not shown).

Evaluation of the Innate Immune Response

Natural killer cells have been shown to control tumor growth in particular when tumors downregulate MHC I. Because type I IFN can modulate innate immunity, including NK cells (6) by affecting their number and cytotoxic capacity (22), an in-depth analysis of the frequency, phenotype, and functional abilities of these cells was carried out. The gating strategy is shown in **Supplementary Figure S2**.

The analysis of the frequencies of total NK ($CD56^+CD3^-$) and NK-like-T (NKT) cells ($CD56^+$ $CD3^+$) showed no differences between pretreatment and posttreatment time points (data not shown). However, the proportion of the different NK subsets changed following treatment. In particular, $CD56^{bright}CD16^{neg}$ NK cell subset was significantly increased after treatment in disease-free patients, whereas in relapsing patients only a trend toward increase was observed (**Figure 5A**). Following *in vitro* activation with PMA/ionomycin, these cells were able to differentiate toward a more mature phenotype, that is, $CD56^{dim}CD16^{neg}$ (**Figure 5B**) more efficiently in NED ($P = 0.043$) than in relapsing patients, and their functional ability increased following treatment only in disease-free patients. In fact, when challenged with MHC devoid target cells (K562 cells), the proportion of $CD56^{dim}CD16^{neg}$ cells expressing CD107a, as marker of degranulation, was significantly expanded ($P = 0.028$) (**Figure 5C**), whereas the percentage of cells expressing IFN-γ did not change (data not shown). In **Figure 5D**, the increase in the percentage of $CD56^{dim}CD16^{neg}$-expressing CD107a between pretreatment and 4 months after treatment is shown for one representative patient (patient 28).

DISCUSSION

The incidence rate of malignant melanoma is constantly increasing, reaching five cases per 100,000 persons (95% CI, 4–7) worldwide and 16 cases per 100,000 persons (95% CI, 11–20) in Western Europe in 2015 (35). Stage III–IV patients have high risk of recurrence after primary melanoma resection (36, 37). Insights into the complex relationship between the host immune response and the tumor have led to the approval of different immunotherapies to prevent recurrence in high-risk patients.

The first adjuvant treatment approved by the Food and Drug Administration (FDA) and the European Medicines Agency (EMA) for stage III patients with high risk of recurrence was high-dose IFN-α (IFN-α2b). Pegylated IFN-α2b was approved by FDA in 2011. The 4-year RFS rate in patients treated with pegylated IFN was 45.6% as compared to 38.9% in the observational group, whereas inconsistent increases in the OS were observed. The treatment was also associated to substantial toxic effects (30).

Starting in 2015, three CPIs have been approved for the adjuvant treatment of melanoma by FDA and EMA, that is, ipilimumab (38, 39), nivolumab (40), and pembrolizumab (41). Later on, the combination of the BRAF inhibitor (dabrafenib) and the MEK inhibitor (trametinib) was shown to improve survival of stage III patients with BRAF V600 mutations (42, 43) and was approved for the adjuvant treatment of melanoma. Although showing impressive antitumor effects, CPIs and kinase inhibitors are characterized, up to now, by some toxicity (especially for ipilimumab at the FDA-approved dose of 10 mg/kg) and by elevated costs, which limit their full utilization on a wide number of patients, such as resected high-risk patients. Moreover, not all patients respond to checkpoint blockade or kinase inhibitors, and not all responses are long-lasting (3). Thus, effective, low-cost, and low-toxicity therapies are still needed in melanoma, especially in the adjuvant setting; thus, it is still of great interest to investigate novel combinations of immunotherapies based on solid scientific rationales.

The present phase II study was designed to provide preliminary evidence of the efficacy of peptide-based vaccination in combination with IFN-α2b, preceded or not by DTIC, to prevent relapse of completely resected melanoma patients with high risk of recurrence (stage III/IV). When the present study began, no FDA/EMA–approved adjuvant treatment was available for stage III–IV melanoma patients. Therefore, no active control could have been used in this study.

The primary endpoint of this study was to assess whether the combination of vaccination and IFN-α2b (with or without DTIC) could increase the 1-year RFS rate from the 60% observed in the untreated control arm of a phase III study (30) to 80%. Because an interim analysis showed a 1-year RFS rate of 58.8% (95% CI, 35.5%−82.1%) in arm 1 patients and of 41.2% (95% CI, 17.9%−64.5%) in arm 2, patient enrollment was stopped at 17 patients per arm, before reaching the preplanned sample size of 24. Notably, this goal and, accordingly, the sample size were chosen based on a phase III clinical study including only stage III resected patients (30), which are characterized by a more favorable prognosis than a mixed population of stage III/IV patients. In hindsight, this goal was indeed overestimated, considering that, in a recently published phase III clinical trial, the 1-year RFS rate of resected stage III/IV patients was 60.8% in ipilimumab-treated patients and 70.5% in the nivolumab group (40).

The intention-to-treat analysis showed interesting results with regard to the clinical outcome of patients treated with melanoma peptides plus IFN-α. In fact, the 4.5-year RFS rate of patients

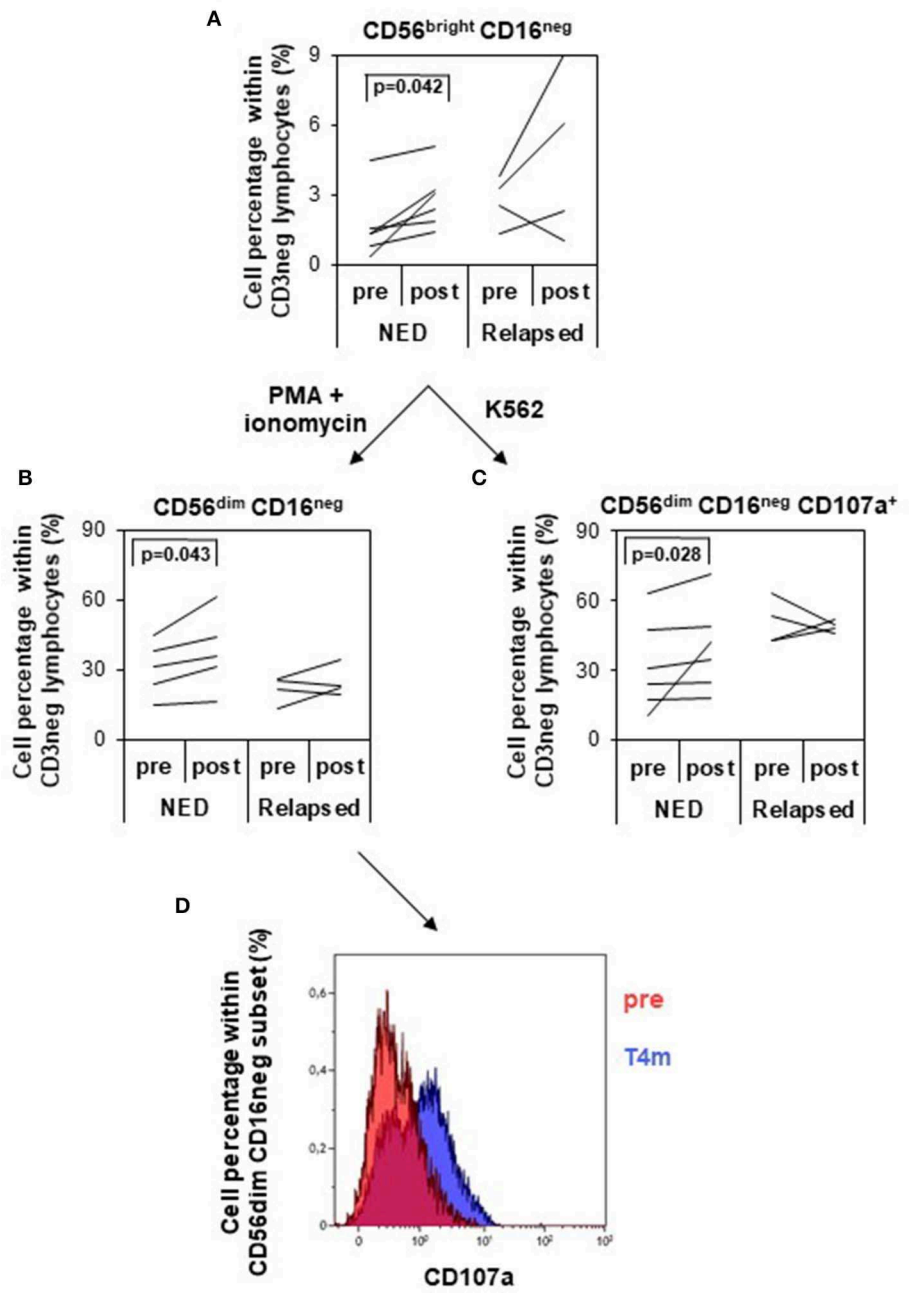

FIGURE 5 | Analysis of natural killer (NK) cell subsets and of their functionality. NK cells were identified and divided into four different subsets based on the expression of CD56 and CD16 within the CD3 negative lymphocytes (gating strategy depicted in **Supplementary Figure S2**). **(A)** Variation of the percentage of $CD56^{bright}$ $CD16^{neg}$ NK cells (logarithmic scale) between pretreatment and posttreatment (4 months) in patients with no evidence of disease (NED) ($n = 6$) vs. relapsed patients ($n = 4$). **(B,C)** NK cells were *in vitro* cultured with PMA/ionomycin **(B)** or with K562 target cells **(C)**, and $CD56^{dim}$ $CD16^{neg}$ NK cells were analyzed for their percentage variation **(B)** and CD107a expression **(C)** pretreatment and posttreatment in NED ($n = 6$) and relapsed patients ($n = 4$). *p* values by Wilcoxon signed-rank test. **(D)** Functional analysis of CD56dim CD16neg NK cells in response to K562 target cells pretherapy and 4 months after therapy in one representative patient (patient 28). CD107a-positive cells increased after treatment.

receiving vaccination with Melan-A and NY-ESO-1 peptides in combination with IFN-α2b was 52.9%, and the 4.5-year OS rate was 68.8%. The RFS and OS curves became stable starting from 18 and 40 months, respectively, and, noticeably, remained stable up to 4.5 years (median follow-up time). After 4.5 and 6.5 years, the estimates of RFS and OS are less reliable, respectively, because fewer than five patients are at risk in one of the two arms. However, it is interesting to note that no further relapses or death

were observed in the patients with longer follow-up (up to 8 years). Although comparisons between different studies should be interpreted with carefulness and despite the limited robustness of our data derived from a small phase II study, the clinical results obtained here appear to be comparable to those observed in randomized phase III studies. As a matter of fact, resected patients treated with pegylated IFN-α2b showed a 4-year RFS rate of 45.6% and an OS rate of 71% (30). In the ipilimumab trial, the 5-year RFS rate was 40.8% in the ipilimumab group vs. 30.3% in the placebo group and OS rate of 65.4% vs. 54.4 (39). In a more recent phase III trial the 3- and 4-year RFS rates were, respectively, 59 and 54% in the dabrafenib plus trametinib arm and 40 and 38% in the placebo arm, whereas the 3-year OS rate were 86% in treated patients vs. 77% in the placebo group (42, 43). Noteworthy, patients included in these three studies were all stage III, whereas those enrolled in our study were stage III (65%) and IV (35%), thus presenting a higher risk of recurrence. Promising results of recently published phase III study in stage III/IV resected patients treated with nivolumab showed improved 1-year RFS rates with respect to ipilimumab (70.5% in the nivolumab group as compared to 60.8% in the ipilimumab group) (40). Recent pembrolizumab results are also highly promising (1-year rate of RFS 75.4% vs. 61.0% in the placebo group) (41), but longer follow-up are still needed. In a small melanoma vaccine trial testing the combination of high-dose IFN-α with autologous DC, transduced with three shared/nonmutated melanoma antigens, it was observed that among the 11 stage III/IV resected patients NED at baseline, seven recurred, and four remained NED (36.3 %) up to 3 years (3.7–37.5+ months). No indications of the OS of these patients are given in the article (44).

Of note, with regard to the present study, it is worth underlining that our combination strategy was devoid of major toxic effects.

Contrary to what we expected based on results of our previous phase I clinical trial (16), pretreatment with DTIC before each vaccination cycle significantly increased neither RFS nor OS. One possible explanation for this discrepancy may rely on the different dose of IFN-α administered in the two studies, that is, 3 MU in the phase I trial (16) and 6 MU in the present phase II study. Immunodominance is a property of $CD8^+$ T cell responses to viruses and vaccines, which determines the skewing of the T cell response toward a few epitopes. $CD8^+$ T cells recognizing their cognate ligand were shown to inhibit the proliferation of other $CD8^+$ T cells engaged with the same APC (45, 46). Based on the hypothesis that the separate administration of the two vaccine peptides could avoid their competition for MHC binding and $CD8^+$ T cell cross-competition (47, 48), in the present study we injected Melan-A and NY-ESO-1 into distant sites, and because each peptide administration was associated with the nearby injection of 3 MU IFN-α2b, the total IFN-α dosage was doubled. As we previously observed that DTIC itself induces an IFN-I–related gene signature (16), possibly responsible for its immunomodulatory properties, we suppose that doubling the dose of IFN-α2b rendered the addition of DTIC irrelevant. Furthermore, the analysis of the vaccine-specific immune response showed no differences between the two treatment arms, indicating that the immune adjuvanticity of 3 MU IFN-α2b + DTIC is similar to that of 6 MU IFN-α2b alone.

Because no significant differences were observed between arm 1 and arm 2 patients either in terms of clinical outcome or of Melan-A–specific immune responses, the immunological analyses were conducted cumulatively in arm 1 and arm 2 patients. Overall, our combination strategies enhanced the vaccine-specific $CD8^+$ T cell frequencies in ∼69% of patients, but this rise did not correlate with the patient clinical outcome [similar to results obtained by Butterfield et al. (44)]. On the contrary, the investigation of the quality of the immune response, carried out by means of a functional multiparameter assay (34), showed that the polyfunctionality of Melan-A–specific T cells is associated with disease control. Indeed, an increase of Melan-A–specific T cells producing simultaneously two and three functions at T92 (i.e., after nine vaccination doses) was observed only in patients who did not relapse thereafter. Similarly, the production of IL-2 by activated Melan-A–specific T cells 4 months after treatment onset positively correlated with the patient clinical outcome, suggesting that these cells are skewed toward a central memory phenotype, which is characterized by high levels of IL-2 production and proliferative ability.

Taking into account the pleiotropic effect of IFN-I (21), in the present study we analyzed not only the vaccine-specific immune responses, like in most immunotherapy clinical trials, but also the modulation of innate immunity. In particular, we focused on NK cells, because studies in IFN-α receptor (IFNAR)–deficient mice demonstrated that IFN-I plays an important role for NK maturation and cytotoxic activity and NK-mediated antitumor effect (22).

Natural killer cells can be distinguished in different subsets based on surface density of CD56 and CD16 (FCγ receptor III) (49). $CD56^{bright}$ NK cells, characterized by high proliferative potential and low cytotoxic ability, are immediate precursors of less proliferating $CD56^{dim}$ NK cells, in which the expression of CD16 increases along with cytotoxicity (49). In our study, an expansion of $CD56^{dim}CD16^{neg}$ NK-producing CD107 was observed in nonrelapsing patients following treatment. Of note, these cells exhibit an intermediate maturation level (in terms of proliferating and cytotoxic activity) and are believed to be responsible for natural cytotoxicity against tumor targets.

Overall, findings from this study suggest that the combination of peptide-based vaccination and IFN-α2b can represent a valuable, nontoxic, and nonexpensive strategy to prevent relapse in stage III/IV resected melanoma patients, which may deserve further controlled clinical studies. Mechanistic studies suggest that this novel therapeutic strategy acts through the induction of both adaptive and innate immunity, that is, of polyfunctional Melan-A–specific $CD8^+$ T cells and NK cells.

Interferons are currently considered by the majority of clinicians as "old drugs" replaced by the new emerging therapies. However, some novel and promising therapeutic opportunities from new insights stemming from the most recent progress on IFN and cancer research have recently been underlined (8, 21, 50). Of note, the use of old drugs for either new therapeutic uses or with qualitatively new modalities and rationales may exhibit advantages in terms of costs and impact on public health systems

(51, 52), as the expenses and time needed for their full clinical development are much lower with respect to those necessary for the all process from drug discovery to the registration of new drugs. We believe that further studies, based on the use of cancer vaccines, together with a local and transient IFN-α treatment and/or IFN-α alone (administered according to our original dosage and schedule), in combination with subsequent CPI administration, can open new perspectives for recurrence prevention in melanoma as well as in other malignant diseases.

DATA AVAILABILITY STATEMENT

The raw data supporting the conclusions of this article will be made available by the authors, without undue reservation, to any qualified researcher.

ETHICS STATEMENT

The studies involving human participants were reviewed and approved by Regina Elena Cancer Institute ethics committee. The patients/participants provided their written informed consent to participate in this study.

AUTHOR CONTRIBUTIONS

FM, VF, PN, IC, FB, and EP designed the study. IC, EP, and FB wrote the clinical protocol. VF, CN, AT, CC, and FC provided and managed patients. BP, PN, IM, FU, and FM developed the methodologies. VF, CN, AT, BP, IM, FU, CB, LC, SB, and NG acquired data. AP and AL prepared drugs and vaccines in the hospital pharmacy. GV performed blood tests. PP, DG, FU, IM, and FM performed statistical analyses and data interpretation. MS, PR, and FU prepared eCRF. FU, VF, IM, PN, BP, FM, FB, and EP wrote or reviewed the manuscript. All authors approved the final version of the manuscript.

FUNDING

The present study was funded by the Italian Ministry of Public Health (Special Project ISS for Alleanza Contro il Cancro and ISS Ricerca Corrente) and, in part, by grants of the Italian Association for Cancer Research (AIRC IG16891).

ACKNOWLEDGMENTS

We would like to thank Dr. Serena Cecchetti, Dr. Giuseppina D'Agostino, Dr. Caterina Lapenta, Dr. Stefano Santini, Dr. Silvia Vendetti and Dr. Eleonora Aricò for their precious scientific advice; IFO-IRE Hospital Pharmacia nurses for investigational drugs labeling and preparation; Daniela Diamanti and Fabiola Diamanti for their punctual technical support; the support staff at the clinical sites. We thank the patients who participated in this trial and their families.

SUPPLEMENTARY MATERIAL

The Supplementary Material for this article can be found online at: https://www.frontiersin.org/articles/10.3389/fonc.2020.00202/full#supplementary-material

REFERENCES

1. Queirolo P, Boutros A, Tanda E, Spagnolo F, Quaglino P. Immune-checkpoint inhibitors for the treatment of metastatic melanoma: a model of cancer immunotherapy. *Sem Cancer Biol.* (2019) 59:290–7. doi: 10.1016/j.semcancer.2019.08.001
2. Spagnolo F, Boutros A, Tanda E, Queirolo P. The adjuvant treatment revolution for high-risk melanoma patients. *Sem Cancer Biol.* (2019) 59:283–9. doi: 10.1016/j.semcancer.2019.08.024
3. Havel JJ, Chowell D, Chan TA. The evolving landscape of biomarkers for checkpoint inhibitor immunotherapy. *Nat Rev Cancer.* (2019) 19:133–50. doi: 10.1038/s41568-019-0116-x
4. Karaki S, Anson M, Tran T, Giusti D, Blanc C, Oudard S, et al. Is there still room for cancer vaccines at the era of checkpoint inhibitors. *Vaccines.* (2016) 4:4. doi: 10.3390/vaccines4040037
5. Peng M, Mo Y, Wang Y, Wu P, Zhang Y, Xiong F, et al. Neoantigen vaccine: an emerging tumor immunotherapy. *Mol Cancer.* (2019) 18:128. doi: 10.1186/s12943-019-1055-6
6. Moschella F, Proietti E, Capone I, Belardelli F. Combination strategies for enhancing the efficacy of immunotherapy in cancer patients. *Ann N Y Acad Sci.* (2010) 1194:169–78. doi: 10.1111/j.1749-6632.2010.05464.x
7. Proietti E, Moschella F, Capone I, Belardelli F. Exploitation of the propulsive force of chemotherapy for improving the response to cancer immunotherapy. *Mol Oncol.* (2012) 6:1–14. doi: 10.1016/j.molonc.2011.11.005
8. Bracci L, Sistigu A, Proietti E, Moschella F. The added value of type I interferons to cytotoxic treatments of cancer. *Cytok Growth Factor Rev.* (2017) 36:89–97. doi: 10.1016/j.cytogfr.2017.06.008
9. Proietti E, Greco G, Garrone B, Baccarini S, Mauri C, Venditti M, et al. Importance of cyclophosphamide-induced bystander effect on T cells for a successful tumor eradication in response to adoptive immunotherapy in mice. *J Clin Invest.* (1998) 101:429–41. doi: 10.1172/JCI1348
10. Lutsiak ME, Semnani RT, De Pascalis R, Kashmiri SV, Schlom J, Sabzevari H. Inhibition of CD4(+)25+ T regulatory cell function implicated in enhanced immune response by low-dose cyclophosphamide. *Blood.* (2005) 105:2862–8. doi: 10.1182/blood-2004-06-241011.
11. Moschella F, Valentini M, Arico E, Macchia I, Sestili P, D'Urso MT, et al. Unraveling cancer chemoimmunotherapy mechanisms by gene and protein expression profiling of responses to cyclophosphamide. *Cancer Res.* (2011) 71:3528–39. doi: 10.1158/0008-5472.CAN-10-4523
12. Buccione C, Fragale A, Polverino F, Zicchedda G, Arico E, Belardelli F, et al. Role of interferon regulatory factor 1 in governing Treg depletion, Th1 polarization, inflammasome activation and antitumor efficacy of cyclophosphamide. *Int J Cancer.* (2018) 142:976–87. doi: 10.1002/ijc.31083
13. Ding ZC, Blazar BR, Mellor AL, Munn DH, Zhou G. Chemotherapy rescues tumor-driven aberrant CD4+ T-cell differentiation and restores an activated polyfunctional helper phenotype. *Blood.* (2010) 115:2397–406. doi: 10.1182/blood-2009-11-253336
14. Bracci L, Moschella F, Sestili P, La Sorsa V, Valentini M, Canini I, et al. Cyclophosphamide enhances the antitumor efficacy of adoptively transferred immune cells through the induction of cytokine expression, B-cell and T-cell homeostatic proliferation, and specific tumor infiltration. *Clin Cancer Res.* (2007) 13:644–53. doi: 10.1158/1078-0432.CCR-06-1209
15. Schiavoni G, Sistigu A, Valentini M, Mattei F, Sestili P, Spadaro F, et al. Cyclophosphamide synergizes with type I interferons through systemic dendritic cell reactivation and induction of immunogenic tumor apoptosis. *Cancer Res.* (2011) 71:768–78. doi: 10.1158/0008-5472.CAN-10-2788
16. Nistico P, Capone I, Palermo B, Del Bello D, Ferraresi V, Moschella F, et al. Chemotherapy enhances vaccine-induced antitumor immunity

in melanoma patients. *Int J Cancer.* (2009) 124:130–9. doi: 10.1002/ijc.23886
17. Moschella F, Torelli GF, Valentini M, Urbani F, Buccione C, Petrucci MT, et al. Cyclophosphamide induces a type I interferon-associated sterile inflammatory response signature in cancer patients' blood cells: implications for cancer chemoimmunotherapy. *Clin Cancer Res.* (2013) 19:4249–61. doi: 10.1158/1078-0432.CCR-12-3666
18. Zicchedda G, Proietti E, Moschella F. The Janus face of cyclophosphamide: A sterile inflammatory response that potentiates cancer immunotherapy. *Oncoimmunology.* (2013) 2:e25789. doi: 10.4161/onci.25789
19. Santini SM, Lapenta C, Logozzi M, Parlato S, Spada M, Di Pucchio T, et al. Type I interferon as a powerful adjuvant for monocyte-derived dendritic cell development and activity in vitro and in Hu-PBL-SCID mice. *J Exp Med.* (2000) 191:1777–88. doi: 10.1084/jem.191.10.1777
20. Moschella F, Bisikirska B, Maffei A, Papadopoulos KP, Skerrett D, Liu Z, et al. Gene expression profiling and functional activity of human dendritic cells induced with IFN-alpha-2b: implications for cancer immunotherapy. *Clin Cancer Res.* (2003) 9:2022–31.
21. Rizza P, Moretti F, Capone I, Belardelli F. Role of type I interferon in inducing a protective immune response: perspectives for clinical applications. *Cytokine Growth Factor Rev.* (2015) 26:195–201. doi: 10.1016/j.cytogfr.2014.10.002
22. Muller L, Aigner P, Stoiber D. Type I interferons and natural killer cell regulation in cancer. *Front Immunol.* (2017) 8:304. doi: 10.3389/fimmu.2017.00304
23. Fuertes MB, Kacha AK, Kline J, Woo SR, Kranz DM, Murphy KM, et al. Host type I IFN signals are required for antitumor CD8+ T cell responses through CD8{alpha}+ dendritic cells. *J Exper Med.* (2011) 208:2005–16. doi: 10.1084/jem.20101159
24. Diamond MS, Kinder M, Matsushita H, Mashayekhi M, Dunn GP, Archambault JM, et al. Type I interferon is selectively required by dendritic cells for immune rejection of tumors. *J Exper Med.* (2011) 208:1989–2003. doi: 10.1084/jem.20101158
25. Miquilena-Colina ME, Lozano-Rodriguez T, Garcia-Pozo L, Saez A, Rizza P, Capone I, et al. Recombinant interferon-alpha2b improves immune response to hepatitis B vaccination in haemodialysis patients: results of a randomised clinical trial. *Vaccine.* (2009) 27:5654–60. doi: 10.1016/j.vaccine.2009.07.014
26. Di Pucchio T, Pilla L, Capone I, Ferrantini M, Montefiore E, Urbani F, et al. Immunization of stage IV melanoma patients with Melan-A/MART-1 and gp100 peptides plus IFN-alpha results in the activation of specific CD8(+) T cells and monocyte/dendritic cell precursors. *Cancer Res.* (2006) 66:4943–51. doi: 10.1158/0008-5472.CAN-05-3396
27. Palermo B, Del Bello D, Sottini A, Serana F, Ghidini C, Gualtieri N, et al. Dacarbazine treatment before peptide vaccination enlarges T-cell repertoire diversity of melan-a-specific, tumor-reactive CTL in melanoma patients. *Cancer Res.* (2010) 70:7084–92. doi: 10.1158/0008-5472.CAN-10-1326
28. Franzese O, Palermo B, Di Donna C, Sperduti I, Ferraresi V, Stabile H, et al. Polyfunctional Melan-A-specific tumor-reactive CD8(+) T cells elicited by dacarbazine treatment before peptide-vaccination depends on AKT activation sustained by ICOS. *Oncoimmunology.* (2016) 5:e1114203. doi: 10.1080/2162402X.2015.1114203
29. Gnjatic S, Nishikawa H, Jungbluth AA, Gure AO, Ritter G, Jager E, et al. NY-ESO-1: review of an immunogenic tumor antigen. *Adv Cancer Res.* (2006) 95:1–30. doi: 10.1016/S0065-230X(06)95001-5
30. Eggermont AM, Suciu S, Santinami M, Testori A, Kruit WH, Marsden J, et al. Adjuvant therapy with pegylated interferon alfa-2b versus observation alone in resected stage III melanoma: final results of EORTC 18991, a randomised phase III trial. *Lancet.* (2008) 372:117–26. doi: 10.1016/S0140-6736(08)61033-8
31. A'Hern RP. Sample size tables for exact single-stage phase II designs. *Stat Med.* (2001) 20:859–66. doi: 10.1002/sim.721
32. Rozera C, Cappellini GA, D'Agostino G, Santodonato L, Castiello L, Urbani F, et al. Intratumoral injection of IFN-alpha dendritic cells after dacarbazine activates anti-tumor immunity: results from a phase I trial in advanced melanoma. *J Trans Med.* (2015) 13:139. doi: 10.1186/s12967-015-0473-5
33. Hartmann FJ, Babdor J, Gherardini PF, Amir ED, Jones K, Sahaf B, et al. Comprehensive immune monitoring of clinical trials to advance human immunotherapy. *Cell Reports.* (2019) 28:819–31 e4. doi: 10.1016/j.celrep.2019.06.049
34. Macchia I, Urbani F, Proietti E. Immune monitoring in cancer vaccine clinical trials: critical issues of functional flow cytometry-based assays. *BioMed Res Int.* (2013) 2013:726239. doi: 10.1155/2013/726239
35. Karimkhani C, Green AC, Nijsten T, Weinstock MA, Dellavalle RP, Naghavi M, et al. The global burden of melanoma: results from the Global Burden of Disease Study 2015. *Bri J Dermatol.* (2017) 177:134–40. doi: 10.1111/bjd.15510
36. Balch CM, Gershenwald JE, Soong SJ, Thompson JF, Atkins MB, Byrd DR, et al. Final version of 2009 AJCC melanoma staging and classification. *J Clin Oncol.* (2009) 27:6199–206. doi: 10.1200/JCO.2009.23.4799
37. Gershenwald JE, Scolyer RA, Hess KR, Sondak VK, Long GV, Ross MI, et al. Melanoma staging: evidence-based changes in the American Joint Committee on Cancer eighth edition cancer staging manual. *Cancer J Clin.* (2017) 67:472–92. doi: 10.3322/caac.21409
38. Eggermont AM, Chiarion-Sileni V, Grob JJ, Dummer R, Wolchok JD, Schmidt H, et al. Adjuvant ipilimumab versus placebo after complete resection of high-risk stage III melanoma (EORTC 18071): a randomised, double-blind, phase 3 trial. *Lancet Oncol.* (2015) 16:522–30. doi: 10.1016/S1470-2045(15)70122-1
39. Eggermont AM, Chiarion-Sileni V, Grob JJ, Dummer R, Wolchok JD, Schmidt H, et al. Prolonged survival in stage III melanoma with ipilimumab adjuvant therapy. *N Engl J Med.* (2016) 375:1845–55. doi: 10.1056/NEJMoa1611299
40. Weber J, Mandala M, Del Vecchio M, Gogas HJ, Arance AM, Cowey CL, et al. Adjuvant nivolumab versus ipilimumab in resected stage III or IV melanoma. *N Engl J Med.* (2017) 377:1824–35. doi: 10.1056/NEJMoa1709030
41. Eggermont AMM, Blank CU, Mandala M, Long GV, Atkinson V, Dalle S, et al. Adjuvant pembrolizumab versus placebo in resected stage III melanoma. *N Engl J Med.* (2018) 378:1789–801. doi: 10.1056/NEJMoa1802357
42. Long GV, Hauschild A, Santinami M, Atkinson V, Mandala M, Chiarion-Sileni V, et al. Adjuvant dabrafenib plus trametinib in stage III BRAF-mutated melanoma. *N Engl J Med.* (2017) 377:1813–23. doi: 10.1056/NEJMoa1708539
43. Hauschild A, Dummer R, Schadendorf D, Santinami M, Atkinson V, Mandala M, et al. Longer follow-up confirms relapse-free survival benefit with adjuvant dabrafenib plus trametinib in patients with resected BRAF V600-mutant stage III melanoma. *J Clin Oncol.* (2018) JCO1801219. doi: 10.1200/JCO.18.01219
44. Butterfield LH, Vujanovic L, Santos PM, Maurer DM, Gambotto A, Lohr J, et al. Multiple antigen-engineered DC vaccines with or without IFNalpha to promote antitumor immunity in melanoma. *J Immunother Cancer.* (2019) 7:113. doi: 10.1186/s40425-019-0552-x
45. Kedl RM, Kappler JW, Marrack P. Epitope dominance, competition and T cell affinity maturation. *Curr Opin Immunol.* (2003) 15:120–7. doi: 10.1016/s0952-7915(02)00009-2
46. Chen W, Anton LC, Bennink JR, Yewdell JW. Dissecting the multifactorial causes of immunodominance in class I-restricted T cell responses to viruses. *Immunity.* (2000) 12:83–93. doi: 10.1016/s1074-7613(00)80161-2
47. Bonomi G, Moschella F, Ombra MN, Del Pozzo G, Granier C, De Berardinis P, et al. Modulation of TCR recognition of MHC class II/peptide by processed remote N- and C-terminal epitope extensions. *Hum Immunol.* (2000) 61:753–63. doi: 10.1016/s0198-8859(00)00147-6
48. Galea I, Stasakova J, Dunscombe MS, Ottensmeier CH, Elliott T, Thirdborough SM. CD8+ T-cell cross-competition is governed by

peptide-MHC class I stability. *Eur J Immunol.* (2012) 42:256–63. doi: 10.1002/eji.201142010
49. Moretta L. Dissecting CD56dim human NK cells. Blood (2010) 116:3689–91. doi: 10.1182/blood-2010-09-303057
50. Borden EC. Interferons alpha and beta in cancer: therapeutic opportunities from new insights. *Nat Rev Drug Disc.* (2019) 18:219–34. doi: 10.1038/s41573-018-0011-2
51. Sleire L, Forde HE, Netland IA, Leiss L, Skeie BS, Enger PO. Drug repurposing in cancer. *Pharmacol Res.* (2017) 124:74–91. doi: 10.1016/j.phrs.2017.07.013
52. Bertolini F, Sukhatme VP, Bouche G. Drug repurposing in oncology–patient and health systems opportunities. *Nat Rev Clin Oncol.* (2015) 12:732–42. doi: 10.1038/nrclinonc.2015.169

Conflict of Interest: The authors declare that the research was conducted in the absence of any commercial or financial relationships that could be construed as a potential conflict of interest.

frontiers in Oncology

ORIGINAL RESEARCH
published: 12 May 2020
doi: 10.3389/fonc.2020.00700

Sitravatinib, a Tyrosine Kinase Inhibitor, Inhibits the Transport Function of ABCG2 and Restores Sensitivity to Chemotherapy-Resistant Cancer Cells *in vitro*

Yuqi Yang[1], Ning Ji[1,2], Qiu-Xu Teng[1], Chao-Yun Cai[1], Jing-Quan Wang[1], Zhuo-Xun Wu[1], Zi-Ning Lei[1], Sabrina Lusvarghi[3], Suresh V. Ambudkar[3] and Zhe-Sheng Chen[1]**

[1] Department of Pharmaceutical Sciences, College of Pharmacy and Health Sciences, St. John's University, Queens, NY, United States, [2] State Key Laboratory of Experimental Hematology Institute of Hematology and Hospital of Blood Diseases, Chinese Academy of Medical Science and Peking Union Medical College, Tianjin, China, [3] Laboratory of Cell Biology, Center for Cancer Research, National Cancer Institute, NIH, Bethesda, MD, United States

OPEN ACCESS

Edited by:
Nehad M. Ayoub,
Jordan University of Science and Technology, Jordan

Reviewed by:
Xiang Chen,
Central South University, China
Vishwa Khare,
Eurofins Viracor, United States
Hua Zhu,
The Ohio State University, United States

***Correspondence:**
Ning Ji
jining@ihcams.ac.cn
Zhe-Sheng Chen
chenz@stjohns.edu

Specialty section:
This article was submitted to Pharmacology of Anti-Cancer Drugs, a section of the journal Frontiers in Oncology

Received: 19 January 2020
Accepted: 14 April 2020
Published: 12 May 2020

Citation:
Yang Y, Ji N, Teng Q-X, Cai C-Y, Wang J-Q, Wu Z-X, Lei Z-N, Lusvarghi S, Ambudkar SV and Chen Z-S (2020) Sitravatinib, a Tyrosine Kinase Inhibitor, Inhibits the Transport Function of ABCG2 and Restores Sensitivity to Chemotherapy-Resistant Cancer Cells in vitro. Front. Oncol. 10:700. doi: 10.3389/fonc.2020.00700

Sitravatinib, also called MGCD516 or MG-516, is a broad-spectrum tyrosine kinase inhibitor (TKI) under phase III clinical evaluation. Herein, we explored the activity of sitravatinib toward multidrug resistance (MDR) by emphasizing its inhibitory effect on ATP-binding cassette super-family G member 2 (ABCG2). ABCG2 is a member of ATP-binding cassette (ABC) transporter family and plays a critical role in mediating MDR. Sitravatinb received an outstanding docking score for binding to the human ABCG2 model (PDB code: 6ETI) among thirty screened TKIs. Also, an MTT assay indicated that sitravatinib at 3 μM had the ability to restore the antineoplastic effect of various ABCG2 substrates in both drug-selected and gene-transfected ABCG2-overexpressing cell lines. In further tritium-labeled mitoxantrone transportation study, sitravatinib at 3 μM blocked the efflux function mediated by ABCG2 and as a result, increased the intracellular concentration of anticancer drugs. Interestingly, sitravatinib at 3 μM altered neither protein expression nor subcellular localization of ABCG2. An ATPase assay demonstrated that ATPase activity of ABCG2 was inhibited in a concentration-dependent manner with sitravatinib; thus, the energy source to pump out compounds was interfered. Collectively, the results of this study open new avenues for sitravatinib working as an ABCG2 inhibitor which restores the antineoplastic activity of anticancer drugs known to be ABCG2 substrates.

Keywords: sitravatinib, tyrosine kinase inhibitor, multidrug resistance, ATP-binding cassette (ABC) transporters, ATP-binding cassette super-family G member 2 (ABCG2)

INTRODUCTION

Evidence from clinical studies showed that patients with multidrug resistant (MDR) tumors have a poorer prognosis and decreased likelihood of survival compared to cancer patients with drug sensitive tumors (1). Cancer patients develop cross-resistance to various structurally and functionally unrelated chemotherapeutic agents, resulting in treatment failure (2, 3). Overexpression of ATP-binding cassette (ABC) transporters is a leading cause of MDR (4). ABC

transporters can be divided into seven subfamilies (ABCA to ABCG). The overexpression of certain transporters leads to MDR, including, but not limited to, ABCB1 (P-glycoprotein, P-gp), ABCG2 (breast cancer resistance protein, BCRP/MXR) and ABCC1 (multidrug resistance-associated protein 1, MRP1) (4, 5). Functionally, ABCB1 and ABCG2 work as efflux pumps, and are located in the lipid raft of specific cell lines (1, 6), reducing the intracellular level of various antineoplastic agents accumulating in cancer cells.

Currently, there are several approaches to circumvent MDR and to enhance the efficacy of antineoplastic drugs such as chemosensitizers (7), gene therapy (8, 9), immune-oncology (10), nanotechnology (11), or traditional Chinese medicine (12). The chemosensitizers, fumitremorgin C (FTC) and its derivative Ko143 are commonly used reference inhibitors of the ABCG2 transporter (13). However, FTC has neurotoxic effects and was withdrawn from clinical use (13). Furthermore, Ko143 was shown to lack specificity for the ABCG2 transporter at high concentrations and it was metabolically unstable in plasma (14). Therefore, more specific and less toxic inhibitors of ABC transporters are urgently needed for both preclinical and clinical evaluation.

In vitro studies have shown that some, but not all, novel tyrosine kinase inhibitors (TKIs) have ability to inhibit the ABCG2 transporter (15, 16). Clinically, TKIs are used as first- or second- line treatments for certain metastatic cancers (16, 17). However, TKIs have non-specific and "off-target" effects (18), thereby probably explaining why TKIs [1] are used as alternative treatments in the clinical setting and [2] restore the anticancer efficacy of chemotherapeutic drugs in the ABCG2-mediated MDR model.

Sitravatinib, also called MGCD516 or MG-516, is a broad-spectrum TKI targeting MET, TAM (TYRO3, AXL, MerTK), and members of vascular endothelial growth factor receptor (VEGFR), platelet-derived growth factor receptor (PDGFR), and Eph families (17, 19, 20). Notably, it has been reported that sitravatinib has potent antitumor efficacy, that may be due, in part, to altering the tumor microenvironment and restoring the efficacy of immune checkpoint blockade (PD-1) in diverse cancer models (20). Dolan et al. reported that sitravatinib could combat drug resistance caused by sunitinib and axitinib in metastatic human and mouse models (17). Together, all these studies provide us with a clue that sitravatinib has the capability to antagonize MDR in cancer cells. Thus, various studies indicate that sitravatinib is efficacious in reversing or antagonizing MDR in cancer cells. Furthermore, sitravatinib is under nine ongoing clinical trials for various indications, with one being a phase III study (NCT03906071). To date, these studies have proved that intolerable adverse effects or unacceptable toxicity profile are not found under sitravatinib treatment in preclinical or clinical model. In this article, we focus on the antagonizing activity of sitravatinib toward MDR mediated by ABCG2.

MATERIALS AND METHODS

Chemicals and Reagents

Sitravatinib was purchased from ChemieTek (Indianapolis, IN). Gilteritinib, BMS-777607, merestinib, and LOXO-101 were kindly provided as free samples from Selleckchem (Houston, TX). Topotecan was purchased from Selleckchem (Houstin, TX). Fetal bovine serum (FBS) was purchased from Atlanta Biologicals (Atlanta, GA). Dulbecco's modified Eagle medium (DMEM), antibiotics (penicillin/streptomycin [P/S]), and trypsin were obtained from Corning (Corning, NY). Mitoxantrone and SN-38 were purchased from Medkoo Sciences (Chapel Hill, NC). Phosphate buffered saline (PBS) (pH 7.4) was obtained from VWR Chemicals (Solon, OH). Ko143, cisplatin, and G418 were obtained from Enzo Life Sciences (Farmingdale, NY). Dimethyl sulfoxide (DMSO), 3-(4,5-dimethylthiazol-yl)-2,5-diphenyltetrazolium bromide (MTT) and Triton X-100 were purchased from Sigma-Aldrich (St. Louis, MO). Formaldehyde was obtained from J.T. Baker Chemical (Phillipsburg, NJ). Bovine serum albumin (BSA), 4′,6-diamidino-2-phenylindole (DAPI), PageRuler^{TM} plus pre-stained protein ladder, GAPDH loading control monoclonal antibody (GA1R), Pierce^{TM} ECL Western blotting substrate, Alexa Fluor 488 conjugated goat anti-mouse IgG secondary antibody, and liquid scintillation cocktail were purchased from Thermo Fisher Scientific (Rockford, IL). HRP-conjugated rabbit anti-mouse IgG secondary antibody was purchased from Cell Signaling Technology (Dancers, MA). The monoclonal anti-BCRP antibody (BXP-21) was obtained from Millipore (Billerica, MA). [^{3}H]-Mitoxantrone (0.5 Ci·mmol^{-1}) were purchased from Moravek Biochemicals (Brea, CA).

Cell Lines and Cell Culture

The non-small cell lung cancer (NSCLC) cell line, NCI-H460, and the corresponding mitoxantrone-selected NCI-H460/MX20 cells were used. The NCI-H460/MX20 cells were developed and maintained in complete medium containing 20 nM of mitoxantrone and these cells were shown to overexpress the wild-type ABCG2 protein (21). The human colon carcinoma cell line, S1, and its corresponding mitoxantrone-selected S1-M1-80 cells were used. The S1-M1-80 cells were selected and maintained in complete medium containing 80 μM of mitoxantrone and were shown to overexpress a mutant allele (R482G) in the ABCG2 gene (22, 23). In addition, transfected cells were also used in this article. HEK293/pcDNA3.1, HEK293/ABCG2-482-R2, HEK293/ABCG2-482-G2, and HEK293/ABCG2-482-T7 were transfected with either an empty vector pcDNA3.1 or a pcDNA3.1 vector containing a full length ABCG2 encoding arginine (R), glycine (G), or threonine (T) for amino acid at position 482 (24). All transfected cell lines were selected and cultured in complete medium with 2 mg·ml^{-1} of G418. All cell lines were cultured in DMEM complete medium containing 10% FBS and 1% P/S at 37°C in a humidified incubator supplied with 5% CO_2. All drug-resistant cells were grown in drug-free medium for more than 3 weeks and passaged at least 3 generations before experimental use. All drug-selected and gene-transfected cell lines used in this article were kindly provided by Drs. Susan Bates and Robert Robey (NCI, NIH, Bethesda, MD).

Induced-Fit Docking Analysis and Molecular Dynamic Simulations for ABCG2

Previously reported protocol was used for the molecular docking simulations (16) by using Maestro v11.1 software (Schrödinger, LLC, New York, NY). The structure of sitravatinib after

preparation by LigPrep v4.1 to simulate the low-energy pose was subjected to the Glide XP (extra precision) docking default protocol (Schrödinger, LLC, New York, NY) with a pre-prepared cryo-EM structure of the human ABCG2 model (PDB code: 6ETI). The human ABCG2 protein model was confined to the docking grid at the drug-binding cavity by selecting specific amino acids that were deemed to be involved in specific interactions (25). The following induced-fit docking (IFD) was generated based on the best scored results from the Glide XP analysis. The docked sitravatinib-ABCG2 complex simulated based on IFD was then subjected to another 10 ns molecular dynamic (MD) simulation using a previously reported default protocol (26). The docking scores were calculated and reported as kcal·mol^{-1} and the highest-scoring result was used for further graphical analysis.

Cell Viability Assay

A modified MTT colorimetric assay was conducted to determine the cytotoxic efficacy of the chemotherapeutic agents with or without ABCG2 inhibitors, as described previously (26). In short, each cell line was harvested and seeded evenly into a 96-well plate with a density of 5×10^3 cell·well^{-1}. The next day, cells were pretreated for 2 h with or without sitravatinib, or Ko143, at the indicated concentrations. Following pretreatment, cells were co-cultured with anticancer drugs (mitoxantrone, SN-38, topotecan or cisplatin) at serial concentrations. After a 68 h incubation period, an MTT solution (4 mg·ml^{-1} in PBS) was added to each well and the cells were further incubated at 37°C for 4 h in the dark. The supernatant was removed, and the resulting formazan crystals were dissolved with DMSO. An accuSkan^{TM} GO UV/Vis Microplate Spectrophotometer (Fisher Sci., Fair Lawn, NJ) was used to measure the absorbance at 570 nm. The half maximal inhibitory concentration (IC_{50}) for each anticancer drug was calculated as previously described (27). DMSO was used as an effective solvent to prepare stock solution (stock concentration is 10 mM) of all compounds. As the highest final concentration in cell viability assay was 100 μM, the final concentration of solvent was 1% in treatment medium (DMEM complete medium containing 10% FBS and 1% P/S). Notably, the control group was treated with solvent only. All experiments were performed independently at least three times performed in triplicate.

[^{3}H]-Mitoxantrone Accumulation and Efflux Assay

The detailed protocol as previously stated was followed (28). Briefly, ABCG2-mediated MDR cells (1×10^6 cell·well^{-1}) were seeded into a 24-well plate and incubated 1 day prior to further study. After 2 h of incubation in a drug-free medium, sitravatinib (0.75 and 3 μM) or a known inhibitor (3 μM), cells were co-incubated with [^{3}H]-mitoxantrone at 37°C for another 2 h. The cells were then washed twice with ice-cold PBS, trypsinized, harvested, and placed in 5 ml of a liquid scintillation cocktail. Radioactivity was measured using a Packard TRI-CARB 1,900 CA liquid scintillation analyzer (Packard Instrument, Downers Grove, IL).

To determine the effect of sitravatinib on the efflux function of the ABCG2 transporter, the tritium-labeled mitoxantrone efflux assay was performed as previously stated (29). As described in the accumulation phase above, cells were pretreated with or without an ABCG2 inhibitor for 2 h followed by 2 h co-treatment with [^{3}H]-mitoxantrone. The cells were then incubated in the presence or absence of an inhibitor at serial time points (0, 30, 60, and 120 min). Subsequently, the cells were washed twice with iced PBS, trypsinized, and transferred into a 5 ml liquid scintillation cocktail. Finally, radioactivity was measured as described above. In this assay, Ko143 served as the reference ABCG2 inhibitor for MDR cell lines. All the experiments were conducted independently three times.

Immunoblotting Analysis

Immunoblotting analysis (i.e., Western blotting) was conducted to detect the protein expression level of ABCG2 after up to 72 h of incubation with or without sitravatinib at 3 μM using a previously reported protocol (26). Briefly, following incubation with the highest non-toxic concentration of sitravatinib for 0, 24, 48, or 72 h, cells were harvested and lysed with lysis buffer (10 mM Tris, 1 mM EDTA, 0.1% SDS, 150 mM NaCl, 1% Triton X-100 and protease inhibitor cocktail) on ice for 20 min, followed by centrifugation at 4°C at 15,000 G for 20 min. The supernatant was collected and a bicinchoninic acid (BCA) Protein Kit (Thermo Scientific, Waltham, MA) was used to quantify the total concentration of protein in each sample. Equal amounts of total protein (20 μg) were loaded and separated by sodium dodecyl sulfate polyacrylamide gel electrophoresis (SDS-PAGE), followed by transfer onto a polyvinylidene fluoride (PVDF) membrane (Millipore, Billerica, MA). After blocking with 4% non-fat milk for 2 h at room temperature, the membrane was incubated with primary monoclonal antibodies against ABCG2 (at 1:500 dilution) and GAPDH (at 1:2,000 dilution) at 4°C overnight. The next day, after washing three times with Tris buffered saline containing 0.4% Tween 20 (TBST), the membrane was incubated with an HRP-conjugated secondary antibody (at 1:2,000 dilution) for 2 h at room temperature. Finally, the chemiluminescence signal of protein-antibody complex was developed by ECL substrate as per manufacturer's instruction. The relative density of each protein band was analyzed by ImageJ software (NIH, Bethesda, MD). All experiments were repeated three times independently.

Immunofluorescence Assay

Immunofluorescence assay was performed to assess the subcellular localization of membrane protein ABCG2 as previously described (30). In short, each cell line (1×10^4 cell·well^{-1}) was seeded onto a 24-well plate and treated with or without sitravatinib at 3 μM for several time frames (0, 24, 48, and 72 h). After the treatment period, cells were washed with PBS three times, fixed in 4% paraformaldehyde for 15 min, and permeabilized by 0.1% Triton X-100 for 15 min before being blocked with 6% BSA for 2 h. Subsequently, the presence of ABCG2 was detected using anti-BCRP monoclonal antibody (at 1:1,000 dilution) followed by Alexa Fluor 488 conjugated secondary antibody (at 1:1,000 dilution). Finally, 1 μg·ml^{-1} DAPI was used to counterstain the nuclei. The immunofluorescence images were captured via an EVOS FL Auto

fluorescence microscope (Thermo Scientific, Waltham, MA). All the experiments were performed three times independently.

ATPase Assay

The ATPase activity was determined by quantifying the amount of product (inorganic phosphate, P_i) produced after ATP hydrolysis. High Five insect cells expressing ABCG2 were used to prepare membrane vesicles (4). Next, membrane vesicles (10 μg total protein) were combined with assay buffer containing 50 mM MES (pH 6.8), 50 mM KCl, 5 mM sodium azide, 2 mM EGTA, 2 mM DTT, 1 mM ouabain, and 10 mM $MgCl_2$, final volume 100 μL. Then sitravatinib was incubated with the membrane vesicles for 3 min at 37°C. The ATP hydrolysis was initiated by addition of 5 mM of Mg-ATP. After incubation at 37°C for 20 min, the reaction was terminated by addition of 100 μl 5% SDS solution. The amount of P_i was quantified using the method modified from Murphy and Riley (31), which is based on the complex formation of phosphate with potassium-antimonyl-tartarate in acidic ammonium molybdate. After reduction induced by ascorbic acid, the complex displays a stable blue color that was quantified by measuring the absorbance at 880 nm using a spectrophotometer (Bio-Rad, Hercules, CA).

Data and Statistical Analysis

All data are presented as the mean ± SD (standard deviation) obtained from three independent experiments performed in triplicate. Comparisons were made between the control group and the corresponding treatment group. The results were analyzed with one-way or two-way analysis of variance (ANOVA) following Tukey *post hoc* analysis. The statistical analysis was performed by GraphPad Prism version 6.02 for Windows (GraphPad Software, La Jolla, CA). The *a priori* significance level was $p < 0.05$.

RESULTS

Pre-selecting TKIs Using a Molecular Simulation Analysis and a Modified Cell Viability Assay

To predict and compare the possible interaction between thirty TKIs and the human ABCG2 model, an *in silico* screening was conducted. The glide gscores of all screened TKIs are shown in **Table S1**. Based on the results from a preliminary study, sitravatinib had a higher docking score for binding to ABCG2 (**Figure 1A**) and a greater efficacy in reversing the anticancer efficacy of mitoxantrone in ABCG2-overexpressing cell line compared to other TKIs (BMS-777607, LOXO-101, gilteritnib, and merestinib) (**Figure 1B**). Based on these results, we conducted experiments to determine if sitravatinib was efficacious in attenuating ABCG2-mediated drug resistance in cell lines overexpressing the ABCG2 transporter.

Molecular Docking Sitravatinib in the Drug-Binding Pocket of ABCG2

The IFD was carried out to simulate the interactions between sitravatinib and the atomic structure of human ABCG2 homodimer (chain A and B). As shown in **Figure 2A**, the lowest energy binding pose of sitravatinib was predicted in the drug-binding cavity through hydrophobic interactions with nearby amino acids. Two hydrogen bonds were formed between the ethylamino group and SER440 of ABCG2 chain A, and between the nitrogen in the pyridine ring of sitravatinib and ASN436 of ABCG2 chain A, respectively. Sitravatinib produced the best glide gscore out of all TKIs with a gscore of -13.248 kcal·mol^{-1}, which is indicative of the free binding energy of the ligand. **Figure 2B** shows that the best-scored pose of sitravatinib occurs in the ABCG2 transmembrane domain with residues GLN 398, VAL 401, THR 402, PHE431, PHE 432, ASN 436, GLN 437, PHE 439, SER 440, SER 441, ARG 482, SER 486, PRO 485, PHE 489, ALA 517, VAL 546, and MET 549 in protein chain A, and PHE 431, PHE 432, THR 435, ASN 436, and MET 549 in protein chain B. Further molecular dynamic simulations of the sitravatinib-ABCG2 complex, as shown in **Figures 2C,D**, indicated that the position of sitravatinib in binding pocket did not show significant movements or changes after 10 ns. By analyzing the root mean square deviation (RMSD) of protein-drug complex, both the backbone of the protein and the complex were shown to be in a stable conformation after the first 2 ns and maintained this conformation until the end of the simulation (**Figure 2E**).

Effect of Sitravatinib on the Efficacy of Antineoplastic Drugs in ABCG2-Mediated MDR Cell Lines

An MTT assay was used to obtain concentration-dependent cell viability curves (concentration range for sitravatinib from 0 to 100 μM) and the non-toxic concentrations for further reversal study. Based on cytotoxicity results, 3 μM concentration was chosen as the highest non-toxic concentration of sitravatinib for further reversal studies (chemical structure of the compound is shown in **Figure 3A**). At this concentration, the cell survival rate was more than 80% after 72 h treatment period (indicated as dash line in **Figures 3B–D**).

The reversal study showed that sitravatinib made the NCI-H460/MX20 and S1-M1-80 cells became more sensitive to mitoxantrone, SN-38 and topotecan in a concentration-dependent manner (**Figures 4A–F**). Additionally, it increased the efficacy of these antineoplastic agents in ACBG2-transfected HEK293 cell lines, including HEK293/ABCG2-482-R2, HEK293/ABCG2-482-G2, and HEK293/ABCG2-482-T7 (**Figures 5A–C**). Importantly, sitravatinib had a significant reversal effect on both wild-type and mutant ABCG2 overexpressing cells, whereas this effect could not be found in corresponding parental cells NCI-H460, S1, or HEK293/pcDNA3.1. It is notable that the reversal activity in ABCG2-overexpressing cell lines is comparable to its counterpart positive control treatment Ko143 at the same concentration level, which served as a reference inhibitor of ABCG2. In addition, sitravatinib did not affect the anticancer effect of cisplatin, a drug that is not the substrate of ABCG2, in neither drug-sensitive nor ABCG2-overexpressing cell lines (**Figures 4G,H**, **5D**). The fold-reduction of IC_{50} values for chemotherapeutic drugs with or without inhibitors are shown in **Tables S2, S3**.

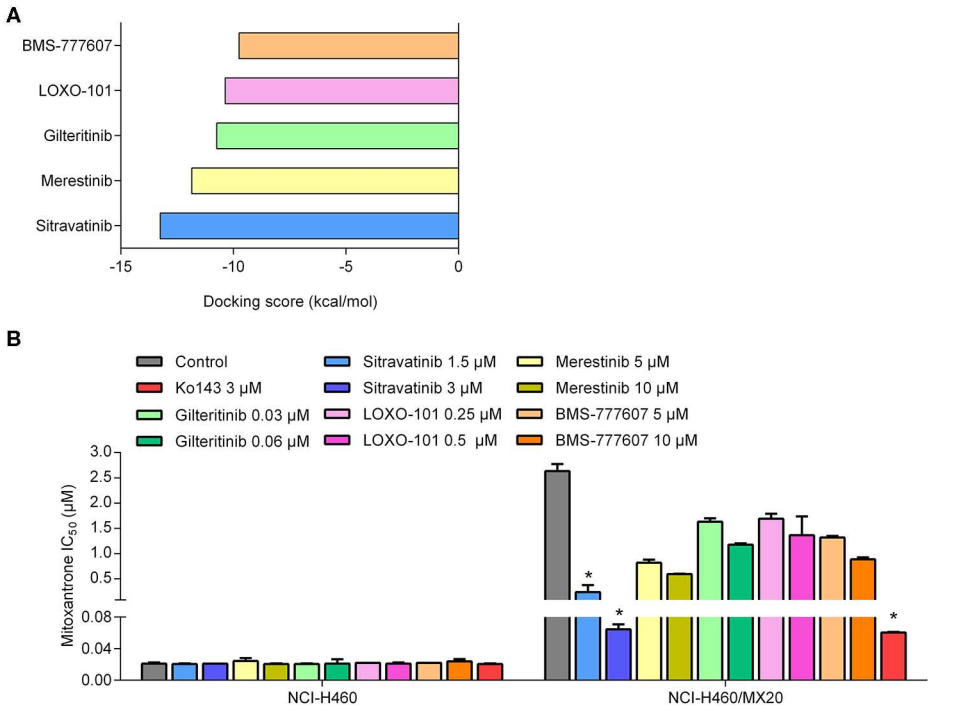

FIGURE 1 | The preliminary study to pre-select possible ABCG2 inhibitor. **(A)** The docking scores of TKIs were screened by computational simulation analysis. **(B)** The antagonizing activity of TKIs toward MDR cell lines mediated by ABCG2. Data are represented as mean ± SD from at least three independent assays. *$p < 0.05$ compared with control group.

Overall, these results denoted that sitravatinib can improve the efficacy of multiple chemotherapeutic agents in ABCG2-mediated MDR cell lines in a concentration-dependent manner.

Modulation of ABCG2-Mediated Efflux of [^{3}H]-Mitoxantrone in MDR Cell Lines

In order to understand the mechanism of action of sitravatinib in reversing MDR, several mechanism-based assays were performed. To evaluate the function of ABCG2, the intracellular concentration of tritium-labeled chemotherapeutic drug was quantified in parental cells and cells overexpressing ABCG2 with or without an inhibitor.

Sitravatinib at 3 μM concentration significantly increased the intracellular [^{3}H]-mitoxantrone accumulation level from 38.7 to 129.2% or from 31.6 to 91.0% in NCI-H460/MX20 or S1-M1-80 cells, respectively, but not in the corresponding parental cell line counterparts (NCI-H460 and S1), as shown in **Figures 6A,B**. In this study, Ko143 served as reference ABCG2 inhibitor. Hence, these results suggested that sitravatinib increases the intracellular accumulation of [^{3}H]-mitoxantrone in ABCG2-mediated MDR cells.

Furthermore, in order to further understand the enhanced intracellular accumulation of [^{3}H]-mitoxantrone in MDR cells, a time-course study was conducted to assess the efflux function of ABCG2 by quantifying the level of intercellular [^{3}H]-substrate at serial time points in the presence or absence of inhibitors. As shown in **Figures 6E,F**, after 120 min, NCI-H460/MX20 and S1-M1-80 cells without ABCG2 inhibitor treatment maintained only 30 and 55% of [^{3}H]-mitoxantrone, respectively. On the contrary, when treated with 3 μM sitravatinib, 68 and 91% [^{3}H]-mitoxantrone was accumulated in NCI-H460/MX20 and S1-M1-80 cells, respectively. In contrast, sitravatinib did not significantly change the efflux function in parental cells (NCI-H460 or S1) at different time points (**Figures 6C,D**).

Taken together, these results demonstrated that sitravatinib could enhance the intracellular accumulation of a tritium-labeled chemotherapeutic drug by blocking the efflux function mediated by ABCG2.

Effect of Sitravatinib on Expression and Localization of ABCG2 in ABCG2-Mediated MDR Cell Lines

It is known that the reversal mechanism of action could involve either downregulation of protein expression level and/or alternation of subcellular localization of the transporter (4). Therefore, immunoblotting analysis and immunofluorescence assay were conducted to detect the expression and localization of ABCG2 protein, respectively.

The expression level of ABCG2 in NCI-H460/MX20 and S1-M1-80 was not significantly altered even after 72 h treatment with 3 μM sitravatinib, **Figures 7A,B**. In addition, ABCG2 was detected on the cell membrane surface after the cells treated with 3 μM sitravatinib for 0, 24, 48, or 72 h, **Figures 7C,D**.

Therefore, long-term treatment at the highest non-toxic concentration of sitravatinib (3 μM) neither downregulates the

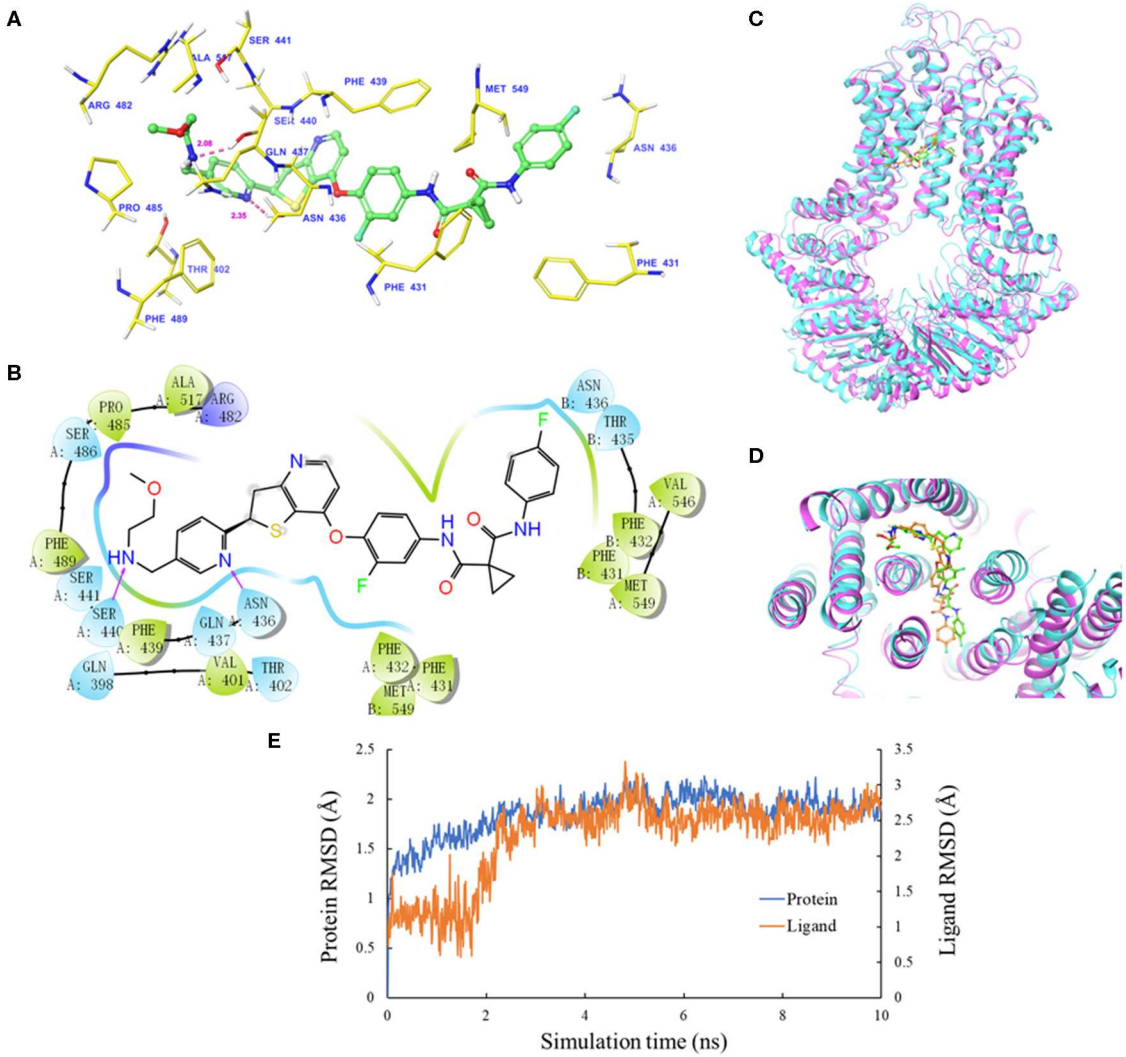

FIGURE 2 | Molecular docking analysis with sitravatinib. **(A)** The docked conformation of sitravatinib (ball-and-stick model) is shown within the ABCG2 drug-binding cavity, with the atoms colored as follows: carbon, green; hydrogen, white; oxygen, red; nitrogen, blue. Important amino acid residues are described with the same color scheme as above for all atoms, except for carbon atoms in yellow. Dotted pink lines represent hydrogen-bonding interactions and the values of the correlation distances are indicated in Å. **(B)** The 2D schematic diagram of ligand–receptor interaction between sitravatinib and the human ABCG2 model. Amino acids within 3 Å are indicated as colored bubbles, polar residues are light blue, hydrophobic residues are green, and the positive charged residue is dark blue. Purple arrows denote H-bonds. **(C,D)** The superimposition of MD pose of sitravatinib within the binding cavity of ABCG2. Sitravatinib molecules are depicted as ball and stick model in faded green or orange for pre- and post-MD, respectively. The ABCG2 structure is in ribbon diagram in faded magenta or faded cyan for pre- and post-MD, respectively. **(E)** RMSD trajectory of ABCG2 and sitravatinib in sitravatinib-ABCG2 complex over the 10 ns simulation run.

expression level nor affects the subcellular localization of ABCG2 in ABCG2-mediated MDR cell lines.

Effect of Sitravatinib on ABCG2 ATPase Activity

It is documented that ATP hydrolysis is the energy source for ABC transporters to pump out endogenous and exogenous toxicants (32, 33). Hence, the effect of sitravatinib on ABCG2 ATPase activity was evaluated. Herein, the ABCG2-mediated ATP hydrolysis was measured in membrane vesicles after incubation with serial concentrations of sitravatinib (0–20 μM). Sitravatinib inhibited 56.2% of the basal ATPase activity, and the inhibitory effect reached 50% at 0.9 μM, see **Figure 8**. These results indicate that sitravatinib inhibits ABCG2 ATPase activity in a concentration-dependent manner. ATPase data combined with molecular docking suggest that sitravatinib interacts with the drug-binding pocket of the ABCG2.

DISCUSSION AND CONCLUSION

It is well-known that ABC transporters contribute to MDR and as a result, limit the anticancer efficacy of numerous

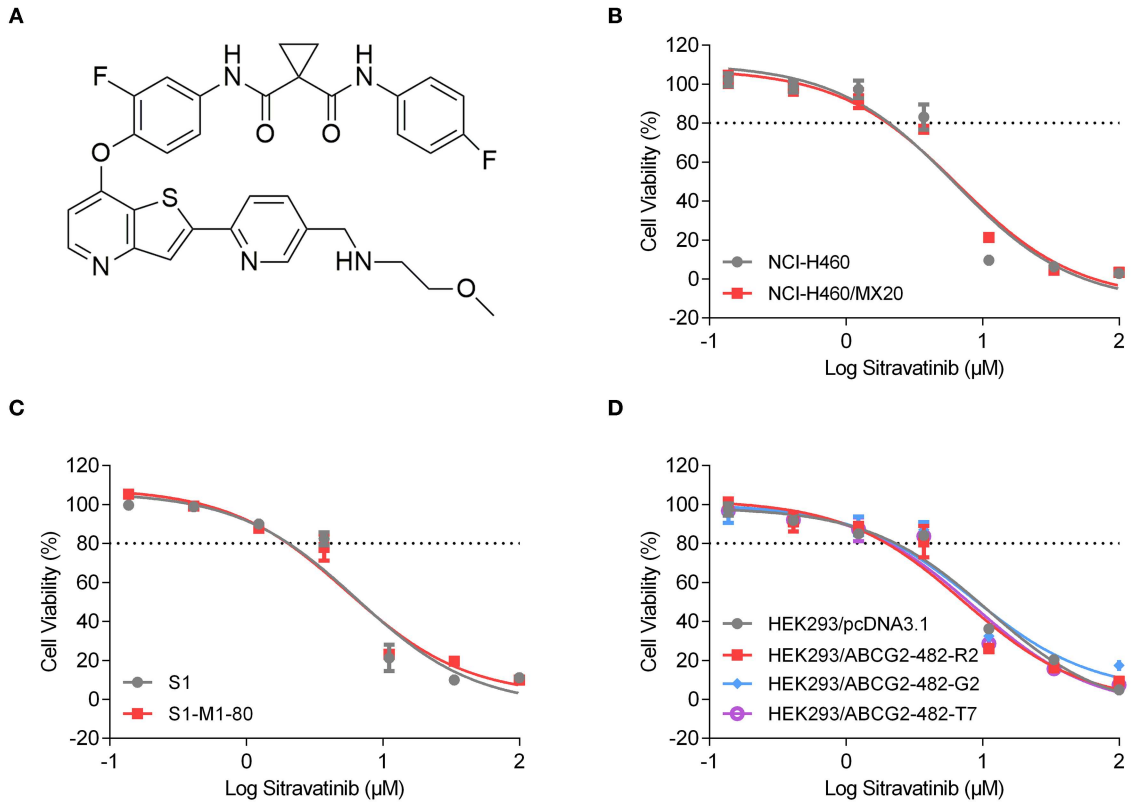

FIGURE 3 | Chemical structure and the cytotoxic activity of sitravatinib in ABCG2-overexpressing cell lines and their corresponding sensitive cell lines. **(A)** Chemical structure of sitravatinib. The cell viability-concentration curves for NCI-H460/MX20 and NCI-H460 **(B)**, S1-M1-80 and S1 **(C)**, HEK293 cell lines transfected with full length ABCG2 or empty vector **(D)** after treatment with serial concentrations of sitravatinib for 72 h. Data are shown as mean ± SD, obtained from at least three experiments performed independently.

chemotherapeutic agents in the clinical setting. Due to their efflux function, ABC transporters can extrude many structurally and functionally unrelated anticancer drugs (34), resulting in poor prognosis and low survival rates in cancer patients. In the past decades, many researchers have attempted to synthesize or screen potential inhibitors of ABC transporters to reverse MDR (16, 35–38). However, high toxicity and drug-drug interactions remain to be a challenge (39). To date, many researchers using *in vivo* and *ex vivo* models have demonstrated that TKIs have ability to restore the sensitivity of substrate antineoplastic drugs of ABC transporters for effective chemotherapy (40–43). Most recently, Chen et al. conducted a phase I clinical evaluation in a population of patients to reveal that cyclosporine A (CsA), a competitive ABCB1 inhibitor, could combat drug resistance caused by brentuximab vedotin in relapsed/refractory Hodgkin lymphoma with tolerable and feasible profile (44). These studies provided growing evidence that inhibitors of ABC transporters have promising possibility in the future preclinical and clinical use. Thus, it is meaningful to find potential inhibitors of ABC transporters even though many obstacles exist. It has been documented that some TKIs could behave as substrates or inhibitors of ABC transporters depending on different settings (45). Collectively, this suggests that TKIs with inhibitory activity toward ABCG2 in combination with conventional chemotherapeutic agents can be a promising strategy to circumvent MDR.

Using molecular docking and cell viability assay we first screened thirty TKIs that share active pharmacophoric features of ABC transporter inhibitors, such as the aromatic system, benzamido groups, or methoxyphenyl groups (46). The five compounds with the highest glide gscores were chosen to further examine their MDR reversal activity in cell lines expressing ABCG2. These screening assays showed that sitravatinib had an outstanding docking score within the drug-binding pocket in the transmembrane domain of the homodimer of human ABCG2, and also demonstrated excellent inhibitory activity in the ABCG2-mediated MDR cell lines.

In silico analysis of the simulated molecular docking showed specific interactions between sitravatinib and the human ABCG2 drug-binding pocket. The high glide gscore (−13.248 kcal·mol^{-1}) suggested strong affinity of sitravatinib. The best-scored pose of other known ABCG2 inhibitors, such as selonsertib, ulixertinib and NVP-TAE684, received glide gscores of −12.278, −11.501, and −12.929 kcal·mol^{-1}, respectively (4, 28, 47), which indicates that the affinity of sitravatinib and ABCG2 protein model may be comparable to other known

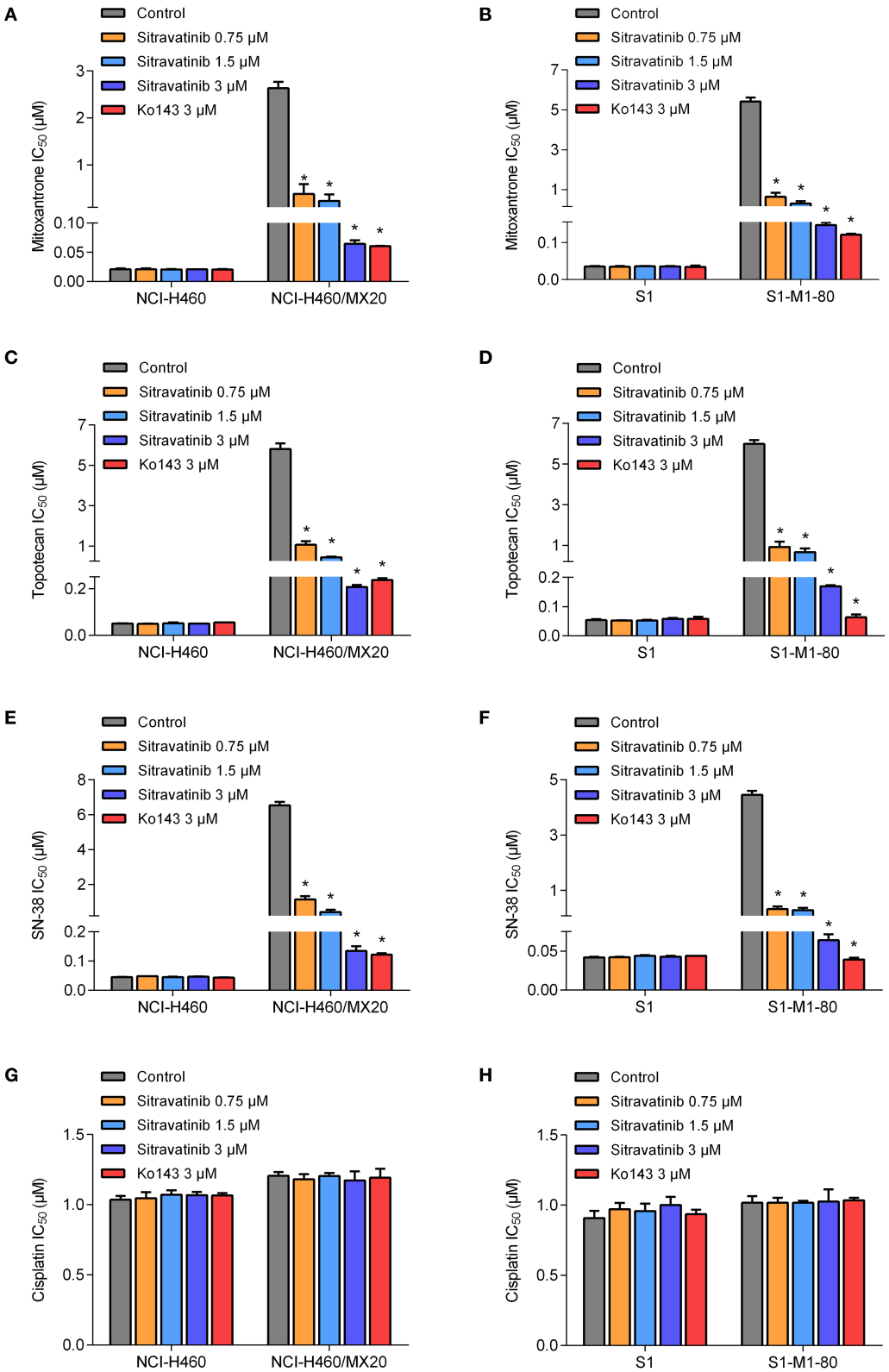

FIGURE 4 | Drug sensitivity of drug-selected ABCG2-overexpressing cell lines to various chemotherapeutic agents in the absence or presence of sitravatinib. The IC_{50} values of mitoxantrone **(A,B)**, topotecan **(C,D)**, SN-38 **(E,F)**, and cisplatin **(G,H)** in NCI-H460 and its mitoxantrone-selected resistance cell line (NCI-H460/MX20), S1 and its mitoxantrone-selected resistance cell line (S1-M1-80). Data were collected from independent experiments repeated at least three times and are shown as mean ± SD. *$p < 0.05$ compared with control group.

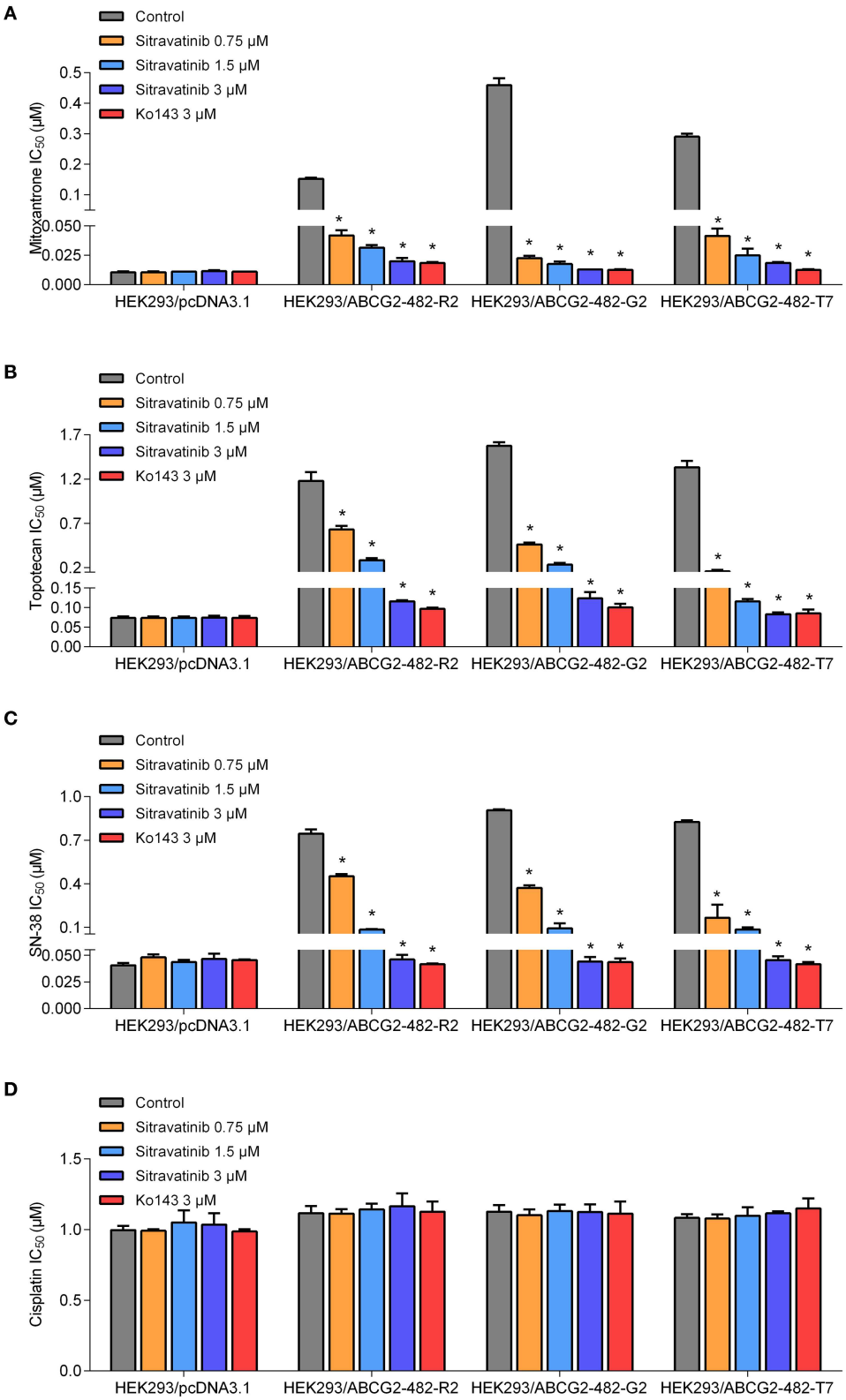

FIGURE 5 | The antagonizing effect of sitravatinib in ABCG2-transfected HEK293 cell lines and the parental cell line HEK293/pcDNA3.1. The IC_{50} values of mitoxantrone **(A)**, topotecan **(B)**, SN-38 **(C),** and cisplatin **(D)** in transfected cell lines. Data are presented as mean ± SD. All data were obtained from at least three independent assays. *$p < 0.05$ compared with control group.

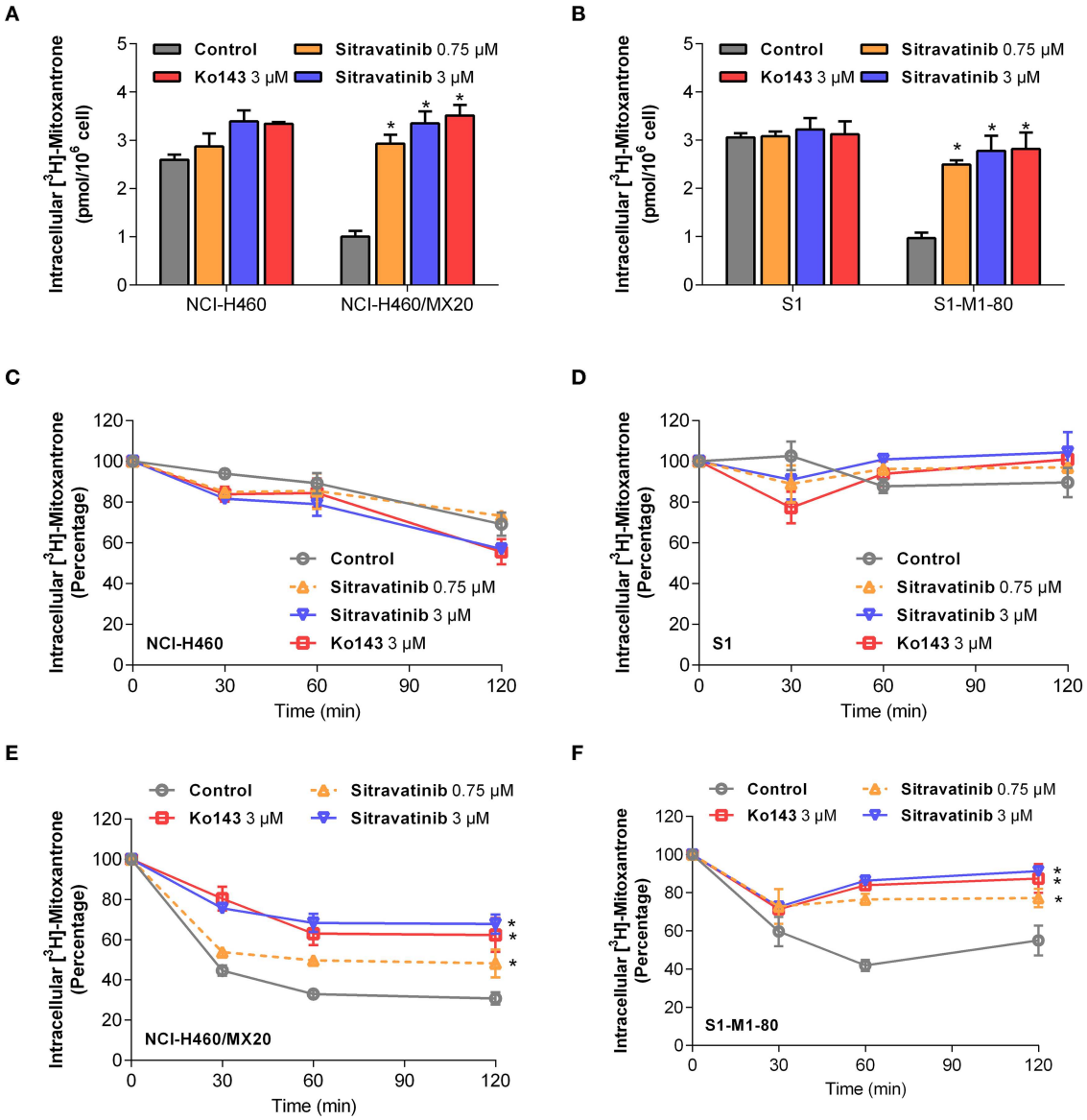

FIGURE 6 | Sitravatinib inhibits ABCG2-mediated mitoxantrone transport. The accumulation of tritium-labeled mitoxantrone in NCI-H460 and NCI-H460/MX20 **(A)**, S1 and S1-M1-80 **(B)**. The ABCG2-mediated efflux activity in NCI-H460 **(C)**, S1 **(E)** and their corresponding mitoxantrone-selected cell line NCI-H460/MX20 **(D)**, S1-M1-80 **(F)** at a series of time points (0, 30, 60, 120 min). Data from at least three independent experiments are shown as mean ± SD. *$p < 0.05$ compared with control group.

ABCG2 inhibitors. To verify whether this docking ligand could be removed from the binding pocket, further MD simulations were performed. The MD simulations indicated that the binding complex did not change significantly in 10 ns, with the maximal RMSD of sitravatinib being approximately 2 Å. These results suggested that sitravatinib could bind stably to the substrate-binding cavity of human ABCG2 with high affinity.

Cell viability assay demonstrated that the highest non-toxic concentration of sitravatinib was 3 μM. Furthermore, the modified MTT colorimetric assay on ABCG2-mediated MDR cell lines supported the conclusion that the inhibitory effect of sitravatinib was strictly associated with the expression of ABCG2. This was further corroborated using ABCG2-transfected HEK293 cell lines, in which ABCG2 is the solo contributor to MDR. By contrast, the reversal effect of sitravatinib was not found in any of the sensitive cell lines. Notably, sitravatinib did not change the IC_{50} values of cisplatin, which is not a substrate of ABCG2.

A mechanism-based assay was conducted to examine the underlying mechanism of action of the antagonizing activity of sitravatinib in ABCG2-overexpressing cell lines. ABCG2 was shown as an efflux pump (48). Hence, tritium-labeled

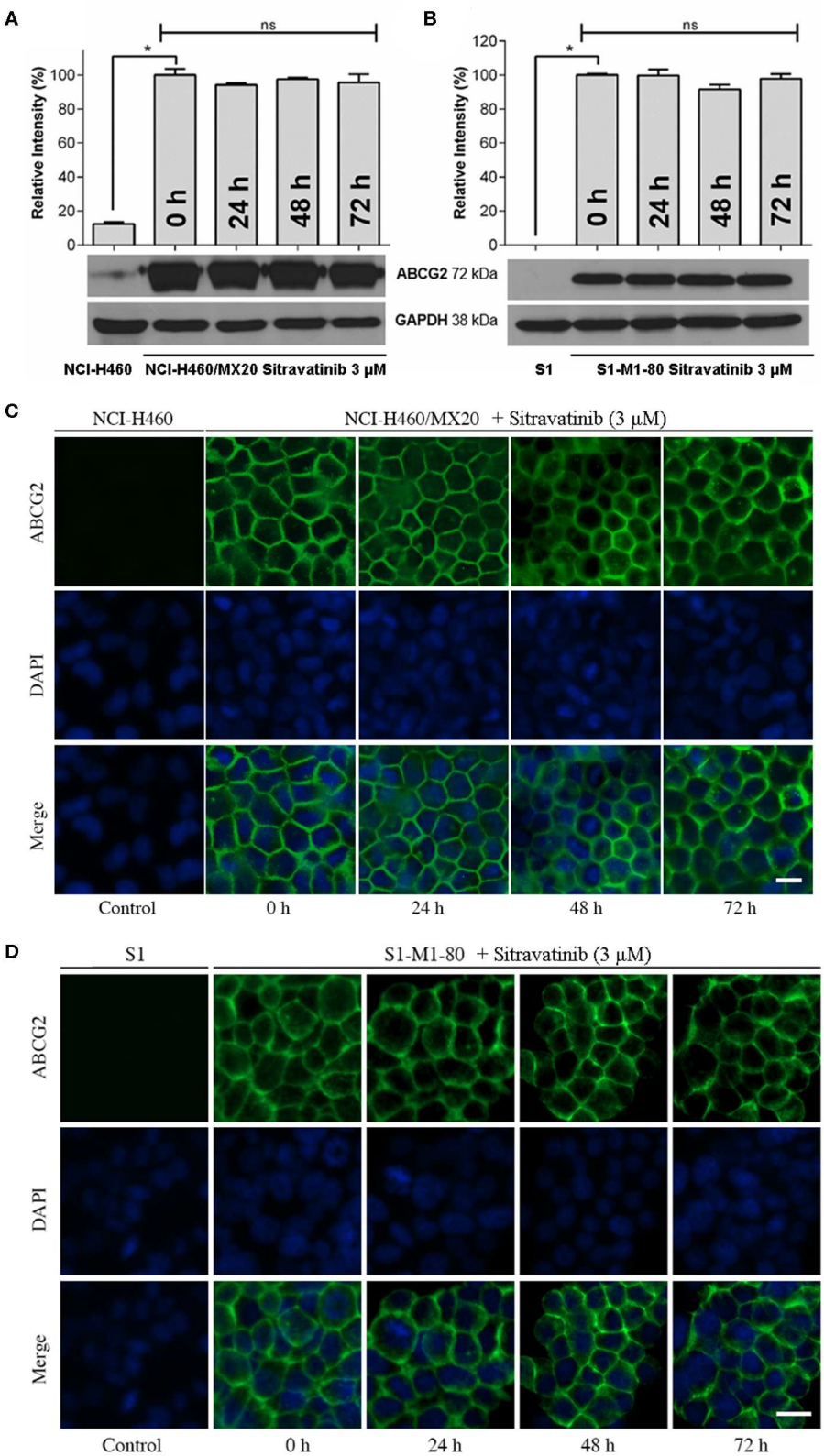

FIGURE 7 | Sitravatinib does not affect protein expression level nor the subcellular localization of ABCG2. Immunoblotting analysis showing the expression level of ABCG2 in MDR cell lines overexpressing ABCG2 NCI-H460/MX20 **(A)** and S1-M1-80 **(B)** compared to the corresponding parental cell lines. The relative density of each band is shown as mean ± SD, collected from at least three independent assays. *$p < 0.05$ compared with control group. Immunofluorescence assay indicating the subcellular localization of membrane protein ABCG2 of NCI-H460/MX20 **(C)** and S1-M1-80 **(D)** and the corresponding parental cell lines. Color: ABCG2 (Green), DAPI (Blue). Scale bar:10 μm.

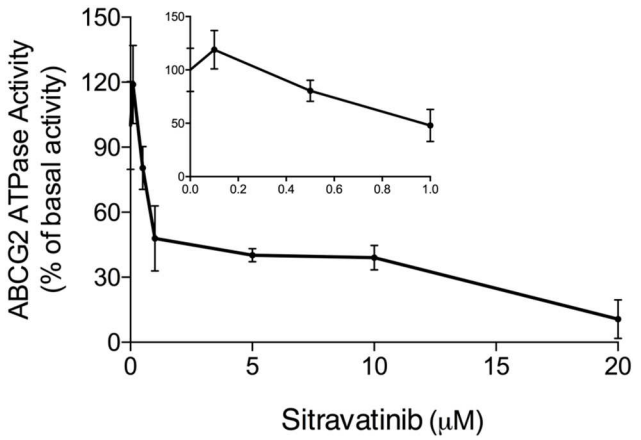

FIGURE 8 | Sitravatinib inhibits ABCG2 ATPase activity in a concentration-dependent manner. The effect of sitravatinib on ATPase activity of ABCG2 in insect cell membrane vesicles was determined as described in the Materials and Methods Section. Data were obtained from independent assays repeated at least three times and are presented as mean ± SD.

mitoxantrone-mediated accumulation and efflux assays were conducted to evaluate the pump function of ABCG2. Pre-treatment of the ABCG2 overexpressing cell lines with sitravatinib significantly improved the intracellular accumulation of mitoxantrone, which is a well-established substrate of ABCG2, but not in the corresponding sensitive cell lines. In addition, the ABCG2-expressing cell lines effluxed less amount of the chemotherapeutic drug after incubation with sitravatinib at non-toxic concentrations, compared with their counterparts in parental cell lines. This demonstrated that sitravatinib could impede the ABCG2 efflux function and in turn increase the intracellular accumulation of anticancer drug; thus, sitravatinib at non-toxic concentrations could remarkably antagonize ABCG2-mediated MDR and improve the antineoplastic efficacy of chemotherapeutic agents.

Mechanistically, it is well-documented that several MDR inhibitors downregulate the level of ABCG2 in the plasma membrane to hinder its pump function (4, 15, 49). To evaluate if this is the case with sitravatinib, Western blotting and immunofluorescence assays were conducted. Our results show that sitravatinib did not alter the expression level or the subcellular localization of ABCG2 in ABCG2-expressing cell lines. Collectively, we summarized that sitravatinib directly inhibits the pump function of ABCG2 without changing the expression level or its subcellular localization. Furthermore, the hydrolysis of ATP is the energy source for ABC transporter-mediated efflux of endogenous and exogenous toxicants (32, 33). Therefore, an ATPase assay was performed to determine the effect of sitravatinib on the ATPase activity of ABCG2. The results demonstrated that sitravatinib could partially inhibit ABCG2 ATPase activity suggesting that sitravatinib has the ability to interfere with the transport function of ABCG2 by interfering with its ATPase activity.

In conclusion, our study revealed that sitravatinib is a potential ABCG2 inhibitor with an acceptable toxicity profile. The sensitizing effect of sitravatinib toward different MDR cell lines is due to inhibition of ABCG2 function. In the future, we will focus on long-term exposure to sitravatinib *in vivo* and *ex vivo* to further evaluate the antagonizing effect and its toxicity profile as an ABCG2 inhibitor.

DATA AVAILABILITY STATEMENT

The datasets generated for this study are available on request to the corresponding author.

AUTHOR CONTRIBUTIONS

YY and Z-SC designed the study. YY, NJ, Q-XT, and J-QW gave contribution to perform experiments. C-YC, Z-NL, Z-XW, SL, and SA provided technical and material support. YY wrote the first draft. All authors discussed the results and implications and developed the manuscript at all stages.

FUNDING

This work was supported by NIH (No. 1R15GM116043-01) to Z-SC, SL, and SA were supported by the Intramural Research Program of the National Institutes of Health, National Cancer Institute, Center for Cancer Research.

ACKNOWLEDGMENTS

Authors are grateful to Drs. Susan Bates and Robert Robey (NCI, NIH, Bethesda, MD) for providing drug-selected and transfected cell lines we used in this article. We also thank Dr. Tanaji T. Talele (St. John's University, New York, NY) for providing the computing resources for the docking analysis. We thank Dr. Charles R. Ashby Jr. (St. John's University, New York, NY) for editing the article.

SUPPLEMENTARY MATERIAL

The Supplementary Material for this article can be found online at: https://www.frontiersin.org/articles/10.3389/fonc.2020.00700/full#supplementary-material

REFERENCES

1. Kartal-Yandim M, Adan-Gokbulut A, Baran Y. Molecular mechanisms of drug resistance and its reversal in cancer. *Crit Rev Biotechnol.* (2016) 36:716–26. doi: 10.3109/07388551.2015.1015957
2. Fletcher JI, Haber M, Henderson MJ, Norris MD. ABC transporters in cancer: more than just drug efflux pumps. *Nat Rev Cancer.* (2010) 10:147–56. doi: 10.1038/nrc2789
3. Amiri-Kordestani L, Basseville A, Kurdziel K, Fojo AT, Bates SE. Targeting MDR in breast and lung cancer: discriminating its potential importance

from the failure of drug resistance reversal studies. *Drug Resist Updat*. (2012) 15:50–61. doi: 10.1016/j.drup.2012.02.002
4. Ji N, Yang Y, Cai CY, Lei ZN, Wang JQ, Gupta P, et al. Selonsertib. (GS-4997), an ASK1 inhibitor, antagonizes multidrug resistance in ABCB1- and ABCG2-overexpressing cancer cells. *Cancer Lett*. (2019) 440–1:82–93. doi: 10.1016/j.canlet.2018.10.007
5. Dean M, Allikmets R. Complete characterization of the human ABC gene family. *J Bioenerg Biomembr*. (2001) 33:475–9. doi: 10.1023/A:1012823120935
6. Klappe K, Hummel I, Hoekstra D, Kok JW. Lipid dependence of ABC transporter localization and function. *Chem Phys Lipids*. (2009) 161:57–64. doi: 10.1016/j.chemphyslip.2009.07.004
7. Tong CWS, Wu WKK, Loong HHF, Cho WCS, To KKW. Drug combination approach to overcome resistance to EGFR tyrosine kinase inhibitors in lung cancer. *Cancer Lett*. (2017) 405:100–10. doi: 10.1016/j.canlet.2017.07.023
8. Shi R, Peng H, Yuan X, Zhang X, Zhang Y, Fan D, et al. Down-regulation of c-fos by shRNA sensitizes adriamycin-resistant MCF-7/ADR cells to chemotherapeutic agents via P-glycoprotein inhibition and apoptosis augmentation. *J Cell Biochem*. (2013) 114:1890–900. doi: 10.1002/jcb.24533
9. Lage H. Gene therapeutic approaches to overcome ABCB1-mediated drug resistance. *Recent Results Cancer Res*. (2016) 209:87–94. doi: 10.1007/978-3-319-42934-2_6
10. Dempke WCM, Fenchel K, Uciechowski P, Dale SP. Second- and third-generation drugs for immuno-oncology treatment-The more the better? *Eur J Cancer*. (2017) 74:55–72. doi: 10.1016/j.ejca.2017.01.001
11. Yin J, Lang T, Cun D, Zheng Z, Huang Y, Yin Q, et al. pH-sensitive nano-complexes overcome drug resistance and inhibit metastasis of breast cancer by silencing akt expression. *Theranostics*. (2017) 7:4204–16. doi: 10.7150/thno.21516
12. Xu WL, Shen HL, Ao ZF, Chen BA, Xia W, Gao F, et al. Combination of tetrandrine as a potential-reversing agent with daunorubicin, etoposide and cytarabine for the treatment of refractory and relapsed acute myelogenous leukemia. *Leuk Res*. (2006) 30:407–13. doi: 10.1016/j.leukres.2005.08.005
13. Toyoda Y, Takada T, Suzuki H. Inhibitors of human ABCG2: from technical background to recent updates with clinical implications. *Front Pharmacol*. (2019) 10:208. doi: 10.3389/fphar.2019.00208
14. Weidner LD, Zoghbi SS, Lu S, Shukla S, Ambudkar SV, Pike VW, et al. The inhibitor Ko143 is not specific for ABCG2. *J Pharmacol Exp Ther*. (2015) 354:384–93. doi: 10.1124/jpet.115.225482
15. Zhang GN, Zhang YK, Wang YJ, Gupta P, Ashby CR Jr, Alqahtani S, et al. Epidermal growth factor receptor (EGFR) inhibitor PD153035 reverses ABCG2-mediated multidrug resistance in non-small cell lung cancer: *in vitro* and *in vivo*. *Cancer Lett*. (2018) 424:19–29. doi: 10.1016/j.canlet.2018.02.040
16. Zhang YK, Wang YJ, Lei ZN, Zhang GN, Zhang XY, Wang DS, et al. Regorafenib antagonizes BCRP-mediated multidrug resistance in colon cancer. *Cancer Lett*. (2019) 442:104–12. doi: 10.1016/j.canlet.2018.10.032
17. Dolan M, Mastri M, Tracz A, Christensen JG, Chatta G, Ebos JML. Enhanced efficacy of sitravatinib in metastatic models of antiangiogenic therapy resistance. *PLoS ONE*. (2019) 14:e0220101. doi: 10.1371/journal.pone.0220101
18. Mastri M, Lee CR, Tracz A, Kerbel RS, Dolan M, Shi Y, et al. Tumor-independent host secretomes induced by angiogenesis and immune-checkpoint inhibitors. *Mol Cancer Ther*. (2018) 17:1602–12. doi: 10.1158/1535-7163.MCT-17-1066
19. Patwardhan PP, Ivy KS, Musi E, de Stanchina E, Schwartz GK. Significant blockade of multiple receptor tyrosine kinases by MGCD516 (Sitravatinib), a novel small molecule inhibitor, shows potent anti-tumor activity in preclinical models of sarcoma. *Oncotarget*. (2016) 7:4093–109. doi: 10.18632/oncotarget.6547
20. Du W, Huang H, Sorrelle N, Brekken RA. Sitravatinib potentiates immune checkpoint blockade in refractory cancer models. *JCI Insight*. (2018) 3. doi: 10.1172/jci.insight.124184
21. Henrich CJ, Bokesch HR, Dean M, Bates SE, Robey RW, Goncharova EI, et al. A high-throughput cell-based assay for inhibitors of ABCG2 activity. *J Biomol Screen*. (2006) 11:176–83. doi: 10.1177/1087057105284576
22. Miyake K, Mickley L, Litman T, Zhan Z, Robey R, Cristensen B, et al. Molecular cloning of cDNAs which are highly overexpressed in mitoxantrone-resistant cells: demonstration of homology to ABC transport genes. *Cancer Res*. (1999) 59:8–13.
23. Honjo Y, Hrycyna CA, Yan QW, Medina-Perez WY, Robey RW, van de Laar A, et al. Acquired mutations in the MXR/BCRP/ABCP gene alter substrate specificity in MXR/BCRP/ABCP-overexpressing cells. *Cancer Res*. (2001) 61:6635–9.
24. Robey RW, Honjo Y, Morisaki K, Nadjem TA, Runge S, Risbood M, et al. Mutations at amino-acid 482 in the ABCG2 gene affect substrate and antagonist specificity. *Br J Cancer*. (2003) 89:1971–8. doi: 10.1038/sj.bjc.6601370
25. Jackson SM, Manolaridis I, Kowal J, Zechner M, Taylor NMI, Bause M, et al. Structural basis of small-molecule inhibition of human multidrug transporter ABCG2. *Nat Struct Mol Biol*. (2018) 25:333–40. doi: 10.1038/s41594-018-0049-1
26. Zhang YK, Zhang XY, Zhang GN, Wang YJ, Xu H, Zhang D, et al. Selective reversal of BCRP-mediated MDR by VEGFR-2 inhibitor ZM323881. *Biochem Pharmacol*. (2017) 132:29–37. doi: 10.1016/j.bcp.2017.02.019
27. Carmichael J, DeGraff WG, Gazdar AF, Minna JD, Mitchell JB. Evaluation of a tetrazolium-based semiautomated colorimetric assay: assessment of chemosensitivity testing. *Cancer Res*. (1987) 47:936–42.
28. Ji N, Yang Y, Lei ZN, Cai CY, Wang JQ, Gupta P, et al. Ulixertinib. (BVD-523) antagonizes ABCB1- and ABCG2-mediated chemotherapeutic drug resistance. *Biochem Pharmacol*. (2018) 158:274–85. doi: 10.1016/j.bcp.2018.10.028
29. Ji N, Yang Y, Cai CY, Wang JQ, Lei ZN, Wu ZX, et al. Midostaurin reverses ABCB1-mediated multidrug resistance, an *in vitro* study. *Front Oncol*. (2019) 9:514. doi: 10.3389/fonc.2019.00514
30. Ji N, Yang Y, Cai CY, Lei ZN, Wang JQ, Gupta P, et al. VS-4718 antagonizes multidrug resistance in ABCB1- and ABCG2-overexpressing cancer cells by inhibiting the efflux function of ABC transporters. *Front Pharmacol*. (2018) 9:1236. doi: 10.3389/fphar.2018.01236
31. Ojida A, Mito-oka Y, Sada K, Hamachi I. Molecular recognition and fluorescence sensing of monophosphorylated peptides in aqueous solution by bis(zinc(II)-dipicolylamine)-based artificial receptors. *J Am Chem Soc*. (2004) 126:2454–63. doi: 10.1021/ja038277x
32. Teodori E, Dei S, Martelli C, Scapecchi S, Gualtieri F. The functions and structure of ABC transporters: implications for the design of new inhibitors of Pgp and MRP1 to control multidrug resistance. (MDR). *Curr Drug Targets*. (2006) 7:893–909. doi: 10.2174/138945006777709520
33. Han LW, Gao C, Mao Q. An update on expression and function of P-gp/ABCB1 and BCRP/ABCG2 in the placenta and fetus. *Expert Opin Drug Metab Toxicol*. (2018) 14:817–29. doi: 10.1080/17425255.2018.1499726
34. Theodoulou FL, Kerr ID. ABC transporter research: going strong 40 years on. *Biochem Soc Trans*. (2015) 43:1033–40. doi: 10.1042/BST20150139
35. Cui H, Zhang AJ, Chen M, Liu JJ. ABC transporter inhibitors in reversing multidrug resistance to chemotherapy. *Curr Drug Targets*. (2015) 16:1356–71. doi: 10.2174/1389450116666150330113506
36. Hsiao SH, Murakami M, Yeh N, Li YQ, Hung TH, Wu YS, et al. The positive inotropic agent DPI-201106 selectively reverses ABCB1-mediated multidrug resistance in cancer cell lines. *Cancer Lett*. (2018) 434:81–90. doi: 10.1016/j.canlet.2018.07.022
37. Cui Q, Cai CY, Gao HL, Ren L, Ji N, Gupta P, et al. Glesatinib, a c-MET/SMO dual inhibitor, antagonizes P-glycoprotein mediated multidrug resistance in cancer cells. *Front Oncol*. (2019) 9:313. doi: 10.3389/fonc.2019.00313
38. Wang JQ, Wang B, Lei ZN, Teng QX, Li JY, Zhang W, et al. Derivative of 5-cyano-6-phenylpyrimidin antagonizes ABCB1- and ABCG2-mediated multidrug resistance. *Eur J Pharmacol*. (2019) 863:172611. doi: 10.1016/j.ejphar.2019.172611
39. Wu CP, Murakami M, Hsiao SH, Liu TC, Yeh N, Li YQ, et al. SIS3, a specific inhibitor of Smad3 reverses ABCB1- and ABCG2-mediated multidrug resistance in cancer cell lines. *Cancer Lett*. (2018) 433:259–72. doi: 10.1016/j.canlet.2018.07.004
40. Zhao XQ, Xie JD, Chen XG, Sim HM, Zhang X, Liang YJ, et al. Neratinib reverses ATP-binding cassette B1-mediated chemotherapeutic drug resistance *in vitro*, *in vivo*, and *ex vivo*. *Mol Pharmacol*. (2012) 82:47–58. doi: 10.1124/mol.111.076299
41. Zhang H, Patel A, Ma SL, Li XJ, Zhang YK, Yang PQ, et al. In vitro, in vivo and ex vivo characterization of ibrutinib: a potent inhibitor of the efflux function of the transporter MRP1. *Br J Pharmacol*. (2014) 171:5845–57. doi: 10.1111/bph.12889

42. Yang K, Chen Y, To KK, Wang F, Li D, Chen L, et al. Alectinib (CH5424802) antagonizes ABCB1- and ABCG2-mediated multidrug resistance *in vitro, in vivo* and *ex vivo*. *Exp Mol Med*. (2017) 49:e303. doi: 10.1038/emm.2016.168
43. Yang L, Li M, Wang F, Zhen C, Luo M, Fang X, et al. Ceritinib enhances the efficacy of substrate chemotherapeutic agent in human abcb1-overexpressing leukemia cells *in vitro, in vivo* and *ex-vivo*. *Cell Physiol Biochem*. (2018) 46:2487–99. doi: 10.1159/000489655
44. Chen R, Herrera AF, Hou J, Chen L, Wu J, Guo Y, et al. Inhibition of MDR1 overcomes resistance to brentuximab vedotin in hodgkin lymphoma. *Clin Cancer Res*. (2020) 26:1034–44. doi: 10.1158/1078-0432.CCR-19-1768
45. Beretta GL, Cassinelli G, Pennati M, Zuco V, Gatti L. Overcoming ABC transporter-mediated multidrug resistance: the dual role of tyrosine kinase inhibitors as multitargeting agents. *Eur J Med Chem*. (2017) 142:271–89. doi: 10.1016/j.ejmech.2017.07.062
46. Nicolle E, Boumendjel A, Macalou S, Genoux E, Ahmed-Belkacem A, Carrupt PA, et al. QSAR analysis and molecular modeling of ABCG2-specific inhibitors. *Adv Drug Deliv Rev*. (2009) 61:34–46. doi: 10.1016/j.addr.2008.10.004
47. Wang J, Wang JQ, Cai CY, Cui Q, Yang Y, Wu ZX, et al. Reversal effect of ALK inhibitor NVP-TAE684 on ABCG2-overexpressing cancer cells. *Front Oncol*. (2020) 10:228. doi: 10.3389/fonc.2020.00228
48. Robey RW, Pluchino KM, Hall MD, Fojo AT, Bates SE, Gottesman MM. Revisiting the role of ABC transporters in multidrug-resistant cancer. *Nat Rev Cancer*. (2018) 18:452–64. doi: 10.1038/s41568-018-0005-8
49. Fan YF, Zhang W, Zeng L, Lei ZN, Cai CY, Gupta P, et al. Dacomitinib antagonizes multidrug resistance. (MDR) in cancer cells by inhibiting the efflux activity of ABCB1 and ABCG2 transporters. *Cancer Lett*. (2018) 421:186–98. doi: 10.1016/j.canlet.2018.01.021

Conflict of Interest: The authors declare that the research was conducted in the absence of any commercial or financial relationships that could be construed as a potential conflict of interest.

frontiers in Oncology

ORIGINAL RESEARCH
published: 12 May 2020
doi: 10.3389/fonc.2020.00674

M3814, a DNA-PK Inhibitor, Modulates ABCG2-Mediated Multidrug Resistance in Lung Cancer Cells

Zhuo-Xun Wu[1], Zheng Peng[2], Yuqi Yang[1], Jing-Quan Wang[1], Qiu-Xu Teng[1], Zi-Ning Lei[1], Yi-Ge Fu[1], Ketankumar Patel[1], Lili Liu[3], Lizhu Lin[4], Chang Zou[2] and Zhe-Sheng Chen[1]**

[1] Department of Pharmaceutical Sciences, College of Pharmacy and Health Sciences, St. John's University, Queens, NY, United States, [2] The Second Clinical Medical College of Jinan University, The First Affiliated Hospital of Southern University of Science and Technology, Shenzhen People's Hospital, Shenzhen, China, [3] Guangdong Provincial Key Laboratory of Occupational Disease Prevention and Treatment, Guangdong Province Hospital for Occupational Disease Prevention and Treatment, Guangzhou, China, [4] Cancer Center, The First Affiliated Hospital of Guangzhou University of Chinese Medicine, Guangzhou, China

OPEN ACCESS

Edited by:
Khalid A. El Sayed, University of Louisiana at Monroe, United States

Reviewed by:
Csilla Özvegy-Laczka, Institute of Enzymology, Hungary
Kamlesh Sodani, Avon, United States
Gary Piazza, University of South Alabama, United States

***Correspondence:**
Chang Zou
zou.chang@szhospital.com
Zhe-Sheng Chen
chenz@stjohns.edu

Specialty section:
This article was submitted to Pharmacology of Anti-Cancer Drugs, a section of the journal Frontiers in Oncology

Received: 19 January 2020
Accepted: 09 April 2020
Published: 12 May 2020

Citation:
Wu Z-X, Peng Z, Yang Y, Wang J-Q, Teng Q-X, Lei Z-N, Fu Y-G, Patel K, Liu L, Lin L, Zou C and Chen Z-S (2020) M3814, a DNA-PK Inhibitor, Modulates ABCG2-Mediated Multidrug Resistance in Lung Cancer Cells. Front. Oncol. 10:674. doi: 10.3389/fonc.2020.00674

M3814, also known as nedisertib, is a potent and selective DNA-dependent protein kinase (DNA-PK) inhibitor under phase 2 clinical trials. ABCG2 is a member of the ATP-binding cassette (ABC) transporter family that is closely related to multidrug resistance (MDR) in cancer treatment. In this study, we demonstrated that M3814 can modulate the function of ABCG2 and overcome ABCG2-mediated MDR. Mechanistic studies showed that M3814 can attenuate the efflux activity of ABCG2 transporter, leading to increased ABCG2 substrate drugs accumulation. Furthermore, M3814 can stimulate the ABCG2 ATPase activity in a concentration-dependent manner without affecting the ABCG2 protein expression or cell surface localization of ABCG2. Moreover, the molecular docking analysis indicated a high affinity between M3814 and ABCG2 transporter at the drug-binding cavity. Taken together, our work reveals M3814 as an ABCG2 modulator and provides a potential combination of co-administering M3814 with ABCG2 substrate-drugs to overcome MDR.

Keywords: ATP-binding cassette (ABC) transporter, M3814, nedisertib, ABCG2, multidrug resistance (MDR)

INTRODUCTION

Lung cancer remains the leading cause of cancer-related mortality worldwide (1). Approximately 85% of the cases are characterized as non-small cell lung cancer (NSCLC) (2). Currently, the clinical treatment strategies include surgery, radiotherapy, and chemotherapy (3). Adjuvant chemotherapy including cisplatin, paclitaxel, docetaxel, gemcitabine, and irinotecan, has been accepted as standard treatment especially for patients with advanced NSCLC (4, 5). Another promising option is the usage of small-molecule inhibitors such as gefitinib and erlotinib (6). However, the high rate of metastasis and drug resistance maintains the continued high mortality rates of lung cancer.

Chemotherapy and radiotherapy can lead to DNA damage, the mechanism by which some anticancer drugs, such as etoposide and doxorubicin, exert their anticancer effect (7). DNA-dependent protein kinase (DNA-PK) is actively involved in the repair of DNA double-strand breaks (DSBs), thereby positioning it as a promising target for cancer treatment (8). Several potent DNA-PK inhibitors have been developed, such as VX-984, NU7427, and M3814 (nedisertib)

(9, 10). Among all, M3814 is a clinical-stage, highly potent and selective DNA-PK inhibitor that demonstrated high activity in preclinical models (11, 12). M3814 has shown promising activity in combination with etoposide and cisplatin in lung cancer xenograft models (7, 13). It is also being investigated as monotherapy for solid tumors and chronic lymphocytic leukemia (CLL, ClinicalTrials.gov ID: NCT02316197), and as part of a combination treatment with radio-chemotherapy (NCT02516813, NCT03770689).

ATP-binding cassette (ABC) transporter family is composed of membrane proteins that serve multiple biological functions. ABC transporters are widely expressed in different organs such as the blood-brain barrier (BBB), placenta, and small intestines, to protect the organs by extrusion of xenobiotics and toxins. However, several ABC transporters are associated with multidrug resistance (MDR) and confer resistance to multiple chemotherapeutic agents as well as some tyrosine kinase inhibitors (TKIs) (14–16). Studies have shown that ABCB1 (P-glycoprotein, MDR1) and ABCG2 (BCRP, MXR) are associated with drug resistance in the clinical setting (17–19). ABCG2 overexpression can render cancer cells resistant to conventional chemotherapeutic agents, in particular topotecan, irinotecan, mitoxantrone, and doxorubicin (20–22), making it a prominent factor leading to MDR.

In lung cancer patients, clinical studies have shown a correlation between therapeutic outcome and ABCG2 expression level (23–26). In one of these studies, the response rate to chemotherapy of patients with ABCG2-negative tumors was 44% compare to 24% in patients with ABCG2-positive tumors (27). Due to the critical role that ABCG2 plays in MDR, the search for effective ABCG2 modulators became pertinent to overcoming drug resistance. To date, several drugs have been identified as ABCG2 modulators, namely fumitremorgin C (28), Ko143 (29), gefitinib (30), and erlotinib (31).

In this study, we aimed to investigate whether M3814 can modulate ABCG2-mediated MDR in lung cancer. We hypothesized that combining M3814 with ABCG2 substrate-drugs can overcome MDR and provide a new treatment strategy for MDR cancer patients.

MATERIALS AND METHODS

Reagents

M3814 was kindly provided by ChemieTek (Indianapolis, IN, USA). FBS, penicillin/streptomycin, DMEM, and trypsin EDTA were purchased from Corning Incorporated (Corning, NY, USA). Mitoxantrone, [^{3}H] (2.5 Ci/mmol) was purchased from Moravek Biochemicals, Inc. (Brea, CA, USA). The Alexa Fluor 488 conjugated IgG secondary antibody and GAPDH monoclonal antibody (GA1R) (catalog number MA5-15738) were obtained from Thermo Fisher Scientific Inc (Rockford, IL, USA). Primary antibody against ABCG2, clone BXP-21 (catalog number MAB4146), was obtained from Millipore (Billerica, MA, USA). Anti-mouse IgG, HRP-linked antibody (catalog number 7076S) was purchased from Cell Signaling Technology Inc (Danvers, MA, USA). PBS and BSA were purchased from VWR chemicals, LLC (Solon, OH, USA). Ko143 was purchased from Enzo Life Sciences (Farmingdale, NY, USA). Paraformaldehyde, triton X-100, 4',6-diamidino-2-phenylindole (DAPI), mitoxantrone, doxorubicin, vincristine, verapamil, cisplatin, methylthiazolyldiphenyl-tetrazolium bromide (MTT), DMSO, and all other chemicals were requested from Sigma Chemical Co (St. Louis, MO, USA).

Cell Lines and Cell Culture

The ABCG2-overexpressing subline NCI-H460/MX20 was originally established by selecting and maintaining parental NSCLC cell line NCI-H460 with mitoxantrone up to 20 nM (32). Another ABCG2-overexpressing subline A549/MX10 was originally established by selecting and maintaining parental NSCLC cell line A549 with mitoxantrone up to 10 nM (32). NCI-H460, NCI-H460/MX20, A549, and A549/MX10 were kindly provided by Drs. Susan Bates and Robert Robey (NCI, NIH, Bethesda, MD).The human embryonic kidney HEK293/pcDNA3.1 and HEK293/ABCG2 were generated by transfecting the cells with either an empty vector pcDNA3.1 or a pcDNA3.1 vector containing a full length ABCG2 gene. Transfected cells were selected with DMEM containing G418 (2 mg/mL). The ABCB1-overexpressing subline KB-C2 was established by introducing increasing concentrations of colchicine to parental cell line KB-3-1 and maintained in DMEM with 2 μg/mL colchicine (33). Both resistant KB-C2 and parental KB-3-1 cells were kindly provided by Dr. Shin-Ichi Akiyama (Kagoshima University, Kagoshima, Japan). All cells were cultured in DMEM with 10% FBS and 1% penicillin/streptomycin and maintained at 37°C incubator supplied with 5% CO_2. The drug-selected cells were cultured in drug-free DMEM for at least 2 weeks before the experiment.

MTT Assay

The cytotoxicity of M and other ch3814emotherapeutic agents was determined by MTT assay (34). Briefly, after cells were harvested and re-suspended in DMEM, cells were seeded evenly into 96-well plates at a density of 5,000–6,000 cells/well and incubated overnight to allow for attachment. For combination studies, an ABCG2 substrate drug and a reversal agent were added to the designated wells on the second day. After 72 h of treatment, cells were incubated with MTT. After 4 h incubation with MTT, the medium was aspirated and DMSO was used to dissolve the resulting formazan crystals. Absorbance at 570 nm was measured using the accuSkanTM GO UV/Vis Microplate Spectrophotometer (Fisher Sci., Fair Lawn, NJ, USA). Resistance-fold was calculated by dividing the IC_{50} value in resistant cells, in the presence or absence of M3814 or Ko143, by the IC_{50} value of the parental cells.

Western Blotting Analysis

The cell lysates were collected from drug-sensitive NCI-H460 and drug-resistant NCI-H460/MX20 cells after treatment with M3814 for different time points. After protein quantitation using Pierce™ BCA Protein Assay Kit (Thermo Scientific, Rockford, IL), the protein samples were separated by PAGE then transferred onto PVDF membranes. After blocking with 5% non-fat milk, the membranes were incubated with primary antibodies against

ABCG2 or GAPDH (1:1000) at 4°C overnight. Next, the blots were further incubated with HRP-linked secondary antibody (1:1000) for 2 h at room temperature. Pierce™ ECL Western blotting substrate (Thermo Scientific, Rockford, IL) was used to develop and visualize the protein bands. The results were analyzed by ImageJ software. The expression levels of ABCG2 relative to GAPDH were calculated.

Immunocytochemistry

Cells were seeded into 24-well plates at a density of 2×10^4 cells per well and incubated overnight. The cells were then treated with 1 μM of M3814 for different time points. Thereafter, the cells were fixed with 4% formaldehyde, permeabilized by 0.25% Triton X-100, and blocked with 6% BSA. Cells were then incubated with primary antibody against ABCG2 (1:1000). At the following day, primary antibody was removed, and the cells were further incubated with Alexa Fluor 488 conjugated secondary antibody (1:1000) at room temperature for 2 h. DAPI solution was added to stain the cell nuclei. Cell images were taken using a Nikon TE-2000S fluorescence microscope (Nikon Instruments Inc., Melville, NY, USA).

Tritium-Labeled Mitoxantrone Accumulation and Efflux Assay

NCI-H460 and NCI-H460/MX20 cells were seeded at a density of 2×10^5 cells per well into 24-well plates and incubated overnight to allow for attachment. Each plate was incubated with M3814 or Ko143, a positive control inhibitor of ABCG2, for 2 h at 37°C. Subsequently, cells were incubated with complete DMEM containing 10 nM of [^{3}H]-mitoxantrone with or without a reversal agent for different time points. For accumulation and efflux assay in the presence of 2,4-dinitrophenol, cells were incubated in glucose-free DMEM with 1 mM 2,4-dinitrophenol for 10 min before the addition of M3814 and [^{3}H]-mitoxantrone (35). Thereafter, the cells were rinsed with PBS and collected with scintillation vials. The radioactivity was read using the Packard TRICARB 1900CA liquid scintillation analyzer (Packard Instrument, Downers Grove, IL).

Evaluation of ABCG2 ATPase Activity

The ABCG2 ATPase activity was determined using PREDEASY ATPase Kits (TEBU-BIOnv, Boechout, Belgium) with modifications as previous described (36). Briefly, different concentrations of M3814 with or without $Na_3VO_4^-$ were added to the ABCG2 membrane suspension. The mixtures were incubated at 37°C for 5 min and the reaction was initiated by the addition of 5 mM Mg^{2+}ATP. After a 40-min incubation at 37°C, the inorganic phosphate (Pi) released was determined colorimetrically. The changes of relative light units were determined by comparing $Na_3VO_4^-$-treated group with the corresponding M3814-treated groups.

M3814 Accumulation Assay

Cells were seeded at a density of 2×10^5 cell per well into a 6-well-plate with a total volume of 2 mL complete DMEM. The plates were then incubated for 2 days before assay. At the day of treatment, the media was replaced by plain media (DMEM without FBS) for each well-before the drug exposure, cells were incubated with 10 mg/mL M3814 for 2 h. Thereafter, cells were washed twice with PBS followed by adding 0.5% Sodium dodecyl sulfate and acetonitrile to lyse the cells for the drug extraction. Samples were collected and centrifuged for 10 min at 14,000 rpm. The supernatant was collected and the intracellular concentration of drug was analyzed by HPLC.

Molecular Docking

The previously reported human ABCG2 cryo-EM structure model (PDB code: 6ETI) was used for docking analysis (37). The molecular docking was performed as described (38, 39) using the Maestro v11.1 software (Schrödinger, LLC, New York, NY, USA). The best docked-conformation of M3814 and ABCG2 transporter was established through the Glide XP (extra precision) docking analysis after the ligands were prepared in the low-energy pose. The top-score results were selected and subjected to induced-fit docking with the default protocol.

Statistical Analysis

At least 3 independent experiments were performed for each assay. Data are expressed as mean ± SD and analyzed using Graph Pad prism software 7. The data were analyzed using one-way ANOVA and statistical significance level was set as $p < 0.05$.

RESULTS

M3814 Reversed ABCG2-Mediated Drug Resistance in Cancer Cells

The chemical structure of M3814 is presented in **Figure 1A**. Firstly, the cytotoxicity of M3814 was determined by MTT assay. From the viability curve (**Figures 1B,E**), non-toxic concentrations were selected to circumvent the additive toxicity of M3814 combined with chemotherapeutic agents. Then the reversal effect was evaluated in the presence of an ABCG2 substrate drug, mitoxantrone or doxorubicin. As shown in **Figures 1C-G**, ABCG2-overexpressing NCI-H460/MX20 and A549/MX10 cells were highly resistant to both mitoxantrone and doxorubicin. Combining one of these substrates with M3814 or Ko143, a well-established ABCG2 inhibitor, was able to significantly sensitize the drug-resistant cells to ABCG2 substrate drugs. Furthermore, the reversal effect of M3814 at 1 μM was comparable to that of Ko143. On the other hand, M3814 did not affect the antiproliferative effect of cisplatin, a drug that is not a substrate of ABCG2, in neither drug-sensitive NCI-H460 nor drug-resistant NCI-H460/MX20 cells (**Figure 1H**). The cytotoxicity of cisplatin was also unaltered in drug-sensitive A549 and drug-resistant A549/MX10 cells (data not shown).

M3814 Reversed ABCG2-Mediated Drug Resistance in Transfected Cells

In order to further validate the reversal effect of M3814, HEK293 transfected cells in which ABCG2 is the sole contributor to MDR were used. In short, HEK293 cells transfected with an empty vector pcDNA3.1 were regarded as the parental cells, and cells transfected with a vector containing wild-type (R482R) or mutant

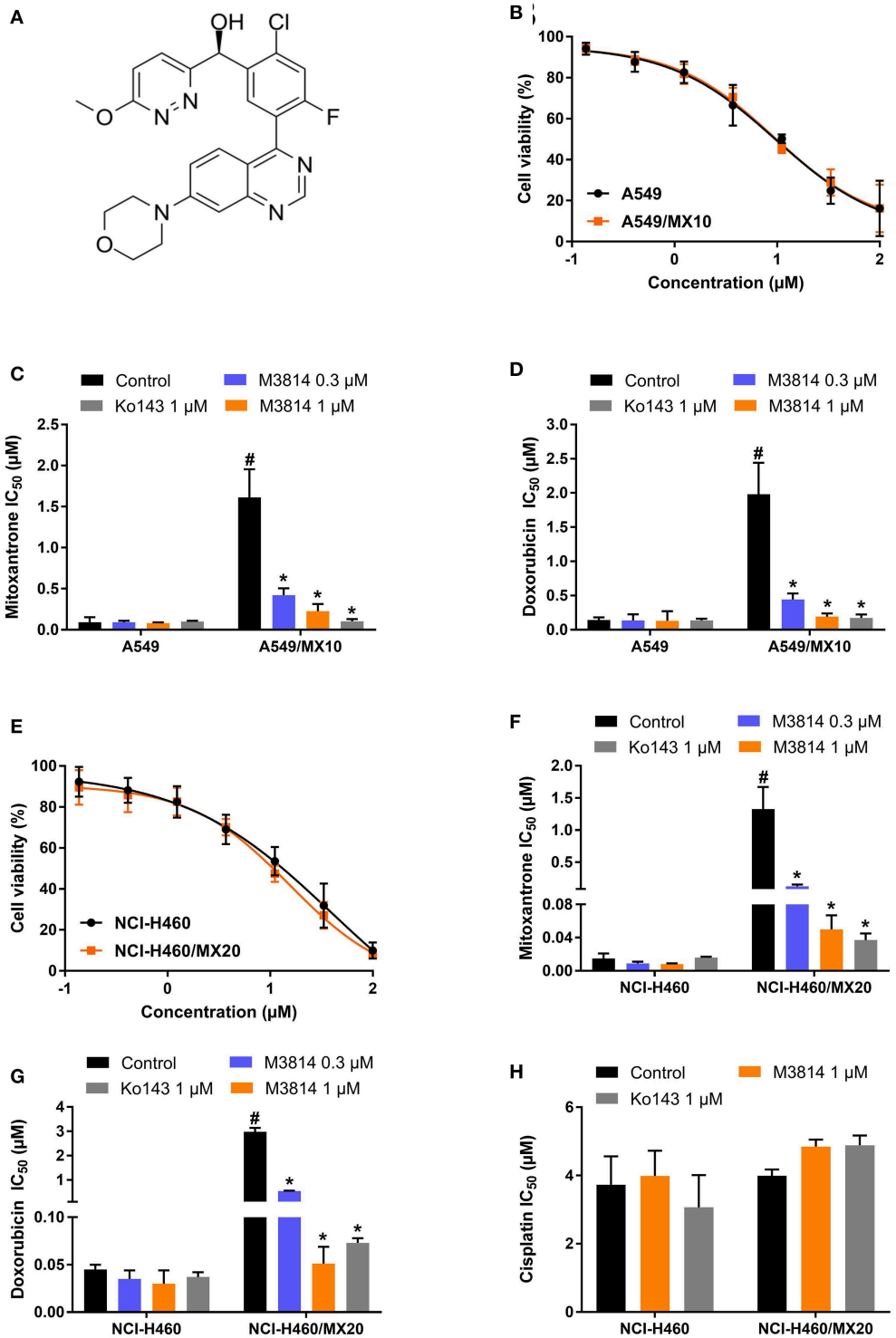

FIGURE 1 | Chemical structure and the effect of M3814 on the cytotoxicity of anticancer drugs in ABCG2-overexpressing cancer cells. **(A)** Chemical structure of M3814; **(B)** Cell viability curves for A549 and A549/MX10 cells; The effect of M3814 on the cytotoxicity of mitoxantrone **(C)**, doxorubicin **(D)** in A549 and A549/MX10 cells; **(E)** Cell viability curves for NCI-H460 and NCI-H460/MX20 cells; The effect of M3814 on the cytotoxicity of mitoxantrone **(F)**, doxorubicin **(G)**, and cisplatin **(H)** in NCI-H460 and NCI-H460/MX20 cells. Data are expressed as mean ± SD from a representative of three independent experiments. $^{*}p < 0.05$ vs. the control group, $^{\#}p < 0.05$ vs. the control group in parental cell lines.

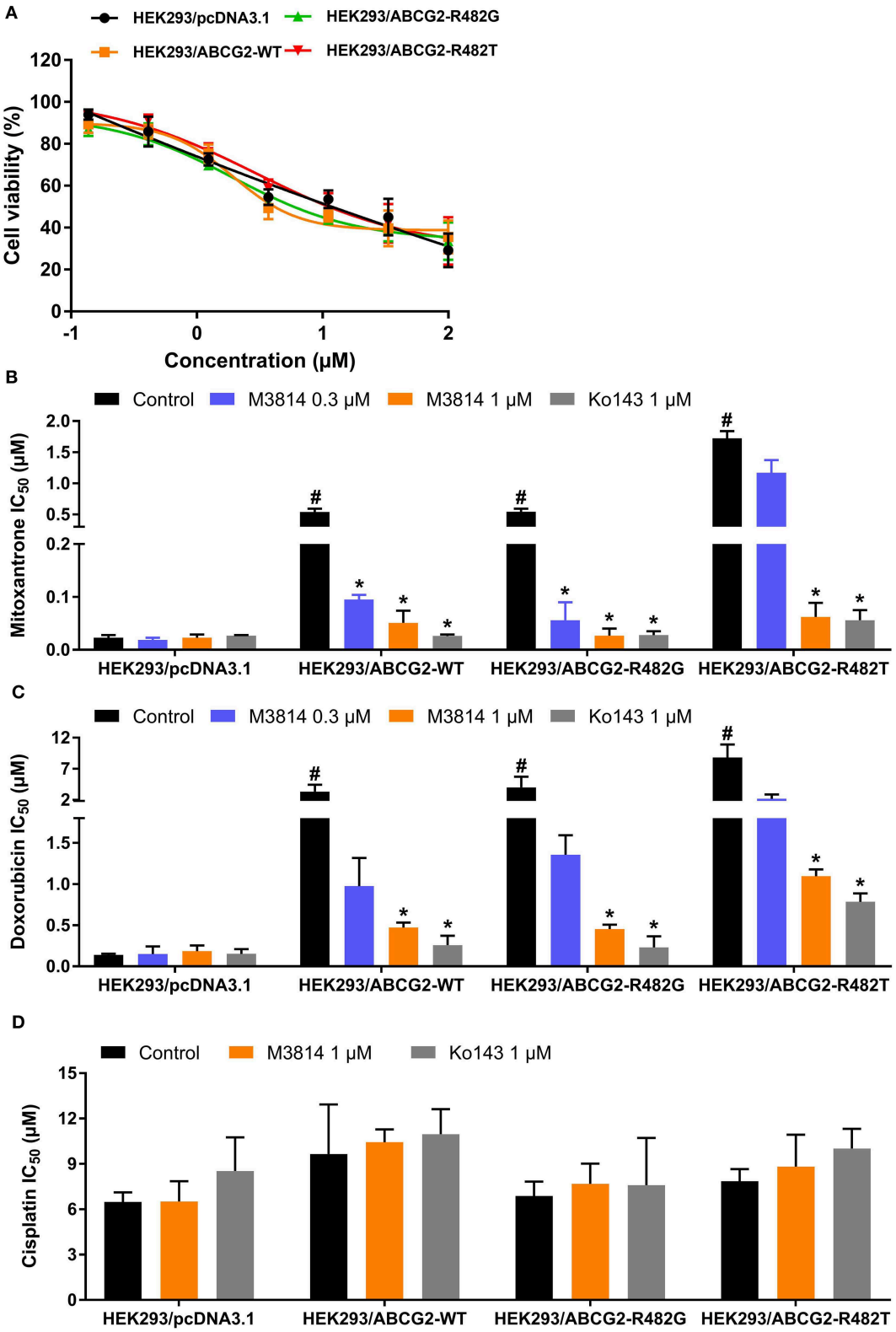

FIGURE 2 | The effect of M3814 on the cytotoxicity of different anticancer drugs in ABCG2-overexpressing HEK293 transfected cells. **(A)** Cell viability curves for HEK293/pcDNA3.1, HEK293/ABCG2-WT, HEK293/ABCG2-R482G, and HEK293/ABCG2-R482T cells; The effect of M3814 on the cytotoxicity of mitoxantrone **(B)**, doxorubicin **(C)**, and cisplatin **(D)**. Data are expressed as mean ± SD from representative of three independent experiments. $^{*}p < 0.05$ vs. the control group, $^{\#}p < 0.05$ vs. the control group in parental cell lines.

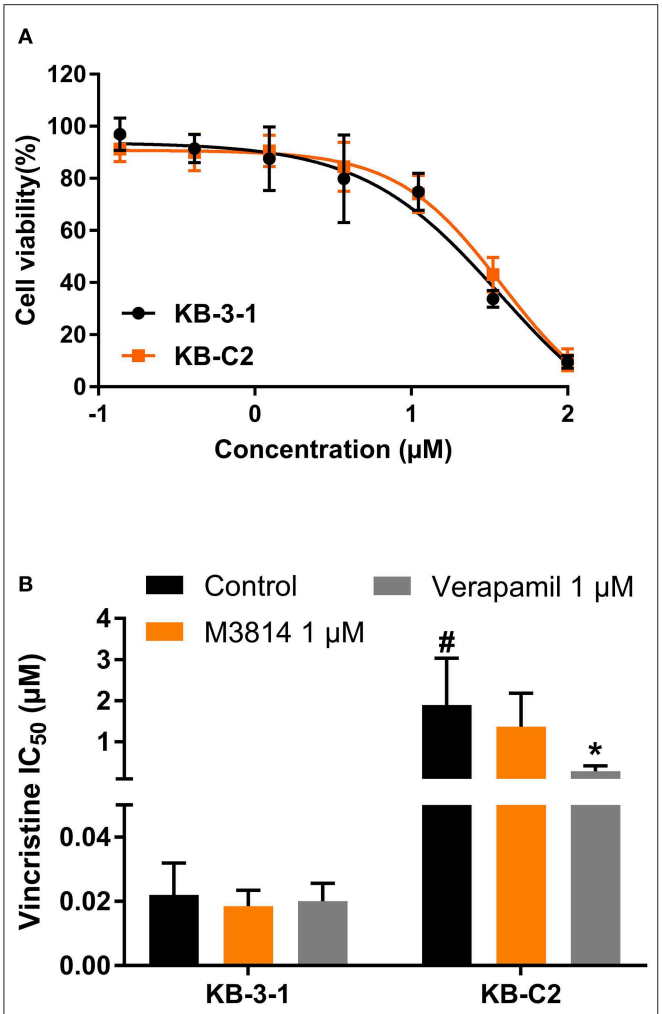

FIGURE 3 | The effect of M3814 on the cytotoxicity of different anticancer drugs in ABCB1-overexpressing cancer cells. **(A)** Cell viability curves for KB-3-1 and KB-C2 cells; **(B)** The effect of M3814 on the cytotoxicity of vincristine. Data are expressed as mean ± SD from a representative of three independent experiments. *$p < 0.05$ vs. the control group. #$p < 0.05$ vs. the control group in parental cell lines.

(R482G/R482T) ABCG2 were regarded as the drug-resistant cells. The cytotoxicity results are presented in **Figure 2**. Likewise, M3814 showed similar cytotoxicity in HEK293 transfected cells to cancer cells. Consistently, M3814 was able to significantly reverse drug resistance in both wild-type and mutant ABCG2 overexpressing HEK293 cells. The results support our initial finding that M3814 is a potential ABCG2 modulator.

M3814 Did Not Affect ABCB1-Mediated MDR

To evaluate the selectivity of M3814 as an ABC drug transporter modulator, we examined whether M3814 can reverse ABCB1-mediated MDR. As shown in **Figure 3A**, the antiproliferative effect of M3814 in parental KB-3-1 and drug-resistant KB-C2 cells were identical and no significant toxicity was observed at 1 μM. Reversal studies showed that M3814, at 1 μM, failed to sensitize drug-resistant KB-C2 cells to vincristine, indicating that M3814 is not an effective modulator of ABCB1 (**Figure 3B**). Therefore, the modulatory effect of M3814 may be specific to the ABCG2 transporter.

M3814 Increased Intracellular Accumulation and Decreased Efflux of [^{3}H]-Mitoxantrone

M3814 showed the ability to reverse ABCG2-mediated MDR, and we therefore, sought to further investigate its modulatory mechanisms. [^{3}H]-mitoxantrone accumulation and efflux assays were performed to measure the intracellular concentration of mitoxantrone. As shown in **Figure 4A**, the intracellular concentration of [^{3}H]-mitoxantrone was lower in drug-resistant NCI-H460/MX20 cells than in drug-sensitive NCI-H460 cells without the presence of a reversal agent. The addition of M3814 or Ko143 increased the accumulation of [^{3}H]-mitoxantrone in drug-resistant NCI-H460/MX20 cells without affecting accumulation in drug-sensitive NCI-H460 cells. The results provided evidence that M3814 can increase the accumulation of [^{3}H]-mitoxantrone in ABCG2-overexpressing cells. Since there are multiple factors that can result in increased mitoxantrone accumulation, we first explored whether M3814 can inhibit the efflux function of ABCG2. As shown in **Figures 4B,C**, without altering the efflux process in drug-sensitive cells, M3814 was able to hinder the efflux of [^{3}H]-mitoxantrone in drug-resistant cells. 2,4-dinitrophenol is an uncoupling agent that blocks the phosphorylation of ADP to ATP. We measured the efflux process of [^{3}H]-mitoxantrone in NCI-H460/MX20 cells in glucose-free DMEM in the presence of 2,4-dinitrophenol. As presented in **Figure 4D**, the efflux of [^{3}H]-mitoxantrone was decreased in NCI-H460/MX20 cells by 2,4-dinitrophenol while the addition of Ko143 or M3814 had no significant effect. Taken together, the results suggested M3814 can inhibit the efflux activity of the ABCG2 transporter, which leads to the increased intracellular concentration of mitoxantrone.

M3814 Stimulated ABCG2 ATPase Activity

The [^{3}H]-mitoxantrone accumulation and efflux assay suggested that M3814 can interact with the ABCG2 transporter. We postulated that M3814 may be a direct ABCG2 inhibitor or an ABCG2 substrate that can inhibit or stimulate the ATPase function, respectively. Therefore, the ABCG2 ATPase assay was conducted to evaluate the role of M3814. As presented in **Figure 5A**, M3814 showed a concentration-dependent stimulation of ATPase activity at 0–20 μM. The stimulatory effect reached 50% maximal effect at 1.64 μM with a maximum stimulation of 371.02% of the basal activity. In this study, topotecan was used as a positive substrate control that can stimulate the activity of ABCG2 ATPase. Combined with the results of the accumulation and efflux assay, M3814 may be a transported substrate and competitively inhibit the transportation of other ABCG2 substrates.

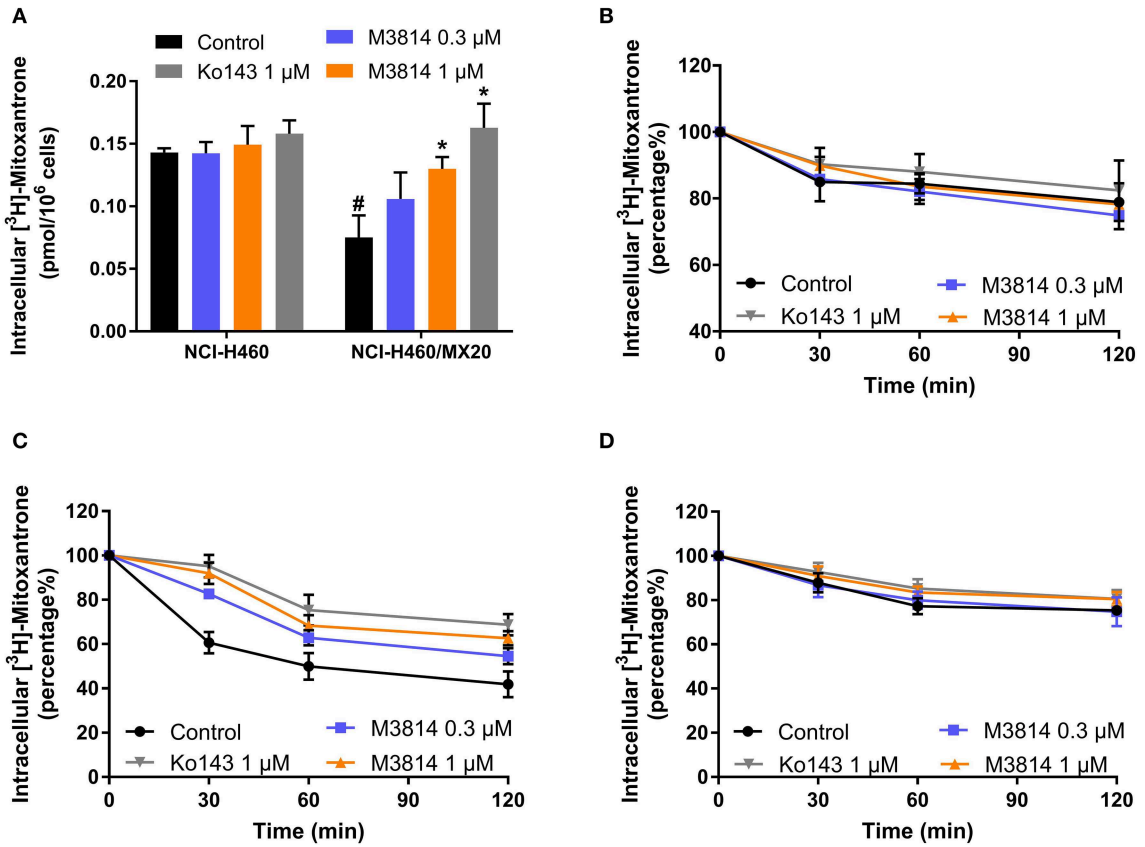

FIGURE 4 | Effect of M3814 on the accumulation and efflux of [^{3}H]-mitoxantrone. **(A)** The effect of M3814 on the accumulation of [^{3}H]-mitoxantrone in NCI-H460 and NCI-H460/MX20 cells. **(B)** The effect of M3814 on the efflux of [^{3}H]-mitoxantrone in NCI-H460 cells. **(C)** The effect of M3814 on the efflux of [^{3}H]-mitoxantrone in NCI-H460/MX20 cells. **(D)** The effect of M3814 on the efflux of [^{3}H]-mitoxantrone in NCI-H460/MX20 cells with 2,4-dinitrophenol pretreatment. Ko143 at 1 μM was used as a positive control inhibitor of ABCG2. Data are expressed as mean ± SD from a representative of three independent experiments. $^*p < 0.05$ vs. the control group, $^\#p < 0.05$ vs. the control group in parental cell lines.

The Intracellular Accumulation of M3814 Was Consistent in Parental and Drug-Resistant Cells

Since M3814 can stimulate ABCG2 ATPase activity, we examined whether M3814 can be pump out of the cells by ABCG2. By performing HPLC analysis, it is found that the intracellular accumulation of M3814 showed no significant different in parental NCI-H460 and ABCG2-overexpressing NCI-H460/MX20 cells (**Figure 5B**). These results suggest that M3814 can bind to ABCG2 transporter without being pump out of the cells.

M3814 Did Not Affect ABCG2 Protein Level or Cell Surface Localization

Since a reversal agent may exert its effect through multiple mechanisms, we investigated whether M3814 can alter ABCG2 protein expression or cell surface localization. As shown in **Figure 6A**, M3814 did not alter the expression level of ABCG2. Furthermore, the immunofluorescent assay (**Figure 6B**) clearly showed that ABCG2 continued to be localized at cell surface after 72 h of M3814 treatment. These results indicated that the modulatory effect of M3814 may be due solely to the inhibition of substrate efflux. Similarly, ABCG2 expression level and cell surface localization were not changed in A549/MX10 cells after M3814 treatment (data not shown).

Molecular Docking Analysis of M3814 With the Human ABCG2 Homology Model

The interactions between M3814 and human ABCG2 model were stimulated by the induced-fit docking analysis. The Glide gscore of the best docked pose of M3814-ABCG2 was −14.035 kcal/mol, which indicated that M3814 has a good affinity to the drug-binding pocket of ABCG2. **Figure 7A** depicted the general docking pose of M3814, which was predicted in the drug-binding cavity of human ABCG2 model with the detailed interactions between M3814 and some specific residues of the protein model. As shown in **Figure 7B**, the best-scored pose of M3814 was mainly stable in the ABCG2 transmembrane domain, demonstrating hydrophobic interactions with specific residues including Leu555, Phe431, Phe432, and Phe439 in protein chain A. Other hydrophobic interactions include Leu555,

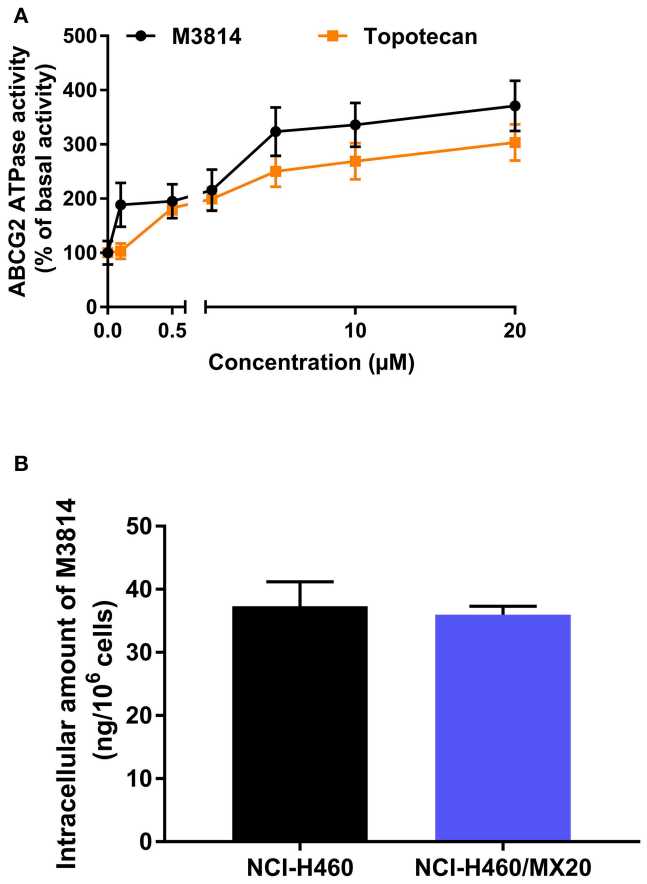

FIGURE 5 | M3814 stimulates ABCG2 ATPase activity without being transported out of the resistant cells **(A)** The effect of M3814 and topotecan on the ATPase activity of ABCG2 transporter. **(B)** The intracellular accumulation of M3814 in NCI-H460 and NCI-H460/MX20. Data are expressed as mean ± SD from three independent experiments.

Val546, Met549, Phe431, Phe432, and Phe439 in protein chain B. Furthermore, **Figure 7B** also depict that a hydrogen bond was formed between the ether group in morpholine of M3814 and Asn436 of ABCG2 chain A. In addition, M3814 formed two hydrogen bonds with protein chain B: one between Phe432 and the methanol group of M3814, another one between Asn436 and the same methanol group. Two π-π stacking interactions were formed between the quinazoline ring of M3814 and Phe431 of both ABCG2 chain A and chain B, respectively. The molecular docking analysis of mitoxantrone with ABCG2 model was shown in **Figure 7C**. M3814 only have two overlapping binding residues, indicating M3814 may not bind to the same substrate-binding site as mitoxantrone.

DISCUSSION

As one of the more well-known members of the ABC transporter family, ABCG2 can be both beneficial and deleterious. By eliminating xenobiotics from cells, ABCG2 acts as a gatekeeper in normal tissue but as an MDR mediator in many tumors (40). ABCG2 overexpression can confer cancer cells resistant to a wide range of chemotherapeutic agents such as irinotecan, doxorubicin, and mitoxantrone. Due to its pivotal role, tremendous effort has been devoted to investigating ABCG2 inhibitors. Even though the clinical effect of these ABCG2 inhibitors remains inconclusive, an appropriate modulation of ABCG2 activity may strengthen the efficacy of substrate-drugs by overcoming MDR and improving their pharmacokinetics (41–43). Recent studies suggest that the combination of several TKIs with substrate-drugs can achieve desired effect and reverse drug resistance (44–46).

Lung cancer accounts for a large proportion of cancer incidences and mortalities. About 85% of the cases are characterized as NSCLC. Clinical data have shown that ABCG2 overexpression may attenuate the response of NSCLC patients to anticancer drug. M3814 is developed as a potent and selective DNA-PK inhibitor. It is now under several clinical trials for advanced solid tumors and CLL, as well as in combination treatment with radio-chemotherapy. In this study, the ABCG2 modulatory effect of M3814 was evaluated in two ABCG2-overexpressing NSCLC cell lines, NCI-H460/MX20 and A549/MX10. We report that M3814 can effectively modulate the function of ABCG2 and reverse MDR in combination treatment.

The cytotoxicity of M3814 was examined in both parental and ABCG2-overexpressing cell lines to select the appropriate concentrations for reversal studies. The results showed that no significant toxicity was observed up to 1 μM in both sets of NSCLC cell lines. Therefore, the reversal experiments were carried out using 0.3 and 1 μM of M3814 to evaluate its reversal effect. The data showed that M3814 can significantly sensitize the drug-resistant cells to ABCG2 substrates (mitoxantrone and doxorubicin) but this phenomenon was not observed in the drug-sensitive parental cells, suggesting that the effect may be due to ABCG2 efflux inhibition. Furthermore, it was documented that a mutation at the position 482 of the ABCG2 protein can result in a distinct substrate-binding and efflux profile (47, 48). By conducting reversal studies in gene-transfected HEK293 cells, we confirmed that M3814 can reverse both wild-type and mutant ABCG2-mediated MDR in cellular models. Comparing with other established ABCG2 modulators, the effective concentration of M3814 is lower than ulixertinib (49), selonsertib (50), ribociclib (51), PD1530353 (52), and comparable to Ko143, olmutinib (53), SIS3 (54). M3814 did not alter the toxicity of cisplatin, a non-substrate drug of ABCG2, nor did it reverse ABCB1-mediated MDR. Therefore, M3814 may be a modulator specific to ABCG2. Although we uncovered that M3814 may not be a reversal agent for ABCB1-mediated MDR, future studies are needed to assess the interaction of M3814 with other MDR-associated proteins such as ABCC1 and ABCC10 (55, 56).

Further studies were conducted to gain insight into the reversal mechanisms. [^{3}H]-mitoxantrone accumulation and efflux assays were conducted. By introducing the tritium-labeled mitoxantrone, it allowed for a direct measurement of intracellular concentration of mitoxantrone to assess the efflux process of ABCG2. From the results of the accumulation assay, we found that M3814 can increase the accumulation of mitoxantrone only

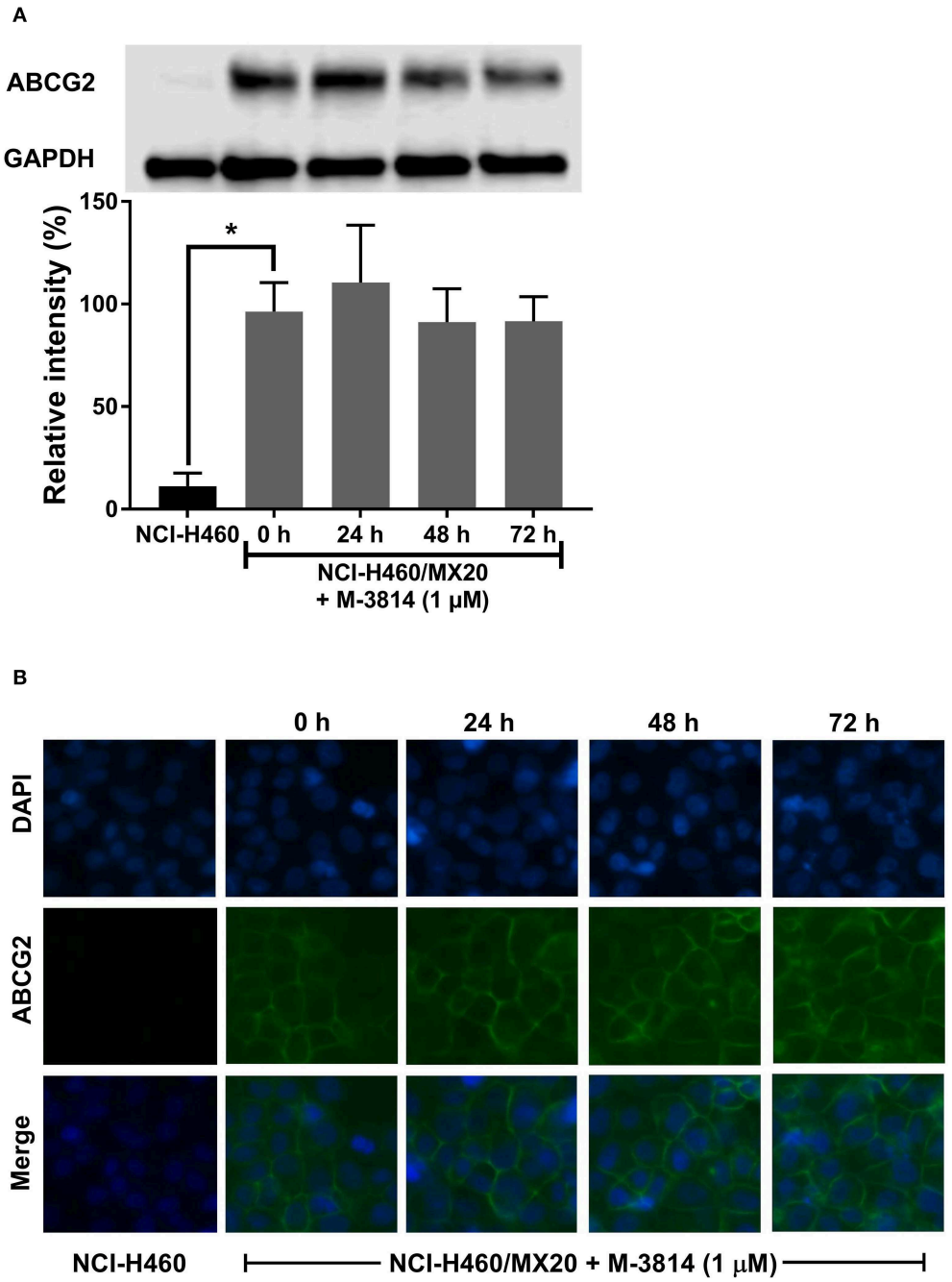

FIGURE 6 | M3814 did not affect the ABCG2 protein expression or cell surface localization. **(A)** The effect of M3814 on the expression level of ABCG2 in NCI-H460 and NCI-H460/MX20 cells. **(B)** Cell surface localization of ABCG2 expression in NCI-H460/MX20 cells incubated with 1 μM of M3814 for up to 72 h. Data are expressed as mean ± SD from three independent experiments. *$p < 0.05$ vs. the control group.

in ABCG2-overexpressing cells in a concentration-dependent manner, indicating that M3814 can interact with an ABCG2 transporter to interfere with its efflux function. Consistently, in the [^{3}H]-mitoxantrone efflux assay, M3814 was able to hinder the efflux process in ABCG2-overexpressing cells and the effect was comparable with the well-established ABCG2 inhibitor Ko143. To determine if the enhanced mitoxantrone accumulation is due to the decreased active efflux or increased drug uptake by the cells, we introduced 2,4-dinitrophenol which can prevent the synthesis of ATP and thereby can deplete the intracellular ATP. As ABCG2 efflux function requires energy from ATP hydrolysis, pretreatment with 2,4-dinitrophenol can significantly

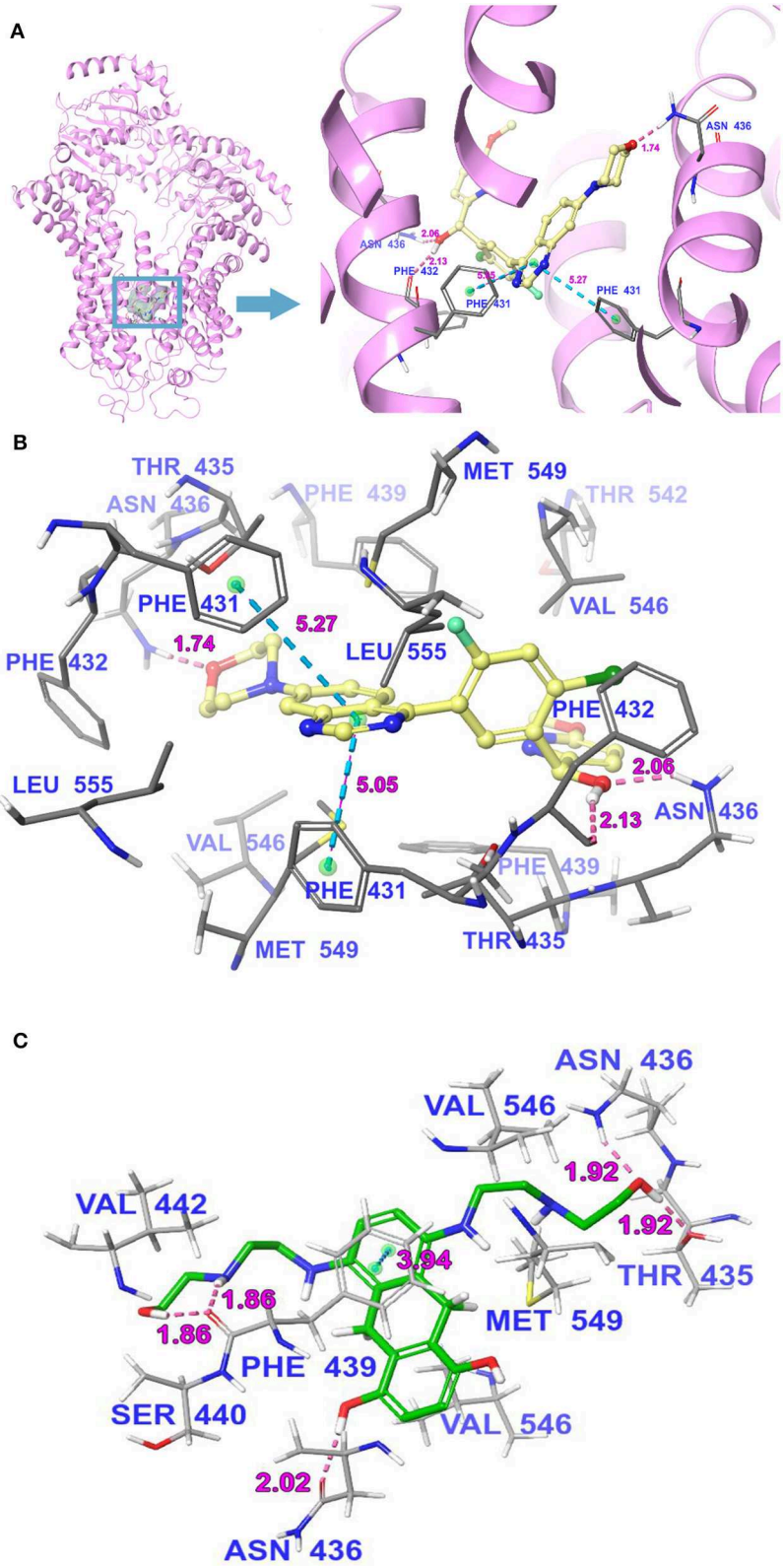

FIGURE 7 | The molecular binding mode of M3814 to the human ABCG2 model as predicted by induced-fit docking. **(A)** The superimposition of the best-scored pose of M3814 within the binding cavity of ABCG2. Ligand is depicted as a ball-and-stick model with a transparent gray surface and the ABCG2 structure as a ribbon diagram in faded pink. The detailed depiction of M3814 and nearby residues inside the ABCG2 binding cavity are depicted with the atoms colored as follows: carbon,

(Continued)

FIGURE 7 | faded yellow; hydrogen, white; nitrogen, blue; oxygen, red; fluorine, light green; chlorine, dark green; and important amino acid residues are described (sticks model) with the same color scheme as above for all atoms but carbon atoms in gray. The values of the relevant distances are indicated in Å. **(B)** The docked conformation of M3814 (ball-and-stick model) is shown within the ABCG2 drug-binding cavity, and specific amino acids residues within 3 Å are indicated as a sticks model, with the same color scheme as **(A)**. Dotted pink lines represent hydrogen-bonding interactions, while dotted light blue lines represent π-π stacking interactions. The values of the correlation distances are indicated in Å. **(C)** The docked conformation of mitoxantrone (ball and stick model) is shown within the ABCG2 drug-binding cavity with the atoms and important amino acid residues are described (sticks model) with the same color scheme as above for all atoms but carbon atoms in green. Dotted pink lines represent hydrogen-bonding interactions, while dotted light blue lines represent π-π stacking interactions. The values of the correlation distances are indicated in Å.

decrease the drug efflux process. Our results showed that, in the presence of 2,4-dinitrophenol, ABCG2-overexpressing NCI-H460/MX20 cells showed significant decreased efflux of mitoxantrone, suggesting the efflux function of ABCG2 is impaired. Furthermore, adding reversal agents M3814 or Ko143 did not contribute to the accumulation of mitoxantrone after cells were pretreated with 2,4-dinitrophenol. These results suggest that M3814 can hinder the ABCG2 efflux function without facilitating mitoxantrone uptake by the cells. Therefore, the modulatory effect of M3814 may be in part due to the inhibition of ABCG2 efflux function, which leads to increased substrate accumulation and enhanced cytotoxic effect.

Since we demonstrated that M3814 can attenuate the efflux activity of ABCG2, it may act by inhibiting the ATPase, hindering ABCG2 from utilizing the energy from ATP hydrolysis. Another explanation, according to several previous studies (49, 50, 57), is that the modulator may act as a substrate of ABCG2 and compete with other substrates for the transporter. To determine the mechanism of M3814 as an ABCG2 modulator, ABCG2 ATPase activity was measured in the presence of M3814. ABCG2 is characterized as a "half-transporter" with a transmembrane domain to which a substrate binds and a nucleotide-binding domain where ATP binds and hydrolyzes. If the drug is an ATPase inhibitor, a trend toward decreased ATPase activity would be observed (36). In contrast, a substrate can bind to the substrate-binding pocket and stimulate the ATPase to provide energy for drug efflux. The results indicated that M3814 can stimulate the activity of ABCG2 ATPase in a concentration-dependent manner, confirming its role as a transported substrate of ABCG2. Some ABCG2 substrate inhibitors can act as competitive inhibitors that bind to a distinct substrate-binding site and inhibit the efflux of a particular class of substrates (58). Another possibility is that some substrate inhibitors can interact with ABCG2 on sites other than the substrate-binding sites and cause conformational changes in the binding pocket which allosterically affect the transportation of some substrates (59). It should be noted that, although several ABCG2 inhibitors were identified as substrates through ATPase assay, overexpression of ABCG2 does not necessarily confer drug resistance to these inhibitors (49, 54, 60–62). Hitherto, the detailed mechanism of this inhibitory effect remained inconclusive and desire further exploration. To explore the possible mechanism of the reversal effect achieved by M3814, we performed HPLC to detect the intracellular accumulation of M3814 in parental and drug-resistant cells. The results showed that ABCG2-overexpressing cells did not 14. Sinc necessarily efflux M38e M3814 can stimulate the activity of ABCG2 ATPase, we hypothesized that M3814 can bind to the drug-binding pocket of ABCG2, causing the protein conformational changes and therefore inhibit the efflux of other substrates. Further studies are needed to verify this possible mechanism of action.

Subsequently, we examined two additional possible mechanisms: alteration of ABCG2 protein expression or cell surface localization. Some reversal agents can downregulate the ABCG2 expression, leading to decreased drug resistance (52). The reversal effect can be achieved by translocating the transporter into cytoplasm, which also decreases the number of efflux pumps on the cell membrane. By performing a Western blot and immunofluorescent assay, we confirmed that M3814 did not affect the expression level of ABCG2, and the transporter remained on the cell membrane after M3814 treatment. Hence, we inferred that M3814 can inhibit the efflux function of ABCG2. Further studies are needed to explore other potential mechanisms.

Molecular docking has been extensively used in the field of structural molecular biology, and helps to predict the predominant binding interaction between a ligand and a protein. The cryo-EM structures of ABCG2 bound with an ABCG2 inhibitor Ko143 (37) were used as the basis for investigating the interaction between ABCG2 modulators and the transporter. M3814 obtained a high docking score of−14.035 kcal/mol compared to several other ABCG2 modulators such as ulixertinib (−11.501 kcal/mol) (49), PD153035 (−7.015 kcal/mol) (52), and TMP195 (−12.7 kcal/mol) (63), suggesting that M3814 has potent binding affinity with the drug-binding cavity of ABCG2. Of note, the molecular docking is not meant to be accurate affinity predictor, thereby the bound conformation may not represent the actual binding situation and is therefore used as a reference for this study (64).

In conclusion, our study highlights M3814 as a modulator of ABCG2 function. The combination of M3814 and ABCG2 substrate drugs may allow additional benefit for cancer patients with high ABCG2 expression.

DATA AVAILABILITY STATEMENT

The datasets generated for this study are available on request to the corresponding author.

AUTHOR CONTRIBUTIONS

Z-XW, Z-SC, CZ, and LLin: Conceptualization. Z-XW, ZP, YY, Q-XT, J-QW, Z-NL, Y-GF, KP, and LLiu: methodology. Z-XW: writing - original draft preparation. Z-XW, YY, LLin, CZ, and Z-SC: writing - review and editing. Z-SC and CZ: supervision.

FUNDING

This project was partially supported by Science and Technology Science Foundation of Guangzhou (201804010005) The project was also partially supported by Department of Pharmaceutical Science, St. John's University.

ACKNOWLEDGMENTS

The authors would like to thank Chemietek for kindly provided the M3814 compound. We would like to thank Drs. Robert W. Robey and Susan E. Bates (NCI, NIH, Bethesda, MD) for providing the NCI-H460, NCI-H460/MX20, A549, and A549/MX10 cell lines. We thank Dr. Shin-Ichi Akiyama (Kagoshima University, Kagoshima, Japan) for the gift of KB-3-1 and KB-C2 cell lines. Thanks are also given to Dr. Tanaji T. Talele (St. John's University, Queens, NY) for providing the computational resource for the molecular docking analysis. This project was partially support by Science and Technology Science Foundation of Guangzhou (201804010005) and Department of Pharmaceutical Sciences, St. John's University. We thank Dr. Yangmin Chen for editing the article.

REFERENCES

1. Ferlay J, Soerjomataram I, Dikshit R, Eser S, Mathers C, Rebelo M, et al. Cancer incidence and mortality worldwide: sources, methods and major patterns in GLOBOCAN 2012. *Int J Cancer*. (2015) 136:E359–86. doi: 10.1002/ijc.29210
2. Ke B, Wei T, Huang Y, Gong Y, Wu G, Liu J, et al. Interleukin-7 resensitizes non-small-cell lung cancer to cisplatin via inhibition of ABCG2. *Media Inflamm*. (2019) 2019:7241418. doi: 10.1155/2019/7241418
3. Ramalingam SS, Dahlberg SE, Belani CP, Saltzman JN, Pennell NA, Nambudiri GS, et al. Pemetrexed, bevacizumab, or the combination as maintenance therapy for advanced nonsquamous non-small-cell lung cancer: ECOG-ACRIN 5508. *J Clin Oncol*. (2019) 37:2360–7. doi: 10.1200/JCO.19.01006
4. Bunn PA Jr, Kelly K. New combinations in the treatment of lung cancer: a time for optimism. *Chest*. (2000) 117:138S−43. doi: 10.1378/chest.117.4_suppl_1.138S
5. Kubota K, Kunitoh H, Seto T, Shimada N, Tsuboi M, Ohhira T, et al. Randomized phase II trial of adjuvant chemotherapy with docetaxel plus cisplatin versus paclitaxel plus carboplatin in patients with completely resected non-small cell lung cancer: TORG 0503. *Lung Cancer*. (2019) 141:32–6. doi: 10.1016/j.lungcan.2019.11.009
6. Baselga J, Hammond LA. HER-targeted tyrosine-kinase inhibitors. *Oncology*. (2002) 63(Suppl. 1):6–16. doi: 10.1159/000066198
7. Wise HC, Iyer GV, Moore K, Temkin SM, Gordon S, Aghajanian C, et al. Activity of M3814, an oral DNA-PK inhibitor, in combination with topoisomerase II inhibitors in ovarian cancer models. *Sci Rep*. (2019) 9:18882. doi: 10.1038/s41598-019-54796-6
8. Harnor SJ, Brennan A, Cano C. Targeting DNA-dependent protein kinase for cancer therapy. *ChemMedChem*. (2017) 12:895–900. doi: 10.1002/cmdc.201700143
9. Hardcastle IR, Cockcroft X, Curtin NJ, El-Murr MD, Leahy JJJ, Stockley M, et al. Discovery of potent chromen-4-one inhibitors of the DNA-dependent protein kinase (DNA-PK) using a small-molecule library approach. *J Med Chem*. (2005) 48:7829–46. doi: 10.1021/jm050444b
10. Timme CR, Rath BH, O'neill JW, Camphausen K, Tofilon PJ. The DNA-PK inhibitor VX-984 enhances the radiosensitivity of glioblastoma cells grown *in vitro* and as orthotopic xenografts. *Mol Cancer Therap*. (2018) 17:1207–16. doi: 10.1158/1535-7163.MCT-17-1267
11. Damstrup L, Zimmerman A, Sirrenberg C, Zenke F, Vassilev L. M3814, a DNA-dependent protein kinase inhibitor (DNA-PKi), potentiates the effect of ionizing radiation (IR) in xenotransplanted tumors in nude mice. *Int J Radiat Oncol Biol Phys*. (2016) 94:940–1. doi: 10.1016/j.ijrobp.2015.12.268
12. Zenke FT, Zimmermann A, Sirrenberg C, Dahmen H, Vassilev L, Pehl U, et al. Abstract 1658: M3814, a novel investigational DNA-PK inhibitor: enhancing the effect of fractionated radiotherapy leading to complete regression of tumors in mice. *Cancer Res*. (2016) 76:1658. doi: 10.1158/1538-7445.AM2016-1658
13. Sirrenberg C, Zimmermann A, Grombacher T, Vassilev LT, Damstrup L, Zenke FT, et al. Abstract 4183: A novel selective DNA-PK inhibitor, M3814, as a potential combination partner of etoposide and cisplatin in the therapy of lung cancer. *Cancer Res*. (2017) 77:4183. doi: 10.1158/1538-7445.AM2017-4183
14. Szakács G, Paterson JK, Ludwig JA, Booth-Genthe C, Gottesman MM. Targeting multidrug resistance in cancer. *Nat Rev Drug Disc*. (2006) 5:219–34. doi: 10.1038/nrd1984
15. Alisi A, Cho WC, Locatelli F, Fruci D. Multidrug resistance and cancer stem cells in neuroblastoma and hepatoblastoma. *Int J Mol Sci*. (2013) 14:24706–25. doi: 10.3390/ijms141224706
16. Kartal-Yandim M, Adan-Gokbulut A, Baran Y. Molecular mechanisms of drug resistance and its reversal in cancer. *Critical Rev Biotechnol*. (2016) 36:716–26. doi: 10.3109/07388551.2015.1015957
17. Linton KJ, Higgins CF. Structure and function of ABC transporters: the ATP switch provides flexible control. *Pflugers Archiv Eur J Physiol*. (2007) 453:555–67. doi: 10.1007/s00424-006-0126-x
18. Robey RW, Pluchino KM, Hall MD, Fojo AT, Bates SE, Gottesman MM. Revisiting the role of ABC transporters in multidrug-resistant cancer. *Nat Rev Cancer*. (2018) 18:452–64. doi: 10.1038/s41568-018-0005-8
19. Bighetti-Trevisan RL, Sousa LO, Castilho RM, Almeida LO. Cancer stem cells: powerful targets to improve current anticancer therapeutics. *Stem Cells Int*. (2019) 2019:9618065. doi: 10.1155/2019/9618065
20. Doyle LA, Yang W, Abruzzo LV, Krogmann T, Gao Y, Rishi AK, et al. A multidrug resistance transporter from human MCF-7 breast cancer cells. *Proc Natl Acad Sci USA*. (1998) 95:15665–70. doi: 10.1073/pnas.95.26.15665
21. Nakatomi K, Yoshikawa M, Oka M, Ikegami Y, Hayasaka S, Sano K, et al. Transport of 7-ethyl-10-hydroxycamptothecin (SN-38) by breast cancer resistance protein ABCG2 in human lung cancer cells. *Biochem Biophys Res Commun*. (2001) 288:827–32. doi: 10.1006/bbrc.2001.5850
22. Robey RW, Medina-Pérez WY, Nishiyama K, Lahusen T, Miyake K, Litman T, et al. Overexpression of the ATP-binding cassette half-transporter, ABCG2 (Mxr/BCrp/ABCP1), in flavopiridol-resistant human breast cancer cells. *Clin Cancer Res*. (2001) 7:145–52.
23. Han J-Y, Lim H-S, Yoo Y-K, Shin ES, Park YH, Lee SY, et al. Associations of ABCB1, ABCC2, and ABCG2 polymorphisms with irinotecan-pharmacokinetics and clinical outcome in patients with advanced non-small cell lung cancer. *Cancer*. (2007) 110:138–47. doi: 10.1002/cncr.22760
24. Lemos C, Giovannetti E, Zucali PA, Assaraf YG, Scheffer GL, Van Der Straaten T, et al. Impact of ABCG2 polymorphisms on the clinical outcome and toxicity of gefitinib in non-small-cell lung cancer patients. *Pharmacogenomics*. (2011) 12:159–70. doi: 10.2217/pgs.10.172
25. Li F, Zeng H, Ying K. The combination of stem cell markers CD133 and ABCG2 predicts relapse in stage I non-small cell lung carcinomas. *Med Oncol*. (2011) 28:1458–62. doi: 10.1007/s12032-010-9646-5
26. Sun J, Zhu M, Shen W, Wang C, Dai J, Xu L, et al. A potentially functional polymorphism in ABCG2 predicts clinical outcome of non-small cell lung cancer in a Chinese population. *Pharmacogeno J*. (2017) 17:280–5. doi: 10.1038/tpj.2016.2
27. Yoh K, Ishii G, Yokose T, Minegishi Y, Tsuta K, Goto K, et al. Breast cancer resistance protein impacts clinical outcome in platinum-based

chemotherapy for advanced non-small cell lung *Cancer*. (2004) 10:1691–7. doi: 10.1158/1078-0432.CCR-0937-3
28. Rabindran SK, Ross DD, Doyle LA, Yang W, Greenberger LM. Fumitremorgin C reverses multidrug resistance in cells transfected with the breast cancer resistance protein. *Cancer Res*. (2000) 60:47–50.
29. Allen JD, Van Loevezijn A, Lakhai JM, Van Der Valk M, Van Tellingen O, Reid G, et al. Potent and specific inhibition of the breast cancer resistance protein multidrug transporter *in vitro* and in mouse intestine by a novel analogue of fumitremorgin C. *Mol Cancer Therap*. (2002) 1:417–25.
30. Ozvegy-Laczka C, Hegedus T, Várady G, Ujhelly O, Schuetz JD, Váradi A, et al. High-affinity interaction of tyrosine kinase inhibitors with the ABCG2 multidrug transporter. *Mol Pharmacol*. (2004) 65:1485–95. doi: 10.1124/mol.65.6.1485
31. Shi Z, Peng X-X, Kim I-W, Shukla S, Si Q-S, Robey RW, et al. Erlotinib (Tarceva, OSI-774) antagonizes ATP-binding cassette subfamily B member 1 and ATP-binding cassette subfamily G member 2-mediated drug resistance. *Cancer Res*. (2007) 67:11012–20. doi: 10.1158/0008-5472.CAN-07-2686
32. Robey RW, Honjo Y, Van De Laar A, Miyake K, Regis JT, Litman T, et al. A functional assay for detection of the mitoxantrone resistance protein, MXR (ABCG2). *Biochim Biophys Acta*. (2001) 1512:171–82. doi: 10.1016/S0005-2736(01)00308-X
33. Lyall RM, Hwang JL, Cardarelli C, Fitzgerald D, Akiyama S, Gottesman MM, et al. Isolation of human KB cell lines resistant to epidermal growth factor-pseudomonas exotoxin conjugates. *Cancer Res*. (1987) 47:2961–6.
34. Carmichael J, Degraff WG, Gazdar AF, Minna JD, Mitchell JB. Evaluation of a tetrazolium-based semiautomated colorimetric assay: assessment of chemosensitivity testing. *Cancer Res*. (1987) 47:936–42.
35. Fujii R, Mutoh M, Niwa K, Yamada K, Aikou T, Nakagawa M, et al. Active efflux system for cisplatin in cisplatin-resistant human KB cells. *Japan J Cancer Res*. (1994) 85:426–33. doi: 10.1111/j.1349-7006.1994.tb02376.x
36. Wu Z-X, Teng Q-X, Cai C-Y, Wang J-Q, Lei Z-N, Yang Y, et al. Tepotinib reverses ABCB1-mediated multidrug resistance in cancer cells. *Biochem Pharmacol*. (2019) 166:120–7. doi: 10.1016/j.bcp.2019.05.015
37. Jackson SM, Manolaridis I, Kowal J, Zechner M, Taylor NMI, Bause M, et al. Structural basis of small-molecule inhibition of human multidrug transporter ABCG2. *Nat Struct Mol Biol*. (2018) 25:333–40. doi: 10.1038/s41594-018-0049-1
38. Zhang Y-K, Wang Y-J, Lei Z-N, Zhang G-N, Zhang X-Y, Wang D-S, et al. Regorafenib antagonizes BCRP-mediated multidrug resistance in colon cancer. *Cancer Lett*. (2019) 442:104–12. doi: 10.1016/j.canlet.2018.10.032
39. Wu Z-X, Yang Y, Teng Q-X, Wang J-Q, Lei Z-N, Wang J-Q, et al. Tivantinib, A c-met inhibitor in clinical trials, is susceptible to ABCG2-mediated drug resistance. *Cancers*. (2020) 12:186. doi: 10.3390/cancers12010186
40. Toyoda Y, Takada T, Suzuki H. Inhibitors of human ABCG2: from technical background to recent updates with clinical implications. *Front Pharmacol*. (2019) 10:208. doi: 10.3389/fphar.2019.00208
41. Mizuno N, Suzuki M, Kusuhara H, Suzuki H, Takeuchi K, Niwa T, et al. Impaired renal excretion of 6-hydroxy-5,7-dimethyl-2-methylamino-4-(3-pyridylmethyl) benzothiazole (e3040) sulfate in breast cancer resistance protein (BCRP1/ABCG2) knockout mice. *Drug Metab Disposit*. (2004) 32:898.
42. Jonker JW, Merino G, Musters S, Van Herwaarden AE, Bolscher E, Wagenaar E, et al. The breast cancer resistance protein BCRP (ABCG2) concentrates drugs and carcinogenic xenotoxins into milk. *Nat Med*. (2005) 11:127–9. doi: 10.1038/nm1186
43. Ando T, Kusuhara H, Merino G, Alvarez AI, Schinkel AH, Sugiyama Y. Involvement of breast cancer resistance protein (ABCG2) in the biliary excretion mechanism of fluoroquinolones. *Drug Metab Disposit*. (2007) 35:1873. doi: 10.1124/dmd.107.014969
44. Ji N, Yang Y, Cai C-Y, Wang J-Q, Lei Z-N, Wu Z-X, et al. Midostaurin reverses ABCB1-mediated multidrug resistance, an *in vitro* study. *Front Oncol*. (2019) 9:514. doi: 10.3389/fonc.2019.00514
45. Wang J-Q, Wang B, Lei Z-N, Teng Q-X, Li JY, Zhang W, et al. Derivative of 5-cyano-6-phenylpyrimidin antagonizes ABCB1- and ABCG2-mediated multidrug resistance. *Eur J Pharmacol*. (2019) 863:172611. doi: 10.1016/j.ejphar.2019.172611
46. Wen Y, Zhao R, Gupta P, Fan Y, Zhang Y, Huang Z, et al. The epigallocatechin gallate derivative Y(6) reverses drug resistance mediated by the ABCB1 transporter both *in vitro* and *in vivo*. *Acta Pharm Sinica B*. (2019) 9:316–23. doi: 10.1016/j.apsb.2018.10.001
47. Chen Z-S, Robey RW, Belinsky MG, Shchaveleva I, Ren X-Q, Sugimoto Y, et al. Transport of methotrexate, methotrexate polyglutamates, and 17β-estradiol 17-(β-d-glucuronide) by ABCG2: effects of acquired mutations at R482 on methotrexate transport. *Cancer Res*. (2003) 63:4048.
48. Pozza A, Perez-Victoria JM, Sardo A, Ahmed-Belkacem A, Di Pietro A. Purification of breast cancer resistance protein ABCG2 and role of arginine-482. *Cell Mol Life Sci CMLS*. (2006) 63:1912–22. doi: 10.1007/s00018-006-6159-7
49. Ji N, Yang Y, Lei Z-N, Cai C-Y, Wang J-Q, Gupta P, et al. Ulixertinib (BVD-523) antagonizes ABCB1- and ABCG2-mediated chemotherapeutic drug resistance. *Biochem Pharmacol*. (2018) 158:274–85. doi: 10.1016/j.bcp.2018.10.028
50. Ji N, Yang Y, Cai C-Y, Lei Z-N, Wang J-Q, Gupta P, et al. Selonsertib (GS-4997), an ASK1 inhibitor, antagonizes multidrug resistance in ABCB1- and ABCG2-overexpressing cancer cells. *Cancer Lett*. (2019) 440–1:82–93. doi: 10.1016/j.canlet.2018.10.007
51. Sorf A, Hofman J, Kučera R, Staud F, Ceckova M. Ribociclib shows potential for pharmacokinetic drug-drug interactions being a substrate of ABCB1 and potent inhibitor of ABCB1, ABCG2 and CYP450 isoforms *in vitro*. *Biochem Pharmacol*. (2018) 154:10–7. doi: 10.1016/j.bcp.2018.04.013
52. Zhang G-N, Zhang Y-K, Wang Y-J, Gupta P, Ashby CR Jr, Alqahtani S, et al. Epidermal growth factor receptor (EGFR) inhibitor PD153035 reverses ABCG2-mediated multidrug resistance in non-small cell lung cancer: *in vitro* and *in vivo*. *Cancer Lett*. (2018) 424:19–29. doi: 10.1016/j.canlet.2018.02.040
53. Zhang Z, Guo X, To KKW, Chen Z, Fang X, Luo M, et al. Olmutinib (HM61713) reversed multidrug resistance by inhibiting the activity of ATP-binding cassette subfamily G member 2 *in vitro* and *in vivo*. *Acta Pharm Sinica B*. (2018) 8:563–74. doi: 10.1016/j.apsb.2018.06.002
54. Wu C-P, Murakami M, Hsiao S-H, Liu T-C, Yeh N, Li Y-Q, et al. SIS3, a specific inhibitor of Smad3 reverses ABCB1- and ABCG2-mediated multidrug resistance in cancer cell lines. *Cancer Lett*. (2018) 433:259–72. doi: 10.1016/j.canlet.2018.07.004
55. Cole SP, Bhardwaj G, Gerlach JH, Mackie JE, Grant CE, Almquist KC, et al. Overexpression of a transporter gene in a multidrug-resistant human lung cancer cell line. *Science*. (1992) 258:1650–4. doi: 10.1126/science.1360704
56. Oguri T, Ozasa H, Uemura T, Bessho Y, Miyazaki M, Maeno K, et al. MRP7/ABCC10 expression is a predictive biomarker for the resistance to paclitaxel in non-small cell lung cancer. *Mol Cancer Ther*. (2008) 7:1150–5. doi: 10.1158/1535-7163.MCT-07-2088
57. Zhang W, Fan Y-F, Cai C-Y, Wang J-Q, Teng Q-X, Lei Z-N, et al. Olmutinib (BI1482694/HM61713), a novel epidermal growth factor receptor tyrosine kinase inhibitor, reverses ABCG2-mediated multidrug resistance in cancer cells. *Front Pharmacol*. (2018) 9:1097. doi: 10.3389/fphar.2018.01097
58. Giri N, Agarwal S, Shaik N, Pan G, Chen Y, Elmquist WF. Substrate-dependent breast cancer resistance protein (Bcrp1/Abcg2)-mediated interactions: consideration of multiple binding sites in *in vitro* assay design. *Drug Metab Disposit*. (2009) 37:560–70. doi: 10.1124/dmd.108.022046

59. Mao Q, Unadkat JD. Role of the breast cancer resistance protein (BCRP/ABCG2) in drug transport–an update. *AAPS J*. (2015) 17:65–82. doi: 10.1208/s12248-014-9668-6
60. Zhang G-N, Zhang Y-K, Wang Y-J, Barbuti AM, Zhu X-J, Yu X-Y, et al. Modulating the function of ATP-binding cassette subfamily G member 2 (ABCG2) with inhibitor cabozantinib. *Pharmacol Res*. (2017) 119:89–98. doi: 10.1016/j.phrs.2017.01.024
61. Ge C, Wang F, Cui C, Su X, To KKW, Wang X, et al. PCI29732, a bruton's tyrosine kinase inhibitor, enhanced the efficacy of conventional chemotherapeutic agents in ABCG2-overexpressing cancer cells. *Cell Physiol Biochem*. (2018) 48:2302–17. doi: 10.1159/000492647
62. Wu C-P, Lusvarghi S, Wang J-C, Hsiao S-H, Huang Y-H, Hung T-H, et al. Avapritinib: a selective inhibitor of KIT and PDGFRα that reverses ABCB1 and ABCG2-mediated multidrug resistance in cancer cell lines. *Mol Pharm*. (2019) 16:3040–52. doi: 10.1021/acs.molpharmaceut.9b00274
63. Wu C-P, Lusvarghi S, Wang J-C, Hsiao S-H, Huang Y-H, Hung T-H, et al. The selective class IIa histone deacetylase inhibitor TMP195 resensitizes ABCB1- and ABCG2-overexpressing multidrug-resistant cancer cells to cytotoxic anticancer drugs. *Int J Mol Sci*. (2019) 21:E238. doi: 10.3390/ijms21010238
64. Ramírez D, Caballero J. Is it reliable to take the molecular docking top scoring position as the best solution without considering available structural data? *Molecules*. (2018) 23:1038. doi: 10.3390/molecules23051038

Conflict of Interest: The authors declare that the research was conducted in the absence of any commercial or financial relationships that could be construed as a potential conflict of interest.

frontiers in Pharmacology

SYSTEMATIC REVIEW
published: 27 May 2020
doi: 10.3389/fphar.2020.00788

Protective Role of Enalapril in Anthracycline-Induced Cardiotoxicity: A Systematic Review

Yili Zhang[1†], Junjie Liu[2†], Yuan Li[2†], Nannan Tan[1†], Kangjia Du[1], Huihui Zhao[1,3], Juan Wang[1,3], Jian Zhang[4], Wei Wang[1,3*] and Yong Wang[1*]*

[1] School of Traditional Chinese Medicine, Beijing University of Chinese Medicine, Beijing, China, [2] Dongzhimen Hospital, Beijing University of Chinese Medicine, Beijing, China, [3] Ministry of Education Key Laboratory of TCM Syndrome and Formula & Beijing Key Laboratory of TCM Syndrome and Formula, Beijing, China, [4] School of Life Science, Beijing University of Chinese Medicine, Beijing, China

OPEN ACCESS

Edited by:
Khalid A El Sayed, University of Louisiana at Monroe, United States

Reviewed by:
Sri Krishna Chaitanya Arudra, Sanford Medical Center, United States
Daniela Cardinale, European Institute of Oncology (IEO), Italy
Timothy C. Tan, Westmead Hospital, Australia

***Correspondence:**
Jian Zhang
zhangjian@bucm.edu.cn
Wei Wang
wangwei@bucm.edu.cn
Yong Wang
wangyong0201@163.com

[†]These authors have contributed equally to this work

Specialty section:
This article was submitted to Pharmacology of Anti-Cancer Drugs, a section of the journal Frontiers in Pharmacology

Received: *01 February 2020*
Accepted: *12 May 2020*
Published: *27 May 2020*

Citation:
Zhang Y, Liu J, Li Y, Tan N, Du K, Zhao H, Wang J, Zhang J, Wang W and Wang Y (2020) Protective Role of Enalapril in Anthracycline-Induced Cardiotoxicity: A Systematic Review. Front. Pharmacol. 11:788. doi: 10.3389/fphar.2020.00788

Background: Evidence of the preventive and therapeutic effects of enalapril on cardiotoxicity caused by chemotherapy needs to be further confirmed and updated.

Methods: We performed a systematic review of studies from electronic databases that were searched from inception to January 29, 2019, and included relevant studies analyzing enalapril as a cardioprotective agent before or during the use of anthracyclines by oncology patients. Homogeneous results from different studies were pooled using RevMan 5.3 software. The Cochrane risk-of-bias tool was used to determine the quality of the studies.

Results: We examined and screened 626 studies according to specific criteria and ultimately included seven studies that were relevant to the indicated topic. Among them, three studies reported the incidence of death during 6- and 12-month follow-up periods. Six of the seven included studies showed possible positive results, suggesting that enalapril plays a cardioprotective role, while five of these studies showed that there was a significant difference in the left ventricular ejection fraction (LVEF) between an enalapril group and a control group (weighted mean difference (WMD) = 7.18, 95% CI: 2.49–11.87, $I^2 = 96\%$, $P < .001$). Moreover, enalapril was beneficial in reducing troponin I (TnI), creatine kinase myocardial band (CK-MB) and N-terminal pro-b-type natriuretic peptide (NT-proBNP) levels in cancer patients treated with anthracycline.

Conclusions: Although a protective effect of enalapril on myocardial toxicity was observed in terms of the LVEF values and TnI, CK-MB and NT-proBNP levels, its use in the prevention and treatment of cardiotoxicity caused by anthracycline needs to be investigated by more scientific research.

Keywords: cardioprotection, onco-cardiology, chemotherapy, evidence-based medicine, anthracycline

INTRODUCTION

With the rapid increase in the global population and the development of an aging society, cancer is becoming increasingly prominent as a leading cause of death (GBD 2016 Causes of Death Collaborators, 2017). According to statistics from the International Agency for Research on Cancer, there were an estimated 18.1 million new cancer cases and 9.6 million cancer-related deaths in 2018 (Rebecca et al., 2018). Nevertheless, the great progress in therapeutic strategies for various tumors has led to a longer life and a higher quality of life (Rohit and Yeh, 2016), which has enabled observations of the side effects of anticancer therapy and increased morbidity and mortality from other causes.

The antibiotic anthracycline (represented by doxorubicin (DOX)) is highly effective and is currently the most commonly used chemotherapeutic drug for various cancers, including leukemia, solid tumors, soft tissue sarcomas and breast cancer (Damiani et al., 2016; Songbo et al., 2019). However, anthracycline-related cardiac toxicity is reportedly as high as 57%, and the mortality rate from these heart diseases is reportedly 8.2 times higher than that in normal persons (Brewster et al., 2014), substantially limiting its clinical application. Only one drug, dexrazoxane, is approved by the US Food and Drug Administration (FDA) to be indicated for contributing a certain protective effect in patients with cardiotoxicity; however, its use is limited to patients receiving a high cumulative dose of anthracyclines (Tomlinson et al., 2019). In July 2011, the FDA released a declaration restricting the use of dexrazoxane to adult patients with cancer who receive >300 mg/m^2 doxorubicin (an anthracycline) or >540 mg/m^2 epirubicin (another chemotherapeutic agent) and have general approval for the use of dexrazoxane for cardioprotection (Tebbi et al., 2007; Salzer et al., 2010). Furthermore, several previous studies have shown that dexrazoxane may increase the incidence of myelodysplastic syndrome and secondary cancers (Tebbi et al., 2007). The Committee for Medicinal Products for Human Use (CHMP) in the UK even recommended a few restrictions on the use of dexrazoxane in both children and adults with cancer (EMA, 2019). Therefore, there is an urgent need to identify the underlying mechanism and novel therapeutic agents that can prevent and/or reverse cancer treatment-induced cardiovascular adverse effects.

Angiotensin-converting enzyme inhibitors (ACEIs) (Cardinale et al., 2006; Zamani et al., 2018) are considered promising cardioprotective agents that can be used for cardiac protection during chemotherapy. The mechanism of cardiac protection is mainly related to the SDF-1a/CXCR4 axis (Wen et al., 2012), hypoxia-inducible factor-1a (HIF-1a) upregulation (Luft, 2017; Zhang and Lin, 2010), nuclear factor kappa-light-chain-enhancer of activated B cells axis (Puddighinu et al., 2018) and a decrease in ROS (Heusch, 2012).

At present, some new clinical trials and meta-analyses (Conway et al., 2015; Gupta et al., 2018) assessing the use of ACEIs for anthracycline-induced cardiotoxicity have been published and may provide higher quality evidence suggesting that ACEIs are effective as cardioprotective agents. Given that existing evidence, therefore, we have the opportunity to perform this systematic review of randomized controlled trials (RCTs) to expand and update knowledge of cardioprotective role of ACEIs on anthracycline-induced cardiotoxicity. We hope that the findings of this study strengthen the evidence of the effectiveness of enalapril with regard to the prevention and treatment of anthracycline-induced cardiotoxicity.

MATERIALS AND METHODS

This study was registered at PROSPERO (registration number: CRD42019124671; http://www.crd.york.ac.uk/PROSPERO). This meta-analysis was conducted based on the Preferred Reporting Items for Systematic Reviews and Meta-analysis (PRISMA) criteria.

Types of Studies

We included all prospective RCTs focusing on enalapril as a strategy for the treatment of cardiotoxicity caused by anthracycline. Crossover trials, quasi-RCTs, animal experiments and other studies published repeatedly or without access to complete data were excluded.

Types of Participants

Participants who accepted conventional chemotherapy were eligible. All participants were included in this review regardless of age, race, sex and cancer type.

Types of Interventions

We only included studies in which interventions, including enalapril alone or combined with other agents, were used to prevent the toxic effects of anthracycline on the heart regardless of duration or dosage.

Types of Comparisons

Control groups that could be used to show the cardioprotective role of enalapril were considered.

Types of Outcomes

The primary outcomes were death from any cause and changes in the left ventricular ejection fraction (LVEF) measured by conventional echocardiographic parameters. The secondary outcomes mainly focused on conventional echocardiographic parameters (except for LVEF), cardiac biomarkers (plasma brain natriuretic peptide, plasma myocardial enzyme, and troponin I (TnI) levels) and adverse events.

Information Sources and Search Strategy

A comprehensive search strategy was carried out that included searches of PubMed/Medline (from inception to January 2019), EMBASE (from inception to January 2019), the Cochrane Library (from inception to January 2019) and ClinicalTrials.gov (from inception to January 2019). The studies that met the inclusion criteria were searched. The following search terms were searched individually or jointly at the time of retrieval: 'enalapril', 'ace-inhibitor', 'angiotensin-

converting enzyme inhibitors', 'ace inhibitor', 'angiotensin converting enzyme inhibitors', 'angiotensin-converting enzyme antagonists', 'angiotensin converting enzyme antagonists', 'ACE inhibitors', 'cancer', 'tumor', 'malignant', and 'solid tumor'. Only studies published in English were considered. NoteExpress 3.0 Software was used to manage the literature.

Study Selection and Study Quality Assessment

Two reviewers independently screened the literature and recorded the reasons for exclusion. At the time of data extraction, a "table of characteristics" was generated to extract information regarding the included trials, including the author, age of the participants, diagnostic criteria, sample size of the experimental group and control group, intervention applied to the two groups, outcomes and adverse events. The methodological quality of the RCTs was assessed independently per the Cochrane Handbook for Systematic Review of Interventions, Version 5.1.0., including randomness, blindness, outcome reporting and other bias. The evaluation degree of each item was divided into the following three grades: low bias risk, high bias risk and unclear bias risk. The evaluation of the methodological quality was performed independently by two reviewers, and discrepancies were solved through mutual consensus.

Data Analysis

RevMan 5.3 software was used for the meta-analytic calculations. The Q test was conducted to estimate the total percentage of variation in each study derived from heterogeneity rather than chance, and the I^2 statistic was used to quantify the heterogeneity. The model used to synthesize the data needed to consider the existence and degree of heterogeneity. For instance, if the I^2 statistic was less than 50% and the P-value was more than 0.1, the fixed-effects model was chosen. If the P-value was less than 0.1, the treatment effects were calculated with a random-effects model. Random effect models were used for the subgroup analysis and when significant heterogeneity existed among the studies. According to the Cochrane Handbook version 5.1.0, a random-effects meta-analysis model involves an assumption that the effects being estimated in the different studies are not identical but follow some distribution. The model represents our lack of knowledge about why real, or apparent, intervention effects differ by considering the differences as if they were random. The center of this distribution describes the average of the effects, while its width describes the degree of heterogeneity.

For the dichotomous variables, the pooled relative risk (RR) and 95% CI were used as the effect measures. For the continuous outcomes, the weighted mean difference (WMD) was used when the units of the outcomes were the same, while the standardized mean difference (SMD) was used when the units and/or measurement methods of the outcomes were inconsistent. If fewer than two studies reported the same results or the heterogeneity among the studies was obvious, the results of our systematic review are narratively reported.

Subgroup Analysis and Sensitivity Analysis

To solve the problems of heterogeneity and secondary analysis, the subgroup analysis was very important. A sensitivity analysis was also implemented from the methodological, statistical and clinical aspects to explore potential sources of heterogeneity. When the results of different experiments greatly varied and the heterogeneity test showed significant differences, we removed one trial that significantly differed from the other trials (due to clinical, methodological, or other factors) and then combined the remaining studies to compare the before and after results. For any meta-analysis involving 10 or more studies, we used funnel diagrams to assess the possibility of publication bias (Kakia et al., 2016).

RESULTS

Search Results and Study Characteristics

Initially, the literature search yielded 626 citations concerning enalapril for the treatment or prevention of cardiotoxicity from an electronic database (**Figure 1**). After the two reviewers screened the title, abstract and full text of each citation according to the inclusion criteria, 619 articles were excluded as duplicates, non-RCTs, reviews, retrospective studies or studies with objectives that differed from the aim of this review. Ultimately, seven RCTs were included, and we analyzed the quantitative data reported in five studies.

In total, 848 participants were included in this systematic review. Of these participants, 382 were treated with enalapril. In addition, 137 patients in Cardinale's study (Cardinale et al., 2018) started taking enalapril only during or after an increase in troponin was evident during chemotherapy. Forty-five patients in one trial (Bosch et al., 2013) received a combination treatment of enalapril and carvedilol. The trials included patients with pediatric cancer, breast cancer, lymphoma, multiple myeloma, lung cancer and other malignancies. The baseline LVEF was comparable between the experimental and control groups in all studies. The duration of follow-up in the selected studies ranged from 6 to 36 months. Seven trials were conducted in different countries, including the US, Italy, Greece, Spain, Iran, and India. The details of the characteristics of the seven included trials are provided in **Table 1**.

Methodological Quality

Regarding random sequence generation, three studies (Cardinale et al., 2006; Bosch et al., 2013; Cardinale et al., 2018) were conducted with appropriate randomization based on numbers generated with an electronic computer. The other trials only briefly mentioned 'random' without providing a detailed description of the specific method. Three studies (Cardinale et al., 2006; Bosch et al., 2013; Cardinale et al., 2018) described the details of the allocation concealment (using central dispensation or numbered envelopes). Two open-labeled trials (Cardinale et al., 2006; Cardinale et al., 2018) were classified as 'high risk' in terms of blinding. Except for the studies by Silber

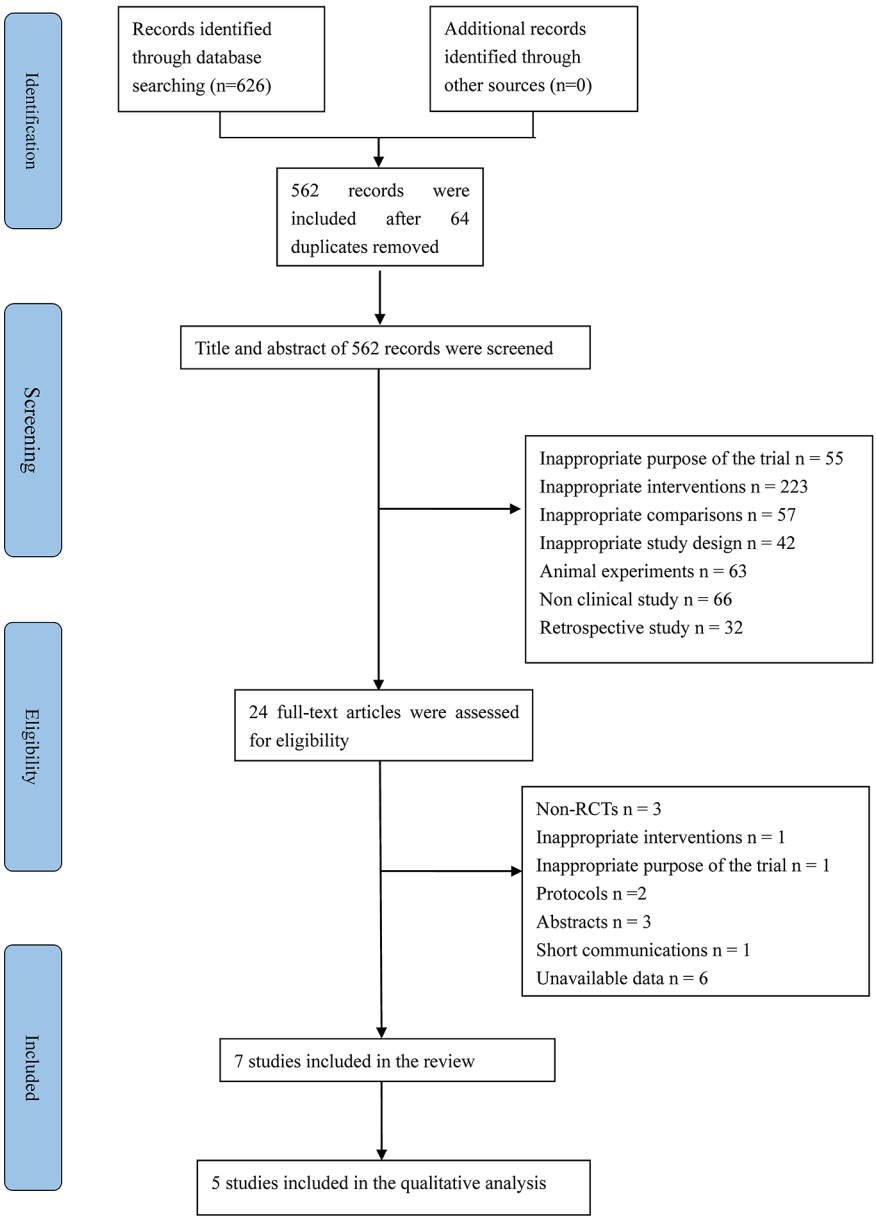

FIGURE 1 | PRISMA flow diagram. RCTs, randomized controlled trials; PRISMA, Preffered Reporting Items for Systematic review and Meta-Analysis.

et al. (2004), Janbabai et al. (2017) and Gupta et al. (2018), the other studies did not report the methods used to blind the participants, researchers or outcome assessments. All studies claimed to have good baseline consistency with a trial registration number, and the attrition in both groups seemed balanced such that incomplete outcome data and selective reporting were deemed to be at a low risk. Additionally, none of the studies mentioned the other bias items. A risk-of-bias graph is shown in **Figure 2**.

Effects of Therapy

Death From Any Cause

Three studies (Bosch et al., 2013; Janbabai et al., 2017; Cardinale et al., 2018) reported the incidence of death during 6- and 12-month follow-up periods. Considering the potential clinical heterogeneity of the interventions (enalapril plus carvedilol vs. no treatment; enalapril vs. placebo; and enalapril in all patients started before chemotherapy vs. enalapril started only in patients with an increase in troponin during or after chemotherapy) and

TABLE 1 | Characteristics of the included trials.

Study ID	Sample size (EG/CG)	Median age	Types of cancer	Patients and detailed chemo-therapy or radiotherapy	Intervention		Baseline LVEF		Follow-up duration	Outcomes
					EG	CG	EG	CG		
Silber et al., 2004	69/66	EG: 17.8 ± 5.60 CG: 18.9 ± 6.17	Long-term survivors of pediatric cancers	The target population consisted of patients aged 8 years and older who developed cancer before the age of 20 years and had been treated with anthracyclines.	Enalapril	Placebo	NR	NR	Mean follow-up duration of 34.6 months	The rate of change in the MCI and LVESWS, stress-velocity index, left ventricular shortening fraction, adverse events, functional status, and quality of life
Cardinale et al., 2006	56/58	45 ± 12	Breast cancer, acute myeloid leukemia, etc.	High-dose chemotherapy including carmustine, etoposide, cytarabine, melphalan, daunorubicin, carboplatin, idarubicin, mitoxantrone, epirubicin, etc.	Enalapril	None	NR	NR	12 months	The occurrence of cardiotoxicity, efficacy of enalapril on LVEF, and adverse cardiac events
Georgakopoulos et al., 2010	43/40	EG: 47.4 ± 16.2 CG: 49.1 ± 19.4	Lymphoma	The CT regimen consisted of 6–8 cycles of the "ABVD schema" for HL as follows: doxorubicin (25 mg/m^2), bleomycin (10 mg/m^2), vinblastine (6 mg/m^2), and dacarbazine (375 mg/m^2) intravenously on day 1 and day 15 every 4 weeks. The NHL patients received the "R-CHOP schema" as follows: rituximab (375 mg/m^2), cyclophosphamide (750 mg/m^2), doxorubicin (50 mg/m^2), and vincristine (1.4 mg/m^2) intravenously on day 1 and prednisolone (100 mg/m^2) orally on days 1–5 every 3 weeks.	Enalapril	None	65.2 ± 7.1	67.6 ± 7.1	36 months	Echocardiographic evaluations
Bosch et al., 2013	45/45	50 ± 13	Acute leukemia, relapsed or refractory; Hodgkin's and non-Hodgkin's lymphoma; and multiple myeloma	NR	Enalapril and carvedilol	None	NR	NR	6 months	Global LVEF, TnI and BNP levels, incidence of death, heart failure or significant LVSD, diastolic function, and incidence of severe life-threatening adverse events
Janbabai et al., 2017	34/35	EG: 47.76 ± 11.81 CG: 47.06 ± 12.39	Breast cancer (60 patients), Hodgkin's lymphoma (six patients), Wilms tumor (one patient), lung cancer (one patient) and bone sarcoma (one patient)	Sixty patients had breast cancer and received doxorubicin and cyclophosphamide; six patients had Hodgkin's lymphoma and underwent R-CHOP chemotherapy, which included rituximab, cyclophosphamide, doxorubicin, vincristine, and prednisolone; one patient had a Wilms tumor and received vincristine, dactinomycin, doxorubicin, cyclophosphamide, and etoposide; one patient had lung cancer and received vincristine, doxorubicin, and cyclophosphamide; and one patient had bone sarcoma and received cisplatin and doxorubicin. All patients received doxorubicin, and most patients received cyclophosphamide. None of the patients received trastuzumab or radiotherapy during the 6-month follow-up period.	Enalapril	Placebo	59.39 ± 6.95	59.61 ± 5.70	6 months	Changes from baseline in LVEF, troponin I and CK-MB levels and the incidences of death, HF, significant LV systolic dysfunction, diastolic dysfunction, and severe life-threatening adverse events

(Continued)

TABLE 1 | Continued

Study ID	Sample size (EG/CG)	Median age	Types of cancer	Patients and detailed chemotherapy or radiotherapy	Intervention		Baseline LVEF		Follow-up duration	Outcomes
					EG	CG	EG	CG		
Cardinale et al., 2018	136/137	51 ± 12	Breast cancer; acute leukemia, non-Hodgkin's lymphoma; Hodgkin's lymphoma; lymphoma, unspecified type; sarcoma; etc.	The median number of cycles of anthracyclines was four cycles delivered over 65 days. Epirubicin and doxorubicin were the most commonly prescribed anthracyclines with a median cumulative dose of 360 and 240 mg/m^2, respectively. In total, 63% of the patients with breast cancer were treated with taxanes, and 22.5% of the patients were treated with trastuzumab. In total, two patients were treated with a tyrosine-kinase inhibitor, imatinib.	Enalapril in all patients was started before chemotherapy	Enalapril started only in patients with an increase in troponin during or after chemotherapy	63.5 ± 5.9	63.9 ± 6.1	12 months	An incidence of troponin elevation above the threshold, LVEF <50% and >10% LVEF reduction, death from cardiovascular causes, death from any cause, hospitalization for cardiovascular causes, and major adverse cardiovascular events
Gupta et al., 2018	44/40	EG: 8.85 ± 3.15 CG: 8.77 ± 2.86	Acute lymphoblastic leukemia/lymphoma	Projected cumulative anthracycline dose was ≥200 mg/m^2.	Enalapril	Placebo	65.73 ± 5.41	64.85 ± 4.94	6 months	LVEF, changes in cardiac biomarkers, and the development of heart failure or arrhythmias

CG, control group; CK-MB, creatinine kinase-MB; EG, experimental group; NR, not reported; FS, fractional shortening; LVESWS, left ventricular end-systolic wall stress; MCI, maximum cardiac index; HL, Hodgkin lymphoma; NHL, non-Hodgkin lymphoma; HF, heart failure; LA, left atrium; LVEDD, left ventricular end-diastolic dimension; LVEDS, left ventricular end-systolic dimension; LVEDV, left ventricular end-diastolic volume; LVEF, left ventricular ejection fraction; LVESV, left ventricular end-systolic volume; LVSD, left ventricular systolic dysfunction.

the different characteristics of the participants, these studies were examined as separate individual studies in the assessment. During the study implementation (Bosch et al., 2013), 11 patients were excluded from the study due to their deaths (four cancer-related deaths and seven infection-related deaths). In the ICOS-ONE trial (Cardinale et al., 2018), 10 patients died (3.7%) during the 1-year follow-up period, including eight patients in the experimental group and two patients in the control group. These deaths were all due to non-cardiovascular causes and were related to cancer progression (70%) or infection (30%). However, none of the patients died during the follow-up period in Janbabai's study (Janbabai et al., 2017) in which the patients seemed to have a better risk control state. In addition, this finding may be related to the regimen and duration of chemotherapy.

Therefore, based on the studies examined, no conclusion can be drawn regarding the influence on cardiac-related mortality.

Changes in Cardiac Function: LVEF Value

Five studies (Cardinale et al., 2006; Georgakopoulos et al., 2010; Bosch et al., 2013; Janbabai et al., 2017; Gupta et al., 2018) reported changes in the LVEF values *via* different control measurements. Of these studies, three studies (Cardinale et al., 2006; Georgakopoulos et al., 2010; Bosch et al., 2013) combined enalapril with no treatment, and each of the other two studies had different participants. Therefore, we combined the three studies into a subgroup while separately calculating the effects of the other two studies to generate an overall meta-analysis. The data of the five combined studies showed that the LVEF value in the intervention group after chemotherapy was significantly higher than that in the control group (WMD = 7.18, 95% CI: 2.49–11.87, P < .001) (**Figure 3**). However, substantial heterogeneity still existed among the studies after the subgroup analysis. The sensitivity analysis found that the results of one study (Georgakopoulos et al., 2010) contradicted those of the other studies, which affected the robustness of the pooling effect. After excluding this study, there was no significant change in the LVEF value compared to the original result. Furthermore, a tendency toward the opposite result did not occur when any of the studies were excluded, indicating that the stability of the current results is trustworthy.

Conventional Echocardiographic Parameters (Other Than LVEF)

Three RCTs (Cardinale et al., 2006; Georgakopoulos et al., 2010; Janbabai et al., 2017) evaluated the morphology and function of the heart by conventional echocardiography, but the selection of evaluation indexes was inconsistent. A meta-analysis could only be performed on the E/A index but showed no statistically significant differences between the two groups. A summary of the conventional echocardiographic parameters is provided in **Table 2**.

Cardiac Biomarkers: Troponin I

An Italian trial (Cardinale et al., 2006) reported that compared with the ACEI group, a percentage of patients in the control group showed an increased TnI value during follow-up, and the

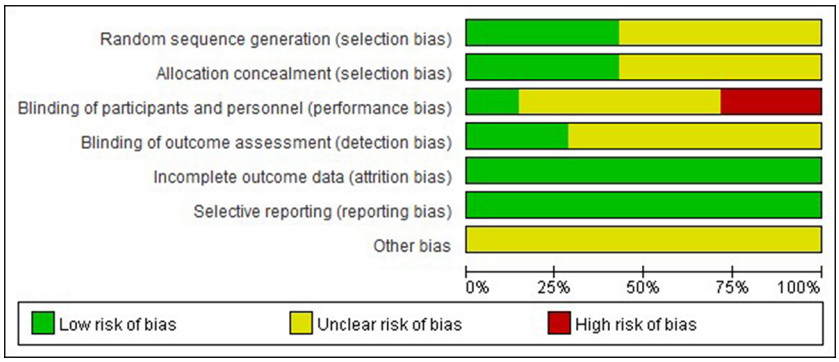

FIGURE 2 | Risk of bias graph.

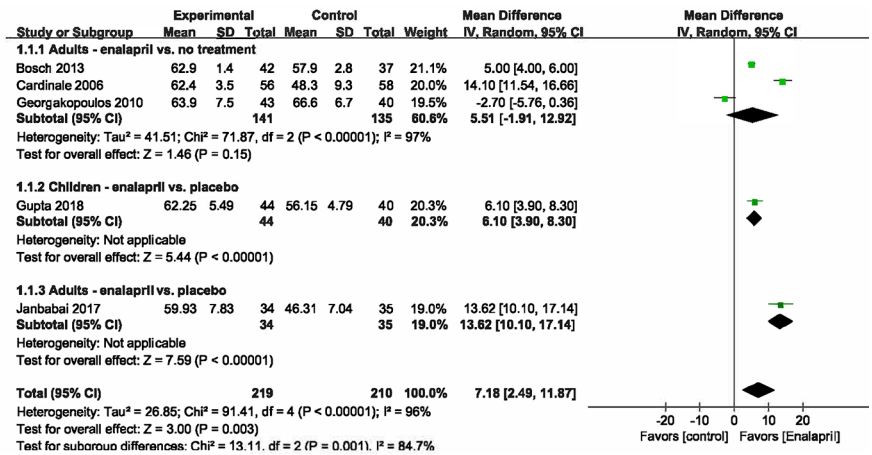

FIGURE 3 | Meta analysis for LVEF value.

TABLE 2 | Summary of the conventional echocardiographic parameters reported (other than the LVEF).

Parameter	Studies	WMD (95% CI)	*P*-value	P of heterogeneity	I^2
EDV	Cardinale et al., 2006	–3.10 [–12.65, 6.45]	0.52	–	–
ESV	Cardinale et al., 2006	15.90 [9.90, 21.90]	P < 0.00001	–	–
LVEDD	Georgakopoulos et al., 2010	0.20 [–0.02, 0.42]	0.07	–	–
LVESD	Georgakopoulos et al., 2010	0.20 [0.01, 0.39]	0.04	–	–
FS %	Georgakopoulos et al., 2010	–1.60 [–3.82, 0.62]	0.16	–	–
E/A, ratio	Georgakopoulos et al., 2010; Janbabai et al., 2017	0.00 [–0.11, 0.11]	1.00	1.00	0%
E/E a	Georgakopoulos et al., 2010	–0.30 [–0.91, 0.31]	0.33	–	–
LVEDV (cm^3)	Janbabai et al., 2017	–10.65 [–19.57, –1.73]	0.02	–	–
LVESV (cm^3)	Janbabai et al., 2017	–19.39 [–25.56, –13.22]	P < 0.00001	–	–
LA	Janbabai et al., 2017	–0.07 [–0.25, 0.11]	0.45	–	–
AR (m/s)	Janbabai et al., 2017	–0.02 [–0.06, 0.02]	0.33	–	–

AR, aortic regurgitation; EDV, end-diastolic volume; ESV, end-systolic volume; FS, fractional shortening; LA, left atrium; LVEDD, left ventricular end-diastolic dimension; LVEDS, left ventricular end-systolic dimension; LVEDV, left ventricular end-diastolic volume; LVESV, left ventricular end-systolic volume.

mean TnI value was higher in the control group (WMD = −0.02, 95% CI: −0.04 – −0.00, P =.01). Bosch's trial (Bosch et al., 2013) demonstrated no statistically significant differences between the two groups in the incidence of troponin I elevation at the end of or soon after a cycle of chemotherapy. One pediatric study (Gupta et al., 2018) showed elevated cTnI levels at 6 months in both groups, whereas the cTnI levels in the placebo group were significantly higher than those in the enalapril group.

Other Biomarkers

One study (Bosch et al., 2013) reported the b-type natriuretic peptide (BNP) levels after 6 months of follow-up. However, the results suggested that there were no significant differences between the two groups when the BNP levels were >80 ng/l or >200 ng/l. Another study (Janbabai et al., 2017) showed that enalapril reduced the creatine kinase myocardial band (CK-MB) levels more favorably using a Mann–Whitney U-test (control group median = 20.27 ng/ml, 95% CI: 18.75–21.25; enalapril group median = 16.44 ng/ml, 95% CI: 15.46–18.75, P =.006). The only pediatric study (Gupta et al., 2018) in this analysis reported proBNP and CK-MB levels. There was a significant difference in the proBNP level at 6 months (49.60 ± 35.97 vs. 98.60 ± 54.24, P < .001) between the two groups, but no difference was found in the levels of CK-MB (P =.08).

Adverse Events

Five included studies (Silber et al., 2004; Cardinale et al., 2006; Bosch et al., 2013; Janbabai et al., 2017; Cardinale et al., 2018) described adverse events during the trial. Silber's study reported that the side effects of enalapril include dizziness or low blood pressure (22% vs. 3% in the placebo group; P < .001) and fatigue (10% vs. 0%; P =.01). In another study, in total, 31 cardiac adverse events occurred during follow-up. Overall, the number of events, including sudden death, cardiac death, and acute pulmonary edema, in the control group was higher than that in the enalapril group. Bosch's trial showed that nine patients and 15 patients in the intervention group and control group, respectively, had life-threatening adverse events due to sepsis. The results of the other two studies showed that safety was relatively good. One study did not find any adverse events possibly because the participants had a more favorable risk profile. Another study found that only 15% of the entire population stopped treatment with the drug, and no serious adverse drug reactions (ADRs) were reported.

DISCUSSION

Based on the results of different individual original studies, regarding the LVESV value, the rate of change in the left ventricular end-systolic wall stress (LVESWS), and troponin I, proBNP and CK-MB levels, enalapril still has a protective effect on the chemotherapy cycles of cancer patients. However, a conclusion regarding whether angiotensin antagonist-based prevention translates into a reduction in adverse events cannot be clearly drawn from our study, although the incidence of cardiac events in the general analysis was nominally better in the prevention group.

The current work is a comprehensive systematic review focusing on the use of enalapril in the treatment or prevention of cardiotoxicity. Prior to this, some systematic reviews have described the role of ACEIs as preventive agents for health problems, such as heart failure (Turgeon et al., 2019) and hypertension (Dimou et al., 2018). Over the past decade, cardiologists have carried out multiple small clinical trials with drugs typically used for heart failure therapy, such as ACEIs, to provide either primary or secondary prevention for anthracycline-induced cardiotoxic effects (Kaya et al., 2013). These studies have shown benefits; however, the short-term benefits may be due to hemodynamic changes rather than real heart protection. Therefore, larger and longer-term clinical studies are needed to demonstrate the true efficacy of these drugs. In addition, to meet the needs of an increasing number of cancer survivors, new insight based on mechanistic research or genetic discovery is needed to pave the way for better prevention, diagnosis and treatment of cardiovascular complications caused by cancer treatment.

In recent years, strain imaging based on echocardiography has been used identify early subclinical changes in left ventricular systolic function during cancer treatment. A number of studies have shown that global longitudinal strain (GLS) can be used as a predictor of cardiotoxicity and can detect early declines in ventricular mechanics prior to an overt reduction in LVEF (El-Sherbeny et al., 2019; Arciniegas Calle et al., 2018; Potter and Marwick, 2018). In clinical practice, GLS can also help reconcile the significance of asymptomatic fluctuations in LVEF, which occur during serial imaging (Robert et al., 2019). However, it is regrettable that there is still a lack of studies that have evaluated the effect of enalapril on GLS. Further investigation is needed to determine whether the inclusion of GLS measurements in current clinical practice will improve cardiac outcomes among patients receiving cardiotoxic cancer therapy.

Although the association between cardiotoxicity and the use of anthracyclines has been known for many decades, five of the seven studies included in this review were published in the last decade, demonstrating the increased interest in this topic in recent years. However, since all studies were single-center studies and the sample sizes were small, the generalizability of these studies is limited despite the similar results obtained by most groups. In addition, although more than two major databases were searched to identify published studies, there was no guarantee that all studies that meet the inclusion criteria were retrieved for this systematic review. Additionally, Bosch's study used carvedilol in combination with enalapril as an intervention; thus, the efficacy of enalapril could not be analyzed separately. However, given the scientific value and methodological robustness of the study, we included this study in the evaluation.

ACEIs are widely used in the clinic because of their class effect. The reason we focused on enalapril in this study was that different ACEIs may involve combinations of drugs, indications and applicable objects in clinical practice. The ultimate purpose of this study was to provide high-quality evidence to inform

clinical decision making regarding specific drugs. If all the specific drugs had been included in the analysis, the extrapolation of the study results may not have been accurate. However, if any new study is carried out in the future, it will be meaningful to conduct a comprehensive analysis of the class effect. Furthermore, the duration of treatment in this work may limit the generalizability of the results. Most studies did not analyze the persistence of left ventricular dysfunction, and the patients were followed up for only 6 months. Long-term results may enhance scientific consistency in the use of ACEIs in this setting and may have the potential to demonstrate sustained and lasting benefits. Although the research carried out to date has been excellent and the preliminary results are considered satisfactory, normative research with sufficient robustness to indicate the routine use of ACEIs to prevent cardiotoxicity induced by anthracycline drugs is still lacking.

AUTHOR CONTRIBUTIONS

YW and WW conceived the idea for this study. YZ and YL conducted the search. JL, NT, and KD interpreted the data and drafted the figures. YZ, YL, and HZ drafted the manuscript. JW and JZ conducted the quality check on inclusion criteria. YZ and NT performed the statistical tests. All authors read and approved the final manuscript.

FUNDING

This study was funded by the National Natural Science Foundation of China (81822049, 81673712, 81673802), Beijing Nova program (Z171100001117028), Fok Ying Tung Education Foundation (151044), and the National Key R&D Program of China (2017YFC1700100, 2017YFC1700102), The funders had no role in the study design, data collection and analysis, the decision to publish, or the preparation of the manuscript.

ACKNOWLEDGMENTS

The authors gratefully acknowledge the assistance of Dr. Xiaoguang Lu in the revision of the manuscript.

REFERENCES

Arciniegas Calle, M. C., Sandhu, N. P., Xia, H., Cha, S. S., Pellikka, P. A., Ye, Z., et al. (2018). Two-dimensional speckle tracking echocardiography predicts early subclinical cardiotoxicity associated with anthracycline-trastuzumab chemotherapy in patients with breast cancer. *BMC Cancer* 18, 1037.

Barbosa, R. R., Bourguignon, T. B., Torres, L. D., Arruda, L. S., Jacques, T. M., Serpa, R. G., et al. (2018). Anthracycline-associated cardiotoxicity in adults: systematic review on the cardioprotective role of beta-blockers. *Rev. Assoc. Med. Bras.* 64, 745–754. doi: 10.1590/1806-9282.64.08.745

Bosch, X., Rovira, M., Sitges, M., Domènech, A., Ortiz-Pérez, J. T., de Caralt, T. M., et al. (2013). Enalapril and carvedilol for preventing chemotherapy-induced left ventricular systolic dysfunction in patients with malignant hemopathies: the OVERCOME trial. *J. Am. Coll. Cardiol.* 61, 2355–2362. doi: 10.1016/j.jacc.2013.02.072

Brewster, D. H., Clark, D., Hopkins, L., Bauer, J., Wild, S. H., Edgar, A. B., et al. (2014). Subsequent hospitalisation experience of 5-year survivors of childhood, adolescent, and young adult cancer in Scotland: a population based, retrospective cohort study. *Br. J. Cancer* 110, 1342–1350. doi: 10.1038/bjc.2013.788

Cardinale, D., Colombo, A., Sandri, M. T., Lamantia, G., Colombo, N., Civelli, M., et al. (2006). Prevention of high-dose chemotherapy–induced cardiotoxicity in high-risk patients by angiotensin-converting enzyme inhibition. *Circulation.* 114, 2474–2481. doi: 10.1161/CIRCULATIONAHA.106.635144

Cardinale, D., Ciceri, F., Latini, R., Franzosi, M. G., Sandri, M. T., Civelli, M., et al. (2018). Anthracycline-induced cardiotoxicity: A multicenter randomised trial comparing two strategies for guiding prevention with enalapril: The International CardioOncology Society-one trial. *Eur. J. Cancer* 94, 126–137. doi: 10.1016/j.ejca.2018.02.005

Conway, A., McCarthy, A. L., Lawrence, P., and Clark, R. A. (2015). The prevention, detection and management of cancer treatment-induced cardiotoxicity: a meta-review. *BMC Cancer* 15, 366. doi: 10.1186/s12885-015-1407-6

Damiani, R. M., Moura, D. J., Viau, C. M., Caceres, R. A., Henriques, J. A. P., and Saffi, J. (2016). Pathways of cardiactoxicity: comparison between chemotherapeutic drugs doxorubicin and mitoxantrone. *Arch. Toxicol.* 90, 2063–2076. doi: 10.1007/s00204-016-1759-y

Dimou, C., Antza, C., Akrivos, E., Doundoulakis, I., Stabouli, S., Haidich, A. B., et al. (2018). A systematic review and network meta-analysis of the comparative efficacy of angiotensin-converting enzyme inhibitors and angiotensin receptor blockers in hypertension. *J. Hum. Hypertens* 33, 188–201. doi: 10.1038/s41371-018-0138-y

El-Sherbeny, W. S., Sabry, N. M., and Sharbay, R. M. (2019). Prediction of trastuzumab-induced cardiotoxicity in breast cancer patients receiving anthracycline-based chemotherapy. *J. Echocardiogr.* 17, 76–83. doi: 10.1007/s12574-018-0394-4

EMA. European Medicines Agency. (2019). *Assessment report. Dexrazoxane-containing medicinal products (EMEA/H/A-31/1275)*. London, United Kingdom. www.ema.europa.eu/docs/en GB/document library/Referrals document/Dexrazoxane 31/WC500120340.pdf Accessed April 13, 2019.

GBD 2016 Causes of Death Collaborators (2017). Global, regional, and national age-sex specific mortality for 264 causes of death, 1980-2016: a systematic analysis for the Global Burden of Disease Study 2016. *Lancet* 390, 1151–1210. doi: 10.1016/S0140-6736(17)32152-9

Georgakopoulos, P., Roussou, P., Matsakas, E., Karavidas, A., Anagnostopoulos, N., Marinakis, T., et al. (2010). Cardioprotective effect of metoprolol and enalapril in doxorubicin-treated lymphoma patients: a prospective, parallel-group, randomized, controlled study with 36-month follow-up. *Am. J. Hematol.* 85, 894–896. doi: 10.1002/ajh.21840

Gupta, V., Kumar Singh, S., Agrawal, V., and Bali, S. T. (2018). Role of ACE inhibitors in anthracycline-induced cardiotoxicity: A randomized, double-blind, placebo-controlled trial. *Pediatr. Blood Cancer* 65, e27308. doi: 10.1002/pbc.27308

Heusch, G. (2012). HIF-1α and paradoxical phenomena in cardioprotection. *Cardiovasc. Res.* 96, 214–215. doi: 10.1093/cvr/cvs145

Janbabai, G., Nabati, M., Faghihinia, M., Azizi, S., Borhani, S., and Yazdani, J. (2017). Effect of Enalapril on Preventing Anthracycline-Induced Cardiomyopathy. *Cardiovasc. Toxicol.* 17, 130–139. doi: 10.1007/s12012-016-9365-z

Kakia, A., Wiysonge, C. S., Ochodo, E. A., Awotedu, A. A., Ristic, A. D., and Mayosi, B. M. (2016). The efficacy and safety of complete pericardial drainage by means of intrapericardial fibrinolysis for the prevention of complications of pericardial effusion: a systematic review protocol. *BMJ Open* 1, e007842. doi: 10.1136/bmjopen-2015-007842

Kaya, M. G., Ozkan, M., Gunebakmaz, O., et al. (2013). Protective effects of nebivolol against anthracycline-induced cardiomyopathy: a randomized control study. *Int. J. Cardiol.* 167, 2306–2310. doi: 10.1016/j.ijcard.2012.06.023

Luft, F. C. (2017). The promise of stromal cell-derived factor-1 in novel heart disease treatments. *J. Mol. Med.* 95, 821–823. doi: 10.1007/s00109-017-1569-6

Potter, E., and Marwick, T. H. (2018). Assessment of left ventricular function by echocardiography: the case for routinely adding global longitudinal strain to ejection fraction. *JACC Cardiovasc. Imaging* 11 (2), 260–274. doi: 10.1016/j.jcmg.2017.11.017

Puddighinu, G., D'Amario, D., Foglio, E., Manchi, M., Siracusano, A., Pontemezzo, E., et al. (2018). Molecular mechanisms of cardioprotective effects mediated by transplanted cardiac ckit+ cells through the activation of an inflammatory hypoxia-dependent reparative response. *Oncotarget.* 9, 937. doi: 10.18632/oncotarget.22946

Rebecca, L. S., Torre, L. A., and Jemal, A. (2018). Global Cancer Statistics 2018: GLOBOCAN Estimates of Incidence and Mortality Worldwide for 36 Cancers in 185 Countries. *CA Cancer J. Clin.* 68, 394–424. doi: 10.3322/caac.21492

Robert, S. C.-H., Liu, J. E., and Yu, A. F. (2019). Cardiotoxicity of HER2-targeted therapies. *Curr. Opin. Cardiol.* 34, 451–458. doi: 10.1097/HCO.0000000000000637

Rohit, M., and Yeh, E. T. H. (2016). Mechanisms of cardiotoxicity of cancer chemotherapeutic agents: Cardiomyopathy and beyond. *Can. J. Cardiol.* 32, 1–28. doi: 10.1016/j.cjca.2016.01.027

Salzer, W. L., Devidas, M., Carroll, W. L., Winick, N., Pullen, J., Hunger, S. P., et al. (2010). Long-term results of the pediatric oncology group studies for childhood acute lymphoblastic leukemia 1984-2001: a report from the children's oncology group. *Leukemia.* 24, 355–370. doi: 10.1038/leu.2009.261

Silber, J. H., Cnaan, A., Clark, B. J., Paridon, S. M., Chin, A. J., Rychik, J., et al. (2004). Enalapril to prevent cardiac function decline in long-term survivors of pediatric cancer exposed to anthracyclines. *J. Clin. Oncol.* 22, 820–828. doi: 10.1200/JCO.2004.06.022

Songbo, M., Lang, H., Xinyong, C., Bin, X., Ping, Z., and Liang, S. (2019). Oxidative stress injury in doxorubicin-induced cardiotoxicity. *Toxicol. Lett.* 307, 41–48. doi: 10.1016/j.toxlet.2019.02.013

Tebbi, C. K., London, W. B., Friedman, D., Villaluna, D., De Alarcon, P. A., Constine, L. S., et al. (2007). Dexrazoxane-associated risk for acute myeloid leukemia/myelodysplastic syndrome and other secondary malignancies in pediatric Hodgkin's disease. *J. Clin. Oncol.* 25, 493–500. doi: 10.1200/JCO.2005.02.3879

Tomlinson, L., Lu, Z. Q., Bentley, R. A., Colley, H. E., Murdoch, C., Webb, S. D., et al. (2019). Attenuation of doxorubicin-induced cardiotoxicity in a human in vitro cardiac model by the induction of the NRF-2 pathway. *Biomed. Pharmacother.* 112, 108637. doi: 10.1016/j.biopha.2019.108637

Turgeon, R. D., Kolber, M. R., Loewen, P., Ellis, U., and McCormack, J. P. (2019). Higher versus lower doses of ACE inhibitors, angiotensin-2 receptor blockers and beta-blockers in heart failure with reduced ejection fraction: Systematic review and meta-analysis. *PloS One* 14, e0212907. doi: 10.1371/journal.pone.0212907

Wen, J., Zhang, J. Q., Huang, W., and Wang, Y. (2012). SDF-1α and CXCR4 as therapeutic targets in cardiovascular disease. *Am. J. Cardiovasc. Dis.* 2, 20–28.

Zamani, B., Salehi, R., and Esfahani, A. (2018). Protective effect of carvedilol against anthracycline-induced cardiomyopathy on patients with breast cancer and lymphoma. *Int. J. Adv. Med.* 5, 16–20. doi: 10.18203/2349-3933.ijam20180061

Zhang, W., and Lin, M. (2010). e0098 HIF-1α, SDF-1α and VEGF gene expression affected by HIF-1α siRNA in MSCs. *Heart.* 96, A32–A33. doi: 10.1136/hrt.2010.208967.98

Conflict of Interest: The authors declare that the research was conducted in the absence of any commercial or financial relationships that could be construed as a potential conflict of interest.

frontiers in Oncology

SYSTEMATIC REVIEW
published: 28 May 2020
doi: 10.3389/fonc.2020.00868

Chemotherapeutic Effectiveness of Combining Cetuximab for Metastatic Colorectal Cancer Treatment: A System Review and Meta-Analysis

Rong Li[1†], *Minqing Liang*[2†], *Xiao Liang*[1], *Lu Yang*[1], *Min Su*[1] *and Keng Po Lai*[1,3*]

[1] Guangxi Key Laboratory of Tumor Immunology and Microenvironmental Regulation, Guilin Medical University, Guilin, China, [2] Department of Pharmacy, Guigang City People's Hospital, The Eighth Affiliated Hospital of Guangxi Medical University, Guigang, China, [3] Department of Chemistry, City University of Hong Kong, Hong Kong, China

This meta-analysis used the database including PubMed, Medline, Cochrane Library, CNKI, Chinese-Cqvip, and Wanfang for randomized controlled trials (RCTs) to investigate the clinical effectiveness for combining cetuximab treatment with chemotherapy for treating metastatic colorectal cancer (mCRC). A total of 12 RCTs involved 7,108 patients with mCRC were included. The patients received chemotherapy with (3,521 cases) or without cetuximab (3,587 cases). Outcomes were overall survival (OS), progression-free survival (PFS), disease control rate (DCR), overall response rate (ORR), odd ratio (OR), and risk ratio (HR). Our results showed that the chemotherapy alone group has shorter OS, PFS, and ORR than the chemotherapy plus cetuximab group, with significant differences (PFS:HR = 0.77, 95% CI = 0.72–0.82, $P < 0.00001$; OS:HR = 0.88, 95% CI = 0.79–0.99, $P = 0.03$; ORR:OR = 1.79, 95% CI = 1.30–2.47; $P = 0.0003$). Results of subgroup analysis showed that cetuximab treatment prolonged PFS and OS in KRAS wild-type patients, with statistically significant differences (PFS:HR = 0.79, 95% CI = 0.65–0.95, $P = 0.01$; OS:HR = 0.85, 95% CI = 0.74–0.98, $P = 0.02$). Combining cetuximab with chemotherapy, the PFS and OS of wild-type KRAS patients and the ORR of all patients were significantly improved.

Keywords: cetuximab, chemotherapy, colorectal cancer, metastasis, meta-analysis

OPEN ACCESS

Edited by:
Nehad M. Ayoub, Jordan University of Science and Technology, Jordan

Reviewed by:
Angelique Nyinawabera, L.E.A.F. Pharmaceuticsls, United States
Hemlata Sukhija, City of Hope National Medical Center, United States

***Correspondence:**
Keng Po Lai
glmu_kengplai@yeah.net;
kengplai@cityu.edu.hk

[†] *These authors have contributed equally to this work*

Specialty section:
This article was submitted to Pharmacology of Anti-Cancer Drugs, a section of the journal Frontiers in Oncology

Received: *17 January 2020*
Accepted: *04 May 2020*
Published: *28 May 2020*

Citation:
Li R, Liang M, Liang X, Yang L, Su M and Lai KP (2020) Chemotherapeutic Effectiveness of Combining Cetuximab for Metastatic Colorectal Cancer Treatment: A System Review and Meta-Analysis. Front. Oncol. 10:868. doi: 10.3389/fonc.2020.00868

INTRODUCTION

Globally, colorectal cancer (CRC) refers to one of top 3 fatal cancers, characterized with poor prognosis and high metastasis (1). However, the early symptoms of CRC are inconspicuous, and then around 15–25% of patients with CRC were diagnosed as advanced stage in initial check-up (2). As a result, 50% of patients with metastatic colorectal cancer (mCRC) are inoperable, thus having recurrence and metastasis after treatment (3). The traditional concept of mCRC chemotherapy is continuous treatment until the disease progresses, but the cumulative toxicity of the drug limits the continued use of chemotherapy. Therefore, measures to reduce toxicity during chemotherapy, prolong PFS and OS have become the key to treatment options. Thanks to the new generation of drugs with less toxicity and better targeting, they have gradually entered the clinical stage, and advanced tumor maintenance treatment has gradually demonstrated its clinical application advantages and have been successfully used in solid tumors, such as blood tumors, lung cancer and

breast cancer (4–7). In the past two decades, with the progress of tumor molecular biology and new drug research, molecularly targeted drugs that specifically interfere with the biological behavior of tumors have gradually demonstrated clinical application advantages in tumor therapy due to their high selectivity and high therapeutic index. The NCCN guidelines recommend combining targeted drugs with mFOLFOX, FOLFIRI and XELOX as first-line treatments for mCRC (8). At present, there are mainly two types of drugs targeting EGFR, monoclonal antibodies and small molecule tyrosine kinase inhibitors (TKIs) have reached the mature stage of clinical application (9). Monoclonal antibodies are highly homogeneous antibodies derived from a single B-cell clone that targets only a specific epitope. Compared with chemotherapeutic drugs, monoclonal antibodies have the advantages of strong therapeutic effect, fewer adverse reactions, and high patient tolerance (10). Sirotnak et al. (11) have found that combining gefitinib with paclitaxel or docetaxel can significantly inhibit the growth of A431, LX-1, SK-LC-16, TSU-PR1, and PC-3 tumor cells as compared to single drugs; doxorubicin combined with gefitinib has 10-fold induction of A549 inhibitory effect. Ciardiello et al. (12) found that the combined effect of gefitinib and chemotherapeutic agents can significantly enhance apoptosis and synergistically inhibit tumor growth in mice with colon cancer (GEO) transplanted tumors and the tumor suppressive effect of gefitinib on tumor-bearing mice was reversible; but after the end of treatment, the tumor growth rate in the control group was still able to recover, while the tumors in the combination group started to grow slowly 4–8 weeks after the treatment.

Cetuximab, as a novel monoclonal antibody, was marketed in 2003 to target epidermal growth factor (EGFR) receptors and block intracellular signal transduction, thereby inhibiting proliferation of cancer cell (13). The main indication described in its drug insert (Merck, Germany) is mCRC which is resistant to chemotherapy with irinotecan-based drugs. Previous studies have found that mCRC is often accompanied with genetic mutations, such as K-Ras mutations, and the mutated mCRC is no longer regulated by EGFR (14, 15). At this point, the drugs that target EGFR will become ineffective. Therefore, EGFR inhibitors are only suitable for the treatment of K-Ras wild type mCRC. Cetuximab combined with chemotherapy is currently the standard protocol for first-line treatment of RAS wild-type mCRC patients (16). Several studies have shown that cetuximab significantly improves objective response rate (ORR), progression-free survival (PFS) and overall survival (OS) in patients with wild-type RAS mCRC, especially those with primary lesions on the left (17, 18). However, even in patients with left half colorectal cancer where the efficacy of cetuximab is dominant, about 30% of patients have failed (19). Besides, its clinical application time is relatively short. In addition, the clinical trial results of cetuximab in the treatment of mCRC in recent years are inconsistent. At present, there is no definitive agreement on its efficacy and adverse reactions. To further explore the use of cetuximab in mCRC, this article used meta-analysis combined with current published data to study the efficacy of cetuximab in combination with chemotherapy for mCRC treatment, so as to provide more reliable evidence-based medical evidence for its clinical use.

METHODS AND MATERIALS

Search Strategy

We conducted database search and data analysis based on the criteria published in the Systematic Review and the Meta-analytical of Preferred Reporting Items (PRISMA) guidelines. Search for PubMed, Medline, Cochrane Library, CNKI, Chinese-Cqvip and Wanfang Database, time range from January 2004 to July 2018, extracting overall survival (OS), progression-free survival (PFS), disease control rate (DCR), overall response rate (ORR), odd ratio (OR), and risk ratio (HR) from literature reports related to mCRC patients result. The disease in these

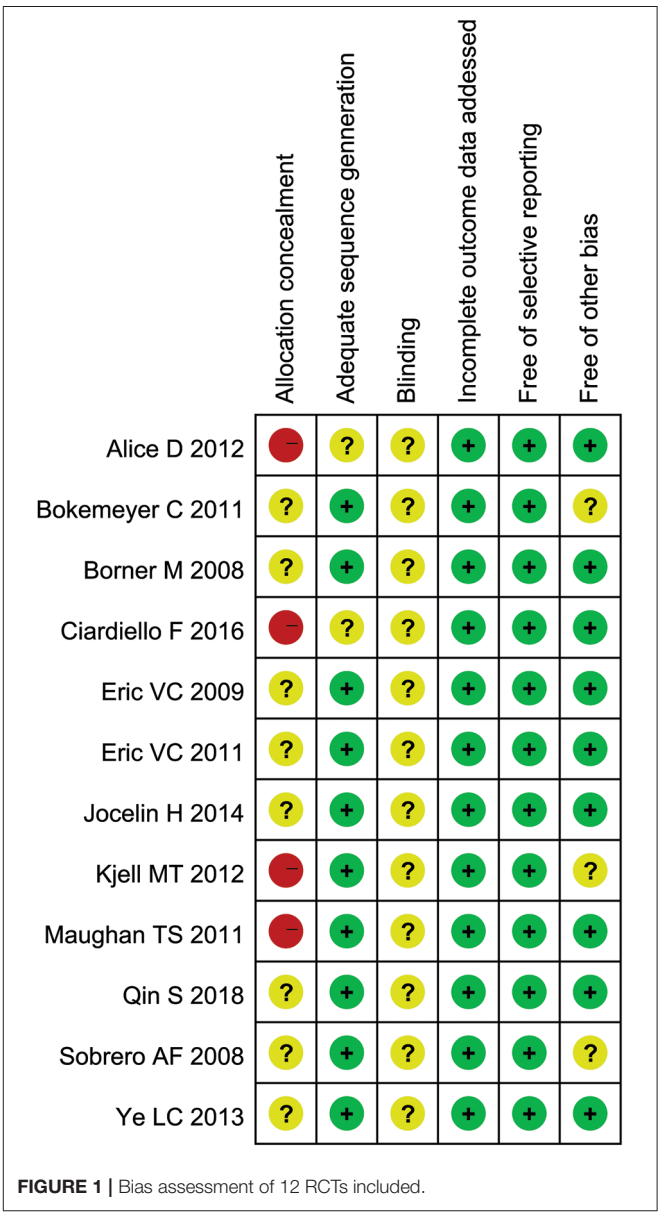

FIGURE 1 | Bias assessment of 12 RCTs included.

mCRC patients originated from KRAS wild-type or mutant colorectal cancer, and they were treated with or without cetuximab in a randomized controlled trial (RCT). The key words for searched were "metastatic colorectal cancer" (or "carcinoma" or "malignant tumor") and cetuximab (or "erbitux"). In addition, there are some full text of the literatures were retrieved by reference of the retrieved literature. And all the articles had no limit for language. In addition, we conducted extensive searches and the articles were further verified in the list of references.

Inclusion and Exclusion Criteria

Patient

Eligible patients were confirmed as mCRC and age 18 years or older with Eastern Cooperative Oncology Group performance status of 0, 1, or 2, and histologically proven stage III (any T, N1 or N2, M0) adenocarcinoma of the colon. Unlimited metastases, and no limit on the number of metastases; no geographical or gender restrictions; and renal and bone marrow hematopoiesis are normal. Life expectancy $\geq$12 weeks. All participants provided written informed consent before study enrollment and were required to submit blood and tumor tissue before randomization.

Intervention

Experimental group: cetuximab combined with chemotherapy; control group: chemotherapy.

Type of Design of Experime

The experiment should be a randomized controlled clinical trial. For studies with multiple intervention groups, relevant data are selected for inclusion. Exclude crossover trials and semi-randomized controlled trials by date or admission. When duplicate or repeating data appears in multiple reports, the data including the most comprehensive information is selected.

Outcomes

Overall survival (OS), progression-free survival (PFS), disease control rate (DCR), overall response rate (ORR), odd ratio (OR), and risk ratio (HR).

Quality Assessment

The abstracts of all documents identified in the original search were screened and two researchers (Xiaoliu Liang and Yujia Liang) excluded studies that violated the inclusion criteria. Another author (Shiyuan Xie) post-evaluated the full-text article. If different opinions were generated, the third researcher was asked to evaluate such research and reach a consensus through discussion. Finally, the risk of selective biased project is recommended according to the Cochrane Handbook for Systematic Reviews of Interventions. Risks of biased items included: blinding, allocation concealment, proper sequence generation, incomplete outcome data, non-selective reporting, and other biases (**Figure 1**). If the article did not display the

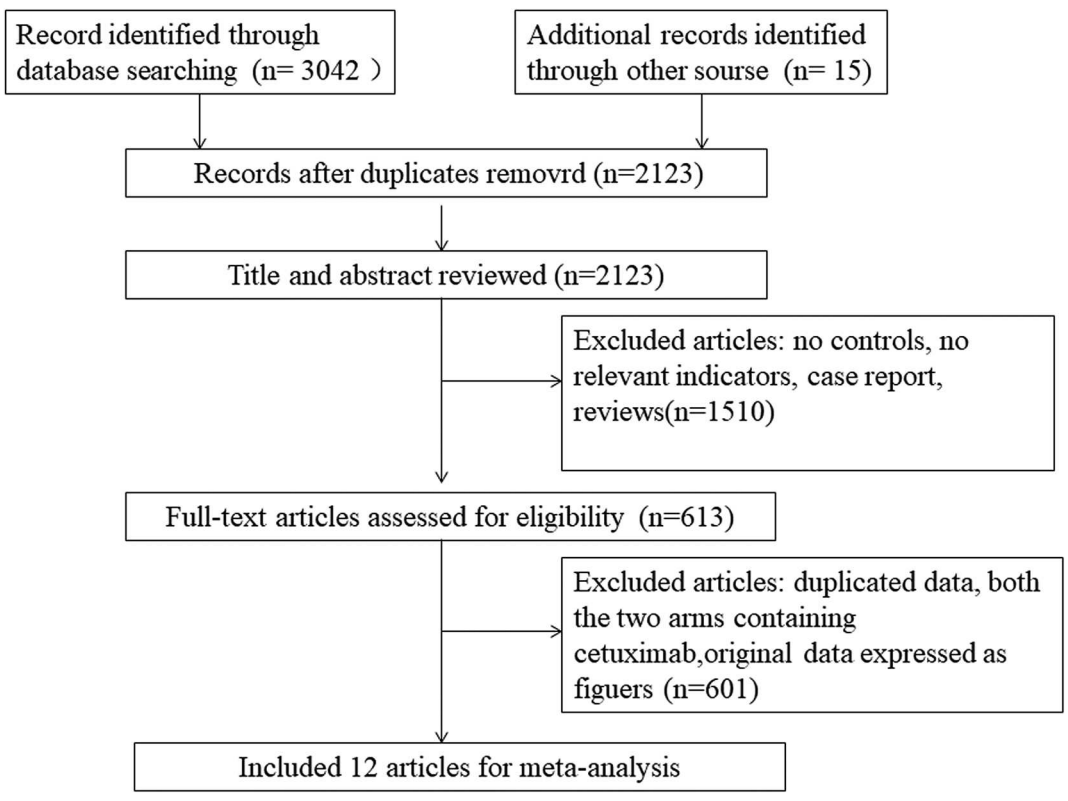

FIGURE 2 | The flowchart of this study setting.

original data, contact the corresponding author of the study by email using a separately customized application form.

Data Extraction

The following information was independently extracted from each study by two investigators (Xiaoliu Liang and Yujia Liang). When a disagreement occurs, it is resolved by consensus. Gather the following information from each eligible study: the first author's name, country, male/female ratio, age range, sample size, treatment regimens, ending index, publication year, intentionality therapy (Intention-to-treat, ITT) in patients with OS and PFS, HRs with corresponding 95% Cis, period of treatment, KRAS wild-type and KRAS-type mutations in OS and PFS patients, etc.

Statistical Analysis

RevMan 5.0 software was used for all statistical analyses. Efficacy in a regimen of chemotherapy with mCRC in combination with

TABLE 1 | Characteristics of the RCT studies included in our meta-analysis.

References	Sex (male/female)	Country	Treatments		Age (median, range)		A period of treatment(d)	Duration
			Control	Experiment	Control	Experiment		
Bokemeyer et al. (16)	181/156	Europe	FOLFOX	FOLFOX +cetuximab	60 (30-82)	62 (24-82)	14	Depending on disease progression and severity of adverse reactions
Huang et al. (28)	78/68	Europe	FOLFIRI	FOLFIRI +cetuximab	57 (25-82)	59 (30-82)	14	6 months
Dewdney et al. (29)	101/63	Multicenter	CAPOX	CAPOX +cetuximab	65 (28-79)	61 (28-79)	14	2 months
Van Cutsem et al. (27)	725/473	Europe	FOLFIRI	FOLFIRI +cetuximab	61 (19-84)	61 (22-82)	14	Depending on disease progression and severity of adverse reactions
Van Cutsem et al. (24)	725/473	Europe	FOLFIRI	FOLFIRI +cetuximab	61 (19-84)	61 (22-82)	14	Depending on the disease progression, the degree of adverse reactions or the informed consent was withdrawn
Tveit et al. (31)	220/159	Multicenter	FLOX	FLOX +cetuximab	61.2 (29.9–74.8)	60.8 (24.1–74.4)	14	Depending on disease progression and severity of adverse reactions
Ye et al. (26)	88/50	Europe or North America	FOLFOX or FOLFIRI	FOLFOX or FOLFIRI +cetuximab	59 (35–75)	57 (26–75)	14	Depending on the reaction after liver metastasis of cancer, disease progression or the degree of adverse reactions
Borner et al. (20)	44/30	Multicenter	CAPOX	CAPOX+cetuximab	63 (47–80)	60 (37–81)	21	4.5 months or disease progression
Maughan et al. (21)	1068/562	UK	CAPOX or FOLFOX	CAPOX or FOLFOX +cetuximab	63 (56–69)	63 (58–70)	14	Depending on disease progression
Ciardiello et al. (23)	72/81	Chinese	FOLFOX	FOLFOX+cetuximab	49–59	49–59	14	Depending on the disease progression, the degree of adverse reactions or the informed consent was withdrawn
Qin et al. (22)	266/127	Multicenter	FOLFOX	FOLFOX +cetuximab	56 (21-78)	56 (21–83)	14	Depending on disease progression and severity of adverse reactions
Sobrero et al. (25)	816/482	Multicenter	Irinotecan	Irinotecan +cetuximab	62 (21-90)	61 (23–85)	21	Depending on disease progression and severity of adverse reactions

cetuximab was evaluated based on data from RCT. DCR and ORR were analyzed by relative risk (RR) or odds ratio (OR); if RR > 1 or > 1, the experimental group (chemotherapy with cetuximab) was higher than the control group (chemotherapy without cetuximab); vice versa, if RR < 1 or < 1, the experimental group was lower than the control group. In addition, PFS and OS

TABLE 2 | Characteristics of the RCT studies included in our meta-analysis.

References	Number of cases		HR (95%CI)	
	Control	Experiment	PFS	OS
Bokemeyer et al. (16)	168	169	0.931(0.705,1.23)	1.105(0.791,1.303)
Huang (28)	106	40	0.53(0.26,1.1)	0.45(0.17,1.16)
Dewdney (29)	81	83	0.81(0.45,1.44)	0.53(0.26,1.10)
Van Cutsem (27)	599	599	0.851(0.726,0.998)	0.878(0.774,0.995)
Van Cutsem (24)	599	599	0.85(0.72,0.99)	0.93(0.81,1.07)
Tveit (31)	185	194	0.89(0.72,1.11)	1.06(0.83,1.35)
Ye et al. (26)	68	70	0.6(0.41, 0.87)	0.54 (0.33, 0.89)
Borner et al. (20)	37	37	NR	NR
Maughan et al. (21)	815	815	NR	NR
Ciardiello et al. (23)	79	74	0.56(0.33, 0.94)	0.57(0.32, 1.02)
Qin et al. (22)	200	193	0.69(0.54, 0.89)	0.76(0.61, 0.96)
Sobrero et al. (25)	650	648	0.692(0.617, 0.776)	0.975(0.854, 1.114)

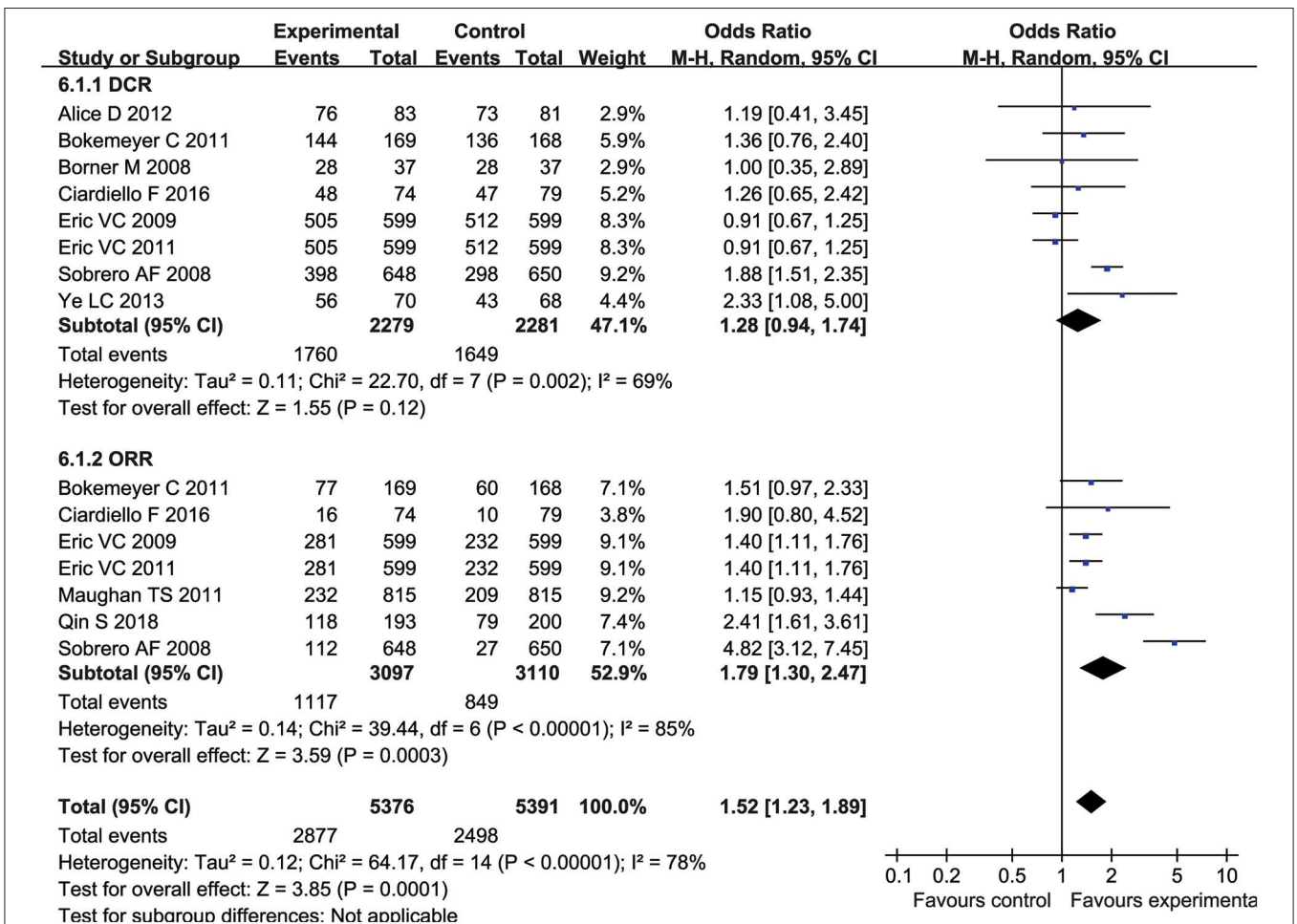

FIGURE 3 | The ORR and DCR of forest plots with fixed effect model.

were the primary endpoints of pooled analysis, and expression of HR at the primary endpoint of each study was 95% CI. If the literature did not provide HR, it could be extracted according to the survival curve method (KM). Chi-square test and I^2 statistics were used when estimating statistical heterogeneity. When $p < 0.05$ or $I^2 > 50\%$, a random effects model was used; otherwise a fixed effect model was used. If the heterogeneity was large, a descriptive analysis was performed. The stability of the test results was determined by sensitivity analysis if necessary.

RESULTS

Selection and Characteristics of Study

The overall flowchart of the study was shown in **Figure 2**. At the beginning, we included 3,057 potential studies. Due to the duplication, 934 publications were excluded. In addition, 1,510 articles with no controls, no relevant indicators, case reports, or no association with mCRC were excluded. Then, 601 articles with no relevant raw data, original data expressed as figures and duplicated data were excluded. Besides, study with the two arms containing cetuximab or the study with dual targeted drugs were also excluded. Finally, 12 articles met the requirements for this meta-analysis, involving 12 RCTs (20–31) (the experimental group: 3,587 cases and the control group: 3,521 cases). The characteristics of the 12 articles were shown in **Tables 1,2**.

Meta-Analysis of DCR and ORR

Eight studies (4,560 patients) reported DCR, and seven studies (6,207 patients) reported ORR. The results showed heterogeneity between studies (DCR: $P = 0.002$, $I^2 = 69\%$; ORR: $P < 0.00001$, I2 = 85%) (**Figure 3**), so a random effects model was used for meta-analysis. Meta-analysis showed no significant

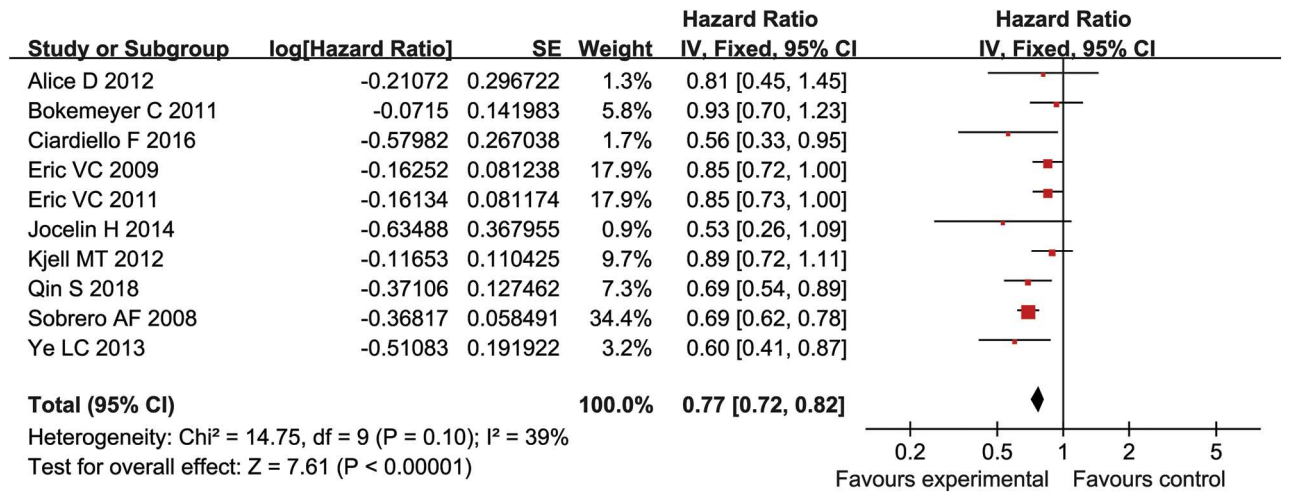

FIGURE 4 | The PFS of forest plots with fixed effect model.

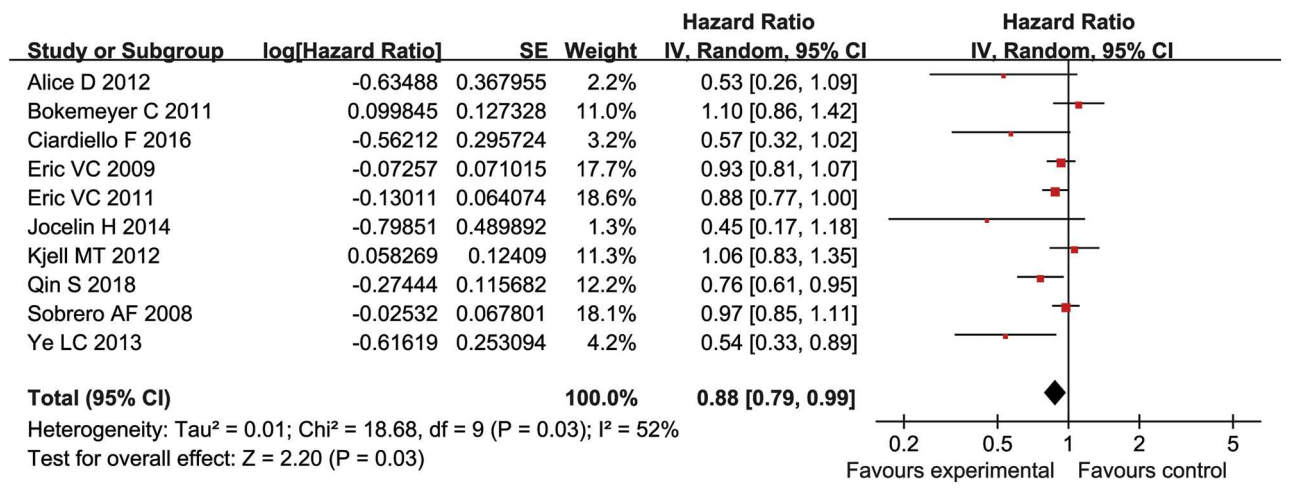

FIGURE 5 | The OS of forest plots with fixed effect model.

difference in DCR between the experimental group and the control group (OR = 1.28, 95% CI = 0.94-1.74, $P = 0.12$) (**Figure 3**). However, patients receiving combination therapy with cetuximab had higher ORR (OR = 1.79, 95% CI = 1.30–2.47; $P = 0.0003$) (**Figure 3**).

Meta-Analysis of PFS

PFS was reported in ten studies (5,404 patients) and there was no statistical heterogeneity between each study ($P = 0.1$, $I^2 = 39\%$) (**Figure 4**). The log HR values of PFS were analyzed by fixed effect model and inverse variance method. The results suggested that the PFS of experimental group was significantly longer than that of control group (HR = 0.77, 95% CI = 0.72–0.82, $P < 0.00001$) (**Figure 4**).

Meta-Analysis of OS

There were 10 studies reported OS (5,404 patients). There was heterogeneity between the studies ($P = 0.03$, $I^2 = 52\%$) (**Figure 5**). Therefore, for the log HR values of the OS, a fixed effect model and an inverse variance method were used for meta-analysis. Analysis showed that the experimental group had significant advantages in improving OS, as compared to the control group (HR = 0.88, 95% CI = 0.79–0.99, $P = 0.03$), (**Figure 5**).

Subgroup Analysis

Patients were divided into mutant KRAS and wild type KRAS according to their KRAS genotypes. The HR with 95% CI were extracted from KRAS wild-type and mutant KRAS of patients in each study, followed by the subgroup analysis. Our result showed that cetuximab can significantly prolonged PFS and OS in patients with KRAS wild type (PFS:HR = 0.79, 95% CI = 0.65–0.95, $P = 0.01$; OS:HR = 0.85, 95% CI = 0.74–0.98, $P = 0.02$) (**Figures 6**, **7**), but there was no significant change of PFS and OS in patients with KRAS mutations when chemotherapy was used in combination with cetuximab (PFS:HR = 1.12, 95% CI = 0.73–1.72), $P = 0.6$; OS:HR = 1.35, 95% CI = 0.96–1.90, $P = 0.09$) (**Figures 6, 7**).

Publication Bias

The PFS was used as the index to draw the inverted funnel plot. The result showed that the arrangement of each study around the Central Line was not completely symmetrical, suggesting that there was a certain publication bias in the included articles (**Figure 8**).

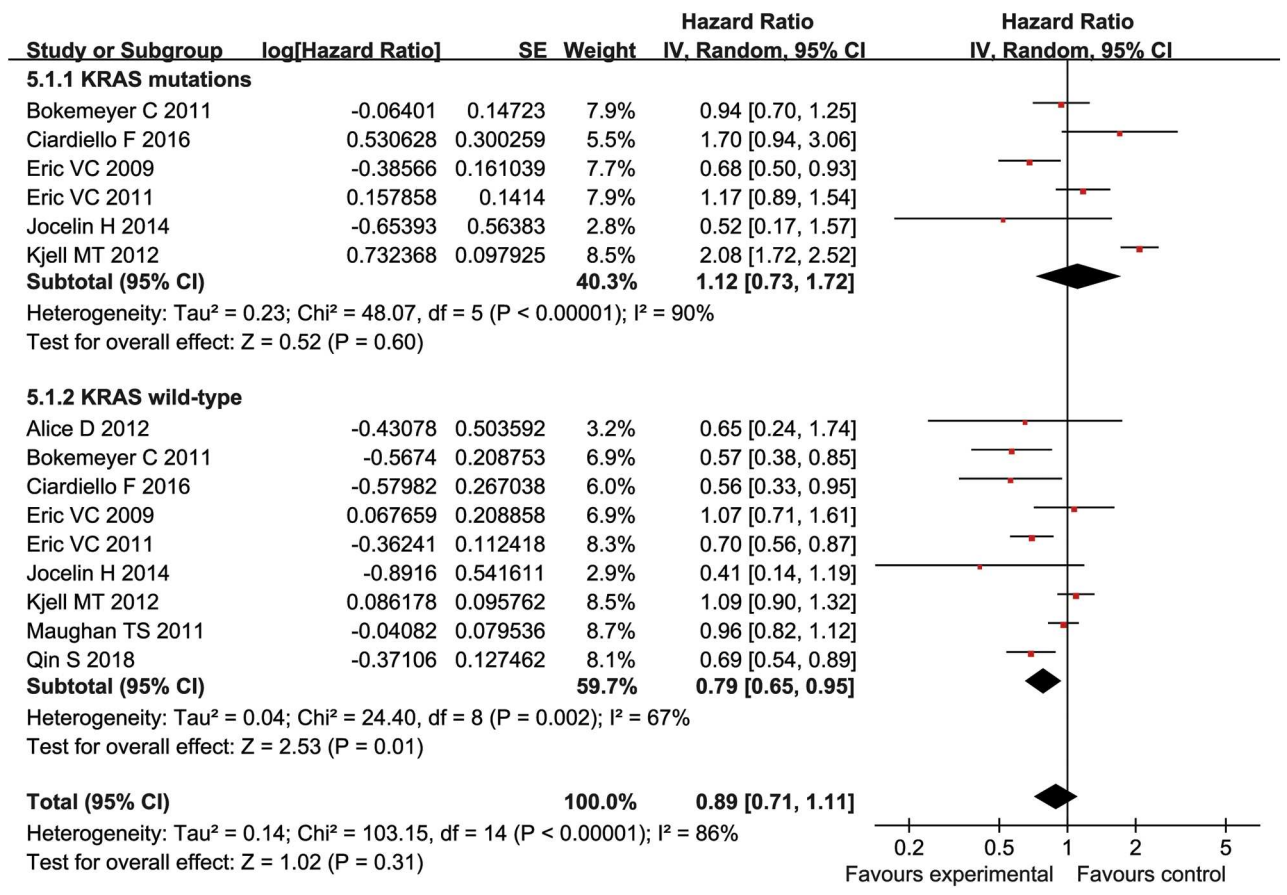

FIGURE 6 | OS forest plot.

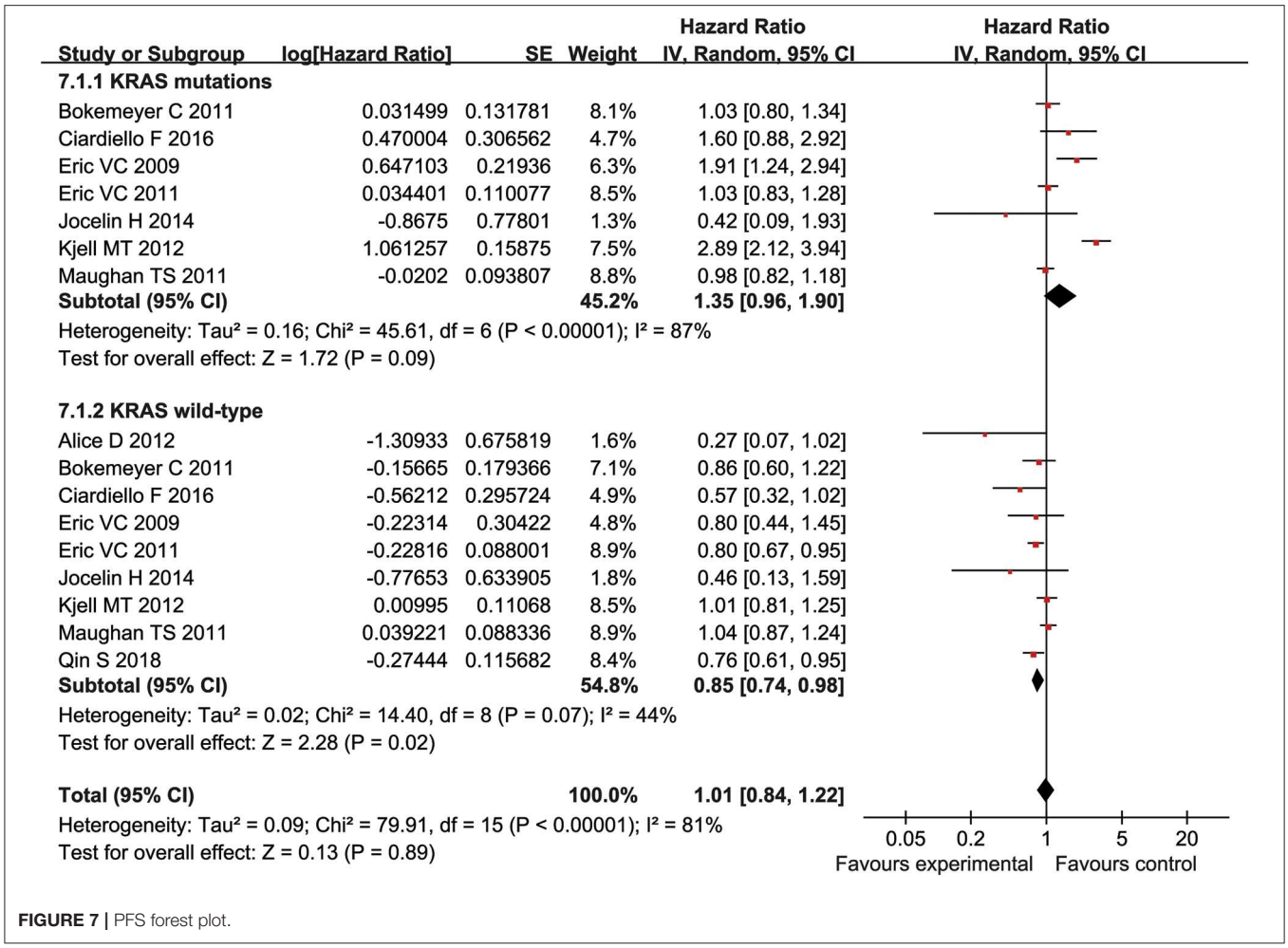

FIGURE 7 | PFS forest plot.

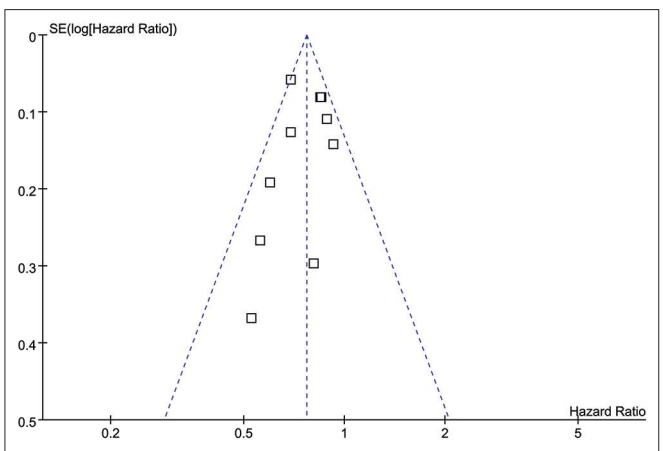

FIGURE 8 | Funnel plot.

DISCUSSION

A total of 12 studies involving 5,404 patients were included in our meta-analysis. Our analysis used a large number of enrolled patients, strict inclusion and exclusion criteria, and similar outcome indicators among studies. Our results showed that cetuximab could significantly prolong PFS and OS in mCRC patients with wild type KRAS, but did not remarkably improve PFS and OS in patients with KRAS mutations. This result was concordant to Wang li's finding that reported the relationship between KRAS gene polymorphism and targeted therapy for colorectal cancer (32). They concluded that cetuximab treatment was ineffective if KRAS gene codon 12 and 13 were mutated. While a meta-analysis conducted by Zhou et al. found that oxaliplatin-based chemotherapy combined with cetuximab or other anti-EGFR monoclonal antibodies could not prolong the survival of mCRC patients (33). It could be explained by the use of different chemotherapeutic drugs. Because in our 12 RCTs studies, five of the studies used folfiri and irinotecan, instead of oxaliplatin-based chemotherapy. For the DCR of intention to treat (ITT) patients, the efficacy of chemotherapy drugs combined with cetuximab was comparable to that of chemotherapy drugs alone, which was consistent with the conclusion of the meta-analysis of 12 RCTS conducted by Wang et al. (34). Our result also indicated that the ORR of the experimental group was significantly higher than that of the

control group, which was consistent with the meta-analysis of Ye et al. (26). Additionally, Qin et al. (22) and Angeles et al. (14) obtained a positive result through RCT, suggesting that the use of cetuximab can be benefit to mCRC patients, while RCT conducted by Yu et al. (19), Sirotnak et al. (11) came to a contrary conclusion. Therefore, there is no consensus on the effective therapeutic significance of cetuximab in mCRC patients with ITT. This may be caused by different sample sources and different experimental methods among different studies.

The KRAS gene polymorphism is a biomarker that reflects changes in EGFR receptors and is associated with the efficacy of cetuximab (27). Foreign CRC diagnostic and therapeutic guidelines suggested that the genetic status of KRAS should be tested before CRC patients treated with cetuximab, while cetuximab is indicated for CRC patients with wild-type KRAS (28). To further elucidate the efficacy relationship between cetuximab and KRAS genotyping, this study performed a meta-analysis of OS and PFS in mCRC patients with wild-type or mutant KRAS, and the conclusions were similar to the finding from Dewdney et al. (29). Another RCT study performed by Christos SK indicated that the use of cetuximab is more effective in patients with wild-type KRAS than that of patients with KRAS mutations (30). References included in this study were all from foreign databases. In addition, the title and abstract attributives of the literature searched in this study were in English, and the literature published in other languages were not included, so there was a database retrieval bias. In the process of literature screening, software screening and manual screening are adopted. The software screening is simple and easy to operate, but it is mechanical, with low recognition ability and the possibility of omission. Manual screening has a large workload and high recognition ability, but it is possible to wrongly reject some negative conclusions, both of which will lead to bias in literature screening. Inverted funnel plot analysis showed that the included studies were not completely symmetrical, which also suggested some publication bias. In addition, due to the designs of the study, there is no information on the number of prior treatments patients have completed, so the information on successful treatment outcome is still not firmly confirmed.

CONCLUSIONS

In summary, compared with chemotherapy alone, combined with cetuximab can significantly prolong PFS and OS in mCRC patients. Limited by the quality and sample size of included studies, this conclusion needs to be verified by a larger sample of RCTs with strict design and long-term follow-up.

DATA AVAILABILITY STATEMENT

The datasets generated for this study are available on request to the corresponding author.

AUTHOR CONTRIBUTIONS

RL and ML collected and assayed the data. RL, XL, and LY conducted statistical analysis and plotted figures. XL and MS discussed the data. KL designed this study, discussed the findings and drafted the manuscript.

FUNDING

This study was supported by the grants from the National Natural Science Foundation of China (No. 81560134, 81660091). KL was supported by Hong Kong SAR, Macao SAR and Taiwan Province Talent Young Scientist Program of Guangxi.

REFERENCES

1. Chen W, Zheng R, Zhang S, Zhao P, Li G, Wu L, et al. Report of incidence and mortality in China cancer registries, 2009. *Chin J Cancer Res.* (2013) 25:10–21. doi: 10.3978/j.issn.1000-9604.2012.12.04
2. Siegel RL, Miller KD, Jemal A. Cancer statistics, 2019. *CA Cancer J Clin.* (2019). 69:7–34. doi: 10.3322/caac.21551
3. Tsai HL, Chu KS, Huang YH, Su YC, Wu JY, Kuo CH, et al. Predictive factors of early relapse in UICC stage I-III colorectal cancer patients after curative resection. *J Surg Oncol.* (2009) 100:736–43. doi: 10.1002/jso.21404
4. Österborg A, Wierda WG, Mayer J, Hess G, Hillmen P, Schetelig J, et al. Ofatumumab retreatment and maintenance in fludarabine-refractory chronic lymphocytic leukaemia patients. *Br J Haematol.* (2015) 170:40–9. doi: 10.1111/bjh.13380
5. Lu Y, Fan Y. [Research progression of maintenance therapy in small cell lung cancer]. *Chinese J Lung Cancer.* (2015) 18:559–64. doi: 10.3779/j.issn.1009-3419.2015.09.06
6. Wu YL, Lee JS, Thongprasert S, Yu CJ, Zhang L, Ladrera G, et al. Intercalated combination of chemotherapy and erlotinib for patients with advanced stage non-small-cell lung cancer (FASTACT-2): a randomised, double-blind trial. *Lancet Oncol.* (2013) 14:777–86. doi: 10.1016/S1470-2045(13)70254-7
7. Lim S, Lee S, Han J, Park BW, Kim S, Park S, et al. Prolonged clinical benefit from the maintenance hormone therapy in patients with metastatic breast cancer. *Breast.* (2013) 22:1205–9. doi: 10.1016/j.breast.2013.08.013
8. Benson AB, Bekaii-Saab T, Chan E, Chen YJ, Choti MA, Cooper HS, et al. Localized colon cancer, version 3.2013: featured updates to the NCCN guidelines. *J Natl Compr Cancer Netw.* (2013) 11:519–28. doi: 10.6004/jnccn.2013.0069
9. Zhang W, Zhang W. Progression of EGFR targeted drugs and chemotherapy in the treatment of malignant tumors. *J Progress Mod Biomed.* (2011) 2011:5171–4.
10. Li Y, Liu H, Huizhen W. Research progress of monoclonal antibodies in targeted therapy of gastric cancer. *J Chin J N Drugs.* (2018) 2018:2557–63.
11. Sirotnak FM, Zakowski MF, Miller VA, Scher HI, Kris MG. Efficacy of cytotoxic agents against human tumor xenografts is markedly enhanced by coadministration of ZD1839 (Iressa), an inhibitor of EGFR tyrosine kinase. *Clin Cancer Res.* (2000) 6:4885–92.
12. Ciardiello F, Caputo R, Bianco R, Damiano V, Pomatico G, De Placido S, et al. Antitumor effect and potentiation of cytotoxic drugs activity in human cancer cells by ZD-1839 (Iressa), an epidermal growth factor receptor-selective tyrosine kinase inhibitor. *Clin Cancer Res.* (2000) 6:2053–63.
13. Sihver W, Pietzsch J, Krause M, Baumann M, Steinbach J, Pietzsch HJ. Radiolabeled cetuximab conjugates for EGFR targeted cancer diagnostics and therapy. *Pharmaceuticals.* (2014) 7:311–38. doi: 10.3390/ph7030311
14. Angeles A, Hung W, Cheung WY. Eligibility of real-world patients with chemo-refractory, K-RAS wild-type, metastatic colorectal cancer for palliative intent regorafenib monotherapy. *Med Oncol.* (2018) 35:114. doi: 10.1007/s12032-018-1176-6

15. Elez E, Argilés G, Tabernero J. First-line treatment of metastatic colorectal cancer: interpreting FIRE-3, PEAK, and CALGB/SWOG 80405. *Curr Treat Options Oncol*. (2015) 16:52. doi: 10.1007/s11864-015-0369-x
16. Bokemeyer C, Bondarenko I, Hartmann JT, de Braud F, Schuch G, Zubel A, et al. Efficacy according to biomarker status of cetuximab plus FOLFOX-4 as first-line treatment for metastatic colorectal cancer: the OPUS study. *Ann Oncol*. (2011) 22:1535–46. doi: 10.1093/annonc/mdq632
17. Stintzing S, Modest DP, Rossius L, Lerch MM, von Weikersthal LF, Decker T, et al. FOLFIRI plus cetuximab versus FOLFIRI plus bevacizumab for metastatic colorectal cancer (FIRE-3): a *post-hoc* analysis of tumour dynamics in the final RAS wild-type subgroup of this randomised open-label phase 3 trial. *Lancet Oncol*. (2016) 17:1426–34. doi: 10.1016/S1470-2045(16)30269-8
18. Khattak MA, Martin H, Davidson A, Phillips M. Role of first-line anti-epidermal growth factor receptor therapy compared with anti-vascular endothelial growth factor therapy in advanced colorectal cancer: a meta-analysis of randomized clinical trials. *Clin Colorectal Cancer*. (2015) 14:81–90. doi: 10.1016/j.clcc.2014.12.011
19. Yu Y, Zhang W, Sun Y, Cheng YJ, Li XY, Li NN, et al. Efficacy and prognostic factors of cetuximab combined with first-line chemotherapy for KRAS / RAS wild-type metastatic colorectal cancer. *Zhongguo Yi Xue Ke Xue Yuan Xue Bao*. (2019) 40:660–6. doi: 10.3881/j.issn.1000-503X.10125
20. Borner M, Koeberle D, Von Moos R, Saletti P, Rauch D, Hess V., et al. Adding cetuximab to capecitabine plus oxaliplatin (XELOX) in first-line treatment of metastatic colorectal cancer: a randomized phase II trial of the Swiss group for clinical cancer research SAKK. *Ann Oncol*. (2008) 19:1288–92. doi: 10.1093/annonc/mdn058
21. Maughan TS, Adams RA, Smith CG, Meade AM, Seymour MT, Wilson RH, et al. Addition of cetuximab to oxaliplatin-based first-line combination chemotherapy for treatment of advanced colorectal cancer: results of the randomised phase 3 MRC COIN trial. *Lancet*. (2011) 377:2103–14. doi: 10.1016/S0084-3873(11)00194-5
22. Qin S, Li J, Wang L, Xu J, Cheng Y, Bai Y, et al. Efficacy and tolerability of first-line cetuximab plus leucovorin, fluorouracil, and oxaliplatin (FOLFOX-4) versus FOLFOX-4 in patients with RAS wild-type metastatic colorectal cancer: the open-label, randomized, phase III TAILOR trial. *J Clin Oncol*. (2018) 36:3031–9. doi: 10.1200/JCO.2018.78.3183
23. Ciardiello F, Normanno N, Martinelli E, Troiani T, Pisconti S, Cardone C, et al. Cetuximab continuation after first progression in metastatic colorectal cancer (CAPRI-GOIM): a randomized phase II trial of FOLFOX plus cetuximab versus FOLFOX. *Ann Oncol*. (2016) 27:1055–61.
24. van Cutsem E, Kohne CH, Hitre E, Zaluski J, Chang Chien C-R, Makhson A, et al. Cetuximab and chemotherapy as initial treatment for metastatic colorectal cancer. *N Engl J Med*. (2009) 360:1408–17. doi: 10.1056/NEJMoa0805019
25. Sobrero AF, Maurel J, Fehrenbacher L, Scheithauer W, Abubakr YA, Lutz MP, et al. EPIC: phase III trial of cetuximab plus irinotecan after fluoropyrimidine and oxaliplatin failure in patients with metastatic colorectal cancer. *J Clin Oncol*. (2008) 26:2311–9. doi: 10.1200/JCO.2007.13.1193
26. Ye LC, Liu TS, Ren L, Wei Y, Zhu DX, Zai SY, et al. Randomized controlled trial of cetuximab plus chemotherapy for patients with KRAS wild-type unresectable colorectal liver-limited metastases. *J Clin Oncol*. (2013) 31:1931–8. doi: 10.1200/JCO.2012.44.8308
27. Van Cutsem E, Köhne C-H, Láng I, Folprecht G, Nowacki MP, Cascinu S, et al. Cetuximab plus irinotecan, fluorouracil, and leucovorin as first-line treatment for metastatic colorectal cancer: updated analysis of overall survival according to tumor KRAS and BRAF mutation status. *J Clin Ocol*. (2011) 29:2011–9. doi: 10.1200/JCO.2010.33.5091
28. Huang J, Nair SG, Mahoney MR, Nelson GD, Shields AF, Chan E, et al. Comparison of FOLFIRI with or without cetuximab in patients with resected stage III colon cancer; NCCTG (Alliance) intergroup trial N0147. *Clin Colorectal Cancer*. (2014) 13:100–9. doi: 10.1016/j.clcc.2013.12.002
29. Dewdney A, Cunningham D, Tabernero J, Capdevila J, Glimelius B, Cervantes A, et al. Multicenter randomized phase II clinical trial comparing neoadjuvant oxaliplatin, capecitabine, and preoperative radiotherapy with or without cetuximab followed by total mesorectal excision in patients with high-risk rectal cancer (EXPERT-C). *J Clin Oncol*. (2012) 30:1620–7. doi: 10.1200/JCO.2011.39.6036
30. Guo GF, Xia LP, Qiu HJ, Xu RH, Zhang B, Jiang WQ, et al. [Efficacy of cetuximab combined with chemotherapy for patients with advanced colorectal cancer and unclear K-ras status]. *Zhonghua zhong liu za zhi*. (2010) 32:777–81.
31. Tveit KM, Guren T, Glimelius B, Pfeiffer P, Sorbye H, Pyrhonen S, et al. Phase III trial of cetuximab with continuous or intermittent fluorouracil, leucovorin, and oxaliplatin (Nordic FLOX) versus FLOX alone in first-line treatment of metastatic colorectal cancer: the NORDIC-VII study. *J Clin Oncol*. (2012) 30:1755–62. doi: 10.1200/JCO.2011.38.0915
32. Wang L, Yu Y. Current status of research on k-ras gene detection and targeted therapy for colorectal cancer. *World Chin J Digestol*. (2011) 19:62-7.
33. Zhou SW, Huang YY, Wei Y, Jiang ZM, Zhang YD, Yang Q, et al. No survival benefit from adding cetuximab or panitumumab to oxaliplatin-based chemotherapy in the first-line treatment of metastatic colorectal cancer in KRAS wild type patients: a meta-analysis. *PLoS ONE*. (2012) 7:e50925. doi: 10.1371/journal.pone.0050925
34. Wang C. Meta-analysis of the efficacy of cetuximab combined with chemotherapeutics versus chemotherapy alone in the treatment of metastatic colorectal cancer. *China Pharm*. (2015) 26.

Conflict of Interest: The authors declare that the research was conducted in the absence of any commercial or financial relationships that could be construed as a potential conflict of interest.

frontiers in Oncology

ORIGINAL RESEARCH
published: 24 June 2020
doi: 10.3389/fonc.2020.00694

Targeting SphK2 Reverses Acquired Resistance of Regorafenib in Hepatocellular Carcinoma

Weiwei Shi[1,2†], *Shan Zhang*[1,2†], *Ding Ma*[1,2], *Dongliang Yan*[3], *Guang Zhang*[1,2,3], *Yin Cao*[1,2,3], *Zhongxia Wang*[1,2,3*], *Junhua Wu*[2*] *and Chunping Jiang*[1,2,3*]

[1] *Department of Hepatobiliary Surgery, The Affiliated Drum Tower Hospital of Nanjing University Medical School, Nanjing, China,* [2] *Jiangsu Key Laboratory of Molecular Medicine, Medical School, Nanjing University, Nanjing, China,* [3] *Department of Hepatobiliary Surgery, Drum Tower Clinical College of Nanjing Medical University, Nanjing, China*

OPEN ACCESS

Edited by:
Nehad M. Ayoub, Jordan University of Science and Technology, Jordan

Reviewed by:
Milankumar Prajapati, Brown University, United States
Md Kamal Hossain, University of Michigan, United States

****Correspondence:***
Zhongxia Wang
freud_t@126.com
Junhua Wu
wujunhua@nju.edu.cn
Chunping Jiang
chunpingjiang@163.com

† These authors have contributed equally to this work

Specialty section:
This article was submitted to Pharmacology of Anti-Cancer Drugs, a section of the journal Frontiers in Oncology

Received: *04 January 2020*
Accepted: *14 April 2020*
Published: *24 June 2020*

Citation:
Shi W, Zhang S, Ma D, Yan D, Zhang G, Cao Y, Wang Z, Wu J and Jiang C (2020) Targeting SphK2 Reverses Acquired Resistance of Regorafenib in Hepatocellular Carcinoma. Front. Oncol. 10:694. doi: 10.3389/fonc.2020.00694

Background: Regorafenib is a second-line therapy drug used for advanced hepatocellular carcinoma (HCC). Unfortunately, the survival benefit of the patients receiving this treatment is modest, which may be attributed to drug resistance. In the present study, sphingosine kinase 2 (SphK2) was targeted to reverse regorafenib resistance in HCC.

Methods: The functions of SphK2 and sphingosine-1-phosphate (S1P), the catalytic product of SphK2 in regorafenib resistance of HCC cells, were evaluated by cell counting kit-8 assay, colony formation, cell cycle evaluation, and annexin V–fluorescein isothiocyanate/propidium iodide double-staining assay. The antitumor activity of combined treatment of regorafenib and the SphK2-specific inhibitor ABC294640 was examined in HCC cells *in vitro* and xenograft model *in vivo*. The molecular mechanisms of SphK2/S1P-mediating regorafenib resistance were investigated using cell line establishment and Western blot analysis.

Results: Well-developed regorafenib-resistant HCC cells indicated high expression levels of SphK2. The sensitivity to regorafenib of regorafenib-resistant HCC cells was restored following SphK2 knockdown or pharmacological inhibition by ABC294640. In addition, ectopic expression of SphK2 and exogenous addition of S1P decreased the sensitivity of HCC cells to regorafenib. Furthermore, the combination treatment with ABC294640 sensitized resistant tumor to regorafenib in xenograft model of HCC. The phosphorylation levels of nuclear factor κB (NF-κB), as well as those of signal transducer and activator of transcription 3 (STAT3), were positively associated with SphK2 and S1P.

Conclusions: SphK2/S1P mediates regorafenib resistance of HCC through NF-κB and STAT3 activation. Targeting SphK2 by ABC294640 potently reduces regorafenib resistance of HCC cells both *in vitro* and *in vivo*. The combination of ABC294640 and regorafenib could be developed as a novel potential treatment strategy for advanced HCC.

Keywords: sphingosine kinase 2, sphingosine-1-phosphate, ABC294640, regorafenib, resistance, hepatocellular carcinoma

INTRODUCTION

With 841,000 newly diagnosed cases and 782,000 deaths annually, liver cancer ranked as the sixth most common cancer and the fourth leading cause for cancer-related deaths worldwide (1). Hepatocellular carcinoma (HCC), which accounts for 75 to 85% cases of primary liver cancer, is the most common pathological type of this deadly disease (2).

The majority of HCC patients are diagnosed at an advanced stage, which limited the applicability and efficacy of potentially curative therapies, including surgical resection and liver transplantation (3). Therefore, patients with advanced HCC rely mainly on systemic therapy. Approved by the US Food and Drug Administration in April 2017, regorafenib is currently used as a second-line systemic therapy for advanced HCC (4). Similar with the first-line systemic drug sorafenib, regorafenib is also an oral tyrosine kinase inhibitor that targets vascular endothelial growth factor receptors (VEGFR1, VEGFR2, and VEGFR3), platelet-derived growth factor receptor, Fibroblast Growth Factor Receptor 1, Raf, TIE-2, and the kinases KIT, RET, and BRAF (5). Despite the fact that regorafenib prolonged the survival of patients who had disease progression following sorafenib failure, the efficacy of this drug was still limited by primary or acquired therapy resistance (6). Therefore, it is essential to investigate the mechanisms underlying the resistance to regorafenib and to further explore strategies to enhance drug efficacy in HCC (7).

Sphingosine kinases (SphKs) are the key regulatory enzymes catalyzing the formation of sphingosine-1-phosphate (S1P) (8). With increasing evidence of the roles of SphKs in cell survival, proliferation, apoptosis, and chemoresistance, these enzymes are considered as significant therapeutic targets in various solid tumors (9). To date, SphK1 and SphK2 have been identified as the two isoforms of SphKs. Considerable attention has been devoted to the involvement of SphK1 in multiple cancers including HCC (10). Recently, the other isoform of SphK, SphK2, also received increasing attention and may be an important regulator of cancer development and progression (11). Accumulating evidence has revealed that SphK2 is overexpressed in tumor tissues and cell lines (12, 13). Knockdown or pharmacological inhibition of SphK2 can decrease tumor proliferation and metastasis and increase apoptosis *in vivo* and *in vitro* (14, 15). It is interesting to note that data from certain studies have shown that SphK2 is closely associated with antitumor drug resistance. Overexpression of SphK2 has been suggested to contribute to gefitinib resistance in non-small cell lung cancer (NSCLC) and all-*trans* retinoic acid (ATRA) resistance in colon cancer (13, 16). However, whether SphK2 is involved in regorafenib resistance in HCC remains unclear.

ABC294640 is a highly selective and orally available small molecule inhibitor of SphK2 that can dose-dependently compete with sphingosine for binding to the enzyme. ABC294640 displayed significant antitumor activity in various solid cancers, including breast (17), lung (15), prostate (18), and liver (19) cancers. Currently, ABC294640 is under evaluation in a phase II clinical trial as a therapy for advanced HCC. Administration of ABC294640 can further enhance the effects of antitumor drugs including sorafenib (20). By coadministration of ABC294640, the potency of sorafenib in HCC, cholangiocarcinoma, pancreatic adenocarcinoma, and kidney carcinoma cells was increased (21). Therefore, it is interesting to investigate whether ABC294640 could also enhance the effects of regorafenib and even reverse regorafenib resistance in HCC.

In the present study, we explored the role and potential molecular mechanisms of SphK2 in regorafenib-resistant HCC cells. ABC294640 was used to investigate the efficacy of targeting SphK2 for reversing regorafenib resistance *in vitro and vivo*. The study aimed to provide experimental evidence for the clinical application of ABC294640 in combination with regorafenib.

RESULTS

Acquired Resistance Develops After Long-Term Exposure to Regorafenib

The SMMC-7721 and MHCC97H cell lines were used to establish cell lines resistant to regorafenib. After the establishment of the resistant cell lines, we characterized their resistant phenotype. Initially, the CCK-8 assay was used, and the data demonstrated that the growth-suppressive effect of regorafenib was significantly higher in parental cells than in regorafenib-resistant cells (**Figure 1A**). The IC_{50} values for regorafenib (**Table 1**) were considerably higher in resistant cells (97H-R: 16.85 μM, 7721-R: 12.27 μM) than in parental cells (97H: 5.378 μM, 7721: 5.431 μM). In addition, the total percentage of apoptotic regorafenib-resistant cells treated with 10 μM regorafenib was significantly lower than that of the parental cells as shown by flow cytometry analysis (**Figure 1B**, $p < 0.001$). Cell cycle analysis demonstrated that regorafenib induced G1 phase arrest in parental cells but not in regorafenib-resistant cells at a dose of 10 μM (**Figure 1C**). We also observed using a colony formation assay that the proliferative potential of regorafenib-resistant cells treated with or without 5 μM regorafenib was significantly higher than that of parental cells (**Figure 1D**). In addition, the differential effects of regorafenib in parental and regorafenib-resistant cells were confirmed by measurement of the expression levels of two apoptotic cascade-related proteins, B-cell leukemia/lymphoma 2 (Bcl2) and poly(ADP-ribose) polymerase (PARP). The effect of regorafenib on cell proliferation was also verified by the expression of cyclin D1 and cyclin-dependent kinase 2 and 4 (CDK2, CDK4). These results indicated that the regorafenib-resistant cells showed less response to regorafenib exposure as compared to parental cells (**Figure 1E**). Collectively, our data confirmed the establishment of stable regorafenib-resistant cells.

SphK2 Expression Is Negatively Associated With Regorafenib Sensitivity in HCC Cells and Is Upregulated in Regorafenib-Resistant HCC Cells

To investigate the potential involvement of SphK2 in regorafenib resistance, five HCC cell lines were used, namely, BEL-7402, HuH-7, PLC/PRF/5, SMMC-7721, and MHCC97H. The characteristics of these cells including the origin, morphology, doubling time, tumorigenicity, metastatic potential, and cellular

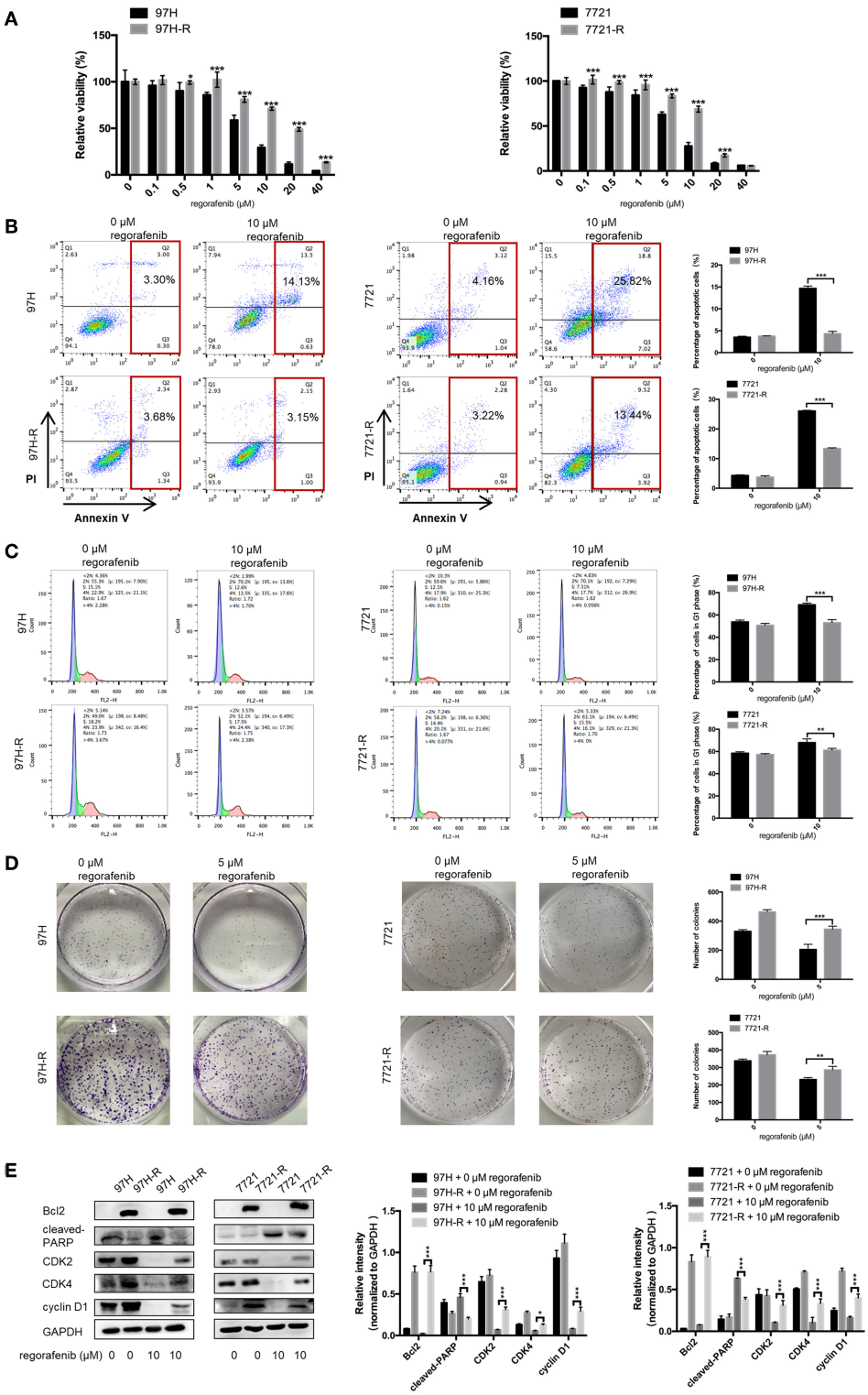

FIGURE 1 | Establishment of regorafenib-resistant HCC cells. **(A)** The CCK-8 assay was used to compare the effects of regorafenib on cell proliferation between parental and regorafenib-resistant HCC cells. **(B)** The percentage of apoptotic parental and regorafenib-resistant HCC cells treated with or without 10 μM regorafenib for 48 h was determined by annexin V/PI staining. **(C)** The cell cycle distribution of parental and regorafenib-resistant HCC cells treated with or without 10 μM

(Continued)

FIGURE 1 | regorafenib for 48 h was detected by flow cytometry. **(D)** The colony formation activity and the cell proliferation of parental and regorafenib-resistant HCC cells treated with or without 5 μM regorafenib (14 days for SMCC-7721 and 7721-R; 10 days for MHCC-97H and 97H-R, respectively) were measured. **(E)** The expression levels of Bcl2, cleaved PARP, cyclin D1, CDK2, and CDK4 were examined by Western blot analysis. 7721 and 97H indicate SMMC-7721 and MHCC97H parental cells, respectively; 7721-R and 97H-R indicate regorafenib-resistant SMMC-7721 and regorafenib-resistant MHCC97H cells, respectively. The result is representative for three independent experiments. The error bars represent mean ± SD from a representative experiment. $*p < 0.05$, $**p < 0.01$, $***p < 0.001$.

TABLE 1 | IC_{50} values of regorafenib in parental and regorafenib-resistant HCC cells.

Cell line	IC_{50} (μM)
97H	5.378
97H-R	16.85
7721	5.431
7721-R	12.27

products are summarized in **Table 2** (22–26). Among these cell lines, PLC/PRF/5 is the only one originated from African male, and BEL-7402 grows the fastest. MHCC97H was reported to develop massive lung metastasis when inoculated subcutaneously and is considered to have high metastasis potential, whereas HuH-7 is considered to be a non-invasive cell line. Hepatitis B surface antigen, which is known to be associated with the development of HCC, is expressed in PLC/PRF/5 and MHCC97H. The α-fetoprotein (α-FP), which represents the aggressiveness of HCC cells, is expressed in all cell lines except SMMC-7721. Based on the information, no obvious correlation was found between the characteristics and SphK2 expression levels. We evaluated SphK2 expression, as well as regorafenib sensitivity in these cells. As shown in **Figures 2A,B**, the protein levels of SphK2 were apparently higher in HCC cells with higher regorafenib IC_{50} values (**Table 3**). In addition, the SphK2 protein levels and the IC_{50} values exhibited a strong correlation, with a Pearson correlation coefficient (R^2) of 0.8889 (**Figure 2C**), indicating that SphK2 expression was negatively associated with regorafenib sensitivity in HCC cell lines. Furthermore, SphK2 was significantly upregulated in regorafenib-resistant cells compared with the corresponding expression noted in parental cells (**Figure 2D**), whereas the expression of SphK1 remained unchanged (**Supplementary Figure 1A**), suggesting that SphK2 expression was positively associated with regorafenib resistance.

Overexpression of SphK2 Promotes Regorafenib Resistance in HCC Cells

To further investigate the role of SphK2 in promoting regorafenib resistance in HCC, SMMC-7721 and MHCC97H HCC cells were stably transfected with LV-SphK2 lentivirus to enhance the expression of SphK2. The increased expression of SphK2 in these two cell lines compared with that in the control cells was confirmed by Western blot analysis (**Figure 3A**). SphK2-overexpressing HCC cells (LV-SphK2 HCC cells) exhibited low sensitivity to regorafenib, as determined by the CCK-8 assay (**Figure 3B**), which was similar to the results demonstrated in HCC cells with acquired regorafenib resistance. The IC_{50} values of SphK2-overexpressing HCC cells were higher than those of the cells in the control group (**Table 4**). In LV-SphK2 HCC cells, exposure to 10 μM regorafenib for 48 h exhibited a limited impact on the percentage of apoptotic cells (**Figure 3C**) and number of G1-phase arrested cells (**Figure 3D**). The proliferative potential of LV-SphK2 cells treated with or without 5 μM regorafenib was significantly higher than that of control cells, as determined by the colony formation assay (**Figure 3E**). In addition, overexpression of SphK2 reversed the changes in Bcl2, cleaved PARP, cyclin D1, CDK2, and CDK4 (**Figure 3F**) expression following incubation of the cells with regorafenib.

Knockdown of SphK2 Restores Regorafenib Sensitivity in Regorafenib-Resistant HCC Cells

Because the previous results suggested that enhanced SphK2 expression may be a cause of acquired resistance to regorafenib in HCC cells, we attempted to knock down SphK2 in 97H-R and 7721-R cells to determine whether regorafenib resistance could be reversed. SphK2 small interfering RNA (siRNA) transfection resulted in significantly decreased expression of SphK2 in both regorafenib-resistant cell lines, as verified by Western blot analysis (**Figure 4A**). Transfection of SphK2 siRNA into HCC cells enhanced the inhibitory effect of regorafenib on the viability of regorafenib-resistant cells (**Figure 4B**), as the IC_{50} values of SphK2-knockdown regorafenib-resistant cells were lower than those of control group cells (**Table 5**). In contrast, siRNA-mediated knockdown of SphK1 (**Supplementary Figure 1B**) showed little impact on the sensitivity of regorafenib (**Supplementary Figure 1C**) and the IC_{50} values (**Supplementary Table 1**) in both resistant cell lines. The apoptosis assay performed on regorafenib-resistant cells demonstrated that incubation with regorafenib (10 μM) alone induced apoptosis only slightly, and SphK2 knockdown mildly increased the percentage of apoptotic cells. However, the combined effect of the two treatments was superior to the effect of either treatment alone (**Figure 4C**). Similar results were found in the cell cycle (**Figure 4D**) and colony formation assays (**Figure 4E**). Furthermore, the combination of SphK2 knockdown and regorafenib decreased Bcl2, cyclin D1, CDK2, and CDK4 expression levels and increased cleaved PARP expression levels. These results indicated that SphK2 knockdown successfully enhanced the effects of regorafenib and restored regorafenib sensitivity in regorafenib-resistant HCC cells.

Exogenous Addition of S1P Increases the Resistance of HCC Cells to Regorafenib

Since the main biological function of SphK2 is to catalyze the generation of S1P, we hypothesized that the effect of SphK2

TABLE 2 | General characteristics of 5 HCC cell lines.

Cell line	Origin	Cell morphology	Doubling time	Tumorigenicity	Metastatic potential	HBsAg	α-FP
BEL-7402	Human HCC Asian male	Epithelial	20 h	Yes	Low	Neg	Pos
HuH-7	Human HCC Asian male	Epithelial	38 h	Yes	Non	Neg	Pos
PLC/PRF/5	Human HCC African male	Epithelial	43 h	Yes	Low	Pos	Pos
SMMC-7721	Human HCC Asian male	Epithelial	40 h	Yes	Low	Neg	Neg
MHCC97H	Human HCC Asian male	Epithelial	31 h	Yes	High	Pos	Pos

HBsAg, hepatitis B surface antigen; α-FP, α-fetoprotein; Neg, negative; Pos, positive.

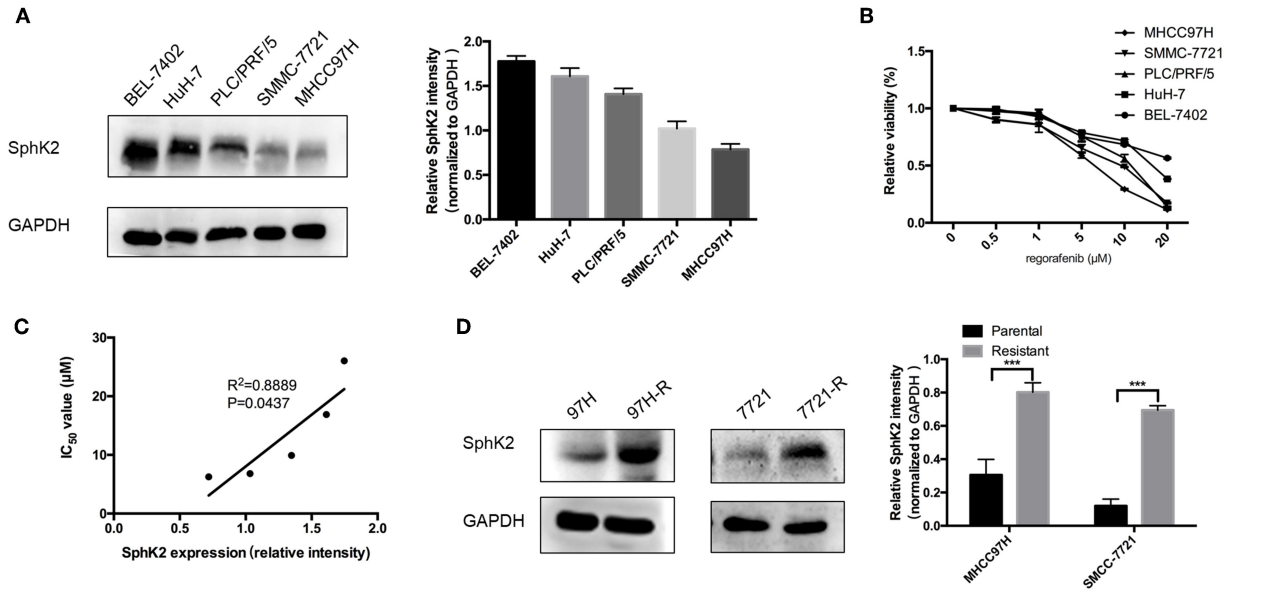

FIGURE 2 | Association between SphK2 expression and regorafenib sensitivity in HCC cells. **(A)** The protein expression of SphK2 in five HCC cell lines was determined by Western blot analysis. **(B)** Hepatocellular carcinoma cells were incubated with regorafenib for 48 h, and regorafenib sensitivity was determined by the CCK-8 assay. **(C)** The correlation between SphK2 expression and the regorafenib IC_{50} value in HCC cell lines was assessed by the Pearson correlation coefficient. **(D)** SphK2 protein expression in parental and regorafenib-resistant HCC cells. The result is representative for three independent experiments. The error bars represent mean ± SD from a representative experiment. ***$p < 0.001$.

TABLE 3 | IC_{50} values of regorafenib in 5 HCC cell lines.

Cell line	IC_{50} (μM)
BEL-7402	26.04
HuH-7	16.90
PLC/PRF/5	9.91
SMMC-7721	6.81
MHCC97H	6.26

on acquired regorafenib resistance was achieved via S1P. To determine whether S1P could increase regorafenib resistance of HCC cells, we added 1 μM exogenous S1P to stimulate HCC cells. The concentration of S1P was determined based on physiological S1P content in human blood and a dose-dependent HCC cell viability analysis (**Supplementary Figure 2**). Sphingosine-1-phosphate stimulation decreased regorafenib sensitivity in HCC cells. The IC_{50} values of regorafenib in 97H and 7721 cells incubated with S1P were 13.13 and 10.67 μM, respectively. However, the IC_{50} values of regorafenib in 97H and 7721 cells that were not incubated with S1P were only 6.157 and 6.245 μM, respectively (**Table 6**). In addition, S1P stimulation decreased the influence of regorafenib on cell viability (**Figure 5A**), apoptosis (**Figure 5B**), and cell cycle progression (**Figure 5C**) in HCC cells. Following S1P stimulation, the proliferative potential of HCC cells was increased significantly (**Figure 5D**), and the changes noted in Bcl2, cleaved PARP, cyclin D1, CDK2, and CDK4 expression following regorafenib treatment of the cells were partly diminished (**Figure 5E**). Collectively, these data suggested that exogenous S1P stimulated the development of regorafenib resistance, indicating that SphK2 could promote

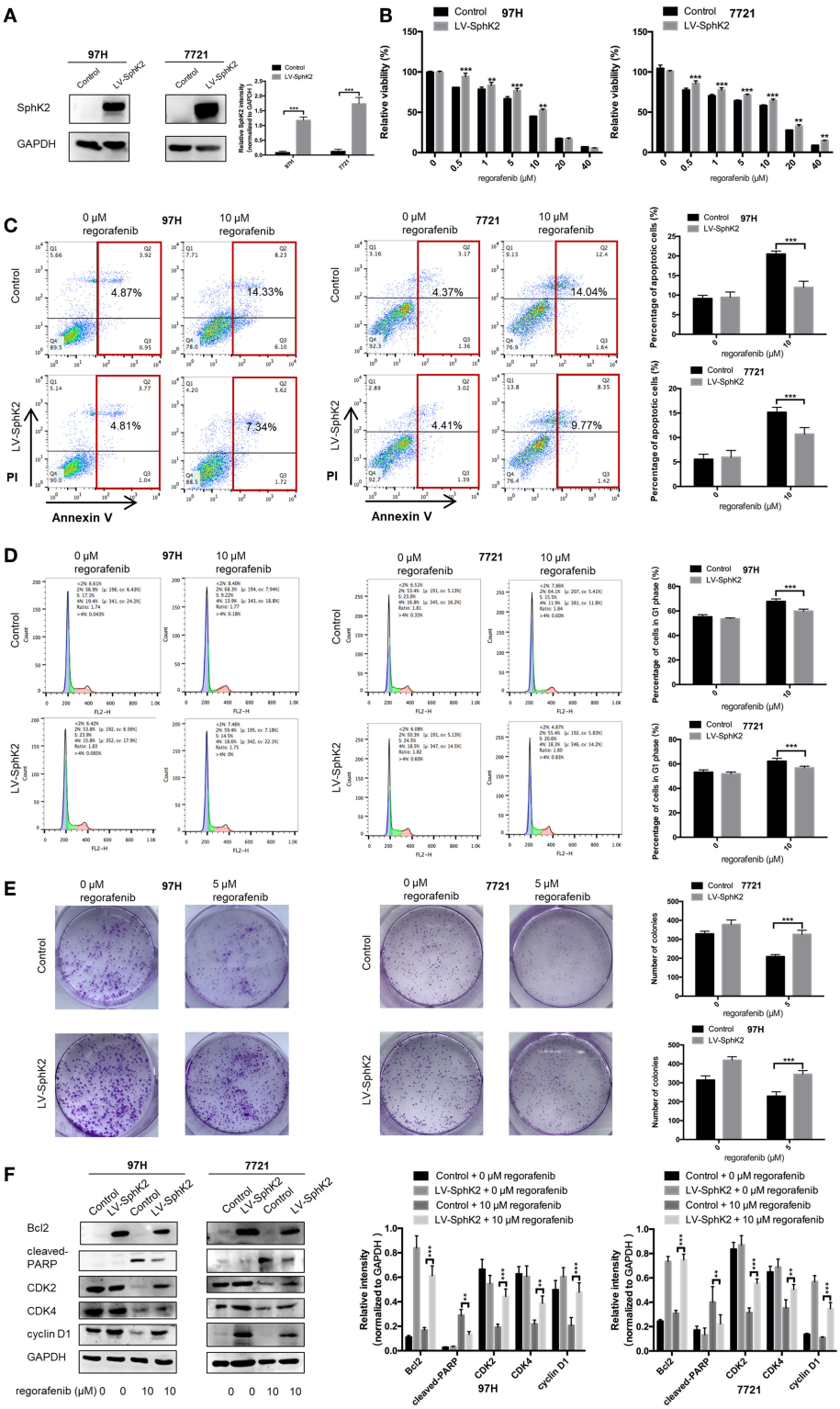

FIGURE 3 | Effects of SphK2 overexpression on the sensitivity of HCC cells to regorafenib. **(A)** The protein expression of SphK2 in HCC cells transfected with LV-SphK2 lentivirus or control vector was measured by Western blot analysis. **(B)** Regorafenib sensitivity of HCC cells transfected with LV-SphK2 lentivirus or control lentivirus was assessed by the CCK-8 assay, and regorafenib IC_{50} values were calculated accordingly. **(C)** The annexin V–FITC/propidium iodide double-staining assay, **(D)** cell cycle analysis, and **(E)** colony formation assay were applied to compare regorafenib sensitivity of HCC cells in the two different groups. **(F)** The

(Continued)

FIGURE 3 | expression levels of Bcl2, cleaved PARP, cyclin D1, CDK2, and CDK4 were examined by Western blot analysis. The dose of regorafenib treatment in the assays was 10 μM for 48 h, with the exception of the colony formation assay (5 μM, 14 days for SMCC-7721 and 10 days for MHCC-97H, respectively). The result is representative for three independent experiments. The error bars represent mean ± SD from a representative experiment. $^{**}p < 0.01$, $^{***}p < 0.001$.

TABLE 4 | IC_{50} values of regorafenib in SphK2-overexpressing HCC cells and control group cells.

Cell line	Group	IC_{50} (μM)
97H	Control	6.145
	LV-SphK2	9.592
7721	Control	6.36
	LV-SphK2	10.22

regorafenib resistance in HCC by catalyzing the generation of S1P.

Pharmacological Inhibition of SphK2 Leads to Regorafenib Sensitization in HCC Cells

In the present study, SphK2 was targeted by its selective inhibitor ABC294640, to evaluate the effects of SphK2 on regorafenib resistance and to explore the potential efficacy of combination treatment with regorafenib and SphK2 inhibitors. The CCK-8 assay was used to determine the effects of ABC294640 on the viability of regorafenib-resistant HCC cells. Treatment with 20 μM of ABC294640 showed little inhibition on cell viability. Therefore, this dose was selected for the SphK2 inhibitory experiments (**Figure 6A**). The representative images of cell morphology demonstrated that the number of cells treated with combination of ABC294640 and regorafenib was considerably decreased compared with that in other groups (**Figure 6B**). The CCK-8 assay results indicated that the viability of 97H-R and 7721-R cells (**Figure 6C**) and their regorafenib IC_{50} values (**Table 7**) were significantly decreased following combination treatment with ABC294640 and regorafenib for 48 h. In contrast, coadministration of selective SphK1 inhibitor PF-543 did not sensitize resistant cells to regorafenib treatment (**Supplementary Figure 1D** and **Supplementary Table 2**). Furthermore, the induction of apoptosis (**Figure 6D**), cell cycle arrest (**Figure 6E**), and the inhibition of colony formation (**Figure 6F**) in regorafenib-resistant cells was dramatically enhanced by concomitant exposure to ABC294640 and regorafenib, while treatment with either drug alone exhibited only marginal effects. The alterations in the expression levels of Bcl2, cleaved PARP, cyclin D1, CDK2, and CDK4 (**Figure 6G**) further confirmed the effects of ABC294640 on reversing regorafenib resistance. These data indicated that the application of ABC294640 could reduce regorafenib resistance of HCC cells.

The Combined Treatment of Regorafenib and ABC294640 Suppressed Tumor Growth in Xenograft Animal Model of HCC

The present study further evaluated the potential therapeutic efficacy of combination treatment with ABC294640 and regorafenib in a nude mice xenograft model established by regorafenib-resistant MHCC97H cells. There was no significant difference in body weight between mice treated with drugs and mice treated with vehicle, and no mice died during the treatment, indicating little systemic toxicity of these drugs (**Figure 7A**). As shown in **Figures 7B,C**, compared with vehicle control, treatment of either regorafenib or ABC294640 showed mild tumor inhibitory effects, whereas combination treatment with both drugs dramatically suppressed the growth of tumor. The measurement of the volume and weight (**Figure 7D**) of tumors also confirmed that coadministration of AB294640 with regorafenib sensitized the resistant cells to treatment.

SphK2/S1P Regulates Regorafenib Resistance of HCC Cells by Inducing the Activation of Nuclear Factor κB and Signal Transducer and Activator of Transcription 3

Currently, the molecular mechanisms of SphK2-mediated regorafenib resistance in HCC remain unknown. Because nuclear factor κB (NF-κB) and signal transducer and activator of transcription 3 (STAT3) are targets of regorafenib and ABC294640, we hypothesized that SphK2/S1P could regulate regorafenib resistance in HCC cells through NF-κB and STAT3 activation. Therefore, we determined the phosphorylation levels of NF-κB p65 and STAT3 in HCC cells following different treatments. Western blot analysis indicated that the phosphorylation levels of NF-κB p65 and STAT3 were increased in regorafenib-resistant HCC cells (**Figure 8A**) and SphK2-overexpressing HCC cells (**Figure 8D**), whereas they were decreased in regorafenib-resistant HCC cells following SphK2 knockdown or inhibition (**Figures 8B,C**). In addition, exogenous S1P treatment promoted the phosphorylation of NF-κB p65 and STAT3 (**Figure 8E**). Based on these experimental data, the present study confirmed that NF-κB and STAT3 activation was involved in SphK2/S1P-mediated regorafenib resistance in HCC cells.

DISCUSSION

Chemoresistance is a complex process that develops in the majority of cancer types and causes poor therapeutic responses along with treatment failure (27). Regorafenib is a crucial drug for treating metastatic colorectal cancer (CRC), advanced gastrointestinal stromal tumors, and HCC (28). To date, only a limited number of studies have been carried out on regorafenib resistance, and most in CRC (5). This is the first study that demonstrated SphK2/S1P was the key regulator in mediating regorafenib resistance of HCC by the activation of NF-κB and STAT3. Moreover, ABC294640, a selective inhibitor of SphK2, exhibited high potential to increase the sensitivity of regorafenib-resistant HCC cells to regorafenib.

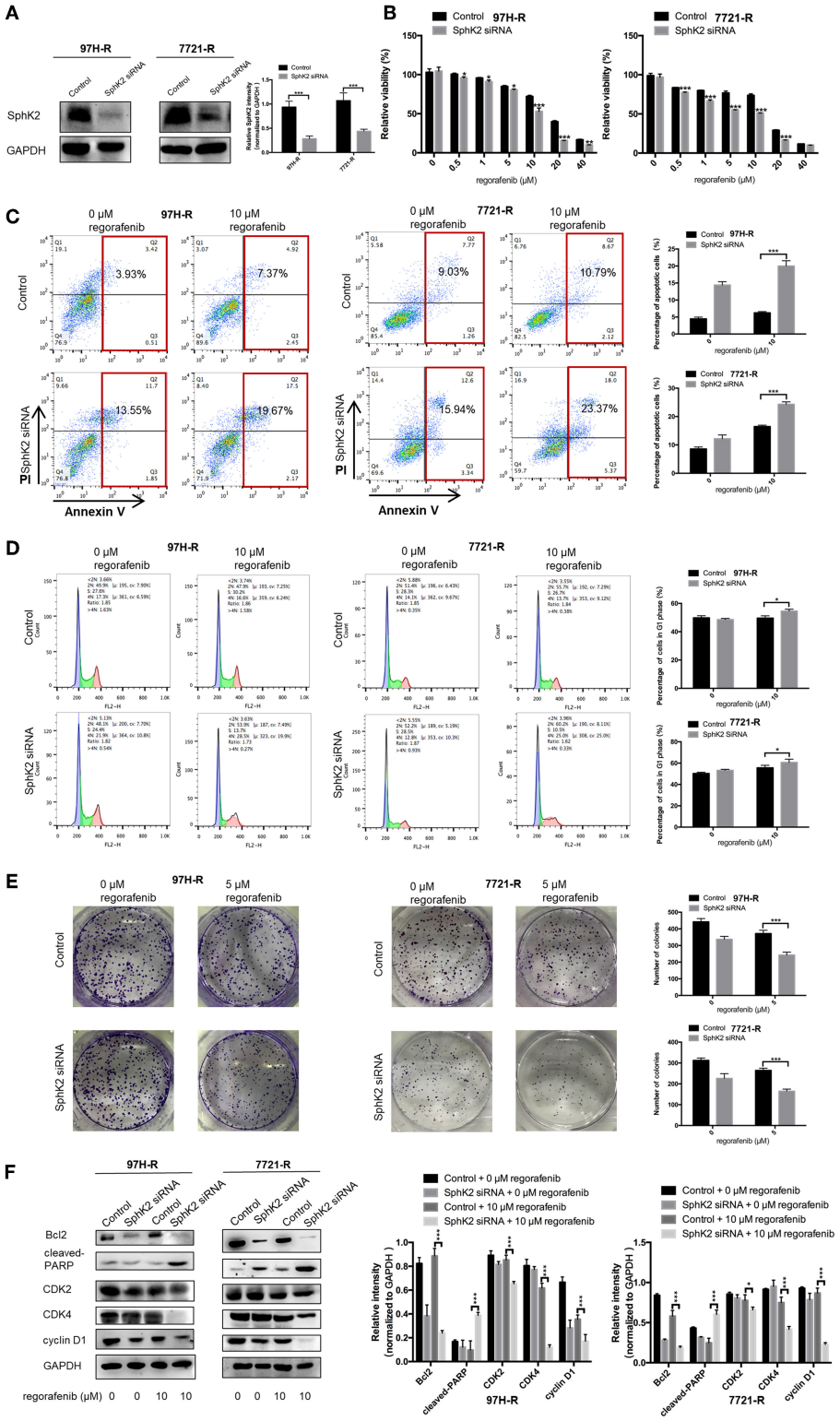

FIGURE 4 | Effects of SphK2 knockdown on regorafenib resistance in HCC cells. **(A)** The protein expression levels of SphK2 in HCC cells transfected with SphK2 siRNA or control vector were determined by Western blot analysis. **(B)** The viability of regorafenib-resistant HCC cells transfected with SphK2 siRNA or control vector was determined by the CCK-8 assay, and IC_{50} values were calculated accordingly. **(C)** The induction of apoptosis of regorafenib-resistant HCC cells transfected with SphK2 siRNA or control vector was assessed by the annexin V–FITC/propidium iodide double-staining assay. **(D)** The cell cycle distribution of regorafenib-resistant

(Continued)

FIGURE 4 | HCC cells transfected with SphK2 siRNA or control vector was assessed by flow cytometry. **(E)** The proliferation of regorafenib-resistant HCC cells transfected with SphK2 siRNA or control vector was evaluated by the colony formation assay. **(F)** The expression levels of Bcl2, cleaved PARP, cyclin D1, CDK2, and CDK4 were examined by Western blot analysis. The dose of regorafenib treatments in all assays was 10 μM for 48 h, except for the colony formation assay (5 μM, 14 days for 7721-R and 10 days for 97H-R, respectively). The result is representative for three independent experiments. The error bars represent mean ± SD from a representative experiment. $^{*}p < 0.05$, $^{**}p < 0.01$, $^{***}p < 0.001$.

TABLE 5 | IC_{50} values of regorafenib in SphK2 knockdown HCC cells and control group cells.

Cell line	Group	IC_{50} (μM)
97H-R	Control	15.24
	SphK2 siRNA	10.08
7721-R	Control	11.13
	SphK2 siRNA	6.243

TABLE 6 | IC_{50} values of regorafenib in S1P-stimulated HCC cells and control group cells.

Cell line	Group	IC_{50} (μM)
97H	0 μM S1P	6.157
	1 μM S1P	13.13
7721	0 μM S1P	6.245
	1 μM S1P	10.67

Dysregulation of sphingolipid metabolism and signaling has recently been shown to be associated with chemoresistance. Lower levels of ceramide and higher levels of S1P were simultaneously observed in gemcitabine-resistant pancreatic cancer cells than in gemcitabine-sensitive pancreatic cancer cells, whereas increasing ceramide concentrations or decreasing S1P concentrations sensitized pancreatic cancer cells to gemcitabine-induced cell death (29). In addition, the ceramide: S1P ratio was also decreased in docetaxel-resistant cells (30) and imatinib-resistant cells (31). In the present study, SphK2, the rate-limiting enzyme in sphingolipid metabolism, was found to play a vital role in regorafenib resistance in HCC. In well-established regorafenib-resistant HCC cells, the expression levels of SphK2 were substantially higher than those in parental cells. Significantly increased SphK2 expression levels were also observed in chemoresistant breast cancer cells (32). In addition, a negative correlation between SphK2 protein levels and the sensitivity to regorafenib was noted in the five HCC cell lines. These results were similar to those reported from the study by Yang et al. (20) demonstrating that SphK2 expression correlated negatively with tumor necrosis factor-related apoptosis-inducing ligand (TRAIL) sensitivity in three NSCLC cell lines.

To further investigate the role of SphK2 in promoting regorafenib resistance in HCC, we inhibited the expression of SphK2 in regorafenib-resistant cells and increased the SphK2 expression in normal HCC cells. Knockdown of SphK2 restored regorafenib sensitivity of regorafenib-resistant HCC cells. A previous study demonstrated that knockdown of SphK2 could induce the apoptosis of gefitinib-resistant NSCLC cells, which is consistent with the results reported in present study (13). Our results also showed that overexpression of SphK2 increased regorafenib resistance of normal HCC cells. Consistently, Shi et al. (16) reported that the increased levels of SphK2 expression led to ATRA therapy resistance in human colonic adenocarcinoma HCT-116 cells. Taking these data together, we demonstrated the important role of SphK2 in mediating regorafenib resistance in HCC, which could be a potential target to overcome regorafenib resistance.

In the present study, we further explored the role of SphK1 in regorafenib resistance of HCC cells. There was no obvious difference in the expression levels of SphK1 between parental cells and regorafenib-resistant cells. In addition, inhibition of SphK1 did not restore the sensitivity of HCC cells to regorafenib. These results indicated that SphK1 may not be involved in regorafenib resistance, and SphK2 was the specific SphK mediating regorafenib resistance.

Because S1P is the main product of SphK2, the present study revealed that S1P mediates regorafenib resistance in HCC cells. Accumulating evidence demonstrated that in addition to its role as a sphingosine metabolite, S1P is a critical secondary messenger that mediates chemoresistance (30). A high level of S1P was detected in camptothecin-resistant PC-3 prostate cancer cells, and inhibition of the S1P receptor signaling significantly decreased cell growth (33). Sphingomab, a neutralizing antibody against S1P, also showed inhibitory effect on sunitinib-resistant renal carcinoma cell growth (34). The present data indicated that the supplementation of S1P reduced the sensitivity of HCC cells to regorafenib. However, the IC_{50} values of regorafenib in HCC cells stimulated with S1P were not as high as those in HCC cells with acquired regorafenib resistance. Possibly, the intracellular S1P levels in HCC cells stimulated with 1 μM S1P were different from those in regorafenib-resistant cells. In previous studies (35), the doses of S1P used to stimulate HCC cells were 1, 3, and 10 μM, which were all higher than that used in our study. Alternatively, exogenous addition of S1P may not influence endogenous ceramide production, which has inhibitory effects on chemoresistance of HCC cells. In contrast to the effects of S1P on chemoresistance, exogenous addition of ceramide (1 μM) to pancreatic cancer cells increased their sensitivity to gemcitabine (30). In addition, it has been shown that 20 μM S1P treatment exhibited no effects on ceramide production in leukemia HL-60 cells (36). Therefore, we hypothesized that the ratio of ceramide to S1P in HCC cells treated with 1 μM S1P was not as low as that in HCC cells with acquired regorafenib resistance. Subsequently, we will further explore the changes and the function of complex sphingolipid metabolism in regorafenib resistance in HCC.

As we demonstrated the promoting effect of SphK2/S1P on the regorafenib resistance of HCC cells, we aimed to reverse

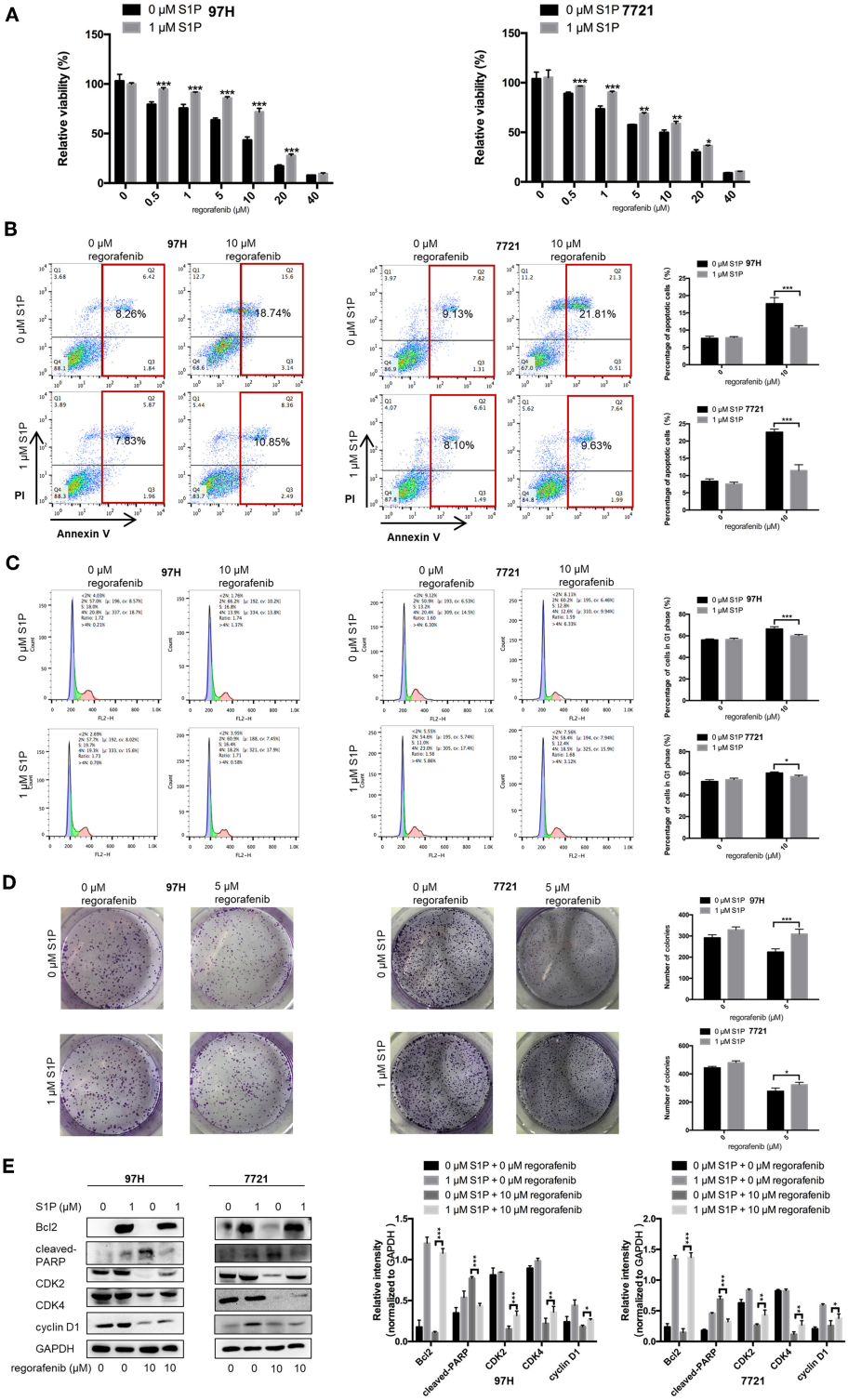

FIGURE 5 | Effects of exogenous S1P on the sensitivity of HCC cells to regorafenib. **(A)** The regorafenib sensitivity of HCC cells stimulated with 1 μM S1P was examined by the CCK-8 assay. We further used the **(B)** annexin V–FITC/propidium iodide double-staining assay, **(C)** cell cycle analysis, and **(D)** colony formation assay to measure regorafenib effects on HCC cells in different groups. **(E)** The expression levels of Bcl2, cleaved PARP, cyclin D1, CDK2, and CDK4 were examined by Western blot analysis. The dose of regorafenib treatment in all assays was 10 μM for 48 h, with the exception of the colony formation assay (5 μM, 14 days for SMCC-7721 and 10 days for MHCC-97H, respectively). The result is representative for three independent experiments. The error bars represent mean ± SD from a representative experiment. $^{*}p < 0.05$, $^{**}p < 0.01$, $^{***}p < 0.001$.

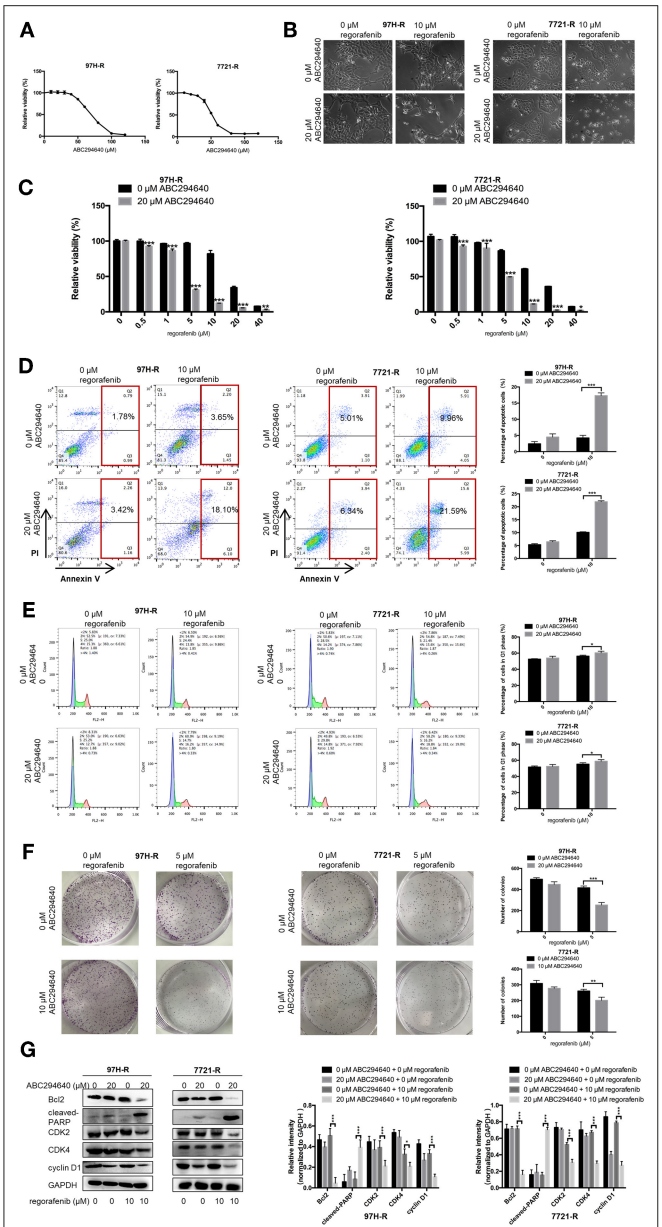

FIGURE 6 | Effects of SphK2 inhibition on regorafenib resistance in HCC cells. **(A)** The effects of ABC294640 on regorafenib-resistant HCC cell viability were evaluated by the CCK-8 assay. **(B)** Regorafenib-resistant HCC cells were treated with ABC294640 and regorafenib for 48 h. Representative images of cell morphology were acquired. Subsequently, **(C)** cell viability was evaluated by the CCK-8 assay, **(D)** whereas the apoptosis rate was determined by the annexin V–FITC/propidium iodide double-staining assay. **(E)** The cell cycle distribution was measured by flow cytometry, and **(F)** cell proliferation was evaluated by the colony formation assay. **(G)** The expression levels of Bcl2, cleaved PARP, cyclin D1, CDK2, and CDK4 were examined by Western blot analysis. The doses of regorafenib and ABC294640 treatment in all assays were 10 and 20 μM, respectively, for 48 h, with the exception of the colony formation assay (5 and 10 μM, respectively, 14 days for 7721-R and 10 days for 97H-R). The result is representative for three independent experiments. The error bars represent mean ± SD from a representative experiment. *$p < 0.05$, **$p < 0.01$, ***$p < 0.001$.

TABLE 7 | IC_{50} values of regorafenib in regorafenib-resistant HCC cells exposed to ABC294640 and control group cells.

Cell line	Group	IC_{50} (μM)
97H-R	0 μM ABC294640	15.99
	20 μM ABC294640	3.101
7721-R	0 μM ABC294640	12.84
	20 μM ABC294640	4.672

regorafenib resistance by targeting SphK2. ABC294640 is a novel selective inhibitor of SphK2 that has been found to exert broad anticancer activity. The application of ABC294640 enhanced the effects of specific antitumor drugs, such as TRAIL-induced apoptosis in NSCLC cells (20) and paclitaxel-induced apoptosis in Caov-3 ovarian cancer cells (37). The present study is the first to explore the biological effects of ABC294640 on regorafenib-resistant HCC cells. We investigated the efficacy of the combination treatment with ABC294640 and regorafenib toward regorafenib-resistant HCC. The combination of ABC294640 with regorafenib increased the induction of apoptosis and decreased the proliferation of regorafenib-resistant HCC cells. The dose of ABC294640 used in our study was 20 μM in most assays and 10 μM in the colony formation assay, which was considerably lower than that used in previous studies (37). By using 20 or 10 μM ABC294640 alone, only a mild effect was noted on proliferation and apoptosis of regorafenib-resistant cells. However, the combination of regorafenib with ABC294640 remarkably inhibited cell proliferation and promoted apoptosis in regorafenib-resistant HCC cell lines *in vitro*. In addition, the combined treatment of regorafenib and ABC294640 suppressed tumor growth of HCC resistant cells in a xenograft tumor model. The combination significantly reduced the volume and weight of developed tumors compared to individual treatments and the vehicle control animals. These findings suggest the potential of the SphK2 inhibitor ABC294640 to reverse regorafenib resistance and provide a high clinical value for the treatment of regorafenib-resistant HCC patients.

Although we demonstrated that SphK2/S1P plays important roles in mediating regorafenib resistance in HCC, the molecular mechanism of its action remains unclear. The present study indicated that NF-κB and STAT3 were involved in regorafenib resistance and that they were the downstream effectors of SphK2/S1P signaling. Western blot analysis demonstrated that the phosphorylation levels of NF-κB p65 and STAT3 were higher in regorafenib-resistant cells compared to parental cells. In addition, SphK2 overexpression and S1P addition increased the phosphorylation levels of NF-κB p65 and STAT3, which were decreased following inhibition of SphK2. The involvement of NF-κB in chemoresistance has been reported in doxorubicin-resistant breast cancer cells (38). In addition, STAT3 is significantly activated in sorafenib-resistant cells (39) and multidrug-resistant myeloma cells (40). Our findings further support previous evidence indicating that NF-κB and STAT3

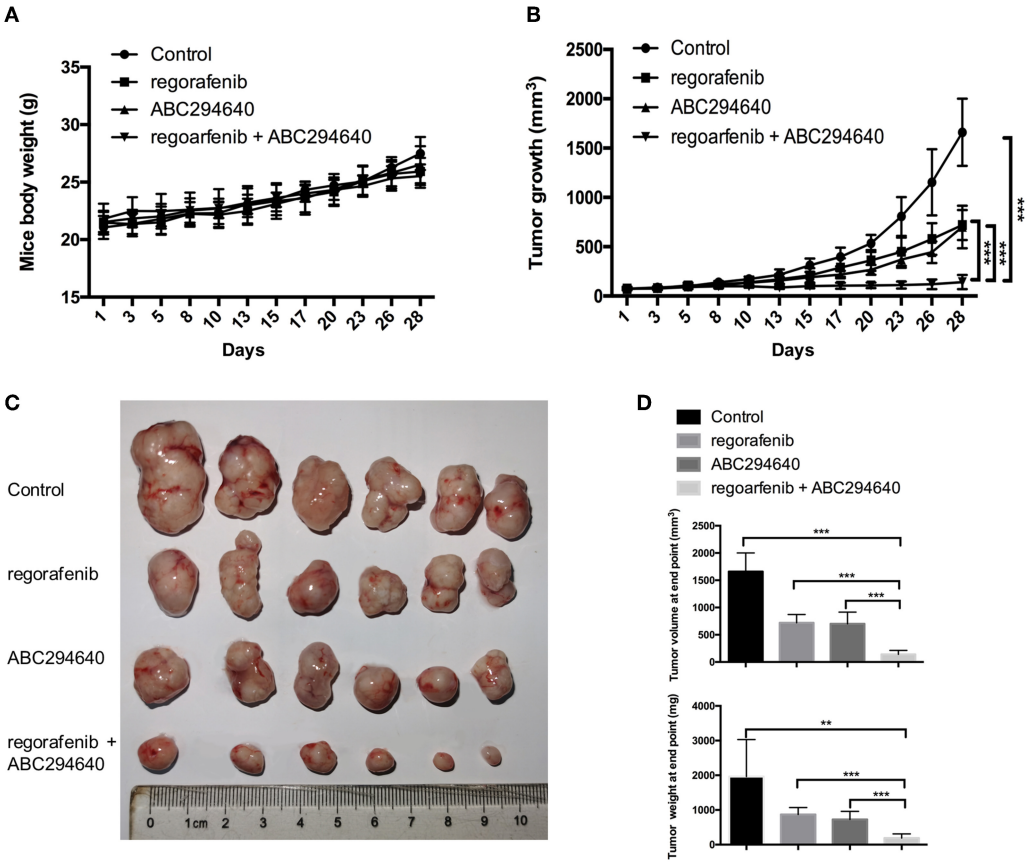

FIGURE 7 | The antitumor effects of the combination treatment of ABC294640 and regorafenib in xenograft nude mice model of HCC. **(A)** Body weight of nude mice during drug treatment. **(B)** Tumor growth of subcutaneous xenograft tumors in nude mice during drug treatment. **(C)** Image of tumors harvested from nude mice treated with vehicle, regorafenib, ABC294640, and the combination with regorafenib and ABC294640. **(D)** Average volume and weight of subcutaneous xenograft tumors harvested from nude mice at the end point of the study. The error bars represent mean ± SD. $^{**}p < 0.01$, $^{***}p < 0.001$.

are important mediators of chemoresistance. In addition, the results indicating that NF-κB and STAT3 are the downstream effectors of SphK2/S1P signaling have been observed in earlier studies. For example, S1P promoted the activation of STAT3 in cardiomyocytes (41), and ABC294640 blocked NF-κB activity in multidrug-resistant breast cancer cells (32).

CONCLUSIONS

Collectively, our data indicated that SphK2/S1P mediated regorafenib resistance of HCC cells. The activation of NF-κB and STAT3 played an important regulatory role in regorafenib resistance. The two key proteins serve as downstream effectors of SphK2/S1P, elucidating a novel mechanism, which links SphK2/S1P to NF-κB and STAT3 in regorafenib-resistant HCC cells. Most notably, the combination treatment of regorafenib with ABC294640 inhibited the proliferation and promoted the apoptosis of regorafenib-resistant HCC cells, providing new insights to overcome acquired resistance to regorafenib treatment and enhancing therapeutic outcomes for patients with advanced HCC.

MATERIALS AND METHODS

Cell Culture, Antibodies, Chemicals, and Reagents

The human HCC cell lines BEL-7402, HuH-7, PLC/PRF/5, and SMMC-7721 were purchased from the Cell Bank of the Chinese Academy of Sciences (Shanghai, China). The HCC cell line MHCC97H was kindly provided by Prof. Jia Fan from Zhongshan Hospital of Fudan University. The cells were maintained in Dulbecco modified Eagle medium (DMEM) supplemented with 10% fetal bovine serum (FBS), 100 U/mL penicillin, and 100 μg/mL streptomycin sulfate in a humidified incubator at 37°C in an atmosphere containing 5% CO_2 in air. The suppliers and catalog numbers of all antibodies, chemicals, and reagents used in this study are listed in **Supplementary Table 3**.

Establishment of Acquired Resistance to Regorafenib

Resistant cell lines (7721-R and 97H-R) were established by treating cells with stepwise increasing concentrations of

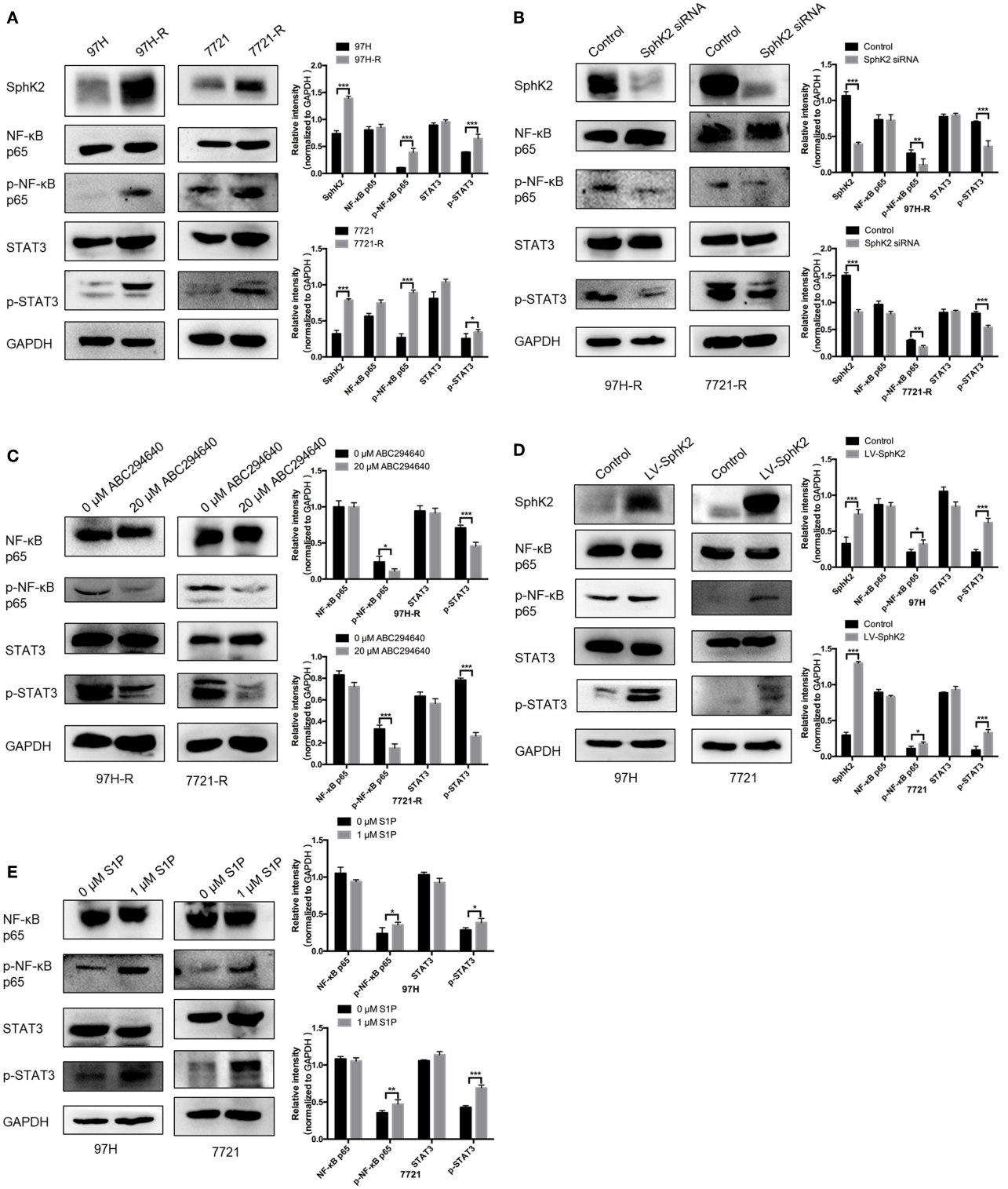

FIGURE 8 | Phosphorylation of NF-κB p65 and STAT3 in HCC cells. **(A)** The phosphorylation of NF-κB p65 and STAT3 in parental and regorafenib-resistant HCC cells was examined by Western blot analysis. **(B)** The phosphorylation of NF-κB p65 and STAT3 in regorafenib-resistant HCC cells transfected with SphKK2 siRNA. **(C)** The phosphorylation of NF-κB p65 and STAT3 in regorafenib-resistant HCC cells treated with ABC294640. **(D)** The phosphorylation of NF-κB p65 and STAT3 in SphK2-overexpressing parental HCC cells. **(E)** The phosphorylation of NF-κB p65 and STAT3 in HCC cells exposed to S1P. The density of each band was measured and normalized to respective GAPDH. The result is representative for three independent experiments. The error bars represent mean ± SD from a representative experiment. $^{*}p < 0.05$, $^{**}p < 0.01$, $^{***}p < 0.001$.

regorafenib. The protocol was modified from the establishment of sorafenib-resistant cell lines described in a previous study (42). Briefly, 1×10^6 cells were cultured in 6-mm plates and were incubated with regorafenib at a concentration just below their respective IC_{50} (5 μM for both SMCC-7721 and MHCC97H). The concentration of regorafenib was slowly increased by 0.5 μM per week. Dead cells were washed, and viable cells were cultured in fresh medium containing stepwise increasing concentrations of regorafenib. In parallel, control wild-type cells were treated with the corresponding vehicle. After 6 months, the IC_{50} to regorafenib was determined to confirm the establishment of regorafenib-resistant HCC cells. Regorafenib-resistant HCC cells were continuously maintained by culturing them in the presence of 4 μM regorafenib.

siRNA Transfection

SphK2 and SphK1 expression was downregulated by transfection with sequence-specific siRNAs. siRNA against human SphK2 (targeted sequence: GGGUAGUGCCUGAUCAAUGTT, 5′ to 3′), human SphK1 (targeted sequence: GGGCAAGGCCUUGCA GCUCTT, 5′ to 3′), and scrambled control siRNA (GenePharma, Shanghai, China) were used. The siRNAs were diluted in 150 μL of OptiPro™ SFM. Lipofectamine™ 2000 (Thermo Fisher Scientific, Waltham, MA, USA) was mixed gently before use, and the appropriate amount was subsequently diluted in 150 μL of OptiPro™ SFM. The solution was incubated for 5 min at room temperature. Following 5 min of incubation, the diluted DNA was combined with diluted Lipofectamine™ 2000 (total volume = 300 μL). The solution was mixed gently for 20 min at room temperature. The complexes (300 μL) were added to a six-well dish containing cells and medium. The cells were incubated at 37°C in a CO_2 incubator for 18 to 48 h prior to further assays.

Lentiviral Transfection

Lentiviral transfection was used to obtain HCC cells with stable ectopic SphK2 overexpression. Lentivirus expressing SphK2 and corresponding negative control virus, both with puromycin resistant gene, were purchased from Shanghai GeneChem Company Ltd. (Shanghai, China). Hepatocellular carcinoma cells were plated in 6-well plates at a density of 2×10^5 cells per well and were subsequently transfected with lentivirus at a multiplicity of infection of 10. Following 48 h of incubation, the antibiotic-resistant transfected cells were selected and enriched by applying culture medium containing puromycin.

CCK-8 Assay

For CCK-8 assay, the powder of regorafenib, ABC294640, and S1P were dissolved in dimethyl sulfoxide (DMSO) to make stock solutions containing 50, 100, and 10 mM indicated chemicals, respectively. The final concentration of DMSO in the treatment medium was <0.1%. Hepatocellular carcinoma cells in DMEM containing 10% FBS were seeded into 96-well plates at a concentration of 1×10^4 cells per well and incubated for 24 h. The culture medium was replaced with fresh medium containing vehicle or testing reagents at indicated concentrations. After treating cells with different reagents or vehicle for 48 h, CCK-8 solution (10 μL/well) was added to the 96-well plates and incubated for 1 h to detect the viability of HCC cells. The absorbance values at 450 nm were measured in a microplate reader (Bio-Rad, Hercules, CA, USA), and cell viability was determined. Relative viability was normalized to the vehicle-treated control cells after background subtraction and was expressed as $OD_{test}/OD_{control} \times 100\%$. The IC_{50} value was defined as the drug concentration that inhibits 50% cell viability compared with vehicle-treated controls and calculated by GraphPad Prism 6.0 software (GraphPad Software, La Jolla, CA, USA). Each treatment was performed in triplicate wells, and three independent repeats of experiments were performed.

Colony Assay

Hepatocellular carcinoma cells were plated in 6-well plates at a density of 1×10^3 cells per well in DMEM containing 10% FBS and allowed to adhere overnight. The culture media was replaced with fresh media containing vehicle or testing reagents every 3 days. The concentration of regorafenib, ABC294640 and S1P for colony assay was 5, 10, and 1 μM, respectively. After incubation (14 days for SMCC-7721 and 7721-R, 10 days for MHCC-97H and 97H-R), the cells were washed and fixed with 4% paraformaldehyde (20 min). The plates were incubated with 0.4% crystal violet solution (30 min) and washed with phosphate-buffered saline (PBS) and dried. The total number of colonies (≥30 cells) (32) in each well was counted manually. Three independent repeats of experiments were performed.

Cell Cycle Assay

The cell cycle distribution of different cells was determined by flow cytometry. The cells (approximately 1×10^6 cells per well) were harvested following different treatments and fixed overnight in 70% ethanol at 4°C. Following fixation, the cells were centrifuged at 1,000 × g for 5 min to remove the ethanol, washed, and stained with propidium iodide (PI) (10 μg/mL) and RNase A (100 μg/mL) at room temperature for 30 min. Propidium iodide detection was achieved with a BD FACSCalibur flow cytometer (Becton–Dickinson, San Jose, CA, USA). The distribution of the cells in the different phases of the cell cycle was analyzed and calculated using the FlowJo software (Tree star, San Carlos, CA, USA). The blue, green, and red parts in the figure of cell cycle distribution represent cells in G1 phase, S phase, and G2/M phase, respectively. Three independent repeats of experiments were performed.

Annexin V–Fluorescein Isothiocyanate/PI Double-Staining Assay

Cells (approximately 1×10^6 cells per well) were collected and centrifuged at 1,000 × g for 5 min at room temperature, resuspended in ice-cold PBS, centrifuged at 1,000 × g for 5 min, and washed. The cells were resuspended by adding 500 μL of 1× binding buffer. Subsequently, 5 μL annexin V–fluorescein isothiocyanate (FITC) staining solution and 5 μL PI staining solution were added to the suspension, mixed well, and incubated for 30 min at room temperature. Fluorescence intensity was measured using a BD FACSCalibur cytometer (Becton–Dickinson), and the apoptotic rates of cells were analyzed using the FlowJo software (Tree Star). The cells in Q1 (left upper quadrant), Q2 (right upper quadrant), Q3 (right lower quadrant), and Q4 (left lower quadrant) represent dead cells, late

apoptotic cells, early apoptotic cells, and living cells, respectively. Three independent repeats of experiments were performed.

Protein Isolation and Western Blot Analysis

The cells were lysed with 150 μL lysis buffer (Beyotime, Shanghai, China) containing 1% protease inhibitors (Thermo Fisher Scientific) on ice for 5 min following washing twice with ice-cold PBS. The cells were harvested and centrifuged at 12,000 × g for 5 min at 4°C. The protein concentrations were determined using a BCA Kit (Beyotime). Equal amounts of protein (20 μg/lane) dissolved in 20 μL loading buffer (Beyotime) were separated by sodium dodecyl sulfate–polyacrylamide gel electrophoresis (Beyotime), transferred to polyvinylidene difluoride (Roche Applied Science, Mannheim, Germany) membranes, and blocked with 5% non-fat dry milk for 1 h at room temperature. Immunoblotting was carried out by incubation overnight at 4°C with the indicated primary antibodies. Catalog numbers and suppliers of antibodies used are listed in **Supplementary Table 3**. The dilution of primary antibodies against SphK1 and SphK2 was 1:500. Other primary antibodies were diluted at 1:1,000. After the incubation with primary antibodies, membranes were washed and incubated with HRP-linked secondary antibodies (1:5,000 dilution) at room temperature for 1 h. The signals were developed with an enhanced chemiluminescence reagent (Biosharp, Beijing, China) under a chemiluminescence camera (Tanon, Beijing, China). The density of each band was measured using ImageJ software (National Institutes of Health, Maryland, MD, USA) and was normalized to internal loading control (GAPDH) from the same sample. Three independent repeats of experiments were performed.

Tumor Xenograft Model

Six-week-old male BALB/c nude mice, weighing ∼20 g, were purchased from the Model Animal Research Center of Nanjing University. Mice were housed in sterile cages in laminar airflow hoods in a specific pathogen-free environment at 22 to 25°C, relative humidity 40°C to 60% with a 12:12-h day–night light cycle. The mice had free access to autoclaved water and commercial mice food (Xietong Biological, Nanjing, China). The protocol of this study was approved by the Institutional Ethics Committee of the Affiliated Drum Tower Hospital of Nanjing University Medical School. Regorafenib-resistant MHCC-97H (97H-R) cells (1×10^7 cells in 100 μL PBS) were injected subcutaneously to nude mice. When the long diameter of tumors reached 5 mm, mice were randomly assigned to four groups ($n = 6$ per group) and were orally treated with vehicle, regorafenib, ABC294640, or both regorafenib and ABC294640, respectively. Regorafenib and ABC294640 were suspended in an oral vehicle containing 2% DMSO + 30% PEG300 (Selleck, Mattapoisett, MA, USA) + 5% Tween 80 (Selleck) + ddH_2O. Mimicking the clinically recommended administration schedule of regorafenib in human, 20 mg/kg regorafenib was given orally once daily for the first 21 days. ABC294640 was given 40 mg/kg orally, three times a week for 4 weeks according to a previously published study (43). Tumors were measured with a digital caliper three times a week, and the volume was calculated by the formula: length × width^2 × 0.5. The body weight of animals was also measured three times a week. All mice were sacrificed by cervical dislocation under general anesthesia with isoflurane (RWD Life Science, Shenzhen, China) after 4 weeks of treatment, and the tumors were harvested.

Statistical Analysis

The data were analyzed using SPSS 19.0 statistical software (IBM, Chicago, IL, USA) and expressed as the mean ± SD of a representative independent experiment. The comparisons between two groups were performed with Student *t*-test, whereas the comparisons among multiple groups were performed with one-way analysis of variance followed by the Student–Newman–Keuls *post-hoc* test. $P < 0.05$ was considered to indicate a statistically significant difference.

DATA AVAILABILITY STATEMENT

All datasets generated for this study are included in the article/**Supplementary Material**.

ETHICS STATEMENT

The animal study was reviewed and approved by Institutional Ethics Committee of the Affiliated Drum Tower Hospital of Nanjing University Medical School.

AUTHOR CONTRIBUTIONS

CJ, JW, ZW, and WS conceived and designed the experiments. WS, SZ, DM, DY, GZ, and YC performed the experiments. WS, SZ, DM, DY, GZ, and YC analyzed the data. WS and SZ wrote the original manuscript. JW and ZW reviewed and edited the manuscript. CJ, JW, and ZW acquired the funding. All authors contributed to the article and approved the submitted version.

FUNDING

This research was supported by the National Natural Science Foundation of China, nos. 81572393, 81972888, and 81602093; the Natural Science Foundation of Jiangsu Province, nos. BK20160118 and BK20141324; the Key Project supported by the Medical Science and Technology Development Foundation, Nanjing Municipality Health Bureau, nos. ZKX15020 and ZKX17022; the Fundamental Research Funds for the Central Universities, nos. 021414380215, 021414380242, 021414380258, and 14380329/3; the Jiangsu Provincial Key Research and Development Program, no. BE2018701.

ACKNOWLEDGMENTS

We thank the Translational Medicine Core facilities of the Medical School of Nanjing University for instrumentation support.

SUPPLEMENTARY MATERIAL

The Supplementary Material for this article can be found online at: https://www.frontiersin.org/articles/10.3389/fonc.2020.00694/full#supplementary-material

REFERENCES

1. Bray F, Ferlay J, Soerjomataram I, Siegel RL, Torre LA, Jemal A. Global cancer statistics 2018: GLOBOCAN estimates of incidence and mortality worldwide for 36 cancers in 185 countries. *CA Cancer J Clin*. (2018) 68:394–424. doi: 10.3322/caac.21492
2. Ayuso C, Rimola J, Vilana R, Burrel M, Darnell A, Garcia-Criado A, et al. Diagnosis and staging of hepatocellular carcinoma (HCC): current guidelines. *Eur J Radiol*. (2018) 101:72–81. doi: 10.1016/j.ejrad.2018.01.025
3. Kim DW, Talati C, Kim R. Hepatocellular carcinoma (HCC): beyond sorafenib-chemotherapy. *J Gastrointest Oncol*. (2017) 8:256–65. doi: 10.21037/jgo.2016.09.07
4. Rimassa L, Pressiani T, Merle P. Systemic treatment options in hepatocellular carcinoma. *Liver Cancer*. (2019) 8:427–46. doi: 10.1159/000499765
5. Mirone G, Perna S, Shukla A, Marfe G. Involvement of notch-1 in resistance to regorafenib in colon cancer cells. *J Cell Physiol*. (2016) 231:1097–105. doi: 10.1002/jcp.25206
6. Bruix J, Qin S, Merle P, Granito A, Huang YH, Bodoky G, et al. Regorafenib for patients with hepatocellular carcinoma who progressed on sorafenib treatment (RESORCE): a randomised, double-blind, placebo-controlled, phase 3 trial. *Lancet*. (2017) 389:56–66. doi: 10.1016/S0140-6736(16)32453-9
7. Tutusaus A, Stefanovic M, Boix L, Cucarull B, Zamora A, Blasco L, et al. Antiapoptotic BCL-2 proteins determine sorafenib/regorafenib resistance and BH3-mimetic efficacy in hepatocellular carcinoma. *Oncotarget*. (2018) 9:16701–17. doi: 10.18632/oncotarget.24673
8. Xie Z, Liu H, Geng M. Targeting sphingosine-1-phosphate signaling for cancer therapy. *Sci China Life Sci*. (2017) 60:585–600. doi: 10.1007/s11427-017-9046-6
9. Plano D, Amin S, Sharma AK. Importance of sphingosine kinase (SphK) as a target in developing cancer therapeutics and recent developments in the synthesis of novel SphK inhibitors. *J Med Chem*. (2014) 57:5509–24. doi: 10.1021/jm4011687
10. Wang F, Wu Z. Sphingosine kinase 1 overexpression is associated with poor prognosis and oxaliplatin resistance in hepatocellular carcinoma. *Exp Ther Med*. (2018) 15:5371–6. doi: 10.3892/etm.2018.6086
11. Hasanifard L, Sheervalilou R, Majidinia M. New insights into the roles and regulation of SphK2 as a therapeutic target in cancer chemoresistance. *J Cell Physiol*. (2019) 234:8162–81. doi: 10.1002/jcp.27612
12. Liu J, Zhou Q, Wu CP, Xu YW, Liu WL, Zhao HF, et al. SPHK2 protein expression, Ki-67 index and infiltration of tumor-associated macrophages (TAMs) in human glioma. *Histol Histopathol*. (2018) 33:987–94. doi: 10.14670/HH-11-995
13. Liu W, Ning J, Li C, Hu J, Meng Q, Lu H, et al. Overexpression of Sphk2 is associated with gefitinib resistance in non-small cell lung cancer. *Tumour Biol*. (2016) 37:6331–6. doi: 10.1007/s13277-015-4480-1
14. Sun E, Zhang W, Wang L, Wang A, Ma C, Lei M, et al. Down-regulation of Sphk2 suppresses bladder cancer progression. *Tumour Biol*. (2016) 37:473–8. doi: 10.1007/s13277-015-3818-z
15. Dai L, Smith CD, Foroozesh M, Miele L, Qin Z. The sphingosine kinase 2 inhibitor ABC294640 displays anti-non-small cell lung cancer activities *in vitro* and *in vivo*. *Int J Cancer*. (2018) 142:2153–62. doi: 10.1002/ijc.31234
16. Shi WN, Cui SX, Song ZY, Wang SQ, Sun SY, Yu XF, et al. Overexpression of SphK2 contributes to ATRA resistance in colon cancer through rapid degradation of cytoplasmic RXRalpha by K48/K63-linked polyubiquitination. *Oncotarget*. (2017) 8:39605–17. doi: 10.18632/oncotarget.17174
17. Antoon JW, White MD, Meacham WD, Slaughter EM, Muir SE, Elliott S, et al. Antiestrogenic effects of the novel sphingosine kinase-2 inhibitor ABC294640. *Endocrinology*. (2010) 151:5124–35. doi: 10.1210/en.2010-0420
18. Venant H, Rahmaniyan M, Jones EE, Lu P, Lilly MB, Garrett-Mayer E, et al. The sphingosine kinase 2 inhibitor ABC294640 reduces the growth of prostate cancer cells and results in accumulation of dihydroceramides *in vitro* and *in vivo*. *Mol Cancer Ther*. (2015) 14:2744–52. doi: 10.1158/1535-7163.MCT-15-0279
19. Beljanski V, Lewis CS, Smith CD. Antitumor activity of sphingosine kinase 2 inhibitor ABC294640 and sorafenib in hepatocellular carcinoma xenografts. *Cancer Biol Ther*. (2011) 11:524–34. doi: 10.4161/cbt.11.5.14677
20. Yang J, Yang C, Zhang S, Mei Z, Shi M, Sun S, et al. ABC294640, a sphingosine kinase 2 inhibitor, enhances the antitumor effects of TRAIL in non-small cell lung cancer. *Cancer Biol Ther*. (2015) 16:1194–204. doi: 10.1080/15384047.2015.1056944
21. Beljanski V, Knaak C, Zhuang Y, Smith CD. Combined anticancer effects of sphingosine kinase inhibitors and sorafenib. *Invest New Drugs*. (2011) 29:1132–42. doi: 10.1007/s10637-010-9452-0
22. Tang ZY, Sun FX, Tian J, Ye SL, Liu YK, Liu KD, et al. Metastatic human hepatocellular carcinoma models in nude mice and cell line with metastatic potential. *World J Gastroenterol*. (2001) 7:597–601. doi: 10.3748/wjg.7.597
23. Tian J, Tang ZY, Ye SL, Liu YK, Lin ZY, Chen J, et al. New human hepatocellular carcinoma (HCC) cell line with highly metastatic potential (MHCC97) and its expressions of the factors associated with metastasis. *Br J Cancer*. (1999) 81:814–21. doi: 10.1038/sj.bjc.6690769
24. Tobita K, Ohori K. Polypeptide analysis of hepatitis-virus type-B surface-antigen 559 produced by a human hepatoma-cell line, PLC-PRF-5. *Acta Virol*. (1980) 24:367-&.
25. Jung CW, Song T-J, Lee K-O, Choi SB, Kim WB, Suh SO, et al. Characterization of hepatocellular carcinoma cell lines based on cell adhesion molecules. *Int J Mol Med*. (2012) 29:1158–64. doi: 10.3892/ijmm.2012.951
26. Wang F, He L, Dai W-Q, Xu Y-P, Wu D, Lin C-L, et al. Salinomycin inhibits proliferation and induces apoptosis of human hepatocellular carcinoma cells *in vitro* and *in vivo*. *PLoS ONE*. (2012) 7:638. doi: 10.1371/journal.pone.0050638
27. Holohan C, Van Schaeybroeck S, Longley DB, Johnston PG. Cancer drug resistance: an evolving paradigm. *Nat Rev Cancer*. (2013) 13:714–26. doi: 10.1038/nrc3599
28. Sherman M. Regorafenib for treatment of hepatocellular carcinoma. *Hepatology*. (2018) 67:1162–5. doi: 10.1002/hep.29598
29. Guillermet-Guibert J, Davenne L, Pchejetski D, Saint-Laurent N, Brizuela L, Guilbeau-Frugier C, et al. Targeting the sphingolipid metabolism to defeat pancreatic cancer cell resistance to the chemotherapeutic gemcitabine drug. *Mol Cancer Ther*. (2009) 8:809–20. doi: 10.1158/1535-7163.MCT-08-1096
30. Ponnusamy S, Meyers-Needham M, Senkal CE, Saddoughi SA, Sentelle D, Selvam SP, et al. Sphingolipids and cancer: ceramide and sphingosine-1-phosphate in the regulation of cell death and drug resistance. *Fut Oncol*. (2010) 6:1603–24. doi: 10.2217/fon.10.116
31. Baran Y, Salas A, Senkal CE, Gunduz U, Bielawski J, Obeid LM, et al. Alterations of ceramide/sphingosine 1-phosphate rheostat involved in the regulation of resistance to imatinib-induced apoptosis in K562 human chronic myeloid leukemia cells. *J Biol Chem*. (2007) 282:10922–34. doi: 10.1074/jbc.M610157200
32. Antoon JW, White MD, Slaughter EM, Driver JL, Khalili HS, Elliott S, et al. Targeting NF kappa B mediated breast cancer chemoresistance through selective inhibition of sphingosine kinase-2. *Cancer Biol Ther*. (2011) 11:678–89. doi: 10.4161/cbt.11.7.14903
33. Akao Y, Banno Y, Nakagawa Y, Hasegawa N, Kim TJ, Murate T, et al. High expression of sphingosine kinase 1 and S1P receptors in chemotherapy-resistant prostate cancer PC3 cells and their camptothecin-induced up-regulation. *Biochem Biophys Res Commun*. (2006) 342:1284–90. doi: 10.1016/j.bbrc.2006.02.070
34. Zhang L, Wang X, Bullock AJ, Callea M, Shah H, Song J, et al. Anti-S1P Antibody as a novel therapeutic strategy for VEGFR TKI-resistant renal cancer. *Clin Cancer Res*. (2015) 21:1925–34. doi: 10.1158/1078-0432.CCR-14-2031
35. Cheng JC, Wang EY, Yi Y, Thakur A, Tsai SH, Hoodless PA. S1P Stimulates proliferation by upregulating CTGF expression through S1PR2-mediated YAP activation. *Mol Cancer Res*. (2018) 16:1543–55. doi: 10.1158/1541-7786.MCR-17-0681
36. Taniguchi M, Kitatani K, Kondo T, Hashimoto-Nishimura M, Asano S, Hayashi A, et al. Regulation of autophagy and its associated cell death by "sphingolipid rheostat": reciprocal role of ceramide and sphingosine 1-phosphate in the mammalian target of rapamycin pathway. *J Biol Chem*. (2012) 287:39898–910. doi: 10.1074/jbc.M112.416552
37. White MD, Chan L, Antoon JW, Beckman BS. Targeting ovarian cancer and chemoresistance through selective inhibition of sphingosine kinase-2 with ABC294640. *Anticancer Res*. (2013) 33:3573–9.
38. Meiyanto E, Putri DD, Susidarti RA, Murwanti R, Sardjiman, Fitriasari A, et al. Curcumin and its analogues (PGV-0 and PGV-1) enhance sensitivity of resistant MCF-7 cells to doxorubicin through inhibition of

HER2 and NF-kB activation. *Asian Pac J Cancer Prev*. (2014) 15:179–84. doi: 10.7314/APJCP.2014.15.1.179
39. Tai WT, Cheng AL, Shiau CW, Liu CY, Ko CH, Lin MW, et al. Dovitinib induces apoptosis and overcomes sorafenib resistance in hepatocellular carcinoma through SHP-1-mediated inhibition of STAT3. *Mol Cancer Ther*. (2012) 11:452–63. doi: 10.1158/1535-7163.MCT-11-0412
40. Shi L, Wang S, Zangari M, Xu H, Cao TM, Xu C, et al. Over-expression of CKS1B activates both MEK/ERK and JAK/STAT3 signaling pathways and promotes myeloma cell drug-resistance. *Oncotarget*. (2010) 1:22–33. doi: 10.18632/oncotarget.105
41. Deshpande GP, Imamdin A, Lecour S, Opie LH. Sphingosine-1-phosphate (S1P) activates STAT3 to protect against *de novo* acute heart failure (AHF). *Life Sci*. (2018) 196:127–32. doi: 10.1016/j.lfs.2018.01.023
42. He C, Dong X, Zhai B, Jiang X, Dong D, Li B, et al. MiR-21 mediates sorafenib resistance of hepatocellular carcinoma cells by inhibiting autophagy via the PTEN/Akt pathway. *Oncotarget*. (2015) 6:28867–81. doi: 10.18632/oncotarget.4814
43. French KJ, Zhuang Y, Maines LW, Gao P, Wang W, Beljanski V, et al. Pharmacology and antitumor activity of ABC294640, a selective inhibitor of sphingosine kinase-2. *J Pharmacol Exp Ther*. (2010) 333:129–39. doi: 10.1124/jpet.109.163444

Conflict of Interest: The authors declare that the research was conducted in the absence of any commercial or financial relationships that could be construed as a potential conflict of interest.

frontiers in Oncology

ORIGINAL RESEARCH
published: 07 August 2020
doi: 10.3389/fonc.2020.01274

Phosphodiesterase Type 5 Inhibitors Synergize Vincristine in Killing Castration-Resistant Prostate Cancer Through Amplifying Mitotic Arrest Signaling

Jui-Ling Hsu[1,2], Wohn-Jenn Leu[1], Lih-Ching Hsu[1], Chen-Hsun Ho[3,4], Shih-Ping Liu[5] and Jih-Hwa Guh[1]**

[1] School of Pharmacy, College of Medicine, National Taiwan University, Taipei, Taiwan, [2] Department of Pharmacy, New Taipei Municipal TuCheng Hospital, Chang Gung Memorial Hospital, New Taipei city, Taiwan, [3] Department of Urology, Shuang Ho Hospital, Taipei Medical University, Taipei, Taiwan, [4] Department of Urology, School of Medicine, College of Medicine, Taipei Medical University, Taipei, Taiwan, [5] Department of Urology, National Taiwan University Hospital College of Medicine, Taipei, Taiwan

OPEN ACCESS

Edited by:
Khalid A El Sayed, University of Louisiana at Monroe, United States

Reviewed by:
Victor M. Bolanos-Garcia, Oxford Brookes University, United Kingdom
William Taylor, University of Toledo, United States

***Correspondence:**
Shih-Ping Liu
spliu@ntuh.gov.tw
Jih-Hwa Guh
jhguh@ntu.edu.tw

Specialty section:
This article was submitted to Pharmacology of Anti-Cancer Drugs, a section of the journal Frontiers in Oncology

Received: *09 February 2020*
Accepted: *19 June 2020*
Published: *07 August 2020*

Citation:
Hsu J-L, Leu W-J, Hsu L-C, Ho C-H, Liu S-P and Guh J-H (2020) Phosphodiesterase Type 5 Inhibitors Synergize Vincristine in Killing Castration-Resistant Prostate Cancer Through Amplifying Mitotic Arrest Signaling. Front. Oncol. 10:1274. doi: 10.3389/fonc.2020.01274

Combination therapies that display cancer-killing activities through either coexistent targeting of several cellular factors or more efficient suppression of a specific pathway are generally used in cancer treatment. Sildenafil, a specific phosphodiesterase type 5 (PDE5) inhibitor, has been suggested to display both cardioprotective and neuroprotective activities that provide a rationale for the combination with vincristine on the treatment against castration-resistant prostate cancer (CRPC). In the present work, vincristine arrested cells in the metaphase stage of mitosis. Vincristine-induced mitotic arrest was identified by Cdk1 activation (i.e., increased $Cdk1^{Thr161}$ phosphorylation and decreased $Cdk1^{Tyr15}$ phosphorylation), cyclin B1 upregulation, and increased phosphorylation of multiple mitotic proteins and stathmin. Sildenafil synergistically potentiated vincristine-induced mitotic arrest and a dramatic increase of mitotic index. Furthermore, sildenafil potentiated vincristine-induced mitochondrial damage, including Mcl-1 downregulation, Bcl-2 phosphorylation and downregulation, Bak upregulation and loss of mitochondrial membrane potential, and sensitized caspase-dependent apoptotic cell death. Sildenafil-mediated synergistic effects were mimicked by other PDE5 inhibitors including vardenafil and tadalafil, and also by *PDE5A* knockdown in cells, suggesting PDE5-involved mechanism. Notably, sildenafil amplified vincristine-induced phosphorylation and cleavage of BUBR1, a protein kinase in spindle assembly checkpoint (SAC) function and chromosome segregation. Sildenafil also significantly decreased kinetochore tension during SAC activation. Moreover, sildenafil synergized with vincristine on suppressing tumor growth in an *in vivo* model. In conclusion, the data suggest that sildenafil, in a PDE5-dependent manner, potentiates vincristine-induced mitotic arrest signaling, and sensitizes mitochondria damage–involved apoptosis in CRPC. Both *in vitro* and *in vivo* data suggest the combination potential of PDE5 inhibitors and vincristine on CRPC treatment.

Keywords: sildenafil, vincristine, castration-resistant prostate cancer, spindle assembly checkpoint, kinetochore tension

INTRODUCTION

Prostate cancer is the second most commonly occurring cancer in men worldwide. Prostate cancer that keeps growing regardless of androgen-deprivation therapy in the situation of very low serum testosterone levels is considered castration-resistant prostate cancer (CRPC). New therapies have emerged for treating CRPC because of better understanding of the molecular signaling pathways underlying the progression and development of CRPC (1, 2). However, even though numerous treatment options have been provided, the patients only have limited survival benefit (3, 4). Recently, several therapeutic agents have been introduced to treat CRPC to improve overall survival; the clinicians still face the critical challenge in choice of the best treatment sequencing (2). In fact, the therapy is still in evolution and new clinical insights need to be proposed. *Vinca* alkaloids (e.g., vincristine, vinblastine, vinorelbine, and vindesine) are a family of anti-mitotic and anti-microtubule agents widely used in cancer chemotherapy. The combination of *Vinca* alkaloids with several anticancer drugs in CRPC treatment has been demonstrated to display favorable activity and a low toxicity profile in several clinical studies (5–7). These combination therapies fulfill the purpose of mechanism-based killing cancer and reduction of toxic effect through decreased doses of individual drugs and suggest that *Vinca* alkaloids are options in combination with other therapeutic drugs in CRPC treatment.

Sildenafil, which acts by inhibiting phosphodiesterase type 5 (PDE5), is a medication for the treatment of erectile dysfunction and pulmonary arterial hypertension (8, 9). Recent evidence has demonstrated the cardioprotective activity of sildenafil against myocardial injury by ischemia/reperfusion, heart failure, cardiac hypertrophy, and diabetic cardiomyopathy (10, 11). Furthermore, a variety of studies have revealed the neuroprotective role of sildenafil and have suggested that sildenafil could be repurposed as a potential therapeutic drug for the treatment of several neuronal disorders (12, 13). Moreover, the anti-inflammatory effects of sildenafil have been proposed to show therapeutic benefit in cardiac and inflammatory complications (10). Notably, sildenafil has been reported to induce apoptotic sensitization of several types of cancer to chemotherapeutic drugs, including prostate cancer, breast cancer, and small cell and non-small cell lung cancers (10, 14–16). It has been suggested that co-treatment of sildenafil and vincristine increases apoptotic sensitization of halaven-resistant KBV20C cancer cells (17). Combination of sildenafil with standard chemotherapy agents (vincristine/etoposide/cisplatin) significantly enhances anticancer effect against medulloblastoma (18). These studies suggest the feasibility and therapeutic anticancer potential between the combination of sildenafil with vincristine. There is an ongoing interest by both basic and clinical oncologic investigators in discovering their clinical uses. In the present work, the anticancer sensitization of sildenafil on vincristine-treated CRPC has been studied. To the best of our knowledge, this is the first study dealing with the underlying mechanism related to perturbation of spindle checkpoint protein and microtubule–kinetochore interactions in sildenafil-sensitized anticancer effect.

MATERIALS AND METHODS

Materials

Human prostate adenocarcinoma cell lines, PC-3 and DU-145, were obtained from American Type Culture Collection (Rockville, MD, USA). RPMI 1640 medium, fetal bovine serum (FBS), penicillin, and streptomycin were purchased from GIBCO/BRL Life Technologies (Grand Island, NY). Antibodies of PARP-1, Bcl-2, Bcl-xL, Bak, Mcl-1, α-tubulin, cyclin A, cyclin B, cyclin-dependent kinase (Cdk) 1, and GAPDH were obtained from Santa Cruz Biotechnology (Santa Cruz, CA). Antibodies of cleaved caspase-9, caspase-8, β-tubulin (Alexa Fluor 594 Conjugate), p-Cdk1^{Thr161}, and p-Cdk1^{Tyr15} were from Cell Signaling Technologies (Boston, MA). Stathmin-1, BUBR1, and CENP-A were from Abcam (Cambridge, UK). MPM2 was from Millipore (Bedford, MA, USA). Caspase-3 was purchased from Imgenex (San Diego, CA). Antibody of PDE5 was from OriGene Technologies (Rockville, MD, USA). PDE5 small interfering RNA (siRNA) was from GE Healthcare Dharmacon (Chicago, USA). JC-1 and DAPI were from Molecular Probes (Eugene, OR, USA). Anti-mouse and anti-rabbit IgGs were from Jackson ImmunoResearch Laboratories (West Grove, PA, USA). Leupeptin, phosphatase inhibitors (NaF and Na_3VO_4), dithiothreitol, phenylmethylsulfonylfluoride (PMSF), propidium iodide (PI), and all other chemical compounds were purchased from Sigma-Aldrich (St. Louis, MO, USA).

Cell Culture

PC-3 and DU145 cells were cultured in RPMI 1640 medium supplemented with 5% FBS (*v*/*v*), penicillin (100 U/ml), and streptomycin (100 μg/ml). Cultures were maintained in a 37°C incubator with 5% CO_2. Adherent cultures were passaged using 0.05% trypsin–EDTA after reaching 80% confluence.

Flow Cytometric Assay With PI Staining

Cells were harvested by trypsinization, fixed with 70% (*v*/*v*) alcohol at 4°C for 30 min and washed with phosphate-buffered saline (PBS). After centrifugation, cells were centrifuged and re-suspended with 0.3 ml PI solution containing Triton X-100 (0.1% *v*/*v*), RNase (100 μg/ml), and PI (80 μg/ml). DNA content was analyzed with the FACScan and CellQuest software (Becton Dickinson, Mountain View, CA).

DNA Fragmentation Assay

DNA fragmentation was determined using commercial Cell Death Detection ELISA^{PLUS} kit (Roche, Mannheim, Germany) which was based on the examination of cytoplasmic histone-associated DNA fragments (mono- and oligo-nucleosomes) in cells after the induction of cell apoptosis. After the indicated treatment, the cells were lysed and centrifuged, and the supernatant was used for the detection of nucleosomal DNA fragments according to the manufacturer's protocol.

Cell-Cycle Synchronization

Synchronization of the cells was performed by double thymidine block. Briefly, the cells were treated with 2 mM thymidine in medium/10% FBS for 12 h. After washing cells with PBS, the block was released by the incubation of cells in the medium

without thymidine and then followed by another 12-h thymidine block. The cells were harvested at the indicated times. The cell-cycle progression was detected by flow cytometric analysis and analyzed with CellQuest software (Becton Dickinson).

Western Blotting

After the treatment, cells were harvested with trypsinization, centrifuged, and lysed in 50 μl of lysis buffer containing 10 mM Tris–HCl (pH 7.4), 150 mM NaCl, 1 mM EGTA, 1% Triton X-100, 1 mM PMSF, 10 μg/ml leupeptin, 1 mM dithiothreitol, 1 mM NaF, and 1 mM sodium orthovanadate. Total protein was quantified, mixed with sample buffer, and boiled at 90°C for 5 min. An equal amount of protein (30 μg) was separated by electrophoresis in 8 or 12% SDS-PAGE, transferred to PVDF membranes. After 1-h incubation at room temperature in PBS/0.1% Tween 20/5% non-fat milk, the membrane was washed with PBS/0.1% Tween 20 for 1 h and immuno-reacted with the indicated antibody for 1 h at room temperature. After three washings with PBS/0.1% Tween 20, the anti-mouse or anti-rabbit IgG (dilute 1:8000) was applied to the membranes for 1 h at room temperature. The membranes were washed with PBS/0.1% Tween 20 for 1 h and the detection of signal was performed with an enhanced chemiluminescence detection kit (Amersham, Buckinghamshire, UK).

Measurement of Mitochondrial Membrane Potential ($\Delta\Psi_m$)

JC-1, a mitochondrial dye staining mitochondria in living cells in a membrane potential–dependent fashion, was used to determine $\Delta\Psi_m$. Cells were treated with or without the compound. Thirty minutes before termination of incubation, cells were incubated with JC-1 (5 μM) at 37°C for 10 min. Accumulation of JC-1 was determined using flow cytometry analysis (Becton Dickinson, Mountain View, CA).

siRNA Transfection

Cells were seeded into a six-well-plate with 30% confluence and grown for 24 h to 50% confluence. Each well was washed twice with PBS and 1 ml of serum-free Opti-MEM (Life Technologies, Ground Island, NY) was added. Aliquots containing control or PDE5 siRNA (a pooled siRNA sequence other than a single sequence) in serum-free Opti-MEM were transfected into cells using Lipofectamine 2000 according to the manufacturer's instructions. After transfection for 6 h, cells were washed twice with PBS and incubated in 10% FBS-containing RPMI-1640 medium for 48 h, and the subsequent experiments were performed.

Confocal Immunofluorescence Microscopic Examination

For β-tubulin and CENP-A staining, cells were fixed with 100% methanol (−20°C) for 5 min and incubated in 1% bovine serum albumin (BSA)/PBS containing 0.1% Triton X-100 at 37°C for 30 min. Cells were washed and stained with β-tubulin antibody at 37°C for 1 h or stained with CENP-A antibody at 4°C overnight. Cells were next incubated with FITC-conjugated secondary antibody at room temperature for 1 h. For BUBR1 staining, cells were fixed with 4% paraformaldehyde in PBS for 20 min, permeabilized with 0.1% Triton X-100 for 10 min, and blocked with 5% BSA/PBS for 1 h. Cells were washed and stained with BUBR1 antibody at 4°C and then FITC-conjugated secondary antibody at room temperature for 1 h. Nuclear identification was performed by DAPI staining. The air-dried coverslips were next mounted onto glass slides using ProLongR Diamond Antifade Mountant (Thermo Fisher Scientific, Waltham, MA, USA). The cells were analyzed by a confocal microscope Zeiss LSM88 (Carl Zeiss, Jena, Germany). As for the measurement of a mitotic index, the number of cells in mitosis (prophase, metaphase, anaphase, and telophase) was divided by the total number of cells. As for the measurement of sister kinetochore distance, distances between paired kinetochores ($n = 50$) were measured at individual z planes using the ZEN 2012 (black edition) software (19).

In vivo Anti-tumor Study

PC-3-derived cancer xenografts in nude mice were used as an *in vivo* model. The nude mice were subcutaneously injected with PC-3 cells (10^7 cells/mouse). When the tumor volume reached 400–600 mm^3, the mice were divided into four groups ($n = 7$–9) and compound treatment was initiated. The animals received intraperitoneal injections of 5% DMSO (for control), vincristine alone (0.5 mg/kg, once weekly), sildenafil alone (10 mg/kg, 5 on 2 off), or vincristine plus sildenafil. The tumor length (l) and width (w) were measured to obtain tumor volume as $lw^2/2$. The protocols of the *in vivo* study were approved by the Animal Care and Use Committee at National Taiwan University. All animal procedures and protocols were approved by an AAALAC-accredited facility.

Data Analysis

Data are presented as mean ± SEM. Statistical analysis was performed and two-group comparisons were done with Student's t-test. $P < 0.05$ was considered statistically significant.

RESULTS

Sildenafil Sensitizes Vincristine-Induced Cell Death and an Increase of Mitotic Index

Vincristine is a natural alkaloid working predominantly by binding to tubulin proteins, preventing their polymerization and microtubule formation, leading to failure of chromosome separation during the metaphase and eventually causing cell apoptosis. The cell morphology analysis via microscopic examination in **Figure 1A** shows that vincristine induced morphological change and cell shrinkage, a hallmark of apoptotic mode of programmed cell death, of PC-3 cells. Sildenafil profoundly exacerbated vincristine-induced effect. The data were substantiated using flow cytometric quantitation of DNA content showing that sildenafil synergistically increased vincristine-induced apoptotic sub-G1 cell population in PC-3 cells (**Figure 1B**). Sildenafil-induced apoptotic potentiation was substantiated by the detection of nucleosomal DNA fragments. The synergism between vincristine and sildenafil was assessed through constructing isobolograms and calculating combination index (CI) values using Chou–Talalay method (20). The

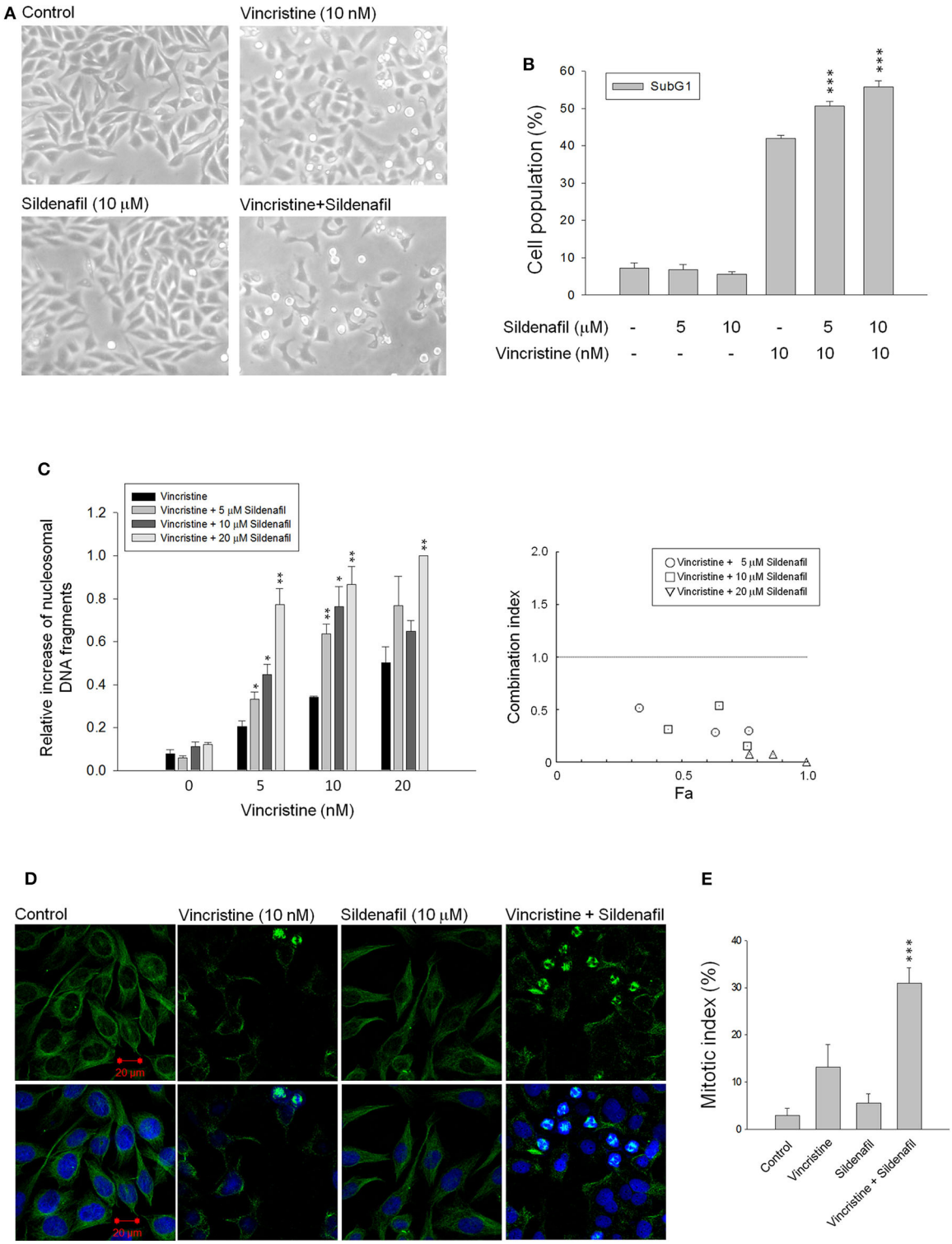

FIGURE 1 | Effect of vincristine and sildenafil on cell morphology, apoptosis, and mitotic index in PC-3 cells. The cells were incubated in the absence or presence of the indicated agent for 24 h **(A,C–E)** or 48 h **(B)**. The cell morphology was observed under microscopic examination **(A)**, or the cells were harvested for propidium iodide staining to analyze the distribution of cell populations at sub-G1 (apoptosis) phase using FACScan flow cytometric analysis **(B)**, or the cell apoptosis was examined through measuring the level of nucleosomal DNA fragments **(C)**. The confocal immunofluorescence examination was performed to detect microtubule (green) and chromosome (blue) using β-tubulin antibody and DAPI **(D)**, and the quantitative mitotic index was obtained accordingly **(E)**. Data are expressed as mean ± SEM of three to nine independent determinations. $^{*}P < 0.05$, $^{**}P < 0.01$, and $^{***}P < 0.001$ compared with vincristine alone.

resulting CI values were <1.0 confirming the synergistic effects. Similar data of synergistic apoptotic effect also were obtained in DU-145 cells (**Supplementary Figure 1**). Furthermore, the mitotic abnormalities, key characteristics of anti-mitotic agents, were detected using double staining of mitotic spindle and chromosome. The images depicted in **Figure 1C** show that vincristine induced mitotic arrest with abnormal features of mitosis. The effect was dramatically exacerbated in the presence of sildenafil. To further substantiate the effect on mitotic arrest, the cells were synchronized using double thymidine block to arrest cell at G1/S boundary. After the release from double thymidine block, cell-cycle progression, and cell population at distinct phase were detected at different time points (**Supplementary Figure 2**). The data showed that in the presence of vincristine at 17, 21, and 24-h treatment, about 23–31% of the cell population was capable of entering G1 phase. In contrast, the population was significantly reduced in the combinatory treatment of vincristine and sildenafil; furthermore, sildenafil significantly increased vincristine-induced G2/M population (**Supplementary Figure 2**).

The levels of mitotic arrest in cells responsive to microtubule-targeting agents are proportional to those of subsequent cell death. Accordingly, the mitotic index was measured showing that sildenafil significantly increased vincristine-induced mitotic arrest (**Figure 1D**) and mitotic index (**Figure 1E**). The mitotic index was defined in detail in characteristics of several mitotic phases, including prophase, metaphase, anaphase, and telophase. The data in **Table 1** demonstrated that vincristine caused predominantly an increase of cell population in metaphase, such as unaligned chromosome, tripolar spindle, multiple spindle poles, and asymmetrical bipolar spindle. The presence of sildenafil dramatically increased the probability of cells at metaphase, in particular tripolar spindle and multiple spindle poles, in cells (**Table 1**). Besides, it has been evident that cells can survive metaphase arrest at a sublethal concentration of vincristine possibly through completing cytokinesis normally (21). Our data showed that sildenafil decreased, although not significantly, the level of cytokinesis in cells responsive to vincristine (**Table 1**).

Sildenafil Exacerbates Vincristine-Induced Mitotic Arrest Signaling and Mitochondrial Damage Response

It has been widely recognized that exposure of cells to anti-tubulin agents always leads to prolonged activation of spindle assembly checkpoint (SAC), resulting in mitotic arrest and eventually cell apoptosis (22, 23). Cdk1 activation needs a multiple process including Cdk1/cyclin B1 complex formation and nuclear relocation, and is based on phosphorylation/dephosphorylation. Dephosphorylation of both Thr14 and Tyr15 is necessary for kinase activity. On the contrary, Thr161 must be phosphorylated for activity (24, 25). As expected, vincristine induced the upregulation of cyclin B1 protein expression associated with a decrease of cyclin A protein levels, and caused an increase of $Cdk1^{Thr161}$ phosphorylation and a decrease of $Cdk1^{Tyr15}$ phosphorylation suggesting the induction of mitotic arrest (**Figure 2A**). Increased phosphorylation of multiple mitotic proteins (MPM-2) and stathmin, which regulate the dynamics of microtubule polymerization and depolymerization, further validate the mitotic arrest to vincristine action. Notably, vincristine-mediated signaling in mitotic arrest was significantly amplified in the presence of sildenafil (**Figure 2A**).

Several lines of evidence suggest a link between the network of SAC and mitochondrial functions that may regulate cellular signaling to cell death (26). Accordingly, JC-1 mitochondrial membrane potential assay was performed and the data demonstrated that vincristine induced a loss of mitochondrial membrane potential that was significantly exacerbated in the presence of sildenafil, suggesting further mitochondrial damage to sildenafil action (**Figure 2B**). Mitochondrial outer membrane potential permeabilization, which is controlled by Bcl-2 family members, is a key event in apoptotic insult because it induces the release of proapoptotic proteins to the cytosol. Vincristine

TABLE 1 | Effect of vincristine alone and combined with sildenafil on several mitotic phases in PC-3 cells.

Cell phase	Feature	Control	Vincristine	Sildenafil	Vincristine + Sildenafil
Prophase	Normal	0.79 ± 0.06	1.23 ± 0.42	1.08 ± 0.23	1.05 ± 0.16
	Monopolar	0	1.02 ± 0.83	0	0.26 ± 0.26
Metaphase	Normal	1.47 ± 0.73	0.58 ± 0.085	1.05 ± 0.53	0.34 ± 0.20
	Unaligned chromosome	0	2.44 ± 0.21	0.23 ± 0.19	1.30 ± 0.39
	Tripolar	0	2.00 ± 1.28	0	7.98 ± 0.45[a]
	Multiple spindle poles	0	4.30 ± 0.72	0	18.40 ± 1.02[b]
	Asymmetrical bipolar spindle	0	0.50 ± 0.32	0	0.11 ± 0.11
Anaphase	Normal	0.25 ± 0.25	0.18 ± 0.18	0	0.11 ± 0.11
	Lagging chromosomes	0	0.22 ± 0.22	0	0.24 ± 0.12
Telophase	Normal	0.48 ± 0.48	0.23 ± 0.23	3.23 ± 0.99	0.11 ± 0.11
Cytokinesis		2.02 ± 0.86	0.45 ± 0.45	5.58 ± 1.27	0.13 ± 0.13

[a] *P < 0.05 compared with vincristine alone.*
[b] *P < 0.001 compared with vincristine alone.*

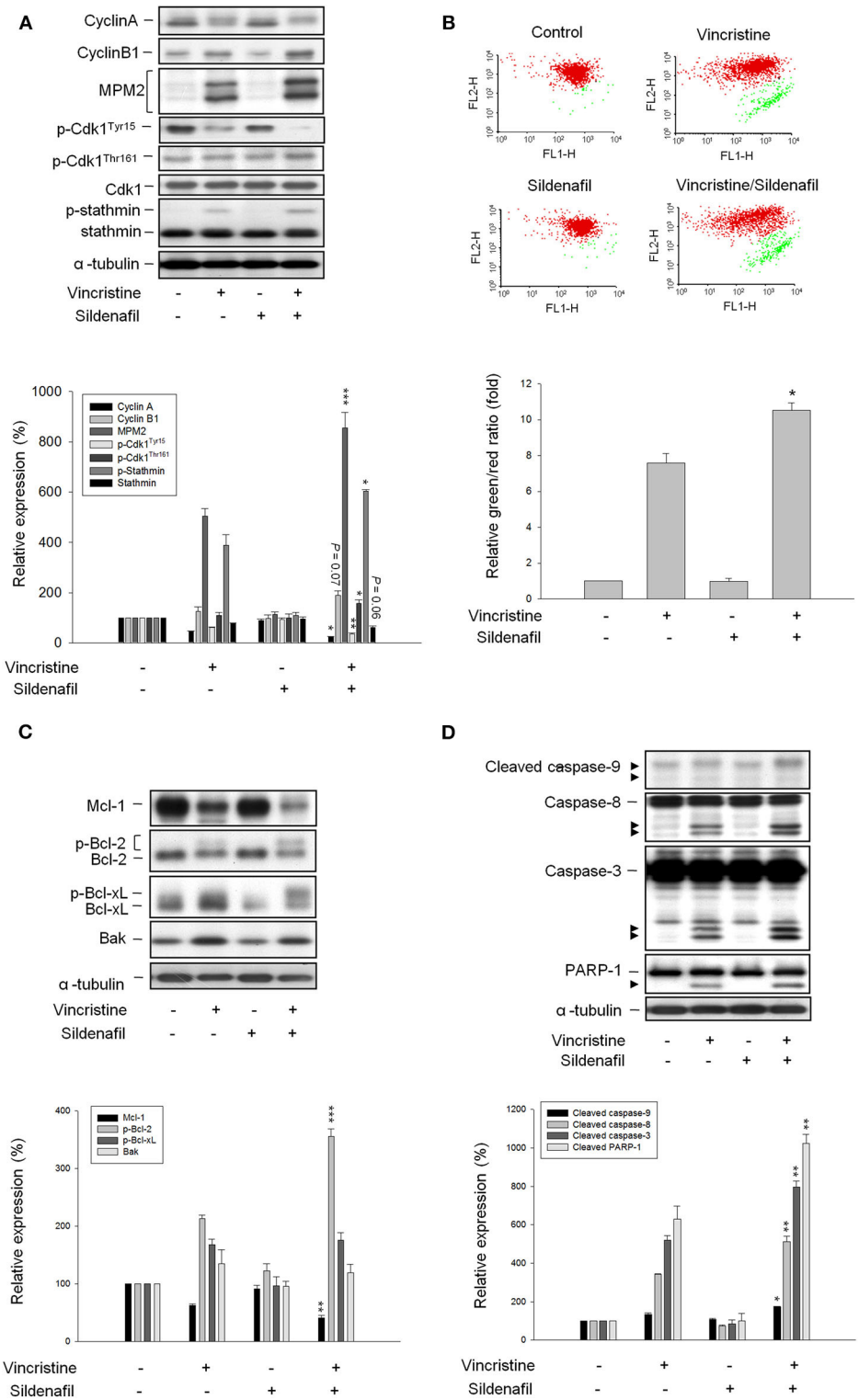

FIGURE 2 | Effect of vincristine and sildenafil on cell-cycle regulators and mitochondria-involved signaling pathway. PC-3 cells were treated in the absence or presence of vincristine (10 nM) and sildenafil (10 μM) for 24 h **(A,C,D)** or 48 h **(B)**. After the treatment, the cells were harvested and lysed for the detection of protein expressions of cell-cycle regulators **(A,C,D)** by Western blot analysis or the cells were harvested for JC-1 staining to detect mitochondrial membrane potential using FACScan flow cytometric analysis **(B)**. Data are expressed as mean ± SEM of three to six determinations. $^{*}P < 0.05$, $^{**}P < 0.01$, and $^{***}P < 0.001$ compared with vincristine alone.

induced downregulation of Mcl-1 and Bcl-2 (two anti-apoptotic Bcl-2 family members) and upregulation of Bak (a pro-apoptotic member) that explained the mitochondrial damage (**Figure 2C**). Moreover, Bcl-2 phosphorylation was evoked (**Figure 2C**) that further verifies the mitotic arrest because it has been evident that Cdk1/cyclin B1-mediated Bcl-2 phosphorylation serves as a functional link coupling mitotic arrest and cell death (27). Of note, sildenafil profoundly aggravated vincristine-mediated effects, in particular the Bcl-2 phosphorylation (**Figure 2C**). The data together with the amplification of caspase activation including caspase-8, -9, and -3, and increased cleavage of PARP-1 (a caspase-3 substrate) (**Figure 2D**) confirmed the synergistic effect on mitotic arrest and apoptotic cell death.

Other PDE5 Inhibitors Mimic Sildenafil on Potentiating Vincristine-Induced Effects

The effect of other PDE5 inhibitors including vardenafil and tadalafil on vincristine-induced cell apoptosis and related signaling pathway was examined. Both vardenafil and tadalafil sensitized apoptotic cell death to vincristine action in PC-3 cells (**Figure 3A**) and DU-145 cells (**Supplementary Figure 3**); the activation of caspase cascade also was potentiated (**Figure 3B**). Both vardenafil and tadalafil synergistically exaggerated vincristine-induced signaling pathways on mitotic arrest effects, including downregulation of cyclin A whereas upregulation of cyclin B1 protein expression, increased mitotic-specific MPM-2 phosphorylation, increased Cdk1 activity (i.e., decreased $Cdk1^{Tyr15}$ phosphorylation associated with increased $Cdk1^{Thr161}$ phosphorylation), and increased phosphorylation of Bcl-2 and Bcl-xL (**Figure 3C**).

Vincristine-Induced Effects Are Amplified in Cells With PDE5A Gene Knockdown by siRNA

Because the PDE5 inhibitors used in this study (i.e., sildenafil, vardenafil, and tadalafil) displayed similar sensitization activity to vincristine action, the *PDE5A* gene knockdown by siRNA in PC-3 cells was performed to realize its functional role. The data showed an efficient knockdown of PDE5A gene and, therefore, a dramatic reduction of PDE5A protein expression was observed (**Figure 4A**). The inhibition of PDE5A protein expression significantly amplified several cellular signals stimulated by vincristine, including caspase-3 activation, PARP-1 cleavage, downregulation of cyclin A protein expression, decreased phosphorylation of $Cdk1^{Tyr15}$, and increased Bcl-2 phosphorylation. The upregulation of cyclin B1 and an increase of mitotic-specific MPM-2 phosphorylation, although not significantly, also were observed in PDE5A knockdown cells (**Figure 4A**). Vincristine-induced mitotic arrest of the cell cycle was markedly increased in PDE5A knockdown cells although sub-G1 population was not augmented (**Figure 4B**). Altogether, the data indicated that knockdown of *PDE5A* played a crucial role on sensitizing vincristine-induced mitotic arrest and subsequent signaling pathway. However, it was noteworthy that none of the conditions, including vincristine alone, sildenafil alone, or their combination, significantly induced an increase of intracellular cGMP levels in PC-3 cells. In contrast, the positive control (the phosphodiesterase inhibitor 3-isobutyl-1-methylxanthine plus the nitric oxide donor sodium nitroprusside) produced a 23-fold increase of intracellular cGMP (data not shown). The data questioned the functional role of cGMP.

Sildenafil Potentiates Vincristine-Induced Phosphorylation and Cleavage of BUBR1 and Loss of Tension Across the Sister Kinetochores

BUBR1, a multidomain protein kinase involving in SAC function and chromosome segregation (26), localizes to kinetochore and plays a crucial role in inhibiting anaphase-promoting complex/cyclosome (APC/C), delaying the anaphase onset in guaranteeing accurate chromosome segregation. BUBR1 is expressed with a high mitotic index and its phosphorylation is regulated during mitotic checkpoint activation (28). The images in **Figure 5A** show that vincristine and in combination with sildenafil induced profound BUBR1 expression. Besides, the phosphorylation of BUBR1 was induced by vincristine and was markedly amplified in the presence of sildenafil. The cleavage of BUBR1 was significantly evoked as well (**Figure 5B**). Furthermore, BUBR1 phosphorylation was validated by the absence of phosphatase inhibitors or the presence of phosphatase. Both conditions almost completely abolished the phosphorylation of BUBR1 (**Figure 5B**).

The kinetochore provides signaling function to modify the properties of spindle checkpoint and evokes signal transduction leading to the blockade of anaphase-promoting complex and cell-cycle arrest (29). The images in **Figure 5C** show that all attached kinetochores on the chromosomes were properly aligned at metaphase plate in control cells, whereas vincristine alone and vincristine combined with sildenafil caused misalignment of chromosomes and attached kinetochores (**Figure 5C**). Because the tension generated between paired kinetochores was suggested to be proportional to their distance, the distance between sister kinetochore pairs was examined accordingly. The data demonstrated $1.039 \pm 0.018\,\mu m$ in control group. In contrast, the distance was decreased to $0.784 \pm 0.023\,\mu m$ in vincristine alone group. Vincristine combined with sildenafil further significantly reduced the distance to $0.720 \pm 0.018\,\mu m$ (**Figure 5D**). The data indicated that sildenafil exacerbated vincristine-induced perturbation of microtubule–kinetochore interactions.

Sildenafil Dramatically Potentiates Vincristine in Suppressing Tumor Growth in Mouse Xenograft Models

The tumor xenografts in nude mice after subcutaneous PC-3 inoculation were performed. The mice were administered with vehicle, vincristine, sildenafil, or vincristine plus sildenafil when the tumor size reached to an average of about 500 mm^3 (control group, 403 ± 51; vincristine group, 542 ± 55; sildenafil group, 561 ± 57; combination group, 600 ± 39). Vincristine alone and combined with sildenafil inhibited tumor growth with T/C

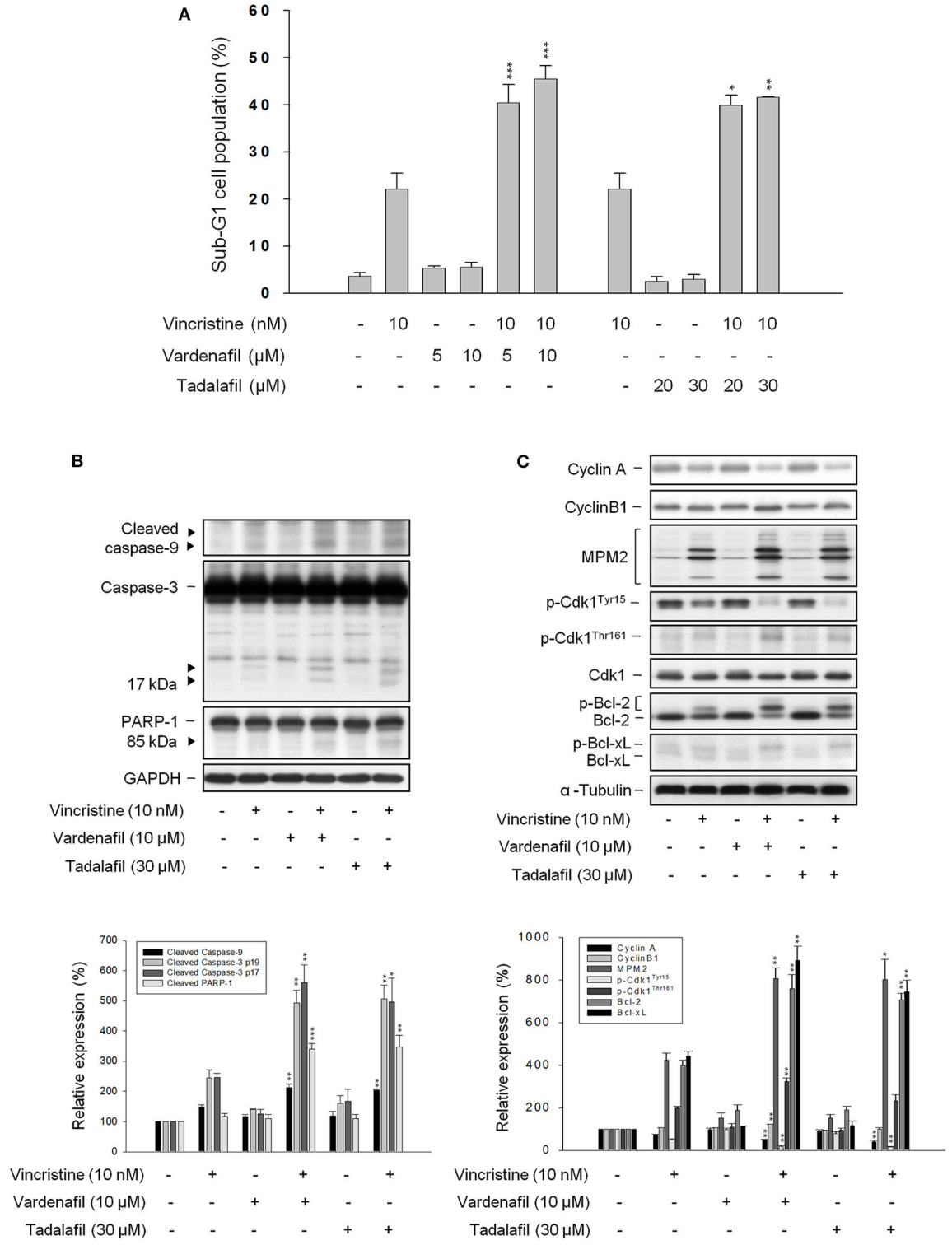

FIGURE 3 | Effect of vardenafil and tadalafil on vincristine-induced sub-G1 population and protein expression. PC-3 cells were incubated in the absence or presence of the indicated agent for 48 h **(A)** or 24 h **(B,C)**. The cells were harvested for propidium iodide staining to analyze the distribution of cell populations at sub-G1 (apoptosis) phase using FACScan flow cytometric analysis **(A)**, or the cells were harvested and lysed for the detection of protein expression by Western blot analysis **(B,C)**. Data are expressed as mean ± SEM of three independent determinations. $^{*}P < 0.05$, $^{**}P < 0.01$, and $^{***}P < 0.001$ compared with vincristine alone.

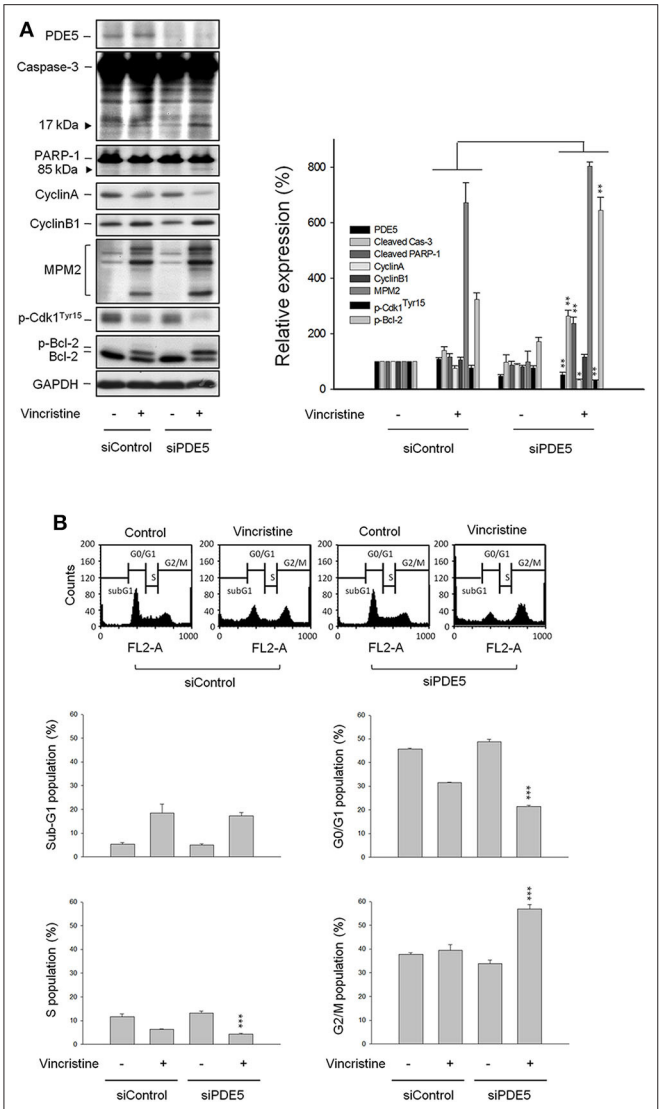

FIGURE 4 | Effect of PDE5 knockdown on vincristine-induced cell-cycle distribution and protein expression. PC-3 cells were transfected with control or PDE5 siRNA as described in the Materials and methods section. After the transfection, the cells were incubated in the absence or presence of vincristine (10 nM) for 24 h and then the cells were harvested and lysed for the detection of protein expression by Western blot analysis **(A)** or the cells were harvested for propidium iodide staining to analyze the distribution of cell populations at various phases using FACScan flow cytometric analysis **(B)**. Data are expressed as mean ± SEM of four independent determinations. $^{*}P < 0.05$, $^{**}P < 0.01$, $^{***}P < 0.001$ compared with vincristine alone at siControl group.

(treatment/control) ratios of 0.69 and 0.25, respectively, at end-of-treatment (**Figure 6A**). The average tumor weights at end-of-treatment were 994.7 ± 116.8, 623.5 ± 132.2, 969.9 ± 92.2, and 207.6 ± 36.7 mg in control group, vincristine group, sildenafil group, and combination group, respectively. The median tumor weights were 1101.7, 641.6, 1046.5, and 225.1 mg, respectively (**Figure 6B**). The data suggested that sildenafil synergized with vincristine on suppressing tumor growth in an *in vivo* model. There was a progressive loss of weight in all experimental animal groups; however, no significant between-group difference was detected (**Figure 6C**).

DISCUSSION

Microtubule-targeting agents, such as taxanes and *Vinca* alkaloids, are used in treating a wide variety of cancers through disturbing microtubule dynamics, resulting in mitotic arrest and cell death. The data in this study showed that vincristine induced mitotic arrest with abnormal features of mitosis. The mitotic index was provided demonstrating that vincristine caused predominantly an increase of abnormality in metaphase of the cell cycle. Vincristine induced several cellular events that are crucial during mitotic arrest, including the activation of Cdk1, upregulation of cyclin B1, and phosphorylation of MPM-2 and stathmin. Furthermore, vincristine induced the alteration of several Bcl-2 family members, the loss of mitochondrial membrane potential, and activation of caspase cascades. Altogether, the data suggested that vincristine induced the mitotic arrest of the cell cycle and apoptotic cell death. However, accumulating evidence shows that vincristine treatment is limited by its side effects, in particular several forms of neuropathy. Combination therapy is an efficient therapeutic approach to achieve drug efficacy through lower doses that produce lower toxicity. Sildenafil has been suggested to improve nerve function and to ameliorate long-term peripheral neuropathy (30, 31). Because of its beneficial role, the study aims to repurpose sildenafil as a supportive anticancer agent when combined with vincristine to sensitize tumor killing efficacy. The data demonstrated that sildenafil dramatically increased the mitotic index to vincristine action. All the cellular signals during SAC activation and mitochondrial damage in response to vincristine were synergistically amplified. Notably, other PDE5 inhibitors, such as vardenafil and tadalafil, mimicked sildenafil on potentiating vincristine-induced mitotic arrest and caspase-dependent apoptosis. The data together with PDE5A gene knockdown study supported that the inhibition of PDE5A played a crucial role on sensitizing vincristine-induced mitotic arrest and subsequent apoptotic signaling pathway. However, either sildenafil alone or vincristine plus sildenafil did not induce an increase of intracellular cGMP levels. The data questioned the functional role of cGMP. Because it is reported that sildenafil sensitivity of PDE5 can be regulated by cGMP-independent mechanisms (32), the role of PDE5 and its dependence on cGMP needs further elucidation.

Not only mitotic cell death, vincristine has been suggested to induce cytotoxicity by interfering with interphase microtubules, such as G1 phase (33). It remained unclear whether G1 interphase cytotoxicity was related to vincristine-induced neuropathy. However, our data by double thymidine block and cell synchronization assay revealed that sildenafil significantly reduced G1 cell population in response to vincristine, and increased cells in mitotic arrest and apoptotic death. The data also provided a rationale for the consideration of combination therapy. Nevertheless, it is noteworthy that cells may die in mitosis or exit mitosis as mitotic slippage. Two cellular networks

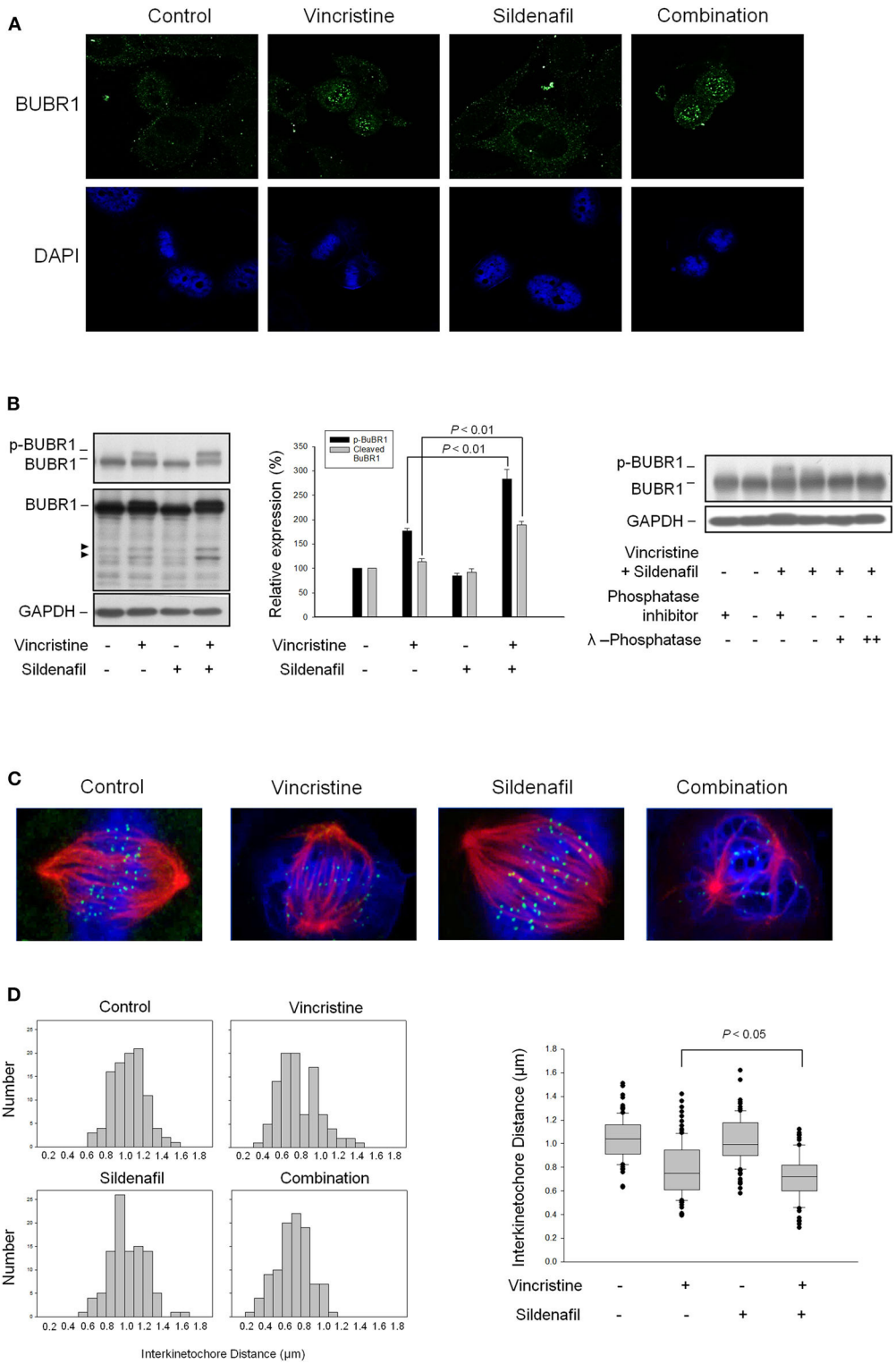

FIGURE 5 | Effect of sildenafil and vincristine on BUBR1 expression and the distance between kinetochore pairs in PC-3 cells. The cells were incubated in the absence or presence of sildenafil (10 μM) and/or vincristine (10 nM) for 24 h. The confocal immunofluorescence examination was performed to detect BUBR1 (green) and chromosome (blue) using BUBR1 antibody and DAPI, respectively **(A)**, or the cells were harvested and lysed for the detection of protein expression by Western blot analysis **(B)**. Data are expressed as mean ± SEM of three independent determinations. Furthermore, BUBR1 phosphorylation was validated by the absence of phosphatase inhibitors or the presence of phosphatase. Both conditions significantly decreased the phosphorylation levels. **(C)** Confocal immunofluorescence microscopic examination was performed to detect kinetochore (green), microtubule (red), and chromosome (blue) using CENP-A antibody, β-tubulin antibody, and DAPI, respectively. **(D)** The distances between paired kinetochores ($n = 100$) were blindly measured at individual z planes, scored from 5 to 8 cells.

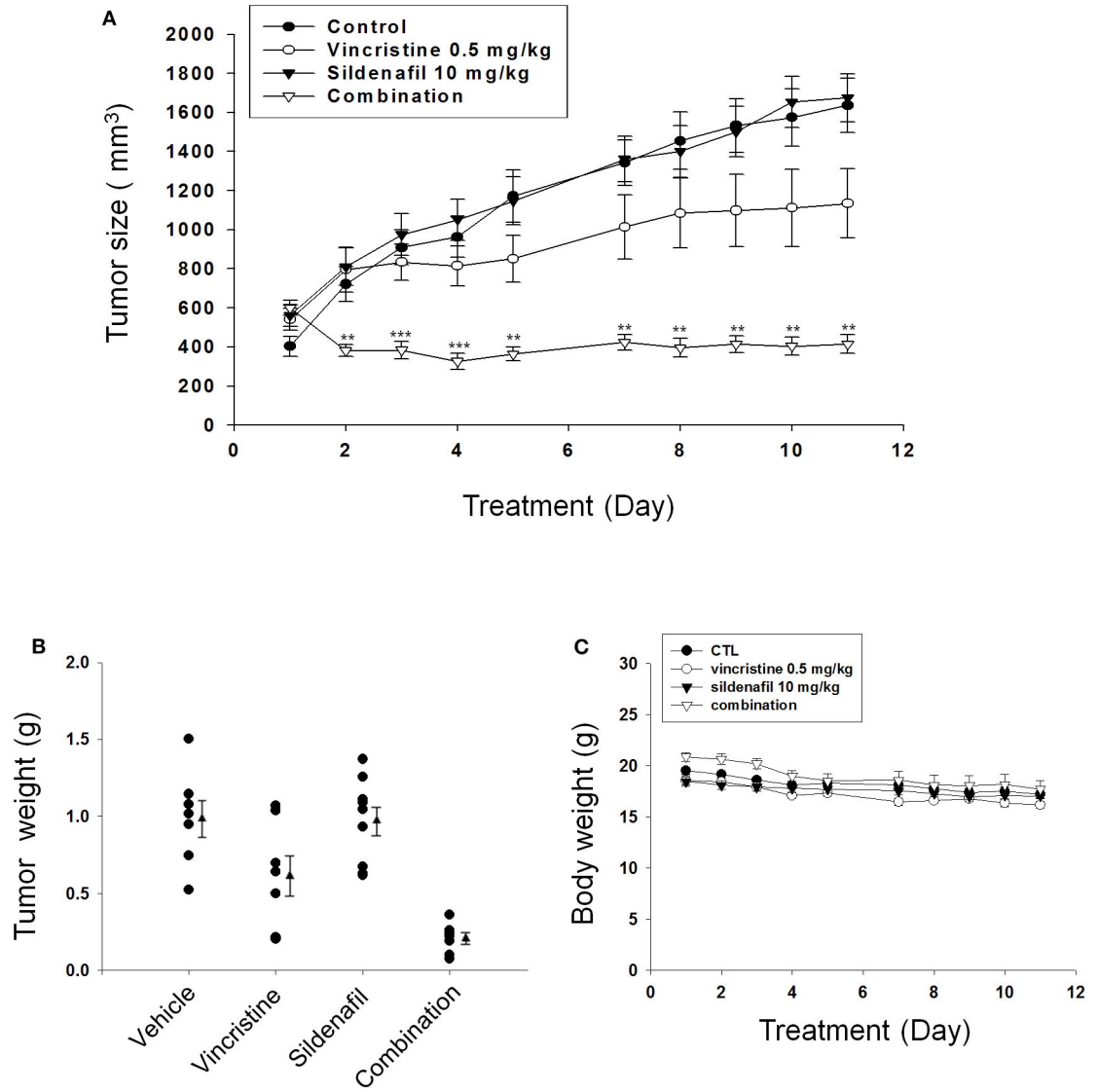

FIGURE 6 | Effect of sildenafil and vincristine on tumor growth in an *in vivo* anti-tumor xenograft model. The nude mice were subcutaneously injected with PC-3 cells (10^7 cells/mouse). The tumors were measured every day. When the tumors reached to a volume of 400–600 mm^3, the mice were divided into four groups and the drug administration was initiated as described in the Materials and methods section. **(A)** The length (*l*) and width (*w*) of the tumor were measured, and tumor volume was calculated as $lw^2/2$. The tumor weights **(B)** and the body weights **(C)** also were measured. Data are expressed as mean ± SEM. $^{**}P < 0.01$ and $^{***}P < 0.001$ compared with vincristine alone.

are key players to dictate the cell fate either to death in mitosis or undergoing mitotic slippage: one involving caspase activation and the other is protecting cyclin B1 from degradation (33, 34). Gascoigne and Taylor have reported an excellent study showing that slowing down caspase activation leads to the delay of mitotic cell death; during this time, cyclin B1 keeps progressively being degraded that ultimately permits slippage. In contrast, cyclin B1 overexpression prolongs the duration of mitotic arrest that gives more time for accumulating death signals and ensures cell death (34). Our data were consistent with the notion showing that sildenafil profoundly amplified vincristine-induced cyclin B1 upregulation, which mediated Bcl-2 phosphorylation as a functional link to mitochondrial damage and caspase-dependent cell death. The data validated that sildenafil delayed the mitotic slippage during vincristine exposure and guaranteed longer mitotic arrest and more cell death.

SAC supervises microtubule and kinetochore interactions during the transition of metaphase to anaphase, working on keeping genome stability through delaying cell division only when precise chromosome segregation can be ensured. Mitotic checkpoint complex, the main effector of SAC, is composed of Bub3 (Budding Uninhibited by Benzimidazole 3), BubR1, Mad2 (Mitotic arrest deficient), and CDC20 (Cell division cycle 20). The mitotic checkpoint complex inhibits APC/C activity (an E3 ubiquitin ligase) and prevents proteolytic degradation of securin (an inhibitor of separase) and cyclin B1 (a Cdk1

activator), resulting in the inhibition of separase activity and sustained Cdk1 activity (26, 35, 36). Because cohesin cleavage by separase is required for anaphase and cytokinesis, the mitotic checkpoint complex acts to prevent cohesin cleavage and sister chromatid separation. SAC is induced in the presence of unattached kinetochores and/or a lack of tension between sister kinetochores (26, 36, 37). Our data showed that vincristine reduced the distance between sister kinetochore pairs, indicating the perturbation of microtubule–kinetochore interactions and SAC activation. Notably, sildenafil markedly exacerbated vincristine-induced effects, reinforcing the mitotic arrest at metaphase and subsequent cell death.

BubR1 phosphorylation is critical for checkpoint inhibition of APC/C. During SAC, BubR1 phosphorylation by several kinases including Cdk1, polo-like kinase (Plk1), Aurora B, and monopolar spindle 1 (Mps1) is necessary to supervise the microtubule–kinetochore binding and to detect kinetochore tension, suggesting the key role on kinetochore attachments and checkpoint regulation (38). Moreover, BubR1 has been implicated in drug resistance. Kita et al. reported that BubR1 knockdown in Hela cells showed reduced formation of mitotic checkpoint complex and mitotic arrest induced by thio-dimethylarsinic acid. The mitotic index was significantly decreased associated with almost completely abolished cyclin B1 protein expression in the BubR1 knockdown cells, leading to an increased cell survival when exposed to thio-dimethylarsinic acid (39). Our data were consistent with this notion showing that sildenafil significantly amplified vincristine-mediated BubR1 phosphorylation and mitotic index, increasing cyclin B1 protein levels and ultimately sensitizing cell apoptosis. Furthermore, Kim et al. reported that the inhibition of caspase activity blocked BubR1 cleavage and prolonged mitosis. They showed that the mutation of caspase cleavage sites in BubR1 which prevented BubR1 from the cleavage led to increased aneuploidy and also reduced the rate of cell death when exposed to nocodazole (40). Our data showed that the cleavage of BubR1 was apparent, in particular in cells exposed to vincristine plus sildenafil that also triggered massive caspase activation. The data supported the caspase activation as a determinant of BubR1 cleavage.

It was noteworthy that our supplementary data showed that sildenafil did not synergize both paclitaxel- and docetaxel-mediated effect (**Supplementary Figure 4**). Precise chromosome segregation is dependent on the SAC. Aurora B plays a key role in the SAC to trigger rapid kinetochore localization of Mps1, granting Mps1 to generate the SAC signals. Anti-mitotics work through disturbing the spindle assembly that induces the SAC and mitotic arrest. However, it is not clear whether there is discrepancy in SAC signals between the stresses of microtubule stabilizing agents and polymerization inhibitors. Gurden et al. have reported that Mps1 inhibition can rapidly override both a nocodazole- and paclitaxel-induced arrest, whereas Aurora B inhibition can only override a paclitaxel-induced arrest through the detection of mitotic index and formation of mitotic checkpoint complex (41). Furthermore, it has been reported that weakened spindle checkpoint with decreased BUBR1 expression is associated with acquired paclitaxel resistance in ovarian carcinoma cells (42). Currently, our study has not yet explained why sildenafil does not synergize both paclitaxel- and docetaxel-mediated effect. However, there exists a discrepancy with the SAC signaling in cells exposed to different anti-mitotics. The sildenafil-mediated different regulation on anti-mitotic sensitivity in this study needs further investigation.

Finally, nude mice xenograft model was used to determine the *in vivo* anti-tumor efficacy. The present work showed that the administration of vincristine combined with sildenafil dramatically inhibited the tumor growth with a low T/C of 0.25 and about 80% inhibition of tumor growth by detecting both average and median tumor sizes.

CONCLUSIONS

The data suggest that sildenafil, in a PDE5-dependent manner, potentiates vincristine-induced mitotic arrest signaling, and sensitizes mitochondria damage–involved apoptosis in CRPC. Both *in vitro* and *in vivo* data suggest the combination potential of PDE5 inhibitors and vincristine on CRPC treatment.

DATA AVAILABILITY STATEMENT

All datasets generated for this study are included in the article/**Supplementary Material**.

ETHICS STATEMENT

The animal study was reviewed and approved by The Animal Care and Use Committee at National Taiwan University. All animal procedures and protocols were approved by AAALAC-accredited facility.

AUTHOR CONTRIBUTIONS

S-PL and J-HG contributed to the conception and design of the experiments. J-LH performed the experiments and analyzed the data. W-JL, L-CH, and C-HH participated in the progress reports and troubleshooting in experiments. J-HG wrote the article. All authors contributed to the article and approved the submitted version.

FUNDING

This work was supported by the Ministry of Science and Technology in Taiwan (MOST 107-2320-B-002-018-MY3 and 106-2320-B-002-005-MY3).

ACKNOWLEDGMENTS

We acknowledge the support by the Center for Innovative Therapeutics Discovery at National Taiwan University and thank the staff of the imaging core at the First Core Labs, National Taiwan University College of Medicine, for technical assistance.

SUPPLEMENTARY MATERIAL

The Supplementary Material for this article can be found online at: https://www.frontiersin.org/articles/10.3389/fonc.2020.01274/full#supplementary-material

REFERENCES

1. Dellis AE, Papatsoris AG. Perspectives on the current and emerging chemical androgen receptor antagonists for the treatment of prostate cancer. *Expert Opin Pharmacother*. (2019) 20:163–72. doi: 10.1080/14656566.2018.1548611
2. Tucci M, Caffo O, Buttigliero C, Cavaliere C, D'aniello C, Di Maio M, et al. Therapeutic options for first-line metastatic castration-resistant prostate cancer: Suggestions for clinical practise in the CHAARTED and LATITUDE era. *Cancer Treat Rev*. (2019) 74:35–42. doi: 10.1016/j.ctrv.2019.01.002
3. Tannock IF, de Wit R, Berry WR, Horti J, Pluzanska A, Chi KN, et al. Docetaxel plus prednisone or mitoxantrone plus prednisone for advanced prostate cancer. *N Engl J Med*. (2004) 351:1502–12. doi: 10.1056/NEJMoa040720
4. Kantoff PW, Higano CS, Shore ND, Berger ER, Small EJ, Penson DF, et al. Sipuleucel-T immunotherapy for castration-resistant prostate cancer. *N Engl J Med*. (2010) 363:411–22. doi: 10.1056/NEJMoa1001294
5. Piatek CI, Raja GL, Ji L, Gitlitz BJ, Dorff TB, Quinn DI, et al. Phase I clinical trial of temsirolimus and vinorelbine in advanced solid tumors. *Cancer Chemother Pharmacol*. (2014) 74:1227–34. doi: 10.1007/s00280-014-2600-z
6. Joly F, Delva R, Mourey L, Sevin E, Bompas E, Vedrine L, et al. Clinical benefits of non-taxane chemotherapies in unselected patients with symptomatic metastatic castration-resistant prostate cancer after docetaxel: the GETUG-P02 study. *BJU Int*. (2015) 115:65–73. doi: 10.1111/bju.12552
7. Di Desidero T, Derosa L, Galli L, Orlandi P, Fontana A, Fioravanti A, et al. Clinical, pharmacodynamic and pharmacokinetic results of a prospective phase II study on oral metronomic vinorelbine and dexamethasone in castration-resistant prostate cancer patients. *Invest New Drugs*. (2016) 34:760–70. doi: 10.1007/s10637-016-0385-0
8. Hrometz SL, Shields KM. Sildenafil citrate for the treatment of pulmonary hypertension. *Drugs Today*. (2006) 42:771–84. doi: 10.1358/dot.2006.42.12.1032057
9. Aversa A, Bruzziches R, Pili M, Spera G. Phosphodiesterase 5 inhibitors in the treatment of erectile dysfunction. *Curr Pharm Des*. (2006) 12:3467–84. doi: 10.2174/138161206778343046
10. Das A, Durrant D, Salloum FN, Xi L, Kukreja RC. PDE5 inhibitors as therapeutics for heart disease, diabetes and cancer. *Pharmacol Ther*. (2015) 147:12–21. doi: 10.1016/j.pharmthera.2014.10.003
11. Di Luigi L, Corinaldesi C, Colletti M, Scolletta S, Antinozzi C, Vannelli GB, et al. Phosphodiesterase Type 5 inhibitor sildenafil decreases the proinflammatory chemokine CXCL10 in human cardiomyocytes and in subjects with diabetic cardiomyopathy. *Inflammation*. (2016) 39:1238–52. doi: 10.1007/s10753-016-0359-6
12. Son Y, Kim K, Cho HR. Sildenafil protects neuronal cells from mitochondrial toxicity induced by β-amyloid peptide via ATP-sensitive K^+ channels. *Biochem Biophys Res Commun*. (2018) 500:504–10. doi: 10.1016/j.bbrc.2018.04.128
13. Tawfik KM, Moustafa YM, El-Azab MF. Neuroprotective mechanisms of sildenafil and selenium in PTZ-kindling model: implications in epilepsy. *Eur J Pharmacol*. (2018) 833:131–44. doi: 10.1016/j.ejphar.2018.05.035
14. Domvri K, Zarogoulidis K, Zogas N, Zarogoulidis P, Petanidis S, Porpodis K, et al. Potential synergistic effect of phosphodiesterase inhibitors with chemotherapy in lung cancer. *J Cancer*. (2017) 8:3648–56. doi: 10.7150/jca.21783
15. Greish K, Fateel M, Abdelghany S, Rachel N, Alimoradi H, Bakhiet M, et al. Sildenafil citrate improves the delivery and anticancer activity of doxorubicin formulations in a mouse model of breast cancer. *J Drug Target*. (2018) 26:610–5. doi: 10.1080/1061186X.2017.1405427
16. Chang JF, Hsu JL, Sheng YH, Leu WJ, Yu CC, Chan SH, et al. Phosphodiesterase Type 5 (PDE5) inhibitors sensitize Topoisomerase II inhibitors in killing prostate cancer through PDE5-independent impairment of HR and NHEJ DNA repair systems. *Front Oncol*. (2019) 8:681. doi: 10.3389/fonc.2018.00681
17. Kim JY, Son JY, Lee BM, Kim HS, Yoon S. Aging-related repositioned drugs, donepezil and sildenafil citrate, increase apoptosis of anti-mitotic drug-resistant KBV20C cells through different molecular mechanisms. *Anticancer Res*. (2018) 38:5149–57. doi: 10.21873/anticanres.12837
18. Roberts JL, Booth L, Conley A, Cruickshanks N, Malkin M, Kukreja RC, et al. PDE5 inhibitors enhance the lethality of standard of care chemotherapy in pediatric CNS tumor cells. *Cancer Biol Ther*. (2014) 15:758–67. doi: 10.4161/cbt.28553
19. Zeeshan M, Pandey R, Ferguson DJP, Tromer EC, Markus R, Abel S, et al. Real-time dynamics of Plasmodium NDC80 reveals unusual modes of chromosome segregation during parasite proliferation. *J Cell Sci*. (2021) 134:jcs245753. doi: 10.1242/jcs.245753
20. Chou TC. Drug combination studies and their synergy quantification using the Chou-Talalay method. *Cancer Res*. (2010) 70:440–6. doi: 10.1158/0008-5472.CAN-09-1947
21. Klein HO. Cell kinetic alterations in normal and neoplastic cell populations *in vitro* and *in vivo* following vincristine: a reply to Dr Camplejohn's review article. *Cell Tissue Kinet*. (1980) 13:425–34. doi: 10.1111/j.1365-2184.1980.tb00481.x
22. D'Angiolella V, Mari C, Nocera D, Rametti L, Grieco D. The spindle checkpoint requires cyclin-dependent kinase activity. *Genes Dev*. (2003) 17:2520–5. doi: 10.1101/gad.267603
23. Mena AL, Lam EW, Chatterjee S. Sustained spindle-assembly checkpoint response requires de novo transcription and translation of cyclin B1. *PLoS ONE*. (2010) 5:e13037. doi: 10.1371/journal.pone.0013037
24. Atherton-Fessler S, Liu F, Gabrielli B, Lee MS, Peng CY, Piwnica-Worms H. Cell cycle regulation of the p34cdc2 inhibitory kinases. *Mol Biol Cell*. (1994) 5:989–1001. doi: 10.1091/mbc.5.9.989
25. Timofeev O, Cizmecioglu O, Settele F, Kempf T, Hoffmann I. Cdc25 phosphatases are required for timely assembly of CDK1-cyclin B at the G2/M transition. *J Biol Chem*. (2010) 285:16978–90. doi: 10.1074/jbc.M109.096552
26. Ruan W, Lim HH, Surana U. Mapping mitotic death: functional integration of mitochondria, spindle assembly checkpoint and apoptosis. *Front Cell Dev Biol*. (2019) 6:177. doi: 10.3389/fcell.2018.00177
27. Terrano DT, Upreti M, Chambers TC. Cyclin-dependent kinase 1-mediated Bcl-xL/Bcl-2 phosphorylation acts as a functional link coupling mitotic arrest and apoptosis. *Mol Cell Biol*. (2010) 30:640–56. doi: 10.1128/MCB.00882-09
28. Li W, Lan Z, Wu H, Wu S, Meadows J, Chen J, et al. BUBR1 phosphorylation is regulated during mitotic checkpoint activation. *Cell Growth Differ*. (1999) 10:769–75.
29. Bloom K, Yeh E. Tension management in the kinetochore. *Curr Biol*. (2010) 20:R1040–8. doi: 10.1016/j.cub.2010.10.055
30. Farooq MU, Naravetla B, Moore PW, Majid A, Gupta R, Kassab MY. Role of sildenafil in neurological disorders. *Clin Neuropharmacol*. (2008) 31:353–62. doi: 10.1097/WNF.0b013e31815cd94c
31. Wang L, Chopp M, Szalad A, Jia L, Lu X, Lu M, et al. Sildenafil ameliorates long term peripheral neuropathy in type II diabetic mice. *PLoS ONE*. (2015) 10:e0118134. doi: 10.1371/journal.pone.0118134
32. Rybalkina IG, Tang XB, Rybalkin SD. Multiple affinity states of cGMP-specific phosphodiesterase for sildenafil inhibition defined by cGMP-dependent and cGMP-independent mechanisms. *Mol Pharmacol*. (2010) 77:670–7. doi: 10.1124/mol.109.062299
33. Kothari A, Hittelman WN, Chambers TC. Cell cycle-dependent mechanisms underlie vincristine-induced death of primary acute lymphoblastic leukemia cells. *Cancer Res*. (2016) 76:3553–61. doi: 10.1158/0008-5472.CAN-15-2104
34. Gascoigne KE, Taylor SS. Cancer cells display profound intra-and interline variation following prolonged exposure to antimitotic drugs. *Cancer Cell*. (2008) 14:111–22. doi: 10.1016/j.ccr.2008.07.002
35. Sudakin V, Chan GK, Yen TJ. Checkpoint inhibition of the APC/C in HeLa cells is mediated by a complex of BUBR1, BUB3, CDC20, and MAD2. *J Cell Biol*. (2001) 154:925–36. doi: 10.1083/jcb.200102093
36. Lara-Gonzalez P, Westhorpe FG, Taylor SS. The spindle assembly checkpoint. *Curr Biol*. (2012) 22:R966–80. doi: 10.1016/j.cub.2012.10.006
37. Hauf S, Waizenegger IC, Peters JM. Cohesin cleavage by separase required for anaphase and cytokinesis in human cells. *Science*. (2001) 293:1320–3. doi: 10.1126/science.1061376
38. Huang H, Hittle J, Zappacosta F, Annan RS, Hershko A, Yen TJ. Phosphorylation sites in BubR1 that regulate kinetochore attachment, tension, and mitotic exit. *J Cell Biol*. (2008) 183:667–80. doi: 10.1083/jcb.200805163

39. Kita K, Imai Y, Asaka N, Suzuki T, Ochi T. BubR1 is essential for thiodimethylarsinic acid-induced spindle assembly checkpoint and mitotic cell death for preventing the accumulation of abnormal cells. *Biol Pharm Bull*. (2019) 42:1089–97. doi: 10.1248/bpb.b18-00638
40. Kim M, Murphy K, Liu F, Parker SE, Dowling ML, Baff W, et al. Caspase-mediated specific cleavage of BubR1 Is a determinant of mitotic progression. *Mol Cell Biol.* (2005) 25:9232–48. doi: 10.1128/MCB.25.21.9232-9248.2005
41. Gurden MD, Anderhub SJ, Faisal A, Linardopoulos S. Aurora B prevents premature removal of spindle assembly checkpoint proteins from the kinetochore: a key role for Aurora B in mitosis. *Oncotarget*. (2016) 9:19525–42. doi: 10.18632/oncotarget.10657
42. Fu Y, Ye D, Chen H, Lu W, Ye F, Xie X. Weakened spindle checkpoint with reduced BubR1 expression in paclitaxel-resistant ovarian carcinoma cell line SKOV3-TR30. *Gynecol Oncol*. (2007) 105:66–73. doi: 10.1016/j.ygyno.2006.10.061

Conflict of Interest: The authors declare that the research was conducted in the absence of any commercial or financial relationships that could be construed as a potential conflict of interest.

frontiers in Oncology

ORIGINAL RESEARCH
published: 30 September 2020
doi: 10.3389/fonc.2020.532285

Overcoming Limitations of Cisplatin Therapy by Additional Treatment With the HSP90 Inhibitor Onalespib

Anja Charlotte Lundgren Mortensen[1†], Tabassom Mohajershojai[1†], Mehran Hariri[1], Marika Pettersson[1] and Diana Spiegelberg[1,2]*

[1] Department of Immunology, Genetics and Pathology, Uppsala University, Uppsala, Sweden, [2] Department of Surgical Sciences, Uppsala University, Uppsala, Sweden

Rational: Cisplatin based cancer therapy is an affordable and effective standard therapy for several solid cancers, including lung, ovarian and head and neck cancers. However, the clinical use of cisplatin is routinely limited by the development of drug resistance and subsequent therapeutic failure. Therefore, methods of circumventing cisplatin resistance have the potential to increase therapeutic efficiency and dramatically increase overall survival. Cisplatin resistance can be mediated by alterations to the DNA damage response, where multiple components of the repair machinery have been described to be client proteins of HSP90. In the present study, we have investigated whether therapy with the novel HSP90 inhibitor onalespib can potentiate the efficacy of cisplatin and potentially reverse cisplatin resistance in ovarian and head and neck cancer cells.

Methods: Cell viability, cancer cell proliferation and migration capacity were evaluated *in vitro* on models of ovarian and head and neck cancer cells. Western blotting was used to assess the downregulation of HSP90 client proteins and alterations in downstream signaling proteins after exposure to cisplatin and/or onalespib. Induction of apoptosis and DNA damage response were evaluated in both monotherapy and combination therapy groups.

Results: Results demonstrate that onalespib enhances the efficiency of cisplatin in a dose-dependent manner. Tumor cells treated with both drugs displayed lower viability and a decreased migration rate compared to vehicle-control cells and cells treated with individual compounds. An increase of DNA double strand breaks was observed in both cisplatin and onalespib treated cells. The damage was highest and most persistent in the combination group, delaying the DNA repair machinery. Further, the cisplatin and onalespib co-treated cells had greater apoptotic activity compared to controls.

Conclusion: The results of this study demonstrate that the reduced therapeutic efficacy of cisplatin due to drug-resistance could be overcome by combination treatment with onalespib. We speculate that the increased apoptotic signaling, DNA damage as well as the downregulation of HSP90 client proteins are important mechanisms promoting increased sensitivity to cisplatin treatment.

Keywords: cisplatin, Hsp90 inhibition, drug resistance, synergy, combination treatment, chemo-sensitization, AT13387, CDDP

OPEN ACCESS

Edited by:
Nehad M. Ayoub, Jordan University of Science and Technology, Jordan

Reviewed by:
Roberta Manuela Moretti, University of Milan, Italy
Diwakar Bastihalli Tukaramrao, University of Toledo, United States

***Correspondence:**
Diana Spiegelberg
diana.spiegelberg@igp.uu.se

† These authors have contributed equally to this work

Specialty section:
This article was submitted to Pharmacology of Anti-Cancer Drugs, a section of the journal Frontiers in Oncology

Received: *03 February 2020*
Accepted: *10 September 2020*
Published: *30 September 2020*

Citation:
Mortensen ACL, Mohajershojai T, Hariri M, Pettersson M and Spiegelberg D (2020) Overcoming Limitations of Cisplatin Therapy by Additional Treatment With the HSP90 Inhibitor Onalespib. Front. Oncol. 10:532285. doi: 10.3389/fonc.2020.532285

INTRODUCTION

Cisplatin (cis-diamminedichloridoplatinum(II), CDDP) is one of the most commonly used antineoplastic drugs worldwide. The platinum-based compound has been in clinical use for more than 40 years and is a cost-effective first-in-line treatment against several solid cancers including ovarian, head and neck and testicular cancer (1). The main mechanism of action of cisplatin and other platinum-based analogs involves inter-or intra-strand crosslinks mediated by binding to reactive metal-binding sites on the DNA, primarily the N7 atoms of guanine and adenine in the major groove (2). These crosslinks disrupt DNA transcription and replication and can result in the induction of cytotoxic processes such as apoptosis. Furthermore, cisplatin is highly electrophilic and thus interacts with numerous nucleophilic non-DNA targets in the cytoplasm upon entering the cell. These interactions account for additional antineoplastic effects of the drug (2).

Though cisplatin is one of the most effective anticancer drugs, issues of acquired or innate resistance along with the serious adverse effects of the drug limit its curative potential (3, 4). However, the efficacy varies among the different types of cancer, in which ovarian and head and neck cancers present the greatest challenge. Development of cisplatin resistance is frequent, and linked to multiple mechanisms. One primary resistance mechanism is the reduction of uptake and accumulation of the compound in cancer cells (5). Although a large fraction of cisplatin is believed to enter the cell through passive diffusion, recent studies have indicated that copper transporters 1 and 2 (CTR1 and CTR2) are involved in the active transport of cisplatin (6). Studies have shown that cisplatin therapy downregulates CTR1 and CTR2, resulting in reduced uptake and subsequently decreased intracellular accumulation of cisplatin (7). Similarly, proteins involved in copper efflux, ATP7A and ATP7B, regulate the efflux of cisplatin, resulting in decreased intracellular cisplatin levels (8). Additionally, increased cisplatin-binding to glutathione S-transferase (GSH), metallothioneins and other cytoplasmic nucleophilic scavengers can decrease reactive intracellular levels of cisplatin (2, 5). Altered DNA-repair pathways further contribute to cisplatin resistance (4, 9). The primary repair mechanism utilized by cells following cisplatin-induced DNA damage is nucleotide excision repair (NER). NER involves more than thirty proteins but cisplatin resistance is most commonly associated with ERCC1, which is essential to catalyze the DNA excision step. High levels of ERCC1 have been associated with cisplatin resistant cancers, whereas low levels of ERCC1 are found in cisplatin sensitive cancers (10). Additionally, alterations in general stress response pathways including the heat shock response can promote cisplatin resistance (2, 5).

Heat shock proteins (HSP) are highly conserved molecular chaperones that play important roles in the formation and maturation of proteins involved in a wide diversity of cellular pathways, and subsequently have noticeable effects on the biology of normal and cancer cells. Among the HSP, HSP90 is a promising target in cancer therapy (11). HSP90 plays an essential role in signal transduction, conformational folding and cellular localization and stabilization of its client proteins (12, 13), which in turn are involved in processes such as transcriptional regulation, chromatin remodeling, cellular homeostasis, and DNA repair. So far, more than 300 HSP90 clients have been discovered. Among the clients are members of the epidermal growth factor receptor family (EGFR), signal transduction proteins (AKT and ERK) or DNA damage response proteins such as ATM (14). Many HSP90 client proteins are cancer-related, and elevated levels of HSP90 are often found in cancer. As a result, the malignancy is retained with the help of HSP90 and becomes particularly dependent on its activity, leading to an "HSP90 addiction" (15, 16). However, this dependency of HSP90 makes the cancer more susceptible to HSP90 inhibition. Therefore, inhibition of HSP90 offers the unique opportunity to overcome HSP90 dependency and to shut down several oncogenic processes simultaneously.

Several HSP90 inhibitors are currently undergoing clinical trials as cancer therapies, both as monotherapy and in combination with common antineoplastic therapies or radiation therapy (17, 18). HSP90 inhibitors mainly target the N-terminal ATPase on HSP90 and are able to displace ATP, blocking HSP90 function (11, 19). HSP90 inhibitors have been investigated as antineoplastic drugs since 1998, and in the intervening decades even more efficient inhibitors have been developed. Although promising on a preclinical level, the clinical usage of the first HSP90 inhibitors such as 17-AAG was limited due to issues with solubility, hepatotoxicity and the potential formation of toxic metabolites (20). Newer generations of HSP90 inhibitors such as AUY922, KW2478, STA-9090, and ONALESPIB387 display lower toxicities and improved function. Among them, onalespib (AT13387) is a potent second-generation compound, currently undergoing phase II studies in advanced solid tumors (13, 17). Studies have demonstrated potent radiosensitizing effects of onalespib both *in vitro* and *in vivo*, an effect likely mediated by impairment of the DNA damage response (13, 21, 22). Here, combination therapy of onalespib and radiotherapy resulted in a substantial increase in DNA double breaks (DSBs) as well as delay in DNA repair measured by the DSB markers γH2AX and 53BP1 (22). These findings raise the question whether HSP90 inhibition may also enhance the cytotoxic effect of cisplatin, due to similarities between the effects of cisplatin and ionizing radiation on tumor cells.

The frequent development of cisplatin resistance in monotherapy has encouraged fruitful research on cisplatin combination therapies. Subsequently, cisplatin has become the backbone of several combination therapies for a wide range of solid tumors including bladder, cervical, ovarian, lung, gastric, breast, and head and neck cancers. However, combination therapy with HSP90 inhibitors is still under investigation and ongoing clinical trials are evaluating the combination of onalespib, cisplatin and radiotherapy (13, 21, 23). Combination treatments with cisplatin are of great interest, both due to its aforementioned wide range of activity, high initial level of activity and the ubiquity and low cost of treatment. Whereas there currently are many novel and highly advanced cancer drugs under investigation, many new compounds are exorbitantly expensive once they reach clinical use. This results in an unavailability for large sections of the worldwide patient

population, resulting in an increased global and socio-economic gap in quality of cancer care. Focusing on restoring or enhancing the efficacy of widely available and affordable drugs by innovative use of combination therapy is therefore an attractive prospect for reducing this gap.

In the present study, we have evaluated whether therapy with the novel HSP90 inhibitor onalespib can potentiate the efficacy of cisplatin and reverse cisplatin resistance *in vitro*. We examined the efficacy of the drugs in H314, a head and neck squamous cell carcinoma cell line, and in the ovarian cancer cell lines SKOV3, A2780 and its cisplatin resistant clone A2780CIS. Furthermore, the underlying molecular mechanisms for the combination treatment were investigated.

MATERIALS AND METHODS

Cell Lines and Culture Conditions

The human ovarian cancer cell line SKOV3 (doubling time 24 h) obtained from American Type Culture Collection (ATCC, Manassas, VA, United States) was cultured in RPMI 1640 medium (Biochrom GmbH, Berlin, Germany) supplemented with 10% fetal bovine serum (FBS) (Sigma Aldrich, St. Louis, United States), 2 mM L-glutamine (Biochrom GmbH) and antibiotics (100 IU penicillin and 100 μg/ml streptomycin, Biochrom GmbH) (24). The human head and neck squamous cell carcinoma cell line H314 (doubling time 34 h) was obtained from The European Collection of Authenticated Cell Cultures (ECACC, Salisbury, United Kingdom) and was cultured in Dulbecco's Modified Eagle Medium/Ham's F-12 medium (1:1, Biochrom GmbH) with the previously described supplements (25). The human ovarian cancer cell lines A2780 and the cisplatin resistant clone A2780CIS (doubling times of 18 h) were obtained from The European Collection of Authenticated Cell Cultures and cultured in RPMI 1640 medium with the previously described supplements (26). In order to retain cisplatin resistance for the clone, 1 μM cisplatin was added to the media every 2–3 passages. All four cell lines were incubated at 37°C with 5% CO_2 and split two-to-three times a week using Trypsin/EDTA (Biochrom GmbH) when cells reached 80–90% confluency. All cell lines have been cultured for less than 3 months.

Drug Preparation

Onalespib (Selleck Chemicals, Houston, TX, United States) was dissolved in DMSO to a stock concentration of 61.0471 mM and stored in aliquots at −20°C. The stock concentration of cisplatin from EBEWE Pharma (Unterach am Attersee, Austria) was 1 mg/ml and was stored at room temperature. Both cisplatin and onalespib were diluted further in complete media for assay dependent concentrations. The final DMSO concentration was 0.005% (v/v) for 3000 nM Onalespib, 0.0002% (v/v) and 0.00008% (v/v) for 100 nM for 50 nM, respectively.

XTT Cell Viability Assays

A defined number of cells were seeded in flat-bottomed 96-well plates (SKOV3: 2000 cells/well, H314: 15000 cells/well, A2780: 2000 cells/well and A2780CIS 3000 cells/well) and incubated at 37°C and 5% CO_2 for 48 h prior to drug incubation with 0–3000 nM onalespib and 500 nM, 10 μM and 25 μM cisplatin. Cells were incubated at 37°C and 5% CO_2 for 24 h or 72 h. XTT Activation Reagent and XTT Reagent were added according manufacturer's instructions (American Type Culture Collection protocol 30–1011 K, Manassas, VA, United States). Plates were incubated for 4 h (SKOV3, A2780, and A2780CIS) and 3 h (H314) at 37°C and 5% CO_2 and absorbance was measured using a BioMark Microplate Reader (Bio-Rad Laboratories AB, Solna, Sweden). Significance was determined using two-way ANOVA followed by Sidak's multiple comparison's test. The number of replicates within each experimental group was 3 or more. Each experiment was repeated three times.

Clonogenic Survival Assay

Clonogenic survival assays were performed as described previously (27). In short, SKOV3, H314, A2780, and A2780CIS cells were seeded in 6-well plates and treated 24 h after seeding, with either cisplatin (100 and 250 nM) or onalespib (50 and 100 nM) as well as with combined treatment (100 nM of cisplatin with 50 nM of onalespib, 100 nM of cisplatin with 100 nM of onalespib, 250 nM of cisplatin with 50 nM onalespib, and 250 nM of cisplatin with 100 nM onalespib). After a drug incubation time of 24 h, the medium was replaced with complete media corresponding to the cell line and cells were incubated until colonies of >50 cells/colony were formed. After colony formation time (H314: 20 days, SKOV3: 10 days, A2780: 14 days, A2780CIS: 14 days), cells were fixed with 95% ethanol and stained with crystal violet. Colonies containing >50 cells were scored manually and plating efficiency (PE) and survival fraction (SF) were calculated. One-way ANOVA followed by Tukey's multiple comparison's test determined significance. Data were expressed as mean ± SD and $p < 0.05$ considered to be statistically significant. The number of replicates within each experimental group was 3. Each experiment was repeated three times.

Wound Healing Assay

Wound healing assay was performed as per published protocol (28). Briefly, cells were seeded in 48 well-plates (H314) or 6 well-plates (SKOV3). After 24 h, the confluent cell monolayer was scratched with a p10 pipette tip and was immediately treated with either cisplatin (100, 250, and 500 nM), onalespib (50 and 100 nM) or combinations thereof. Images from the same scratch location (three areas for each concentration) were obtained directly after scratching, 8 h and 24 h for SKOV3 cells and 24, 48, and 72 h of incubation for H314 cells using an inverted microscope Nikon Diaphot (Nikon, Japan) mounted with a Canon EOS 700D camera (Canon Inc., Japan). Migration distance was measured and analyzed using ImageJ 1.51k software (NIH, Bethesda, MD, United States). One-way ANOVA followed by Tukey's multiple comparison's test determined significance. Data were expressed as mean ± SD and $p < 0.05$ considered to be statistically significant. The number of replicates within each experimental group was three. Each experiment was repeated three times.

Trans-Well Migration Assay

Trans-well migration assay was performed using 24-well plates with inserts of 8 μm filter (Thermo Fisher Scientific, Sweden). Cells were starved for 24 h before adding cell suspension in FBS^{-} media (1×10^5 cells/chamber) and 250 nM cisplatin and/or 50 and 100 nM onalespib into the upper chamber with a total volume of 100 μl. 500 μl 10% FBS containing media was placed in lower chamber. After overnight incubation at 37°C, remaining cells in the upper chamber were removed and the migrated cells on the bottom side of the filter were fixed in 99.7% ethanol for 10 min and stained with 1% crystal violet for 2 min. Five images of each insert were captured with microscope at ×200 magnification. and ImageJ (version 2.0, NIH, United States) was used for manual scoring of the migrated cells and for analysis. One-way ANOVA followed by Tukey's multiple comparison's test determined significance. The experiments were repeated at least two times ($N > 2$).

Western Blotting

After a 24 h or 96 h drug incubation with either 250 or 500 nM cisplatin, 50 or 100 nM onalespib or combinations thereof, whole cell lysates of SKOV3 and H314 cells were prepared as follows: cells were washed once with 1x cold PBS and incubated with Pierce® IP Lysis Buffer containing 1x phosphatase and protease inhibitor cocktail (Thermo Fisher Scientific, Sweden) for 15 min on a tilting ice bed. The cell lysates were centrifuged for 15 min at 15000 rpm at 4°C and subsequently stored at −20°C. Following protein quantification (Pierce BCA Protein Assay Kit, Thermo Scientific, Sweden) samples were separated on an SDS-PAGE using 4–12% Bis-Tris gels in MES or MOPS SDS running buffer or 3–8% Tris–Acetate gels in Tris–Acetate SDS running buffer (Novex™, NuPAGE®, Invitrogen, Thermo Fisher Scientific, Sweden). Thereafter, the separated proteins were transferred to a PVDF membrane (Merck Millipore, Darmstadt, Germany) using wet transfer for 2 h with the constant voltage of 100 V at room temperature using an insert ice block for cooling. The membranes were blocked in Western Blot fluorescent Blocking Buffer (ThermoFisher Scientific, Sweden) or 5% bovine serum albumin in PBS-Tween (0.1%) for 60 min. The membranes were incubated with the primary antibody targeting EGFR (2232S Rabbit polyclonal antibody, Cell Signaling Technology, United States), AKT1,2,3 (ab179463 Rabbit monoclonal antibody, Abcam, United Kingdom), Anti-AKT (phospho T308) (Rabbit polyclonal antibody, Abcam, United Kingdom), Anti-AKT1 + AKT2 + AKT3 (phospho Y312 + Y315 + Y316) (Rabbit polyclonal antibody, Abcam, United Kingdom), H2AX (Rabbit polyclonal antibody, Abcam, United Kingdom), γH2AX (Rabbit monoclonal antibody, Abcam, United Kingdom and Mouse monoclonal antibody, JBW clone 301, Millipore GmbH, Germany), ATM (Rabbit monoclonal antibody, Abcam, United Kingdom) and DNA-PKcs (Rabbit monoclonal antibody, Abcam, United Kingdom), overnight at 4°C. Beta-actin (Mouse monoclonal, Sigma Aldrich, Sweden) or sodium-potassium ATPase (ab76020, Abcam, United Kingdom) was used as loading control. The following day, the membranes were incubated with secondary antibodies (Invitrogen) in 0.1% PBS-Tween for 60 min and developed using the Amersham™ Imagequant™ 800 (ThermoFisher Scientific, Sweden). The bands were quantified by using ImageJ software. One-way ANOVA followed by Tukey's multiple comparison's test determined significance where $p < 0.05$ was considered significant. The experiments were repeated at least three times ($N = 3$).

Analysis of Apoptosis via Flow Cytometry

SKOV3 and A2780CIS cells were plated in T25 flasks 24 h before drug exposure. Afterward, samples were treated with 37°C warm media mixed with 100 nM onalespib, 500 nM cisplatin, or a combination of onalespib and cisplatin for 96 h before flow cytometry. Harvested cells were washed in cold PBS and stained with propidium iodide (PI) and Alexa Fluor 488 annexin V (Alexa Fluor®488 Annexin V/Dead Cell Apoptosis Kit with Alexa Fluor 488 annexin V and PI for flow cytometry, ThermoFisher Scientific, Sweden) according to manufactures instructions. CellEvent™ Caspase-3/7 Green Flow Cytometry Assay Kit (Thermo Fisher Scientific, Sweden) was used to analyze caspase 3/7 activity. Caspase activity inhibition on SKOV3 and A2780CIS apoptosis were evaluated by pan-caspase inhibitor z-VAD-FMK (Selleckchem, Germany). Cells were pretreated with or without 20 μM z-VAD-FMK for 1 h followed by incubation with 500 nM cisplatin and 100 nM onalespib. Apoptotic cells were visualized using a CytoFLEX (Beckman Coulter, Krefeld, Germany). Obtained data were analyzed by FlowJo™ Software for Windows (Version 10.6.1. Becton, Dickinson and Company, Ashland, OR, United States). One-way ANOVA followed by Tukey's multiple comparison's test determined significance, where $p < 0.05$ was considered significant. The number of replicates within each experimental group was two. Each experiment was repeated three times.

Cell-Cycle Distribution Analysis via Flow Cytometry

After 96 h exposure to 500 nM cisplatin, 100 nM onalespib, or the combination thereof SKOV3 and A2780CIS cells were harvested and washed with ice-cold PBS followed by resuspension in 0.5 mL PBS. Cells were fixed by adding 5 mL of ice-cold 70% EtOH drop-wise and incubated at −20°C overnight. Afterwards, the cells were centrifuged at 1200 rpm for 5 min and washed once with 2 mL ice-cold PBS. After removing the supernatant, cells were centrifuged again at 1200 rpm for 5 min followed by removing the supernatant and adding 0.5 mL RNase (100 μg/mL) and 100 μL of PI (50 μg/mL). The cells were incubated for 30 min at RT in the dark before analysis using a CytoFLEX (Beckman Coulter, Krefeld, Germany). The data analysis and peaks recognition performed in FlowJo™ Software for Windows (Version 10.6.1. Becton, Dickinson and Company, Oregon, United States).

Analysis of γH2AX and 53BP1 Expression via Immunofluorescence Staining (Confocal Microscopy)

SKOV3 and A2780CIS cells were seeded in 4-well cell culture chamber slides (Nunc A/S, Roskilde, Denmark) and incubated

for 24 h before drug treatment for a confluency of 60% prior to start of treatment. Thereafter, cells were incubated with either mono-or combination treatments of 500 nM cisplatin and 100 nM onalespib for 96 h. After treatment, slides were washed with 1x PBS followed by 99% methanol fixation at −20°C. Cell membrane permeability was induced by ice-cold acetone exposure for 10–15 s (Millipore, Merck, United States). Non-specific protein blocking was performed in 10% FBS-PBS for 60 min at room temperature to reduce background interference. Cells were incubated with primary Rabbit anti-53BP1 (Abcam, Cambridge, United Kingdom) and mouse anti-γH2AX (EMD Millipore Merck Darmstadt, Germany) antibodies overnight at 4°C and secondary antibody incubation [master mix of Alexa flour 488 (ab150117, Abcam, Cambridge, United Kingdom) and Alexa flour 555 (ab150086, Abcam, Cambridge, United Kingdom)] were done the following day for 60 min in the dark. DAPI (ThermoFisher Scientific, Sweden) was used for nucleus staining in the dark for 2 min followed by 10 washes with 1x PBS and milli-Q water. After air-drying, the VectaShield (Vectorlabs, Burlingame, CA, United States) were mounted on slides and covered with a coverslip. Slides were imaged at three randomly chosen fields of view with a Zeiss LSM 700 confocal microscope (Zeiss, Oberkochen, Germany). The accuracy of foci image acquisition was confirmed by Z-stacking with different magnifications. Image processing and foci counting were performed using Image J software. One-way ANOVA followed by Tukey's multiple comparison's test determined significance, where $p < 0.05$ was considered significant. The experiments were repeated three times ($N = 3$).

RESULTS

Cisplatin and Onalespib Monotherapy Decreases Viability of Cancer Cells While Co-treatment Potentiates the Effects

The growth inhibitory effects of monotherapy with cisplatin and the HSP90 inhibitor onalespib were first assessed in ovarian cancer cell lines SKOV3, A2780, and A2780CIS cells as well as head and neck cancer cells (H314) following both 24 h and 72 h drug incubations (**Figures 1A,B** and **Supplementary Figure 1**). Increasing concentrations of cisplatin decreased the viability as measured by XTT metabolic assay in all cell lines in a concentration dependent manner (**Figure 1A**). In the XTT assays 500 nM cisplatin did not affect the viability of SKOV3, H314, or A2780CIS cells using a drug incubation time of 72 h. However, the A2780 cells demonstrated a decrease in viability by about >50% as a result of a 72 h drug incubation time. Concentrations of 10 μM decreased the viability by 57.5% and 53% and 25 μM cisplatin by 70 and 71% in SKOV3 and H314 cells, respectively. Similarly, the A2780CIS cells was greatly affected by 10 and 25 μM cisplatin, resulting in a decrease in viability by 58 and 98%, respectively.

Increasing concentrations of onalespib also decreased the viability as measured by XTT. 100 nM onalespib decreased the viability by 11% and 45%, and 1 μM onalespib by 60% and 90% in SKOV3 and H314 cells in the XTT analysis, respectively (**Figure 1B**). The A2780 and A2780CIS cells were more sensitive to onalespib monotherapy than SKOV3 and H314 cells. Following incubation with 100 nM of onalespib, the viability of A2780 and A2780CIS cells decreased by 80% and 70%, respectively. 1 μM of onalespib resulted in a nearly undetectable signal, nearing 100% decrease in viability.

At 24 h, the viability of SKOV3 and H314 cells was not significantly affected by cisplatin monotherapy at either concentration (**Supplementary Figure 1A**, dotted lines), whereas onalespib monotherapy resulted in decreased viability at concentrations exceeding 100 nM for both cell lines (**Supplementary Figure 1A**). Analysis of the later time point (72 h) demonstrated greater effects in both SKOV3, H314 and A2780CIS cells treated with 10 μM cisplatin, where viability had decreased to less than 50% of untreated controls, compared with 90–100% of untreated controls at 24 h post treatment (dotted lines in **Figures 2A,B**). Similarly, the effects of onalespib increased over time, resulting in significantly decreased viability of samples treated with 30 nM or higher (**Supplementary Figures 1A**, **2A,B**).

The potency of the combination of cisplatin and onalespib was greater at the later time point (72 h) and the high cisplatin concentration (10 μM). In these samples, a significant decrease in viability was measured in all combination treated samples compared to monotherapy in both cell lines. In H314 cells, the combination of 10 μM of cisplatin and doses ≥300 nM onalespib resulted in nearly indistinguishable absorbance levels (13% for onalespib monotherapy at 1000 and 3000 nM and 2% for combination therapy at the same concentrations), effectively reducing survival of the cells to near zero. For SKOV3 and A2780CIS cells, the same pattern was observed, resulting in a viability of the combination of 10 μM cisplatin and 100 or 300 nM onalespib below 15% (**Figure 2B**). Interestingly, H314 samples treated with 500 nM of cisplatin were unaffected and there were no differences between onalespib monotherapy and combination treated samples. SKOV3 and A2780 cells treated with 500 nM cisplatin were affected by the combination therapy, with significant differences between onalespib monotherapy and combination treated samples at onalespib concentrations ≤100 nM (**Figure 2A**).

Combination Therapy Significantly Impairs Clonogenic Survival

The efficacy of cisplatin and onalespib combination therapy was also studied in clonogenic survival assays. The highest concentration of cisplatin (500 nM) significantly decreased the survival fraction of SKOV3, H314, A2780, and A2780CIS cells (**Figures 3A–D**, left hand graph). Monotreatment with 100 nM onalespib decreased the survival of H314, A2780, and A2780CIS cells, but not of SKOV3 cells. However, the combination of cisplatin and onalespib significantly affected the survival fractions of all cell lines compared to untreated controls and cells treated with onalespib alone (**Figures 3A–D** middle and right-hand graphs). Generally, A2780 and H314 cells were more sensitive to the treatments than SKOV3 and A2780CIS cells (**Figures 3A–D**, middle). Cisplatin in combination with 50 nM onalespib displayed a clear increase in effect, where all

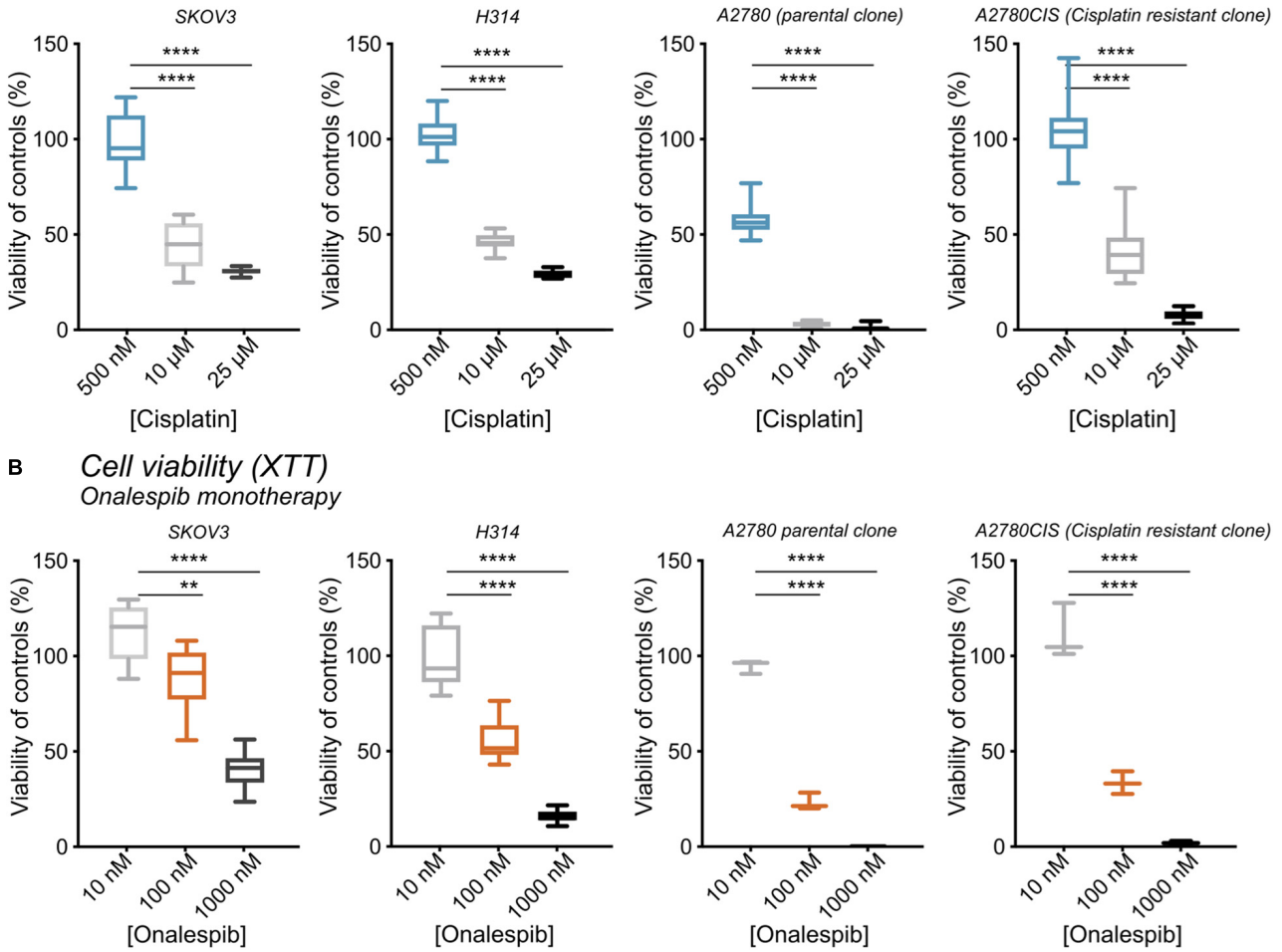

FIGURE 1 | (A) XTT cell viability from left to right of SKOV3, H314, A2780, and A2780CIS cells following treatment with 500 nM, 10 μM, or 25 μM cisplatin normalized to untreated controls. **(B)** XTT cell viability from left to right of SKOV3, H314, A2780, and A2780CIS cells following treatment with 10, 100, or 1000 nM onalespib normalized to untreated controls. $N = 3$, error bars represent SD. $^{**}p < 0.01$, $^{****}p < 0.0001$.

survival fractions of all combination treatments were significantly decreased compared to both untreated controls and onalespib monotherapy. For 100 nM onalespib, the difference between combination treatment and monotreatment was lower, due to the high effect of onalespib alone. Here, all four cell lines treated with 100 nM onalespib were significantly affected compared to untreated controls ($p \leq 0.001$). Furthermore, the combination of 500 nM cisplatin and 100 nM onalespib was significantly decreased from onalespib monotherapy in all cell lines ($p \leq 0.05$). Combination therapy of H314 and A2780 cells decreased the survival fraction in all tested combinations ($p \leq 0.0001$). Besides the effects on the survival fraction, the shape and size of the colonies was affected by the drug treatment. In general, cells treated with increasing drug combinations showed smaller colony sizes. Furthermore, colonies of the combination treatment groups were more irregular in shape (**Figures 3A–D**, right hand).

Combination Therapy of Cisplatin and Onalespib Delayed Wound Healing and Decreased the Migration of Cancer Cells

Wound Healing Assay

To further study whether onalespib treatment can augment cisplatin therapy, the migration capacity of SKOV3 and H314 cells was studied in wound healing assays. Cisplatin monotherapy did not affect the wound healing ability of SKOV3 cells (**Supplementary Figure 1C**), whereas a dose-dependent decrease in migration capacity/healing was observed for onalespib (50 and 100 nM) monotherapy samples (**Figures 4A–C**). The combination of 50 nM onalespib with 500 nM cisplatin (**Figure 4A**) resulted in a significant ($p \leq 0.01$) delay in wound healing in compared to either monotherapy at 24 h post start of the assay (**Figure 4B**, bar chart). A similar trend in inhibitory effect was observed for the combination with 100 nM onalespib,

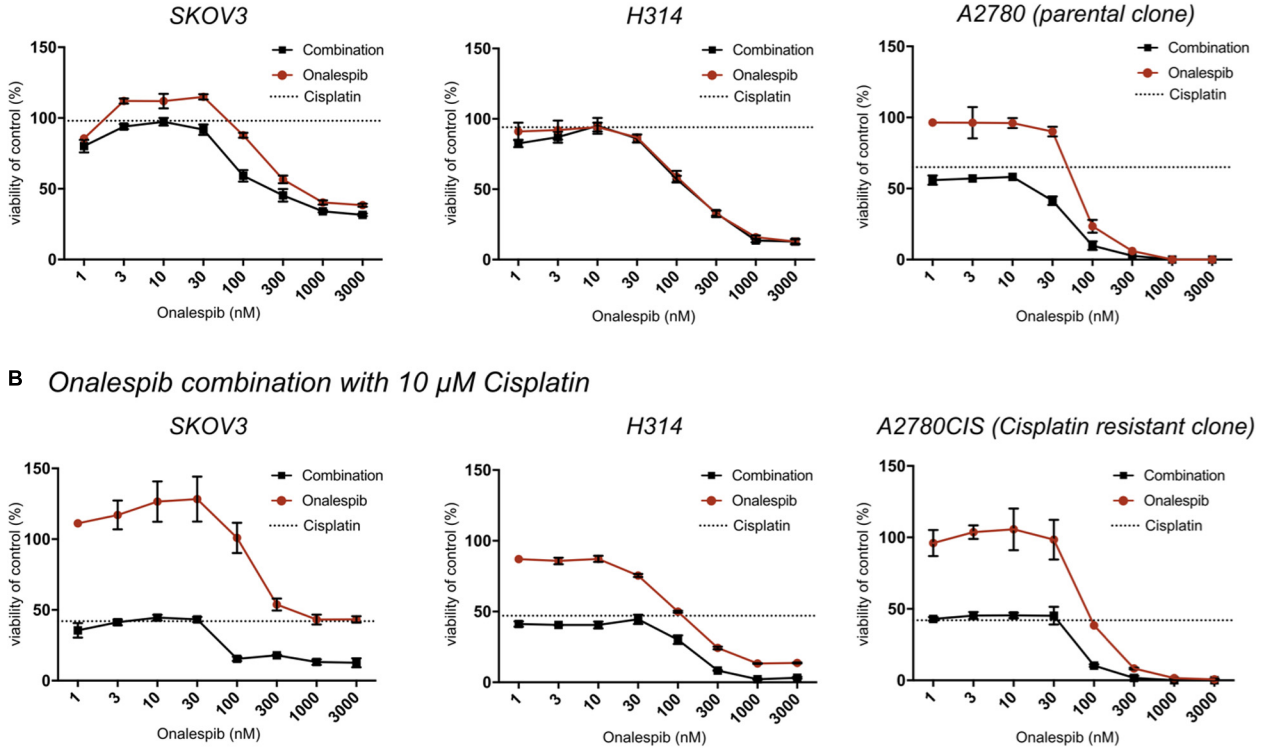

FIGURE 2 | (A) XTT cell viability normalized to untreated controls of SKOV3, H314, and A2780 cells treated with 0–3000 nM onalespib or the combination of onalespib with 500 nM cisplatin **(A)** 72 h post treatment. **(B)** XTT cell viability normalized to untreated controls of SKOV3, H314 and A2780CIS cells treated with 0–3000 nM onalespib or the combination of onalespib with 10 μM cisplatin at 72 h post treatment. *N* = 3, error bars represent SEM. Dotted lines represent the viability of cisplatin monotherapy at either 500 nM or 10 μM.

though not statistically significant (**Figures 4B,C**). H314 cells did not migrate as fast as SKOV3 cells. Therefore, this cell line was followed up to 72 h. H314 cells were unaffected by cisplatin monotherapy (**Supplementary Figure 1C**) after 72 h, but onalespib monotherapy displayed a dose-dependent decrease in healing. However, the onalespib combination therapy had a more potent effect compared to monotherapy in the H314 cells (**Figures 4D–F**). The combination of cisplatin and onalespib resulted in a significant delay in wound healing for the combination of 50 nM of onalespib with 250 nM cisplatin ($p \leq 0.001$), but paradoxically not for 500 nM cisplatin. Similarly to SKOV3 cells, the greatest inhibitory effect was seen in the 100 nM onalespib and 500 nM cisplatin group, though the difference to monotherapy was not statistically significant (**Figure 4E**). Representative images of the scratches are shown in **Figure 4C** for SKOV3 cells and in **Figure 4F** for H314 cells.

Trans-Well Migration Assay

Since the wound healing assays measure a mixture of migration and proliferation, the migrating potential of serum-starved SKOV3 and H314 cells was specifically investigated using *trans*-well migration assays with a pore size 0.8 μm. Increasing doses of cisplatin decreased the number of migrated SKOV3 cells, with significant decrease measured at 250 nM (63.3 ± 9.2%) and 500 nM cisplatin (17.1 ± 2.1%) compared to control cells. Similarly, increasing doses of onalespib resulted in a significantly lower number of migrated SKOV3 cells at concentrations ≥100 nM (54.1 ± 8% and 21 ± 3.7% for 100 and 200 nM, respectively) compared to untreated controls. Moreover, the combination of cisplatin and onalespib resulted in additionally lowered migration (**Table 1**), although none of the tested combination treatments resulted in significant changes compared to monotherapies. Microscopic images of the migrated cells are displayed in **Supplementary Figure 1D**. H314 cells were unable to migrate in the *trans*-well migration assays, where as few as ten cells had migrated after 48 h in the control samples (data not shown).

Onalespib and Cisplatin Treatment Downregulate Cell Signaling and HSP90 Client Proteins

Western blotting was used to study the effect of onalespib and cisplatin on HSP90 client proteins, downstream signaling cascades and DNA damage response proteins in SKOV3 and H314 cells (**Figures 5A–C**). In order to investigate DNA

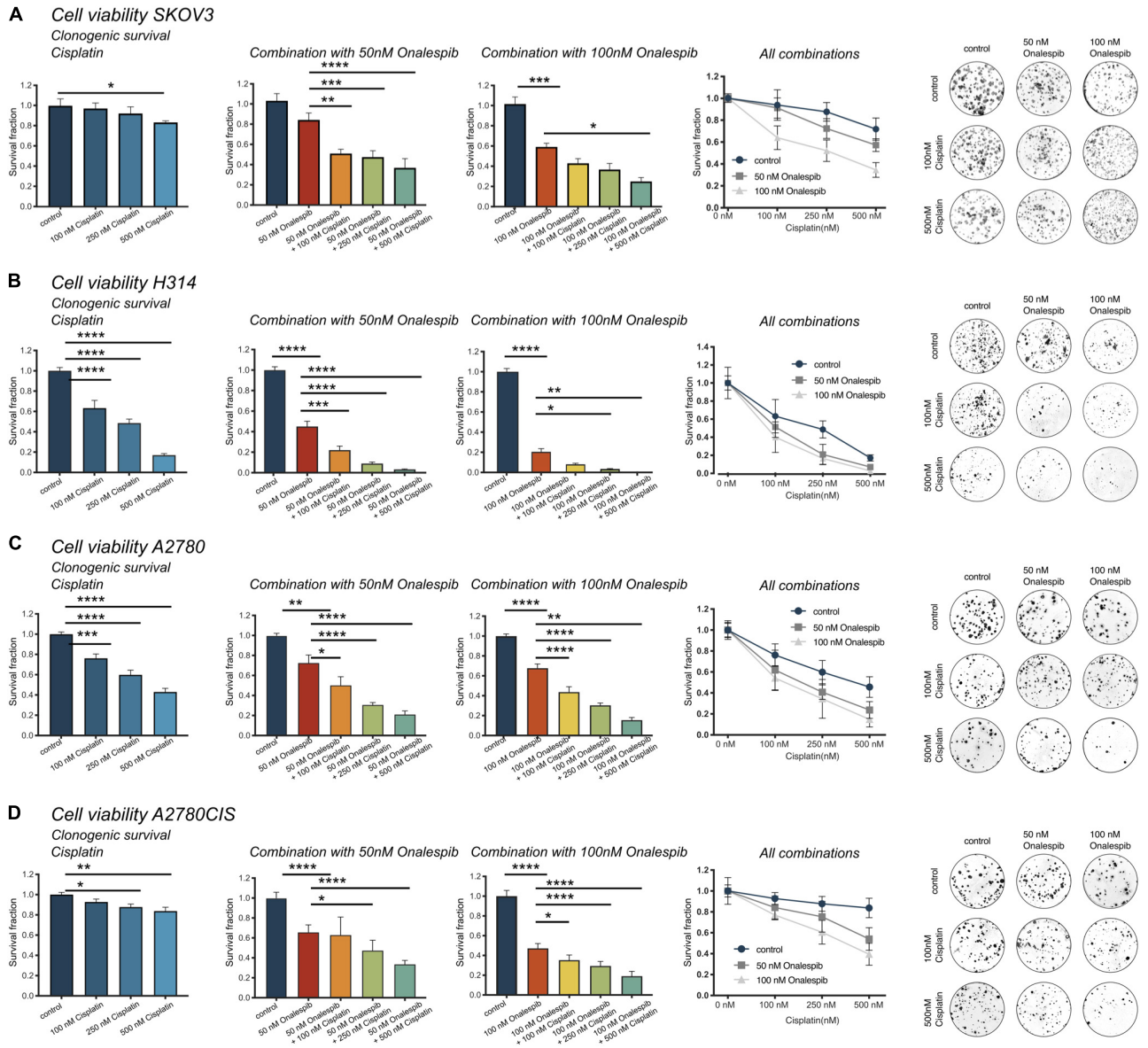

FIGURE 3 | (A) Clonogenic survival of SKOV3 cells treated with 0, 100, 250, and 500 nM cisplatin as monotherapy or in combination with 50 or 100 nM onalespib. Note that combination samples are normalized to 0, 50, or 100 nM of onalespib to compensate for the effect on survival by onalespib alone. **(B)** Clonogenic survival of H314 cells treated with 0, 100, 250, and 500 nM cisplatin as monotherapy or in combination with 50 or 100 nM onalespib. Note that combination samples are normalized to 0, 50, or 100 nM of onalespib to compensate for the effect on survival by onalespib alone. **(C)** Clonogenic survival of A2780 cells treated with 0, 100, 250, and 500 nM cisplatin as monotherapy or in combination with 50 or 100 nM onalespib. **(D)** Clonogenic survival of A2780CIS cells treated with 0, 100, 250, and 500 nM cisplatin as monotherapy or in combination with 50 or 100 nM onalespib. Note that combination samples are normalized to 0, 50, or 100 nM of onalespib to compensate for the effect on survival by onalespib alone. $N = 3$, error bars represent SD. $^{*}p < 0.05$, $^{**}p < 0.01$, $^{***}p < 0.001$, $^{****}p < 0.0001$.

damage response, the expression of the repair proteins ATM and DNAPKcs were investigated. Treatment with onalespib reduced ATM and DNAPKcs expression, most pronounced at highest concentrations (100 nM onalespib) with and without cisplatin treatment (**Figures 5A,B**). Incubation with onalespib reduced ATM expression to a high degree, and no band was observed in H314 cells at highest concentrations (**Figure 5C**). To investigate whether the non-phosphorylated form of the DNA double strand break marker γH2AX is changed by onalespib and / or cisplatin, we examined the expression of the histon H2AX. At the 24 h time point, the level of H2AX expression was nearly constant for both cell lines in all treatment groups and in the control. At 96 h, a slight increase in the H2AX level was found for both cell lines, but not significant (**Figure 5C**).

The AKT expression levels for both cell lines decreased significantly in the onalespib and the combination treatment group compared to control and cisplatin monotherapy. For

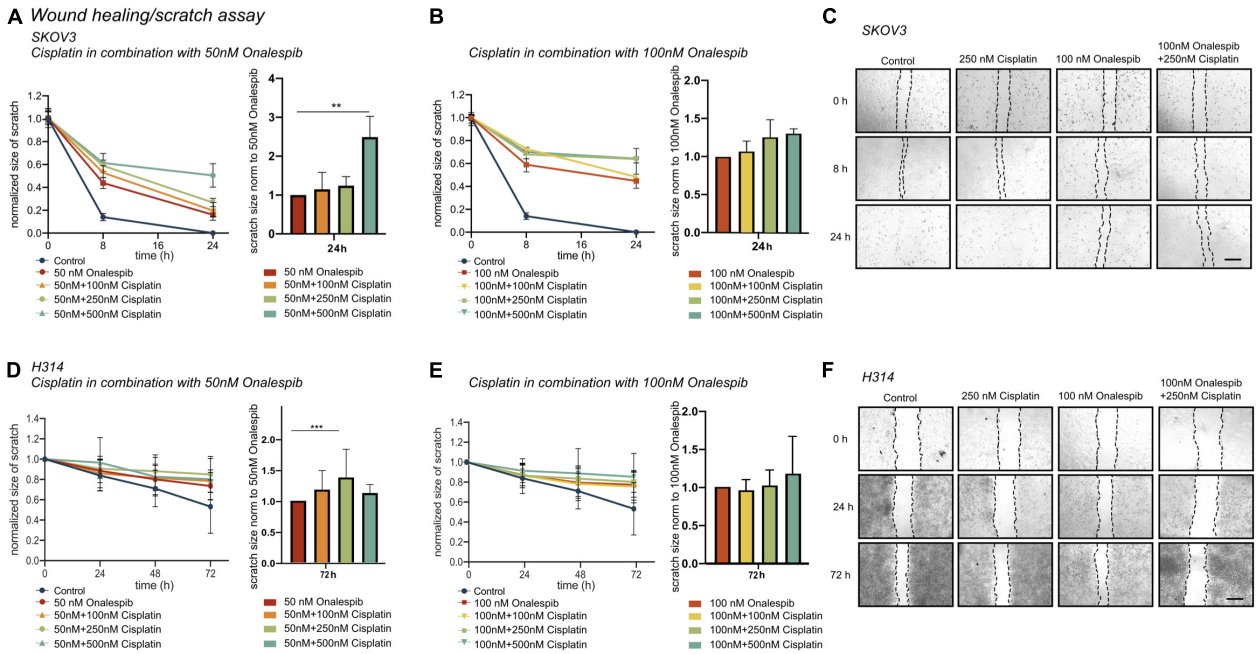

FIGURE 4 | (A) Effect of 50 nM onalespib and the combination with 100, 250, or 500 nM cisplatin and **(B)** effect of 100 nM onalespib and the combination with 100, 250, or 500 nM cisplatin at 24 h on the wound healing ability of SKOV3 cells. Note that in figure [**(A)** – right] and [**(B)** – right], wound/scratch sizes are normalized to 50 nM onalespib **(A)** or 100 nM onalespib **(B)**. **(C)** Representative images of SKOV 3 wound/scratch of control, 250 nM cisplatin, 100 nM onalespib and the combination at 0, 8, and 24 h post scratch. **(D)** effect of 50 nM onalespib and the combination with 100, 250, or 500 nM cisplatin and **(E)** effect of 100 nM onalespib and the combination with 100, 250, or 500 nM cisplatin at 24 h on the wound healing ability of H314 cells at 72 h. Note that in figure [**(D)** – right] and [**(E)** – right], wound/scratch sizes are normalized to 50 nM onalespib **(D)** or 100 nM onalespib **(E)**. **(F)** Representative images of H314 wound/scratch of control, 250 nM cisplatin, 100 nM onalespib and the combination at 0, 24, and 72 h post scratch. $N = 3$, error bars represent SD. $^{**}p < 0.01$, $^{***}p < 0.001$. The size bar in **(C,F)** corresponds to 4 μm.

SKOV3 cells, only the combination of 250 nM cisplatin and 100 nM onalespib resulted in a significant decrease compared to cisplatin monotherapy (**Figures 5A,B**). For H314 cells, all combination treatments showed a significantly lower AKT expression compared to cisplatin monotherapy. For both cell lines, pAKT was not detected by Western blot at any time point (data not shown).

Cisplatin monotherapy at concentration <500 nM did not affect the expression of EGFR in both SKOV3 and H314 cells, whereas monotherapy with 50 nM and 100 nM onalespib significantly downregulated EGFR levels in a concentration-dependent manner (**Figures 5A,B**).

TABLE 1 | Mean, SEM, and 95% confidence intervals (CI) of migrated SKOV3 cells treated with 250 or 500 nM cisplatin, 50 or 100 nM onalespib or the combination during the *trans*-well migration assays, $N = 3$.

Treatments	Mean of migrated cells ± SEM	95% CI
Control	100 ± 4	8.4
250 nM Cisplatin	63.3 ± 9.2	19.2
500 nM Cisplatin	17.1 ± 2.1	4.8
50 nM Onalespib	80.6 ± 5.5	11.9
100 nM Onalespib	54.1 ± 8	18.1
200 nM Onalespib	21 ± 3.7	8.5
250 nM Cisplatin + 50 nM Onalespib	65.3 ± 9	19.4
250 nM Cisplatin + 100 nM Onalespib	51.4 ± 7	16
250 nM Cisplatin + 200 nM Onalespib	23 ± 4	9.7
500 nM Cisplatin + 50 nM Onalespib	24.2 ± 4	13.8
500 nM Cisplatin + 100 nM Onalespib	26.5 ± 7	20.3
500 nM Cisplatin + 200 nM Onalespib	18.2 ± 2	4.6

Combination Therapy With Cisplatin and Onalespib Leads to G2/M Phase Arrest

Flow cytometric analysis of cell cycle distribution of SKOV3 cells using PI staining after exposure to 500 nM cisplatin, 100 nM onalespib, or combination for 96 h showed increasing number of cells in G2/M phase (32.5%) in the combination group compared to the monotreatment groups (onalespib 26.6% and cisplatin 12.1%) (**Figures 5D,E**). The percentage of cells in the G2/M phase of the combination group was significantly ($p \leq 0.01$) higher than the cisplatin and ($p \leq 0.001$) control group (6%). The percentage of cells in the S phase was significantly ($p \leq 0.01$) higher in the combination group (45%) compared to onalespib (20.5%) and cisplatin (18.2%) and control (20%) samples. The G1 phase was decreased from 73.9% in the control group to 71.1% in the cisplatin group followed by 50.5% in the onalespib group and 31.7% in the combination group. Representative histograms are presented in **Figure 5E**.

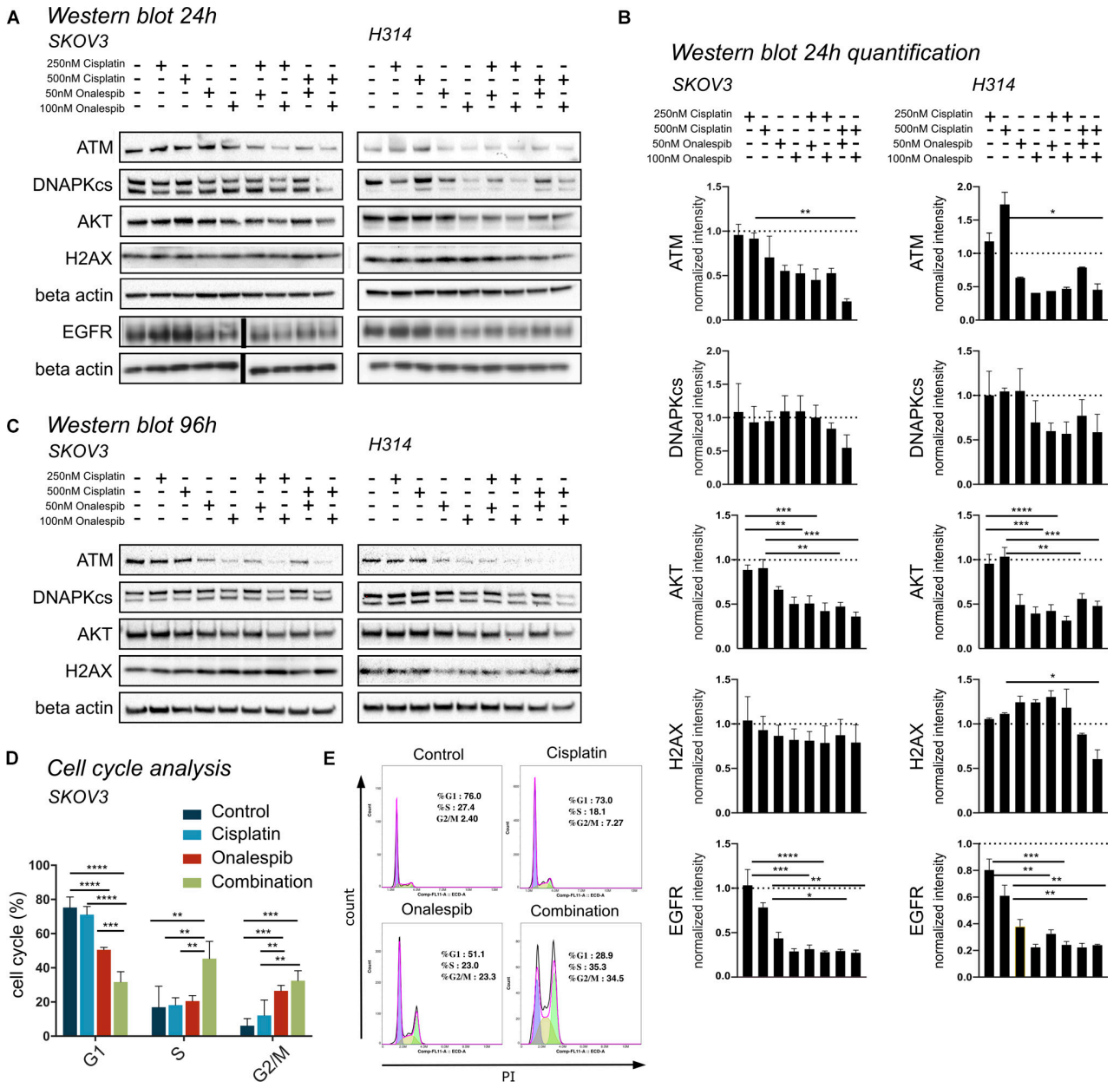

FIGURE 5 | (A) Representative Western blot membrane of the analysis of ATM, DNAPKcs, AKT, H2AX, and EGFR expression levels of SKOV3 and H314 cells following 24 h incubation with cisplatin and onalespib and their combinations. Note for EGFR analysis is from a separate membrane and the beta actin below is the loading control for this particular membrane. The black bar inserted in the middle of the membrane is due to removal of an overexposed size marker **(B)** Quantification of Western blot at 24 h incubation of SKOV3 and H314 cells. **(C)** Representative Western blot membrane of the analysis of ATM, DNAPKcs, AKT and H2AX expression levels of SKOV3 and H314 cells following 96 h incubation with cisplatin and onalespib and their combinations. **(D,E)** Cell cycle distribution in SKOV3 cells after exposure to cisplatin, onalespib, and their combinations as percentage of cells in G1, S, and G2M phases. **(E)** Representative flow cytometry graphs. Combination treatment led to cell cycle arrest and elevated G2/M peak compare to monotherapy groups. $N = 3$, error bars represent SEM. $^{*}p < 0.05$, $^{**}p < 0.01$, $^{***}p < 0.001$, $^{****}p < 0.0001$.

Combination Therapy of Cisplatin and Onalespib Increased Apoptotic Activity in Cancer Cells

SKOV3 and A2780CIS cells were treated with 500 nM cisplatin and 100 nM onalespib monotherapy and combination therapy for 96 h to investigate cell apoptosis by flow cytometry (**Figure 6**). Mean fluorescence intensity graphs are presented in **Supplementary Figure 2**.

Annexin V, a specific apoptotic cell membrane marker, revealed increased levels of apoptotic cells for both cell lines following all treatments (**Figures 6A,B,E,F**). In SKOV3 cells,

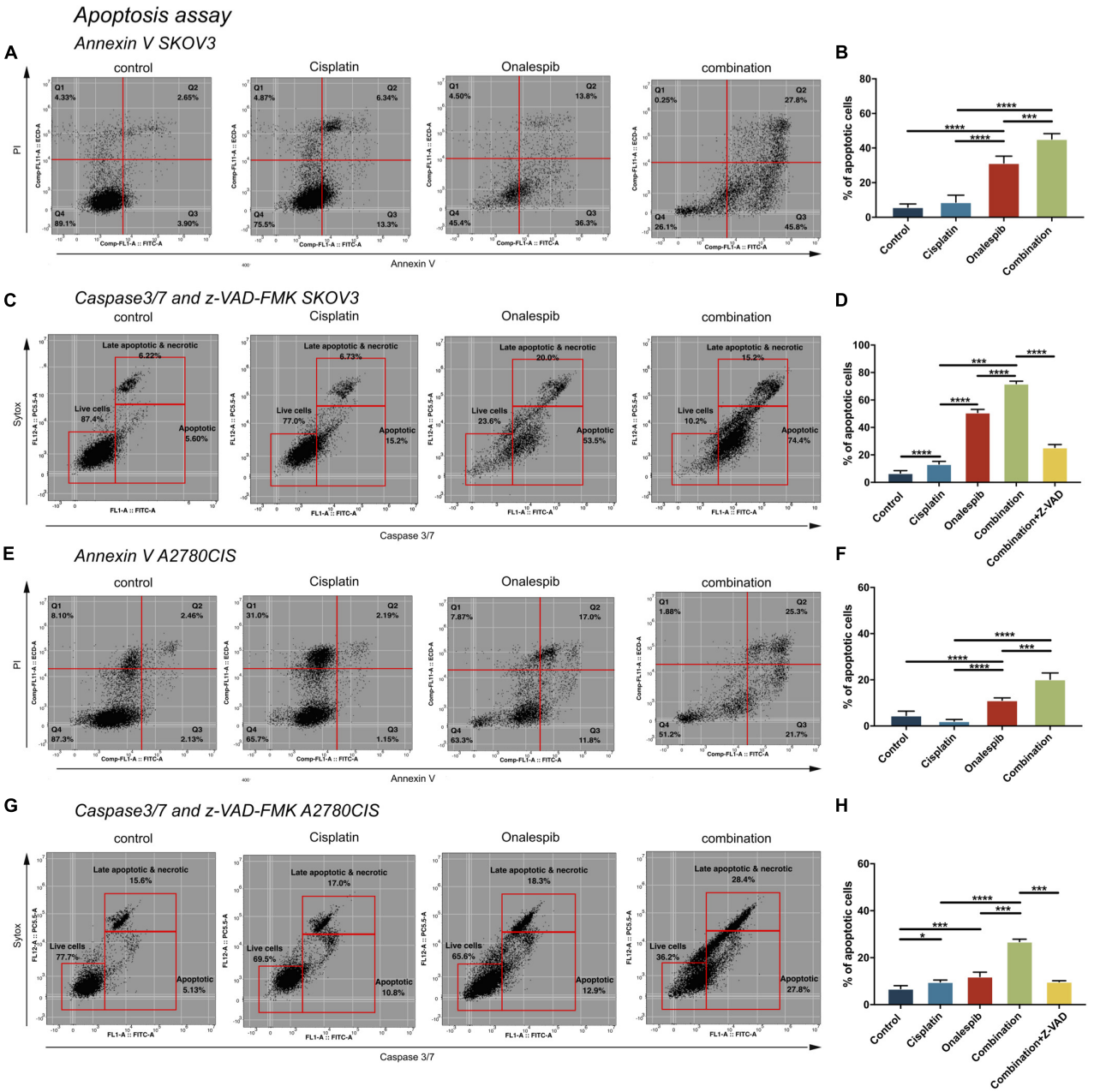

FIGURE 6 | Flow cytometric analysis of apoptosis of untreated controls, 500 nM cisplatin, 100 nM onalespib and the combination using Annexin V/PI staining of **(A,B)** SKOV3 and **(E,F)** A2780CIS cells following 96 h incubation. The lower left square shows the percentage of live cells, the lower right square shows the percentage of apoptotic cells and the upper right square shows late apoptotic and necrotic cells. Flow cytometric analysis of caspase 3/7 of untreated controls, 500 nM cisplatin, 100 nM onalespib and the combination of **(C,D)** SKOV3 and **(G,H)** A2780CIS cells after 96 h incubation. Note that in **(C,D,G,H)**, the effects of combination therapy were also evaluated in combination with 20 μM of the z-VAD-FMK pan-caspase inhibitor. The lower left square shows the percentage of live cells, the lower right square shows the percentage of apoptotic cells and the upper right square shows late apoptotic and necrotic cells. $N = 3$, error bars represent SEM. *$p < 0.05$, ***$p < 0.001$, ****$p < 0.0001$.

combination treatment significantly elevated Annexin V activity to 45% compared to 31% in the onalespib treated group ($p = 0.0003$) and 9% in the cisplatin group ($p < 0.0001$). Similarly, albeit somewhat lower for A2780CIS cells than SKOV3 cells, Annexin V activity was significantly elevated to 20% in the combination group compared to 11% in the onalespib and 2% in the cisplatin monotherapy groups ($p < 0.0001$). The apoptotic response in the onalespib group was significantly higher than cisplatin treated and control cells ($p < 0.0001$) (**Figures 6E,F**).

To further characterize the apoptotic activity flow cytometric analysis of caspase 3/7-sytox and the pan-caspase inhibitor z-VAD-FMK were performed (**Figures 6C,D,G,H**). Similarly

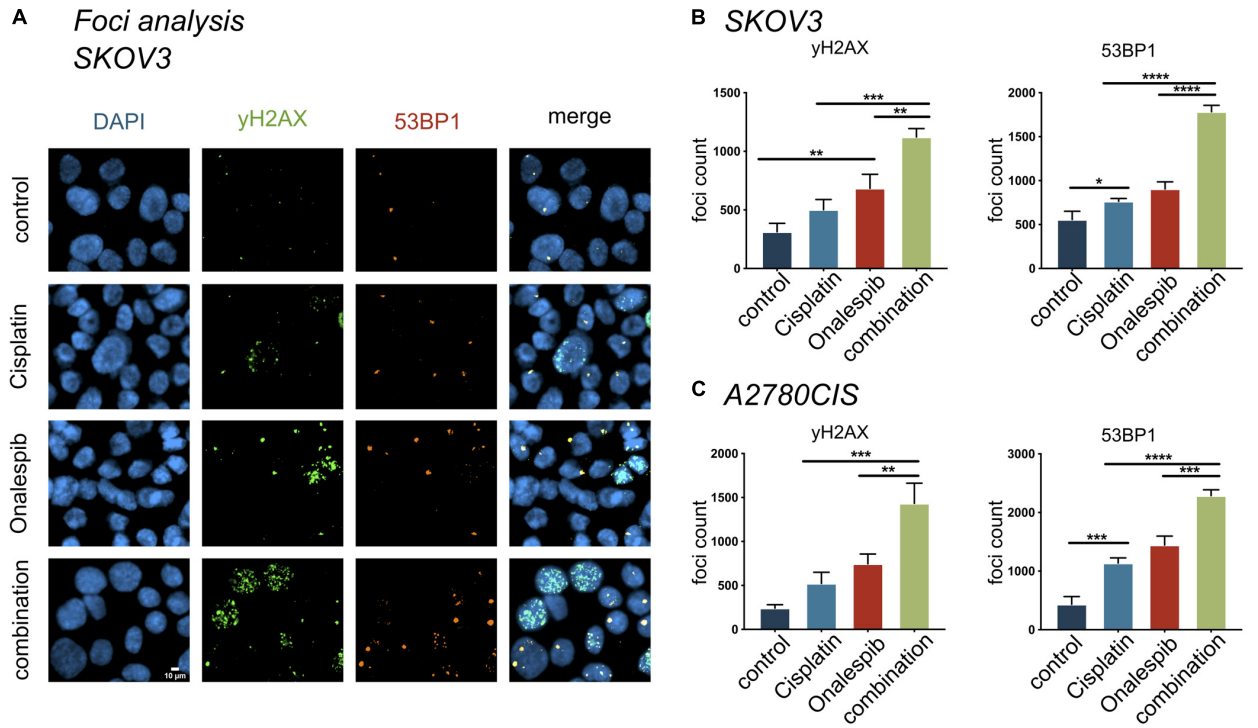

FIGURE 7 | The compartmentalization of γH2AX, 53BP1 foci in SKOV3 cells *in vitro* exposed to mono- and combined treatment of cisplatin and onalespib. **(A)** Representative high-resolution images of γH2AX and 53BP1 foci units formation in SKOV3 cells *in vitro* exposed to 500 nM cisplatin, 100 nM onalespib, or a combination of cisplatin and onalespib for 96 h. The images panel demonstrate green stain for γH2AX, orange for 53BP1, and blue for stained nuclei with DAPI **(B,C)**. $N = 3$, foci counts are presented as the mean @ SD, $^{*}p < 0.05$, $^{**}p < 0.01$, $^{***}p < 0.001$, $^{****}p < 0.0001$.

to the Annexin V results, apoptotic activation was greatest in SKOV3 cells compared to A2780CIS cells. In SKOV3 cells, caspase 3/7 increased significantly to 72% in the combination group compared to 51% and 13% in the onalespib and cisplatin monotherapy groups, respectively ($p < 0.0001$). Caspase activity in onalespib monotherapy samples was significantly higher than in cisplatin monotherapy samples ($p < 0.0001$). Treatment with the z-VAD-FMK pan-caspase inhibitor significantly reduced apoptotic activity to 25% in the combination group ($p < 0.0001$) (**Figure 6C** and **Supplementary Figure 2E**). The percentage of caspase 3/7 positive A2780CIS cells was significantly increased to 27% in the combination group compared to 12% in onalespib and 10% in cisplatin monotherapy groups ($p < 0.0001$). Here, the pan-caspase inhibitor significantly inhibited apoptotic activity to 10% in the combination group ($p < 0.0001$) (**Figure 6H** and **Supplementary Figure 2J**).

Onalespib and Cisplatin Combination Treatment Increased Number of DNA Double Strand Breaks

The effect of onalespib and cisplatin combination treatment on the induction of DNA damage was studied by confocal microscopy through γH2AX foci and 53BP1 foci analyses of 300 SKOV3 and A2780CIS cells per replica (**Figure 7**). As demonstrated in **Figure 7A**, exposure of SKOV3 and A2780CIS cells to 500 nM cisplatin induced DSBs as measured by the number of γH2AX and 53BP1 foci. Monotherapy with 100 nM onalespib significantly increased the DNA damage, as measured by number of foci. In SKOV3 cells, the total number of 53BP1 foci was higher than that of γH2AX in all samples (**Figures 7A,B**). The number of 53PB1 foci was significantly elevated in the combination compared to onalespib and cisplatin monotherapy ($p < 0.0001$). The number of γH2AX foci significantly increased in the combination compared to onalespib ($p = 0.0015$) and cisplatin ($p = 0.0001$) monotherapy. The same DSBs induction trend was seen in A2780CIS cells. The combination produced significantly greater numbers of 53PB1 foci than onalespib ($p = 0.0001$) and cisplatin ($p < 0.0001$) monotherapy. The γH2AX foci number significantly increased in the combination therapy compared to onalespib ($p = 0.0017$) and cisplatin ($p = 0.0002$) monotherapy (**Figure 7C**).

Foci analysis was also performed on H314 cells, however, due to its different growth phenotype (in clusters, spheroid like) it was not possible to get quantifiable data on foci numbers (data not shown).

DISCUSSION

Forty years after the introduction of cisplatin, it remains a cornerstone cancer drug, widely used as a first-in-line treatment in many solid cancers. The initial response to cisplatin is high, as for all platinum-based drugs. The majority of patients will relapse

with cisplatin-resistant disease, however, as rapid resistance development is one of the main limitations of cisplatin and related platinum-based analogs. Additional clinically important limitations include severe adverse side effects, which restrict the possibility of achieving efficient doses in patients (3). These important limitations have encouraged extensive exploration of cisplatin combination therapies, of which several are in wide clinical use today. Combination therapies in general are becoming increasingly important within the field of cancer therapy, due to multiple factors such as the potential of re-sensitizing resistant cancers, potentiating the effects of therapy, and/or reducing side effects by facilitating lowered therapeutic doses without compromising the outcome (9). Multiple studies have demonstrated that combination therapies including HSP90 inhibitors can overcome or reverse drug resistance in several cancers due to the wide involvement of HSP90 client proteins in many fundamental aspects of cancer, especially DNA damage response and repair (19, 29, 30). Accordingly, preclinical studies suggest that the HSP90 inhibitor onalespib display radiosensitizing effects, and an ongoing clinical trial is exploring the combination of cisplatin, radiotherapy and onalespib (13, 21, 23). However, little is known about the mechanisms behind the reversal of cisplatin resistance in combination with onalespib and other HSP90 inhibitors.

The four cell lines used in this study were chosen as representatives of types of cancers that are traditionally considered challenging to treat with cisplatin, specifically ovarian and head and neck cancer. Three of the tested cell lines (SKOV3, H314, and A2780CIS) were selected due to their relatively high innate cisplatin resistance (**Figure 1**), and one was selected as cisplatin sensitive (A2780). As A2780CIS is derived from A2780 a direct comparison of differences in cisplatin sensitivity is possible.

Interestingly, while all cell lines were sensitive to onalespib monotherapy, H314 proved more sensitive than SKOV3, while the A2780 cell lines demonstrated even greater sensitivity. This relationship was consistent in both XTT cytotoxicity and clonogenic survival assays (**Figures 1**, **3**). In this work, however, the combination therapy has been generally found to be more potent than either monotherapy, an effect likely caused by onalespib-mediated inhibition of DNA repair mechanisms activated in response to cisplatin-mediated DNA damage (**Figures 2**, **3**). Combination treatment with 10 μM cisplatin resulted in significantly reduced cell viability for all cell lines at all tested onalespib concentrations as measured by XTT assays (**Figure 2**). Moreover, combination treatment virtually eliminated H314 and A2780 cell viability and significantly reduced SKOV3 and A2780CIS cell colony formation ability (**Figure 3**). These findings are in line with previous studies on cisplatin in combination with other HSP90 inhibitors, and are encouraging for the prospect of utilizing cisplatin against types of cancer typically not considered sensitive (30).

Recent studies indicate that the HSP90 inhibitors 17-AAG and AUY922 also can affect cancer cell motility and migration (31–34). To investigate whether these effects translate to onalespib, the effects of cisplatin and/or onalespib on migration and wound healing were investigated in two separate migration assays (**Figure 4**). Onalespib indeed affected the rate of wound healing while cisplatin did not, thus indicating a reduction in migration and proliferation in both tested cell lines. This reduction was amplified in combination with cisplatin in a dose-dependent manner. Interestingly, H314 cells were unable to migrate in the *trans*-well migration assay, whereas SKOV3 cell migration was impaired in a dose-dependent manner following both cisplatin and onalespib treatment (**Table 1**). This strongly indicates that the effects on the H314 cells in the wound healing assay were primarily due to reduced proliferation and not impaired migration, which was not the case for the SKOV3 cells.

Interestingly, cisplatin itself inhibits HSP90 by binding to the ATP-binding domain on the C-terminal of HSP90 (2). This raises the question of why HSP90 inhibition prevents or reverses cisplatin resistance when cisplatin itself acts as an HSP90 inhibitor. In light of this, the current findings may seem implausible. Our data clearly demonstrates that the tested HSP90 client proteins are not significantly affected by cisplatin treatment alone, however (**Figure 5**), whereas expression of HSP90 client proteins EGFR and its downstream target protein AKT were significantly downregulated by onalespib monotherapy at both 50 and 100 nM doses (**Figure 5**). The high potency of onalespib in terms of downregulation of HSP90 client proteins made it difficult to assess potential combination effects through Western blotting, which has a low dynamic range. There was a trend toward slightly greater downregulation in combination treatments observed for the measured EGFR-expression levels, however, most notably evident in the highest dose combinations. These results indicate that cisplatin-induced DNA damage does not significantly affect HSP90 client protein expression levels. Interestingly, only combination therapy managed to significantly increase the number of apoptotic SKOV3 cells (**Figure 6**). This finding is consistent with the HSP90 inhibitor geldanamycin demonstrating depletion of essential anti-apoptotic proteins and resulting in greater levels of apoptosis in combination with cisplatin, as demonstrated elsewhere (35). In general, apoptotic cell death is induced by stress, e.g., the withdrawal of stimulating growth factors, hypoxia and DNA damage. The same stimuli induce the expression and accumulation of members of the HSP family, however, including HSP70 and HSP90, which shows that a death stimulus can cause a protective response in the cell (36). HSP90 associates with essential stress-signal- and apoptotic molecules, thereby blocking programmed cell death and promoting survival, proliferation, migration and differentiation, which can be reversed by HSP90 inhibition.

Cisplatin induces DNA intra-strand crosslinks that activate a cascade of DNA damage response (DDR) pathways such as cell cycle arrest, DNA repair and apoptosis (37). The main repair mechanism for cisplatin-induced cross-links is nucleotide excision repair (NER) (38). ERCC1 is a central component of NER and ERCC1 overexpression correlates with cisplatin resistance, indicating its role in the repair of cisplatin-induced DNA damage (39). Excision of cisplatin-induced DNA-adducts through NER can produce DSBs, which are harder to repair for the cell compared to single strand breaks. DNA repair proteins such as ATM, ATR and DNA-PKcs are known client proteins of HSP90, which was also confirmed by Western blotting in this study (**Figure 5**). Therefore, onalespib-induced HSP90 inhibition

may further impair DDR pathways, resulting in increased conversion of single strand breaks to DSBs and a switch from NER to DSB repair mechanisms. The two primary DSB repair mechanisms are homologous recombination (HR) and non-homologous end joining (NHEJ) and the choice of mechanism is strongly connected to cell cycle phases (40). One of the earliest events in the DSB repair is the phosphorylation of H2AX and subsequent phosphorylation of 53BP1 (41, 42). Our studies demonstrate a significant increase in γH2AX and 53BP1 foci and therefore an increase in DSBs of SKOV3 and A2780CIS cells in the combination therapy compared to cisplatin and onalespib monotherapy (**Figure 7**). This observation proves that the SKOV3 and A2780CIS cells were unable to successfully repair DSBs induced by cisplatin when combined with onalespib, whereas repair in the monotherapy groups was more successful.

CONCLUSION

In conclusion, our findings support HSP90 inhibition as a potentially valuable mechanism for enhancing cisplatin efficacy; by increasing the cytotoxic effect, restoring sensitivity in innately resistant cells and possibly preventing development of cisplatin resistance. Further development of this concept has the potential to increase cure rates, prolong survival and increase quality of life for a broad population of patients, and follow-up studies exploring optimal dosing intervals and *in vivo* efficacy are therefore warranted.

DATA AVAILABILITY STATEMENT

The datasets generated for this study are available on request to the corresponding author.

AUTHOR CONTRIBUTIONS

AM contributed to experimental studies with focus on the XTT assays and western blotting, analyzed and interpreted the data, and drafted and revised the manuscript. TM contributed to experimental studies with focus on the western blotting, viability, and migration assays, analyzed and interpreted the data, and drafted and revised the manuscript. MH contributed to experimental studies with focus on the microscopy and flow cytometry assays, analyzed and interpreted the data, and drafted and revised the manuscript. MP contributed to experimental studies with focus on the viability assays, contributed to the data interpretation, and revised the manuscript. DS initiated and designed the study, contributed to data analysis and interpretation, and drafted and revised the manuscript. All authors have read and approved the final manuscript.

FUNDING

This study was supported by grants from Lions Cancer Society at Uppsala University Hospital, Åke Wiberg Foundation and Erik, Karin, and Gösta Selanders Foundation.

ACKNOWLEDGMENTS

The authors would like to thank Hanna Berglund and Preeti Jha for the assistance with the XTT and the western blotting as well as Bo Stenerlöw for his valuable advice regarding DNA damage pathways. Microscopic imaging was performed with equipment maintained by the BioVis Platform, Uppsala.

SUPPLEMENTARY MATERIAL

The Supplementary Material for this article can be found online at: https://www.frontiersin.org/articles/10.3389/fonc.2020.532285/full#supplementary-material

FIGURE S1 | XTT cell viability normalized to untreated controls of **(A)** SKOV3 and **(B)** H314 cells treated with 0–3000 nM onalespib or the combination of onalespib with 500 nM cisplatin 24 h post treatment. $N = 3$, error bars represent SEM. Dotted lines represent the viability of cisplatin monotherapy at either 500 nM or 10 μM. **(C)** Wound healing/scratch assay. Effect of Cisplatin monotreatment on SKOV3 and H314 cells. **(D)** Representative *trans*-well migration assay images of SKOV3 cells after treatment with onalespib, cisplatin and their combination. The size bar corresponds to 4 μm.

FIGURE S2 | Flow cytometric analysis. **(A,B)** Annexin V median fluorescent intensity (MFI) expression (FITC.A+) in SKOV3 cells and **(F,G)** A2780CIS cells after 96 h exposure to 500 nM cisplatin, 100 nM onalespib, or a combination. **(C,D)** Caspase 3/7 median fluorescent intensity (MFI) expression (FITC.A+) in SKOV3 cells and **(F,G)** A2780CIS cells after 96 h exposure to 500 nM cisplatin, 100 nM onalespib, or a combination. Z-VAD-FMK analysis in **(E)** SKOV3 cells and **(J)** A2780CIS cells. $N = 3$, error bars represent SEM. $^{*}p < 0.05$, $^{**}p < 0.01$, $^{***}p < 0.001$, $^{****}p < 0.0001$.

TABLE S1 | Average plating efficiency (PE) and standard deviation (SD) of SKOV3, H314, A2780 parental, and A2780 cisplatin resistant cells, $N > 3$.

REFERENCES

1. Dasari S, Tchounwou PB. Cisplatin in cancer therapy: molecular mechanisms of action. *Eur J Pharmacol*. (2014) 740:364–78. doi: 10.1016/j.ejphar.2014.07.025
2. Fuertes MA, Castilla J, Alonso C, Pérez JM. Cisplatin biochemical mechanism of action: from cytotoxicity to induction of cell death through interconnections between apoptotic and necrotic pathways. *Curr Med Chem*. (2003) 10:257–66. doi: 10.2174/0929867033368484
3. Oun R, Moussa YE, Wheate NJ. The side effects of platinum-based chemotherapy drugs: a review for chemists. *Dalton Trans*. (2018) 47:6645–53. doi: 10.1039/c8dt00838h
4. Holmes D. Ovarian cancer: beyond resistance. *Nature*. (2015) 527:S217–217.
5. Galluzzi L, Senovilla L, Vitale I, Michels J, Martins I, Kepp O, et al. Molecular mechanisms of cisplatin resistance. *Oncogene*. (2012) 31:1869–83.
6. Holzer AK, Manorek GH, Howell SB. Contribution of the major copper influx transporter CTR1 to the cellular accumulation of cisplatin, carboplatin, and oxaliplatin. *Mol Pharmacol*. (2006) 70:1390–4. doi: 10.1124/mol.106.022624

7. Holzer AK, Howell SB. The internalization and degradation of human copper transporter 1 following cisplatin exposure. *Cancer Res*. (2006) 66:10944–52. doi: 10.1158/0008-5472.can-06-1710
8. Kuo MT, Chen HHW, Song I-S, Savaraj N, Ishikawa T. The roles of copper transporters in cisplatin resistance. *Cancer Metastasis Rev*. (2007) 26:71–83. doi: 10.1007/s10555-007-9045-3
9. Amable L. Cisplatin resistance and opportunities for precision medicine. *Pharmacol Res*. (2016) 106:27–36. doi: 10.1016/j.phrs.2016.01.001
10. Li Q, Yu JJ, Mu C, Yunmbam MK, Slavsky D, Cross CL, et al. Association between the level of ERCC-1 expression and the repair of cisplatin-induced DNA damage in human ovarian cancer cells. *Anticancer Res*. (2000) 20: 645–52.
11. Ma L, Sato F, Sato R, Matsubara T, Hirai K, Yamasaki M, et al. Dual targeting of heat shock proteins 90 and 70 promotes cell death and enhances the anticancer effect of chemotherapeutic agents in bladder cancer. *Oncol Rep*. (2014) 31:2482–92. doi: 10.3892/or.2014.3132
12. Taipale M, Jarosz DF, Lindquist S. HSP90 at the hub of protein homeostasis: emerging mechanistic insights. *Nat Rev Mol Cell Biol*. (2010) 11:515–28. doi: 10.1038/nrm2918
13. Spiegelberg D, Dascalu A, Mortensen AC, Abramenkovs A, Kuku G, Nestor M, et al. The novel HSP90 inhibitor AT13387 potentiates radiation effects in squamous cell carcinoma and adenocarcinoma cells. *Oncotarget*. (2015) 6:35652–66. doi: 10.18632/oncotarget.5363
14. Picard D. *HSP90 Facts & Literature*. (2020). Available online at: https://www.picard.ch/downloads/Hsp90facts.pdf (accessed 2020 July 29).
15. Koga F, Kihara K, Neckers L. Inhibition of cancer invasion and metastasis by targeting the molecular chaperone heat-shock protein 90. *Anticancer Res*. (2009) 29:797–807.
16. Ory B, Baud'huin M, Verrecchia F, Royer BB-L, Quillard T, Amiaud J, et al. Blocking HSP90 addiction inhibits tumor cell proliferation, metastasis development, and synergistically acts with zoledronic acid to delay osteosarcoma progression. *Clin Cancer Res*. (2016) 22:2520–33. doi: 10.1158/1078-0432.ccr-15-1925
17. Yuno A, Lee M-J, Lee S, Tomita Y, Rekhtman D, Moore B, et al. Clinical evaluation and biomarker profiling of Hsp90 inhibitors. In: Calderwood SK, Prince TL editors. *Chaperones: Methods and Protocols*. New York, NY: Springer (2018). p. 423–41. doi: 10.1007/978-1-4939-7477-1_29
18. Kryeziu K, Bruun J, Guren TK, Sveen A, Lothe RA. Combination therapies with HSP90 inhibitors against colorectal cancer. *Biochim Biophys Acta*. (2019) 1871:240–7. doi: 10.1016/j.bbcan.2019.01.002
19. Jhaveri K, Modi S. HSP90 inhibitors for cancer therapy and overcoming drug resistance. *Adv Pharmacol*. (2012) 65:471–517. doi: 10.1016/b978-0-12-397927-8.00015-4
20. Samuni Y, Ishii H, Hyodo F, Samuni U, Krishna MC, Goldstein S, et al. Reactive oxygen species mediate hepatotoxicity induced by the Hsp90 inhibitor geldanamycin and its analogs. *Free Radic Biol Med*. (2010) 48:1559–63. doi: 10.1016/j.freeradbiomed.2010.03.001
21. Lundsten S, Spiegelberg D, Stenerlöw B, Nestor M. The HSP90 inhibitor onalespib potentiates 177Lu-DOTATATE therapy in neuroendocrine tumor cells. *Int J Oncol*. (2019) 55:1287–95.
22. Spiegelberg D, Abramenkovs A, Mortensen ACL, Lundsten S, Nestor M, Stenerlöw B. The HSP90 inhibitor Onalespib exerts synergistic anti-cancer effects when combined with radiotherapy: an in vitro and in vivo approach. *Sci Rep*. (2020) 10:5923.
23. ClinicalTrials.gov. *Onalespib in Treating Patients With Locoregionally Advanced Squamous Cell Carcinoma of the Head and Neck Receiving Radiation Therapy and Cisplatin – Full Text View - ClinicalTrials.gov*. (2020). Available online at: https://clinicaltrials.gov/ct2/show/NCT02381535 (accessed 2020 Jan 30).
24. Paramee S, Sookkhee S, Sakonwasun C, Na Takuathung M, Mungkornasawakul P, Nimlamool W, et al. Anti-cancer effects of Kaempferia parviflora on ovarian cancer SKOV3 cells. *BMC Complement Altern Med*. (2018) 18:178. doi: 10.1186/s12906-018-2241-6
25. Khoo X-H, Paterson IC, Goh B-H, Lee W-L. Cisplatin-resistance in oral squamous cell carcinoma: regulation by tumor cell-derived extracellular vesicles. *Cancers (Basel)*. (2019) 14:1166. doi: 10.3390/cancers11081166
26. Tudrej P, Olbryt M, Zembala-Nożyńska E, Kujawa KA, Cortez AJ, Fiszer-Kierzkowska A, et al. Establishment and characterization of the novel high-grade serous ovarian cancer cell line OVPA8. *Int J Mol Sci*. (2018) 19:2080. doi: 10.3390/ijms19072080
27. Franken NA, Rodermond HM, Stap J, Haveman J, van Bree C. Clonogenic assay of cells in vitro. *Nat Protoc*. (2006) 1:2315–9. doi: 10.1038/nprot.2006.339
28. Liang C-C, Park AY, Guan J-L. In vitro scratch assay: a convenient and inexpensive method for analysis of cell migration in vitro. *Nat Protoc*. (2007) 2:329–33. doi: 10.1038/nprot.2007.30
29. Smyth T, Paraiso KHT, Hearn K, Rodriguez-Lopez AM, Munck JM, Haarberg HE, et al. Inhibition of HSP90 by AT13387 delays the emergence of resistance to BRAF inhibitors and overcomes resistance to dual BRAF and MEK inhibition in melanoma models. *Mol Cancer Ther*. (2014) 13:2793–804. doi: 10.1158/1535-7163.mct-14-0452
30. Zhang Z, Xie Z, Sun G, Yang P, Li J, Yang H, et al. Reversing drug resistance of cisplatin by hsp90 inhibitors in human ovarian cancer cells. *Int J Clin Exp Med*. (2015) 8:6687–701.
31. Taiyab A, Rao CHM. HSP90 modulates actin dynamics: inhibition of HSP90 leads to decreased cell motility and impairs invasion. *Biochim Biophys Acta*. (2011) 1813:213–21. doi: 10.1016/j.bbamcr.2010.09.012
32. Memmel S, Sisario D, Zöller C, Fiedler V, Katzer A, Heiden R, et al. Migration pattern, actin cytoskeleton organization and response to PI3K-, mTOR-, and Hsp90-inhibition of glioblastoma cells with different invasive capacities. *Oncotarget*. (2017) 8:45298–310. doi: 10.18632/oncotarget.16847
33. McCready J, Wong DS, Burlison JA, Ying W, Jay DG. An impermeant ganetespib analog inhibits extracellular Hsp90-mediated cancer cell migration that involves lysyl oxidase 2-like protein. *Cancers (Basel)*. (2014) 6:1031–46. doi: 10.3390/cancers6021031
34. Xiong X, Wang Y, Liu C, Lu Q, Liu T, Chen G, et al. Heat shock protein 90β stabilizes focal adhesion kinase and enhances cell migration and invasion in breast cancer cells. *Exp Cell Res*. (2014) 326:78–89. doi: 10.1016/j.yexcr.2014.05.018
35. Bagatell R, Beliakoff J, David CL, Marron MT, Whitesell L. Hsp90 inhibitors deplete key anti-apoptotic proteins in pediatric solid tumor cells and demonstrate synergistic anticancer activity with cisplatin. *Int J Cancer*. (2005) 113:179–88. doi: 10.1002/ijc.20611
36. Lanneau D, Brunet M, Frisan E, Solary E, Fontenay M, Garrido C. Heat shock proteins: essential proteins for apoptosis regulation. *J Cell Mol Med*. (2008) 12:743–61. doi: 10.1111/j.1582-4934.2008.00273.x
37. Miow QH, Tan TZ, Ye J, Lau JA, Yokomizo T, Thiery J-P, et al. Epithelial-mesenchymal status renders differential responses to cisplatin in ovarian cancer. *Oncogene*. (2015) 34:1899–907.
38. Basu A, Krishnamurthy S. Cellular responses to cisplatin-induced DNA damage. *J Nucleic Acids*. (2010) 2010:201367.
39. Sun Y, Li T, Ma K, Tian Z, Zhu Y, Chen F, et al. The impacts of ERCC1 gene exon VIII alternative splicing on cisplatin-resistance in ovarian cancer cells. *Cancer Invest*. (2009) 27:891–7. doi: 10.3109/07357900902744536
40. Shibata A, Jeggo P. A historical reflection on our understanding of radiation-induced DNA double strand break repair in somatic mammalian cells; interfacing the past with the present. *Int J Radiat Biol*. (2019) 95:945–56. doi: 10.1080/09553002.2018.1564083
41. doi: 10.1016/j.molcel.2017.05.015Blackford AN, Jackson SPATM. ATR, and DNA-PK: the trinity at the heart of the DNA damage response. *Mol Cell*. (2017) 66:801–17.
42. Buisson R, Boisvert JL, Benes CH, Zou L. Distinct but concerted roles of ATR, DNA-PK, and Chk1 in countering replication stress during S phase. *Mol Cell*. (2015) 59:1011–24. doi: 10.1016/j.molcel.2015.07.029

Conflict of Interest: The authors declare that the research was conducted in the absence of any commercial or financial relationships that could be construed as a potential conflict of interest.

frontiers in Oncology

ORIGINAL RESEARCH
published: 22 October 2020
doi: 10.3389/fonc.2020.532292

Activity of Birinapant, a SMAC Mimetic Compound, Alone or in Combination in NSCLCs With Different Mutations

Marika Colombo†, Mirko Marabese†, Giulia Vargiu, Massimo Broggini and Elisa Caiola*

Laboratory of Molecular Pharmacology, Istituto di Ricerche Farmacologiche Mario Negri IRCCS, Milan, Italy

Liver kinase B1 (*LKB1/STK11*) is the second tumor suppressor gene most frequently mutated in non-small-cell lung cancer (NSCLC) and its activity is impaired in about half KRAS-mutated NSCLCs. Nowadays, no effective therapies are available for patients having these mutations. To highlight new vulnerabilities of this subgroup of tumors exploitable to design specific therapies we screened an US FDA-approved drug library using an isogenic system of wild-type (WT) or deleted LKB1. Among eight hit compounds, Birinapant, an inhibitor of the Inhibitor of Apoptosis Proteins (IAPs), was the most active compound in LKB1-deleted clone only compared to its LKB1 WT counterpart. We validated the Birinapant cells response and its mechanism of action to be dependent on LKB1 deletion. Indeed, we demonstrated the ability of this compound to induce apoptosis, through activation of caspases in the LKB1-deleted clone only. Expanding our results, we found that the presence of *KRAS* mutations could mediate Birinapant resistance in a panel of NSCLC cell lines. The combination of Birinapant with Ralimetinib, inhibitor of p38α, restores the sensitivity of LKB1- and KRAS-mutated cell lines to the IAP inhibitor Birinapant. Our study shows how the use of Birinapant could be a viable therapeutic option for patients with LKB1-mutated NSCLCs. In addition, combination of Birinapant and a KRAS pathway inhibitor, as Ralimetinib, could be useful for patients with LKB1 and KRAS-mutated NSCLC.

Keywords: non-small-cell lung cancer, liver kinase B1, KRAS, drug library *in vitro* screening, SMAC mimetic compounds, 3D culture (three-dimensional spheroids), combination therapeutics, Ralimetinib

OPEN ACCESS

Edited by:
Nehad M. Ayoub, Jordan University of Science and Technology, Jordan

Reviewed by:
Milankumar Prajapati, Brown University, United States
Donatella Del Bufalo, Regina Elena National Cancer Institute (IRCCS), Italy

****Correspondence:***
Massimo Broggini
massimo.broggini@marionegri.it

†These authors share first authorship

Specialty section:
This article was submitted to Pharmacology of Anti-Cancer Drugs, a section of the journal Frontiers in Oncology

Received: *03 February 2020*
Accepted: *30 September 2020*
Published: *22 October 2020*

Citation:
Colombo M, Marabese M, Vargiu G, Broggini M and Caiola E (2020) Activity of Birinapant, a SMAC Mimetic Compound, Alone or in Combination in NSCLCs With Different Mutations. Front. Oncol. 10:532292. doi: 10.3389/fonc.2020.532292

INTRODUCTION

Non-small-cell lung cancer (NSCLC) is the leading cause of cancer-related death worldwide (1). In the recent decades, with the discovery of the molecular heterogeneity and oncogene addiction of some NSCLC subtypes, the use of targeted therapies and immunotherapy has improved the outcomes for patients affected by these malignancies (2). Nowadays, in spite of this progress, some mutations frequently present in NSCLCs remain untargetable and the available therapies seem to be not very effective (2, 3). Among these, NSCLC mutated in *Liver kinase B1* (*LKB1/STK11)* gene represent one-third of the cases and *LKB1/STK11* is considered the third most commonly mutated

gene in NSCLC adenocarcinomas, after *TP53* and *KRAS* (4). *LKB1* mutations were found in about 50% of KRAS-mutated NSCLC and it was demonstrated that the co-occurrence of *LKB1/KRAS* mutations significantly increases the tumor burden, mediated by increased resistance to classical anticancer and immunotherapeutic drugs thus corresponding with poor prognosis for patients carrying these alterations (5, 6). Moreover, mutations in *LKB1* is mutually exclusive with mutations in those genes for which a targeted therapy already exists. LKB1 is a master kinase that, acting on AMPK-mTOR pathway, regulates different cellular processes as cell metabolism, cell polarity, growth and autophagy (7). Mutations in this gene almost invariably lead to protein loss of function that reflects in a series of cellular abnormalities (8).

Birinapant is a SMAC mimetic compound and an IAP inhibitor (9). Similar to the endogenous SMAC protein, Birinapant is able to bind IAPs promoting their degradation. In particular, it binds with high affinity to the cellular IAP 1 (c-IAP1) and with a lesser extent to the cellular IAP 2 (c-IAP2) and XIAP (10). IAPs belong to the class of proteins that inhibit the apoptotic process. Indeed, in normal cell conditions, they block the extrinsic apoptotic pathway and promote cell survival and cell growth (11, 12).

Ralimetinib is a selective molecule able to inhibit α and β isoforms of p38 mitogen-activated protein kinase (MAPK), in an ATP-competitive way (13). P38 MAPK belongs to MAPK family, which also includes JNK and ERK (14), and it is downstream the MAPKKK proteins, as KRAS protein. P38 MAPK protein phosphorylates multiple substrates in response to external stimuli. Inhibition of this protein decreases prosurvival, proangiogenic, and proinflammatory soluble factors (15).

In the present study, after an FDA-approved drug library screening, we analyzed the activity of Birinapant alone, or in combination with Ralimetinib, in LKB1-mutated NSCLC cell lines.

MATERIALS AND METHODS

2D Cell Culture and Treatments

The NSCLC cell lines used (H1299, H520, H1975, H2009, H358, LU99, H727, H460, H2030, A549, H23) were obtained from American Type Culture Collection (ATCC) and RIKEN BRC cell bank. They were grown in RPMI1640 (Gibco) with the addition of 10% fetal bovine serum (FBS) (Euroclone) and 2 mM L-Glutamine (Gibco). Two LKB1-deleted clones H1299-LKB1 KO 1 and 2 were derived from H1299 through the Crispr-Cas9 technique, as previously described (16). They were maintained in selection by adding 3 μg/ml of Puromycin to the medium. The NCI-H1299 cells were also genetically manipulated to generate the KRAS G12C mutated (K) and LKB1WT and KRAS G12C-mutated and LKB1-deleted (KL) clones (17–20). For the K and KL clones, 500 μg/ml of Geneticin (G418) were added to the medium. Cell lines were routinely tested for mycoplasma contamination by polymerase chain reaction (PCR), and authenticated with the PowerPlex 16 HS System (Promega) every 6 months by comparing the short tandem repeat (STR) profiles to those deposited in the ATCC and/or in the German Collection of Microorganisms and Cell Cultures (DSMZ) databases.

The day of the treatment, dimethyl sulfoxide (DMSO) stock solutions of all the drugs used (10 mM) were diluted in complete medium at the desired concentrations with a final DMSO concentration of 0.05% for single treatment or 0.15% in combination treatment. In all the cytotoxicity experiments, either single or combination treatments, cells were continuously treated for 72 h.

Cell viability assays were performed independently. For the MTS cell viability assay, MTS was added to each well. Then, plates were incubated at 37°C for about 3 h and the absorbance at 490 nm was read using plate-reading instrument (GloMax discover, Promega). For the CellTiter-Glo viability assay, a volume of CellTiter-Glo reagent equal to the volume present in each well was added and luminescence was read through GloMax instrument. Finally, the sulforhodamine B assay was performed following the manufacturer's instructions and the absorbance was measured at 560 nm.

For each experiment, starting from the absorbance/luminescence values, the mean of at least six biological replicates and the percentage of cell viability (where the 100% of viability were control-treated samples values) were calculated for each dose. The average of at least three independent experiments was then plotted in dose-response curves. The concentration that inhibits 50% of cell viability (IC_{50}) was calculated with PRISM software.

3D Spheroids Culture and Treatments

Procedures involving animals were conducted in conformity with the following laws, regulations, and policies governing the care and use of laboratory animals: Italian Governing Law (D. lg 26/2014; authorization no.19/2008-A issued 6 March 2008 by the Ministry of Health); Mario Negri Institutional Regulations and Policies providing internal authorization for persons conducting animal experiments (Quality Management System Certificate: UNI EN ISO 9001:2008, reg. no. 6121); An institutional review board and the Italian Ministry of Health approved the *in vivo* experiments performed (project authorization #9F5F5.69.EXT.37).

Three dimensional spheroids models were derived from excised H1299 and H1299-LKB1 KO xenografts, obtained by subcutaneously injecting the cell lines in nude mice. When the tumor weight was about 1 mg, the mice were euthanized with CO_2, then, tumors were excised, rinsed with saline solution, mechanically minced and incubated in a flask at 37°C with collagenase. After 30 min, all the flask content was filtered, the tumor mass was recovered and another cycle with collagenase was performed for 60 min. Successively, after filtration, the tumor mass was transferred into a 50 ml falcon where it was resuspended in 10 ml of wash buffer (**Supplementary Material**) and incubated at room temperature for 20 min. The supernatant was removed and the passage was repeated until the solution became clear. After the last wash, the pellet was spun down in 10 ml of wash buffer. The pellet was resuspended in wash buffer and counted with Neubauer chamber. Cells, at a density of 20000 cells/ml, were then resuspended in 50 μl/well of Basement

Membrane Extract (BME, RGF BME, Type 2 PathClear, CULTREX) and seeded in 24-well plate. Once BME was solidified, 500 µl of culture medium (**Supplementary Material**) was added. Spheroids formed in about 1 week and were subsequently subcultured once a week. The procedure of subculture consisted in mechanical detachment of BME with spheroids from the substrate and trypsin addition (TrypLE Express, GIBCO) to favor the disruption of the 3D aggregates. The suspension was then incubated at 37°C for 5 min under mild shaking and trypsin activity was stopped by adding cold basal medium (**Supplementary Material**). Single cells were resuspended in BME and plated in 24-well plates. After BME solidification, warm culture medium was added. Spheroids were replaced with fresh stocks from liquid nitrogen after 4 to 5 months of culture.

To perform cytotoxicity experiments, 3D spheroids were mechanically detached from the 24-well plate and spheroid-derived single cells were then counted by Neubauer chamber and resuspended in an appropriated volume of BME to obtain 100,000 cells/ml as final concentration. They were then seeded in white 96-well plates, 10 µl of BME per well, and 50 µl of culture medium was added to each well. Four days after seeding, they were treated and 72 h after treatment start, CellTiter glo assay was performed, as previously described.

FDA-Approved Drug Library Screening

The FDA approved drug library (Z208828, Selleckchem) is a collection of 1,443 inhibitors belonging to different classes like oncology, anti-inflammation, immunology, neuropsychiatry, analgesia and so on. The library comprises some drugs already approved by FDA and some undergoing clinical trials (21). The compounds were dissolved in DMSO or water at a concentration of 10 mM. Original stock solutions of the library compounds were then diluted in water to a final concentration of 100 µM for each compound.

To perform the screening, cells were detached from flasks by trypsin-EDTA, resuspended at the desired concentration in RPMI1640 medium plus Penicillin and Streptomycin (Pen/Strep, Gibco) and seeded in a volume of 76 µl/well in 384-wells plates by automatic liquid handling (epMotion 5075, Eppendorf). The next day, the plates were treated with the FDA-approved drug library by an automatic liquid handling. Four µl of each drug were transferred to 384-well plates, thus reaching a final concentration of 5 µM for each drug and 0.05% for DMSO. Medium (80 µl/well) was used as a blank. Negative control was composed of 4 µl of H_2O or 4 µl of H_2O + DMSO 0.05% without drug treatment. Finally, a positive control group was composed of adding 4 µl of a drug known to be active only in LKB1-deleted clone. After 72 h of continuous treatment, the cytotoxicity of each compound was evaluated with MTS cell viability assay, as previously described. For each cell line, the absorbance of drug-treated cells (T) was normalized to control-treated cells (C), thus obtaining the T/C ratio.

Western Blot Molecular Analysis

Cells were seeded in petri dishes and, after 48 h, they were treated with drug at the desired concentration. Pellets were collected 24 and 48 h after treatment start. To prepare the pellets, cells were washed twice with ice-cold PBS and then mechanically detached from the plates with scrapers. The suspension was then centrifuged and the pellet resuspended in lysis buffer and incubated on ice for 1 h to permit cells lysis. Successively, insoluble cellular debris were pelleted at 10,000 rpm for 15 min at 4°C and the total protein amount in the supernatant was recovered. An aliquot was used to determine protein concentration at 595 nm at the spectrophotometer Ultrospec 2100 pro (Amersham Bioscences). Protein concentration was obtained using a BSA calibration curve.

Thirty µg of protein total extracts were separated according to their molecular weight with an electrophoretic run in denaturing conditions at about 100V. Then, proteins were transferred on activated PVDF membrane (Millipore) for 2 h at 60V. PVDF membrane was colored with Red Ponceau dye (Sigma) to verify the presence of proteins.

The proteins of interest were detected by exposing PVDF membranes overnight at 4°C to protein-specific primary antibodies diluted in 5% BSA-TBS-T or non-fat dry milk-TBS-T. The next day, the membrane was exposed to the secondary antibodies labelled with horseradish-peroxidase. After several washings, the horseradish-peroxidase substrate (ECL Western Blotting Detection, Amersham-Life Science) was added and the signal revealed through Odyssey Fc instrument (LI-COR). C-IAP1, LKB1, and PARP primary antibodies were purchased from Cell Signaling while XIAP, Caspase-3, Actin, Ran, and Lamin B from Santa Cruz Biothecnology. The anti-mouse and anti-rabbit secondary antibodies were purchased from Biorad whereas the anti-goat secondary antibody was purchased from Santa Cruz Biotechnology.

Realtime-Glo Annexin V Apoptosis Assay

Cells were seeded in white 96-well plates and treated with the drug at the desired concentrations after 24 h. The Realtime-Glo Annexin V detection reagent was added to all wells (the detection reagent was prepared following the datasheet instructions). Plates were maintained at 37°C and luminescence was read at different time points: 0, 24, 48, and 72 h after treatment start. At each concentration and time point, luminescence data were normalized to blank values and the average of six biological replicates was calculated. Control-treated cells were used as reference samples. Results were plotted as histograms, which represented the mean of at least three independent experiments.

Caspase-Glo 3/7 Assay

Cells were seeded in white 96-well plates and, after 24 h, treated with the drug at the desired concentrations. Seventy-two hours after treatment, the Caspase Glo reagent was then added to all wells (the reagent was prepared following the datasheet instructions). Plates were incubated at 37°C and, after 1 h, luminescence was read. Data were analyzed as for Annexin V assay and statistical analysis was performed with PRISM software.

Statistical Analysis

The statistical analyses for each experiment were performed through GraphPad Prism 7.01 software (GraphPad Software,

San Diego California USA, www.graphpad.com). The different tests used are reported in the legends of the figures. Differences with a p-value < 0.05 were considered statistically significant.

RESULTS

FDA-Approved Drug Library Screening and Independent Validation of the Hit Compounds

To find new vulnerabilities of LKB1-mutated NSCLCs, potentially exploitable to design new therapies, we performed a high throughput screening with an FDA-approved drug library. We used NCI-H1299 cell line (LKB1 WT) and a LKB1-deleted clone (H1299-LKB1 KO 1) previously obtained with Crispr-Cas9 technique (16) from H1299. To select compounds more active on LKB1-deleted clone than on the parental cell line, for each compound of the library, the ratio between H1299-LKB1 KO 1 T/C and H1299 T/C was calculated and a cut-off of 0.6 was established (**Supplementary Table 1**). This cut-off permitted to select compounds able to induce at least 40% more cell killing in LKB1-deleted clone than in the WT cell line. Fourteen compounds have achieved the cut-off value but three of them were excluded from hit compounds because of their high toxicity in both cell lines (**Figure 1A**). Among hits, two MEK inhibitors, three antimetabolites, a SYK inhibitor and an ALDH inhibitor, an HMG-CoA reductase inhibitor, an antiseptic, an antibacterial and an IAP inhibitor were present (**Table 1**).

The activity of selected drugs was confirmed by generating, for each compound, a complete dose-response curve on both H1299 and H1299-LKB1 KO 1 cell lines and by calculating the

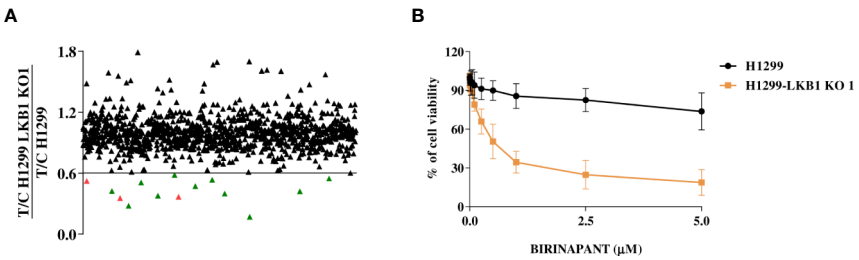

FIGURE 1 | **(A)**, Distribution of the FDA-approved drug library's compounds according to their different activity in H1299 and H1299 LKB1 KO 1 cells. Y-axis refers to H1299-LKB1 KO 1 T/C and H1299 T/C ratio. Each single triangle represents a compound. The eleven hit compounds are below the chosen cut-off value of 0.6 and they are colored in green. The three excluded compounds are in red. **(B)** Dose-response curves of H1299 and H1299-LKB1 KO 1 isogenic system treated with increasing concentrations of Birinapant. The response to the drug was evaluated with MTS assay. The average of three independent experiments is reported. Statistical analysis was carried out through two-way ANOVA and Bonferroni post-test for multiple comparisons and it is reported in **Supplementary Table 2**.

TABLE 1 | Table summarizing the H1299 and H1299-LKB1 KO 1 clone (here reported as LKB1 KO 1) IC_{50} of the eleven hit compounds from the drug library screening.

DRUG	CLASS	H1299 IC_{50} (μM)	LKB1 KO 1 IC_{50} (μM)	IC_{50} H1299 / IC_{50} LKB1 KO 1
Birinapant	IAP inhibitor	>5	0.527 (0.466–0.596)	≥9.48
6-Mercaptopurine	Antimetabolite	>5	0.212 (0.184–0.244)	≥2.36
Clofarabine	Antimetabolite	0.717 (0.559–0.954)	0.332 (0.289–0.385)	2.16
Floxuridine	Antimetabolite	0.106 (0.065–0.178)	0.054 (0.038–0.789)	1.95
Pitavastatin Calcium	HMG-CoA reductase inhibitor	3.114 (1.681–13.159)	1.687 (1.028–3.877)	1.84
Fostamatinib	SYK inhibitor	4.380 (3.904–5.156)	2.660 (2.506–2.819)	1.65
Chloroxine	Antibacterial	3.399 (3.138–3.682)	3.100 (2.878–3.326)	1.10
Disulfiram	ADLH-inhibitor	0.241 (0.136–0.412)	0.289 (0.159–0.514)	0.83
Chlorhexidine HCl	Antiseptic	0.747 (0.626–0.876)	1.942 (1.792–2.101)	0.39
Cobimetinib	MEK inhibitor	>4	>4	–
Pimasertib	MEK inhibitor	>4	>4	–

For each compound the drug class, the IC_{50} in the two cell lines and the ratio between the IC_{50} in the H1299 and H1299-LKB1 KO 1 clone are indicated.

IC_{50}, where it was possible. In addition, the ratio between H1299 IC_{50} and H1299-LKB1 KO 1 IC_{50} was calculated. Eight compounds, out of eleven, confirmed a higher cytotoxicity on the LKB1-deleted clone compared to the parental cell line (**Table 1**, **Supplementary Figure 1**). The antiseptic and antibacterial drugs showed an opposite behavior compared to the screening, while the ALDH inhibitor did not show significant differences between the two cell lines. Although the H1299-LKB1 KO 1 showed a higher sensitivity to MEK inhibitors than the LKB1 WT cell line, drug concentrations chosen for these inhibitors were too low to reach the IC_{50} in both cell lines. Birinapant, an IAP inhibitor, gave the best different responses: H1299-LKB1 KO 1 showed a significant sensitivity to this drug compared to the parental cell line and only for the LKB1-mutated clone we were able to calculate the IC_{50} (0.53 μM; CI: 0.47–0.60 μM) (**Figure 1B**, **Table 1**, and **Supplementary Table 2**).

Therefore, the study continued characterizing the different response observed with this drug.

Analysis of Birinapant Activity With Different Cell Viability Assays and in 3D Models

Birinapant activity was further validated on our isogenic system by two additional cell viability assays. The use of CellTiter-Glo and the sulforodamine B assay confirmed the high sensitivity of the LKB1-deleted clone to Birinapant (IC_{50} 0.52 μM; CI: 0.46–0.58 μM and 0.53 μM; CI: 0.41–0.67 μM, respectively), while the parental cell line remained resistant, with an IC_{50} not calculable for the first assay

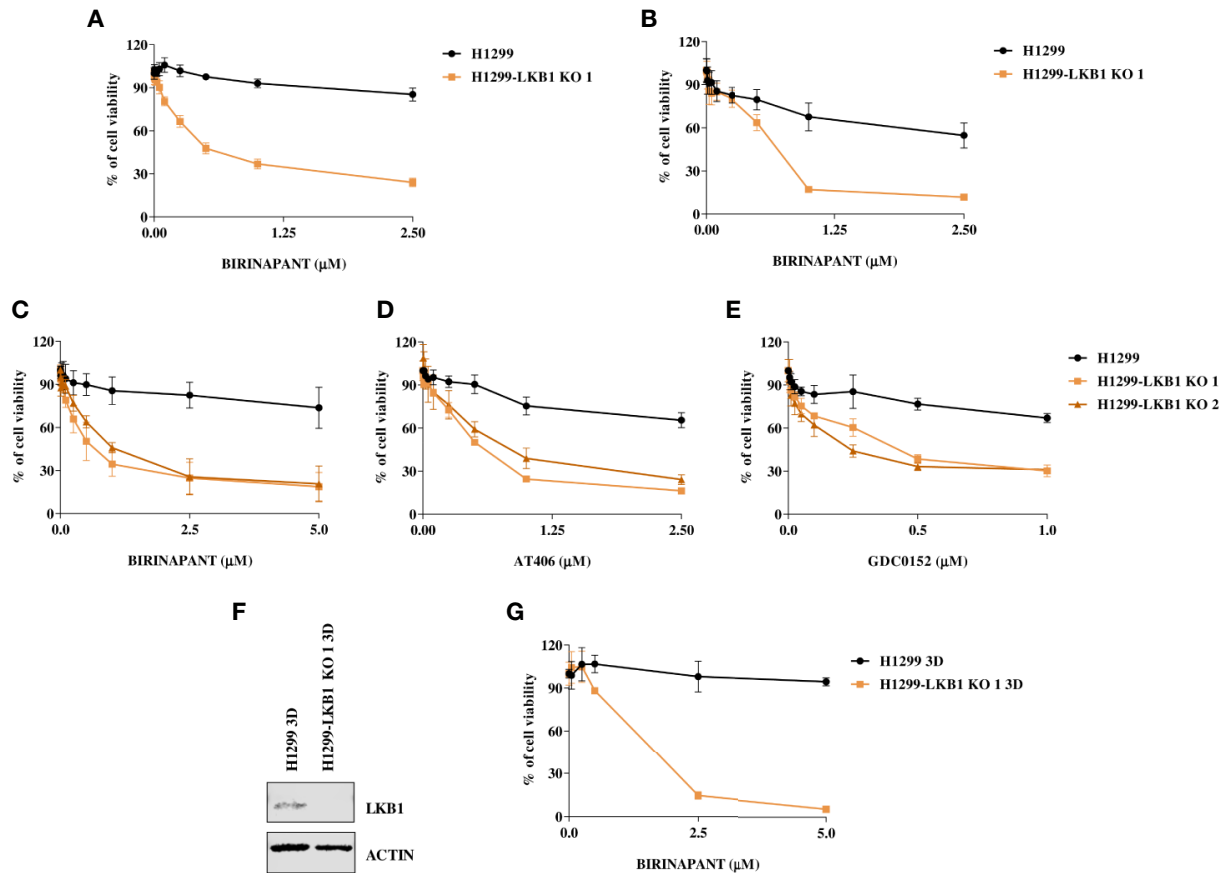

FIGURE 2 | **(A, B)** Evaluation of the H1299 isogenic system response to Birinapant treatment through different cell viability assays: **(A)** CellTiter-Glo viability assay and **(B)** Sulforhodamine B assay. Dose-response curves were generated by treating the H1299 isogenic system with increasing concentrations of Birinapant. The average of three independent experiments is reported. Statistical analysis was carried out through two-way ANOVA and Bonferroni post-test for multiple comparisons and it is reported in **Supplementary Table 3**. **(C–E)** Dose-response curves of H1299 and two H1299-LKB1 KO clones treated with increasing concentrations of **(C)** Birinapant, **(D)** AT406, and **(E)** GDC0152. The response to the drug was evaluated with the MTS assay. The average of three independent experiments is reported. Statistical analysis was carried out through two-way ANOVA and Bonferroni post-test for multiple comparisons and it is reported in **Supplementary Table 4**. **(F)** Western Blot analysis of LKB1 expression levels in H1299 and H1299-LKB1 KO 1 spheroids (3D). Actin was used as a loading control. **(G)** Dose-response curves of H1299 and H1299-LKB1 KO 1 spheroids (3D) treated with increasing concentrations of Birinapant. The response to the drug was evaluated with the CellTiter-Glo viability assay. The average of three independent experiments is reported. Statistical analysis was carried out through two-way ANOVA and Bonferroni post-test for multiple comparisons and it is reported in **Supplementary Table 5**.

and equal to 2.58 μM (CI: 2.0–3.4 μM) for the second (**Figures 2A, B and Supplementary Table 3**). Moreover, the Birinapant activity was confirmed in another independent H1299-derived clone (H1299-LKB1 KO 2) previously obtained with the Crispr-Cas9 technique (**Figure 2C**, **Supplementary Table 4**) (16).

In order to verify that Birinapant activity was correlated to its specific mechanism of action as IAP inhibitor, we treated the cell lines with increasing doses of other two IAP inhibitors, AT406 and GDC0152. For each drug, it was possible to calculate the IC_{50} in both the two LKB1-deleted clones, whereas the drug concentrations used did not permit to reach the 50% of viability inhibition in the LKB1 WT cell line (**Figures 2D, E and Supplementary Table 4**).

Finally, we increased the complexity of our cellular model: 3D spheroids expressing or not LKB1 were generated (**Figure 2F**) and treated with Birinapant. Even in this model, it was possible to calculate the IC_{50} just for the clone lacking LKB1 (1.3 μM; CI: 0.8–2.0 μM) while the WT cells resulted resistant (**Figure 2G** and **Supplementary Table 5**).

Analysis of Apoptosis at Different Levels After Birinapant Treatment

We first excluded that the differences in the sensitivity of H1299 and H1299-LKB1 KO 1 cells to the drug were due to differences in the achievement of its targets. We analyzed the expression of

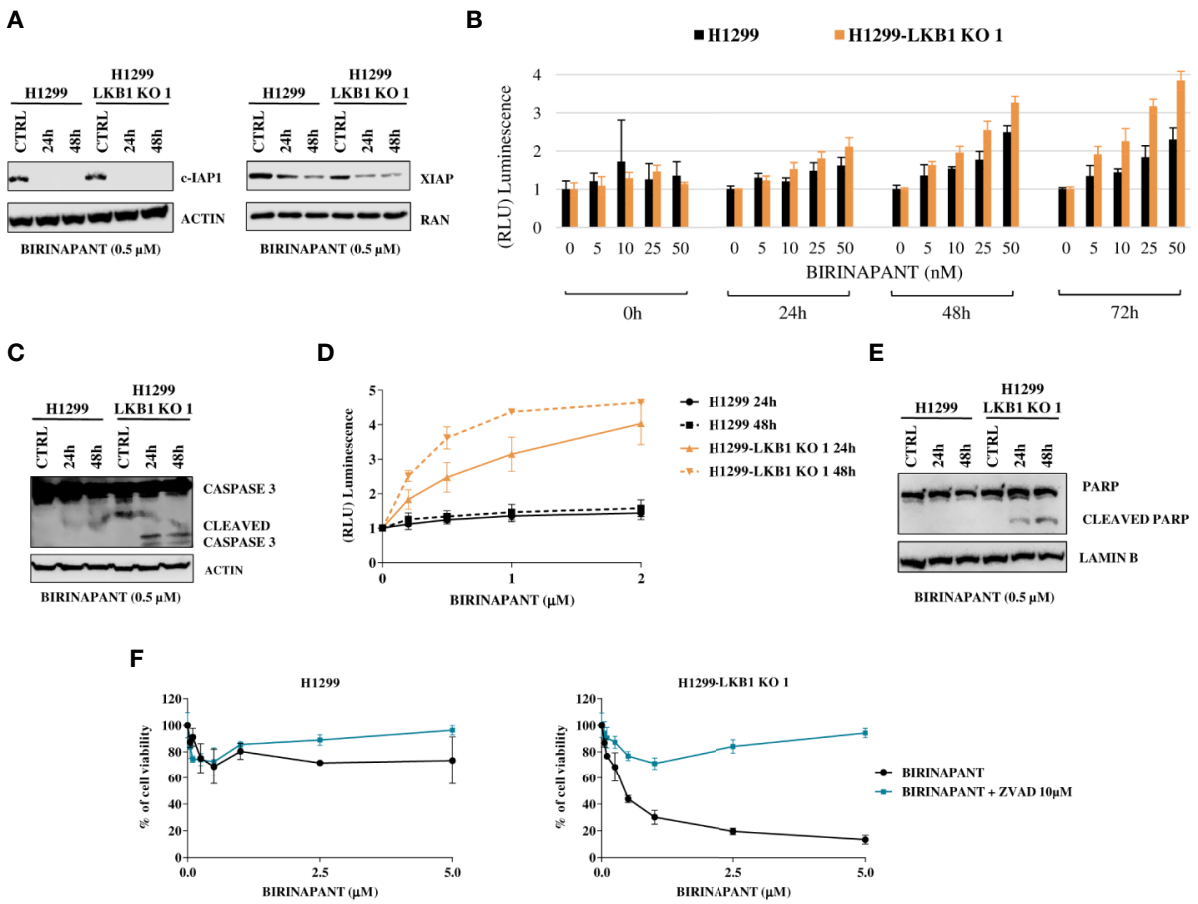

FIGURE 3 | **(A)** Western Blot analysis of c-IAP and XIAP levels after Birinapant treatment, at different time points. Actin and Ran were used as loading controls. **(B)** RealTime-Glo Annexin V assay on H1299 and H1299-LKB1 KO 1 cell lines treated with Birinapant 5, 10, 25, and 50 nM. Annexin V exposure was followed 0, 24, 48, and 72 h from treatment start. The average of three biological replicates with standard deviations are reported. Statistical analysis was carried out through two-way ANOVA and Bonferroni post-test for multiple comparisons and it is reported in **Supplementary Table 6**. **(C)** Analysis of caspase-3 cleavage in H1299 and H1299-LKB1 KO 1. The two cell lines were treated with Birinapant 0.5 μM and protein levels were evaluated 24 and 48 h after treatment start. Actin was used as loading control. **(D)** Evaluation of caspase-3/7 activity in H1299 isogenic system after treatment with different concentrations of Birinapant, 24 and 48 h after treatment start with Caspase-Glo 3/7 assay. The average of two independent experiments is reported. The statistical analysis was carried out through two-way ANOVA and Bonferroni post-test for multiple comparisons and it is reported in **Supplementary Table 7**. **(E)** Analysis of PARP cleavage in H1299 isogenic system after 24 and 48 h from Birinapant treatment start. Lamin B was used as loading control. **(F)** Dose-response curves of H1299 and H1299-LKB1 KO 1 cell lines treated with increasing concentrations of Birinapant, alone or in combination with ZVAD 10 μM. The response to the drugs was evaluated with MTS assay. The average of three independent experiments is reported. Statistical analysis was carried out through two-way ANOVA and Bonferroni post-test for multiple comparisons and it is reported in **Supplementary Table 8**.

c-IAP1 and XIAP, the two main Birinapant targets, after 24 and 48 h from treatment start with a sub-toxic concentration of 0.5 μM. In both cell lines, at the two time points considered, the drug reached its targets but, while the c-IAP1 was completely degraded, the XIAP levels were only (again equally in both cell lines) downregulated (**Figure 3A**).

Being an IAP inhibitor, Birinapant exerts its cytotoxic activity by induction of apoptosis (9), so we analyzed this process at different levels. We evaluated the phosphatidylserine (PS) exposure on the outer leaflet of cell membrane, a signal of induction of apoptosis (22), by detecting Annexin V binding to it. H1299 and H1299-LKB1 KO 1 cells were treated with increasing concentrations of Birinapant and Annexin V binding was measured at different time points. We observed a higher PS exposure in H1299-LKB1 KO 1 clone compared to H1299, after 24 h of treatment. The differences in Annexin V levels between the two cell lines became more marked at 48 and 72 h (**Figure 3B and Supplementary Table 6**).

Then, we studied the effectors of apoptosis, Caspase 3 and 7. We observed the cleaved and active form of the Caspase 3 enzyme after treatment with a sub-toxic dose of Birinapant (0.5 μM), just in H1299-LKB1 KO cell line, while in H1299 only the uncleaved, inactive form of Caspase 3 was present (**Figure 3C**). Further evidence of apoptosis activation only in H1299-LKB1 KO 1 sensitive clone was given by the observation of Caspase 3/7 activity, at both 24 and 48 h from treatment. In the WT cell line, no activity of effector caspases at the two time points considered was detected (**Figure 3D** and **Supplementary Table 7**). In addition, Birinapant treatment induced cleavage of PARP, a substrate of active caspases, once again just in H1299-LKB1 KO 1 cells (**Figure 3E**).

To corroborate these data with a different approach, we treated cells with a combination of Birinapant and ZVAD, a pan caspases inhibitor. As expected, the co-treatment completely restored the resistance to Birinapant in H1299-LKB1 KO 1 clone while the same treatment in H1299 parental cell line did not change the viability of cells. Indeed, while the LKB1-deleted clone displayed an IC_{50} of about 0.5 μM, when treated with Birinapant alone, it was not possible to calculate this parameter when ZVAD was added to the treatment (**Figure 3F** and **Supplementary Table 8**).

TABLE 2 | *LKB1* and *KRAS* mutational status in NSCLC cell lines.

CELL LINES	LKB1	KRAS	REFs
H520	WT	WT	(23)
H1975	WT	WT	(23)
H2009	WT	G12A	(23)
H358	WT	G12C	(23)
LU99	WT	G12C	(24)
H727	Q302P	G12V	(23)
H460	LOSS (Hom Q37*)	Q61H	(23)
H2030	LOSS (Hom E317*)	G12C	(23)
A549	LOSS (Hom Q37*)	G12S	(23)
H23	LOSS (Hom W322*)	G12C	(23)

REFs references of the mutational status reported in the table.

Analysis of Birinapant Activity in NSCLC Cell Lines With Different *LKB1* Status

In order to strengthen our previous results, we expanded the study to a panel of NSCLC cell lines WT or naturally mutated in LKB1 (**Table 2**). As already reported in literature, all the inactivating mutations found in *LKB1* gene invariably lead to protein loss (**Figure 4A**) (7). All the cell lines chosen, together with the H1299-LKB1 KO 1 clone, used as positive control of treatment efficacy, were treated with Birinapant and dose-response curves were plotted. As shown in **Figure 4B**, all the cell lines were resistant to the compound (IC_{50} > 5 μM), independently from their *LKB1* mutational status. These findings were also confirmed by treating a representative panel of cell lines, with increasing concentrations of two other IAP inhibitors previously tested, AT406 (**Figure 4C**) and GDC0152 (**Figure 4D**). Realizing that all LKB1-mutated cell lines in this panel also harbored activating *KRAS* mutations (**Table 2**) we hypothesized that these alterations could impede, in some way, Birinapant action and justify the resistance of LKB1-mutated NSCLC cell lines.

To assess this hypothesis, we used an *ad hoc* isogenic cell system composed by K clone (KRAS G12C/LKB1 WT) and its derived KL clone (KRAS G12C/LKB1-deleted). The K clone was previously obtained starting from H1299 cell line by transfecting KRAS-G12C containing vector, then *LKB1* was disrupted through Crispr-Cas9 technique, thus generating KL clone (17–20). Both clones were resistant to Birinapant as indicated by IC_{50} values higher than 5 μM (**Figure 4E**).

Combination of Birinapant and Ralimetinib in Other KRAS-LKB1 Co-Mutated Cell Lines

Knowing that the unique difference between KL and H1299-LKB1 KO 1 clones is the activating mutation in *KRAS*, we suggested that the inhibition of proteins belonging to pathways downstream of KRAS could restore the sensitivity to Birinapant in KL clone. Therefore, we treated K and KL clones with increasing doses of Birinapant and a sub-toxic dose of some KRAS downstream protein inhibitors: ERK inhibitor, MEK inhibitor, B-RAF inhibitor, AKT inhibitor and p38α inhibitor (data not shown). Among them, only the combination of Birinapant and Ralimetinib (2 μM), the p38α inhibitor, restored the sensitivity in KL clone, with an IC_{50} of 1.55 μM (CI: 1.24–1.99 μM), while the K clone remained resistant (IC_{50} > 5 μM) (**Figure 5A** and **Supplementary Table 9**).

Having confirmed that, in our *ad hoc* isogenic system, the inhibition of a KRAS downstream protein with Ralimetinib restored the sensitivity to Birinapant in the LKB1-deleted KRAS mutated clone, we tried to expand this result to other LKB1 and KRAS mutated cell lines of our previous panel. We chose two KRAS mutated and LKB1 WT cell lines, the H358 and the LU99, and other two naturally mutated both in KRAS and LKB1, the A549 and the H23. All these cell lines were treated with single sub-toxic doses of Birinapant or Ralimetinib and with the combination of the two drugs. The combination treatment did not have a significant impact on cell viability in the LKB1 WT cell lines (**Figure 5B**), while it significantly decreased cell viability in both the LKB1-mutated cell lines (**Figure 5C**).

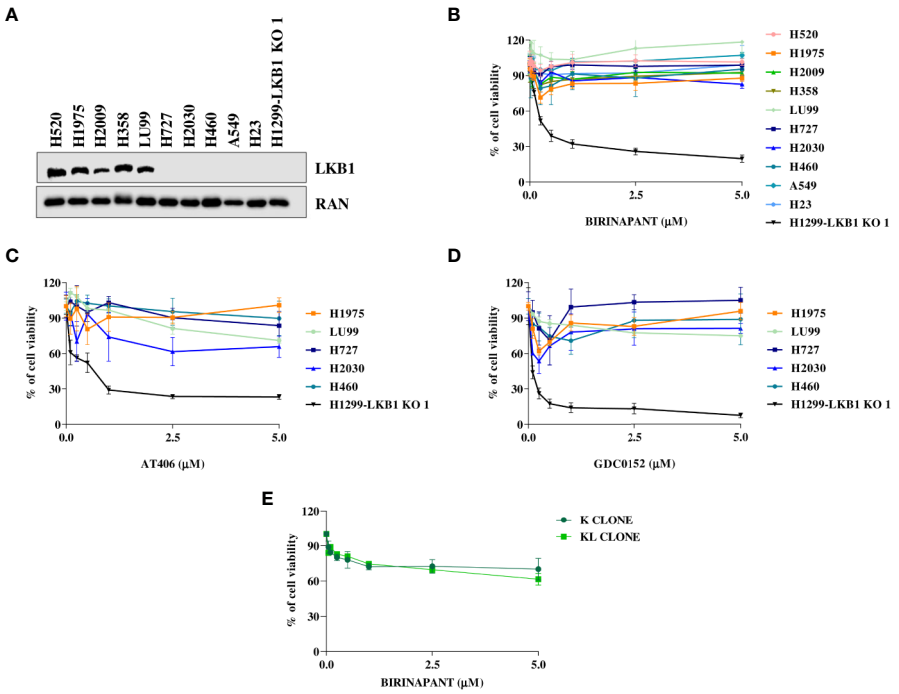

FIGURE 4 | **(A)** Western Blot analysis of LKB1 expression levels in NSCLC cell lines. Ran was used as loading control. **(B–D)** Dose-response curves of NSCLC cell lines treated with increasing concentrations of **(B)** Birinapant, **(C)** AT406, and **(D)** GDC0152. The response to the drugs was evaluated with MTS assay. The average of three independent experiments is reported. **(E)** Dose-response curves of H1299-derived clones, K, and KL, treated with increasing concentrations of Birinapant. The response to the drugs was evaluated with MTS assay. The average of three independent experiments is reported. Statistical analysis was carried out through two-way ANOVA and Bonferroni post-test for multiple comparisons. Data were not reported because no differences were found among all the compared groups.

DISCUSSION

Mutations in *STK11*, the second tumor suppressor gene most frequently mutated in NSCLCs (4), lead to loss of LKB1 protein expression which precludes the possibility to directly targeting the cancer-associated, mutated product. Moreover, the frequent co-presence, in NSCLCs, of *LKB1* and *KRAS* mutations (25) is associated with resistance to the classical anticancer drugs and immunotherapy (5). In addition, the mutual exclusivity of *LKB1* mutations with other targetable mutated genes, such as EGFR and ALK (5), pose great challenges on how to treat patients affected by these tumors. Therefore, highlighting new vulnerabilities of LKB1-mutated NSCLC tumors potentially exploitable to design new therapies is urgently needed. In order to achieve this goal, we have screened an FDA-approved drug library on a NSCLC cell line LKB1 WT and its LKB1-deleted clone, previously obtained in our laboratory with Crispr-Cas9 technique. The FDA-approved library used comprises some drugs already approved by FDA and others under evaluation in clinical trials (21). The screening of FDA-approved library is an interesting technique already used in different fields by researchers (26, 27). Indeed, by examining all the drug classes on the same cellular model it is possible to find new applications for an old drug and, hence, introduce an already existing therapy to a new disease, the so called drug repurposing (28). In addition, drug repurposing allows rapid clinical impact and patient benefit at reduced cost and time requirements than *de novo* drug development as a result of the availability of bioactivity and safety data from clinical trials for each compound used in the screening (21). In our study, the screening and the consequent validation revealed that eight compounds were more active on the LKB1-deleted clone compared to the parental cell line. As already reported in the literature, the LKB1-deleted clone resulted sensitive to the three different MEK inhibitors included in the library (29, 30). The most active compound on LKB1-deleted clone compared to the LKB1 WT cell line was Birinapant, a phase II SMAC mimetic or IAP inhibitor compound. Our results indicate that Birinapant, as a representative compound of IAP inhibitors, inhibited c-IAP1 and XIAP in both cell lines, but just in the LKB1-deleted clone it induced apoptosis through caspase activation. Studies in literature showed that degradation or inhibition of IAPs by Birinapant does not necessarily translate in sensitivity to the drug (31). In our isogenic system, the unique difference between the cell lines is the deletion in LKB1, so we identify a potential role of this protein in determining sensitivity to IAP inhibitors.

In order to enhance the translational impact of our results, we chose to shift from this isogenic system to different LKB1 WT or naturally mutated NSCLC cell lines. All the cell lines tested were resistant to Birinapant, independently from *LKB1* mutations.

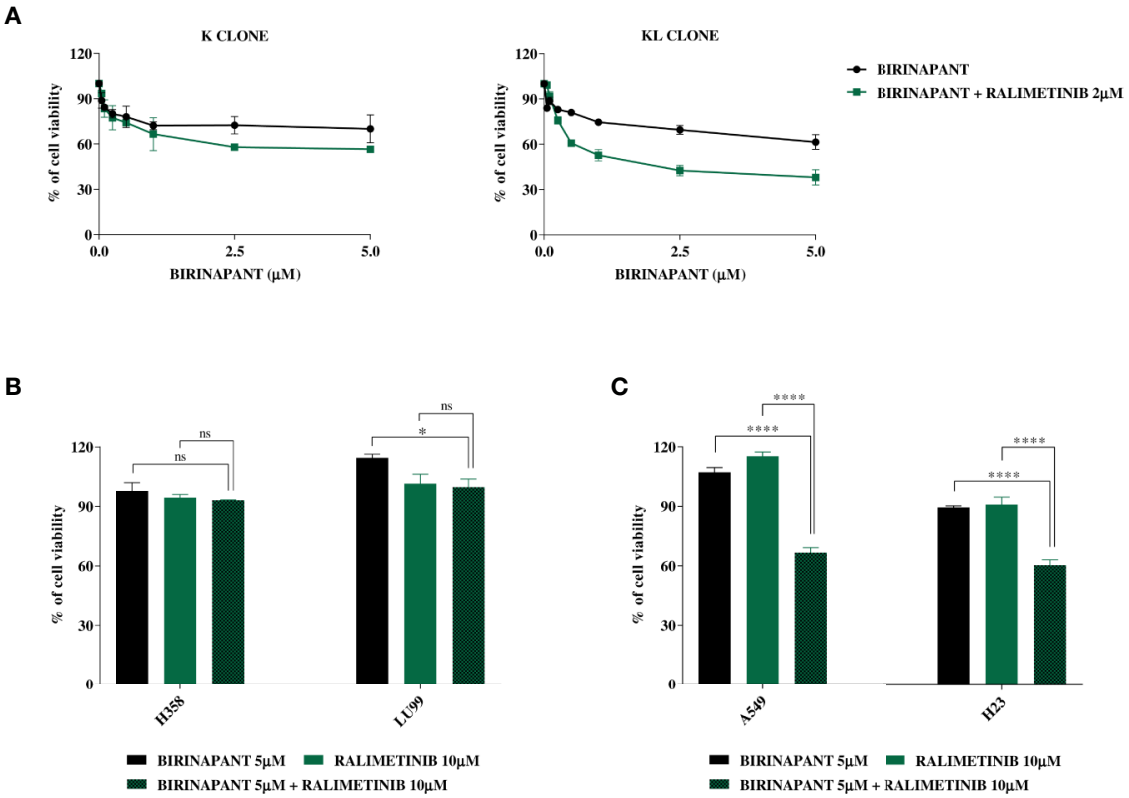

FIGURE 5 | **(A)** Dose-response curves of K and KL clones treated with increasing concentrations of Birinapant, alone or in combination with Ralimetinib 2 μM. The response to the drugs was evaluated with MTS assay. The average of three independent experiments is reported. Statistical analysis was carried out through two-way ANOVA and Bonferroni post-test for multiple comparisons and it is reported in **Supplementary Table 9**. **(B)** Histograms of KRAS mutated/LKB1 WT cell lines, H358 and LU99, treated with Birinapant 5 μM, Ralimetinib 10 μM or the combination of the two drugs. The response to the drugs was evaluated with MTS assay. The average of three independent experiments is reported. Statistical analysis was carried out through one-way ANOVA and Bonferroni post-test for multiple comparisons and it is reported in the graphs. *$p < 0.05$, ns: not statistically significant. **(C)** Histograms of KRAS mutated/LKB1 deleted cell lines, A549 and H23, treated with Birinapant 5 μM, Ralimetinib 10 μM or the combination of the two drugs. The response to the drugs was evaluated with MTS assay. The average of three independent experiments is reported. Statistical analysis was carried out through one-way ANOVA and Bonferroni post-test for multiple comparisons and it is reported in the graphs. ****$p < 0.0001$. Percentage of cell viability of single treated samples was calculated reporting its value to the control-treated sample, considered 100% viable. While, for combination treatment, Ralimetinib treated sample was considered as 100% of viability hence the combination cell viability was normalized on the Ralimetinib cell viability. In this way, the minimum effect of Ralimetinib on cell viability is nulled and the potency of Ralimetinib in sensitizing cells to Birinapant is highlighted.

Due to the fact that all LKB1-deleted cell lines tested in these experiments were also KRAS-mutated, we hypothesized that the latter mutation could constitutively activate downstream pathways to interfere with the sensitivity of LKB1-deleted cell lines to IAP inhibitors. To investigate the hypothesized contribution of *KRAS* mutations in the resistance to Birinapant, we combined subtoxic doses of the IAP inhibitor to different KRAS downstream protein inhibitors. Among them, the combination of Birinapant and Ralimetinib, a p38α inhibitor (13, 14), was able to restore the sensitivity of Birinapant in KRAS- and LKB1-mutated cell lines. Our data are in line with those present in literature where it was shown that targeting p38α, overcomes resistance to Birinapant in primary acute myeloid leukemia (32).

In conclusion, our results highlighted a potential new strategy to specifically treat LKB1-deleted tumors. Pending the verification of our results in LKB1-mutated *in vivo* systems, the use of Birinapant could be a viable therapeutic option for patients with LKB1-mutated NSCLCs, where co-existing alterations which can interfere with Birinapant activity (i.e. *KRAS* activating mutations) have not been found. Moreover, combination of Birinapant and Ralimetinib could be also useful for that number of patients with LKB1- and KRAS-mutated NSCLC, for whom, no targeted therapies are available yet, although the recent introduction of KRAS G12C specific inhibitors could make KRAS druggable (33). Because the results observed with Ralimetinib were based on the assumption that it interferes with KRAS signaling, our data would suggest that a combination of Birinapant and KRAS specific inhibitors, (at least for those patients harboring G12C mutation) could be a further valuable strategy. Finally, considering that Birinapant has been already adopted in phase I-II clinical trials (NCT03803774, NCT01828346, and NCT01681368) (34), the new therapy could be quickly translated to the clinic.

DATA AVAILABILITY STATEMENT

The datasets generated for this study are available on request to the corresponding author.

ETHICS STATEMENT

The animal study was reviewed and approved by The Mario Negri institutional review board and the Italian Ministry of Health.

AUTHOR CONTRIBUTIONS

EC, MM, and MB contributed to the conception and design of the study. MC, MM, GV, and EC organized and performed the experiments. MB and EC performed the statistical analysis. MC and EC wrote the first draft of the manuscript. MC, MM, GV, MB, and EC wrote sections of the manuscript. All authors contributed to the article and approved the submitted version.

FUNDING

This work was supported by Fondazione CARIPLO "Biomedical research conducted by young researchers (2018-0372) grant to EC.

SUPPLEMENTARY MATERIAL

The Supplementary Material for this article can be found online at: https://www.frontiersin.org/articles/10.3389/fonc.2020.532292/full#supplementary-material

REFERENCES

1. Planchard D, Popat S, Kerr K, Novello S, Smit EF, Faivre-Finn C, et al. Metastatic non-small cell lung cancer: ESMO Clinical Practice Guidelines for diagnosis, treatment and follow-up. *Ann Oncol* (2018) 29(Suppl 4):iv192–237. doi: 10.1093/annonc/mdy275
2. Boolell V, Alamgeer M, Watkins D, Ganju V. The Evolution of Therapies in Non-Small Cell Lung Cancer. *Cancers* (2015) 7(3):1815–46. doi: 10.3390/cancers7030864
3. Baxevanos P, Mountzios G. Novel chemotherapy regimens for advanced lung cancer: have we reached a plateau? *Ann Trans Med* (2018) 6(8):139–9. doi: 10.21037/atm.2018.04.04
4. Ding L, Getz G, Wheeler DA, Mardis ER, McLellan MD, Cibulskis K, et al. Somatic mutations affect key pathways in lung adenocarcinoma. *Nature* (2008) 455(7216):1069–75. doi: 10.1038/nature07423
5. Facchinetti F, Bluthgen MV, Tergemina-Clain G, Faivre L, Pignon J-P, Planchard D, et al. LKB1/STK11 mutations in non-small cell lung cancer patients: Descriptive analysis and prognostic value. *Lung Cancer* (2017) 112:62–8. doi: 10.1016/j.lungcan.2017.08.002
6. Ji H, Ramsey MR, Hayes DN, Fan C, McNamara K, Kozlowski P, et al. LKB1 modulates lung cancer differentiation and metastasis. *Nature* (2007) 448 (7155):807–10. doi: 10.1038/nature06030
7. Zhou W, Zhang J, Marcus AI. LKB1 Tumor Suppressor: Therapeutic Opportunities Knock when LKB1 Is Inactivated. *Genes Dis* (2014) 1(1):64–74. doi: 10.1016/j.gendis.2014.06.002
8. Momcilovic M, Shackelford DB. Targeting LKB1 in cancer - exposing and exploiting vulnerabilities. *Br J Cancer* (2015) 113(4):574–84. doi: 10.1038/bjc.2015.261
9. Benetatos CA, Mitsuuchi Y, Burns JM, Neiman EM, Condon SM, Yu G, et al. Birinapant (TL32711), a bivalent SMAC mimetic, targets TRAF2-associated cIAPs, abrogates TNF-induced NF-κB activation, and is active in patient-derived xenograft models. *Mol Cancer Ther* (2014) 13(4):867–79. doi: 10.1158/1535-7163.MCT-13-0798
10. Amaravadi RK, Schilder RJ, Martin LP, Levin M, Graham MA, Weng DE, et al. A Phase I Study of the SMAC-Mimetic Birinapant in Adults with Refractory Solid Tumors or Lymphoma. *Mol Cancer Ther* (2015) 14 (11):2569–75. doi: 10.1158/1535-7163.MCT-15-0475
11. Silke J, Meier P. Inhibitor of apoptosis (IAP) proteins-modulators of cell death and inflammation. *Cold Spring Harb Perspect Biol* (2013) 5(2). doi: 10.1101/cshperspect.a008730
12. Fulda S, Vucic D. Targeting IAP proteins for therapeutic intervention in cancer. *Nat Rev Drug Discovery* (2012) 11(2):109–24. doi: 10.1038/nrd3627
13. Campbell RM, Anderson BD, Brooks NA, Brooks HB, Chan EM, De Dios A, et al. Characterization of LY2228820 Dimesylate, a Potent and Selective Inhibitor of p38 MAPK with Antitumor Activity. *Mol Cancer Ther* (2014) 13(2):364–74. doi: 10.1158/1535-7163.MCT-13-0513
14. Manning G, Whyte DB, Martinez R, Hunter T, Sudarsanam S. The protein kinase complement of the human genome. *Science* (2002) 298(5600):1912–34. doi: 10.1126/science.1075762
15. Patnaik A, Haluska P, Tolcher AW, Erlichman C, Papadopoulos KP, Lensing JL, et al. A First-in-Human Phase I Study of the Oral p38 MAPK Inhibitor, Ralimetinib (LY2228820 Dimesylate), in Patients with Advanced Cancer. *Clin Cancer Res* (2016) 22(5):1095–102. doi: 10.1158/1078-0432.CCR-16-0645
16. Caiola E, Iezzi A, Tomanelli M, Bonaldi E, Scagliotti A, Colombo M, et al. LKB1 Deficiency Renders NSCLC Cells Sensitive to ERK Inhibitors. *J Thorac Oncol* (2019) 15(3):360–70. doi: 10.1016/j.jtho.2019.10.009
17. Brunelli L, Caiola E, Marabese M, Broggini M, Pastorelli R. Comparative metabolomics profiling of isogenic KRAS wild type and mutant NSCLC cells in vitro and in vivo. *Sci Rep* (2016) 6(1). doi: 10.1038/srep28398
18. Caiola E, Brunelli L, Marabese M, Broggini M, Lupi M, Pastorelli R. Different metabolic responses to PI3K inhibition in NSCLC cells harboring wild-type and G12C mutant KRAS. *Oncotarget* (2016) 7(32):51462–72. doi: 10.18632/oncotarget.9849
19. Caiola E, Salles D, Frapolli R, Lupi M, Rotella G, Ronchi A, et al. Base excision repair-mediated resistance to cisplatin in KRAS(G12C) mutant NSCLC cells. *Oncotarget* (2015) 6(30):30072–87. doi: 10.18632/oncotarget.5019
20. Garassino MC, Marabese M, Rusconi P, Rulli E, Martelli O, Farina G, et al. Different types of K-Ras mutations could affect drug sensitivity and tumour behaviour in non-small-cell lung cancer. *Ann Oncol* (2011) 22(1):235–7. doi: 10.1093/annonc/mdq680
21. https://www.selleckchem.com/.
22. Hassan M, Watari H, AbuAlmaaty A, Ohba Y, Sakuragi N. Apoptosis and molecular targeting therapy in cancer. *BioMed Res Int* (2014) 2014:150845. doi: 10.1155/2014/150845
23. https://cancer.sanger.ac.uk/cell_lines.
24. Takata M, Chikumi H, Miyake N, Adachi K, Kanamori Y, Yamasaki A, et al. Lack of AKT activation in lung cancer cells with EGFR mutation is a novel marker of cetuximab sensitivity. *Cancer Biol Ther* (2012) 13(6):369–78. doi: 10.4161/cbt.19238
25. Skoulidis F, Byers LA, Diao L, Papadimitrakopoulou VA, Tong P, Izzo J, et al. Co-occurring Genomic Alterations Define Major Subsets of KRAS-Mutant Lung Adenocarcinoma with Distinct Biology, Immune Profiles, and Therapeutic Vulnerabilities. *Cancer Discovery* (2015) 5(8):860–77. doi: 10.1158/2159-8290.CD-14-1236
26. Wang S, Liu Y, Guo J, Wang P, Zhang L, Xiao G, et al. Screening of FDA-Approved Drugs for Inhibitors of Japanese Encephalitis Virus Infection. Diamond MS, editor. *J Virol* (2017) 91(21). doi: 10.1128/JVI.01055-17
27. Guillotin D, Austin P, Begum R, Freitas MO, Merve A, Brend T, et al. Drug-Repositioning Screens Identify Triamterene as a Selective Drug for the

Treatment of DNA Mismatch Repair Deficient Cells. *Clin Cancer Res* (2017) 23(11):2880–90. doi: 10.1158/1078-0432.CCR-16-1216
28. Hirst J, Pathak HB, Hyter S, Pessetto ZY, Ly T, Graw S, et al. Licofelone Enhances the Efficacy of Paclitaxel in Ovarian Cancer by Reversing Drug Resistance and Tumor Stem-like Properties. *Cancer Res* (2018) 78(15):4370–85. doi: 10.1158/0008-5472.CAN-17-3993
29. Wang Y, Li N, Jiang W, Deng W, Ye R, Xu C, et al. Mutant LKB1 Confers Enhanced Radiosensitization in Combination with Trametinib in KRAS-Mutant Non-Small Cell Lung Cancer. *Clin Cancer Res* (2018) 24(22):5744–56. doi: 10.1158/1078-0432.CCR-18-1489
30. Mahoney CL, Choudhury B, Davies H, Edkins S, Greenman C, van Haaften G, et al. LKB1/KRAS mutant lung cancers constitute a genetic subset of NSCLC with increased sensitivity to MAPK and mTOR signalling inhibition. *Br J Cancer* (2009) 100(2):370–5. doi: 10.1038/sj.bjc.6604886
31. Krepler C, Chunduru SK, Halloran MB, He X, Xiao M, Vultur A, et al. The novel SMAC mimetic birinapant exhibits potent activity against human melanoma cells. *Clin Cancer Res* (2013) 19(7):1784–94. doi: 10.1158/1078-0432.CCR-12-2518
32. Lalaoui N, Hänggi K, Brumatti G, Chau D, Nguyen N-YN, Vasilikos L, et al. Targeting p38 or MK2 Enhances the Anti-Leukemic Activity of Smac-Mimetics. *Cancer Cell* (2016) 29(2):145–58. doi: 10.1016/j.ccell.2016.01.006
33. Hallin J, Engstrom LD, Hargis L, Calinisan A, Aranda R, Briere DM, et al. The KRASG12C Inhibitor MRTX849 Provides Insight toward Therapeutic Susceptibility of KRAS-Mutant Cancers in Mouse Models and Patients. *Cancer Discovery* (2020) 10(1):54–71. doi: 10.1158/2159-8290.CD-19-1167
34. https://clinicaltrials.gov/ct2/home.

Conflict of Interest: The authors declare that the research was conducted in the absence of any commercial or financial relationships that could be construed as a potential conflict of interest.

frontiers in Pharmacology

ORIGINAL RESEARCH
published: 16 December 2020
doi: 10.3389/fphar.2020.532395

Suppression of Esophageal Cancer Stem-like Cells by SNX-2112 Is Enhanced by STAT3 Silencing

Dan-dan Xu[1,2,3†], Su-hong Chen[1,2†], Peng-jun Zhou[2], Ying Wang[4], Zhen-dong Zhao[1], Xia Wang[1], Hui-qing Huang[1], Xue Xue[1], Qiu-ying Liu[2], Yi-fei Wang[2] and Rong Zhang[3]**

[1] Guangdong Food and Drug Vocational College, Guangzhou, China, [2] College of Life Science and Technology, Jinan University, Guangzhou, China, [3] State Key Laboratory of Oncology in South China and Collaborative Innovation Center for Cancer Medicine, SunYat-Sen University Cancer Center, Guangzhou, China, [4] College of Food Science and Technology, Zhongkai University of Agriculture and Engineering, Guangzhou, China

OPEN ACCESS

Edited by:
Nehad M. Ayoub,
Jordan University of Science and Technology, Jordan

Reviewed by:
Shikha Kumari,
University of Nebraska Medical Center, United States
Xiao Wang,
Jinan University, China

***Correspondence:**
Yi-fei Wang
twang-yf@163.com
Rong Zhang
zhangrong@sysucc.org.cn

†These authors have contributed equally to this work

Specialty section:
This article was submitted to Pharmacology of Anti-Cancer Drugs, a section of the journal Frontiers in Pharmacology

Received: 04 February 2020
Accepted: 16 November 2020
Published: 16 December 2020

Citation:
Xu D, Chen S, Zhou P, Wang Y, Zhao Z, Wang X, Huang H, Xue X, Liu Q, Wang Y and Zhang R (2020) Suppression of Esophageal Cancer Stem-like Cells by SNX-2112 Is Enhanced by STAT3 Silencing. Front. Pharmacol. 11:532395. doi: 10.3389/fphar.2020.532395

Many studies have demonstrated that cancer stem cells (CSCs) or tumor-initiating cells (TICs) are responsible for tumor cell proliferation, chemotherapy resistance, metastasis, and relapse in various cancers. We, and others, have previously shown that the signal transducer and activator of transcription 3 (STAT3) signaling pathway is responsible for CSCs and TICs growth. Recent reports have indicated that the heat shock protein 90 (Hsp90) is also essential for the survival of CSCs and TICs. SNX-2112 is an Hsp90 inhibitor. However, it remains unclear whether proliferation of esophageal cancer stem-like cells (ECSLCs) is suppressed by SNX-2112 with knockdown of STAT3 (shSTAT3). Here, we explored the association between SNX-2112 with shSTAT3 and the suppression of ECSLCs growth. We found that the expression level of both STAT3 and p-STAT3 was higher in clinical esophageal cancer tissue than in the adjacent normal tissue, using western blot and qPCR analysis. Furthermore, differential expression analysis demonstrated that STAT3 was overexpressed in clinical specimens. We demonstrated that SNX-2112 inhibited cancer cell proliferation, decreased *ABCB1* and *ABCG2* gene expression levels and reduced the colony formation capacity of ECSLCs, which was enhanced by STAT3 silencing. Flow cytometry analysis revealed that the combination of SNX-2112 and shSTAT3 significantly induced apoptosis and cell cycle arrest at G2/M phase in ECSLCs. Levels of proliferation pathway proteins, including p38, c-Jun N-terminal kinase (JNK), and extracellular signal–regulated kinase (ERK) which were also client proteins of Hsp90, were also reduced. In addition, SNX-2112 with shSTAT3 inhibited the proliferation of ECSLCs *in vivo*. Finally, STAT3 overexpression eliminated the apoptotic and antiproliferative effects of SNX-2112 on ECSLCs. Hence, these results provide a rationale for the therapeutic potential of the combination of SNX-2112 with shSTAT3 in esophageal cancer, and may indicate new targets for clinical intervention in human cancer.

Keywords: SNX-2112, Hsp90, STAT3, suppression, esophageal cancer stem-like cells

INTRODUCTION

Esophageal cancer is the seventh most common cause of cancer-associated death globally (Siegel et al., 2020). The mortality rate for patients with esophageal cancer is high, and the 5-years survival rate is less than 20%, even in developed countries like the United States (Siegel et al., 2020). According to epidemiology and pathology, esophageal cancer is of two types: esophageal squamous cell carcinoma (ESCC) and esophageal adenocarcinoma (EAC) (Middleton et al., 2018). ESCC is the most common type of esophageal cancer, and is highly prevalent in East Asia, East Africa, and South America (Middleton et al., 2018). Although clinicians and researchers have made progress with treatments for esophageal cancer, most patients are diagnosed at a later stage, when metastasis has occurred (Itskoviz et al., 2019). A lack of effective chemotherapeutic drugs is responsible for the high mortality rate.

According to cancer stem cells (CSCs) hypotheses, cancer cells from small subpopulations are responsible for tumor cell proliferation, invasion, metastasis, relapse, and resistance (Jeter et al., 2011; Noh et al., 2012; Song et al., 2017). In addition, CSCs have the ability to self-renew (Noh et al., 2012). To-date, CSCs have been isolated and identified in many types of solid tumors, including breast, prostate, brain, colorectal, and pancreatic cancers (Sancho et al., 2015). CSCs are identified primarily through their aldehyde dehydrogenase (ALDH) activity, along with several surface markers, including CD44, CD90, and CD133 (Zhao et al., 2011; Hang et al., 2012; Wang et al., 2017). In esophageal cancer cells, $CD44^+$ cells are considered to be CSCs (Zhao et al., 2011). In previous studies, esophageal cancer stem-like cells (ECSLCs) were isolated and examined, demonstrating high expression levels of stem-like markers, as well as tumor sphere formation and tumorigenesis induction (Xu et al., 2016).

Molecular chaperones, such as heat shock protein 90 (Hsp90), interact with their client proteins to stabilize them and assist in their folding. They play an essential role in cell stress process, such as during starvation and at low temperatures, to prevent their client proteins from mis-folding (Hoter et al., 2018). Hsp90 helps its client proteins to recover from cell stress, either by protein refolding or by degradation to restore homeostasis. Hsp90 is implicated in carcinogenesis by promoting cancer cell proliferation, as well as inhibiting cell death pathways (Hoter et al., 2018). The client proteins of Hsp90 are associated with the hallmarks of cancer, and inhibition of Hsp90 has been considered an efficient strategy for cancer therapy (Wang et al., 2010). Emerging evidence demonstrates that Hsp90 inhibition is effective in targeting CSCs (White et al., 2016; Nolan et al., 2017). Extracellular Hsp90 upregulates stemness markers, promotes self-renewal, and enhances tumor sphere growth in prostate cancer patients, which suggest that extracellular Hsp90 is a modulator of CSCs in prostate cancer (Nolan et al., 2017). Inhibition of extracellular Hsp90 using the monoclonal antibody mAb4C5 reduced the activity of breast CSC *in vitro* and significantly inhibited the growth of breast cancer cells *in vivo* (Stivarou et al., 2016). Additionally, inhibition of Hsp90 using novel C-terminal inhibitors KU711 and KU757 completely prevented the self-renewal of head and neck squamous cell carcinoma CSCs (Subramanian et al., 2017). At the same time, they found that suppression of Hsp90 effectively targeted the functionality of thyroid CSCs, which prevented their migration and invasion (White et al., 2016). In our previous studies, the Hsp90 inhibitor SNX-2112 demonstrated antitumor activity by induction of apoptosis and cell cycle arrest of melanoma cells, and inhibiting tumor growth *in vivo* (Liu et al., 2012a; Liu et al., 2012b; Wang et al., 2014). In addition, it exerted its inhibitory effect on various cancer cells by binding to the N-terminal adenosine triphosphate binding site of Hsp90 (Wang et al., 2015). Moreover, SNX-2112 is a more effective agent compared to the classic Hsp90 inhibitor, 17-allylamino-17-demethoxygeldanamycin (17-AAG). For example, SNX-2112 inhibited melanoma cell proliferation in a dose-dependent manner to a more significant level than 17-AAG and the IC_{50} values of 17-AAG and SNX-2112 at 48 h were 1.25 and 0.16 μM, respectively (Liu et al., 2012b). The inhibitors of Hsp90 are listed in **Table 1**. These results encouraged us to investigate the effects of SNX-2112 on ECSLCs.

Accumulating evidence has demonstrated that STAT3 signaling is associated with the proliferation of CSCs or TICs (Chung et al., 2013; Kulesza et al., 2019). STAT3 is a key transcription factor with many functions in normal stem cells, CSCs, and embryonic stem cells (ESCs) (Zhong et al., 1994; Marotta et al., 2011; da Hora et al., 2019; Zhang et al., 2019). This transcription factor is necessary for maintaining mouse ESCs in an undifferentiated state, and is regulated via a Myc-dependent mechanism (Wong et al., 2018). STAT3 has been identified as an oncogene, and activated STAT3 can mediate cellular transformation (Bromberg et al., 1999). Indeed, its regulation is complex as it is involved in many signaling pathways, in many types of cancer cells (He et al., 2018; Lin et al., 2018). STAT3 is constitutively activated by tyrosine phosphorylation in numerous cancers, including esophageal cancer (Chen et al., 2013). Aberrant expression of STAT3 has been implicated in malignant transformation and tumor progression (Xiong et al., 2012). Further studies have demonstrated that STAT3 is overexpressed in CSCs in brain cancer, leukemia, and breast cancer (Hosea et al., 2018; Shastri et al., 2018; Han et al., 2019). Consistently, STAT3 level was higher in melanoma samples and it supported maintenance of melanoma CSCs. It is suggested that STAT3 could serve as a potential target to impair tumor progression or recurrence (Kulesza et al., 2019). STAT3 is also overexpressed in ECSLCs (Xu et al., 2016).

Notably, Hsp90 is important for the functional competence of STAT3 which governs the tumor microenvironment and cancer progression (Bocchini et al., 2014; Cho et al., 2019). The association between Hsp90 and STAT3 was identified in tumor cells, and is necessary for STAT3 phosphorylation, dimerization, and nuclear translocation, all of which contribute to cancer cell survival (Chatterjee et al., 2007; Bocchini et al., 2014). Hsp90 inhibition may simultaneously suppress both Hsp90 functionality and STAT3 signaling activity (Cho et al., 2019). However, it remains unclear whether STAT3 inhibition influences the anti-tumor activity of Hsp90 inhibitors.

TABLE 1 | Summary of Hsp90 inhibitors reaching clinical trials.

Hsp inhibitor	Class of compound	Cancer type	Phase	Ref
17-AAG	Geldanamycin analogue	Prostate, papillary, and clear cell RCC, melanoma V600E Harboring BRAF mutation	Phase II	(Solit et al., 2008) NCT00118092
17-DMAG	Geldanamycin analogue	Solid tumors, AML	Phase I	(Lancet et al., 2010) NCT00088868
IPI-504	Geldanamycin analogue	GIST progression after TKI NSCLC progression on EGFR inhibitor	Phase III Phase I/II	(Sequist et al., 2010; Wagner et al., 2013) NCT00606814
AUY922	Resorcinol derivate	NSCLC progression on chemotherapy	Phase II	(Garon et al., 2013) NCT01854034
AT-13387	Resorcinol derivate	CRPC progression on abiraterone	Phase II	(Shapiro et al., 2015) NCT01685268
STA-9090	Resorcinol derivate	Solid and hematological malignancies	Phase I	(Acquaviva et al., 2014) NCT00858572
SNX-5422	Purine and purine-like analogue	$HER2^+$ tumor types NSLC, esophagogastric, breast	Phase I/II	(Rajan et al., 2011) NCT01848756
NVP-HSP990	Purine and purine-like analogue	Advanced solid tumors	Phase I	(Spreafico et al., 2015) NCT00879905
XL -888	Purine and purine-like analogue	Advanced solid tumors	Phase I	(Jhaveri et al., 2012) NCT00796484

RCC, renal cell carcinoma; CRPC, castrate-resistant prostate cancer; GIST, gastrointestinal stromal tumors; NSCLC, non-small cell lung cancer; TKI, tyrosine kinase inhibitor; EGFR, epidermal growth factor receptor.

In the present study, we investigated the molecular mechanisms underlying the ECSLCs-targeting effects of STAT3 knockdown combined with SNX-2112. We found that ECSLCs proliferation was inhibited by combination treatment. We also demonstrated that the expression level of p-STAT3 is higher in clinical esophageal samples than in paired normal cells. Moreover, the levels of Hsp90 client proteins were significantly reduced in ECSLCs after STAT3 depletion and treatment with SNX-2112. Finally, knockdown of STAT3, along with SNX-2112 administration, inhibited the growth of ECSLCs *in vivo*.

MATERIALS AND METHODS

ECSLCs Culture

SNX-2112 was synthesized in our laboratory according to a known procedure, with purity of the compound >98.0% (Barta et al., 2008). SNX-2112 was dissolved in DMSO and 10 mM SNX-2112 stock solution was stored in 4°C. Eca109 cancer cells were obtained from the Cell Bank of the Chinese Academy of Science. Immortalized human esophageal epithelial cells (HEEC) were purchased from BNBIO (Beijing, China). ECSLCs were isolated and identified according to our previous study (Xu et al., 2016). After they were isolated, the ECSLCs were maintained in serum-free DMEM/F12 medium supplemented with B27 supplement (1: 50) (Invitrogen, Carlsbad, CA, United States), 20 ng/ml epidermal growth factor (EGF) (Pepro Tech, Inc. Rocky Hill, United States), 20 ng/ml basic fibroblast growth factor (bFGF) (Pepro Tech, Inc. Rocky Hill, United States) using ultra-low attachment plates (Coring, NY, United States). Clinical esophageal samples were provided by the Cancer Center of Sun Yet-Sen University in October 2014. Primary ESCC tumors and adjacent normal tissues were obtained from eight patients who underwent surgical treatment. The specimen was same with our previous studies (Xu et al., 2016). The patients provided written informed consent to participate in the study. The use of the clinical specimens for research purposes was approved by the Ethics Committee of Guangdong Food and Drug Vocational College.

Cell Viability Assay and Ki-67 Labeling

The proliferation of ECSLCs was evaluated using the MTT (3-(4, 5-dimethylthiazol-2-yl)-2, 5-diphenyltetrazolium bromide) assay. The ECSLCs were stably transduced with lentiviral constructs carrying shGFPctrl or shSTAT3 for 72 h. Next, approximately 4×10^3 cells were seeded into 96-well culture plates and cultured overnight in DMEM/F12 medium containing 20 ng/ml EGF, 20 ng/ml bFGF, and B27 (1: 50). The following day, to the combination treatment group the cells had been transfected with lentiviral and after 72 h, the cells were exposed to SNX-2112 for 24 h. To the shGFPctrl and shSTAT3 groups ECSLCs were treated with lentiviral constructs for 72 h and cell viability was measured. To SNX-2112 group the ECSLCs were treated with SNX-2112 and cell viability was measured. The MTT assay solution (10 μL) was added to each well, and the plates were incubated at 37°C for 4 h. The MTT final concentration in treatment media was 5 mg/ml. Then the medium was removed, and the formazan crystals were dissolved in DMSO. The absorbance (A) was measured at 570 nm using a microplate reader (Elx800, Biotek). To detect the proliferation of ECSLCs using the Ki-67 marker, the cells were treated with SNX-2112 and shSTAT3 for 24 h. The next day, the cells were incubated with the Ki-67 antibody (1:1,000, Cell Signaling Technology, #9449) at room temperature for 1.5 h after the cells were blocked with 10% goat serum at room temperature for 1.0 h. The cells were then washed three times with Tris-buffered containing 01% Tween-20 for 5 min. Next, the cells were incubated with FITC-conjugated secondary antibody (goat anti-mouse/rabbit) (1:8,000, Beyotime, Haimen, Jiangsu, China) at 37°C for 0.5 h. The cells were then washed three times with Tris-buffered saline (TBS) for 5 min and photographed using a fluorescence microscope (Nikon, Japan).

Construction of shRNA-Expressing Vectors and Transfection

The STAT3-specific shRNA carrying lentiviral vectors with GFP were constructed (Genechem, Shanghai, China) in order to silence the expression of STAT3. The shRNA sequence were as follows, shSTAT3, forward primer, 5′-GCCATTGGCCGG AATTAGCGAACGGT-3′, reverse primer, 5′-CCGGTTAAAG GTTCGACTTCCAAGGTA-3′; shSTAT3-1, forward primer, 5′-GCTAAACCGGTGCCAGCTGAGTTCCCA-3′, reverse primer, 5′-TTGGCGTAAGGTTCGTACAGTTGGTCC-3′; shGFP-ctrl, forward primer, 5′-GTCGGAAGTCCCAAGGTTAGTCCGT-3′, reverse primer, 5′-GGTTACGTAAGGTCCGACTGGAC-3′. The complementary oligonucleotides encoding shRNA were designed and packaged. The sequences of plasmids were verified by sequencing. The cells were transfected with a serum-free medium in the presence of 8 μg/ml polybrene to improve the knockdown efficiency for 4 h. After 4 h, the serum-free medium was replaced by normal medium. The silence efficiency of shSTAT3 was evaluated in our previous studies (Xu et al., 2016).

Ribonucleic Acid Sequencing and Quantitative PCR Analysis

The total RNA was extracted from the tumor tissue using Trizol reagent (Invitrogen, CA, United States) following the manufacturer's procedure. RNA integrity was assessed using the RNA Nano 6000 Assay Kit of the Bioanalyzer 2,100 system (Agilent Technologies, CA, United States). After total RNA was extracted, the ribosomal RNA in the total RNA was completely removed using the Ribo-Zero Magnetic Gold Kit (illumina, United States). Subsequently, the RNA was broken into fragments and connected to the sequencing connector using NEB Next Ultra Directional RNA Library Prep Kit for Illumina (NEB, United States) following the manufacturer's procedure. The cDNA libraries were sequenced by Novogene Technologies (Beijing, China) using an Illumina HiSeq Xten platform. Raw data generated by sequencing were recorded. The specific processing steps were as follows: removal of short sequences; removal of contaminated information which cannot be determined; removal of low-quality reads. At the same time, Q20, Q30, and GC content of the clean data were calculated. All of the analyses were based on the clean data with high quality. For Quantitative PCR (qPCR) analysis, total RNA was isolated using TRIzol reagent (Invitrogen) and reverse transcribed into cDNA using a standard protocol (TaKaRa Biotechnology, Dalian, China). qPCR was carried out using the Bio-Rad system (Hercules, CA, United States) and the TaqMan system (Applied Biosystems, Foster City, CA, United States). The PCR primers were synthesized (Sangon Biotech, Shanghai, China). The primer sequences for PCR were as follows: ABCB1, forward primer 5′-CAGCTGTTGTCTTTGGTGCC-3′, reverse primer 5′-TGGCAA TGCGTTGTTTCTGG-3′. ABCG2, forward primer 5′-TGGTGT TCCTTGTGACACTG-3′, reverse primer 5′-TGAGCCTTTGGT TAAGACCG-3′. GAPDH, forward primer 5′-ATTCCACCC ATGGCAAATTC-3′, reverse primer 5′-TGGGATTTCCAT TGATGACAAG-3′. Each sample was analyzed in triplicate. Gene expression level data analysis was performed according to the $2^{-\Delta\Delta Ct}$ method using GAPDH expression as the control. The following PCR procedure was used on the Light Cycler: 95°C for 5 s, 60°C for 5 s, followed by 42 cycles of 95°C for 15 s and 60°C for 1 min, in a 10 μl reaction volume.

Western Blot Analysis

Cells were collected and lyzed with 1% SDS containing phenylmethylsulfonyl fluoride (PMSF), and protein concentration in the samples was measured using the BCA protein assay kit (Beyotime, Haimen, China). Samples containing 20 μg protein were separated by SDS-PAGE and transferred onto 0.22 μm polyvinylidene fluoride membranes (Millipore, Billerica, MA, United States). Membranes were blocked with 5% skimmed milk in TBS containing 0.05% Tween-20 (TBST) for 1.5 h and were incubated with primary antibodies [Bcl2, Cell Signaling Technology (CST), c15071; Bax, CST, #5023; p38, abcam, ab32142; p-p38, abcam, ab126425; ERK, CST, #4695; *p*-ERK, CST, #4370; JNK, CST, #9252; *p*-JNK, CST, #9255; STAT3, CST, #9139; p-STAT3 (Tyr705), CST, #9145; GAPDH, CST, #5174] at 4°C overnight. The following day, the membranes were washed three times with 0.1% TBST. The membranes were incubated with HRP-conjugated secondary antibody (1: 8,000, goat anti-mouse antibody or goat anti-rabbit antibody) for 1.5 h. The signals on the membranes were developed with ECL reagent (Thermo Scientific, Waltham, MA, United States).

Flow Cytometry Assay

For the apoptosis assay, cells were treated with shSTAT3 and SNX-2112. They were then harvested and washed with PBS for 5 min. The cells were incubated with 5 μl of binding reagent and 5 μl of Annexin V-APC (KeyGen BioTech, China). After 30 min, cells were washed three times with PBS and stained with 5 μl of 7-AAD (KeyGen BioTech, China) for 25 min at room temperature, according to the manufacturer's instructions. The experiments were repeated three times. All data were analyzed and calculated using FlowJo software.

TUNEL Assay

ECSLCs apoptosis was analyzed post-treatment using the terminal deoxynucleotidyl transferase–mediated deoxyuridine triphosphate nick end labeling (TUNEL) method, using the *in-situ* cell death detection kit (Beyotime, Haimen, China), according to the manufacturer's instructions. Paraffin sections were dewaxed in xylene for 10 min, followed by soaking in a series of descending alcohol concentrations (EtOH for 5 min, 90% EtOH for 2 min, 70% EtOH for 2 min, distilled water for 2 min). The sections were incubated with 20 mg/ml proteinase K for 20 min at 30°C in an incubator. The sections were washed with PBS three times for 5 min and soaked in 3% H_2O_2 to block endogenous peroxidase. The sections were incubated with TUNEL reagents. The percentage of TUNEL-labeled cells was determined at a magnification of ×400 by counting 500 cells in a random field.

Colony Formation Assay

For colony formation, according to our previous study (Xu et al., 2016), a 6-well plate was coated with a bottom agar layer containing DMEM/F12 medium supplemented with recombinant human EGF, recombinant human bFGF, and B27 supplement (1:50). The top agar layer contained a single cell suspension of 1×10^3 ECSLCs transfected with shSTAT3 in DMEM/F12 medium supplemented with EGF (20 ng/ml), bFGF (20 ng/ml), B27 supplement (1:50), and 0.2 μM SNX-2112. After 14 days, the cells were stained with 0.5% crystal violet for 30 min at 37°C, and colonies of more than 50 cells were counted as positive.

Animal Experiments and Immunohistochemical Analysis

The study protocol was approved and conducted according to the Jinan University Laboratory Animal Ethics Committee. Five-week-old male Balb/c nude mice were purchased from the Animal Center of Huafukang (Beijing, China). These mice were divided randomly into four groups containing six animals each. ECSLCs containing shSTAT3 were washed with PBS three times and counted. The cells (1×10^5) were resuspended in 150 μl PBS, mixed with an equal volume of Matrigel (BD Biosciences, MA, United States), and injected subcutaneously into the neck area of each nude mouse. The tumor size was measured every three days, and the tumor volume was calculated as $L \times W^2 \times 0.5$ (mm^3; L indicates length; W indicates width). After seven days, SNX-2112 was intraperitoneally injected into mice. In addition, in control group the mice were inoculated 1×10^5 cells and seven days later equal volume of PBS was intraperitoneally injected, which was same as the experiment group treatment. Every other day the mice were administrated 10 mg/kg of SNX-2112. After drug treatment for 2 weeks, animals from each group were euthanized, and the tumors were harvested and measured to determine their weight.

For IHC analysis, tumor tissue and adjacent non-tumor esophageal tissue were fixed in 4% paraformaldehyde and paraffin-embedded. Then, the tissues were sectioned at 3–4 μm thickness and deparaffinized. The sections were dewaxed and subjected to antigen retrieval (0.01 M Citrate buffer pH 6.0 and 0.01 M Tris-HCI buffer pH 9.0, respectively). Endogenous peroxidase was blocked using 0.6% H_2O_2 for 30 min, followed by washing steps with TBS. Sections were treated with 10% normal goat serum in 0.1% TBST for 10 min for non-specific antibody binding. Tissue sections were incubated with primary antibodies [p-ERK, CST, #4695, 1:100; *p*-AKT (Ser473), CST, #4060, 1:100; STAT3, CST, #9139; p-STAT3 (Tyr705), CST, #9145]. Secondary antibody incubation was performed at room temperature for 90 min. Chromogen reaction was performed by incubating with diaminobenzidine (DAB) for 5 min. Slides were counterstained with hematoxylin, dehydrated, and permanently mounted using standard procedures. IHC quantification was performed on three randomly selected high power fields (HPF) per slice. Quantification of apoptotic cells was performed manually. Integrated optical density (iod) of Ki-67$^+$, *p*-AKT and *p*-ERK were quantified using Image pro-Plus software by applying the appropriate pixel threshold equally on all selected pictures and using measure function to calculate the covered area. Data is represented as % of covered area.

Statistical Analysis

The SPSS19.0 program (SPSS Inc., Chicago, IL, United States) was used for statistical analysis. The data are presented as the means ± SD of at least three independent experiments. Student's *t*-test was used for two-group comparisons. $p < 0.05$ was considered to indicate a statistically significant difference.

RESULTS

STAT3 Level Was Higher in Clinical Esophageal Cancer Samples

STAT3 is constitutively activated in numerous types of human cancers, including ECSS, and plays a key role in regulating proliferation, chemo-resistance, and relapse.

However, its clinical significance and biological role in the regulation of proliferation remains unexplored. Western blot analysis indicated that both STAT3 and p-STAT3 (Tyr705) protein levels were increased in human ECSS samples compared with adjacent non-tumor tissue samples (**Figure 1A**). qPCR analysis showed that remarkably higher level of STAT3 was detected in clinical cancer samples (**Figure 1B**). IHC results were also consistent with western blot results regarding levels of STAT3 and p-STAT3 (Tyr705) (**Figure 1C**). Additionally, we compared gene expression profiles of eight esophageal cancer cases with those of normal adjacent tissues using RNA sequencing. Differential expression analysis demonstrated that STAT3 was overexpressed in six out of eight cases (**Figure 1D**). Together, these results demonstrated that STAT3 level is higher in esophageal cancer cells, and STAT3 may play an important role in regulating the proliferation of esophageal cancer cells.

shSTAT3 Enhanced SNX-2112 Efficacy by Inhibiting ECSLCs Colony Formation

The chemical structure of SNX-2112 is shown in **Figure 2**. First the cell toxicity of SNX-2112 was studied using HEEC. According to our previous studies (Liu et al., 2012a; Liu et al., 2012b), HEEC were cultured with 20, 40, and 80 μM SNX-2112 for 24, 48, and 72 h. As in the **Supplementary Figure S1**, no significant cell toxicity was observed. In addition, both western blot and qPCR assays demonstrated that the silence efficiency of shSTAT3 was higher than shSTAT3-1 (**Supplementary Figure S2**). Therefore, the shSTAT3 was selected to conduct the following experiments. To investigate the anticancer effects of the combination treatment of SNX-2112 with shSTAT3, ECSLCs viability was analyzed. The ECSLCs was cultured in the presence of a range of concentration of SNX-2112 (0.05, 0.1, 0.2, 0.4, 0.8,1.6 μM) for 24 h. The viability of ECSLCs was inhibited in a concentration-dependent manner

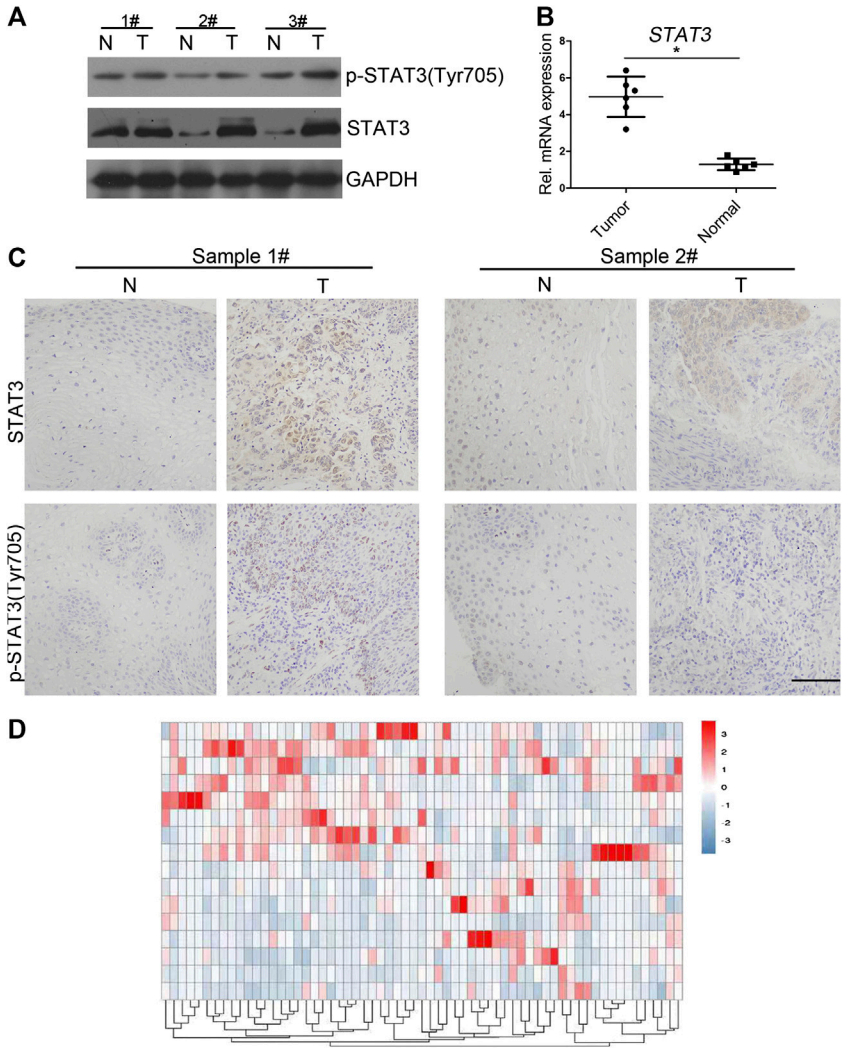

FIGURE 1 | Expression of STAT3 and p-STAT3 in clinical esophageal cancer samples **(A)** Western blot analysis of the STAT3 expression in clinical samples. STAT3 expression in tumor tissues was compared with that in the adjacent normal tissues. T, tumor tissues; N, normal. **(B)** qPCR analysis of the STAT3 expression level in clinical samples. mRNA expression levels of STAT3 in clinical tumor tissue were compared with that in normal tissue. The experiments were repeated three times independently (mean ± SD). **(C)** Expression levels of STAT3 and p-STAT3 in paraffin sections of clinical tumor tissue were analyzed by immunocytochemistry. Representative images of various clinical esophageal cancer specimen sections from eight independent cases and the percentage of samples showing high STAT3 and p-STAT3 expression levels are provided. Scale bar, 50 μm. **(D)** Heat maps of differential expressions of mRNA in clinical esophageal cancer samples.

(**Figure 3A**), and the IC50 value of SNX-2112 at 24 h was 0.19 μM. So for the convenience in the following studies the treatment time and concentration of SNX-2112 was 24 h and 0.20 μM, respectively. SNX-2112, along with shSTAT3, remarkably suppressed cell proliferation compared with shSTAT3 and SNX-2112 alone (**Figure 3B**). Furthermore, a significant downregulation of the mitochondrial protein Bcl2 level was observed with the combination therapy. Bax expression level in the combination treatment group was higher than that in the shSTAT3 and 0.20 μM SNX-2112 alone treatment groups (**Figure 3C**). In addition, the mRNA level of ABC transporter super-family ABCB1 and ABCG2 was significantly reduced following the combination treatment (**Figures 3D,E**).

We further investigated the colony formation capacity of ECSLCs cultured in DMEM/F12 medium supplemented with recombinant human 20 ng/ml EGF, recombinant human 20 ng/ml bFGF and B27 (1: 50). The results demonstrated that the combination treatment of SNX-2112 with shSTAT3 significantly decreased the colony formation ability of ECSLCs (**Figure 3F**). These results indicated that the combination treatment notably reduced the proliferation of the ECSLCs.

SNX-2112 With shSTAT3 Induced Apoptosis and Cell Cycle Arrest in ESCLCs

To explore whether the combination of SNX-2112 with shSTAT3 induced ECSLCs cycle arrest, a flow cytometry assay was

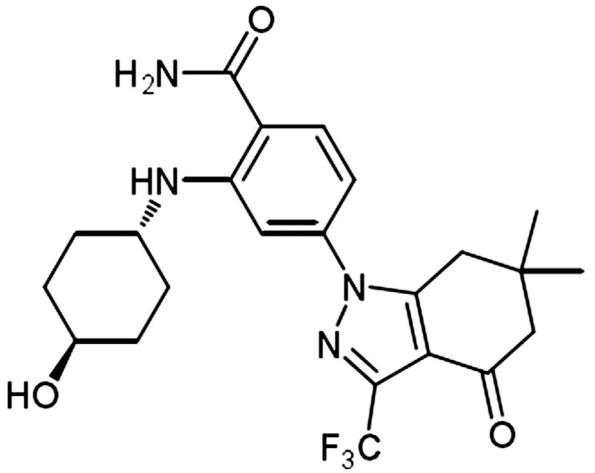

FIGURE 2 | The chemical structure of SNX-2112.

conducted. As shown in **Figure 4A**, the cell cycle was indeed found to be arrested. The relative percentages of G2/M phase cells in the combination treatment, SNX-2112 and shSTAT3 groups were 29.97%, 24.32%, and 16.73%, respectively. In addition, the combination treatment significantly increased the number apoptotic cells compared with the individual treatment (**Figure 4B**). These results suggest that SNX-2112 and shSTAT3 combination remarkably increased G2/M phase arrest compared with SNX-2112 or shSTAT3 alone.

To further investigate whether SNX-2112 combination with shSTAT3 reduced the proliferation and colony formation size of cancer cells, we performed a gain-of-function analysis *in vitro*, using a shSTAT3 lentiviral vector containing GFP. As shown in **Figure 4C**, SNX-2112 combination with shSTAT3 significantly decreased the colony formation size of cells.

To explore the molecular changes in cell proliferation, the levels of p38, JNK and ERK which were client proteins of Hsp90, were measured. We found that p-p38 levels were significantly reduced in the combination group compared with SNX-2112 and shSTAT3 alone groups (**Figure 4D**). Changes were also observed in *p*-JNK and *p*-ERK levels (**Figure 4D**). In addition, the Ki-67 assay showed that intensity of signal of Ki-67 was reduced, which suggested that the proliferation of ECSLCs was inhibited by the combination treatment of SNX-2112 with shSTAT3 (**Figure 4E**). Together, these results demonstrate that STAT3 is required for the proliferation of ECSCLs.

Combination Treatment of SNX-2112 With shSTAT3 Suppressed ECSLCs Tumor Growth *In Vivo*

To investigate the effect of a combination of SNX-2112 with shSTAT3 on esophageal tumor growth *in vivo*, xenograft tumor models with ECSLCs were established. The tumor volume was monitored. The mean weight and volume of tumors in the combination treatment group were smaller than that in the shSTAT3 or SNX-2112 alone groups (**Figure 5A**). The combination treatment of SNX-2112 with shSTAT3 inhibited the tumor growth (**Figure 5A**). In addition, the body weight of animal was not significanty reduced in the combination treatment group (**Figure 5A**). To further investigate the effect of SNX-2112 combination with shSTAT3 on tumor growth, the levels of Ki-67, *p*-ERK and *p*-AKT (Ser473) in the xenograft tumors were examined. It was determined that Ki-67 and *p*-ERK levels were decreased significantly in the combination treatment group. The same effect was observed for *p*-AKT (Ser473) (**Figure 5B**). TUNEL assay revealed higher levels of cancer cell apoptosis in the combination treatment group (**Figure 5B**).

Constitutively Active STAT3 Reduced the Efficacy of SNX-2112 on ECSLCs

Previous studies have demonstrated that STAT3 is overexpressed in many types of tumor cells (Misra et al., 2018; Shastri et al., 2018; Kulesza et al., 2019). To determine whether the STAT3 pathway is required for SNX-2112-induced ECSLCs apoptosis, clinical esophageal cancer samples were collected and the STAT3 and p-STAT3 expression levels were evaluated using IHC. STAT3 and p-STAT3 (Tyr705) levels were higher in tumors than in the adjacent normal tissues (**Figure 6A**). Western blot assay demonstrated that the expression level of p-p38 was reduced with treatment of SNX-2112, and this effect was reversed by STAT3 overexpression (**Figure 6B**). Consistently, these results were observed in *p*-JNK and *p*-ERK (**Figure 6B**). In addition, fluorescence microscopy showed that the proliferation of ECSLCs was inhibited by SNX-2112. However, the proliferation inhibition of the ECSLCs by SNX-2112 was reversed by STAT3 overexpression (**Figure 6C**). These results demonstrated that STAT3 overexpression reduced the efficacy of SNX-2112 on ECSLCs.

STAT3 Overexpression Abolished the Apoptotic Effect of SNX-2112 on ECSLCs

To investigate the effect of STAT3 overexpression on the expression of ABCB1 and ABCG2, the level of ABCB1 and ABCG2 was messured. SNX-2112 reduced the expression level of ABCB1 and ABCG2, which was reversed by STAT3 overexpression (**Figures 7A,B**). In addition, the percentage of total apoptosis in the control, SNX-2112 and STAT3 overexpression groups was 11.68%, 23.60%, and 14.27%, respectively (**Figure 7C**). STAT3 overexpression decreased the percentage of the apoptotic cells. To further confirm the biological role of STAT3 in the regulation of ECSLCs proliferation, the colony formation assay was conducted. The colony formation assay demonstrated that STAT3 overexpression increased colony formation ability of ECSLCs (**Figure 7D**). Collectively, shSTAT3 potentiated the apoptotic effect of SNX-2112 on ECSLCs. Meanwhile, overexpression of STAT3 abolished the apoptosis of ECSLCs induced by SNX-2112. Taken together, these results suggest that SNX-2112 with shSTAT3 inhibited the proliferation of ECSLCs.

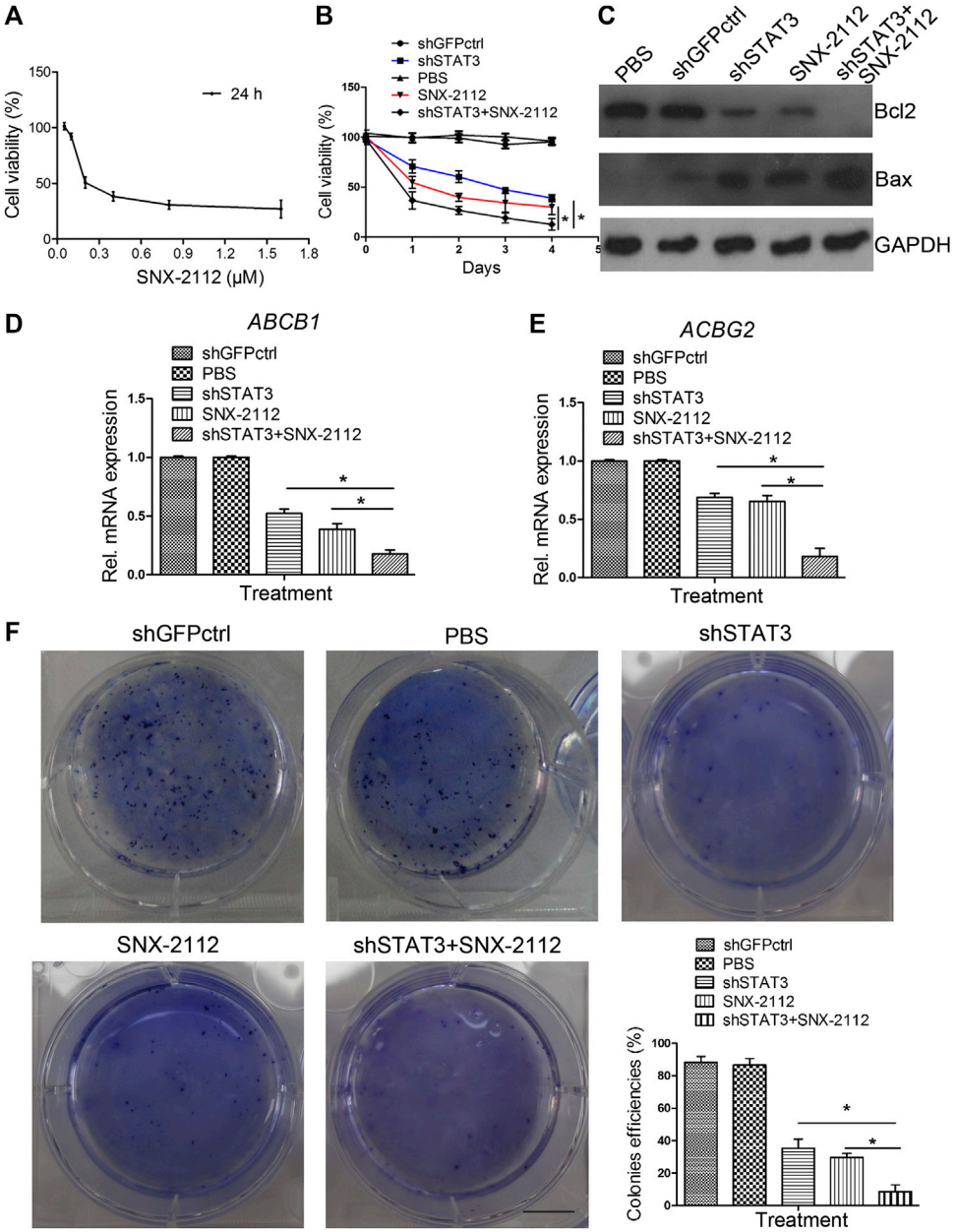

FIGURE 3 | The inhibition of colony formation capacity of ECSLCs by combination treatment of SNX-2112 with shSTAT3 **(A)** Cell viability of ECSLCs treated with SNX-2112 for 24 h. ECSLCs were treated with various concentrations of SNX-2112 fro 24 h and cell viability was assessed using the MTT assay. **(B)** Proliferation curve analysis of ECSLCs after treatment with SNX-2112 and shSTAT3. ECSLCs were stably transduced with lentiviral constructs carrying shGFPctrl and shSTAT3. After 72 h, ECSLCs were treated with 0.2 μM SNX-2112 for 24 h. Then, ECSLCs proliferation was evaluated by MTT assay. The experiments were repeated three times independently. **(C)** Western blot analysis of Bcl2 and Bax expression levels in ECSLCs post treatment with shSTAT3 for 72 h and 0.2 μM SNX-2112 for 24 h. GAPDH was used as a loading control. **(D,E)** qPCR analysis of *ABCB1* and *ABCG2* in ECSLCs. After transfection with shSTAT3 for 72 h, ECSLCs were treated with 0.2 μM SNX-2112 for 24 h. Vertical bars represent mean ± SD. **(F)** The colony forming capacity of ECSLCs was tested using soft agar plates. Approximately 1 × 103 ECSLCs post treatment with shSTAT3 and 0.2 μM SNX-2112 were allowed to grow for approximately 14 days and formed colonies were stained by 0.5% crystal violet and counted. The experiments were repeated three times independently. Scale bar, 10 mm.

DISCUSSION

CSCs have been isolated and identified in many types of tumor cells, including breast, pancreas, brain, and leukemia (Choi et al., 2014; Ross et al., 2015). CSCs have been found to have stem-like cell properties, such as self-renewal, multilineage differentiation potential, and stemness marker expression (Batlle and Clevers, 2017). More importantly, cancer cells have the abilities of invasion, resistance, metastasis, and relapse, mainly due to the presence of these CSCs (Chen et al., 2011; Sainz and Heeschen,

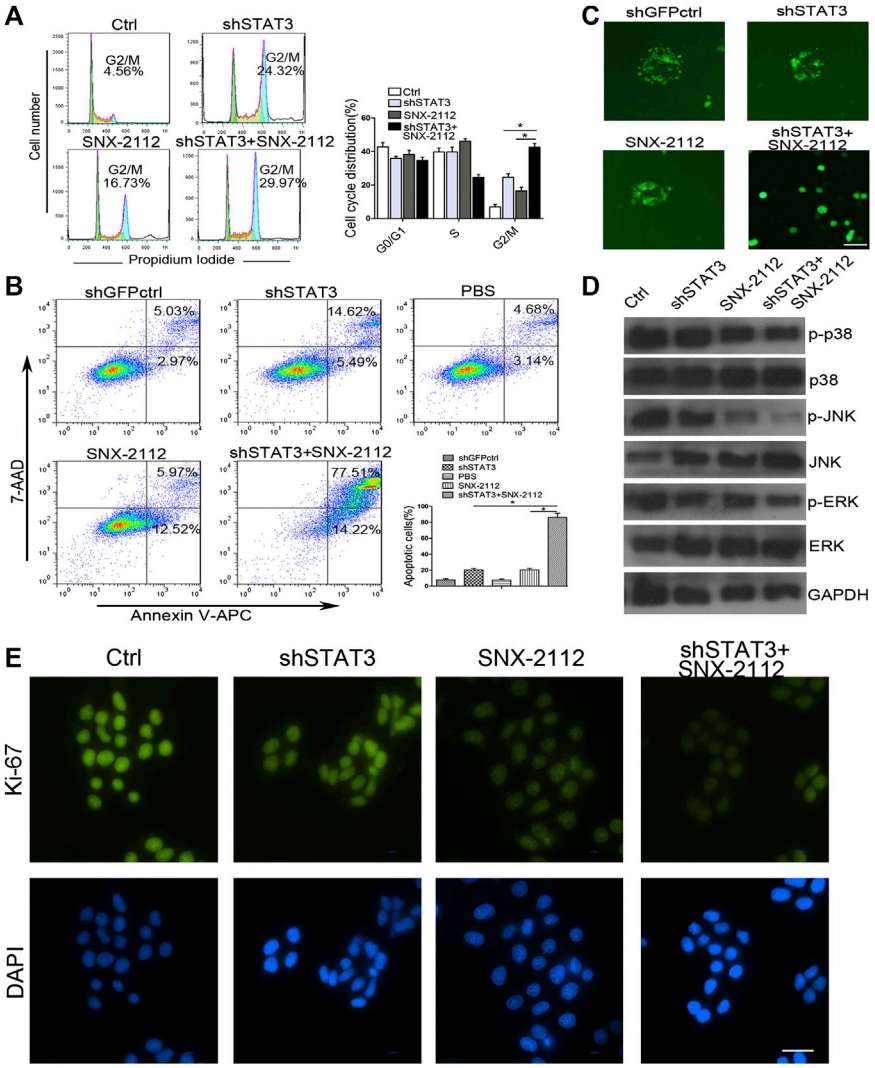

FIGURE 4 | Combination treatment with SNX-2112 and shSTAT3 induced ECSLCs apoptosis and cell cycle arrest **(A)** Flow cytometry analysis of cell cycle of the ECSLCs after treatment with shSTAT3 for 72 h and with 0.2 μM SNX-2112 for 24 h. The cell cycle distribution was analyzed by flow cytometry. Vertical bars represent mean ± SD from three independent experiments. **(B)** The apoptosis of ECSLCs treated with shSTAT3 for 72 h and 0.2 μM SNX-2112 for 24 h was analyzed by flow cytometry. The data were from three independent experiments. **(C)** The sphere formation size detection of ECSLCs. The ECSLCs were treated with shSTAT3 for 72 h and 0.2 μM SNX-2112 for 24 h. Then the ECSLCs were subjected to normal medium for approximately 14 days. The medium was changed every 3 days. Scale bar, 50 μm. **(D)** Western blot analysis of ECSLCs treated with shSTAT3 for 72 h and 0.2 μM SNX-2112 for 24 h. The level of p38, ERK, and JNK were analyzed by western blot. GAPDH was used as a loading control. **(E)** Ki-67 proliferation analysis of ECSLCs treated with shSTAT3 and 0.2 μM SNX-2112 for 24 h. The cells were collected and incubated with Ki-67 antibody. Scale bar, 50 μm.

2013; Williams et al., 2015; Zhao et al., 2015). In this study, we demonstrated that the Hsp90 inhibitor SNX-2112 combined with shSTAT3 suppressed the proliferation of esophageal cancer stem-like cells *in vitro* and *in vivo*. Importantly, the combined treatment of SNX-2112 with shSTAT3 exerted cytotoxic effects against ECSLCs. These results suggest that combined treatment of SNX-2112 with shSTAT3 could be useful for esophageal cancer therapy.

Overexpression of Hsp was found to promote cell survival and protect cellular proteins from the risk of damage or aggregation, such as heat shock, absence of nutrients, and oxidative stress (Pirkkala et al., 2001; Hoter et al., 2018). Hsp90 is known to promote cancer cell survival and anticancer drug resistance by helping their client protein to maintain correct conformation and by enhancing the stability of numerous oncogenic proteins (Taipale et al., 2010; Jego et al., 2013; Le et al., 2018). Hsp90 overexpression is observed in many types of cancer cells, and has emerged as a promising target for anti-tumor drug development (Modi et al., 2011; Le et al., 2018). In addition, several clinical trials are being conducted to evaluate the effectiveness of Hsp90 inhibitors (Modi et al., 2011).

In addition, Hsp90 plays a key role in drug resistance. Cisplatin resistance in bladder cancer-initiating cells was overcome by Hsp90 inhibitor 17-DMAG (Tatokoro et al.,

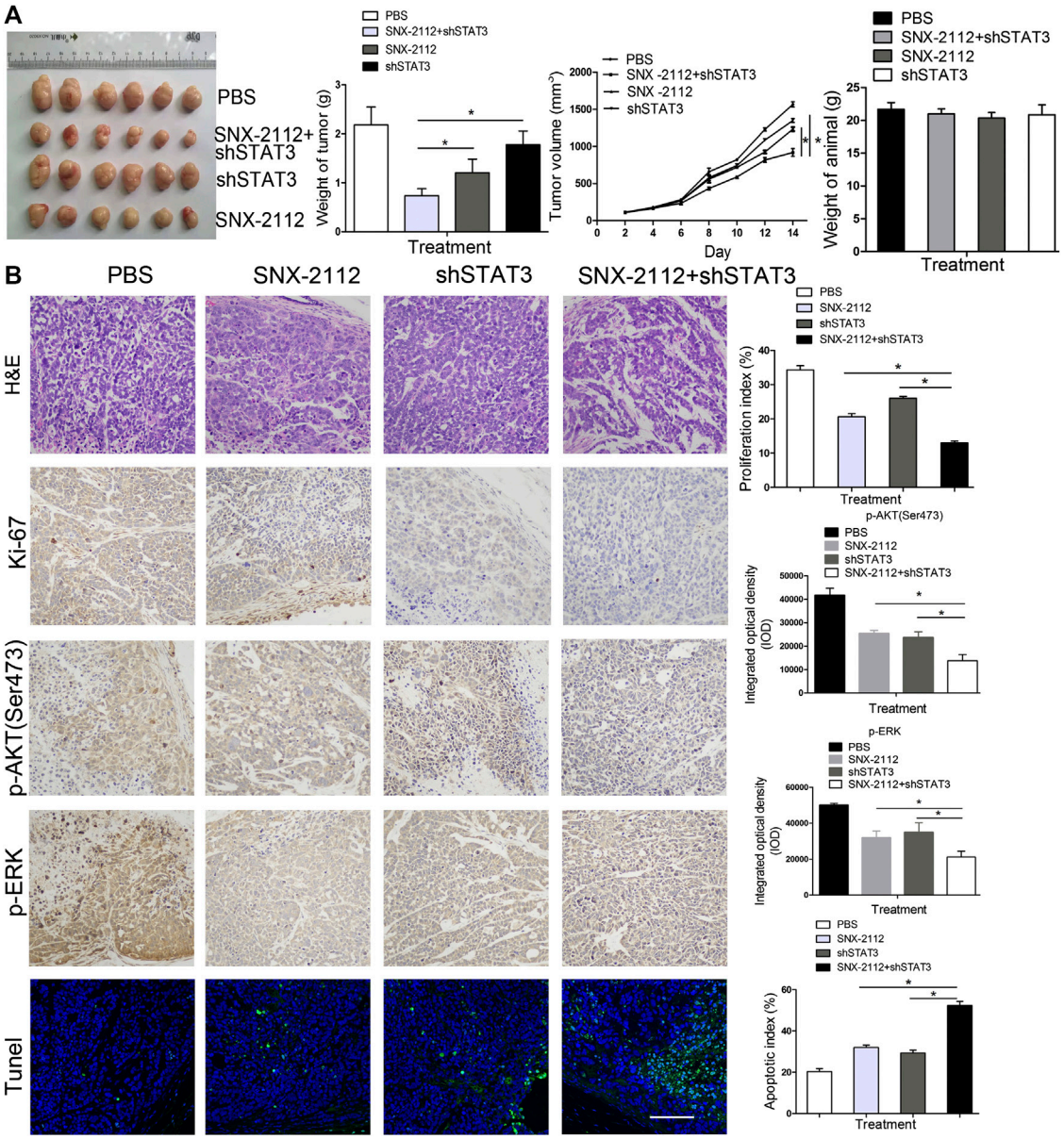

FIGURE 5 | The inhibition of tumorigenicity of ECSLCs by SNX-2112 with shSTAT3 *in vivo* **(A)** Analysis of tumor weight and animal weight. Balb/c nude mice were injected subcutaneously with 1 × 105 ECSLCs transduced with shSTAT3. After 7 days, 10 mg/kg SNX-2112 was intraperitoneally injected into mice. Every other day, the mice were administrated with SNX-2112. Following drug treatment for 2 weeks, animals from each group were euthanized, and the tumors were harvested and measured. Vertical bars represent mean ± SD. **(B)** Expression of Ki-67, *p*-AKT (Ser473) and *p*-ERK proteins in paraffin sections of ECSLCs xenografts analyzed by immunocytochemistry. Sections were counter-stained with hematoxylin (blue nuclei). Representative images of various tumor tissue sections were present. TUNEL analysis of cell apoptosis was present. Scale bar, 100 μm.

2012). In their study, they found that 17-DMAG simultaneously inactivated both AKT and ERK signaling, which were its client proteins, and synergistically potentiated the cytotoxicity of cisplatin (Tatokoro et al., 2012). The glioma tumor-initiating cells were inhibited in a dose-dependent manner by NVP-HSP990, another Hsp90 inhibitor. NVP-HSP990 disrupted cell-cycle control mechanisms by decreased *CDK2* and *CDK4* levels and increased glioma tumor-initiating cell apoptosis levels (Fu et al., 2013). Furthermore, in aggressive hematological tumors, Hsp90 is still a target for anti-tumor therapy. For example, 17-AAG, an Hsp90 inhibitor, induced apoptosis and disrupted transcriptional functionality of HIF1α, which is a client protein of Hsp90, and 17-AAG decreased the colony formation ability of mouse lymphoma CSCs and human myeloid leukemia CSCs (Newman et al., 2012).

Hsp90 inhibitors were initially designed and developed with the rationale that Hsp90 is overexpressed in cancer cells and emerges as a molecular chaperone to many client proteins

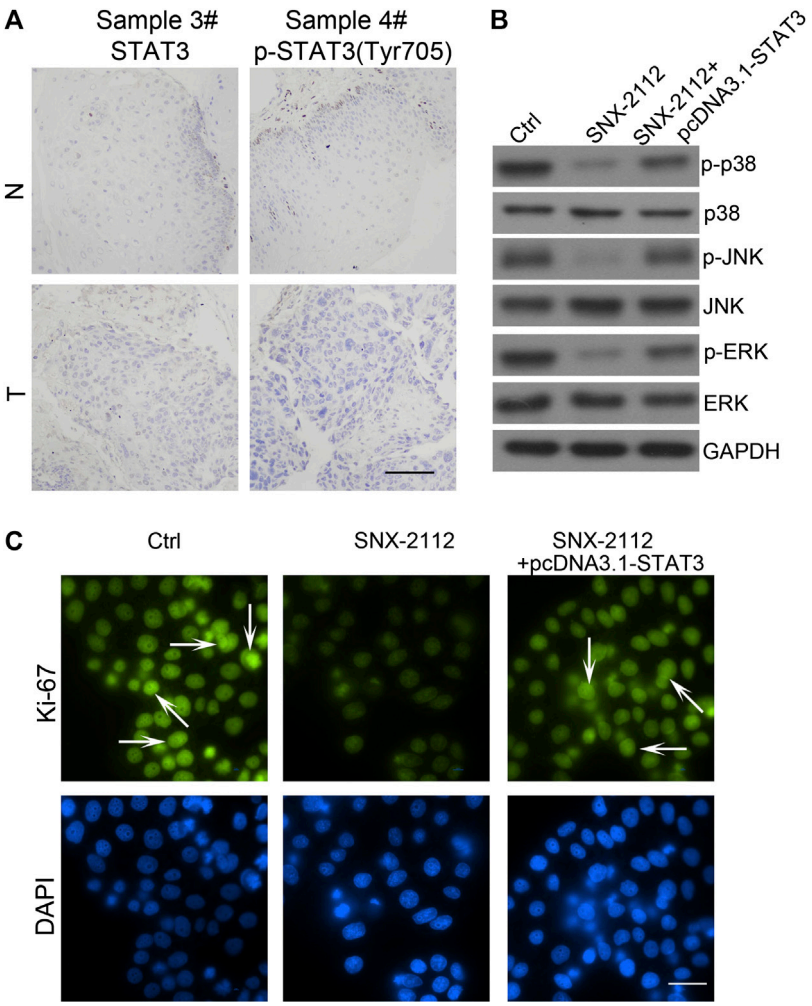

FIGURE 6 | STAT3 overexpression-reducing the efficacy of SNX-2112 **(A)** STAT3 expression was analyzed in tumor specimens compared with adjacent normal tissue. Representative images of various clinical esophageal cancer specimen sections were present. T, tumor tissues; N, normal. Scale bar, 50 μm. **(B)** Western blot analysis of p38, JNK and ERK expression. ECSLCs were transfected with pcDNA3.1-STAT3 vectors for 72 h and then 0.2 μM SNX-2112 for 24 h. GAPDH was used as a loading control. **(C)** The proliferation analysis of ECSLCs treated with pcDNA3.1-STAT3 vectors for 72 h and then 0.2 μM SNX-2112 for 24 h. The cells were collected and incubated with Ki-67 antibody. Scale bar, 50 μm.

(Subramanian et al., 2017). Hsp90-related gene expression is increased in CSCs, which led us to hypothesize that Hsp90 inhibitors may be useful in cancer therapies. Furthermore, Hsp90 inhibitors are more active in tumor cells than in normal tissue, which suggests that these novel inhibitors are likely to preferentially target cancer cell populations and CSCs subpopulations (White et al., 2016; Subramanian et al., 2017). In our study, we demonstrated that treatment with SNX-2112 in combination with shSTAT3 decreased ECSLCs viability and induced ECSLCs apoptosis and cell cycle arrest in G2/M phase. ECSLCs proliferation was significantly inhibited as indicated by reduced colony formation potential and reduced cell viability.

The expression of ABCB1 and ABCG2 was also reduced by treatment with SNX-2112 in combination with shSTAT3. The increased levels of ATP-binding cassette (ABC) transporters is a general mechanism by which cancer cells acquire multidrug resistance in CSCs. High ABCB1 protein expression has been identified as an independent predictor of early recurrence and death for EAC and ESCC patients treated with chemoradiotherapy based on 5-fluorouracil and cisplatin (Zhu et al., 2015). Available studies suggest that expression of several ABC proteins (ABCB1, ABCC2, and ABCG2) correlates with prognosis or response to therapy in esophageal cancer patients (Vrana et al., 2018). Other studies confirmed ABCG2 protein overexpression in the majority (75%) of esophageal cancer tissues and high ABCG2 protein correlates with poor prognosis of ESCC patients (Bharthuar et al., 2014). ABCB1 overexpression has been observed in half of EAC patients whose biopsies were taken before and after treatment with combination of epirubicin, cisplatin and 5-fluorouracil (Narumiya et al., 2011). ABCG2 overexpression accompanied by increased drug efflux rate resulted in resistance

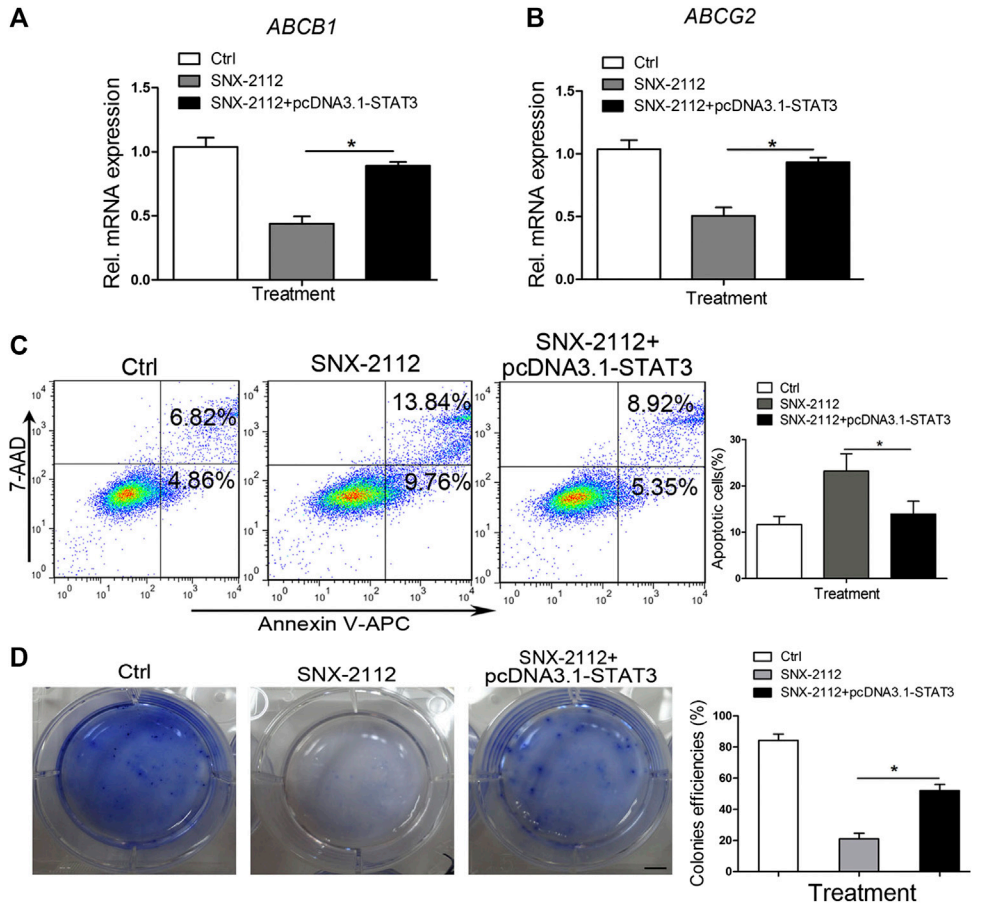

FIGURE 7 | STAT3 overexpression-reversing SNX-2112-induced ECSLCs apoptosis **(A,B)** qPCR analysis of ABCB1 and ABCG2 expression level in ECSLCs. ECSLCs were transfected with pcDNA3.1-STAT3 vectors and after 72 h the ECSLCs were treated with 0.2 μM SNX-2112 for 24 h. **(C)** Flow cytometry analysis of ECSLCs. ECSLCs were treated with pcDNA3.1-STAT3 vectors for 72 h and 0.2 μM SNX-2112 for 24 h. **(D)** The colony formation efficiency analysis of ECSLCs treated with pcDNA3.1-STAT3 vectors and SNX-2112. Approximately 1 × 103 ECSLCs were treated with pcDNA3.1-STAT3 vectors for 72 h and then 0.2 μM SNX-2112 for 24 h. These cells were then cultured on soft agar plates for 14 days, followed by staining with 0.5% crystal violet. Scale bar, 10 mm.

of ECA-109 cell line to doxorubicin *in vitro* (Liu et al., 2014). This resistance could be reversed, through downregulation of ABCG2, by administration of epigallocatechin-3-gallate *in vitro* (Liu et al., 2017). Previous studies have already suggested important role for ABCB1 overexpression in paclitaxel and cisplatin-resistance in radio-resistant EC-9706 ESCC model *in vitro*. Interestingly, the resistance to taxane could be blocked by ABCB1 inhibitor verapamil (Wang et al., 2012). In our studies, we found that ABCB1 and ABCG2 levels were reduced by SNX-2112 with shSTAT3.

Accumulating evidence has demonstrated that STAT3 plays an important role in regulating proliferation, survival, relapse, invasion, and self-renewal of CSCs (Kulesza et al., 2019; Zhang et al., 2019). The JAK/STAT3 axis plays an essential role in promoting tumor initiation and radio-resistance in glioma CSCs (Lin et al., 2018). STAT3 suppression reduced stemness-associated gene expression levels and inhibited colony formation capacity of glioma cells, and the intracranial glioma xenograft growth was effectively impaired (Han et al., 2019). Furthermore, in malignant hematopoietic cell disorders, STAT3 was considered a treatment target, and high STAT3 expression was observed in myelodysplastic syndromes. $CD34^{+}$ cell and STAT3 inhibition by antisense oligonucleotides led to reduced viability and increased apoptosis in leukemic cell lines (Shastri et al., 2018). The targeted delivery of the STAT3 modulator reduced expression levels of several stemness genes, including *MYC*, *BCL2*, *EGFR*, and *MMP9*, and caused a reduction of CD44+/CD24-breast CSCs (Misra et al., 2018). In our previous study, we found that miR-181b and STAT3 interacted and their interaction was key for the proliferation of ECSLCs (Xu et al., 2016). In this study, we found that p-STAT3 (Tyr705) was upregulated in clinical esophageal cancer samples. In addition, we found that the Hsp90 inhibitor combination with shSTAT3 significantly suppressed the proliferation of ECSLCs and induced apoptosis. SNX-2112 with shSTAT3 inhibited ECSLCs tumor growth *in vivo*. Compared with the SNX-2112 group and shSTAT3 group, the tumor weight and volume in the combination group were significantly reduced. The animal body in the combination group was not decreased, which suggested that the reduced tumor weight and volume were due to the effect

of SNX-2112 with shSTAT3. Consistently, The Hsp90 client proteins *p*-ERK and *p*-AKT (Ser473) levels were reduced in the combination group. TUNEL assay demonstrated that the apoptotic effect was obvious in the combination group.

CONCLUSION

In summary, we demonstrated that STAT3 is overexpressed in clinical esophageal cancer samples by RNA sequencing. Combination treatment of SNX-2112 along with shSTAT3 inhibited ECSLCs proliferation, induced ECSLCs apoptosis and cell cycle arrest at G2/M phase, attenuated clonal growth, inhibited phosphorylation of Hsp90 client proteins, and decreased ECSLCs tumorigenicity. STAT3 overexpression reversed the anticancer effects of SNX-2112 in ECSLCs suggesting that the combination treatment of SNX-2112 with shSTAT3 suppresses ECSLCs proliferation through the STAT3 pathway.

DATA AVAILABILITY STATEMENT

The raw data supporting the conclusions of this article will be made available by the authors, without undue reservation, to any qualified researcher.

ETHICS STATEMENT

The patients provided their written informed consent to participate in this study. The use of the clinical specimen for research purposes was approved by the Ethics Committee of Guangdong Food and Drug Vocational College.

AUTHOR CONTRIBUTIONS

D-dX designed the studies, carried out the experiments, performed statistical analyses, and wrote the manuscript; S-hC and Z-dZ read and revised the manuscript; P-jZ and YW analyzed the data and performed bioinformatics analyses. XW and H-qH conceived the study and analyzed the data; Q-yL and XX participated in the design and coordination of the study. Y-fW and RZ designed the study and participated in manuscript development. All authors contributed to manuscript revision and read and approved the submitted version.

FUNDING

This study was supported by the National Natural Science Foundation of China Youth Fund (81702990), Guangdong Medical Research Fund (A2017312, A2018540, A2018238), Science and Technology Project of Guangzhou (201904010050). Natural Science Foundation of Guangdong Province (2017A030313449).

SUPPLEMENTARY MATERIAL

The Supplementary Material for this article can be found online at: https://www.frontiersin.org/articles/10.3389/fphar.2020.532395/full#supplementary-material.

REFERENCES

Acquaviva, J., Smith, D. L., Jimenez, J. P., Zhang, C., Sequeira, M., He, S., et al. (2014). Overcoming acquired BRAF inhibitor resistance in melanoma via targeted inhibition of Hsp90 with ganetespib. *Mol. Cancer Therapeut.* 13(2), 353–363. doi:10.1158/1535-7163.MCT-13-0481

Barta, T. E., Veal, J. M., Rice, J. W., Partridge, J. M., Fadden, R. P., Ma, W., et al. (2008). Discovery of benzamide tetrahydro-4H-carbazol-4-ones as novel small molecule inhibitors of Hsp90. *Bioorg. Med. Chem. Lett.* 18 (12), 3517–3521. doi:10.1016/j.bmcl.2008.05.023

Batlle, E., and Clevers, H. (2017). Cancer stem cells revisited. *Nat. Med.* 23 (10), 1124–1134. doi:10.1038/nm.4409

Bharthuar, A., Saif Ur Rehman, S., Black, J. D., Levea, C., Malhotra, U., Mashtare, T. L., et al. (2014). Breast cancer resistance protein (BCRP) and excision repair cross complement-1 (ERCC1) expression in esophageal cancers and response to cisplatin and irinotecan based chemotherapy. *J. Gastrointest. Oncol.* 5 (4), 253–258. doi:10.3978/j.issn.2078-6891.2014.018

Bocchini, C. E., Kasembeli, M. M., Roh, S. H., and Tweardy, D. J. (2014). Contribution of chaperones to STAT pathway signaling. *JAKSTAT* 3 (3), e970459. doi:10.4161/21623988.2014.970459

Bromberg, J. F., Wrzeszczynska, M. H., Devgan, G., Zhao, Y., Pestell, R. G., Albanese, C., et al. (1999). Stat3 as an oncogene. *Cell* 98 (3), 295–303. doi:10.1016/s0092-8674(00)81959-5

Chatterjee, M., Jain, S., Stuhmer, T., Andrulis, M., Ungethum, U., Kuban, R. J., et al. (2007). STAT3 and MAPK signaling maintain overexpression of heat shock proteins 90alpha and beta in multiple myeloma cells, which critically contribute to tumor-cell survival. *Blood* 109 (2), 720–728. doi:10.1182/blood-2006-05-024372

Chen, X., Lingala, S., Khoobyari, S., Nolta, J., Zern, M. A., and Wu, J. (2011). Epithelial mesenchymal transition and hedgehog signaling activation are associated with chemoresistance and invasion of hepatoma subpopulations. *J. Hepatol.* 55 (4), 838–845. doi:10.1016/j.jhep.2010.12.043

Chen, X., Ying, Z., Lin, X., Lin, H., Wu, J., Li, M., et al. (2013). Acylglycerol kinase augments JAK2/STAT3 signaling in esophageal squamous cells. *J. Clin. Invest.* 123 (6), 2576–2589. doi:10.1172/JCI68143

Cho, T. M., Kim, J. Y., Kim, Y. J., Sung, D., Oh, E., Jang, S., et al. (2019). C-terminal HSP90 inhibitor L80 elicits anti-metastatic effects in triple-negative breast cancer via STAT3 inhibition. *Cancer Lett.* 447, 141–153. doi:10.1016/j.canlet.2019.01.029

Choi, S. A., Lee, J. Y., Phi, J. H., Wang, K. C., Park, C. K., Park, S. H., et al. (2014). Identification of brain tumour initiating cells using the stem cell marker aldehyde dehydrogenase. *Eur. J. Cancer* 50 (1), 137–149. doi:10.1016/j.ejca.2013.09.004

Chung, S. S., Aroh, C., and Vadgama, J. V. (2013). Constitutive activation of STAT3 signaling regulates hTERT and promotes stem cell-like traits in human breast cancer cells. *PLoS One* 8 (12), e83971. doi:10.1371/journal.pone.0083971

da Hora, C. C., Pinkham, K., Carvalho, L., Zinter, M., Tabet, E., Nakano, I., et al. (2019). Sustained NF-kappaB-STAT3 signaling promotes resistance to Smac mimetics in Glioma stem-like cells but creates a vulnerability to EZH2 inhibition. *Cell Death Dis.* 5, 72. doi:10.1038/s41420-019-0155-9

Fu, J., Koul, D., Yao, J., Wang, S., Yuan, Y., Colman, H., et al. (2013). Novel HSP90 inhibitor NVP-HSP990 targets cell-cycle regulators to ablate Olig2-positive glioma tumor-initiating cells. *Cancer Res.* 73 (10), 3062–3074. doi:10.1158/0008-5472.CAN-12-2033

Garon, E. B., Finn, R. S., Hamidi, H., Dering, J., Pitts, S., Kamranpour, N., et al. (2013). The HSP90 inhibitor NVP-AUY922 potently inhibits non-small cell lung cancer growth. *Mol. Cancer Therapeut.* 12 (6), 890–900. doi:10.1158/1535-7163.MCT-12-0998

Han, D., Yu, T., Dong, N., Wang, B., Sun, F., and Jiang, D. (2019). Napabucasin, a novel STAT3 inhibitor suppresses proliferation, invasion and stemness of glioblastoma cells. *J. Exp. Clin. Cancer Res.* 38 (1), 289. doi:10.1186/s13046-019-1289-6

Hang, D., Dong, H. C., Ning, T., Dong, B., Hou, D. L., and Xu, W. G. (2012). Prognostic value of the stem cell markers CD133 and ABCG2 expression in esophageal squamous cell carcinoma. *Dis. Esophagus* 25 (7), 638–644. doi:10.1111/j.1442-2050.2011.01298.x

He, W., Wu, J., Shi, J., Huo, Y. M., Dai, W., Geng, J., et al. (2018). IL22RA1/STAT3 signaling promotes stemness and tumorigenicity in pancreatic cancer. *Cancer Res.* 78 (12), 3293–3305. doi:10.1158/0008-5472.CAN-17-3131

Hosea, R., Hardiany, N. S., Ohneda, O., and Wanandi, S. I. (2018). Glucosamine decreases the stemness of human ALDH(+) breast cancer stem cells by inactivating STAT3. *Oncol. Lett.* 16 (4), 4737–4744. doi:10.3892/ol.2018.9222

Hoter, A., El-Sabban, M. E., and Naim, H. Y. (2018). The HSP90 family: structure, regulation, function, and implications in health and disease. *Int. J. Mol. Sci.* 19 (9), 2560. doi:10.3390/ijms19092560

Itskoviz, D., Tamary, H., Krasnov, T., Yacobovich, J., Sahar, N., Zevit, N., et al. (2019). Endoscopic findings and esophageal cancer incidence among Fanconi Anemia patients participating in an endoscopic surveillance program. *Dig. Liver Dis.* 51 (2), 242–246. doi:10.1016/j.dld.2018.08.010

Jego, G., Hazoume, A., Seigneuric, R., and Garrido, C. (2013). Targeting heat shock proteins in cancer. *Cancer Lett.* 332 (2), 275–285. doi:10.1016/j.canlet.2010.10.014

Jeter, C. R., Liu, B., Liu, X., Chen, X., Liu, C., Calhoun-Davis, T., et al. (2011). NANOG promotes cancer stem cell characteristics and prostate cancer resistance to androgen deprivation. *Oncogene* 30 (36), 3833–3845. doi:10.1038/onc.2011.114

Jhaveri, K., Taldone, T., Modi, S., and Chiosis, G. (2012). Advances in the clinical development of heat shock protein 90 (Hsp90) inhibitors in cancers. *Biochim. Biophys. Acta* 1823 (3), 742–755. doi:10.1016/j.bbamcr.2011.10.008

Kulesza, D. W., Przanowski, P., and Kaminska, B. (2019). Knockdown of STAT3 targets a subpopulation of invasive melanoma stem-like cells. *Cell Biol. Int.* 43 (6), 613–622. doi:10.1002/cbin.11134

Lancet, J. E., Gojo, I., Burton, M., Quinn, M., Tighe, S. M., Kersey, K., et al. (2010). Phase I study of the heat shock protein 90 inhibitor alvespimycin (KOS-1022, 17-DMAG) administered intravenously twice weekly to patients with acute myeloid leukemia. *Leukemia* 24 (4), 699–705. doi:10.1038/leu.2009.292

Le, H. T., Nguyen, H. T., Min, H. Y., Hyun, S. Y., Kwon, S., Lee, Y., et al. (2018). Panaxynol, a natural Hsp90 inhibitor, effectively targets both lung cancer stem and non-stem cells. *Cancer Lett.* 412, 297–307. doi:10.1016/j.canlet.2017.10.013

Lin, J. C., Tsai, J. T., Chao, T. Y., Ma, H. I., and Liu, W. H. (2018). The STAT3/slug Axis enhances radiation-induced tumor invasion and cancer stem-like properties in radioresistant glioblastoma. *Cancers* 10 (12), 512. doi:10.3390/cancers10120512

Liu, K. S., Ding, W. C., Wang, S. X., Liu, Z., Xing, G. W., Wang, Y., et al. (2012a). The heat shock protein 90 inhibitor SNX-2112 inhibits B16 melanoma cell growth *in vitro* and *in vivo*. *Oncol. Rep.* 27 (6), 1904–1910. doi:10.3892/or.2012.1738

Liu, K. S., Liu, H., Qi, J. H., Liu, Q. Y., Liu, Z., Xia, M., et al. (2012b). SNX-2112, an Hsp90 inhibitor, induces apoptosis and autophagy via degradation of Hsp90 client proteins in human melanoma A-375 cells. *Cancer Lett.* 318 (2), 180–188. doi:10.1016/j.canlet.2011.12.015

Liu, L., Zuo, L. F., and Guo, J. W. (2014). ABCG2 gene amplification and expression in esophageal cancer cells with acquired adriamycin resistance. *Mol. Med. Rep.* 9 (4), 1299–1304. doi:10.3892/mmr.2014.1949

Liu, L., Ju, Y., Wang, J., and Zhou, R. (2017). Epigallocatechin-3-gallate promotes apoptosis and reversal of multidrug resistance in esophageal cancer cells. *Pathol. Res. Pract.* 213 (10), 1242–1250. doi:10.1016/j.prp.2017.09.006

Marotta, L. L., Almendro, V., Marusyk, A., Shipitsin, M., Schemme, J., Walker, S. R., et al. (2011). The JAK2/STAT3 signaling pathway is required for growth of CD44(+)CD24(-) stem cell-like breast cancer cells in human tumors. *J. Clin. Invest.* 121 (7), 2723–2735. doi:10.1172/JCI44745

Middleton, D. R. S., Bouaoun, L., Hanisch, R., Bray, F., Dzamalala, C., Chasimpha, S., et al. (2018). Esophageal cancer male to female incidence ratios in Africa: a systematic review and meta-analysis of geographic, time and age trends. *Cancer Epidemiol* 53, 119–128. doi:10.1016/j.canep.2018.01.020

Misra, S. K., De, A., and Pan, D. (2018). Targeted delivery of STAT-3 modulator to breast cancer stem-like cells downregulates a series of stemness genes. *Mol. Cancer Ther.* 17 (1), 119–129. doi:10.1158/1535-7163.MCT-17-0070

Modi, S., Stopeck, A., Linden, H., Solit, D., Chandarlapaty, S., Rosen, N., et al. (2011). HSP90 inhibition is effective in breast cancer: a phase II trial of tanespimycin (17-AAG) plus trastuzumab in patients with HER2-positive metastatic breast cancer progressing on trastuzumab. *Clin. Cancer Res.* 17 (15), 5132–5139. doi:10.1158/1078-0432.CCR-11-0072

Narumiya, K., Metzger, R., Bollschweiler, E., Alakus, H., Brabender, J., Drebber, U., et al. (2011). Impact of ABCB1 C3435T polymorphism on lymph node regression in multimodality treatment of locally advanced esophageal cancer. *Pharmacogenomics* 12 (2), 205–214. doi:10.2217/pgs.10.174

Newman, B., Liu, Y., Lee, H. F., Sun, D., and Wang, Y. (2012). HSP90 inhibitor 17-AAG selectively eradicates lymphoma stem cells. *Cancer Res.* 72 (17), 4551–4561. doi:10.1158/0008-5472.CAN-11-3600

Noh, K. H., Kim, B. W., Song, K. H., Cho, H., Lee, Y. H., Kim, J. H., et al. (2012). Nanog signaling in cancer promotes stem-like phenotype and immune evasion. *J. Clin. Invest.* 122 (11), 4077–4093. doi:10.1172/JCI64057

Nolan, K. D., Kaur, J., and Isaacs, J. S. (2017). Secreted heat shock protein 90 promotes prostate cancer stem cell heterogeneity. *Oncotarget* 8 (12), 19323–19341. doi:10.18632/oncotarget.14252

Pirkkala, L., Nykanen, P., and Sistonen, L. (2001). Roles of the heat shock transcription factors in regulation of the heat shock response and beyond. *FASEB J.* 15 (7), 1118–1131. doi:10.1096/fj00-0294rev

Rajan, A., Kelly, R. J., Trepel, J. B., Kim, Y. S., Alarcon, S. V., Kummar, S., et al. (2011). A phase I study of PF-04929113 (SNX-5422), an orally bioavailable heat shock protein 90 inhibitor, in patients with refractory solid tumor malignancies and lymphomas. *Clin. Cancer Res.* 17 (21), 6831–6839. doi:10.1158/1078-0432.CCR-11-0821

Ross, J. B., Huh, D., Noble, L. B., and Tavazoie, S. F. (2015). Identification of molecular determinants of primary and metastatic tumour re-initiation in breast cancer. *Nat. Cell Biol.* 17 (5), 651–664. doi:10.1038/ncb3148

Sainz, B., Jr., and Heeschen, C. (2013). Standing out from the crowd: cancer stem cells in hepatocellular carcinoma. *Cancer Cell* 23 (4), 431–433. doi:10.1016/j.ccr.2013.03.023

Sancho, P., Burgos-Ramos, E., Tavera, A., Bou Kheir, T., Jagust, P., Schoenhals, M., et al. (2015). MYC/PGC-1alpha balance determines the metabolic phenotype and plasticity of pancreatic cancer stem cells. *Cell Metabol.* 22 (4), 590–605. doi:10.1016/j.cmet.2015.08.015

Sequist, L. V., Gettinger, S., Senzer, N. N., Martins, R. G., Janne, P. A., Lilenbaum, R., et al. (2010). Activity of IPI-504, a novel heat-shock protein 90 inhibitor, in patients with molecularly defined non-small-cell lung cancer. *J. Clin. Oncol.* 28 (33), 4953–4960. doi:10.1200/JCO.2010.30.8338

Shapiro, G. I., Kwak, E., Dezube, B. J., Yule, M., Ayrton, J., Lyons, J., et al. (2015). First-in-human phase I dose escalation study of a second-generation non-ansamycin HSP90 inhibitor, AT13387, in patients with advanced solid tumors. *Clin. Cancer Res.* 21 (1), 87–97. doi:10.1158/1078-0432.CCR-14-0979

Shastri, A., Choudhary, G., Teixeira, M., Gordon-Mitchell, S., Ramachandra, N., Bernard, L., et al. (2018). Antisense STAT3 inhibitor decreases viability of myelodysplastic and leukemic stem cells. *J. Clin. Invest.* 128 (12), 5479–5488. doi:10.1172/JCI120156

Siegel, R. L., Miller, K. D., and Jemal, A. (2020). Cancer statistics, 2020. *CA Cancer J. Clin.* 70 (1), 7–30. doi:10.3322/caac.21590

Solit, D. B., Osman, I., Polsky, D., Panageas, K. S., Daud, A., Goydos, J. S., et al. (2008). Phase II trial of 17-allylamino-17-demethoxygeldanamycin in patients with metastatic melanoma. *Clin. Cancer Res.* 14 (24), 8302–8307. doi:10.1158/1078-0432.CCR-08-1002

Song, K. H., Choi, C. H., Lee, H. J., Oh, S. J., Woo, S. R., Hong, S. O., et al. (2017). HDAC1 upregulation by NANOG promotes multidrug resistance and a stem-like phenotype in immune edited tumor cells. *Cancer Res.* 77 (18), 5039–5053. doi:10.1158/0008-5472.CAN-17-0072

Spreafico, A., Delord, J. P., De Mattos-Arruda, L., Berge, Y., Rodon, J., Cottura, E., et al. (2015). A first-in-human phase I, dose-escalation, multicentre study of HSP990 administered orally in adult patients with advanced solid malignancies. *Br. J. Cancer* 112 (4), 650–659. doi:10.1038/bjc.2014.653

Stivarou, T., Stellas, D., Vartzi, G., Thomaidou, D., and Patsavoudi, E. (2016). Targeting highly expressed extracellular HSP90 in breast cancer stem cells inhibits tumor growth *in vitro* and *in vivo*. *Cancer Biol. Ther.* 17 (8), 799–812. doi:10.1080/15384047.2016.1195041

Subramanian, C., Kovatch, K. J., Sim, M. W., Wang, G., Prince, M. E., Carey, T. E., et al. (2017). Novel C-terminal heat shock protein 90 inhibitors (KU711 and Ku757) are effective in targeting head and neck squamous cell carcinoma cancer stem cells. *Neoplasia* 19 (12), 1003–1011. doi:10.1016/j.neo.2017.09.003

Taipale, M., Jarosz, D. F., and Lindquist, S. (2010). HSP90 at the hub of protein homeostasis: emerging mechanistic insights. *Nat. Rev. Mol. Cell Biol.* 11 (7), 515–528. doi:10.1038/nrm2918

Tatokoro, M., Koga, F., Yoshida, S., Kawakami, S., Fujii, Y., Neckers, L., et al. (2012). Potential role of Hsp90 inhibitors in overcoming cisplatin resistance of bladder cancer-initiating cells. *Int. J. Cancer* 131 (4), 987–996. doi:10.1002/ijc.26475

Vrana, D., Hlavac, V., Brynychova, V., Vaclavikova, R., Neoral, C., Vrba, J., et al. (2018). ABC transporters and their role in the neoadjuvant treatment of esophageal cancer. *Int. J. Mol. Sci.* 19 (3). doi:10.3390/ijms19030868

Wagner, A. J., Chugh, R., Rosen, L. S., Morgan, J. A., George, S., Gordon, M., et al. (2013). A phase I study of the HSP90 inhibitor retaspimycin hydrochloride (IPI-504) in patients with gastrointestinal stromal tumors or soft-tissue sarcomas. *Clin. Cancer Res.* 19 (21), 6020–6029. doi:10.1158/1078-0432.CCR-13-0953

Wang, Y., Trepel, J. B., Neckers, L. M., and Giaccone, G. (2010). STA-9090, a small-molecule Hsp90 inhibitor for the potential treatment of cancer. *Curr. Opin. Invest. Drugs* 11 (12), 1466–1476

Wang, Y., Chen, Q., Jin, S., Deng, W., Li, S., Tong, Q., et al. (2012). Up-regulation of P-glycoprotein is involved in the increased paclitaxel resistance in human esophageal cancer radioresistant cells. *Scand. J. Gastroenterol.* 47 (7), 802–808. doi:10.3109/00365521.2012.683042

Wang, X., Wang, S., Liu, Y., Ding, W., Zheng, K., Xiang, Y., et al. (2014). The Hsp90 inhibitor SNX-2112 induces apoptosis of human hepatocellular carcinoma cells: the role of ER stress. *Biochem. Biophys. Res. Commun.* 446 (1), 160–166. doi:10.1016/j.bbrc.2014.02.081

Wang, S., Du, Z., Luo, J., Wang, X., Li, H., Liu, Y., et al. (2015). Inhibition of heat shock protein 90 suppresses squamous carcinogenic progression in a mouse model of esophageal cancer. *J. Cancer Res. Clin. Oncol.* 141 (8), 1405–1416. doi:10.1007/s00432-014-1896-8

Wang, Y., Zhang, C., Zhu, H., Tang, J., Zhang, S., Luo, J., et al. (2017). CD90 positive cells exhibit aggressive radioresistance in esophageal squamous cell carcinoma. *J. Thorac. Dis.* 9 (3), 610–620. doi:10.21037/jtd.2017.03.28

White, P. T., Subramanian, C., Zhu, Q., Zhang, H., Zhao, H., Gallagher, R., et al. (2016). Novel HSP90 inhibitors effectively target functions of thyroid cancer stem cell preventing migration and invasion. *Surgery* 159 (1), 142–151. doi:10.1016/j.surg.2015.07.050

Williams, K. E., Bundred, N. J., Landberg, G., Clarke, R. B., and Farnie, G. (2015). Focal adhesion kinase and Wnt signaling regulate human ductal carcinoma *in situ* stem cell activity and response to radiotherapy. *Stem Cell.* 33 (2), 327–341. doi:10.1002/stem.1843

Wong, Y. Q., Xu, H., Wu, Q., Liu, X., Lufei, C., Xu, X. Q., et al. (2018). STAT3-Inducible mouse ESCs: a model to study the role of STAT3 in ESC maintenance and lineage differentiation. *Stem Cell. Int.* 2018, 8632950. doi:10.1155/2018/8632950

Xiong, H., Du, W., Wang, J. L., Wang, Y. C., Tang, J. T., Hong, J., et al. (2012). Constitutive activation of STAT3 is predictive of poor prognosis in human gastric cancer. *J. Mol. Med. (Berl.)* 90 (9), 1037–1046. doi:10.1007/s00109-012-0869-0

Xu, D. D., Zhou, P. J., Wang, Y., Zhang, L., Fu, W. Y., Ruan, B. B., et al. (2016). Reciprocal activation between STAT3 and miR-181b regulates the proliferation of esophageal cancer stem-like cells via the CYLD pathway. *Mol. Cancer* 15 (1), 40. doi:10.1186/s12943-016-0521-7

Zhang, Y., Wang, D., Xu, J., Wang, Y., Ma, F., Li, Z., et al. (2019). Stat3 activation is critical for pluripotency maintenance. *J. Cell. Physiol.* 234 (2), 1044–1051. doi:10.1002/jcp.27241

Zhao, J. S., Li, W. J., Ge, D., Zhang, P. J., Li, J. J., Lu, C. L., et al. (2011). Tumor initiating cells in esophageal squamous cell carcinomas express high levels of CD44. *PLoS One* 6 (6), e21419. doi:10.1371/journal.pone.0021419

Zhao, D., Pan, C., Sun, J., Gilbert, C., Drews-Elger, K., Azzam, D. J., et al. (2015). VEGF drives cancer-initiating stem cells through VEGFR-2/Stat3 signaling to upregulate Myc and Sox2. *Oncogene* 34 (24), 3107–3119. doi:10.1038/onc.2014.257

Zhong, Z., Wen, Z., and Darnell, J. E., Jr. (1994). Stat3: a STAT family member activated by tyrosine phosphorylation in response to epidermal growth factor and interleukin-6. *Science* 264 (5155), 95–98. doi:10.1126/science.8140422

Zhu, J., Ling, Y., Xu, Y., Lu, M. Z., Liu, Y. P., and Zhang, C. S. (2015). Elevated expression of MDR1 associated with Line-1 hypomethylation in esophageal squamous cell carcinoma. *Int. J. Clin. Exp. Pathol.* 8 (11), 14392–14400.

Conflict of Interest: The authors declare that the research was conducted in the absence of any commercial or financial relationships that could be construed as a potential conflict of interest.

GLOSSARY

ABC ATP-binding cassette

ALDH aldehyde dehydrogenase

bFGF basic fibroblast growth factor

CSCs cancer stem cells

EAC esophageal adenocarcinoma

ECSLCs esophageal cancer stem-like cells

EGF epidermal growth factor

ERK extracellular signal–regulated kinase

ESCC esophageal squamous cell carcinoma

ESCs embryonic stem cells

HEEC human esophageal epithelial cells

Hsp90 heat shock protein 90

IHC immunohistochemical

JNK c-Jun N-terminal kinase

PMSF phenylmethylsulfonyl fluoride

shSTAT3 knockdown of STAT3

STAT3 signal transducer and activator of transcription 3

TICs tumor-initiating cells

TUNEL terminal deoxynucleotidyl transferase–mediated deoxyuridine triphosphate nick end labeling

17-AAG 17-allylamino-17-demethoxygeldanamycin

frontiers in Oncology

MINI REVIEW
published: 27 January 2021
doi: 10.3389/fonc.2020.539527

Novel Combination Therapies for the Treatment of Bladder Cancer

Mei Peng[1,2†], Di Xiao[2†], Yizhi Bu[2], Jiahui Long[2], Xue Yang[1], Shuhe Lv[1] and Xiaoping Yang[2]*

[1] Department of Pharmacy, Xiangya Hospital, Central South University, Changsha, China, [2] Key Laboratory of Study and Discovery of Small Targeted Molecules of Hunan Province, Department of Pharmacy, School of Medicine, Hunan Normal University, Changsha, China

Bladder cancer is the ninth most frequently diagnosed cancer world-wide and ranks 13th in cancer-related deaths. Two tremendous breakthroughs in bladder cancer therapy over the last decades are the approval of immune checkpoint inhibitors(ICIs)and the fibroblast growth factor receptor tyrosine kinase inhibitor (FGFR-TKI) erdafitinib for treating this deadly disease. Despite the beneficial effects of these approaches, the low response rate and the potential resistance of the cancer are major concerns. Hence, novel combination therapies to overcome these limitations have been investigated. In this context, combining immunotherapy with targeted drugs is an appealing therapeutic option to improve response and reduce the emergence of resistance in the management of bladder cancer. In this review, the rationale of using different therapeutic combinations is discussed according to the mechanistic differences, emphasizing the efficacy and safety based on evidence collected from preclinical and clinical studies. Finally, we highlight the limitations of these combinations and provide suggestions for further efforts in this challenging field.

Keywords: combination therapies, immunotherapy, targeted therapy, chemotherapy, bladder cancer

OPEN ACCESS

Edited by:
Nehad M. Ayoub, Jordan University of Science and Technology, Jordan

Reviewed by:
Yuan Tang, University of Toledo, United States
Hu Liu, Anhui Provincial Cancer Hospital, China

***Correspondence:**
Xiaoping Yang
Xiaoping.Yang@hunnu.edu.cn

†These authors have contributed equally to this work

Specialty section:
This article was submitted to Pharmacology of Anti-Cancer Drugs, a section of the journal Frontiers in Oncology

Received: *01 March 2020*
Accepted: *07 December 2020*
Published: *27 January 2021*

Citation:
Peng M, Xiao D, Bu Y, Long J, Yang X, Lv S and Yang X (2021) Novel Combination Therapies for the Treatment of Bladder Cancer. Front. Oncol. 10:539527. doi: 10.3389/fonc.2020.539527

Abbreviations: ADCs, antibody-drug conjugates; AKT, protein kinase B; APIM, AlkB homologue 2 PCNA-interacting motif; AR, androgen receptor; BCG, bacillus Calmette-Guerin; CTLA-4, cytotoxic T lymphocyte-associated antigen-4; DC, docetaxel with cisplatin; DDR, DNA damage repair; DNMT1, DNA methyltransferase1; EV, enfortumab vedotin; FDA, food and drug administration; FGFR-TKI, fibroblast growth factor receptor tyrosine receptor inhibitor; GC, Gemcitabine plus cisplatin; ICIs, immune checkpoint inhibitors; ICLs, interstrand crosslinks; IFN γ, interferon gamma; IL-15, interleukin-15; IDO, Indoleamine 2,3-dioxygenase; MIBC, muscle invasive bladder cancer; MMC, Mitomycin C; MVAC, methotrexate, vinblastine, doxorubicin and cisplatin; mTOR, mammalian target of rapamycin; NMIBC, non-muscle invasive bladder cancer; NK, natural killer; ORR, objective response rate; OS, overall survival; PARP, poly ADP-ribose polymerase; PD-1, programmed death-1; PD-L1, programmed death-1 ligand 1; PCNA, proliferating cell nuclear antigen; PFS, progression-free survival; PI3K, phosphatidylinositol 3 kinase; PLUMMB, pembrolizumab in muscle-invasive/metastatic bladder cancer; polyICLC, polyinosinic-polycytidylic acid-poly-l-lysine carboxymethylcellulose; PPAR, peroxisome proliferator-activated receptors; pT0, the pathological T0 rate; PTEN, gene of phosphate and tension homology deleted on chromosome ten; RICTOR, Rapamycin-insensitive companion of mTOR; RT, radiation therapy; SoC, standard of care; TAAs, tumor-associated antigens; TACC3, transforming acidic coiled-coil containing protein 3; TAMs, tumor-associated macrophages; TCC, transitional cell carcinoma; Tregs, regulatory T cells; TIL, tumor-infiltrating lymphocytes; TSC, tuberous sclerosis complex; UC, urothelial carcinoma.

INTRODUCTION

Bladder cancer is one of the most prevalent cancers worldwide, with around 430,000 new diagnoses and 150,000 deaths each year (1). Approximately 75% of newly diagnosed patients have non-muscle invasive bladder cancer (NMIBC) with standard treatment of intravesical chemotherapeutic drugs or immune inhibitor after tumor resection (2). However, around 40-50% of patients will experience recurrence within five years of diagnosis with up to 80% in the highest-risk groups (2). The remaining 25% of patients have muscle invasive bladder cancer (MIBC) or metastatic disease and the gold standard therapeutic method is radical cystectomy followed with systemic chemotherapy. However, prognosis in this population of bladder cancer patients is poor and the 5-year overall survival (OS) rate is 15% (3, 4).

The past decade has witnessed the rapid development of combination therapy for improved therapeutic outcomes in bladder cancer. Combination therapy has been a successful strategy to enhance efficacy, increase response, reverse resistance and reduce toxicity as well as address tumor heterogeneity upon using different drugs of different dynamics and molecular targets (5, 6). Previously, the common combination regimens are drugs composed of different chemotherapeutic anticancer drugs or combining chemotherapy with radiotherapy. With comprehensive analysis of bladder cancer cases, molecular characterization is figured out and this provides rationales for novel therapies. NMIBC is primarily presented with FGFR3 alterations while MIBC has a more diverse mutation spectrum (7, 8). High mutational burden in bladder cancer provides implications for the use of targeted and immune checkpoint inhibitors (ICIs). Recently, immunotherapy has become a hot topic since the approval of programmed death-1 (PD-1)/programmed death-1 ligand 1 (PD-L1), cytotoxic T lymphocyte-associated antigen-4 (CTLA-4) ICIs by the U.S. Food and Drug Administration (FDA)with satisfying efficacy in advanced cancers (9, 10). However, low response rate, emergence of drug resistance, and tolerability concerns appeared quickly. The tumor microenvironment significantly influences therapeutic response and efficacy. Thus, combination therapy *via* regulation of immune microenvironment for the purpose of sensitizing drug activity and decreasing doses has been under investigation (11). Another breakthrough is the introduction of erdafitinib, an oral pan-FGFR-targeted tyrosine kinase inhibitor approved by the US FDA in 2019 for treatment of metastatic urothelial carcinoma (UC) patients with susceptible FGFR3 or FGFR2 alterations (12).

In this mini-review, multiple combination regimens including chemotherapy, radiotherapy, targeted therapy, and immunotherapy for treating bladder cancer in preclinical or clinical settings are discussed. This review will provide a comprehensive summary for readers to understand the present and future potential combination therapies in bladder cancer.

IMMUNOTHERAPY

Immune checkpoints refer to inhibitory pathways built into the immune system which are vital to limit collateral tissue damage (that is, the prevention of autoimmunity) under the circumstance of physiological immune responses (13). Immune checkpoints are initiated by ligand-receptor interactions. For example, normal cells harbor PD-L1 bind to PD-1 receptors on T-cells to suppress excessive immune response (14). In addition, the activation of the receptor CTLA-4 located in T cells inhibits the initiation of the immune response by T cells, resulting in the reduction of activated T cells and preventing the formation of memory T cells (15). However, Tumor cells can up-regulate PD-L1 or activate CTLA-4 and this ligand-receptor binding causes inactivation of T cells and tumors escaping the immune response (16). Therefore, the FDA approved ICIs that block the interaction between CTLA-4 and its ligand or block the interaction between PD-1 and PD-L1, thereby restoring cytotoxic T cell immune response in recognizing and destroying cancer cells thus preventing growth of tumors (9, 10). Immunotherapy is approved as a second-line treatment for metastatic urothelial cancer (17). Their use as a first-line agent is only limited to patients who are ineligible for cisplatin-based treatments (17). There is a biological and clinical rationale for using immunotherapy in NMIBC patients. First, the historic use of bacillus Calmette–Guerin(BCG)in NMIBC attests to the effectiveness of immunotherapy for these patients and supports evaluation of other immunotherapy strategies to overcome resistance to BCG. Second, it is well known that genomic and epigenomic alterations drive the pathogenesis of bladder cancer (18), with many alterations thought to provide neoantigens that may elicit potent antitumor immune responses (8, 18). High-grade NMIBC harbors many of the same genomic alterations as muscle invasive and metastatic bladder cancer (8). Tumors with a higher mutational load produce many neoantigens that are recognized as foreign by the immune system, thereby triggering a T-cell mediated antitumor immune response (19). High mutational burden has also been associated with increased efficacy of ICIs (20, 21). From a preclinical perspective, evidence from bladder cancer models in immunocompetent mice supports the use of ICIs alone or in combination with other treatment modalities in bladder cancer (22). From a clinical context, the approval of five inhibitors of the PD-1/PD-L1 axis (atezolizumab, pembrolizumab, nivolumab, durvalumab, and avelumab) for the treatment of advanced or metastatic UC provides a compelling and logical rationale for testing checkpoint blockades in the earlier stage, BCG-unresponsive NMIBC. Although immunotherapy is better tolerated than chemotherapy, autoimmune side effects are be particularly concerning. Simultaneously, based on results from clinical trials, the overall response rate of immunotherapy is ranging from 17% to 23% and indicating that immunotherapy is only effective for a minority of patients. Thus, there is an urgent need to find new therapeutic approaches to improve response rates. Combinations of immunotherapy with conventional agents are being investigated in several preclinical and clinical studies in urothelial cancer. **Table 1** summarizes ongoing clinical trials for ICIs and other novel combination therapies for the management of bladder and urothelial cancers.

Combination of PD-1 With CTLA-4 Inhibitors

It is well established that tumors use PD-1 and CTLA-4 pathways to silence the immune system (16). The CTLA-4 antibody promotes the entry of anti-cancer immune cells into the surrounding tumor

TABLE 1 | Ongoing clinical trials of novel combination therapies in bladder cancer and urothelial cancer.

Study number	Eligibility	Phase	Intervention
NCT01928394	Advanced or metastatic bladder cancer	Phase I/II	Nivolumab and Ipilimumab
NCT03084471	Advanced bladder cancer	Phase III	Durvalumab and Tremelimumab
NCT03219775	Metastatic or advanced transitional cell carcinoma	Phase II	Nivolumab and Ipilimumab
NCT03036098	Unresectable or metastatic UC	Phase III	Nivolumab, Ipilimumab, Gemcitabine/Cisplatin/Carboplatin
NCT02516241	Unresectable stage IV UC	Phase III	Durvalumab and Tremelimumab
NCT04223856	Advanced or metastatic UC	Phase III	EV and Pembrolizumab
NCT03519256	BCG unresponsive high-risk NMIBC	Phase II	Nivolumab, BMS-986205 and BCG
NCT02560636	Advanced bladder cancer	Phase I	Pembrolizumab and radiotherapy
NCT02643303	Bladder cancer	Phase I/II	Tremelimumab, Durvalumab and polyICLC
NCT03473743	Metastatic or advanced UC	Phase Ib-II	Erdafitinib, Cetrelimab and Platinum
NCT03473756	UC	Phase Ib/II	Rogaratinib and Atezolizumba
NCT04172675	High-risk NMIBC	Phase II	Erdafitinib, Gemcitabine/Mitomycin C
NCT03745911	Metastatic UC	Phase II	Paclitaxel and TAK-228
NCT02546661	MIBC	Phase I	Durvalumab, Olaparib, AZD1775 and Vistusertib
NCT03022825	BCG unresponsive high grade NMIBC	Phase II	ALT-803 and BCG

BCG, bacillus Calmette-guerin vaccine; EV, enfortumab vedotin; MIBC, muscle-invasive bladder cancer; NMIBC, non-muscle-invasive bladder cancer; polyICLC, polyinosinic-polycytidylic acid-poly-l-lysine carboxymethylcellulose; UC, urothelial carcinoma.

tissue and eliminates the immunosuppressive cells that promote cancer growth (23). At the same time, the role of PD-1 antibody is to activate these immune cells to prevent tumor cell immune escape (16). Recent data have shown that combination therapy with an anti-PD-1 and anti-CTLA-4 antibodies demonstrated significant preclinical and clinical responses in bladder cancer (24). Duraiswamy et al. provided evidence that reversal of T-cell dysfunction could be achieved by simultaneously targeting effector T cells and regulatory T cells (Tregs). The study showed that co-expression of both PD-1 and CTLA-4 was associated with marked dysfunction of antigen-specific T cells so blockade of PD-1 and CTLA-4 pathways reversed T-cell dysfunction. It proved that adoptive transfer tumor-infiltrating lymphocytes (TIL) that had been pretreated *in vitro* with anti-PD-1 and anti-CTLA-4 antibodies eliminated tumors *in vivo* (25). Furthermore, immunohistochemistry staining for CD3+ T cells in the MC38 tumor model revealed the highest CD3+ T-cell tumor infiltration in the anti-CTLA-4/PD-1 monoclonal antibodies combination setting (26). Higher tumor infiltration likely accounts for CTLA-4/PD synergy. Shi et al. elucidated the underlying tumor rejection mechanisms for the combination therapy of PD-1 with CTLA-4 inhibitors by performing a detailed analysis of human bladder tumor samples together with murine MB49 bladder tumor model (27). The results showed that combination therapy improved tumor rejection by promoting T-cell infiltration into tumors, encouraging the proliferation and polyfunctionality of TILs, and endogenous memory T cells expansion. The interactions among these immune cells are mediated by the interdependent loop between interleukin-7 (IL-7) and interferon gamma (IFN- γ) signaling (27). These provided direct evidence that additional blockade of PD-1 hindered tumor from breaking away from an anti-CTLA-4 inhibitor monotherapy and additional blockade of PD-1 handicapped tumor from getting rid of a-CTLA-4 monotherapy *via* protecting immunity by both T-cell-dependent, and natural killer (NK)/natural killer T (NKT) cell-independent fashions (27). In clinical trials, current PD and CTLA-4 combinations are paired as durvalumab/tremilimumab and nivolumab/ipilimumab. CheckMate-032 assessed nivolumab monotherapy and two combinations of nivolumab and ipilimumab in participants with platinum-refractory advanced bladder cancer. The dosage was variant in the combination groups, with nivolumab 1 mg/kg + ipilimumab 3 mg/kg (n = 26) in one cohort and nivolumab 3 mg/kg + ipilimumab 1 mg/kg (n = 104) in the other. From preliminary data, OS and objective response rate (ORR) were stronger in the cohort receiving a greater ipilimumab dose (10.2 months and 39%) compared to nivolumab monotherapy or the other combination (7.3 months and 26%) (28) (NCT01928394). Optimal sequencing is being tested in TITAN-TCC, in which subjects begin with nivolumab monotherapy induction and, should no response occur, receive boost cycles of nivolumab/ipilimumab (NCT03219775). Potential utility in the first line is being tested in CheckMate-901, previously discussed for its gemcitabine + cisplatin (GC)+ nivolumab arm, is also testing nivolumab/ipilimumab. This combination will be assessed against standard of care (SoC) chemotherapy, and the study aims for an enrollment of 897 (NCT03036098). Multiple umbrella trials are investigating durvalumab/tremelimumab together in advanced cancers. STRONG (NCT03084471) compares a fixed dose regimen of durvalumab 1500 mg + tremelimumab 75 mg to durvalumab 1500 mg monotherapy in advanced cancers including bladder cancer. Subjects will have progressed on prior chemotherapy. Durvalumab/tremelimumab is being compared to SOC chemotherapy in a phase III trial dubbed DANUBE (NCT02516241). Stage IV bladder cancer patients formed the study's population (est. n = 1200) and were randomized 1:1:1 to durvalumab monotherapy, durvalumab with tremelimumab, or chemotherapy (29). This combination was assessed in a phase I/II study of advanced cancers including bladder cancer with the addition of intra-tumoral polyinosinic-polycytidylic acid-poly-l-lysine carboxymethylcellulose, which is a toll-like receptor 3 agonist and a modulator of the tumor microenvironment (NCT02643303).

Combination of Radiation Therapy With Immunotherapy

Radiation therapy (RT) has evolved over the past several decades as a powerful way to treat cancer (30). However, it has some limitations as it alone cannot generate a systemic effect.

Integration of RT with the immunotherapies has been a subject of intense research recently. The rationale behind the combination was initially derived from abscopal effect observations. It is a phenomenon whereby radiation at one site leads to the regression of metastatic cancer at a distant site that has not been exposed to any radiation (31). Advances in immunology have progressed our understanding of the phenomena, and while the mechanism is still not entirely elaborated, the explanation for combining immunotherapy and radiation to increase the frequency of the abscopal effect is irradiation activated cytotoxic T cells to target tumor-associated antigens (TAAs) within human bodies, thereby overcoming the immunosuppressive tumor microenvironment. Furthermore, radiotherapy might increase the response rate of combination by stimulating the accumulation and activation of CD8 + T cells (32) to create a more permissive tumor microenvironment.

Preclinical and clinical trials showed that the combination of the immunotherapy and RT had the potential to provide a synergistic effect in treating cancer, including NMIBC (33). Interestingly, T-cell activity was important for radiation efficacy in tumor control. Wu et al. found that radiation transiently increased PD-L1 expression, and PD-1 or PD-L1 blockade not only led to tumor control, but also enhanced the efficacy of RT, and the combination had increased efficacy compared with either modality alone (34). In addition to improving local control of treated tumors, several recent cases of the abscopal effect with RT published in the literature were in the setting of ICI therapy, suggesting that the combination of ICIs and RT may be the scenario where the abscopal effect may occur with a higher frequency (35, 36). Finally, the combination of immunomodulating agents and RT may result in protective immunologic memory, preventing subsequent recurrences of disease. However, there are many unanswered questions regarding the practical and logistic combination of RT and immunotherapy. For example, the optimal consequence of immunotherapy and RT, the optimal immunotherapy dose, and the duration of radiotherapy need to be clarified. Additionally, details regarding the RT, such as the optimal dose/fractionation, target volume, and site to irradiate are not known (37). Since an inappropriate combination can increase the patient's therapeutic toxicity, the PLUMMB trial (Pembrolizumab in Muscle-invasive/Metastatic Bladder cancer) (NCT02560636) is in a phase I study to test the tolerability of a combination of weekly RT with pembrolizumab in patients with metastatic or locally advanced urothelial cancer of the bladder. In the first dose-cohort, patients received pembrolizumab 100 mg 3-weekly, starting 2 weeks before commencing weekly adaptive bladder RT to a dose of 36 Gy in 6 fractions. The first dose-cohort was stopped after 5 patients, having met the predefined definition of dose-limiting toxicity. Three patients experienced grade 3 urinary toxicities, 2 of which were attributable to therapy. One patient experienced a grade 4 rectal perforation. In view of these findings, the trial had been paused and the protocol would be amended to reduce RT dose per fraction (38). As a result, clinical trials are underway on the optimal combination of radiation and immunotherapy to treat various cancers, including bladder cancer (37). In conclusion, the combination of radiotherapy and immunotherapy has a great prospect (**Figure 1A**).

Combination of IDO1 With Immunotherapy

Indoleamine 2,3-dioxygenase 1(IDO1) enzyme is involved in the catabolism of the essential amino acid tryptophan and plays an important role in immune evasion and tumor growth through production of kynurenine. The IDO1 enzyme is activated in many human cancers including NMIBC (40, 41). Recent data indicate that IDO1 gene expression characterizes a poorly differentiated, more aggressive NMIBC, with IDO1 gene expression in tumor tissues directly correlating with tumor size (R (correlation coefficient) =0.24, p=0.04) and stage (R=0.25, p=0.03) (41). Moreover, there was a trend toward longer OS in patients with tumors that did not express IDO1. IDO inhibitors such as BMS-986205, epacadostat, indoximod, navoximod, and HTl-1090 are in various stages of clinical development in several cancers. There is evidence supporting an interrelationship between the PD-1/PD-L1 and IDO1 axes, with IDO functional activity linked with increased PD-L1 positive cytotoxic T-cells and increased CTLA4 expression by regulatory T cells (42). Therefore, it has been proposed that parallel inhibition of these pathways may lead to a more effective activation of T cell mediated antitumor immune response.

Indeed, in an advanced bladder cancer cohort (n=29) of an ongoing multi-arm, phase I/IIa dose-escalation and expansion study (CA017-003), treatment with oral BMS-986205 (100 or 200 mg once daily) in combination with nivolumab (2 schedules) resulted in an ORR of 34% and disease control rate of 48%. The ORR was 38% in patients with no prior immunotherapy (n=26), 47% in patients with tumor PD-L1 1% (n=15), and 27% in those with tumor PD-L1 <1% (n=11). The authors reported that the combination of BMS-986205 plus nivolumab was well tolerated (43). Preliminary phase I/II results of the ECHO-202/KEYNOTE-037 trial also demonstrated that oral epacadostat plus pembrolizumab was well tolerated and yielded an ORR of 35% in patients with advanced UC (43). Preliminary antitumor signals in the advanced UC cohort of the CA017-003 study and the ECHO-202/KEYNOTE-037 study are suggestive of potential activity in bladder cancer (44). Based on these data, the aforementioned CheckMate 9UT trial has been designed to investigate four different treatment regimens (nivolumab alone, nivolumab plus BCG, nivolumab plus BMS-986205, or nivolumab plus BMS-986205 and BCG) in BCG-unresponsive, high-risk NMIBC (NCT03519256)

Combination of PARP Inhibitors With Immunotherapy

Poly ADP-ribose polymerase (PARP) inhibitors (PARPi), such as Olaparib, amplifies the DNA damage, augments the mutational burden and promotes the immune priming of the tumor by increasing the neoantigen exposure and increasing tumor-infiltrate T lymphocytes (45). Studies also reported that defects in DNA damage repair (DDR) genes could be potential predictive biomarkers of clinical response to ICIs in metastatic urothelial bladder cancer (46, 47). However, the use of PARPi

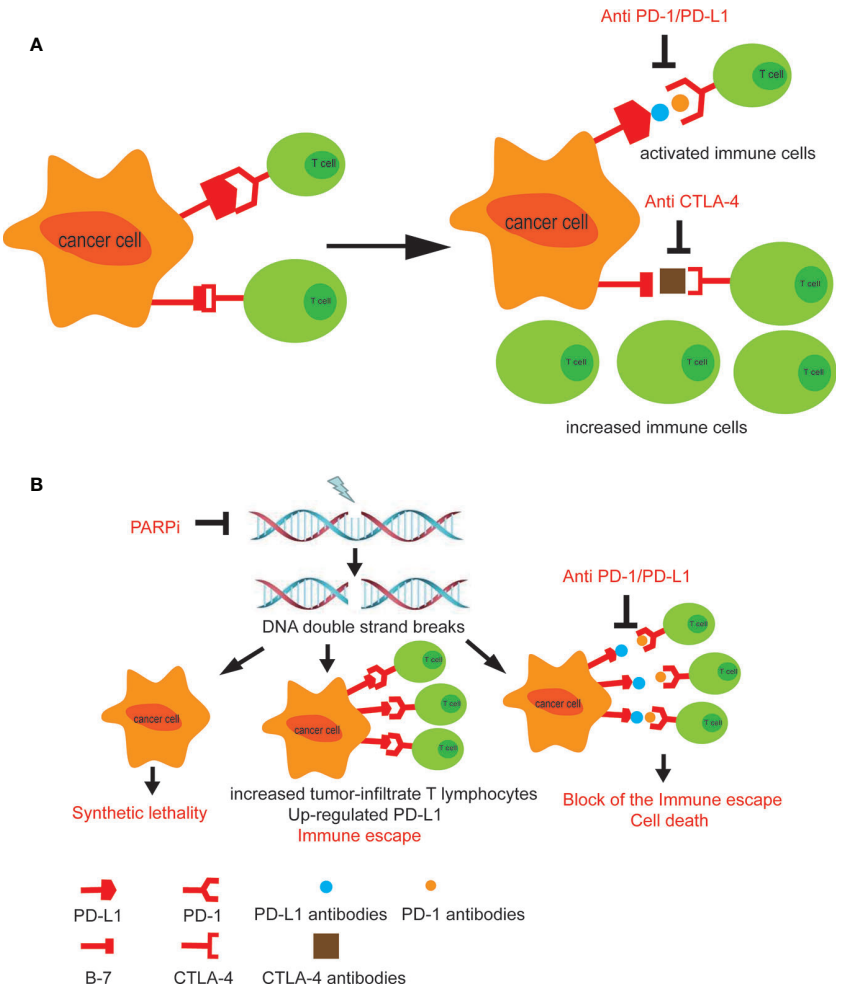

FIGURE 1 | **(A)** The combined use of CTLA-4 and PD-1 inhibitors promotes anti-cancer immune cells to enter the surrounding of the tumor tissue and activates immune response. **(B)** The treatment of PARP inhibitors leads to PD-L1 upregulation in tumor cells. Combining PARP inhibitors with immunosuppressants blocks tumor immune escape (39).

can also lead to upregulation of PD-L1 in tumor cells, leading to tumor immune escape. Therefore, the combination of PARPi and immunosuppressants will benefit patients including those with bladder cancer. Interestingly, a more recent study, in 60 patients with advanced UC, had indicated that defects in DDR pathways may enrich for antitumor responses to anti–PD-1/L1 (48). In this study, patients with a deleterious alteration in at least one of 34 DDR genes showed a response rate of 80% versus only 18.8% in patients lacking these alterations. Thus, the combination of PARPi and the anti-PD/PD-L1 targeting may represent a promising strategy for bladder cancer treatment (39) (NCT02546661). Ross et al. summarized available data and found that combinations of PARPi and anti–PD-1/L1 agents were well tolerated and demonstrated antitumor activity in a range of tumor types (49). An open-label randomized multidrug biomarker-directed phase Ib study, the BISCAY trial, was designed to evaluate the effects of the treatments with the PARPi Olaparib as a single agent therapy, or in association with the ICI durvalumab (anti-PD-L1 antibody), for treatment of urothelial bladder cancer patients who had progressed from prior treatment and also presented defects in DNA-repair genes (NCT02546661) (**Figure 1B**).

Epigenetics is defined as a heritable modification to DNA without alteration in the nucleotide sequence, resulting in altered gene transcription and chromatin structure. Epigenetic modifications include DNA methylation and post-translational histone modifications involving methylation or acetylation are common in bladder tumors. Growing evidence showed that epigenetic drugs, such as DNA methyltransferase inhibitors can upregulate immune signaling through demethylation of endogenous retroviruses and cancer testis antigens. It provides a strong rationale for the combination of epigenetic drugs with ICIs (50, 51). Interestingly, RRx-001, not only a new DNA damage inducer, but also an epigenetic and immunomodulatory drug, has

been recently investigated as single chemotherapeutic agent to re-sensitize tumor to prior therapy (52–54). The low toxicity profile of RRx-001 differentiates this agent from conventional anticancer drugs, such as chemotherapeutics, and epigenetic agents (54, 55). Indeed, RRx-001 is able to trigger DNA damage response in urothelial bladder cancer cells, reducing the DNA methyltransferase1(DNMT1) levels and increasing the transcriptional levels of the interferon type III and the interferon stimulated genes (56). Thus, it enhances the sensitivity to ICIs. Criscuolo D et al. investigated the effects of combining three classes of drugs together with epigenetic agents and immune-checkpoint inhibitors in bladder cancer for the purpose of reducing toxicity and doses of monotherapy alone (39).

Combination of Antibody-Drug Conjugates (ADSs) With Immunotherapy

The response of immunotherapy is a big concern in clinic. The combination of ADCs with immunotherapy attempts to increase patients' overall response rate. ADCs are monoclonal antibodies conjugated to cytotoxic agents through a chemical linker, which can achieve selective targeting of cancer cells (57). In December 2019, the United States Food and Drug Administration (FDA) approved the first ADCs, enfortumab vedotin (EV), for the treatment of platinum-refractory and immune checkpoint blockade-refractory locally advanced or metastatic UC. A phase I study of EV in 112 patients with immunotherapy and platinum refractory metastatic UC treated at the 1.25mg/kg dose level indicate a 43% confirmed ORR, including five complete responses (50).

A phase 1b study (58) investigating combination of EV (1.25 mg/kg) plus pembrolizumab (200mg) for cisplatin-ineligible patients with metastatic UC. The preliminary data showed that patients tolerated it well and achieved a response rate of 73.3% (59). Based on the efficacy observed in the trial, a randomized phase III study (NCT04223856) of EV and pembrolizumab with or without platinum-based chemotherapy for the first-line treatment of locally advanced or metastatic urothelial cancer was initiated (60).

TARGETED THERAPY

Targeted therapy is a revolutionary treatment which can prevent the growth, progression, and metastasis of cancer by interfering with specific molecules. This therapy has achieved satisfactory results in the treatment of various cancers, such as breast cancer and colon cancer (61). However, the contribution of targeted drugs in UC is very limited due to the lack of efficacy or treatment-related toxicity.

Targeted therapies have not been added to the crucial backbone of the treatment in bladder cancer so far. Comprehensive analyses of MIBC samples, expanding from 131 to 412, identified significantly mutated genes, including FGFR3, phosphatidylinositol 3 kinase (PI3K)/protein kinase B (AKT) pathway, Peroxisome proliferator-activated receptors (PPAR) γ mutations, DNA repair, p53 and cell cycle (7, 62). The good news is that, in April of 2019, the US FDA approved erdafitinib as an oral pan-FGFR-targeted agent indicated for metastatic urothelial cancer (UC) patients with susceptible FGFR3 or FGFR2 alterations (12). Despite genomic instability, molecular heterogeneity, and pathway redundancy still presenting challenges to targeted therapies in bladder cancer, researchers are making strategies to improve efficacy. Here, we present the combination effects of targeted therapies with other drugs in preclinical settings (**Figure 2**).

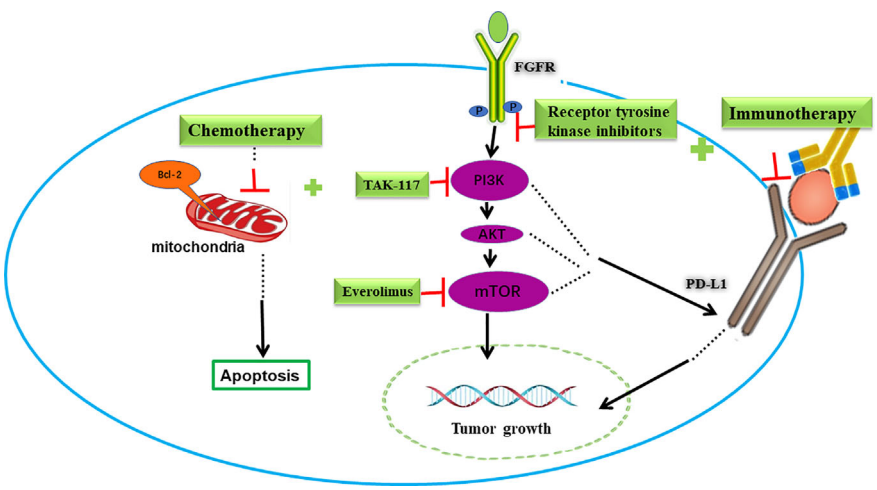

FIGURE 2 | Combination of targeted therapy with immunotherapy or chemotherapy in bladder cancer. FGFR and PI3K/AKT/mTOR signing pathways are potential targets in bladder cancer. Blocking FGFR or PI3K/AKT/mTOR pathway decreased PD-L1 levels and increased immunotherapy response. On the other hand, these targeted drugs increased the pro-apoptotic effect and cytotoxic effect of chemotherapy drugs.

Combination of FGFR Inhibitors With Immunotherapy

Erdafitinib, as the first TKI approved in UC therapy, has been demonstrated to be beneficial in clinical trials. Similar to other targeted drugs, toxicity and drug responses become concerns. Research has suggested that the presence of an antitumor T-cell response is fundamental for the activity of immunotherapy (63). Recently, Sweis et al. showed that UC can be divided into T-cell-inflamed and non-T-cell-inflamed subtypes. The latter phenotype correlated with a resistance to ICIs, but was also linked to FGFR3 mutation, providing a rationale for combining FGFR inhibitors and anti-PD-1/PD-L1 (64). Preliminary data in the FIERCE-22 study showed that the ORR was 36% in the overall population, and a response was observed in both wild type (ORR33%) and mutated (ORR 43%) FGFR3 patients receiving vofatamab (FGFR3 inhibitor) and pembrolizumab (anti-PD-1) (65). Powles et al. conducted a phase I study (NCT02546661) enrolled with platinum-resistant and ICI naïve patients with A/M UC harboring FGFR mutations (66). However, the results showed that AZD4547 (FGFR1-3 inhibitor) plus durvalumab increased response modestly compared to AZD4547 alone (n=21, ORR 29% versus n=15, ORR 20%, respectively), suggesting that the tumor mutations burden might contribute rather small differences to ICI response. A phase Ib/II study of rogaratinib combined with atezolizumab in patients with untreated FGFR-positive UC is currently in progress (NCT03473756). Likewise, the safety and efficacy of erdafitinib plus JNJ-63723283 (an anti-PD-1 monoclonal antibody) are investigated by a phase Ib/II study (NCT03473743) in advanced UC patients with FGFR gene alterations.

FGFR inhibitors may induce tumor environment changes and sensitize ICIs. However, FGFR alterations in UC contribute to intrinsic resistance to FGFR inhibitors. Thus, some patients with FGFR point mutations or fusions did not respond to erdafitinib or other FGFR inhibitors. Lima et al. observed activating FGFR3 mutants and FGFR3-TACC3 (transforming acidic coiled-coil containing protein 3) fusion constitutively elevated Src levels (67). Low dose dasatinib sensitized UC to FGFR TKIs, implying that the combination of FGFR with Src inhibitors may overcome intrinsic resistance compared with FGFR TKI monotherapy.

Combination of PI3K/AKT/mTOR Inhibitors With Immunotherapy or Chemotherapy

The PI3K/AKT/mammalian target of rapamycin (mTOR) pathway is an important signal pathway closely related to protein synthesis, cell growth, survival and tumorigenesis (68). The deregulation of this signaling pathway is present in 42% of UC, including mutations, copy number alterations, or RNA expression changes (62). Despite the frequent deregulation, clinical trials using PI3K/mTOR inhibitors have not shown prominent success. The PIK3CA gene is an oncogene that implicates the overactivation of the PI3K/AKT/mTOR pathway. Recurrent somatic mutations of PIK3CA increase the activity of PI3Ks and the loss of phosphatase and tension homolog (PTEN, a tumor suppressor that inhibits PI3K) also can result in the overactivation of the PI3K/AKT/mTOR pathway (69).

A study in human glioma suggested that the loss of PTEN and the consequent upregulation of the PI3K-AKT pathway increased the expression of PD-L1 post-transcriptionally, thus promoting immune resistance (70). Additionally, other reports validated this resistance in melanoma, prostate and breast cancers, making the inhibition of PI3K-AKT pathway a potential strategy to overcome immunotherapy-resistance (71, 72).

Recently, a study showed that the PIK3CA mutation correlated with immune cell infiltration. In human urothelial bladder cancer samples, the expression of the immune gene signature which represents the immune cell infiltration in PIK3CA-mutated tumors was significantly lower than that of wild type counterparts. It means PIK3CA-mutated tumors may show lower response to ICIs therapy. In a humanized mouse model of bladder cancer with PIK3CA mutation, the treatment of BKM120(a pan-PI3K inhibitor) increases the expression of chemokines and immune genes. Notably, compared to the single treatment, BKM120 combined with Nivolumab (an anti-PD-1antibody) significantly inhibited the growth of PIK3CA-mutated tumors (73). And a clinical trial is now investigating the therapeutic promise of durvalumab (an antibody that blocks PD-L1) in combination with vistusertib (AZD2014) in MIBC patients with rapamycin-insensitive companion of mTOR (RICTOR) amplification, or tuberous sclerosis complex (TSC) 1/1 mutation. (NCT02546661 module E)

Chemotherapy drugs kill tumor cells primarily through the induction of apoptosis. The activation of PI3K/AKT/mTOR pathway in tumor cells reduces the pro-apoptotic effect and the cytotoxic effect of chemotherapy drugs, leading to resistance (74). Therefore, inhibition of this signaling pathway may enhance the sensitivity of chemotherapy drugs.

Zeng et al. reported that in the patient-derived xenograft models with a PI3K mutation or amplification, the combination groups (pictilisib with cisplatin and/or gemcitabine) achieved significant delay of tumor growth and increased survival compared with any single drug (pictilisib/cisplatin/gemcitabine) (75). When combining TAK-228 (an oral mTORC1/2 inhibitor) with TAK-117 (PI3Kα inhibitor) or with paclitaxel, strong synergistic effect was also observed in preclinical bladder cancer models (76). These results facilitate a clinical trial to investigate efficacy of TAK-228 plus paclitaxel in patients with metastatic bladder cancer (NCT03745911). Similar results were obtained through combining the PI3K/mTOR dual inhibitor NVP-BEZ235 with cisplatin in osteosarcoma, triple negative breast cancer and bladder cancer (77, 78). Moon et al. demonstrated that when NVP-BEZ235 was used in combination to treat cisplatin-resistant T24R2 cells, the IC_{50} of cisplatin and NVP-BEZ235 could be reduced by 3.6- and 5.6-fold, respectively (79).

However, the results of clinical trials seem to be inconsistent. A phase II trial of BEZ235 evaluated in 20 advanced bladder cancer patients after failure of platinum-based therapy conveyed a modest activity but a hostile toxicity with 50% grade 3-4 adverse effects (80). Single-agent mTOR inhibitor temsirolimus and everolimus also showed limited efficacy (81, 82), whereas one patient carrying a TSC 1-inactivating mutation treated with

everolimus had notable tumor shrinkage and durable response, suggesting the blockade of the PI3K/mTOR axis could improve outcome in some specific patients (83). The role of paclitaxel/everolimus combination in metastatic UC was investigated in the phase II AUO AB 35/09 trial, and the results were modest (PFS was 2.9 months, 3 months and ORR 13%) (84). Thus, better understanding of the molecular landscape of these tumors and more precise patient selection might be helpful for a more rational design of combination therapy.

CHEMOTHERAPY

Chemotherapy is a routine treatment in cancer. There are two different chemotherapeutic routes in bladder cancer, including intravesical BCG/MMC for NMIBC and systemic chemotherapies for MIBC. Although it has brought benefits to patients in the past decades, intolerant toxicity needs to be improved. Novel combinations of chemotherapeutic drugs with others are studied.

Combination of Interleukin-15 Super-Agonist With BCG

Interleukin-15 (IL-15) is implicated in the development, proliferation, and activation of effector NK cells and CD8+ memory T cells. However, its short half-life, high dose requirement for clinical activity, and prohibitive toxicity represent barriers for successful clinical trial development (85). To overcome these shortcomings, ALT-803 was developed as a novel fusion complex. Recombinant IL-15, a super-agonist due to an activating N72D mutation, is bound to the soluble receptor IL-15RαSushi-Fc. This complex has improved bioavailability, increased serum half-life, longer retention in lymphoid organs, and *in vivo* biological activity up to 25 times that of native IL-15. ALT-803 has demonstrated potent immunostimulatory effects in terms of triggering a local cytokine response as well as activating NK and CD8+ T cells in animal models (85). In a carcinogen-induced rodent NMIBC tumor model, intravesical ALT-803 plus BCG treatment reduced tumor burden by 46% vs ALT-803 (35%) or BCG (15%) alone (86). An ongoing multicenter, open-label, single-arm phase II trial (QUILT-3.032) is evaluating ALT-803 in combination with BCG administered *via* intravesical instillation in patients with BCG-unresponsive NMIBC (NCT03022825). Recently presented preliminary results indicate that six of the seven evaluable patients with BCG-unresponsive carcinoma *in situ* achieved a CR at the 12-week response assessment (87).

Combination of Chemotherapeutic Drug MMC With BCG/Gemcitabine

BCG and Mitomycin C (MMC) are representatives of clinical intravesical immunotherapy and chemotherapy drugs for NMIBC.

A randomized prospective trial involved 407 patients with intermediate- to high-risk NMIBC found that sequential combination of MMC plus BCG is more effective but more toxic than BCG alone. Thus, it was recommended to patients with a high likelihood of recurrence, such as those with recurrent T1 tumors (88). Another study including 151 patients with high-risk NMIBC demonstrated outstanding efficacy for sequential BCG and EMDA-MMC (Electro Motive drug administration of MMC). The complete-response rate was 87%, with 86% and 93% remaining disease-free at one and two years respectively which is better than any previously published outcomes in this disease (89).

Gemcitabine is a pyrimidine analogue that incorporates into actively replicating DNA and thereby prevents further synthesis, whereas MMC cross-links DNA moieties to prevent synthesis (90). In addition, MMC is a vesicant to the urothelium, which could increase permeability to subsequent gemcitabine administration through its irritating action. So, it is available to combine MMC with gemcitabine as a possibly effective way to enhance mutual absorption and control tumor progression (91). Sequential intravesical gemcitabine and MMC in NMIBC patients appeared to be well tolerated and yielded a response in a good proportion of patients with recurrent BCG refractory bladder cancer or who are not surgical candidates (92).

Furthermore, combination of MMC with other novel methods also suggests improved treatment effect. Proliferating cell nuclear antigen (PCNA) is an essential scaffold protein in multiple cellular processes including DNA replication and repair (93). More than 200 proteins, many involved in stress responses, interact with PCNA through the AlkB homologue 2 PCNA-interacting motif (APIM), including several proteins directly or indirectly involved in repair of DNA interstrand crosslinks (ICLs) (94). Gederaas et al. targeted PCNA with a novel peptide drug containing the APIM sequence, ATX-101, to inhibit repair of the DNA damage introduced by the chemotherapeutics. Results showed that ATX-101 increased the anticancer efficacy of the ICL-inducing drug MMC and ATX-101 given intravesically in combination with MMC penetrating the bladder wall and further reducing the tumor growth in both the slow growing endogenously induced and the rapidly growing transplanted tumors (95). Survivin inhibits apoptosis and enables tumor cells to escape from therapy-induced senescence. High expression of survivin is associated with bladder cancer aggressiveness and recurrence. Cui et al. demonstrated that silencing survivin enhanced activity of MMC in human bladder RT4 xenografts, representing a potentially useful chemo-gene therapy for bladder cancer (96). These data indicate that combination of MMC can be a useful approach to improve the effect of chemotherapy.

Platinum-Based Combination Treatment

Chemotherapy with MVAC (methotrexate, vinblastine, doxorubicin, and cisplatin) or GC (Gemcitabine plus cisplatin) are considered the gold standard of care for MIBC. To improve efficacy and reduce toxicity, clinical researchers are still trying to develop new combinations. Taxanes, including paclitaxel, docetaxel and derivatives with taxane structure, are well-known antitumor drugs. Combination of platinum with taxanes has emerged as an alternative option for MIBC patients (97).

Apart from combination of clinically available chemotherapeutic agents, several preclinical trials focusing on novel mechanisms that can improve efficacy and sensitize chemoresistance of cisplatin have been studied. Obatoclax, a BH3 mimetic which inhibits pro-survival Bcl-2 family members, can inhibit cell proliferation, promote apoptosis, and significantly enhance the effectiveness of cisplatin in MIBC cells *via* inhibiting Bcl-2 and Bcl-xL and decreasing cyclin D1 and Cdk4/6 expression levels (98). This finding can help validate Obatoclax as a cell cycle inhibitor and increase the attractiveness of Obatoclax as an anti-cancer drug. Enzalutamide, a synthetic androgen receptor (AR) signaling inhibitor, synergistically inhibited growth of bladder cancer cells more efficiently when combined with cisplatin. This supports the feasibility for future investigation of AR antagonists in combination with standard chemotherapy in MIBC (99). Besides, obtained data *via* an epigenomic approach suggested that Homeobox A9 promoter methylation could serve as a potential predictive biomarker and decitabine might sensitize resistant tumors in patients receiving cisplatin-based chemotherapy, but clinical trials are needed to confirm this conclusion (100).

DISCUSSION

As we stated above, due to the efforts of the scientific community, the management of bladder cancer, especially for advanced patients, has made great progress recently despite the slow rate of development (101). Two milestones, the application of ICIs and approval of oral FGFR-TKI erdafitinib have made tremendous progress (12, 17). ICIs bring a revolutionary impact on patients with durable outcomes in a subset of individuals with tolerable adverse event profiles (12). More importantly, marked advances to understand the molecular interplay within the immune environment have been generated in the past decades (63, 64). Thus, combination of immunotherapy with other therapies has been designed to improve efficacy, increase responses and reduce toxicity. Simultaneously, antibody-drug conjugates represent a new therapeutic modality in urothelial cancer. Enfortumab vedotin (EV), is the first antibody-drug conjugate, which gained approval in December, 2019 in advanced UC. Clinical trials seek to improve its efficacy *via* novel combinations such as combining EV with immunotherapy drugs. There are also new ADCs under investigation and showing promise. Although the results show that combination therapies produce encouraging outcomes, there are still several unsolved issues. First, the detailed mechanisms of each ICIs need to be investigated. Second, biomarkers are required to analyze through molecular diagnosis helping in understanding patient-specific immune-suppression. Third, toxicity should be tolerable with proper drug doses and irradiation duration time.

The approval of FGFR-TKI erdafitinib made a breakthrough for metastatic bladder cancer targeted therapy. Combination of FGFR-TKI with ICIs has the potential to overcome drug-resistance barriers as well as augment immunogenicity of the tumor – even in patients who lack response to ICIs monotherapy (65). As pointed out in the previous section, PI3K/AKT/mTOR pathway plays an important role in bladder tumorigenesis, conferring PI3K/AKT/mTOR potential targets in bladder cancer. Unfortunately, clinical results of these targeted inhibitors, alone or in combination, are not very encouraging so far (80–82). The possible reason is that the molecular landscape and pathophysiology of patients were not fully and deeply understood. Thus, assays such as genome sequencing and immunohistochemical analyses could be employed to select appropriate patients.

Intravesical drugs including BCG and MMC, the clinical guidelines recommended for NMIBC after tumor resection have been clinically used for a long time (102, 103). The past decades witnessed their benefits to patients. However, recurrence has been a big challenge all the time for these administration strategies. New multiagent intravesical chemotherapy regimens

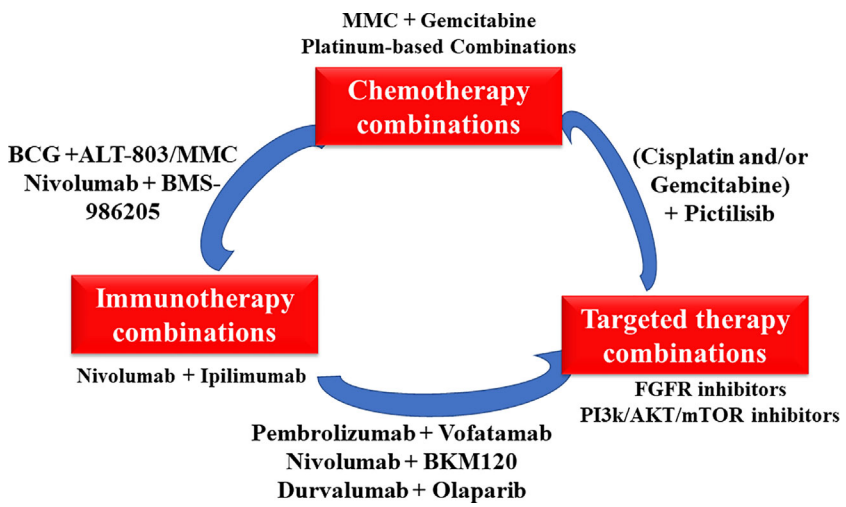

FIGURE 3 | The overview of various novel combinations in bladder cancer.

for instance, either interleukin-15 super-agonist or MMC with BCG have been developed in recent years, dramatically enhancing antitumor activity of BCG (2). Either GC or MVAC is well-accepted neoadjuvant chemotherapies for MIBC (104). As stated above, pathologic information of patients largely helps medical doctors to make the decision to choose either GC or MVAC to treat bladder cancer patients, depending on molecular characteristics of individuals (105).

In addition, intravesical administration route is a particular way for bladder cancer treatment due to the unique physiological features of urinary bladders. The strategy increases the local concentrations within the bladder and avoids the systemic toxicity of drugs. Due to the possible interactions among drugs, the physical and chemical profiles of drugs should be carefully considered when combining.

CONCLUSIONS

In conclusion, combination therapy is a classic and proven strategy to improve patients' survival. Many combination therapies as shown in **Figure 3** such as dual immunotherapies and alternate ICIs with targeted therapies are understudied, holding considerable promise for treating bladder cancer. The revolution of bladder cancer treatment will keep moving forward with a good understanding the biology of bladder cancer based on rapid drug development.

AUTHOR CONTRIBUTIONS

MP and XiY designed this study, wrote and revised the manuscript. DX, YB, JL, XuY, and SL prepared the literatures and drafted the manuscript. All authors contributed to the article and approved the submitted version.

FUNDING

This research was funded by National Natural Science Foundation of China (81703008,81874212), Huxiang High-Level Talent Innovation Team (2018RS3072), Major Scientific and Technological Projects for Collaborative Prevention and Control of Birth Defect in Hunan Province (2019SK1012).

REFERENCES

1. Torre LA, Bray F, Siegel RL, Ferlay J, Lortet-Tieulent J, Jemal A. Global cancer statistics, 2012. *CA Cancer J Clin* (2015) 65(2):87–108. doi: 10.3322/caac.21262
2. Brooks NA, O'Donnell MA. Combination Intravesical Therapy. *Urol Clin* (2020) 47:83–91. doi: 10.1016/j.ucl.2019.09.010
3. Aragon-Ching JB, Ryan PW, Anthony LZ, Gary DS. Multidisciplinary Management of Muscle-Invasive Bladder Cancer: Current Challenges and Future Directions. *ASCO Educ Book* (2018), 307–17. doi: 10.1200/EDBK_201227
4. Gakis G. Management of Muscle-invasive Bladder Cancer in the 2020s: Challenges and Perspectives. *Eur Urol Focus* (2020) 6(4):632–8. doi: 10.1016/j.euf.2020.01.007
5. Babjuk M, Maximilian B, Eva MC, Paolo G, Mostafid AH, Joan P, et al. European Association of Urology Guidelines on Non-muscle-invasive Bladder Cancer (TaT1 and Carcinoma In Situ)- 2019 Update. *Eur Urol* (2019) 76(6):39 –6 57. doi: 10.1016/j.eururo.2019.08.016
6. Khaled D, John T, Jeffrey H. Salvage Therapy for Non–muscle-invasive Bladder Cancer: Novel Intravesical Agents. *Urol Clin North Am* (2020) 47:119–28. doi: 10.1016/j.ucl.2019.09.014
7. Robertson AG, Kim J, Al-Ahmadie H, Bellmunt J, Guo G, Cherniack AD, et al. Comprehensive Molecular Characterization of Muscle-Invasive Bladder Cancer. *Cell* (2017) 171(3):540–56. e25. doi: 10.1016/j.cell.2017.09.007
8. Pietzak EJ, Bagrodia A, Cha EK, Drill EN, Iyer G, Isharwal S, et al. Next-generation Sequencing of Nonmuscle Invasive Bladder Cancer Reveals Potential Biomarkers and Rational Therapeutic Targets. *Eur Urol* (2017) 72(6):952–9. doi: 10.1016/j.eururo.2017.05.032
9. Chen L, Han X. Anti-PD-1/PD-L1 therapy of human cancer: past, present, and future. *J Clin Invest* (2015) 125(9):3384–91. doi: 10.1172/JCI80011
10. Lingel H, Brunner-Weinzierl MC. CTLA-4 (CD152): A versatile receptor for immune-based therapy. *Semin Immunol* (2019) 42:101298. doi: 10.1016/j.smim.2019.101298
11. Klemm F, Joyce JA. Microenvironmental regulation of therapeutic response in cancer. *Trends Cell Biol* (2015) 25(4):198–213. doi: 10.1016/j.tcb.2014.11.006
12. Montazeri K, Bellmunt J. Erdafitinib for the treatment of metastatic bladder cancer. *Expert Rev Clin Pharmacol* (2020) 13(1):1–6. doi: 10.1080/17512433.2020.1702025
13. Haque R, Lei F, Xiong X, Bian Y, Zhao B, Wu Y, et al. Programming of regulatory T cells from pluripotent stem cells and prevention of autoimmunity. *J Immunol* (2012) 189(3):1228–36. doi: 10.4049/jimmunol.1200633
14. Vasekar M, Degraff D, Joshi M. Immunotherapy in Bladder Cancer. *Am J Ther* (2019) 9(3):242–51. doi: 10.2174/1874467208666150716120945
15. Xia Y, Medeiros LJ, Young KH. Immune checkpoint blockade: Releasing the brake towards hematological malignancies. *Blood Rev* (2016) 30(3):189–200. doi: 10.1016/j.blre.2015.11.003
16. Donin NM, Lenis AT, Holden S, Drakaki A, Pantuck A, Belldegrun A, et al. Immunotherapy for the Treatment of Urothelial Carcinoma. *J Urol* (2017) 197(1):14–22. doi: 10.1016/j.juro.2016.02.3005
17. Carosella ED, Ploussard G, Lemaoult J, Desgrandchamps F. A Systematic Review of Immunotherapy in Urologic Cancer: Evolving Roles for Targeting of CTLA-4, PD-1/PD-L1, and HLA-G. *Eur Urol* (2015) 68(2):267–79. doi: 10.1016/j.eururo.2015.02.032
18. Bilgin B, Sendur MA, Hizal M, Yalçın B. An update on immunotherapy options for urothelial cancer. *Expert Opin Biol Ther* (2019) 19(12):1265–74. doi: 10.1080/14712598.2019.1667975
19. Kentaro I. Bladder Cancer: New Insights into Its Molecular Pathology. *Cancers* (2018) 10(4):100. doi: 10.3390/cancers10040100
20. Ricciuti B, Kravets S, Dahlberg SE, Umeton R, Albayrak A, Subegdjo SJ, et al. Use of targeted next generation sequencing to characterize tumor mutational burden and efficacy of immune checkpoint inhibition in small cell lung cancer. *J Immunother Cancer* (2019) 7(1):87. doi: 10.1186/s40425-019-0572-6
21. Schumacher TN, Schreiber RD. Neoantigens in cancer immunotherapy. *Science* (2015) 348(6230):69–74. doi: 10.1126/science.aaa4971
22. Zhu J, Armstrong AJ, Friedlander TW, Kim W, Pal SK, George DJ, et al. Biomarkers of immunotherapy in urothelial and renal cell carcinoma: PD-L1, tumor mutational burden, and beyond. *J Immunother Cancer* (2018) 6 (1):4. doi: 10.1186/s40425-018-0314-1
23. Hahn NM, Necchi A, Loriot Y, Powles T, Plimack ER, Sonpavde G, et al. Role of Checkpoint Inhibition in Localized Bladder Cancer. *Eur Urol Oncol* (2018) 1(3):190–8. doi: 10.1016/j.euo.2018.05.002
24. Curran MA, Montalvo W, Yagita H, Allison JP. PD-1 and CTLA-4 combination blockade expands infiltrating T cells and reduces regulatory T and myeloid cells within B16 melanoma tumors. *Proc Natl Acad Sci U S A* (2010) 107(9):4275–80. doi: 10.1073/pnas.0915174107
25. Duraiswamy J, Kaluza KM, Freeman GJ, Coukos G. Dual Blockade of PD-1 and CTLA-4 Combined with Tumor Vaccine Effectively Restores T-Cell

Rejection Function in Tumors. *Cancer Res* (2013) 73(12):3591–603. doi: 10.1158/0008-5472.CAN-12-4100
26. Selby MJ, Engelhardt JJ, Johnston RJ, Lu LS, Han M, Thudium K, et al. Correction: Preclinical Development of Ipilimumab and Nivolumab Combination Immunotherapy: Mouse Tumor Models, In Vitro Functional Studies, and Cynomolgus Macaque Toxicology. *PloS One* (2016) 11(11): e0167251. doi: 10.1371/journal.pone.0167251
27. Shi LZ, Fu T, Guan B, Chen J, Blando JM, Allison JP, et al. Interdependent IL-7 and IFN-γ signalling in T-cell controls tumour eradication by combined α-CTLA-4+α-PD-1 therapy. *Nat Commun* (2016) 7:12335. doi: 10.1038/ncomms12335
28. Powles T, Necchi A, Rosen G, Hariharan S, Apolo AB. Antia programmed cell death-1/ligand-1 (PD-1/PD-L1) antibodies for the treatment of urothelial carcinoma: state-of-the-art and future development. *Clin Genitourin Cancer* (2017) S1558767317303622. doi: 10.1016/j.clgc.2017.11.002
29. Powles T, Galsky MD, Castellano D, Van Der Heijden MS, Petrylak DP, Armstrong J, et al. A phase 3 study of first-line durvalumab (MEDI4736) ±tremelimumab versus standard of care (SoC) chemotherapy (CT) in patients (pts) with unresectable Stage IV urothelial bladder cancer (UBC): DANUBE. *J Clin Oncol* (2016) 2016(34):15. doi: 10.1200/JCO.2016.34.15_suppl.TPS457
30. Park B, Yee C, Lee KM. The Effect of Radiation on the Immune Response to Cancers. *Int J Mol Sci* (2014) 15(1):927–43. doi: 10.3390/ijms15010927
31. Deng L, Liang H, Burnette B, Beckett M, Darga T, Weichselbaum RR, et al. Irradiation and anti–PD-L1 treatment synergistically promote antitumor immunity in mice. *J Clin Invest* (2014) 124(2):687–95. doi: 10.1172/JCI67313
32. Sundahl N, Wolf KD, Rottey S, Decaestecker K, De Maeseneer D, Meireson A, et al. A phase I/II trial of fixed-dose stereotactic body radiotherapy with sequential or concurrent pembrolizumab in metastatic urothelial carcinoma: evaluation of safety and clinical and immunologic response. *J Trans Med* (2017) 15(1):150. doi: 10.1186/s12967-017-1251-3
33. Teng F, Mu D, Meng X, Kong L, Yu J. Tumor infiltrating lymphocytes (TILs) before and after neoadjuvant chemoradiotherapy and its clinical utility for rectal cancer. *Am J Cancer Res* (2015) 5(6):2064–74.
34. Wu CT, Chen WC, Chang YH, Lin WY, Chen MF. The role of PD-L1 in the radiation response and clinical outcome for bladder cancer. *Sci Rep* (2016) 6 (1):19740. doi: 10.1038/srep19740
35. Abuodeh Y, Venkat P, Kim S. Systematic review of case reports on the abscopal effect. *Curr Probl Cancer* (2016) 40(1):25–37. doi: 10.1016/j.currproblcancer.2015.10.001
36. Grimaldi AM, Simeone E, Giannarelli D, Muto P, Falivene S, Borzillo V, et al. Abscopal effects of radiotherapy on advanced melanoma patients who progressed after ipilimumab immunotherapy. *OncoImmunology* (2014) 3(5): e28780. doi: 10.4161/onci.28780
37. Solanki AA, Bossi A, Efstathiou JA, Lock D, Mondini M, Ramapriyan R, et al. Combining Immunotherapy with Radiotherapy for the Treatment of Genitourinary Malignancies. *Eur Urol Oncol* (2019) 2(1):79–87. doi: 10.1016/j.euo.2018.09.013
38. Claire TA, Kelly J, Shaista H, Azar SMT, Joseph HK, Susan L, et al. Dose-limiting Urinary Toxicity With Pembrolizumab Combined With Weekly Hypofractionated RT in Bladder Cancer. *Int J Radiat Oncol Biol Phys* (2018) 101(5):1168–71. doi: 10.1016/j.ijrobp.2018.04.070
39. Criscuolo D, Francesco M, Riccardo G, Roberta V, Aniello C, Angela C. New combinatorial strategies to improve the PARP inhibitors efficacy in the urothelial bladder Cancer treatment. *J Exp Clin Cancer Res* (2019) 38:91. doi: 10.1186/s13046-019-1089-z
40. Godin-Ethier J, Laïla-Aïcha H, Piccirillo CA, Réjean L. Indoleamine 2,3-Dioxygenase Expression in Human Cancers: Clinical and Immunologic Perspectives. *Clin Cancer Res* (2011) 17(22):6985–91. doi: 10.1158/1078-0432.CCR-11-1331
41. Hudolin T, Mengus C, Coulot J, Kastelan Z, El-Saleh A, Spagnoli GC. Expression of Indoleamine 2,3-Dioxygenase Gene Is a Feature of Poorly Differentiated Non-muscle-invasive Urothelial Cell Bladder Carcinomas. *Anticancer Res* (2017) 37(3):1375. doi: 10.21873/anticanres.11458
42. Smith DC, Gajewski T, Hamid O. Epacadostat plus pembrolizumab in patients with advanced urothelial carcinoma: preliminary phase I/II results of ECHO-202/KEYNOTE-037. *J Clin Oncol suppl* (2017) 36(32):3223–30. doi: 10.1200/JCO.2018.78.9602
43. Meng MV, Gschwend JE, Shore N, Grossfeld GD, Mostafid H, Black PC. Emerging Immunotherapy Options for BCG-unresponsive Non-muscle-invasive Bladder Cancer. *J Urol* (2019) 202(6):1111–9. doi: 10.1097/JU.0000000000000297
44. Ding L, Kim HJ, Wang Q, Kearns M, Jiang T, Ohlson CE, et al. PARP Inhibition Elicits STING-Dependent Antitumor Immunity in Brca1-Deficient Ovarian Cancer. *Cell Rep* (2018) 25(11):2972–2980.e5. doi: 10.1016/j.celrep.2018.11.054
45. Chevolet I, Speeckaert R, Bc S, Neyns B, Brochez L. Characterization of the in vivo immune network of IDO, tryptophan metabolism, PD-L1, and CTLA-4 in circulating immune cells in melanoma. *OncoImmunology* (2015) 4(3):e982382. doi: 10.4161/2162402X.2014.982382
46. Mouw KW, Goldberg MS, Konstantinopoulos PA, D"Andrea AD. DNA Damage and Repair Biomarkers of Immunotherapy Response. *Cancer Discov* (2017) 7(7):675–93. doi: 10.1158/2159-8290.CD-17-0226
47. Van Allen EM, Miao D, Schilling B, Shukla SA, Blank C, Zimmer L, et al. Genomic correlates of response to CTLA4 blockade in metastatic melanoma. *Science* (2015) 350(6257):207–11. doi: 10.1126/science.aad0095 science.aad0095.
48. Oosterlinck W, Kirkali Z, Sylvester R, Silva FCD, Busch C, Algaba F, et al. Sequential Intravesical Chemoimmunotherapy with Mitomycin C and Bacillus Calmette-Guérin and with Bacillus Calmette-Guérin Alone in Patients with Carcinoma in Situ of the Urinary Bladder: Results of an EORTC Genito-Urinary Group Randomized Phase 2 Trial (30993). *Eur Urol* (2011) 59(3):438–46. doi: 10.1016/j.eururo.2010.11.038
49. Stewart RA, Patrick GP, Timothy AY. Development of PARP and Immune-Checkpoint Inhibitor Combinations. *Cancer Res* (2018) 78:OF1–9. doi: 10.1158/0008-5472.CAN-18-2652
50. Sigalotti L, Fratta E, Coral S, Maio M. Epigenetic drugs as immunomodulators for combination therapies in solid tumors. *Pharmacol Ther* (2014) 142(3):339–50. doi: 10.1016/j.pharmthera.2013.12.015
51. Dunn J, Rao S. Epigenetics and immunotherapy: The current state of play. *Mol Immunol* (2017) 87:227–39. doi: 10.1016/j.molimm.2017.04.012
52. Scicinski J, Fisher G, Carter C, Cho-Phan C, Reid T. The Development Of RRx-001, A Novel Nitric-Oxide-Mediated Epigenetically Active Anticancer Agent. *Redox Biol* (2015) 5(C):422–2. doi: 10.1016/j.redox.2015.09.035
53. Zhao H, Ning S, Scicinski J, Oronsky B, Peehl DM. Epigenetic effects of RRx-001: A possible unifying mechanism of anticancer activity. *Oncotarget* (2015) 6(41):43172–81. doi: 10.18632/oncotarget.6526
54. Carter CA, Oronsky BT, Roswarski J, Oronsky AL, Oronsky N, Scicinski J, et al. No Patient Left Behind: The Promise of Immune Priming With Epigenetic Agents. *OncoImmunology* (2017) 6(10):e1315486. doi: 10.1080/2162402X.2017.1315486
55. Das DS, Ray A, Das A, Song Y, Tian Z, Oronsky B, et al. A novel hypoxia-selective epigenetic agent RRx-001 triggers apoptosis and overcomes drug resistance in multiple myeloma cells. *Leukemia*. (2016) 30(11):2187–97. doi: 10.1038/leu.2016.96
56. Morra F, Merolla F, Criscuolo D, Insabato L, Giannella R, Ilardi G, et al. CCDC6 and USP7 expression levels suggest novel treatment options in high-grade urothelial bladder cancer. *J Exp Clin Cancer Res* (2019) 38:90. doi: 10.1186/s13046-019-1087-1
57. Vlachostergios PJ, Jakubowski CD, Niaz MJ, Aileen L, Charlene T, Hackett AL, et al. Antibody-Drug Conjugates in Bladder Cancer. *Bladder Cancer* (2018) 4(3):247–59. doi: 10.3233/BLC-180169
58. Jonathan R, Srikala SS, Zhang JS, David S, Dean R, Thomas WF, et al. EV-101: A Phase I Study of Single-Agent Enfortumab Vedotin in Patients With Nectin-4–Positive Solid Tumors, Including Metastatic Urothelial Carcinoma. *J Clin Oncol* (2020) 38(10):1–9. doi: 10.1200/JCO.19.02044 JCO.19.02044.
59. Rosenberg JE, Flaig TW, Friedlander TW, Friedlander TW, Milowsky MI, Hoimeset CJ. Study EV-103: Durability results of enfortumab vedotin plus pembrolizumab for locally advanced or metastatic urothelial carcinoma. *J Clin Oncol* (2020) 38(15_suppl):5044–4. doi: 10.1200/JCO.2020.38.15_suppl.5044
60. Lattanzi M, Rosenberg JE. The emerging role of antibody-drug conjugates in urothelial carcinoma. *Expert Rev Anticancer Ther* (2020) 20(7):551–61:1782201. doi: 10.1080/14737140.2020

61. Lee YT, Tan YJ, Oon CE. Molecular targeted therapy: Treating cancer with specificity. *Eur J Pharmacol* (2018) 834:188–96. doi: 10.1016/j.ejphar.2018.07.034
62. Cancer Genome Atlas Research N. Comprehensive molecular characterization of urothelial bladder carcinoma. *Nature* (2014) 507 (7492):315–22. doi: 10.1038/nature12965
63. Maleki Vareki S. High and low mutational burden tumors versus immunologically hot and cold tumors and response to immune checkpoint inhibitors. *J Immunother Cancer* (2018) 6(1):157–. doi: 10.1186/s40425-018-0479-7
64. Sweis RF, Spranger S, Bao R, Paner GP, Stadler WM, Steinberg G, et al. Molecular Drivers of the Non-T-cell-Inflamed Tumor Microenvironment in Urothelial Bladder Cancer. *Cancer Immunol Res* (2016) 4(7):563–8. doi: 10.1158/2326-6066.CIR-15-0274
65. Casadei C, Dizman N, Schepisi G, Cursano MC, Basso U, Santini D, et al. Targeted therapies for advanced bladder cancer: new strategies with FGFR inhibitors. *Ther Adv Med Oncol* (2019) 11:1758835919890285–. doi: 10.1177/1758835919890285
66. Qin Q, Patel V, Galsky MD. Urothelial carcinoma: the development of FGFR inhibitors in combination with immune checkpoint inhibitors. *Expert Rev Anticancer Ther* (2020) 20(6):503–12. doi: 10.1080/14737140.2020.1770600
67. Lima NC, Atkinson E, Bunney TD, Katan M, Huang PH. Targeting the Src Pathway Enhances the Efficacy of Selective FGFR Inhibitors in Urothelial Cancers with FGFR3 Alterations. *Int J Mol Sci* (2020) 21(9):3214. doi: 10.3390/ijms21093214
68. Ross RL, McPherson HR, Kettlewell L, Shnyder SD, Hurst CD, Alder O, et al. PIK3CA dependence and sensitivity to therapeutic targeting in urothelial carcinoma. *BMC Cancer* (2016) 16:553–. doi: 10.1186/s12885-016-2570-0
69. Liu ST, Hui G, Mathis C, Chamie K, Pantuck AJ, Drakaki A. The Current Status and Future Role of the Phosphoinositide 3 Kinase/AKT Signaling Pathway in Urothelial Cancer: An Old Pathway in the New Immunotherapy Era. *Clin Genitourin Cancer* (2018) 16(2):e269–e76. doi: 10.1016/j.clgc.2017.10.011
70. Parsa AT, Waldron JS, Panner A, Crane CA, Parney IF, Barry JJ, et al. Loss of tumor suppressor PTEN function increases B7-H1 expression and immunoresistance in glioma. *Nat Med* (2007) 13(1):84–8. doi: 10.1038/nm1517
71. Peng W, Chen JQ, Liu C, Malu S, Creasy C, Tetzlaff MT, et al. Loss of PTEN Promotes Resistance to T Cell-Mediated Immunotherapy. *Cancer Discov* (2016) 6(2):202–16. doi: 10.1158/2159-8290.CD-15-0283
72. Crane CA, Panner A, Murray JC, Wilson SP, Xu H, Chen L, et al. PI(3) kinase is associated with a mechanism of immunoresistance in breast and prostate cancer. *Oncogene* (2009) 28(2):306–12. doi: 10.1038/onc.2008.384
73. Borcoman E, De La Rochere P, Richer W, Vacher S, Chemlali W, Krucker C, et al. Inhibition of PI3K pathway increases immune infiltrate in muscle-invasive bladder cancer. *Oncoimmunology* (2019) 8(5):e1581556–e. doi: 10.1080/2162402X.2019.1581556
74. Workman P, Clarke PA, Raynaud FI, van Montfort RLM. Drugging the PI3 kinome: from chemical tools to drugs in the clinic. *Cancer Res* (2010) 70 (6):2146–57. doi: 10.1158/0008-5472.CAN-09-4355
75. Zeng S-X, Zhu Y, Ma A-H, Yu W, Zhang H, Lin T-Y, et al. The Phosphatidylinositol 3-Kinase Pathway as a Potential Therapeutic Target in Bladder Cancer. *Clin Cancer Res* (2017) 23(21):6580–91. doi: 10.1158/1078-0432.CCR-17-0033
76. Hernández-Prat A, Rodriguez-Vida A, Juanpere-Rodero N, Arpi O, Menéndez S, Soria-Jiménez L, et al. Novel Oral mTORC1/2 Inhibitor TAK-228 Has Synergistic Antitumor Effects When Combined with Paclitaxel or PI3Kα Inhibitor TAK-117 in Preclinical Bladder Cancer Models. *Mol Cancer Res* (2019) 17(9):1931–44. doi: 10.1158/1541-7786.MCR-18-0923
77. Huang J-C, Cui Z-F, Chen S-M, Yang L-J, Lian H-K, Liu B, et al. NVP-BEZ235 synergizes cisplatin sensitivity in osteosarcoma. *Oncotarget* (2017) 9 (12):10483–96. doi: 10.18632/oncotarget.23711
78. Gohr K, Hamacher A, Engelke LH, Kassack MU. Inhibition of PI3K/Akt/mTOR overcomes cisplatin resistance in the triple negative breast cancer cell line HCC38. *BMC Cancer* (2017) 17(1):711–. doi: 10.1186/s12885-017-3695-5
79. Moon DG, Lee SE, Oh MM, Lee SC, Jeong SJ, Hong SK, et al. NVP-BEZ235, a dual PI3K/mTOR inhibitor synergistically potentiates the antitumor effects of cisplatin in bladder cancer cells. *Int J Oncol* (2014) 45(3):1027–35. doi: 10.3892/ijo.2014.2505
80. Seront E, Rottey S, Filleul B, Glorieux P, Goeminne J-C, Verschaeve V, et al. Phase II study of dual phosphoinositol-3-kinase (PI3K) and mammalian target of rapamycin (mTOR) inhibitor BEZ235 in patients with locally advanced or metastatic transitional cell carcinoma. *BJU Int* (2016) 118 (3):408–15. doi: 10.1111/bju.13415
81. Gerullis H, Eimer C, Ecke TH, Georgas E, Freitas C, Kastenholz S, et al. A phase II trial of temsirolimus in second-line metastatic urothelial cancer. *Med Oncol* (2012) 29(4):2870–6. doi: 10.1007/s12032-012-0216-x
82. Milowsky MI, Iyer G, Regazzi AM, Al-Ahmadie H, Gerst SR, Ostrovnaya I, et al. Phase II study of everolimus in metastatic urothelial cancer. *BJU Int* (2013) 112(4):462–70. doi: 10.1111/j.1464-410X.2012.11720.x
83. Iyer G, Hanrahan AJ, Milowsky MI, Al-Ahmadie H, Scott SN, Janakiraman M, et al. Genome sequencing identifies a basis for everolimus sensitivity. *Science (New York NY)* (2012) 338(6104):221–. doi: 10.1126/science.1226344
84. Niegisch G, Retz M, Thalgott M, Balabanov S, Honecker F, Ohlmann CH, et al. Second-Line Treatment of Advanced Urothelial Cancer with Paclitaxel and Everolimus in a German Phase II Trial (AUO Trial AB 35/09). *Oncology* (2015) 89(2):70–8. doi: 10.1159/000376551
85. Kim PS, Kwilas AR, Xu W, Alter S, Jeng EK, Wong HC, et al. Abstract 3245: IL-15 superagonist/IL-15RαSushi-Fc fusion complex (IL-15SA/IL-15RαSu-Fc; ALT-803) markedly enhances specific subpopulations of NK and memory CD8+ T cells, and mediates potent anti-tumor activity of murine breast and colon carcinomas. *Oncotarget* (2016) 7(13):16130–45. doi: 10.18632/oncotarget.7470
86. Evan GG, Makito M, Steve G, Aravindhan S, Ge Z, Lijing Y, et al. Intravesical ALT-803 and BCG Treatment Reduces Tumor Burden in a Carcinogen Induced Bladder Cancer Rat Model; a Role for Cytokine Production and NK Cell Expansion. *PloS One* (2014) 9(6):e96705–. doi: 10.1371/journal.pone.0096705
87. Kaczmarek P, Błaszczyk J, Fijałkowski P, Sierakowska-Fijałek A, Niemirowicz J, Kasprzak A, et al. Assessment of 8-hydroxy-2'-deoxyguanosine concentrations in bladder cancer patients treated with intravesical BCG instillation. *Pol Merkur Lekarski* (2005) 19(112):526–8.
88. Solsona E, Rosario M, Venancio C, Jesus MF, Juan AZ, Jose´ AP, et al. Sequential Combination of Mitomycin C Plus Bacillus Calmette-Gue´rin (BCG) Is More Effective but More Toxic Than BCG Alone in Patients with Non–Muscle-invasive Bladder Cancer. *Eur Urol* (2014) 5865:1–9. doi: 10.1016/j.eururo.2014.09.026
89. Gan C, Amery S, Chatterton K, Khan MS, Thomas K, O'Brien T. Sequential BCG / Electromotive drug administration Mitomycin C (EMDA-MMC) as the standard intravesical regimen in high risk non muscle invasive bladder cancer (HR-NMIBC) – two year outcomes. *J Urol* (2016) 195(6):1697–703. doi: 10.1016/j.juro.2016.01.103
90. Lightfoot AJ, Breyer BN, Rosevear HM, Erickson BA, Konety BR, O'Donnell MA. Multi-institutional analysis of sequential intravesical gemcitabine and mitomycin C chemotherapy for non–muscle invasive bladder cancer. *Urol Oncol* (2014) 32(1):35.e15–9. doi: 10.1016/j.urolonc.2013.01.009
91. Cockerill PA, Knoedler JJ, Frank I, Tarrell R, Karnes RJ. Intravesical gemcitabine in combination with mitomycin C as salvage treatment in recurrent non-muscle-invasive bladder cancer. *BJU Int* (2016) 117(3):456–62. doi: 10.1111/bju.13088
92. Breyer BN, Jared MW, Peter RC, Badrinath RK. Sequential intravesical gemcitabine and mitomycin C chemotherapy regimen in patients with non-muscle invasive bladder cancer. *Urol Oncol* (2010) 28(5):510–4. doi: 10.1016/j.urolonc.2008.11.019
93. Mailand N, Gibbs-Seymour I, Bekker-Jensen S. Regulation of PCNA-protein interactions for genome stability. *Nat Rev Mol Cell Biol* (2013) 14(5):269–82. doi: 10.1038/nrm3562
94. Gilljam KM, Feyzi E, Aas PA, Sousa MM, Müller R, Vågbø CB, et al. Identification of a novel, widespread, and functionally important PCNA-binding motif. *J Cell Biol* (2009) 186(5):645–54. doi: 10.1083/jcb.200903138
95. Gederaas OA, Caroline DS, Trond V, Siri B, Per B, Carl-Jørgen A, et al. Increased Anticancer Efficacy of Intravesical Mitomycin C Therapy when Combined with a PCNA Targeting Peptide. *Trans Oncol* (2014) 7:812–23. doi: 10.1016/j.tranon.2014.10.005
96. Cui M, Jessie L-SA, Guillaume Wientjes M, O'Donnell MA, Kevin RL, Ze L. Intravenous siRNA silencing of survivin enhances activity of mitomycin C in

human bladder RT4 xenografts. *HHS Public Access* (2015) 194(1):230–7. doi: 10.1016/j.juro.2015.02.036

97. Terakawa T, Hideaki M, Naoki Y, Akira M, Hiroyuki T, Takaaki I, et al. Clinical Outcome of Paclitaxel and Carboplatin as Second-Line Chemotherapy for Advanced Urothelial Carcinoma Resistant to First-Line Therapy with Gemcitabine and Cisplatin. *Urol Int* (2014) 92:180–5. doi: 10.1159/000354149
98. Steele TM, CT G, Anhao S, Clifford GT, Paramita MG, Ruth LV. Obatoclax, a BH3 Mimetic, Enhances Cisplatin-Induced Apoptosis and Decreases the Clonogenicity of Muscle Invasive Bladder Cancer Cells via Mechanisms That Involve the Inhibition of Pro-Survival Molecules as Well as Cell Cycle Regulators. *Mol Sci* (2019) 20:1285. doi: 10.3390/ijms20061285
99. Tyagi A, Balaji C, Venkatesh K, Samarpit R, Adrienne CJ, Alatassi H, et al. Combination of androgen receptor inhibitor and cisplatin, an effective treatment strategy for urothelial carcinoma of the bladder. *Urol Oncol* (2019) 37:492–502. doi: 10.1016/j.urolonc.2019.03.008
100. Xylinas E, Melanie RH, Dazhong Z, Martin K, Zeynep E, Brian DR, et al. An Epigenomic Approach to Improving Response to Neoadjuvant Cisplatin Chemotherapy in Bladder Cancer. *Biomolecules* (2016) 6:37. doi: 10.3390/biom6030037
101. Nadal R, Bellmunt J. Management of metastatic bladder cancer. *Cancer Treat Rev* (2019) 76:10–21. doi: 10.1016/j.ctrv.2019.04.002
102. Packiam VT, Scott CJ, Gary DS. Non-Muscle-Invasive Bladder Cancer: Intravesical Treatments Beyond Bacille Calmette-Guerin. *Cancer* (2016), 390–400. doi: 10.1002/cncr.30392
103. Homayoun Z, Jonathan A, Joseph I, Alan S, Peter B. Optimizing intravesical mitomycin C therapy in non-muscle-invasive bladder cancer. *Urology* (2014) 114(4):220–30. doi: 10.1038/nrurol.2014.52
104. Galsky MD, Sumanta KP, Simon C, Lauren CH, Simon JC, Yu-Ning W, et al. Comparative Effectiveness of Gemcitabine Plus Cisplatin Versus Methotrexate, Vinblastine, Doxorubicin, Plus Cisplatin as Neoadjuvant Therapy for Muscle-Invasive Bladder Cancer. *Cancer* (2015), 2586–93. doi: 10.1002/cncr.29387
105. Jinhai H, Mohamed DR-Z, Yong S, Karim C, Stephen AB, Preston K, et al. Discerning Patterns and Quality of Neoadjuvant Chemotherapy Use Among Patients with Muscle-invasive Bladder Cancer. *Eur Urol Oncol* (2019) 2:497–504. doi: 10.1016/j.euo.2018.07.009

Conflict of Interest: The authors declare that the research was conducted in the absence of any commercial or financial relationships that could be construed as a potential conflict of interest.

frontiers in Pharmacology

ORIGINAL RESEARCH
published: 11 March 2021
doi: 10.3389/fphar.2021.487316

Doubling the Dose of Bevacizumab Beyond Progression in Metastatic Colorectal Cancer–the Experience of a Tertiary Cancer Center

Călin Căinap[1,2], Ovidiu-Vasile Bochiş[1†], Cătălin Vlad[1,2†], Raluca Popita[1,3†], Patriciu Achimaş-Cadariu[1,2†], Andrei Havasi[1], Andreea Vidrean[1], Alexandra Dranca[1], Andra Piciu[1,2], Anne-Marie Constantin[4†], Tiberiu Tat[1,5†], Maniu Dana[6†], Ovidiu Crişan[7†], Cosmin Vasile Cioban[8†], Ovidiu Bălăcescu[1†], Ovidiu Coza[1,2†], Loredana Bălăcescu[1†], Monica Mihaela Marta[9†], Madalina Bota[10†] and Simona Căinap[10]*

[1]"Prof Dr Ion Chiricuta" Institute of Oncology, Cluj-Napoca, Romania, [2]Department of Oncology, "Iuliu Hatieganu" University of Medicine and Pharmacy, Cluj-Napoca, Romania, [3]Department of Surgical Specialities, "Iuliu Hatieganu" University of Medicine and Pharmacy, Cluj-Napoca, Romania, [4]Department of Morphological Sciences, "Iuliu Haţieganu" University of Medicine and Pharmacy, Cluj-Napoca, Romania, [5]Department of Anesthesia and Intensive Care I, "Iuliu Hatieganu" University of Medicine and Pharmacy, Cluj-Napoca, Romania, [6]Faculty of Physics, Babes-Bolyai University, Cluj-Napoca, Romania, [7]Faculty of Pharmacy, "Iuliu Hatieganu" University of Medicine and Pharmacy, Cluj-Napoca, Romania, [8]Faculty of Dental Medicine, "Iuliu Hatieganu" University of Medicine and Pharmacy, Cluj-Napoca, Romania, [9]Department of Medical Education, "Iuliu Hatieganu" University of Medicine and Pharmacy, Cluj-Napoca, Romania, [10]Department of Mother and Child, "Iuliu Hatieganu" University of Medicine and Pharmacy, Cluj-Napoca, Romania

Background: Colorectal cancer (CRC) is the third most common cancer in Europe, with an annual increase in incidence ranging between 0.4 and 3.6% in various countries. Although the development of CRC was extensively studied, limited number of new therapies were developed in the last few years. Bevacizumab is frequently used as first- and second-line therapy for management of metastatic CRC (mCRC). The aim of this study is to present our experience with using bevacizumab beyond disease progression at different dosage levels in mCRC patients, in terms of overall survival, progression-free survival, time to treatment failure, and toxicities.

Methods: We performed a consecutive retrospective analysis of patients with confirmed mCRC who were treated with bevacizumab at "Prof Dr. Ion Chiricuta" Institute of Oncology, Cluj-Napoca, Romania. We included patients who had received bevacizumab as first- or second-line therapy and further stratified them according to the dose administered as a second-line (either standard dose of 5 mg/kg every 2 weeks or 7.5 mg/kg every 3 weeks, or double dose of 10 mg/kg every 2 weeks or 15 mg/kg every 3 weeks–depending on the classical chemotherapy partner). All patients had received bevacizumab beyond progression (BYP) which is defined as continuing bevacizumab administration through second-line treatment despite disease progression. In each group, we evaluated the prognostic factors that influenced survival and treatment outcome.

Results: One hundred and fifty-one (151) patients were included in the study. Themedian age of patients receiving double dose bevacizumab (DDB) and standard dose bevacizumab (SDB) was 58 years (range 41–71) and 57 years (range 19–75),

OPEN ACCESS

Edited by:
Nehad M Ayoub,
Jordan University of Science and Technology, Jordan

Reviewed by:
Srinivas V Koduru,
Penn State Milton S. Hershey Medical Center, Hershey, PA, United States
Belal Al-Husein,
Jordan University of Science and Technology, Jordan

***Correspondence:**
Ovidiu Crisan
ovicrisan@umfcluj.ro

[†]These authors have contributed equally to this work and share first authorship

Specialty section:
This article was submitted to Pharmacology of Anti-Cancer Drugs, a section of the journal Frontiers in Pharmacology

Received: 25 July 2019
Accepted: 20 January 2021
Published: 11 March 2021

Citation:
Căinap C, Bochiş O-V, Vlad Că, Popita R, Achimaş-Cadariu P, Havasi A, Vidrean A, Dranca A, Piciu A, Constantin A-M, Tat T, Dana M, Crişan O, Cioban CV, Bălăcescu O, Coza O, Bălăcescu L, Marta MM, Bota M and Căinap S (2021) Doubling the Dose of Bevacizumab Beyond Progression in Metastatic Colorectal Cancer–the Experience of a Tertiary Cancer Center. Front. Pharmacol. 12:487316. doi: 10.3389/fphar.2021.487316

respectively. The median overall survival in the DDB group was 41 months (range 27–49) compared to 25 months (range 23–29) in the SDB group ($p = 0.01$ log-rank test). First-line oxaliplatin-based treatment was used more frequently regardless of group, while irinotecan-based more frequently used as a second-line treatment ($p = 0.014$). Both oxaliplatin- and irinotecan-based regimens were found to be suitable partners for BYP. Statistical analysis revealed that dose intensity, primary tumor location, and cumulative exposure to BYP had significant influence on survival.

Conclusion: Doubling the dose of bevacizumab after first progression may improve survival in mCRC patients. Increasing bevacizumab dose intensity could override the prognostic impact of primary tumor location in patients receiving double the dose of bevacizumab after first disease progression.

Keywords: colorectal, cancer, progression, bevacizumab, metastasis, double dose

INTRODUCTION

According to the latestdata released by GLOBOCAN in 2018, colorectal cancer (CRC) is one of the most common types of cancer worldwide, being the third most frequent and the second most fatal malignancy (Ferlay et al., 2018). In Europe, CRC is the third most common cancer, with the highest incidence rates registered in countries such as Hungary, Slovenia, Slovakia, Norway, and the Netherlands (Ferlay et al., 2018). In Romania, CRC is the second most frequent malignancy after lung cancer in both genders, with a rapidly increasing incidence (Ferlay et al., 2018). The annual increase in incidence in the different European countries ranges from 0.4 to 3.6%.According to the latest reports, the age of disease onset appears to be decreasing. Vuik et al. analyzed the incidence of CRC in the last 25 years in Europe, and revealed an increase in the incidence of the disease among adults aged 20–49 years of age, compared with initial data which showed a predisposition for CRC starting with fifth decade (Vuik et al., 2019).

Since CRC treatment can be curative in the localized and locoregional disease, early diagnosis through national screening programs is essential. However, up to 44% of patients with loco regional disease will develop metastases despite treatment (Bray et al., 2018). In such relapsed cases, as well as in the 20% of CRC patients presenting with metastasis at diagnosis (Edwards et al., 2014), overall survival (OS) can exceed 30 months in fit patients who benefit fromthe triple-agent chemotherapy regimen (FOLFOXIRI) combined with targeted therapy (Qiu et al., 2015).

Despite the discoveries made in the last few years and the research conducted in order to highlight the mechanisms of CRC pathogenesis, the processes that allow cancer cells to migrate, invade and metastasize to other parts of the body have not yet been fully described (Esin and Yalcin, 2016; Coyle et al., 2017).

Although genomic instability—microsatellite instability (MSI), chromosomal instability (CIN), and CpG island methylator phenotype (CIMP) are known to contribute to the development of CRC (Hong, 2018), a limited number of new therapies for metastatic CRC (mCRC) patients have been developed in the last few years. Therapeutic options currently available to treat mCRC include the classical chemotherapy backbone–fluoropyrimidine with oxaliplatin or irinotecan, combined with either an anti-angiogenic agent, or anti-epidermal growth factor receptor (EGFR) antibodies. There are several classesof drugs which target malignant angiogenesis, such as anti-vascular endothelial growth factor (VEGF) antibodies, proteins with binding portions for the extracellular domains of human VEGF receptors 1 and 2, which will retain tumor-released VEGF (a VEGF trap: aflibercept, for example), or protein kinase inhibitors which target angiogenic, stromal and oncogenic receptor tyrosine kinase (RTK) (Stivarga, 2020; Zaltrap, 2020). While anti-EGFR antibodies are used exclusively for mCRC patients with wild-type RAS, anti-angiogenic drugs can be of benefit in all patients regardless of RAS status.Bevacizumab (anti-VEGF antibody) is frequently used as first-orsecond-line therapy for the management of mCRC. Beyond the first progression of the disease, standard dose bevacizumab (SDB) or double dose bevacizumab (DDB) can be administered (Avastin, 2020). New target drugs have been approved for use in patients with mCRC such as immunotherapy like pembrolizumab–approved in MSI-high mCRC patientsas well asunresectable or metastatic solid tumors with MSI-H ordeficient mismatch repair (dMMR). BRAF inhibitors–dabrafenib and MEK inhibitors for mCRC BRAF mutant are still under investigations (Al-Husein et al., 2012; Cutsem et al., 2016; Kuramochi et al., 2017; Keytruda, 2020). Human epidermal growth factor receptor (HER2) amplification seems to be a valuable new target in mCRC. Despite its prevalence of 2% in the general population of mCRC patients, it seems to be linked to primary resistance to anti-EGFR agents (Dienstmann et al., 2018). Although phase III trials are not available, the response rate to anti-HER2 agents reached 38% in the MyPathway study (Dienstmann et al., 2018).

The aim of this study is to present our experience with using bevacizumab beyond disease progression at different dosage levels in mCRC patients, in terms of OS, progression-free survival (PFS), time to treatment failure (TTF), and toxicities.

MATERIALS AND METHODS

Study Population

This study was conducted to generate data from a tertiary care center of excellence in the treatment of mCRC in Romania. We

TABLE 1 | Chemotherapy used in combination with bevacizumab in first and second-line therapy.

Type of chemotherapy	Drug	Dose	Cycle length
FOLFOX4	5-FU	400 mg/m^2 bolus in 15 min day 1 + 2	14 days
	5-FU	600 mg/m^2 continuous perfusion over 22 h day 1 + 2	
	Leucovorin	400 mg/m^2 in 2 h day 1 + 2	
	Oxaliplatin	85 mg/m^2 in 2 h day 1	
FOLFIRI	5-FU	400 mg/m^2 bolus in 15 min day 1 + 2	14 days
	5-FU	600 mg/m^2 continuous perfusion over 22 h day 1 + 2	
	Leucovorin	400 mg/m^2 in 2 h day 1 + 2	
	Irinotecan	180 mg/m^2 day 1	
CAPEOX	Capecitabine	2,000 mg/m^2 days 1–14	21 days
	Oxaliplatin	130 mg/m^2 in 2 h day 1	
CAPIRI	Capecitabine	2,000 mg/m^2 days 1–14	21 days
	Irinotecan	240 mg/m^2 day 1	
Bevacizumab standard dose (SDB)	Bevacizumab + FOLFOX4 or FOLFIRI	5 mg/kg	Every 2 weeks
Bevacizumab standard dose (SDB)	Bevacizumab + CAPEOX or CAPIRI	7.5 mg/kg	Every 3 weeks
Bevacizumab double dose (DDB)	Bevacizumab + FOLFOX4 or FOLFIRI	10 mg/kg	Every 2 weeks
Bevacizumab double dose (DDB)	Bevacizumab + CAPEOX or CAPIRI	15 mg/kg	Every 3 weeks

5FU, 5 fluorouracil; m^2-square meter; mg-milligram, kg-kilogram.

present the treatment strategies, prognostic factors, and survival data of them CRC patients treated between 2009 and 2017 outside of a clinical trial. This study retrospectively included mCRC patients who used bevacizumab as first-line and second-line treatment. Two treatment options are used in our cancer center in which the first is to continue SDB and the other is to consider DDB through second-line treatment. Hence, mCRC patients in this study were classified according to the dose of bevacizumab administered beyond progression. Bevacizumab beyond progression (BYP) was defined as the continuation of bevacizumab treatment in the second-line of systemic therapy despite disease progression proven through imaging techniques. SDB implies that patients continued the same dose of bevacizumab (5 mg/kg every 2 weeks or 7.5 mg/kg every 3 weeks) administered as first-line treatment, while DDB indicates doubling the dose of bevacizumab (10 mg/kg/every 2 weeks or 15 mg/kg every 3 weeks). The decision to maintain SDB or switch to DDB through the second-line treatment was made by oncologists based on bevacizumab toxicity and tolerance through the first-line treatment phase. The study was approved by the Ethics Committee of "Prof.Dr. Ion Chiricuta" Institute of Oncology,Cluj-Napoca,Romania through decision No 42/8 December 2015.

The inclusion criteria were: age of 18 years or older, histologically confirmed diagnosis of CRC, lab tests adequate for chemotherapy and no medical contraindication to chemotherapy, at least one metastatic site, Eastern Cooperative Oncology Group (ECOG) performance status of 0–2, bevacizumab administration in first and second-line treatment, adequate follow-up (at least monthly clinical checkup and CT-scan every 3–4 months).

The exclusion criteria were: previous administration of chemotherapy for the metastatic stage, uncontrolled comorbidities, poor performance status (ECOG ≥3), inadequate labtests, hypersensitivity to the active substance, heart failure (NYHA grade >2), uncontrolled hypertension, acute myocardial infarction (within 6 months prior to start chemotherapy) and pregnancy.

According to the literature, the benefit of systemic treatment in mCRC is controversial especially in patients with poor ECOG performance status, with no survival advantage over the best supportive care (Crosara Teixeira et al., 2015). Therefore, patients with poor performance status were excluded from this study.

Chemotherapy Regimens and Follow-up

The chemotherapeutic regimens used in this study were consistent with international guidelines: capecitabine-based (CAPEOX/XELOX or CAPIRI/XELIRI) 3 weeks regimen or 5-fluorouracil-based (FOLFOX4 or FOLFIRI) 2 weeks regimen, at the dosages displayed in **Table 1**. Dose modifications during treatment were allowed according to guideline recommendations (Cutsem et al., 2016; Messersmith, 2019).

After first-line chemotherapy, most patients underwent maintenance therapy with a reduction in chemotherapy intensity until disease progression or surgical resection. The same standard or double dose bevacizumab was continued beyond disease progression in combination with a different chemotherapy partner. All patients were assessed by CT scan according to RECIST 1.1 (Eisenhauer et al., 2009).

Statistical Analysis

For statistical analysis purposes, we defined overall survival (OS) as the period of time between the first cycle of chemotherapy and death, time to treatment failure (TTF) as the period of time between the first and the last cycle of bevacizumab chemotherapy, progression-free survival after first-line therapy (PFS1) as the time between the first and the last cycle of first-line chemotherapy and progression-free survival during second-line therapy (PFS2) as the time between the first and the last cycle of second-line chemotherapy. These definitions were similar to those in the Simkens CAIRO3 trial with TTF corresponding to the time to second progression (Simkens et al., 2015). We also defined PFS during second-line of therapy in the DDB group.

The main characteristics of the studied population were analyzed using Microsoft Excel 2010, followed by Chi-square test for association. For data reported as mean ± SD, *p*-values were calculated with *t*-test. Survival analyses were performed using R version 3.5.1 [R Core Team (2018). R: A language and

TABLE 2 | Baseline characteristics of mCRC patients in SDB (*N* = 111) and DDB (*N* = 40) groups.

		SDB	DDB	*p*-value
Age **(**years)	Under 65	88 (79.3%)	35 (87.5%)	0.25
	Over 65	23 (20.7%)	5 (12.5%)	
Gender	Male	62 (58.9%)	24 (60.0%)	0.65
	Female	49 (44.1%)	16 (40.0%)	
BMI*(kg/m^2)		25.17 ± 4.47 (14.19–36.51)	27.73 ± 5.03 (19.59–42.24)	**0.01**
Primary tumor	Left-sided	35 (23.17)		0.25
	Right-sided	116 (76.82%)		
Metastasis site	Liver	91 (58.0%)	30 (62.5%)	0.98
	Lung	19 (12.1%)	6 (12.5%)	
	Peritoneum	25 (15.9%)	6 (12.5%)	
	Lymph nodes	6 (3.8%)	2 (4.2%)	
	Bone	6 (3.8%)	1 (2.1%)	
	Other**	10 (6.4%)	3 (6.3%)	
Metastasis–organs involved	1	78 (70.3%)	32 (80.0%)	0.24
	>1	33 (29.7%)	8 (20.0%)	
First-line chemotherapy	Oxaliplatin-based	81 (73.0%)	9 (22.5%)	<**0.01**
	Irinotecan-based	30 (27.0%)	30 (75.0%)	
Second-line chemotherapy	Oxaliplatin -based	33 (29.7%)	20 (50%)	**0.01**
	Irinotecan-based	78 (70.3%)	19 (47.5%)	
RAS	Mutant	11 (9.9%)	6 (15%)	0.06
	Wild type	32 (28.8%)	5 (12.5%)	
	Not available	68 (61.3%)	29 (72.5%)	
T Stage	1	0 (0%)	1 (2.5%)	<**0.01**
	2	3 (2.7%)	1 (2.5%)	
	3	58 (52.3%)	27 (67.5%)	
	4	34 (30.6)	7 (17.5%)	
	Not available	16 (14.4%)	4 (10%)	
N stage	0	8 (7.2%)	6 (15.0%)	0.39
	1	29 (26.1%)	13 (32.5%)	
	2	48 (43.2%)	16 (40.0%)	
	Not available	26 (23.4%)	5 (12.5%)	
M Stage	0***	35 (31.5%)	14 (35%)	0.72
	1	72 (64.9%)	25 (62.5%)	
	Not available	4 (2.5%)	1 (2.5%)	

SDB: standard dose bevacizumab, DDB: double dose bevacizumab; BMI: body mass index; data are n (%); p*-value was calculated with Chi-test.*
**data are mean ± SD (range) and* p*-value was calculated with* t*-test; all tests were conducted at 0.05 level of significance. Bold the significant* p *value when we have multiple values.*
subcutaneous, ovaries.*M0–stage at initial diagnostic.*

environment for statistical computing. R Foundation for Statistical Computing, Vienna, Austria. URLhttp://www.R-project.org/.] in multiple steps. First, we used the Kaplan-Meier method to obtain survival curves. Second, we compared them using the log-rank test. Finally, we used Cox regression to generate Hazard Ratios (HRs) and corresponding 95% Confidence Intervals (CIs). The calculated *p*-values were two-sided, and *p*-values less than 0.05 were considered statistically significant. The Pearson correlation coefficients as well as the corresponding *p*-values were determined using Pearson correlation test, in Microsoft Excel 2010.

RESULTS

Patient Characteristics

In a retrospective analysis of mCRC patients treated with chemotherapy in our institute between 2009 and 2017, we identified 162 patients who met the main inclusion criteria. Out of these, 151 met the criteria for "beyond progression", while 11 were treated with bevacizumab through multiple lines or beyond the third-line of chemotherapy and therefore were excluded from the analysis.

First-line oxaliplatin-based chemotherapy was more frequently used than irinotecan-based therapy in the SDB group compared with the DDB group ($p < 0.001$), while irinotecan was more frequently used in the second-line after disease progression ($p = 0.014$) (**Table 2**). The median age was 57 years (range 19–75) in the SDB group and 58 in the DDB group (range 41–71), while approximately 80% of patients were under the age of 65 in both groups. The primary tumor was in the right side of the colon in 76.8% of cases. The liver, peritoneum and lungs were the most common metastatic sites in both the SDB and DDB groups. About 27.2% of patients had more than one metastatic site. No significant differences were noted between SDB and DDB patients regarding site and number of metastases. More male patients had left-sided cancer compared to female patients. Mean body mass index (BMI) was significantly higher in the DDB group compared to patients receiving SDB ($p = 0.01$). Regarding the RAS status, a reasonable proportion of patients did not have data; however no significant differences were observed between the SDB and DDB groups.

The median values of OS, TTF, PFS1, and PFS2 were significantly higher in the DDB group compared with the SDB group (**Table 3**).

TABLE 3 | Median of OS, PFS, and TTF based on bevacizumab dose.

Endpoint	SDB	DDB	*p*-value
OS	25 (23–29)	41 (27–49)	**0.01**
TTF	19 (16–22)	24 (21–35)	**0.01**
PFS1	12 (11–14)	17 (15–22)	**0.01**
PFS2	5 (4–6)	9 (6–12)	**0.03**

SDB: standard dose bevacizumab, DDB: double dose bevacizumab, OS: overall survival, TTF: time to treatment failure, PFS1: progression-free survival during first-line treatment, PFS2: progression-free survival during second-line treatment; data are median (interquartile range) in months; p-values were calculated with log-rank test at 0.05 level of significance. p value statistical significant.

First and Second-line Chemotherapy Backbone

We investigated the role of first and second-line chemotherapy partners for bevacizumab to improve our understanding for the impact of chemotherapy in mCRC patients.

When comparing the groups regarding the type of standard chemotherapy regimens (irinotecan vs. oxaliplatin backbone) in first- or second-line treatment, a trend toward a greater OS, TTF, PFS1, and PFS2 was observed for irinotecan-based regimens compared to oxaliplatin-based chemotherapy in both groups, however these differences did not reach statistical significance (**Table 6**).

TABLE 4 | Bevacizumab toxicity in SDB and DDB groups.

Type of toxicity		DDB–number of patients (% from total number-40)	SDB- number of patients (% from total number-111)	*p*-value
Proteinuria	Grade 1	7 (17.5%)	10 (9%)	0.69
	Grade 2	4 (10%)	3 (2.7%)	
	Grade 3	3 (7.5%)	5 (4.5%)	
	Any grade	14 (35.0%)	18 (16.2%)	**0.01**
Hypertension	Grade 2	1 (2.5%)	10 (9%)	**0.04**
	Grade 3	7 (17.5%)	8 (7.2%)	
	Any grade	8 (20%)	18 (16.2%)	0.29
Thromboembolic events	Grade 2	1 (2.5%)	3 (2.7%)	0.17
	Grade 3	1 (2.5%)	0 (0%)	
	Any grade	2 (5%)	3 (2.7%)	0.65
Fistula		1 (2.5%)	1 (0.9%)	1.0
Bleeding	Grade 2	1 (2.5%)	3 (2.7%)	1.0
	Grade 3	1 (2.5%)	3 (2.7%)	
	Any grade	2 (5%)	6 (5.4%)	0.92
Cardiopathy		1 (2.5%)	5 (4.5%)	0.10
Treatment delay	Number of patients	3 (7.5%)	7 (6.3%)	0.47
	days delay*	85.33 ± 49.92 (30–127)	69.57 ± 121.45 (8–340)	

DDB: double dose bevacizumab; SDB: standard dose bevacizumab; data are n (%); p-values were calculated with χ2test
**data are mean ± SD (range) and p-value was calculated with t-test; all tests were conducted at 0.05 level of significance. Bold the significant p value when we have multiple values.*

Bevacizumab Toxicity

Regarding toxicity of bevacizumab, hypertension and proteinuria were more frequent in the DDB compared to the SD Bgroup. Of those, only proteinuria and hypertension grade 3 reached statistical significance (**Table 4**). These differences did not lead to significant treatment delays between the SDB and DDB groups.

Survival curves were constructed for OS, TTF, PFS1, and PFS2 according to primary tumor location (data not shown) and the corresponding medians and HR were determined. Statistically significant differences were obtained for OS only with a higher median survival for left-sided vs. right-sided tumors: 29 months (IQR: 25–37) vs. 22 months (IQR: 18–30), respectively, ($p = 0.01$).

In the group of patients having received DDB after first progression, no differences between left- and right-sided mCRC were observed in terms of OS, PFS1, PFS2, and TTF.

Patients receiving SDB had significantly improved OS and PFS2 for left-sided mCRC compared to right-sided disease (**Table 5**). However, TTF and PFS1 were not significantly different between left- and right-sided tumors in patients receiving SDB in second-line treatment.

TABLE 5 | Characteristics of OS, TTF, and PFS depending on primary tumor location in the DDB and SDB groups.

Item	Left-sided*	Right-sided*	HR (CI 95%)	*p*-value
DDB				
OS	46 (35–56)	27 (21–41)	0.57 (0.26–1.24)	0.15
TTF	31 (22–39)	21 (17–28)	0.60 (0.28–1.27)	0.18
PFS1	16 (14–27)	16 (11–20)	0.73 (0.36–1.49)	0.39
PFS2	9 (7–14)	5 (3–10)	0.48 (0.22–1.03)	0.06
SDB				
OS	27 (24–35)	12 (13–32)	0.54 (0.33–0.88)	**0.01**
TTF	19 (16–23)	15 (11–23)	0.99 (0.41–1.08)	0.10
PFS1	12 (11–14)	10 (7–17)	0.84 (0.53–1.33)	0.45
PFS2	6 (5–8)	4 (3–6)	0.55 (0.33–0.9)	**0.02**

*OS: overall survival, TTF: time to treatment failure, PFS1: progression-free survival during first-line treatment, PFS2: progression-free survival during second-line treatment, DDB: double dose bevacizumab, SDB: standard dose bevacizumab; p-values were calculated with log-rank test; HR < 1 means better results in left -sided than in right-sided cases *all values are displayed as medians (interquartile range) in months. Bold the significant p value when we have multiple values.*

TABLE 6 | Median of OS, TTF, and PFS based on type of chemotherapy in the SDB and DDB groups.

		Irinotecan-based*	Oxaliplatin-based*	*p*-value
DDB	OS	43.5 (30–35)	27 (18–44)	0.06
SDB		25 (22–36)	25 (23–30)	0.50
DDB	TTF	25 (21–36)	24 (17–35)	0.60
SDB		21 (16–30)	16 (15–22)	0.30
DDB	PFS1	16 (14–28)	14 (9–19)	0.07
SDB		13 (12–18)	12 (9–13)	0.30
DDB	PFS2	9 (5–19)	8 (6–12)	0.30
SDB		5 (4–6)	6 (4–9)	0.70

OS: overall survival, TTF: time to treatment failure, PFS1: progression-free survival during first-line treatment, PFS2: progression-free survival during second-line treatment, DDB: double dose bevacizumab, SDB: standard dose bevacizumab; p-values were calculated with log-rank test

**data are median (interquartile range) in months.*

outcomes and the total dose of bevacizumab administered ($p < 0.001$). TTF was positively and strongly correlated with total bevacizumab dose, while OS, PFS1, and PFS2 were moderately correlated with total bevacizumab dose, with a tendency toward strong positive correlation in the case of PFS1 in SDB group (**Table 9**).

Subgroup Analysis of Overall Survival

Male gender, age below 65 and an irinotecan-based chemotherapy regimen in first-line were significantly linked to survival advantage among mCRC patients (**Table 10**).

Was OS Influenced by PFS1 or PFS2?

As shown in **Table 11**, OS was significantly and positively correlated with each of TTF, PFS1, and PFS2 among all mCRC patients and each of DDB and SDB patient groups ($p < 0.001$). These correlations were moderate to strong according to the Pearson's correlation analysis.

TABLE 7 | Correlation between treatment outcomes and delayed initiation of bevacizumab in first-line treatment in DDB and SDB groups.

		Delayed bevacizumabinitiation–in months	
		r	*p*-value
OS	DDB	−0.31	0.052
TTF		−0.51	<**0.01**
PFS1		−0.43	<**0.01**
PFS2		−0.39	**0.01**
OS	SDB	−0.19	**0.04**
TTF		−0.41	<**0.01**
PFS1		−0.42	<**0.01**
PFS2		−0.17	0.07

OS: overall survival, TTF: time to tratment failure, PFS1: progression-free survival during first-line treatment, PFS2: progression-free survival during second-line treatment, DDB: double dose bevacizumab, SDB: standard dose bevacizumab; p-value <0.05 indicate statistical significance of Pearson's correlation coefficients (r). Bold the significant p value when we have multiple values.

Timing of Bevacizumab Initiation

We investigated the time of initiation of bevacizumab treatment in terms of months of delay of treatment to see whether it explains the differences in OS, TTF, PFS1, and PFS2 between the DDB and SDB groups; for instance, whether PFS1 could be statistically linked to the initiation of bevacizumab. According to guidelines, bevacizumab must be administrated from the first cycle of systemic treatment, without any delays.

PFS1 and TTF were negatively and significantly correlated with delayed bevacizumab initiation in both the DDB and SDB groups of patients ($p < 0.01$). As shown in **Table 7**, this correlation was moderate.

Bevacizumab dose Intensity

The analysis of bevacizumab dose intensity revealed significant differences in both first and second-line therapy between the DDB and SDB groups. These differences remained also significant for the overall treatment (first and second-line) (**Table 8**).

The Pearson correlation analysis between the total dose of bevacizumab and survival rates is detailed in **Table 9**.

As seen in **Table 9**, both groups (DDB and SDB) had significantly positive correlations between all the treatment

DISCUSSION

Primary Tumor Location

Primary tumor location (PTL) is one of the most important prognostic factors for mCRC. Survival after recurrence was significantly longer in left-sided compared with right-sided colon cancer patients (Cutsem et al., 2016). In first-line treatment with oxaliplatin, fluoropyrimidine and bevacizumab, the laterality of the primary tumor was less important in the maintenance phase of first-line therapy (Jordan et al., 2018). However, PTL remains a significant prognostic factor for second and further lines of treatment (Hegewisch-Becker et al., 2018).

Surprisingly, in our DDB group of patients, no statistically significant differences in terms of OS, TTF, PFS1, and PFS2 in relation with PTL were noted. These results suggest that doubling the dose of bevacizumab overrides the prognostic differences in mCRC according to tumor location. Increasing the dose of bevacizumab could equalize the chance of response to

TABLE 8 | Mean bevacizumab dose intensity in the DDB and SDB patient groups.

	First-line Bev-DI (mg/kg/week)	Second-line Bev-DI (mg/kg/week)	Total Bev-DI (mg/kg/week)
DDB	1.84 ± 0.56 (0.47–3.22)	4.49 ± 2.31 (0.66–12.08)	2.68 ± 1.18 (1.23–7.26)
SDB	1.50 ± 0.64 (0.23–3.06)	2.47 ± 1.05 (0.36–7.74)	1.74 ± 0.52 (0.59–2.97)
p value	**0.004**	<**0.001**	<**0.001**

Bev-DI: bevacizumab dose intensity; DDB: double dose bevacizumab, SDB: standard dose bevacizumab; p-values were calculated with t-test; data are mean ± SD (range). p value statistical significant.

TABLE 9 | Correlation between treatment outcomes and total bevacizumab dose.

Outcome variable		Bevacizumab total dose	
		r	***p*-value**
OS	DDB	0.67	<0.001
TTF		0.77	<0.001
PFS1		0.61	<0.001
PFS2		0.64	<0.001
OS	SDB	0.60	<0.001
TTF		0.80	<0.001
PFS1		0.75	<0.001
PFS2		0.47	<0.001
OS	All	0.59	<0.001
TTF		0.77	<0.001
PFS1		0.68	<0.001
PFS2		0.54	<0.001

OS: overall survival, TTF: time to treatment failure, PFS1: progression-free survival during first-line therapy, PFS2: progression-free survival during second-line therapy, DDB: double dose bevacizumab, SDB: standard dose bevacizumab
**all corresponding p-value are lower than 0.001.*

TABLE 10 | Subgroup analysis of overall survival hazard ratios.

	N	HR	95% CI	*p*-value
All	151	0.62	0.42–0.91	**0.02**
Gender				
Male	86	0.53	0.31–0.90	**0.02**
Female	65	0.65	0.35–1.18	0.16
Age (years)				
<65	123	0.60	0.39–0.91	**0.02**
≥65	28	0.66	0.22–1.97	0.45
First-line chemotherapy				
Oxaliplatin-based	89	0.87	0.40–1.90	0.73
Irinotecan-based	56	0.49	0.27–0.88	**0.02**
PFS1(months)				
≤12	76	0.58	0.31–1.08	0.09

PFS1: progression-free survival after first-line therapy, HR: hazard ratio; CI: confidence interval; p-values were calculated with log-rank test; A hazard ratio< 1 indicate better treatment in double dose bevacizumab group vs. standard dose bevacizumab group. Bold the significant p value when we have multiple values.

TABLE 11 | Correlation between OS and each of PFS and TTF in SDB and DDB groups.

Outcome variable		Overall survival (OS)	
		r	***p*-value**
PFS1	DDB	0.60	<0.001
PFS2		0.47	<0.001
TTF		0.69	<0.001
PFS1	SDB	0.65	<0.001
PFS2		0.56	<0.001
TTF		0.75	<0.001
PFS1	All	0.65	<0.001
PFS2		0.55	<0.001
TTF		0.75	<0.001

OS: overall survival, TTF: time to treatment failure, PFS1: progression-free survival during first-line therapy, PFS2: progression-free survival during second-line therapy, SDB: standard dose bevacizumab, DDB: double dose bevacizumab.

systemic treatment and control of the disease for left-sided and right-sided mCRC patients. However, considering the PTL role in CRC prognosis, Boeckx et al. showed that patients with RAS wild-type left-sided mCRC had a better OS than right-sided disease, regardless of treatment received (Boeckx et al., 2018). In line with this, in a study including 754 patients with first-line therapy of bevacizumab and oxaliplatin backbone regimen, Hegewisch-Becker et al. found significantly better survival in left-sided CRC patients (median survival 24.8 months) compared with right-sided patients (18.4 months), with PTL being the most powerful prognostic factor in multivariate analysis (Hegewisch Becker et al., 2018).

First and Second-line Chemotherapy Backbone Associated With Bevacizumab

The ESMO guidelines recommend the combination of a standard chemotherapy regimen (irinotecan or oxaliplatin-based) with either anti-VEGF or anti–EGFR therapy in the first and second-line treatment in mCRC patients (Schmoll et al., 2012). The NCCN guidelines recommend bevacizumab in first-line therapy in associations with classical chemotherapy regimens but with modest effect on OS, especially when added to oxaliplatin (Messersmith, 2019).

In our study, both chemotherapy regimens–oxaliplatin or irinotecan backbone were equally effective in combination with bevacizumab, as no significant differences were seen between the DDB and SDB groups. The first-line chemotherapy regimen with oxaliplatin backbone was more frequently used in the SDB group compared with DDB in first-line ($p < 0.001$) while irinotecan was more frequently used in the first-line for DDB patients ($p = 0.014$). Similar with our data, two previous studies conducted by Bendell et al. in ARIES study, on 1,550 patients, and Yamazaki et al. on 395 patients, treated in the first-line with FOLFIRI or FOLFOX combined with bevacizumab, retrieved equivalent OS, PFS or rate of response between arms (Bendell et al., 2012; Yamazaki et al., 2014). Moreover, van Cutsem et al. showed similar efficacy of FOLFOX, FOLFIRI or XELOX combined with bevacizumab in the

first-line in the BEAT study on 1914 patients (Van Cutsem et al., 2009). Premature discontinuation of oxaliplatin-based treatment as defined by protocol design altered HR of PFS from 0.63 to 0.83 (Ilic et al., 2016). The main concerns with oxaliplatin-based chemotherapy are its cumulative and slowly reversible neurotoxicity as well as the allergic reactions associated with this regimen (Cetean et al., 2015).

When regimens were compared, the irinotecan-based one seemed to be slightly superior. Ilic et al. and Baraniskin et al. confirmed the advantage of using bevacizumab with chemotherapy (Ilic et al., 2016; Baraniskin et al., 2019).

Bevacizumab dose Intensity and its use Beyond Progression

In clinical practice, according to the European guideline (ESMO) as well as NCCN guideline, a complete genetic characterization of the tumor (all RAS type) and imaging evaluation are required before choosing a systemic regimen for a particular patient (Cutsem et al., 2016; Messersmith, 2019; Veld et al., 2019). The NCCN guidelines draw attention to the existence of preclinical data suggesting a possible rebound effect after bevacizumab cessation (Veld et al., 2019). Our data revealed lower bevacizumab dose intensity in the first but not in the second-line for SDB. The same effect was also recorded for DDB, with an explicable doubling of the intensity in the second-line. The explanation of these facts resides in the administrative constraints existing in our country. In Romania, for more than a decade the national insurance reimbursed the cost of bevacizumab only after a centralized approval. This fact was responsible for widespread and sometimes prolonged delays in optimal bevacizumab administration in the first-line, which were less encountered in second-line administration. We found no significant difference in first-line delays between the SDB and DDB groups. However, our analysis did show significantly negative correlations between PFS1, TTF, and delayed bevacizumab initiation in both the SDB and DDB groups ($p < 0.01$). In DDB group, PFS2 was moderately and negatively correlated with time of bevacizumab delay, while OS was weakly, yet significantly and negatively correlated with delayed bevacizumab administration in the SDB group. Contrary to first-line administration of bevacizumab in our patients, in the second-line we did not observe significant delays in bevacizumab start of administration. Moreover, the dose of bevacizumab was doubled after disease progression in the DDB group with practical aim to overcome tumor resistance which was translated into a prolonged PFS2 for DDB patients compared to SDB. Whether first-line delay of bevacizumab administration could influence PFS2–it must be interpreted with caution, due to the retrospective nature of our analysis with possible bias in patient recruitment and inclusion process. Differences in dose intensity in the first-line treatment may raise questions regarding an excess of bevacizumab or classic chemotherapy partner toxicity in the first-line for the SDB group.

One of the first clinical trials to address the question whether bevacizumab should be continued after disease progression was the ML 18147 phase III trial (Bennouna et al., 2013). The trial was positive in terms of OS, considering the same dose of bevacizumab as in the first-line (2.5 mg/kg body/week). Moreover, in the BRiTE study, Grothey et al. defined "bevacizumab beyond progression" (BYP) differently referring to patients who continued treatment after disease progression within two months at maximum. Median OS and survival after progression were better in patients who received bevacizumab after first progression (19.2 vs. 9.5 months) (Grothey et al., 2014). In the ARIES study on 1,550 patients, Bendell et al. reported that a cumulative dose of bevacizumab represented a significant prognostic factor for survival after first progression (Bendell et al., 2012). The same results were retrieved by Cartwright et al. on 573 patients as determined by improved OS (27.9 vs. 14.6 months) and post-progression survival (21.4 vs. 10.1 months) (Cartwright et al., 2012).

In the same context, in a phase III trial on 185 patients treated with second-line bevacizumab with or without FOLFIRI or FOLFOX (depending on the first-line treatment already administered), Masi et al. found a statistically significant PFS and OS advantage for bevacizumab continuation or reintroduction in the second-line over chemotherapy alone in all the analyzed subgroups (Masi et al., 2015).

Toxicity of Bevacizumab in mCRC Patients

Bevacizumab has some specific adverse effects like hypertension, proteinuria, gastro-intestinal perforation, thrombosis, pulmonary thromboembolism and hemorrhage (Feliu et al., 2015; Dionísio de Sousa et al., 2016).

In our analysis, no statistically significant differences were found in the number of hypertensive cases between the SDB and DDB groups, but in the DDB group grade 3 hypertension was twice as frequent as in the SDB group ($p = 0.04$). Hypertension (grade 3 and 4) is a common adverse event to bevacizumab treatment with an incidence of 0.4 and 17.9% (Dionísio de Sousa et al., 2016). In a small retrospective analysis of 79 patients, grade 2 and 3 of hypertension during bevacizumab administration was predictive of PFS but not OS improvement (Feliu et al., 2015). Our data also revealed that proteinuria was more frequent in the DDB than in the SDB group, reaching statistical significance. Proteinuria was reported in 0.7–54.7% of patients (Feliu et al., 2015). Proteinuria was not correlated with OS or PFS advantage in a phase II trial (Lee et al., 2019). Both hypertension and proteinuria were statistically correlated with the duration of bevacizumab administration, higher doses of bevacizumab may increase the risk, due to a cumulative effect (Loupakis et al., 2018). As for the other bevacizumab adverse events, no significant differences in bleeding, perforation, cardiomyopathy, thrombosis and emboli were found between groups. Treatment was not delayed in the DDB group despite the higher dose in the second-line since no untreatable toxicity occurred. However, perforations were reported in 0.2–1% of patients, bleeding in 10–20% and thrombosis and thromboembolism events in 2.8–17.3% of patients (Feliu et al., 2015).

Subgroup Analysis of Overall Survival

Older age could be a factor for under-treatment reported by Raab et al. (Raab et al., 2019), despite the fact that bevacizumab could improve OS and PFS for this category of patients, as showed by Pinto et al. (Pinto et al., 2017).

In our study, male gender, age below 65 and irinotecan-based chemotherapy in the first-line were significantly linked to a survival advantage. No PFS1 cut-off value was found to be associated with better OS. In the same line, the results of Loupakis et al. that retrospectively analyzed the results of NO 16966 and AVF2107g phase III trials, including patients with mCRC treated in the first-line with bevacizumab and standard chemotherapy showed no OS advantage in any subcategory (Loupakis et al., 2018).

In a pooled analysis of 2,879 patients included in major published trials (COIN, OPUS, AGITG, CRYSTAL, FOCUS 2, and COIN-B), Salem et al. showed that left-sided colon cancer patients were mostly elderly females (over the age of 70 years) (Salem et al., 2018). However, considering the Rahman et al. data, gender was not shown to be predictive for OS (Abdel-Rahman, 2019).

Is OS Influenced by PFS1 or PFS2?

Post-progression survival is a very important factor that may characterize better clinical outcomes after first disease progression. Petrelli et al. showed that in 16,408 patients included in 34 phase III randomized clinical trials, a good correlation between OS and post-progression survival (PFS2) was observed (Petrelli and Barni, 2013).

In our study,PFS1, PFS2, TTF, and OS were all higher in the group of mCRC patients treated with DDB after disease progression (**Table 3**) (Bochis et al., 2020). In previously published data PFS1 was shown to have a strong influence on OS (Petrelli and Barni, 2013). However, in our study, a positive moderate correlation between PFS1, PFS2, and OS with total bevacizumab dose was found in both groups of patients. PFS1 in SDB group showed a tendency to strong positive correlation. All Pearson's correlations examined were statistically significant ($p < 0.001$). PFS1 should not have been dependent on bevacizumab dose intensity since the same first-line doses were administered in both the DDB and SDB groups. The retrospective nature of our study may explain this finding. An analysis of 22,736 patients included in 50 clinical trials found a good correlation between PFS and OS in chemotherapy regimens but less so for trials on monoclonal antibodies (Petrelli and Barni, 2013). Within 20,438 patients, Sidhu et al. observed a weak correlation between the response rate (RR) and OS, lower than the correlation coefficient for PFS and OS (Sidhu et al., 2013).

The limitations of our study may reside in several factors such as the lack of patient randomization at inclusion and variations in the induction treatment and should be considered as a potential source of bias. The unbalanced use of an oxaliplatin backbone regimen in first and second-line therapy in both the SDB and DDB groups may be a factor influencing the general results of our study, due to well-known differences in terms of rate of response, type, and intensity of toxicity compared with irinotecan. The strength of our analysis resides in the data extracted from the medical records of unselected patients with mCRC treated with systemic treatment. The inclusion and exclusion criteria established in this study were meant to create a real-life situation that medical oncologists may be faced with. By avoiding the over-selection of patients imposed by the constraints of a clinical trial, we wished to have a better chance of determining the advantage (if any) of doubling the bevacizumab dose in mCRC patients after first disease progression. In the EMA market-approval for bevacizumab in mCRC, both treatment strategies–standard and double dose–are mentioned, without any recommendation on when to use the double dose. The scarce clinical data available need to be completed with the experience of cancer centers, regional databases, and randomized phase III trials to provide the best proof of efficacy of one of the two strategies. No definitive conclusion can be drawn according to the available data.

CONCLUSION

Our data demonstrated that doubling the dose of bevacizumab after first progression may improve OS, PFS1, PFS2, and TTF. Moreover, an increasing dose of bevacizumab may lead to better outcomes in the DDB group. However, doubling the dose of bevacizumab was not associated with increased toxicities except for grade 3 hypertension, which was manageable, without negative influence on treatment administration. Irinotecan-based chemotherapy regimens in the first-line significantly could be a preferential partner for bevacizumab in mCRC patients.

DATA AVAILABILITY STATEMENT

The datasets generated for this study will not be made publicly available The datasets for this article are not publicly available because: GPDR legislation. Requests to access the datasets should be directed to CC, (calincainap2015@gmail.com).

ETHICS STATEMENT

The studies involving human participants were reviewed and approved by Ethics Committee of the Chiricuta Oncologic Institute, Cluj-Napoca, No 42/8 December 2015. The patients/participants provided their written informed consent to participate in this study.

AUTHOR CONTRIBUTIONS

CC: conceptualization, formal analysis, writing original draft, review and editing; O-VB, CV, RP, PA-C: conceptualization, formal analysis, investigation, data curation, review and editing; A-MC, TT, MD, OC, CVC, OB, OC, LB, MM, MB: investigation, data curation, review and editing; SC: conceptualization, writing original draft, review and editing.

FUNDING

Knowledge transfer of biogenomics in oncology and related domains in clinical applications - BIOGENONCO, MySMIS Code: 105774, Financing contract No: 10/01.09.2016.

REFERENCES

Abdel-Rahman, O. (2019). Impact of sex on chemotherapy toxicity and efficacy among patients with metastatic colorectal cancer: pooled analysis of 5 randomized trials. *Clin. Colorectal Cancer* 18 (2), 110–115.e2. doi:10.1016/j.clcc.2018.12.006

Al-Husein, B., Abdalla, M., Trepte, M., DeRemer, D. L., and Somanath, P. R. (2012). Antiangiogenic therapy for cancer: an update. *Pharmacotherapy* 32 (12), 1095–1111. doi:10.1002/phar.1147

Avastin (2020). European medicines agency. Available from: https://www.ema.europa.eu/en/medicines/human/EPAR/avastin (Accessed Mar 1, 2020).

Baraniskin, A., Buchberger, B., Pox, C., Graeven, U., Holch, J. W., Schmiegel, W., et al. (2019). Efficacy of bevacizumab in first-line treatment of metastatic colorectal cancer: a systematic review and meta-analysis. *Eur. J. Cancer* 106, 37–44. doi:10.1016/j.ejca.2018.10.009

Bendell, J. C., Bekaii-Saab, T. S., Cohn, A. L., Hurwitz, H. I., Kozloff, M., Tezcan, H., et al. (2012). Treatment patterns and clinical outcomes in patients with metastatic colorectal cancer initially treated with FOLFOX-Bevacizumab or FOLFIRI-Bevacizumab: results from ARIES, a bevacizumab observational cohort study. *Oncologist* 17 (12), 1486–1495. doi:10.1634/theoncologist.2012-0190

Bennouna, J., Sastre, J., Arnold, D., Österlund, P., Greil, R., Van Cutsem, E., et al. (2013). Continuation of bevacizumab after first progression in metastatic colorectal cancer (ML18147): a randomised phase 3 trial. *Lancet Oncol.* 14 (1), 29–37. doi:10.1016/s1470-2045(12)70477-1

Bochiş, O-V., Vlad, C., Căinap, C., Achimaş Cadariu, P., Sur, D., Havasi, A., et al. (2020). Treatment beyond progression in metastatic colorectal cancer: to double or not to double the dose of bevacizumab? *J. BUON* 25 (2), 875–883.

Boeckx, N., Koukakis, R., Op de Beeck, K., Rolfo, C., Van Camp, G., Siena, S., et al. (2018). Effect of primary tumor location on second or later-line treatment outcomes in patients with RAS wild-type metastatic colorectal cancer and all treatment lines in patients with RAS mutations in four randomized panitumumab studies. *Clin. Colorectal Cancer* 17 (3), 170–178.e3. doi:10.1016/j.clcc.2018.03.005

Bray, F., Ferlay, J., Soerjomataram, I., Siegel, R. L., Torre, L. A., and Jemal, A. (2018). Global cancer statistics 2018: GLOBOCAN estimates of incidence and mortality worldwide for 36 cancers in 185 countries. *CA A. Cancer J. Clin.* 68 (6), 394–424. doi:10.3322/caac.21492

Cartwright, T. H., Yim, Y. M., Yu, E., Chung, H., Halm, M., and Forsyth, M. (2012). Survival outcomes of bevacizumab beyond progression in metastatic colorectal cancer patients treated in United States community oncology. *Clin. Colorectal Cancer* 11 (4), 238–246. doi:10.1016/j.clcc.2012.05.005

Cetean, S., Ciuleanu, T., Leucuta, D-C., Cainap, C., Constantin, A., Cazacu, I., et al. (2015). Hypersensitivity reactions to platinum derivatives: findings of new predictive markers. *J. BUON* 20 (6), 1617.

Coyle, K. M., Boudreau, J. E., and Marcato, P. (2017). Genetic mutations and epigenetic modifications: driving cancer and informing precision medicine. *Biomed. Res. Int.* 2017, 9620870. doi:10.1155/2017/9620870

Crosara Teixeira, M., Marques, D. F., Ferrari, A. C., Alves, M. F. S., Alex, A. K., Sabbaga, J., et al. (2015). The effects of palliative chemotherapy in metastatic colorectal cancer patients with an ECOG performance status of 3 and 4. *Clin. Colorectal Cancer* 14 (1), 52–57. doi:10.1016/j.clcc.2014.09.010

Cutsem, E. V., Cervantes, A., Adam, R., Sobrero, A., Krieken, J. H. Van., Aderka, D., et al. (2016). ESMO consensus guidelines for the management of patients with metastatic colorectal cancer. *Ann. Oncol.* 27 (8), 1386–1422. doi:10.1093/annonc/mdw235

Dienstmann, R., Salazar, R., and Tabernero, J. (2018). Molecular subtypes and the evolution of treatment decisions in metastatic colorectal cancer. *Am. Soc. Clin. Oncol. Educ. B* (38), 231–238. doi:10.1200/edbk_200929

Dionísio de Sousa, I. J., Ferreira, J., Rodrigues, J., Bonito, N., Jacinto, P., Marques, M., et al. (2016). Association between bevacizumab-related hypertension and response to treatment in patients with metastatic colorectal cancer. *ESMO Open* 1 (3), e000045. doi:10.1136/esmoopen-2016-000045

Edwards, B. K., Noone, A. M., Mariotto, A. B., Simard, E. P., Boscoe, F. P., Henley, S. J., et al. (2014). Annual Report to the Nation on the status of cancer, 1975-2010, featuring prevalence of comorbidity and impact on survival among persons with lung. in colorectal, breast, or prostate cancer. *Cancer* 120, 1290–1314. doi:10.1002/cncr.28509

Eisenhauer, E. A., Therasse, P., Bogaerts, J., Schwartz, L. H., Sargent, D., Ford, R., et al. (2009). New response evaluation criteria in solid tumours: revised RECIST guideline (version 1.1). *Eur. J. Cancer* 45 (2), 228–247. doi:10.1016/j.ejca.2008.10.026

Esin, E., and Yalcin, S. (2016). Maintenance strategy in metastatic colorectal cancer: a systematic review. *Cancer Treat. Rev.* 42, 82–90. doi:10.1016/j.ctrv.2015.10.012

Feliu, J., Salud, A., Safont, M. J., García-Girón, C., Aparicio, J., Losa, F., et al. (2015). Correlation of hypertension and proteinuria with outcome in elderly bevacizumab-treated patients with metastatic colorectal cancer. *PLoS One* 10 (1), e0116527. doi:10.1371/journal.pone.0116527

Ferlay, J., Colombet, M., Soerjomataram, I., Mathers, C., Parkin, D. M., Piñeros, M., et al. (2018). Estimating the global cancer incidence and mortality in 2018: GLOBOCAN sources and methods. *Int. J. Cancer* 144 (8), 1941–1953. doi:10.1002/ijc.31937

Grothey, A., Flick, E. D., Cohn, A. L., Bekaii-Saab, T. S., Bendell, J. C., Kozloff, M., et al. (2014). Bevacizumab exposure beyond first disease progression in patients with metastatic colorectal cancer: analyses of the ARIES observational cohort study. *Pharmacoepidemiol. Drug Saf.* 23 (7), 726–734. doi:10.1002/pds.3633

Hegewisch-Becker, S., Nöpel-Dünnebacke, S., Hinke, A., Graeven, U., Reinacher-Schick, A., Hertel, J., et al. (2018). Impact of primary tumour location and RAS/BRAF mutational status in metastatic colorectal cancer treated with first-line regimens containing oxaliplatin and bevacizumab: prognostic factors from the AIO KRK0207 first-line and maintenance therapy trial. *Eur. J. Cancer* 101, 105–113. doi:10.1016/j.ejca.2018.06.015

Hong, S. N. (2018). Genetic and epigenetic alterations of colorectal cancer. *Intest Res.* 16 (3), 327–337. doi:10.5217/ir.2018.16.3.327

Ilic, I., Jankovic, S., and Ilic, M. (2016). Bevacizumab combined with chemotherapy improves survival for patients with metastatic colorectal cancer: evidence from meta analysis. *PLoS One*. 11 (8), e0161912. doi:10.1371/journal.pone.0161912

Jordan, F., Grundmann, N., Schenkirsch, G., Märkl, B., Messmann, H., Anthuber, M., et al. (2018). Impact of primary tumor localization on the efficacy of bevacizumab in metastatic colorectal cancer. *Anticancer Res.* 38 (9), 5539–5546. doi:10.21873/anticanres.12889

Keytruda (2020). European medicines agency. Available from: https://www.ema.europa.eu/en/medicines/human/EPAR/keytruda (Accessed March 1, 2020).

Kuramochi, H., Ando, M., Itabashi, M., Nakajima, G., Kawakami, K., Hamano, M., et al. (2017). Phase II study of bevacizumab and irinotecan as second-line therapy for patients with metastatic colorectal cancer previously treated with fluoropyrimidines, oxaliplatin, and bevacizumab. *Cancer Chemother. Pharmacol.* 79 (3), 579–585. doi:10.1007/s00280-017-3255-3

Lee, S-P., Hsu, H-C., Tai, Y-J., Chen, Y-L., Chiang, Y-C., Chen, C-A., et al. (2019). Bevacizumab dose affects the severity of adverse events in gynecologic malignancies. *Front. Pharmacol.* 10, 426. doi:10.3389/fphar.2019.00426

Loupakis, F., Hurwitz, H. I., Saltz, L., Arnold, D., Grothey, A., Nguyen, Q. L., et al. (2018). Impact of primary tumour location on efficacy of bevacizumab plus chemotherapy in metastatic colorectal cancer. *Br. J. Cancer* 119 (12):1451–1455. doi:10.1038/s41416-018-0304-6

Masi, G., Salvatore, L., Boni, L., Loupakis, F., Cremolini, C., Fornaro, L., et al. (2015). Continuation or reintroduction of bevacizumab beyond progression to first-line therapy in metastatic colorectal cancer: final results of the randomized BEBYP trial. *Ann. Oncol.* 26 (4), 724–730. doi:10.1093/annonc/mdv012

Messersmith, W. A. (2019). NCCN guidelines updates: management of metastatic colorectal cancer. *J. Natl. Compr. Canc Netw.* 17 (55), 599–601. doi:10.6004/jnccn.2019.5014

Petrelli, F., and Barni, S. (2013). Correlation of progression-free and post-progression survival with overall survival in advanced colorectal cancer. *Ann. Oncol.* 24 (1), 186–192. doi:10.1093/annonc/mds289

Pinto, C., Antonuzzo, L., Porcu, L., Aprile, G., Maiello, E., Masi, G., et al. (2017). Efficacy and safety of bevacizumab combined with fluoropyrimidine monotherapy for unfit or older patients with metastatic colorectal cancer: a systematic review and meta-analysis. *Clin. Colorectal Cancer* 16 (2), e61–e72. doi:10.1016/j.clcc.2016.08.006

Qiu, M., Hu, J., Yang, D., Cosgrove, D. P., and Xu, R. (2015). Pattern of distant metastases in colorectal cancer: a SEER based study. *Oncotarget* 6 (36), 38658–38666. doi:10.18632/oncotarget.6130

Raab, G. T., Lin, A., Hillyer, G. C., Keller, D., O'Neil, D. S., Accordino, M. K., et al. (2019). Use of bevacizumab for elderly patients with stage IV colon cancer: analysis of SEER-medicare data. *Clin. Colorectal Cancer* 18 (3), e294–9. doi:10.1016/j.clcc.2019.05.008

Salem, M. E., Yin, J., Weinberg, B. A., Renfro, L. A., Pederson, L. D., Maughan, T. S., et al. (2018). Clinicopathological differences and survival outcomes with first-line therapy in patients with left-sided colon cancer and rectal cancer: pooled analysis of 2879 patients from AGITG (MAX), COIN, FOCUS2, OPUS, CRYSTAL and COIN-B trials in the ARCAD databas. *Eur. J. Cancer* 103, 205–213. doi:10.1016/j.ejca.2018.08.020

Schmoll, H. J., Cutsem, E. V., Stein, A., Valentini, V., Glimelius, B., Haustermans, K., et al. (2012). ESMO Consensus Guidelines for management of patients with colon and rectal cancer. A personalized approach to clinical decision making. *Ann. Oncol.* 23 (10), 2479–2516. doi:10.1093/annonc/mds236

Sidhu, R., Rong, A., and Dahlberg, S. (2013). Evaluation of progression-free survival as a surrogate endpoint for survival in chemotherapy and targeted agent metastatic colorectal cancer trials. *Clin. Cancer Res.* 19 (5), 969–976. doi:10.1158/1078-0432.ccr-12-2502

Simkens, L. H. J., van Tinteren, H., May, A., Ten Tije, A. J., Creemers, G-J. M., Loosveld, O. J. L., et al. (2015). Maintenance treatment with capecitabine and bevacizumab in metastatic colorectal cancer ({CAIRO}3): a phase 3 randomised controlled trial of the Dutch colorectal cancer group. *Lancet* 385 (9980), 1843–1852. doi:10.1016/S0140-6736(14)62004-3

Stivarga (2020). European medicines agency. Available from: https://www.ema.europa.eu/en/medicines/human/EPAR/stivarga (Accessed March 1, 2020).

Van Cutsem, E., Rivera, F., Berry, S., Kretzschmar, A., Michael, M., DiBartolomeo, M., et al. (2009). Safety and efficacy of first-line bevacizumab with FOLFOX, XELOX, FOLFIRI and fluoropyrimidines in metastatic colorectal cancer: the BEAT study. *Ann. Oncol.* 20 (11), 1842–1847. doi:10.1093/annonc/mdp233

Veld, J. V., Amelung, F. J., Borstlap, W. A. A., Eise van Halsema, E., Consten, E. C. J., Siersema, P. D., et al. (2019). Changes in management of left-sided obstructive colon cancer: national practice and guideline implementation. *J. Natl. Compr. Cancer Netw.* 17 (12), 1512–1520. doi:10.6004/jnccn.2019.7326

Vuik, F. E., Nieuwenburg, S. A., Bardou, M., Lansdorp-Vogelaar, I., Dinis-Ribeiro, M., Bento, M. J., et al. (2019). Increasing incidence of colorectal cancer in young adults in Europe over the last 25 years. *Gut* 68 (10), 18206. doi:10.1136/gutjnl-2018-317592

Yamazaki, K., Nagase, M., Tamagawa, H., Ueda, S., Tamura, T., Murata, K., et al. (2014). A randomized phase III trial of mFOLFOX6 plus bevacizumab versus FOLFIRI plus bevacizumab as first-line treatment for metastatic colorectal cancer: West Japan oncology group study 4407G (WJOG4407G). *J. Clin. Oncol.* 32 (Suppl. 15l), 3534. doi:10.1200/jco.2014.32.15_suppl.3534

Zaltrap (2020). European medicines agency. Available from: https://www.ema.europa.eu/en/medicines/human/EPAR/zaltrap (Accessed Mar 1 2020).

Conflict of Interest: The authors declare that the research was conducted in the absence of any commercial or financial relationships that could be construed as a potential conflict of interest.

Advantages of publishing in Frontiers

OPEN ACCESS
Articles are free to read for greatest visibility and readership

FAST PUBLICATION
Around 90 days from submission to decision

HIGH QUALITY PEER-REVIEW
Rigorous, collaborative, and constructive peer-review

TRANSPARENT PEER-REVIEW
Editors and reviewers acknowledged by name on published articles

Frontiers
Avenue du Tribunal-Fédéral 34
1005 Lausanne | Switzerland

Visit us: www.frontiersin.org
Contact us: frontiersin.org/about/contact

REPRODUCIBILITY OF RESEARCH
Support open data and methods to enhance research reproducibility

DIGITAL PUBLISHING
Articles designed for optimal readership across devices

FOLLOW US
@frontiersin

IMPACT METRICS
Advanced article metrics track visibility across digital media

EXTENSIVE PROMOTION
Marketing and promotion of impactful research

LOOP RESEARCH NETWORK
Our network increases your article's readership